

## รายงานวิจัยฉบับสมบูรณ์

## โครงการ การศึกษาและออกแบบสารประกอบที่มีโครงสร้าง

ในระดับนาโนเมตร

ศ.ดร. จำรัส ลิ้มตระกูล



## รายงานวิจัยฉบับสมบูรณ์

# โครงการ การศึกษาและออกแบบสารประกอบที่มีโครงสร้างใน ระดับนาโนเมตร

คณะผู้วิจัย

สังกัด

ศ.ดร. จำรัส ถิ้มตระกูล ภาควิชาเคมี คณะวิทยาศาสตร์

มหาวิทยาลัยเกษตรศาสตร์

สนับสนุนโดยสำนักงานกองทุนสนับสนุนการวิจัย

(ความเห็นในรายงานนี้เป็นของผู้วิจัย สกว. ไม่จำเป็นต้องเห็นค้วยเสมอไป)

## สารบัญ

บทศัลย่อ/Abstract	1
Executive summary	3
เนื้อหางานวิจัย	6
ผลลัพธ์ที่ใค้จากโครงการ	7
ภาคผนวก	11

## บทคัดย่อ

การศึกษาวิจัยกระบวนการเร่งปฏิกิริยาเคมี ส่งผลต่อการพัฒนาอุตสากรรมเคมือย่างมาก ประกอบกับการวิจัยค้านนาโนเทคโนโลยี ทำให้ค้นพบสารประกอบที่มีโครงสร้างในระดับนาโน เมตร ที่มีคุณสมบัติพีเสษหลายประการ และสามารถประยุกต์ใช้เป็นตัวเร่งปฏิกิริยาเคมีที่มีคุณสมบัติคื ได้ เช่น ซีโอไลต์ ซึ่งเป็นผลิกที่มีรูพรุนที่มีขนาดใกล้เคียงกับขนาดของโมเลกุลของสารเคมี (~0.5 nm) และมีคุณสมบัติในการเลือกเกิดปฏิกิริยาที่จำเพาะกับขนาดและรูปร่างของโมเลกุล และอนุภาคโลหะ ทรานซิชั่น ขนาดนาโนเมตร มีสมบัติเป็นตัวเร่งปฏิกิริยาออกซิเดชันที่ดีและมีความจำเพาะสูงกว่า โลหะทั่วไปมาก การศึกษาวิจัยเกมีของสสารในระดับนาโนเมตรหรือระดับโมเลกุลและความก้าว หน้าค้านนาโนเทคโนโลยีมีความสำคัญและจะช่วยให้เกิดความก้าวหน้าทางวิทยาศาสตร์และ เทคโนโลยีเกมีและอุตสาหกรรมที่เกี่ยวข้อง และการพัฒนาการคำนวณทางเคมีคอมพิวเตอร์และการ จำลองแบบโมเลกุลจะช่วยสนับสนุนการพัฒนาดังกล่าวได้อย่างดียิ่ง

กลุ่มวิจัยเมธิวิจัยอาวุโสนี้จัดตั้งขึ้นเพื่อส่งเสริมการศึกษาวิจัยและรวบรวมความรู้ความ เชี่ยวชาญจากนักวิจัยและนักวิจัยรุ่นใหม่ในสาขาเคมีและวิศวกรรมเคมีจากมหาวิทยาลัยเกษตรศาสตร์ และนักวิจัยรุ่นใหม่จากมหาวิทยาลัย สถาบันเทคโนโลยีพระจอมเกล้า - ลาดกระบัง มหาวิทยาลัย เชียงใหม่ และมหาวิทยาลัยมหิดล เพื่อร่วมกันสร้างสรรค์งานวิจัยและความเป็นเลิศด้านเคมีการเร่ง ปฏิกิริยาในระคับโมเลกุลและวัสดุที่มีโครงสร้างระคับนาโนเมตร กลุ่มวิจัยที่สร้างขึ้นมีผลงานวิจัย จำนวน 25 เรื่องในวารสารวิชาการนานชาติชั้นนำ และเสริมสร้างนักวิจัยวิจัยรุ่นใหม่ จำนวน 12 คน และนักวิจัยรุ่นใหม่ที่เป็นผลผลิตจากกลุ่มวิจัยเมธิวิจัยอาวุโสนี้จะมีส่วนช่วยในการพัฒนาทาง วิทยาศาสตร์และเทคโนโลยีของประเทศต่อไปในอนาคต

#### Abstract

Catalytic and nanostructured materials are perhaps of the utmost importance to areas of research that have direct impact on the chemical industries. Nanochemistry creates a new dimension of chemistry as many materials in small nanometer sizes have significantly different properties from the bulk phases. Zeolites, which are nanostructured crystalline materials, are much better catalysts than normal silica-alumina oxides. Highly dispersed metal clusters show different chemical and electronic properties from large particles of the same metal. Knowledges of nanochemistry or molecular chemistry and nanotechnology are increasingly important and predicted to lead to dramatic impacts to the way we practice and study chemistry and other fields of science and technology. With the advance in computing technology, the computational chemistry and molecular modeling can be an effective route to advancing in chemistry and nanotechnology and related industries.

The proposed "TRF Senior Research Scholar" Unit is designed to provide a unique research environment for the integration of knowledge and expertise from different divisions within the KU faculty of science and engineering. The "Unit" combines the expertise of science and engineering faculties with the talents of new and young members in various universities (Chiang Mai University, and Kasetsart University, and King Mongkut Institute of Technology Lardkrabung, and Mahidol University) to pursue the excellence and integration of research in the areas of Molecular Catalytic and Nanostructured materials. The forming research team has published 25 articles in prestige international journals and fostered 12 young scientists. These outputs of this research unit will contribute to the development and science and technology in Thailand.

## หน้าสรุปโครงการ (Executive Summary) ทุนเมธีวิจัยอาวุโส สกว. (ทุนส่งเสริมกลุ่มวิจัย)

1. ชื่อโครงการ (ภาษาไทย) การศึกษาและออกแบบสารประกอบที่มีโครงสร้างในระดับนาโน เมตร

(ภาษาอังกฤษ) Molecular Design, Structures, and Reaction Mechanisms of Nanostructured Materials Systems

## 2. ชื่อหัวหน้าโครงการ

ศ.คร. จำรัส ลิ้มตระกูล ภาควิชาเคมี คณะวิทยาศาสตร์ มหาวิทยาลัยเกษตรศาสตร์ จตุจักร กรุงเทพฯ 10900

โทรศัพท์: 02-942-8900 ต่อ 304

โทรสาร: 02-942-8900 ต่อ 324

e-mail: fscijrl@ku.ac.th

## 3. สาขาที่ทำการวิจัย เคมีเชิงฟิสิกส์

## 4. ปัญหาที่ทำการวิจัย และความสำคัญของปัญหา

การศึกษาวิจัยกระบวนการเร่งปฏิกิริยาเคมีส่งผลต่อการพัฒนาอุตสากรรมเคมือย่างมาก ประกอบกับการวิจัยค้านนาโนเทคโนโลยี ทำให้ค้นพบสารประกอบที่มีโครงสร้างในระคับนาโน เมตร (Nanomaterials) ซึ่งมีคุณสมบัติพิเศษหลายประการ และสามารถประยุกต์ใช้เป็นตัวเร่งปฏิกิริยา เคมีที่มีคุณสมบัติดีได้ ตัวอย่างเช่น ซีโอไลต์ ZSM-5 ซึ่งเป็นผลึกที่มีรูพรุนที่มีขนาดใกล้เคียงกับขนาด ของโมเลกุลของสารเคมี (~0.5 nm) และมีคุณสมบัติในการเลือกเกิดปฏิกิริยาที่จำเพาะกับขนาดและ รูปร่างของโมเลกุล (Shape Selectivity) และเมื่อเติมอนุภาคโลหะทรานซิชั่น ขนาดเล็กกว่า 1 nm ไป ในซีโอโลต์จะทำให้มีสมบัติเป็นตัวเร่งปฏิกิริยาออกซิเคชัน (selective oxidation) ที่ดีและมี ความจำเพาะสูงกว่าโลหะทรานซิชั่นทั่วไปมาก ตัวอย่างเหล่านี้ แสดงให้เห็นถึงความสำคัญในการ ศึกษาวิจัยสารในระดับนาโนเมตร ซึ่งจะช่วยให้เกิดความก้าวหน้าทางวิทยาศาสตร์และเทคโนโลยีเคมี ได้อย่างดียิ่ง

งานวิจัยนี้ทำการศึกษากลไกปฏิกิริยาเคมีโดยละเอียด อาศัยเทคโนโลยีที่ทันสมัยในค้าน ต่างๆ ได้แก่ ด้าน Spectroscopy โดยได้นำเอาเทกนิกของ IR Raman และ NMR มาใช้ในการวิเคราะห์ และศึกษาสมบัติของตัวเร่งปฏิกิริยาตลอดจนกระบวนการการเร่งปฏิกิริยาที่เกิดขึ้นจริงที่สภาวะต่างๆ ด้าน Reaction Techniques ใค้มีการใช้เทคนิค Temporal Analysis of Products (TAP) และ IR เพื่อ ทำนายที่สทาง และกลไกของการเกิดปฏิกิริยา และได้อาสัยการศึกษาทางทฤษฎีในการจำลองแบบ โมเลกุล (Modeling and Molecular Simulations) โดยใช้ความรู้ทาง Quantum Chemistry, Statistical Mechanics, Reaction Dynamics และ Reaction Engineering ในการจำลองแบบระบบที่สนใจ เพื่อ ศึกษาถึงสมบัติของตัวเร่ง และทำนายกลไกการเกิดปฏิกิริยาที่สภาวะต่างๆ ทำให้เกิดความเข้าใจใน กระบวนการเคมีที่เกิดขึ้นบนพื้นผิวของปฏิกิริยา โครงการวิจัยนี้ได้ทำการศึกษาทั้งโดยการศึกษา ทคลองกับระบบจริงและการศึกษาทางทฤษฎี ด้วยการจำลองแบบโมเลกุลเพื่อให้บรรลุตาม วัตถุประสงค์ คือเกิดความรู้ความเข้าใจปฏิกิริยาเลมีถึงระดับโมเลกุล และเข้าใจผลของโครงสร้างใน ระดับนาโนเมตรของตัวเร่งปฏิกิริยาต่อปฏิกิริยาเคมีที่สนใจศึกษา ซึ่งความรู้ที่ได้ สามารถนำมาใช้ให้ เกิดประโยชน์สูงสุดในการพัฒนาและออกแบบตัวเร่งปฏิกิริยาที่มีประสิทธิภาพ นอกจากนั้นยังได้ทำ การพัฒนาวิธีการสังเคราะห์ซีโอไลต์โดยอาศัยเทคนิคการสังเคราะห์แบบใหม่ และพัฒนาระเบียบ วิธีการคำนวณทางคอมพิวเตอร์เพื่อช่วยในการศึกษาและการออกแบบตัวเร่งปฏิกิริยา เพื่อให้ได้ตัวเร่ง ปฏิกิริยาที่มีประสิทธิภาพสูง สำหรับอุตสาหกรรมเคมีและปีโตรเคมี

## 5. วัตถุประสงค์

- สร้างองค์ความรู้ใหม่ค้านกลไกการเร่งปฏิกิริยาเคมีระคับ โมเลกุล (molecular catalysis) และ nanostructed materials และ computational methodologies
- 2. สร้างกลุ่มวิจัยที่ประกอบด้วยนักวิจัยรุ่นใหม่และนักวิจัยอาวุโส ให้มีศักยภาพสูง ทัดเทียม ระดับสากล และสร้างความร่วมมือในด้านงานวิจัยระหว่างสถาบันการศึกษาทั้งในประเทศ และต่างประเทศ
- สนับสนุนให้มีการวิจัยในระดับสากลเพื่อยกระดับมาตรฐานการศึกษาและวิจัยทาง
   วิทยาศาสตร์ และเทคโนโลยีของประเทศไทย
- 4. ตีพิมพ์ผลงานในวารสารนานาชาติ เพื่อเผยแพร่และประชาสัมพันธ์งานวิจัย

## 6. สรุปผลการดำเนินการของโครงการ

จากการดำเนินการในระยะ 3 ปี ด้วยทุนเมชีวิจัยอาวุโส สกว. (ทุนส่งเสริมกลุ่มวิจัย) ทำให้ เกิดความร่วมมือกันอย่างใกล้ชีดระหว่างนักวิจัย และเสริมสร้างนักวิจัยวิจัยรุ่นใหม่ จำนวน 12 คน จากหลายสถาบันได้แก่ มหาวิทยาลัยเกษตรศาสตร์ มหาวิทยาลัยมหิดล สถาบันเทคโนโลยีพระจอม เกล้าฯ ลาดกระบัง มหาวิทยาลัยเชียงใหม่ โดยร่วมมือกันทำงานวิจัยมุ่งเน้นศึกษาการเร่งปฏิกิริยาใน ระดับโมเลกุล (Molecular Catalysis) บนสารประกอบที่มีโครงสร้างในระดับนาโนเมตร อันได้แก่ สารซีโอไลต์ สารประกอบ TS1 อนุภาคโลหะขนาดเล็ก (Metal Cluster) โดยเน้นศึกษาปฏิกิริยาใน ห้องปฏิบัติการจริง และค้นคว้าวิธีการสังเคราะห์สารประกอบที่โครงสร้างระดับนาโนเมตรแบบใหม่ เพื่อการประยุกด์ใช้ในกระบวนการเคมี ควบคู่ไปกับการใช้วิธีเคมีคอมพิวเตอร์ เพื่อให้เกิดความเข้าใจ ในโครงสร้างและกลไกปฏิกิริยาอย่างลึกซึ้ง และเพื่อเป็นแนวทางในการนำไปใช้ประโยชน์ต่อไป นอกจากนั้นแล้ว ในโครงการวิจัยนี้ ยังมีเป้าหมายเพื่อ ทำการพัฒนาระเบียบวิธีทาง Computational Chemistry ให้ได้วิธีใหม่ ที่มีความถูกต้องและมีประสิทธิภาพสูงยิ่งขึ้น

ผลลัพธ์ของโครงการทำให้เกิดงานวิจัยที่ตีพิมพ์ในวารสารวิชาการนานาชาติ จำนวน 25เรื่อง

## เนื้อหางานวิจัย

จากการศึกษาโดยใช้วิธีทางเคมีทฤษฎีควบคู่กับข้อมูลที่ได้จากการทดลองในห้องปฏิบัติการ จริง ทำให้เข้าใจถึงสมบัติตัวเร่งปฏิกิริยาและกลไกการเร่งปฏิกิริยาเกมีระคับ โมเลกุลของสารประกอบ ที่มีโครงสร้างระคับนาโนเมตรที่มีความสำคัญในอุคสาหกรรม โดยอาศัยหลักการของระเบียบวิธี Hybrid methods ซึ่งเป็นการรวม Density Functional Theory กับ Embedded Structure Theory ศึกษา การคูคซับของสารคูคซับประเภทต่างๆ บนซีโอไลค์ซึ่งถือว่าเป็นขั้นแรกและขั้นสำคัญของ กระบวนการเร่งปฏิกิริยาโดยซีโอไลต์ พบว่าค่าพลังงานคูดซับของสารคูดซับมีความสัมพันธ์โดยตรง กับโครงสร้างและสมบัติเฉพาะทางเคมีของซีโอไลค์ ในกรณีที่สารดูดซับที่มีขนาดของโมเลกูล ใกล้เคียงกับรูพรุนของซี โอ ไลต์และเป็นโมเลกุลไม่มีขั้วจะมีพลังงานการคูคซับที่เกิดจากแรงคึ่งคูค ระหว่างโมเลกุลดูคซับกับผนังรูพรุนของซีโอไลต์ซึ่งส่วนใหญ่เป็นแรง van der Waals อย่างไรก็ตาม เมื่อสารคูคซับเป็นโมเลกุลมีขั้วแรง van der Waals จะมีผลต่อพลังงานการคูคซับน้อยลงแต่ผลของ electrostatic interactions จากโครงผลึกของซีโอไลต์ต่อพลังงานการดูคซับจะเพิ่มขึ้น คังนั้น การเลือก Hybrid methods ให้เหมาะสมกับระบบที่ศึกษาจึงเป็นอีกปัจจัยหนึ่งที่มีผลต่อความน่าเชื่อถือของ ข้อมูลที่ได้ เช่น เมื่อศึกษาการคูดซับของสารประกอบแอ โรมาติกส์บนตัวเร่งซี โอไลต์ ควรเลือกใช้ Hybrid method ที่รวมอิทธิพลของแรง van der Waals ด้วย ซึ่งวิธีหนึ่งที่ประหยัดเวลาและให้ผลที่ เชื้อถือได้คือ DFT:UFF Hybrid method ในขณะที่ระบบมีสารดูคชับเป็นโมเลกุลมีขั้ว เช่น น้ำหรือเม ทานอล ควรเลือกใช้ Hybrid methods ที่รวมผลของ electrostatic interactions ด้วย เช่น SCREEP method ถึงแม้ DFT:UFF และ SCREEP Hybrid methods สามารถใช้ศึกษาการดูคซับของสารดูคซับ บนตัวเร่งซีโอไลต์ได้คื แต่ทั้งสองวิธีนี้ยังมีข้อจำกัด โดยเฉพาะอย่างยิ่งเมื่อต้องการศึกษากลไกการเร่ง ปฏิกิริยาของซีโอไลต์ที่เกี่ยวข้องกับ transition states หรือ intermediates ที่มีโครงสร้างเกะกะและมี ประจุ การใช้แบบจำลองที่มีเพียงแรง van der Waals หรือ electrostatic interactions อย่างใคอย่างหนึ่ง ไม่เพียงพอที่จะอธิบายโครงสร้างที่ไม่เสถียรเหล่านี้ได้ กลุ่มวิจัยจึงได้พัฒนาระเบียบวิธีใหม่บน พื้นฐานของ Hybrid methods เดิม โดยการรวมอิทธิพลของแรง van der Waals และ electrostatic interactions ไว้ในแบบจำลองเคียวกันเพื่อเปรียบเทียบการคูคซับและการเร่งปฏิกิริยาของซีโอไลต์ที่มี โครงผลึกต่างกัน และเรียกแบบจำลองนี้ว่า Embedded ONIOM method

## ผลลัพธ์ที่ได้จากโครงการ

- 1. สรุปผลงานที่ได้รับการตีพิมพ์ในวารสารวิชาการนานาชาติในตลอดระยะเวลา 3 ปี ของการ ดำเนิน โครงการ จำนวน 25 ผลงาน อันได้แก่
  - Pantu, P., Pabchanda, S., and Limtrakul, J. (2004) "Theoretical Investigation of Selective Oxidation of Methane to methanol on Nanostructured Fe-ZSM-5 by ONIOM method", ChemPhysChem, 5, 1901-1906.
  - Namuangruk, S., Pantu, P., Limtrakul, J. (2004) "Alkylation of benzene with ethylene over faujasite zeolite investigated by the ONIOM method", Journal of Catalysis, 2004, 225(2), 523-530.
  - Limtrakul, J., Inntam, C., Truong, T.N. (2004) "Density functional theory study of the ethylene epoxidation over Ti-substituted silicalite (TS-1)", Journal of Molecular Catalysis A: Chemical, 207(2), 139-148.
  - Nokbin, S., Limtrakul, J., Hermansson, K. (2004) "DFT plane-wave calculations of the Rh/MgO(001) interface", Surface Science, 566-568, 977-982.
  - Rungsirisakun, R., Jansang, B., Pantu, P. and Limtrakul, J. (2004) "The adsorption of Benzene on industrially important nanostructured catalysts (H-BEA, H-ZSM-5, and H-FAU): confinement effects", J. Mol. Struct., 733, 239-246.
  - Sirijaraensre, J., Limtrakul, J. (2004) "The influence of the framework to structures
    and energetic profiles of the vapor phase of the Beckmann rearrangement on different
    types of zeolite", Petroleum Chemistry, Preprints, 49(2), 222-226.
  - Chareonpanich, M., Namto, T., Kongkachuichay, P., Limtrakul, J. (2004)
     "Synthesis of ZSM-5 zeolite from lignite fly ash and rice husk ash", Fuel
     Processing Technology, 85(15), 1623-1634.
  - Feil, S., Gluch, K., Matt-Leubner, S., Scheier, P., Limtrakul, J., Probst, M., Deutsch, H., Becker, K., Stamatovic, A., Märk, T.D. (2004) "Partial cross sections for positive and negative ion formation following electron impact on uracil", Journal of Physics B, 37, 3013-3020.
  - Ketrat, S., Limtrakul, J. (2003) "Theoretical study of the ethylene on alkaliexchanged zeolites", International Journal of Quantum Chemistry, 94(6), 333-340.

- Kasuriya, S., Namuangruk, S., Trecsukol, P., Tirtowidjojo, M., Limtrakul, J.,
   (2003) "Adsorption of ethylene, benzene and ethylbenzene over faujasit zeolite investigated by the ONIOM method", Journal of Catalysis, 219, 320-328.
- Bobuatong, K., Limtrakul, J. (2003) "Effects of the zeolite framework on the adsorption of ethylene and benzene on alkali-exchanged zeolite: an ONIOM study", Applied Catalysis A: General, 253, 49-64.
- Sailer, W., Pelc, A., Probst, M., Limtrakul, J., (2003) "Dissociative electron attachment to acetic acid (CH3COOH)", Chemical Physics Letters, 378 (3-4), 250-256.
- 13. Tonmunphean, S., Wijitkosoom, A., Tantirungrotechai, Y., Nuttavut, N., Limtrakul, J. (2003) "Magnetizabilities of Ring-structured Molecules, [8]-cyclacene, [8]-BN-cyclacene and [8]-Collarene, and their Effect on 3He Nuclear Shielding Tensor", Bulletin of the Chemical Society of Japan, 76, 1537-1541.
- Dungsrikaew, V., Limtrakul, J., et. al. (2003) "Comparison of methods for point charge representation of electrostatic fields", International Journal of Quantum Chemistry, 96, 17-22.
- Sailer, W., Pelc, A., Limao-Vieira, P., Mason, N.J., Limtrakul, J, and Probst, M.,
   (2003) "Low energy electron attachment to CH3CN", Chemical Physics Letters,
   381(1,2), 216-222.
- Panjan, W., Limtrakul, J. (2003) "The influence of the framework on adsorption properties of ethylene/H-ZSM-5 system: an ONIOM study", Journal of Molecular Structure, 654(1-3), 35-45.
- Raksakoon, C., Limtrakul, J. (2003) "Adsorption of aromatic hydrocarbon onto H-ZSM-5 zeolite investigated by ONIOM study" THEOCHEM 631, 147-156.
- Boekfa, B., Sirijareansre, J., Pantu, P. and Limtrakul, J., (2004) "A quantum chemical study of the interaction of carbonyls with H-ZSM-5 zeolite", Stud Surf Sci Catal. 154, 1582-1588.
- Wongthong, P., Soonthornpalin, C., Pantu, P. and Limtrakul, J., (2004) "Adsorption of Toluene over Faujasite zeolite investigated by the combined quantum mechanics/molecular mechanics method", Stud Surf Sci Catal., 154, 1817-1822.

- Pabchanda, S., Pantu, P., Tantanak, D. and Limtrakul, J., (2004) "Structure and energetics of nitrous oxide and methane adsorption on the Fe-ZSM-5 zeolite: ONIOM and density functional studies", Stud Surf Sci Catal., 154, 1844-1848.
- Jungsuttiwong, S., Limtrakul, J. and Truong, T.N., (2005) "Theoretical Study of Modes of Adsorption of Water Dimer on H-ZSM-5 and H-Faujasite Zeolites" Journal of Physical Chemistry B, 109, 13342-13351.
- Sirijaraensre, J., Truong, T.N. and Limtrakul J., (2005) "Density Functional Study of the Mechanism of the Beckmann Rearrangement Catalyzed by H-ZSM-5: A Cluster and Embedded Cluster Study" Journal of Physical Chemistry B 109 (24), 12099-12106.
- Treesukol, P., Srisuk, K., Limtrakul J. and Truong T.N, (2005) "Nature of the Metal-Support Interaction in Bifunctional Catalytic Pt/H-ZSM-5 Zeolite" Journal of Physical Chemistry B, 109, 11940-11945.
- Sangthong, W., Probst, M. and Limtrakul J., (2005) "Computational study of the carbonyl-ene reaction of encapsulated formaldehyde in Na-FAU zeolite" Journal of Molecular Structure, 748, 119-127.
- Rujiwatra, A. and Limtrakul, J., (2005) "Ethane-1,2-diaminium hexaaquazinc(II) sulfate" Acta Crystalloraphica, E61, M1403-M1404.

## 2. สรุปผลงานในการประชุมนานาชาติตลอคระยะเวลา 3 ปี ของการคำเนินโครงการ อันได้แก่

- แสดงผลงานในการประชุมนานาชาติในงาน ACS National Meeting ครั้งที่ 225
   ระหว่างวันที่ 23 ถึง 27 มีนาคม 2546 ณ เมือง New Orleans, LA. ประเทศ สหรัฐอเมริกา จำนวน 4 เรื่อง
- 2. แสดงผลงานในการประชุมนานาชาติในงาน Advances in Petrochemicals and Polymers in the New Millennium ครั้งที่ 1 ระหว่างวันที่ 22 ถึง 25 กรกฎาคม 2546 ณ กรุงเทพมหานคร ประเทศไทย จำนวน 4 เรื่อง
- 3. แสดงผลงานในการประชุมนานาชาติในงาน American Chemical Society National Meeting ครั้งที่ 227 ระหว่างวันที่ 28 มีนาคม ถึง 1 เมษายน 2547 ณ เมือง Anaheim, CA. ประเทศสหรัฐอเมริกา จำนวน 5 เรื่อง
- 4. แสดงผลงานในการประชุมนานาชาติในงาน International Zeolite Conference ครั้งที่ 14 ระหว่างวันที่ 25 ถึง 30 เมษายน 2547 ณ เมือง Cape Town, ประเทศแอฟริกาใด้ จำนวน 3 เรื่อง

- 5. แสคงผลงานในการประชุมนานาชาติในงาน American Chemical Society National Meeting ครั้งที่ 229 ระหว่างวันที่ 13 มีนาคม ถึง 17 มีนาคม 2548 ณ เมือง San Diego ประเทศสหรัฐอเมริกา จำนวน 12 เรื่อง
- 3. สรุปกิจกรรมที่เกี่ยวข้อง ตลอคระยะเวลา 3 ปี ของการคำเนิน โครงการ อันได้แก่
  - จัดการประชุมเมธีวิจัยอาวุโส ในหัวข้อเรื่อง การออกแบบโครงสร้างและกลไกการ เกิดปฏิกิริยาของซีโอไลต์และสารประกอบที่มีโครงสร้างในระดับนาโนเมตร เมื่อวันที่ 9-11 พฤศจิกายน 2546 ณ โรงแรมรามาการ์เดน
  - 2. จัดการประชุมเมรีวิจัยอาวุโส ในหัวข้อเรื่อง "Molecular Design, Structure and Reaction Mechanisms of Nanostructured Materials Systems" เมื่อวันที่ 22 มกราคม 2548 ณ โรงแรมซิดี้ปีช รีสอร์ท หัวหิน

# ภาคผนวก

## ภาคผนวก ก.

สรุปผลงานที่ได้รับการตีพิมพ์ ในวารสารวิชาการนานาชาติ จำนวน 25 เรื่อง

# Theoretical Investigation of the Selective Oxidation of Methane to Methanol on Nanostructured Fe-ZSM-5 by the ONIOM Method\*\*

Piboon Pantu, Suwat Pabchanda, and Jumras Limtrakul\*<sup>(a)</sup>

The Intracrystalline nanostructured pore network of zeolites has an astonishing ability to stabilize small metal complexes, leading to extraordinary catalytic activities. Small iron complexes in ZSM-5 (Fe-ZSM-5), for example, have a remarkable redox behavior and received great attention. The Fe-ZSM-5 shows a unique activity in the selective oxidation of methane to methanol at room temperature using nitrous oxide as an oxidant. Due to this catalytic property, the Fe-ZSM-5 has been widely compared with the enzyme methane mono-oxygenase (MMO), whose active site contains a binuclear iron cluster. The Fe-ZSM-5 zeolite also exhibits high activity for the direct partial oxidation of benzene to phenol using nitrous oxide as an oxidant. In and also for selective catalytic reduction of nitrogen oxides. In an also for selective catalytic reduction of nitrogen oxides.

The highly selective and active catalytic site in the Fe-ZSM-5 is generally denoted as a site, of which the exact structure is still not understood, though it has been extensively studied. Generally, the active iron atoms in Fe-ZSM-5 are highly dispersed from complexes, which can form isolated ions, binuclear complexes, or small aggregates of iron atoms, in a zeolite matrix. [6-10] After activation at high temperatures under vacuum or in a flow of steam, the active form of Iron is formed. (6) This active site has a strong affinity for nitrous oxide decomposition. At low temperatures (below 300°C), the decomposition of nitrous oxide leads to deposition of active surface oxygen denoted as α oxygen.<sup>[4]</sup> According to in situ X-ray absorption near edge structure (XANES) and Mössbauer studies, iron atoms at the a site are in a bivalent state (Fe<sup>st</sup>). After decomposition of nitrous oxide, the iron atoms are oxidized to a trivalent state (Fe<sup>ti</sup>). Earlier, proposed structures for the active site mostly were the oxo- or hydroxo-bridged binuclear iron complexes in ZSM-5 pores resembling the structure of the active site of the MMO enzyme. Extended X-ray absorption fine structure (EXAFS) studies have supported the presence of binuclear iron complexes in over-exchanged Fe-ZSM-5 catalysts.<sup>(7)</sup> Recently, it has been reported that the isolated iron cations can be found at the ion exchange site in Fe-ZSM-5 samples, especially at low iron loadings (Fe/Al < 1).[6-10] Based on the infrared spectroscopic results of nitric oxide (NO) adsorption on Fe-ZSM-5, Berlier et al. [8] suggested that the active site is the highly coordinately unsaturated isolated Fe<sup>h</sup> site that is located at the Brønsted acid site. Choi et al. [10] reported EXAFS studies of Fe-ZSM-5 samples with a Fe/Al ratio < 1, which are prepared by solid-state ion exchange with iron species uniformly present in a form of mononuclear iron complexes as either [FeO<sub>3</sub>]<sup>+</sup> or [Fe(OH)<sub>3</sub>]<sup>+</sup>.

Quantum-chemical studies have been utilized to characterize the active site in the Fe-ZSM-5 and to study its activity in various selective oxidation reactions. The first quantum model of active iron species inside zeolites proposed binuclear iron clusters. [11] Yoshizawa et al. [12] proposed a model of mononuclear iron oxide cation in a 3T zeolite cluster and demonstrated that these cations can catalyze the direct oxidation of methane to methanol and of benzene to phenol, although their model involves an unrealistic conversion of Fe<sup>N</sup> to Fe<sup>I</sup> species which has not been experimentally proven. Recently, Ryder et al. [13, 14] and Kachurovskaya et al. [15] proposed a ferryl-type mononuclear iron species in a ZSM-5 zeolite cluster. These two slightly different models demonstrated catalytic decomposition of nitrous oxide<sup>[13]</sup> and direct oxidation of benzene to phenol. [14-15]

However, in earlier reported quantum-chemical studies, electronic properties of zeolites are usually modeled with size-limited cluster fragments of a particular zeolite. With such limited models, the effect of the framework, which can significantly change the structure and energetics of the system, is not taken into account. It has been shown that neglecting the microporous framework effect leads to discrepancies between cluster results and the actual zeolite behavior. [16]

Recent developments in hybrid methods, such as embedded cluster or combined quantum mechanics/molecular mechanics (QM/MM) methods, as well as the more general ONIOM (our own n-layer integrated molecular orbital and molecular mechanics)<sup>(17)</sup> method, have brought large systems within reach of accurate calculation results.

Herein, we report the quantum-chemical study of structure and activity of Fe-ZSM-5 for decomposition of nitrous oxide and oxidation of methane to methanol using an ONIOM method. The active site is modeled as a highly coordinately unsaturated Isolated Fe cation located at the Brønsted acid site of ZSM-5, and the effects of the extended zeolitic framework are explicitly included by utilizing a two-layered ONIOM model. This is one of the first theoretical studies[18-19] adopting the ONIOM scheme for characterizing the reactivity of active sites inside zeolites. The extended structure of the zeolite is found to have profound effects on the structure, the electronic properties and the catalytic activity of the Iron species. These findings are in agreement with a recent FTIR study by Berlier et al., [85] which shows that the Fe<sup>II</sup> species hosted inside the MFI channels exhibits significantly more pronounced coordinative unsaturation than the Fe<sup>®</sup> species anchored on MCM-41 and amorphous silica surfaces and, thus, their higher reactivity towards NO molecules.

<sup>(</sup>a) Or. P. Pantu, S. Pabchanda, Prof. Dr. J. Limtrakul Laboratory for Computational and Applied Chemistry Physical Chemistry Division, Department of Chemistry Kasetsart University, Bangkok 10900 (Thailand) Fax: (4-662)942-8900-324 E-mail: fscijrl@ku.ac.th

<sup>[\*\*]</sup> ONIOM = our own n-layer integrated molecular orbital and molecular mechanics

#### Results and Discussion

#### Model of the a Site [FeO+/ZSM-5-]

The active site in Fe-ZSM-5 is modeled as an isolated mononuclear iron oxide ion at the ion-exchange sites of the ZSM-5. The existence of such an active site has been found by Fourier Transform (FT) IR spectroscopy<sup>89</sup> and was recently confirmed by EXAFS experiments<sup>108</sup> on Fe-ZSM-5 with low iron loadings of Fe/Al = 0.17-0.80. In this model, the active oxygen atom, which is bound to the iron cation, is considered to be an O- radical anion since EPR experiments reported the formation of OT radical anions by decomposition of nitrous oxide on a surface of reduced metal oxides.[20] The effects of nanostructured zeolite pores are included by using the 46T ONIOM2 model in which the active region, consisting of the iron oxide, reactive species and the 5T structure of the ZSM-5 acid site, is modeled by densitiy funtional theory (DFT) calculations, whereas the surrounding ZSM-5 crystal lattice is modeled by the universal force field (UFF) force field with up to 46T atoms in order to cover the cavity at the intersection of the straight and the zigzag pore channels, where reactions normally take place. Since the main interactions between adsorbed molecules and zeolite pore walls are van der Waals Interactions, pil the UFF force field has been found to be adequate in representing the confinement effects of zeolite pore walls. The active model used in this study is similar to that proposed by Ryder et al. in their studies on nitrous oxide decomposition and oxidation of benzene to phenol, 113-141 except that in this study the effects of the extend-

ed zeolite framework is explicitly taken into account by using the ONIOM scheme. Therefore, we will make comparisons wherever possible and point out the effects of the zeolite framework on the reaction inside the zeolite pores.

The optimized structure of the Fe-ZSM-5 model is shown in Figure 1 a. At the active site, the iron cation [FeO]<sup>+</sup> is coordinated with the two bridging oxygen atoms of the zeolite framework which act as Lewis bases exerting bidentate interactions. These interactions are found to be approximately sym-

metric, with almost equal Fe-O bond lengths of 2.02 and 2.03 Å (see Table 1). The distance between the Fe and Al atoms is 2.83 Å. An O" radical anion (O1) is covalently bonded to the Iron atom with a bond distance of 1.66 Å.

#### Oxidation of the $\alpha$ Site by Nitrous Oxide Decomposition

At temperatures below 300 °C, nitrous oxide decomposition can take place on the  $\alpha$  site in Fe-ZSM-5 and leave an active

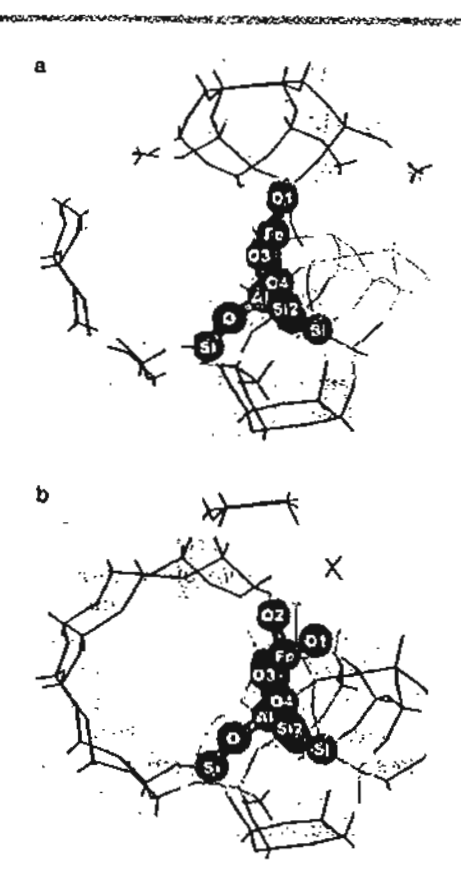


Figure 1. 46T ONIOM model of the Fe-ZSM-5 zeolite, AlSi<sub>a</sub>O<sub>4</sub>H<sub>4</sub>, Atoms belonging to the active region are drawn as sphere: a) FeO-ZSM-5 and b) FeO<sub>2</sub>ZSM-5.

Table 1. The opin	nit in a second	Legimerene	des dille projekt	Cres Oberion	
mediates bod tran		ious estis primis	ысы Деше <b>лк</b> ⊖х	is (Activities (G+10	
Parameters	$N_2O + (FeO)$	N <sub>2</sub> O/(FeO)	TSa	N,/[FeO <sub>2</sub> ]	N,+(FeO <sub>2</sub> )
distances					
Fe-Al	2.83	2.83	2.79	2.80	2.80
Fe-01	1.66	1.67	1.71	1.68	1.67
Fe02	-	2.29	1.90	1.67	1.67
Fe03	2.03	2.04	2.01	1.99	1.98
Fe-04	2.02	2.03	2.01	2.00	1,98
Fe-N1	~	3.10	2.71	2.47	-
N1~02	1.19	1.20	1.56	3.00	(0.65)
N1N2	1.13	1.12	1.12	1.09	3,10
angles					
<b></b> \$01 <b>-</b> Fe-02	-	96.9	101.7	85.4	86.4
<b>₹\$1-03-AI</b>	129.2	129_5	129.9	129.7	129.4
<b>≰Si2O4AJ</b>	130.3	130.4	129.8	128.6	128.9

surface oxygen species (α oxygen) deposited on the active iron center. The reaction pathway is depicted in Figure 2 and selected structural parameters are tabulated in Table 1. First, a nitrous oxide molecule adsorbs on the [FeO]<sup>+</sup> site. It is found that structure and energetics of the adsorbed nitrous oxide molecule are significantly affected by the extended zeolite crystal structure. The steric confinement of the zeolite pore walls included in the 46T ONIOM model causes the adsorbed nitrous oxide molecule to point with its nitrogen end towards the empty space in the intersection cavity of the ZSM-5 zeolite,

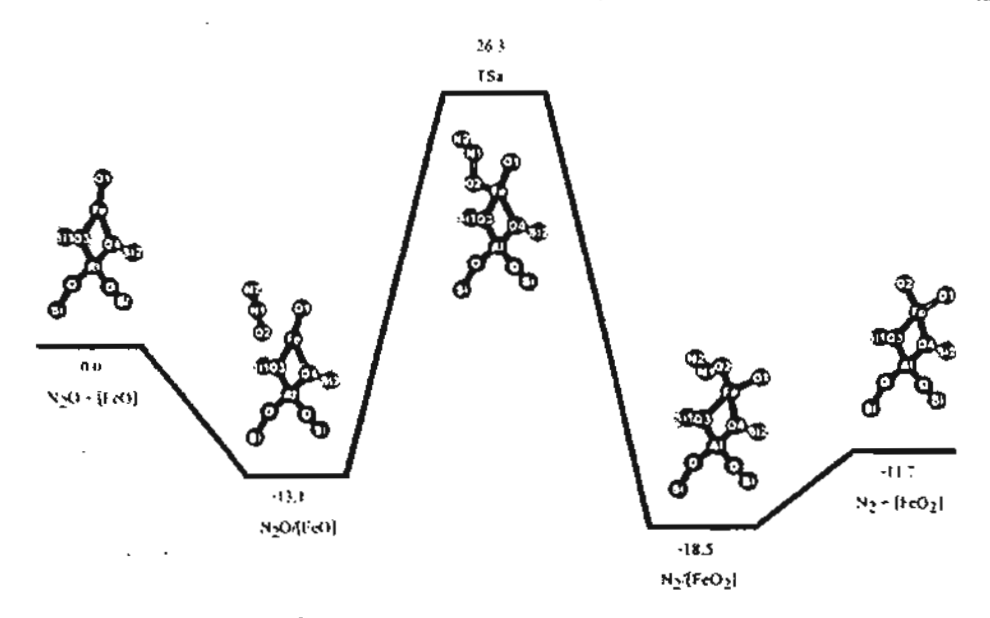


Figure 2. Energy profile [kcalmol $^{-1}$ ] for nitrous axide decomposition over Fe-ZSM-5 by the 46T ONIOM method (B3LYP/6-311 + G(3df,2p):UFF).

whereas in a bare 5T model the nitrogen end of the nitrous oxide leans towards the 5T cluster fragment due to stabilizing electronic interactions. The energetics of the adsorbed molecule is also markedly affected by the extended framework of the zeolite. In the 46T ONIOM model, the adsorption energy is calculated to be -13.1 kcal mol<sup>-1</sup>, which is reasonably close to the averagemental estimate of 15 kcal mol<sup>-1</sup>, which is reasonably close to (CO). The second of the adsorption energy is the average of the adsorption and the α-oxygen atom (CO). The second of the adsorption energy is (CO).

the experimental estimate of -16 kcalmol-1221 whereas, in the case of 5T bare cluster, the computed adsorption energy is only -6.6 kcal mol-1,[13] Subsequently, the adsorbed nitrous oxide can undergo the decomposition reaction by breaking the N-O bond, releasing a nitrogen molecule, and leaving an active surface a oxygen deposited on the active iron site. The activation energy for the nitrous oxide decomposition is evaluated to be 39.4 kcalmol-1, which agrees reasonably with the energy barrier for the same step computed by Ryder et al. of 37.6 kcal mol<sup>-1</sup> [13] However, the apparent activation energy for this step is calculated to be 26.3 kcalmol-1, which is considerably lower than the value of 31.0 kcalmol<sup>-1</sup> reported by Ryder et al.[13] for the same reaction step mainly due to the effects of the extended zeolite framework included ONIOM scheme that stabilizes the reactive complexes inside the zeolite pores.

After decomposition of nitrous oxide, an active  $\alpha$ -oxygen atom is deposited on the active iron center and the optimized structure of the  $\alpha$ -oxygen-loaded site is presented in Figure 1 b. The Fe-Al distance is computed to be 2.80 Å (see Table 1), which agrees well with the Fe-Al distance of  $\approx$  2.9 Å experimentally measured by EXAFS for the mononuclear iron dioxide  $\{\text{FeO}_2\}^+$  or rather the dihydroxide  $\{\text{Fe}(\text{OH})_2\}^+$  at the ion exchanged site of the ZSM-5 zeolite by Choi et al. The Fe-O distances are 1.98 Å between the iron atom and the two bridging atoms of the zeolite framework and 1.67 Å between the iron atom and the  $\alpha$ -oxygen atoms, it is noted that the Fe-O bond distance of 1.67 Å is close to the bond distance of 1.65 Å

between an active oxygen atom bound to the heme iron in the enzyme cytochrome P450cam, D31 but significantly shorter than the normal Fe-O single bond distance of 1.8 Å. The distance between the two oxygen atoms is 2.29 Å, which Indicates that these two OToxides do not form a chemical bond. The configurations of the two oxygen atoms around the iron atom are slightly different. The Fe-O1 bond is close to the zigzag pore wall while the Fe-O2 bond is pointing towards the free space in the intersection cavity. Therefore, the O2 is slightly more accessible to incoming adsorbates.

Methane Selective Oxidation on the  $\alpha\textsc{-Oxygen-Loaded}$  Site [FeO2+/ZSM-5-]

the a-oxygen-loaded site is proposed in Figure 3 and selected structural parameters are presented in Table 2. Initially, methane weakly adsorbs on the active site with one hydrogen atom (H1) pointing towards the iron atom and the α-oxygen atom (O2). The computed adsorption energy is -6.1 kcal mol-1. The weak Interactions between the adsorbed methane and the active site do not significantly disturb the structure of the active site. Nevertheless, the adsorbed methane molecule is apparently activated to some extent as the C-H1 bond distance is slightly elongated from 1.090 Å to 1.095 Å. Then, the adsorbed methane is activated by hydrogen abstraction forming a hydroxyl group on the iron center and a methyl radical. The transition state structure shows the characteristic feature of the direct H-abstraction process with an almost linear angle for the C-H1-Oα angle (172.7 degree). At the transition state, the C-H1 bond of the methane molecule is elongated from 1.095 Å to 1.21 Å and, at the same time, the H1-Oa bond is forming as the H1-Ox distance decreased from 3.30 Å to 1.33 Å. The energy barrier for this step is calculated to be 15.3 kcalmol<sup>-1</sup>, which is close to the energy barrier of 14-18 kcalmol<sup>-1</sup> for Habstraction from methane by the MMO enzymeted and also close to the energy barrier of 16 kcal mol-1 for C-H bond dissociation of methane on the surface O- radical anion of MoO, [25]

The methyl free radical intermediate can rapidly recombine with the surface O<sup>-</sup> radical anion forming a highly stable methoxide species. The bond distances between the iron atom and methoxide as well as between the iron atom and hydroxide are 1.79 and 1.81 Å, respectively reflecting the typical Fe—O single bond distance. The O1—Fe—O2 bond angle Increases from 86.4 to 119.2 degrees to reduce the repulsive interactions between the methoxide and the hydroxide which are situated

## **CHEMPHYSCHEM**

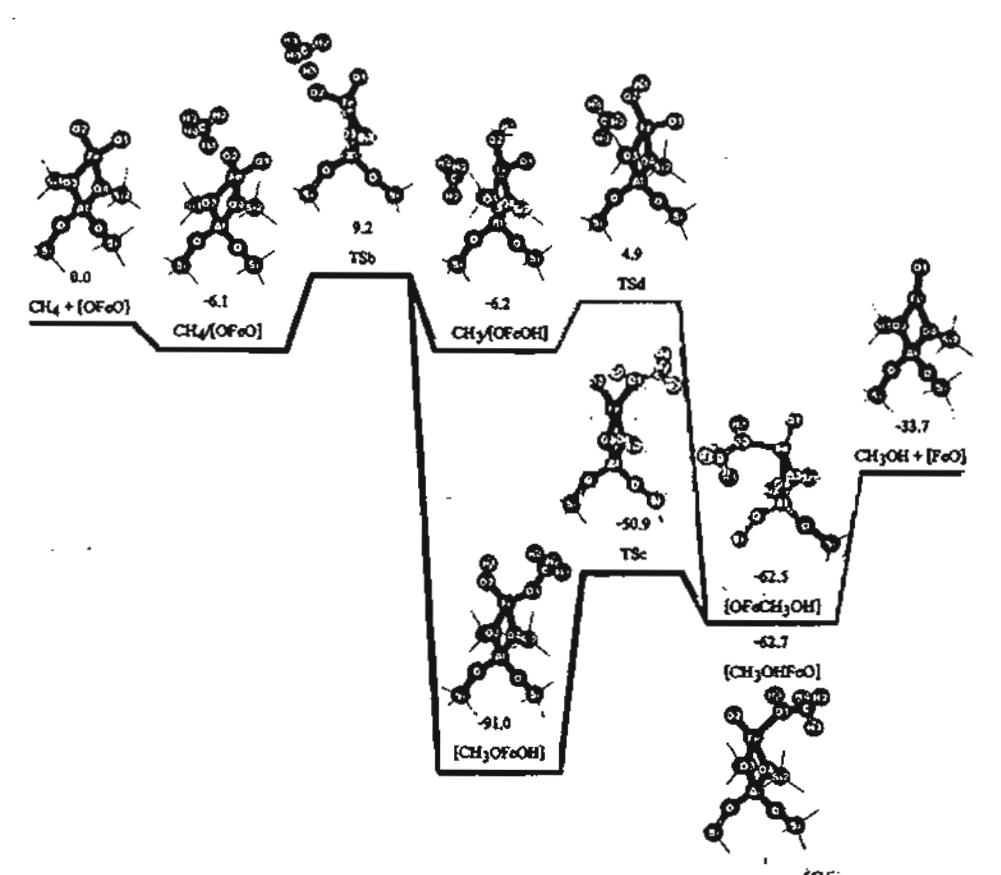


Figure 3. Energy profile [kcal mol<sup>-1</sup>] for selective axidation of methane over Fe-ZSM-5 by the 46T ONIOM method (83LYP/6-311+G(3df,2p):UFF).

on the same iron atom. The methoxide product is more stable than the starting reactants and, therefore, this process is highly exothermic with a reaction energy of -91.0 kcal mol<sup>-1</sup>. This fast radical recombination step is assumed to be a barrierless process, since a transition state for this step cannot be found.

This stable methoxide can be converted to methanol via a hydrogen shift reaction. The transition structure shows that the hydrogen atom of the hydroxyl group is moving to the oxygen atom of the methoxide to form the methanol product. However, the conversion of methoxide to methanol is quite difficult, as this reactions requires a high activation energy of 40.1 kcal mol-1 and is endothermic by 28.5 kcal mol-1. However, the exothermic conversion of methanol back to methoxide is relatively easy achievable and requires a small activation energy of 11.8 kcal mol-1 as the methoxide species is more stable than the adsorbed methanol.

Alternatively, the methyl radical is stabilized by the ZSM-5 framework by forming a loosely bound complex with the iron atom at a Fe--CH<sub>3</sub> distance of 2.78 Å. The formation of strongly bound methyl species on the iron active site with a much shorter bond distance (1.97 Å) as proposed by Yoshizawa et al.<sup>[12]</sup> has not been found in this model, the

space around the active iron atom is more crowded than in the model of Yoshizawa et al. as the iron atom is covalently bound to two oxygen atoms and surrounded by zeolite pore walls. Therefore, the space around the iron atom appears to be too crowded to accommodate a strong bonding of a methyl group. The relative energy of this loosely bound methyl radical complex is evaluated to be -6.2 kcal mol<sup>-1</sup>. The methyl radical

Parameters	$CH_1 + \{OFeO\}$	CH_AOFeO)	†Sb	ĮζΉ <sub>ε</sub> ΟΓεΟΗ[	TS¢	(CH <sub>1</sub> OHFeO)	CH_XOFeOH	TS:d	[QFeCH <sub>2</sub> QI
distances									
e Al	2.80	2.79	2.77	2.64	2.82	2.85	2:64	2.85	2.84
e-01	1.67	1.67	1,61	1.79	2.03	2.13	1.61	1.65	1,67
e-02	1.67	\ <i>i</i> Śፖ	1.75	1.81	1.74	1.67	1.78	1.87	2.12
c-03	1.98	1.98	1.99	2.04	2.03	2:07	2.03	2.07	207
e ∙04	1.96	1.99	2.03	202	2.03	2.06	2-05	2,84	2.07
e-C	_	3.46	3.66	3.09	3.23	3,40	2.78	2.48	3,31
HI	1.09	1.09\$	1.21	-	~		3.87	-	-
)1O2	2.29	2.27	2,58	3.10	2.31	2.76	2.59	2,77	2.98
11-02	-	3.30	1,33	0.96	1,29	2.53	0.97	0.97	0,96
(1 - O)	•	3.33	2.74	3.39	1.20	0.97	2.55	-	-
ngles									
₹01 Fe-02	86,4	85.8	100,1	319.2	75.2	.92.2	99,3	103.5	102,9
£5103 ;Ai	129.4	129.9	129.9	129.1	129.4	129.4	129.3	129.0	129.5
K \$42 - O4 - A1	128.9	128,4	129.1	130.6	129.6	130.4	130.5	130.7	131.0
¢C-R103		84.5	172.7		X-1	· <u>-</u>	_	_	•

## COMMUNICATIONS

can then be transformed to methanol by reacting with the hydroxyl group on the active iron center. This reaction is also highly exothermic with a reaction energy of -56.3 kcal mol<sup>-1</sup> and a calculated activation energy of 11.1 kcal mol<sup>-1</sup>. The resulting adsorbed methanol is strongly attached to the catalyst. Desorption of the adsorbed methanol would require a high activation energy to overcome the strong adsorption energy of 28.8 kcal mol<sup>-1</sup>.

The methoxide and methanol products are both strongly attached to the active site and, thus, are not easy to be desorbed, which is in agreement with experimental observation, which show that the product from the direct oxidation of methane to methanol on Fe-ZSM-5 is so strongly attached to the catalyst surface that it cannot be directly desorbed. A solvent extraction by water or a mixture of water and acetonitrile<sup>[1]</sup> is needed to hydrolyze and remove the adsorbed products from the surface of Fe-ZSM-5.

When we examine the energy profile of the selective oxidation of methane, the activation of methane via hydrogen abstraction is found to be the rate-limiting step in agreement with the kinetic isotope effects, which indicate that a step involving C—H dissociation is the rate-limiting step. The predicted activation energy of 15.3 kcal mol<sup>-1</sup> is comparable to the energy barrier for H abstraction by the MMO enzyme.<sup>[24]</sup> This is also in agreement with the experimental observation that this reaction can occur at room temperature similar to the enzymatic system.<sup>[1-2]</sup> The reaction then preferably proceeds via a rapid recombination of the methyl radical and the surface oxygen radical anion forms the highly stable methoxide which is strongly adsorbed to the active site.

## Conclusions

Using the ONIOM method to investigate the reactivity of Fe-ZSM-5, we observe that the confinement of the zeolite pore structure can stabilize the adsorbed reactive species and affect structures, electronic properties and catalytic activity of the active Iron species. On the active iron center, the oxidation of methane proceeds through the direct hydrogen abstraction of adsorbed methane forming a methyl radical with an energy barrier of 15.3 kcalmol<sup>-1</sup> which is comparable to the energy barrier found in the MMO enzyme system. The methyl radical can undergo the barrier-less recombination with the surface Or radical anion and produces the strongly adsorbed methoxide. Alternatively, the methyl radical can be stabilized by the zeolite framework and, then, react rapidly with the hydroxyl group on the iron center forming the adsorbed methanol. Due to the relative stability, the adsorbed methanol can be easily converted to the more stable methoxide species which should become the dominant product and is strongly adsorbed on the catalyst surface.

## **Computational Methods**

The structure of the duster model was taken from the crystal structure of the ZSM-5 lattice.<sup>[26]</sup> In this study, the Fe-ZSM-5 structure was represented by a 46T ONIOM2 model. The

46T cluster that coveres the three different channel structures (channel intersection, the straight channel and the zigzag channel), where reactions normally take place, was selected with one aluminum atom that substituted a silicon atom at the T12 position. The negative charge of the cluster was balanced by either the [FeO]<sup>+</sup> or the [FeO<sub>2</sub>]<sup>+</sup> ion to form the active center (Figure 1).

The accuracy of the ONIOM method depends significantly on the choice of the level of calculations for high- and lowlevel regions, in the ONIOM2 model the 5T active center was treated quantum chemically at the 83 LYP level of theory using the 6-311+G(3df,2p) basis set for all types of atoms, except for the Iron atom, for which the energy-consistent pseudo-potential (ECP) of Stuttgart and Born in the small-core approximation[27] was used as it has been shown by Ryder et al.[13-14] that this basis set gives reasonable results for catalytic decomposition of nitrous oxide and oxidation of benzene to phenol in the Fe-ZSM-5 catalyst. Using the experimental adsorption energy as a benchmark, we have demonstrated that the UFF method provides reasonable values corresponding to experimental measurements.[10] This is due to the explicit consideration of van der Waals interactions, which are the dominant contribution for adsorption-desorption mechanisms in zeolites. [21] This suggests that the UFF method is a practical choice for the low-level methodology whereas the high-level region is treated by the B3LYP method. Therefore, the rest of the extended framework, up to 46T, was treated at molecular mechanics force field.

Geometry optimizations were done at the B3LYP/6-311 + G(3df,2p) level of theory. The total spin of the system was kept constant at the sextet state throughout all calculations. During the structure optimization, only the 5T portion of the active site region and the adsorbates were allowed to relax while the rest was fixed at the crystallographic coordinates. Normal mode analyses were carried out to verify the transition states to have one imaginary frequency whose mode corresponds to the designated reaction. All calculations have been performed by using the Gaussian 98 code.<sup>[28]</sup>

## Acknowledgements

This work was supported by grants from the Thailand Research Fund (TRF Senior Research Scholar to JL) and the Kasetsart University Research and Development Institute (KURDI) as well as by the Ministry of University Affairs under the Science and Technology Higher Education Development Project (MUA-ADB funds).



a) K. A. Dubkov, V. I. Sobolev, G. I. Panov, Kinet. Catal. 1998, 39, 72-79;
 b) G. I. Panov, V. I. Sobolev, K. A. Dubkov, V. N. Parmon, N. S. Ovanesyan, A. E. Shilov, A. A. Shteinman. React. Kinet. Catal. Lett. 1997, 61, 251-258;
 c) V. I. Sobolev, K. A. Dubkov, O. V. Panna, G. I. Panov, Catal. Today 1995, 24, 251-252.

## **CHEMPHYSCHEM**

- [2] G. L. Panov, V. L. Sobolev, K. A. Dubkov, A. S. Kharitonov, Stud. Surf. Sci. Catal. 1996, 101, 493 – S02.
- [3] a) G. L. Panov, G. A. Sheveleva, A. S. Kharitonov, V. N. Romannikov, L. A. Vostrikova, Appl. Catal. A 1992, 82, 31–36; b) R. Burch, C. Howitt, Appl. Catal. A 1993, 103, 135–162.
- [4] G. I. Panov, V. I. Sobolev, A. S. Kharitonov, J. Mol. Catal. 1990, 61, 85-97.
- [5] a) R. Joyner, M. Stockenhuber, J. Phys. Chem. B 1999, 103, 5963-5976;
   b) V. I. Sobolev, G. I. Panov, A. S. Kharitonov, V. N. Romannikov, A. M. Volodin, K. G. Ione, J. Catal. 1993, 139, 435-443;
   c) X. Feng, W. K. Hall, Catal. Lett. 1996, 41, 45-46;
   d) J. Perez-Ramirez, F. Kapteijn, G. Mul, J. A. Moulijn, Chem. Commun. 2001, 693-694.
- [6] a) G. Berlier, G. Spoto, S. Bordiga, G. Ricchlardi, P. Fiskaro, A. Zecchina, L. Rossetti, E. Seili, L. Forni, E. Giarnello, C. Lamberti, J. Catal. 2002, 208, 64–82; b) J. Jia, Q. Sun, B. Wen, L. X. Chen, W. M. H. Sachtler, Catal. Lett. 2002, 82, 7–11; c) K. A. Dubkov, N. S. Ovanesyan, A. A. Shteinman, E. V. Starokon, G. I. Panov, J. Catal. 2002, 207, 341–352.
- [7] a) A. Battiston, J. H. Bitter, F. M. F. de Groot, A. R. Overweg, O. Stephan, J. A. van Bokhoven, P. J. Kooyman, C. van der Spek, G. Vanko, D. C. Koningsberger, J. Catal. 2003, 213, 251–271; b) K. A. Dubkov, N. S. Ovanesyan, A. A. Shteinman, E. V. Starokon, G. L. Panov, J. Catal. 2002, 207, 341–352; c) T. V. Voskoboinikov, H.-Y. Chen, W. M. H. Sachtler, Appl. Catal. 8 1998, 19, 279–287; d) P. Marturano, L. Drozdova, A. Kogelbauer, R. Prins, J. Catal. 2000, 192, 236–247.
- [8] a) G. Berlier, A. Zecchina, G. Spoto, G. Ricchiardi, S. Bordiga, C. Lamberti, J. Catal. 2003, 215, 264-270; b) G. Berlier, F. Bonino, A. Zecchina, S. Bordiga, C. Lamberti, ChemPhysChem 2003, 4, 1073-1078.
- (9) L. J. Lobree, L.-C. Hwang, J. A. Reimer, A. T. Bell, J. Catal. 1999, 186, 242–253.
- [10] S. H. Chol, B. R. Wood, J. A. Ryder, A. T. Bell, J. Phys. Chem. B 2003, 107, 11843-11851.
- [11] M. J. Filatov, A. G. Peimenschikov, G. M. Zhidomirov, J. Mol. Catal. 1993, 80, 243-251.
- [12] K. Yoshizawa, Y. Shiota, T. Yumura, T. Yamabe, J. Phys. Chem. 8 2000, 104, 734-740.
- [13] J. A. Ryder, A. K. Chakraborty, A. Y. Bell, J. Phys. Chem. 8 2002, 106, 7059-7064.
- [14] J. A. Ryder, A. K. Chakraborty, A. T. Bell, J. Catal. 2003, 220, 84-91.
- [15] N. A. Kachurovskaya, G. M. Zhildomirov, E. J. M. Hensen, R. A. van Santen, Catal. Lett. 2003, 86, 25–31.
- [16] a) P. E. Sinclair, A. H. de Vries, P. Sherwood, C. R. A. Catlow, R. A. van Santen, J. Chem. Soc. Faraday Trans. 1998, 94, 3401-3408; b) M. Brandle, J. Brandle, J. Am. Chem. Soc. 1998, 120, 1556-1570.
- [17] a) M. Svensson, S. Humbel, R. D. J. Froese, T. Matsubara, S. Sieber, K. Morokuma, J. Phys. Chem. 1996, 100, 19357-19363; b) S. Dapprich, I. Komaromi, K. S. Byun, K. Morokuma, M. J. Frisch, J. Mol. Struct. 1999, 461, 1-21.
- [18] a) C. Raksakoon, J. Umtrakul, J. Mol. Struct. 2003, 631, 147-156; b) W. Panjan, J. Limtrakul, J. Mol. Struct. 2003, 654, 35-45; c) S. Kasuriya, S. Namuangruk, P. Treesukol, M. Tirtowidjojo, J. Limtrakul, J. Catal. 2003, 219, 320-328; d) K. Bobuatong, J. Limtrakul, Appl. Catal., A 2003, 253, 49-64.
- [19] a) M. Boronat, P. M. Viruela, A. Corma, J. Am. Chem. Soc. 2004, 126, 3300-3309; b) A. Damín, S. Bordiga, A. Zecchina, C. Lamberti, J. Chem. Phys. 2002, 117, 226-237; c) F. Bonino, A. Damin, G. Ricchiardi, M. Ricci, G. Spano, R. D'Aloisio, A. Zecchina, C. Lamberti, C. Prestipino, S. Bordiga, J. Phys. Chem. B 2004, 108, 3573-3583; d) F. Bonino, A. Damin, S. Bordiga, C. Lamberti, A. Zecchina, Langmulr 2003, 19, 2155-2161; e) S. Bordiga, A. Damin, F. Bonino, A. Zecchina, G. Spano, F. Rivetti, V. Bolís, C. Prestipino, C. Lamberti, J. Phys. Chem. B 2002, 106, 9892-9905.
- [20] a) V. A. Shvets, V. B. Kazanskil, J. Catal. 1972, 25, 123-130; b) Y. B. Taarit, J. H. Lunsford, Chem. Phys. Lett. 1973, 19, 348-350.
- [21] a) X. Rozanska, R. A. van Santen, F. Hutschka, J. Hafner, J. Am. Chem. Soc. 2001, 123, 7655-7667; b) L. A. Clark, M. Slerka, J. Sauer, J. Am. Chem. Soc. 2003, 125, 2136-2141; c) E. G. Derouane, C. D. Chang, Microporous Mesoporous Mater. 2000, 35-36, 425-433; d) A. Pelmenschikov, J. Leszczynski, J. Phys. Chem. 8 1999, 103, 6886-6890.
- [22] B. R. Wood, J. A. Reimer, A. T. Bell. J. Catal. 2002, 209, 151-158.
- [23] L. Schlichting, J. Berendzen, K. Chu, A. M. Stock, S. A. Maves, D. E. Benson, R. M. Sweet, D. Ringe, G. A. Petsko, S. G. Silgar, Science, 2000, 287, 1615–1622.

[24] A.M. Valentine, S.S. Stahl, S.J. Uppard, J. Am. Chem. Soc. 1999, 121, 3876–3887.

- [25] S. P. Mehandru, A. B. Anderson, J. F. Brazdil, R. K. Grasselli, J. Phys. Chem. 1987, 91, 2930 – 2934.
- [26] H. van Koningveld, H van Bekkun, J. C. Jansen, Acta Crystallogr., Sect. 8: Struct. Sci. 1987, 43, 127 – 132.
- [27] M. Dolg, U. Wedig, H. Stoll, H. Preuss, J. Chem. Phys. 1987, 86, 866.
- [28] Gaussian 98 (Revision A.7), M. J. Frisch, G. W. Trucks, H. B. Schlegel, G. E. Scuseria, M. A. Robb, J. R. Cheeseman, V. G. Zakrzewski, J. A. Montgomery, R. E. Stratmann, J. C. Burant, S. Dapprich, J. M. Millam, A. D. Daniels, K. N. Kudin, M. C. Strain, O. Farias, J. Tomasi, V. Barone, M. Cossi, R. Cammi, B. Mennucci, C. Pomelli, C. Adamo, S. Clifford, J. Ochterski, G. A. Petersson, P. Y. Ayala, Q. Cul, K. Morokuma, D. K. Malick, A. D. Rabuck, K. Raghavachari, J. B. Foresman, J. Goslowski, J. V. Ortiz, B. B. Stefanov, G. Liu, A. Liashenko, P. Piskorz, L. Komaromi, R. Gomperts, R. L. Martin, D. J. Fox, T. Keith, M. A. Al-Laham, C. Y. Peng, A. Nanayakkara, C. Gonzalez, M. Challacombe, P. M. W. Gill, B. G. Johnson, W. Chen, M. W. Wong, J. L. Andres, M. Head-Gordon, E. S. Replogle, J. A. Pople, Gaussian, Inc., Pitts-

Received: April 12, 2004

burgh, PA, 2001.

Early View Article
Published online on November 12, 2004

## Cation Mobility and Anion Reorientation in Sodium Trifluoromethyl Sulfonate

Leo van Wüllen, \*\*\*\* Natalia Sofina, \*\*\* and Martin Jansen\*\*\*

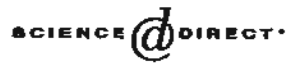
The study of solid electrolytes for use in all solid-state batteries remains an important facet of materials science. Mainly due to their low weight and flexibility, the vast majority of studies in this field has been devoted to polymer-based electrolytes. However, with respect to the key feature, a high ionic conductivity in combination with a more or less vanishing electronic contribution, crystalline materials might evolve as a promising alternative. One route to optimized conductivities in these materials follows a maximization of vacancies via aliovalent doping or replacement as successfully exemplified in  $\text{Li}_{4-2x}\text{Si}_{1-x}\text{S}_2\text{O}_4$  (0.30 < x < 0.45), [II]  $\text{Li}_{3x}\text{La}_{2(3)-y}\text{TiO}_3$  (0.04 < y < 0.14) [2-6] or  $\text{Na}_{3-x}P_{1-x}\text{S}_x\text{O}_4$  (0 = z = 0.6), [2-6] The second route has its starting point with the observation that the phase transition of some alkali salts of complex anions (e.g.,  $\text{NO}_2^-$ ,  $\text{SO}_4^{2-}$ ,  $\text{PO}_4^{3-}$ ,  $\text{Alf}_6^{3-}$ ) into the dynamically disordered high-temperature

- [a] Priv.-Doz. Dr. L. van Wüllen, N. Sofina, Prof. Dr. M. Jansen Max-Planck-Institut für Festkörperforschung Heisenbergstrasse 1, 70569 Stuttgart (Germany) Fax: (+ 49) 711-6891502 E-mail: wullen@unl-muenster.de
- m.jansen@mpi-stuttgart.mpg.de
  [b] Priv.-Ooz. Dr. L. van Wällen
  Institut für Physikalische Chemie
  Westfällische Wilhelms-Universität Münster
  Corrensstr. 30, 48149 Münster (Germany)

Fax: (+49) 251-8329159



Available online at www.sciencedirect.com



Journal of Catalysis 225 (2004) 523-530

JOURNAL OF CATALYSIS

www.elsevier.com/locate/jcat

# Alkylation of benzene with ethylene over faujasite zeolite investigated by the ONIOM method

Supawadee Namuangruk, Piboon Pantu, and Jumras Limtrakul\*

Laboratory for Computational and Applied Chemistry, Physical Chemistry Division, Kasetsart University, Bangkok 10900, Thailand
Received 30 March 2004; accepted 15 April 2004

Available online 2 June 2004

#### Abstract

The alkylation of benzene with ethylene over faujasite zeolite has been investigated using an 84T cluster of faujasite zeolite serving as a nanometer-sized chemical reactor modeled by the ONIOM3 (MP2/6-311++G(d,p):HF/6-31G(d):UFF) method, which gives accurate adsorption energies for the reactants and the product, indicating the accuracy of the model in representing interactions between the adsorbates and the zeolite. The computed adsorption energies are -8.73, -13.91, and -20.11 kcal/mol, which compared well with experimentally reported values of -9.0, -14.0, and -20.4 kcal/mol for ethylene, benzene, and ethylbenzene, respectively. Stepwise and concerted mechanisms of the alkylation reaction are considered. For the stepwise mechanism, the alkylation starts with the protonation of the adsorbed ethylene by an acidic zeolite proton leading to the formation of the ethoxide intermediate and, subsequently, the ethoxide reacts with a benzene molecule forming an ethylbenzene product. The computed activation energies are 30.06 and 38.18 kcal/mol for the first and second step, respectively. For the concerted mechanism, the alkylation of benzene takes place in a single reaction step without prior ethoxide formation. The concerted mechanism has an activation energy of 33.41 kcal/mol which is in between the two energy barriers of the stepwise mechanism.

@ 2004 Elsevier Inc. All rights reserved.

Keywords: Benzene alkylation; Density functional calculations; ONIOM, QM/MM; Zeolite; Reaction mechanism

#### 1. Introduction

Ethylbenzene is an important raw material in the petrochemical industry for the manufacture of styrene, which is one of the most important industrial monomers. Worldwide capacity of ethylbenzene production is about 23 million metric tons per year [1]. Conventionally, ethylbenzene is produced by benzene alkylation with ethylene using mineral acids such as aluminum chloride or phosphoric acid as catalysts. However, these corrosive catalysts cause a number of problems concerning handling, safety, corrosion, and waste disposal. An immense endeavor has been put into developing alternative catalytic systems that are more environmentally friendly. As a result, the ethylbenzene production technology has been progressively moved toward zeolite-based processes. In the past couple of decades, zeolite-based processes have been introduced and licensed by several

manufactures, Mobil-Badger, Lummus-UOP, CDTech, and Dow Chemical [1].

Zeolite catalysts also offer an advantage of high selectivity toward the desired product due to the shape-selective properties of their microcrystalline pore structures. Several types of zeolites have been reported to have high activity for benzene alkylation, for example, faujasite, beta, H-ZSM-5, and MCM-22 [1-11]. Elucidation of the reaction mechanism of benzene alkylation on zeolite catalysts is of great interest. From an industry point of view, understanding the alkylation mechanism could help in optimizing the reaction conditions and designing a new catalyst for a more efficient process. However, the reaction mechanism of alkylation of aromatics with short-chain olefins on zeolites is not yet clearly understood. Venuto et al. [2] and Weitkamp [3] suggested that alkylation of benzene with ethylene over acidic faujasite and ZSM-5 zeolites followed the Eley-Rideal mechanism. Corma et al. [4] reported the Eley-Rideal mechanism for alkylation of benzene with propylene over MCM-22. While the Langmuir-Hinshelwood mecha-

<sup>\*</sup> Corresponding author.

E-mail address: fscijri@ku.ac.th (1. Limtrakul).

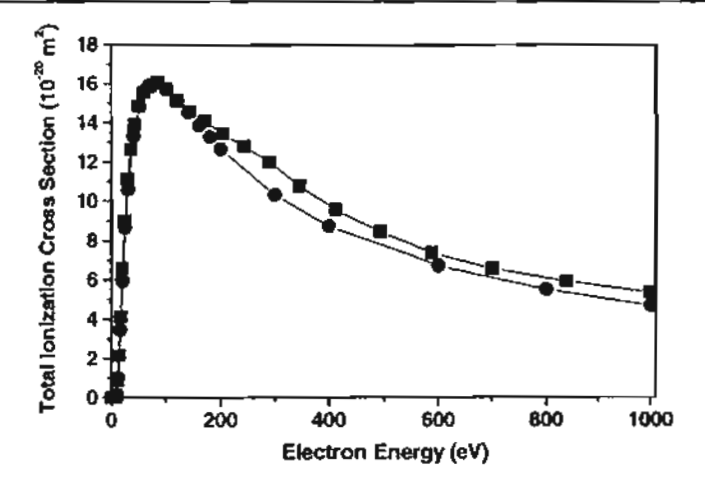


Figure 3. Total single tracil ionization cross section as a function of electron energy. The relative measured cross section was put on an absolute scale by normalization to a calculated cross section using the DM formalism of  $15.7 \times 10^{-20}$  m<sup>2</sup> at 100 eV. The normalized measured cross section (filled squares) is compared with the calculated DM cross section (filled circles) over the entire range of impact energies studied here (threshold to 1000 eV).

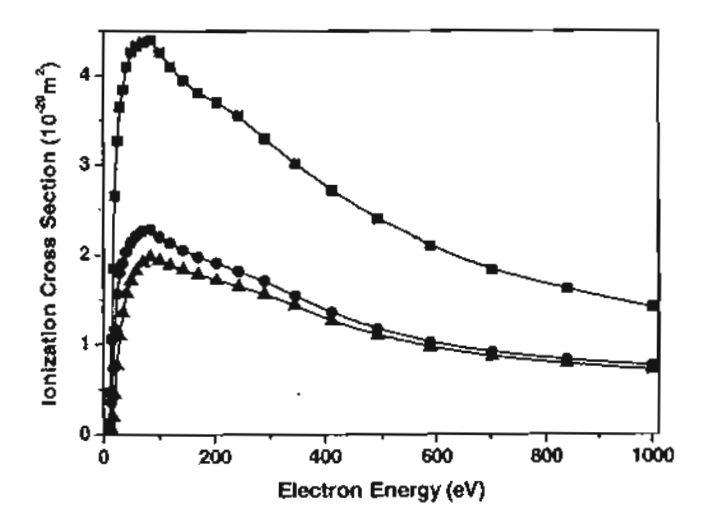


Figure 4. Absolute partial ionization cross sections for the formation of the parent uracil  $C_4H_4N_2O_2^*$  ion (squares) and two fragment ions  $C_3H_3NO^*$  (circles) and OCN\* (triangles) as a function of electron energy following electron impact on uracil.

measured cross section tends to lie slightly above the calculated cross section. The maximum discrepancy in the two cross sections of slightly more than 10% is found in the energy range between 250 and 350 eV. At impact energies from 150 eV to 250 eV and above 400 eV, the deviation between the two curves is generally less than 5%.

Figure 4 shows the three absolute partial ionization cross sections for the parent uracil ion  $C_4H_4N_2O_2^+$  and two fragment ions,  $C_3H_3NO^+$  and  $OCN^+$ . As one would expect on the basis of the mass spectrum depicted in figure 1, the parent ionization cross section has the

The reaction profile involving the reaction between the alkoxide intermediate with benzene to produce ethylbenzene is shown in Fig. 3a and selected structural parameters are tabulated in Table 2. A benzene molecule diffuses into the vicinity to react with the alkoxide. The alkylation of benzene involves concerted bond forming between the carbon atoms of ethylene and benzene and the breaking of a benzene proton giving the proton back to the zeolite-bridging oxygen. The vibrational motion corresponding to the imaginary frequency at the transition is explicitly shown in Fig. 3b, which clearly demonstrates that the C-C bond forming between the ethyl and benzene occurs via interactions of surface ethoxide and benzene. During the transformation, the C-O covalent bond of the surface ethoxide is breaking while the bond between the ethyl and benzene begins to form and a benzene proton is leaving toward the zeolite framework. The activation energy is evaluated to be 38.18 kcal/mol. The adsorbed ethylbenzene product is subsequently desorbed endothermically, requiring energy of 20.11 kcal/mol.

## 3.3.2. Concerted mechanism for benzene alkylation with ethylene

Alternatively, benzene alkylation can proceed via concerted interactions in the coadsorbed complex of ethylene and benzene without the formation of an alkoxide intermediate. The reaction steps can be written as follows:

$$C_{2}H_{4} + H-FAU \rightleftharpoons C_{2}H_{4}-H-FAU, \qquad (5)$$

$$C_{6}H_{6} + C_{2}H_{4}-H-FAU \rightleftharpoons (CH_{3}CH_{2})C_{6}H_{5}-H-FAU, \qquad (6)$$

$$(CH_{3}CH_{2})C_{6}H_{5}-H-FAU \rightleftharpoons (CH_{3}CH_{2})C_{6}H_{5} + H-FAU. \qquad (7)$$

Very recently, DFT cluster calculations of ethylbenzene formation via the concerted reaction of the coadsorbed complex have been reported using DFT quantum cluster calculations by Vos et al. [53] and Arstad et al. [54]. Therefore, a comparison will be made and the effect of inclusion of the extended framework of the zeolite by the ONIOM method will be discussed.

The reaction energy profile is presented in Fig. 4a and the selected geometrical parameters of intermediates and transition state are tabulated in Table 3. The reaction is initiated by coadsorption of benzene on the adsorbed ethylene at the acid site of the zeolite. The coadsorption energy is evaluated to be -16.79 kcal/mol, which is significantly higher than the values previously reported by Vos et al. and Arstad et al. (7.3 and 7.8 kcal/mol, respectively). The difference results mainly from Van der Waals interactions between the adsorbed complex and the zeolite walls, which in this study were taken into account by using the UFF force field to model the extended framework of the zeolite [30-37]. At the transition state, there is an imaginary frequency associated with the transition complex (Fig. 4b) which indicates that the zeolitic proton (H1) is moving toward the ethylene carbon (C1) and the other ethylene carbon (C2) starts forming a bond with the benzene carbon (C3) and, simultaneously, the

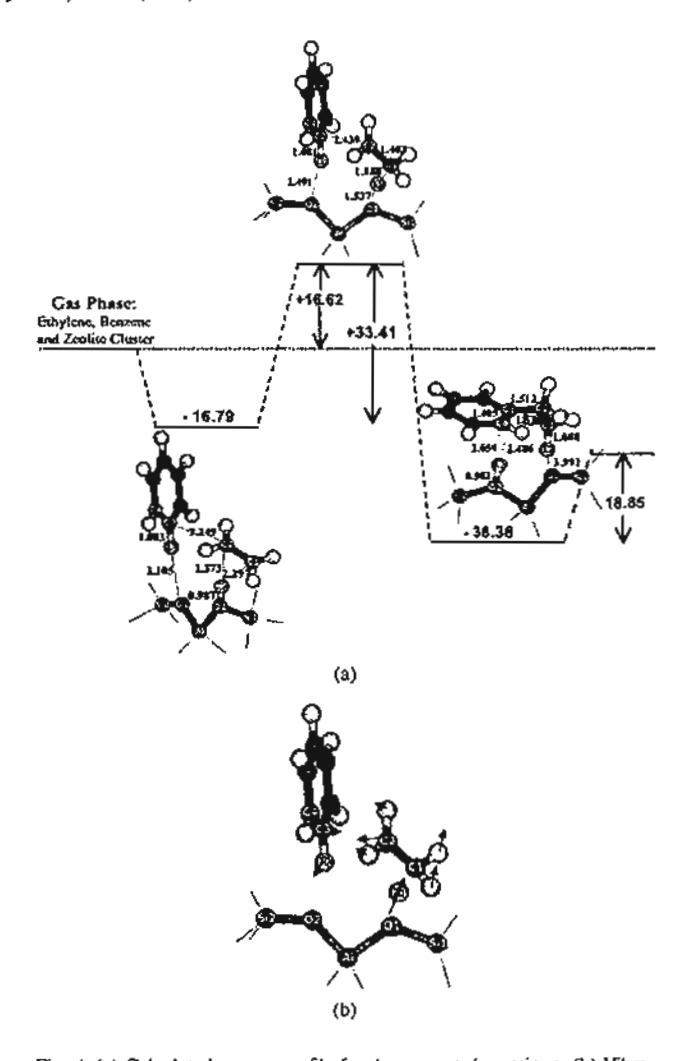


Fig. 4. (a) Calculated energy profile for the concerned reactions. (b) Vibrational movement corresponding to the imaginary frequency at the transition structure.

benzene proton is leaving toward the zeolite-bridging oxygen (O2). The vibrational motion of the transition state complex clearly indicates the concerted mechanism of the alkylation of benzene. The structure of the transition state shows that the Brønsted acid O1-HI distance is greatly lengthened from 0.987 to 1.537 Å and the distance between the zeolitic proton (H1) and the ethylene carbon (C1) becomes 1.188 Å. The ethylene C-C bond distance is significantly lengthened from 1.342 to 1.403 Å, whereas the structure of the benzene molecule does not significantly differ from that of the coadsorbed structure except that the distance between the benzene proton (H2) and the zeolite-bridging oxygen (O2) is shortened from 3.105 to 2.491 Å. The transition-state structure obtained in this model is similar to that of reported by Arstad et al., but slightly different from that reported by Vos et al. in which the ethylene is completely protonated at the transition state. The activation energy is calculated to be 33.41 kcal/mol, very close to the numbers reported by Vos et al. and Arstad et al. (31.6 and 31.3 kcal/mol, respectively).

Table 3

The optimized geometric parameters of isolated molecule, coadsorption complex, transition state (TS), and product of concerted reaction of benzene alkylation on FAU using ONIOM3 (distances are in angestroms and angles are in degrees)

Parameters	Isolated cluster	Coadsorption complex	Transition state	Product
Distances		<u> </u>	<u> </u>	
A)-H1	2.462			
C1-C2	1.335	1.342	1.403	1.529
C2-C3	-	3.249	2,439	1.512
C3-C4	-	1.398	1.408	1.405
C3-H2	_	1.083	1.081	2.486
C4-H2	-	2.147	2.159	2.659
O2-H2	-	3.105	2.491	0.982
CI-HI	-	2.297	1.188	1.088
C2-H1		2.373	2.030	2,165
O1–K1	0.970	0.987	1.537	3.992
A}-O1	1.876	1.861	1.773	1.701
A1-O2	1.694	1.699	1.741	1.886
\$i1-O1	1.669	1.667	1.612	1.601
Si2-O2	1.606	1.602	1.598	1.683
Angles				
ZSilOtAl	123.7	122.9	121.7	116.9
∠\$i2Q2A!	130.4	131.5	134.9	135.1

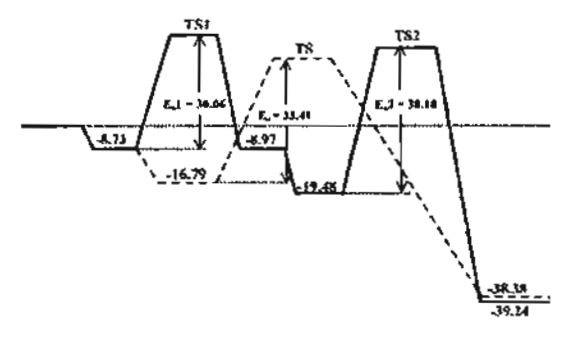


Fig. 5. Calculated energetic profiles for the stepwise (solid line) and concerted (dashed line) reaction mechanisms.

The complete energetic profiles of the two mechanisms are drawn on the same diagram (Fig. 5) for easy comparison. For the stepwise mechanism, the alkoxide formation has a smaller activation energy of 30.06 kcal/mol and the surface reaction step is the rate-determining step with the activation energy of 38.18 kcal/mol. The activation barrier of the concerted mechanism of 33.41 kcal/mol is in between the barriers of the stepwise mechanism. It might appear that the concerted mechanism should dominate the overall alkylation reaction due to the smaller activation energy. However, the stepwise mechanism could also contribute significantly because, from an energetic point of view, the alkoxide formation will occur relatively easily, and after the alkoxide intermediate is formed the stability of the adsorbed benzenealkoxide adduct makes the reverse reaction more difficult to occur than the forward reaction to the ethylbenzene product. When it is considered that both mechanisms can take place under the reaction conditions, the calculated apparent activation energy for the alkylation of benzene with ethylene would be in a range of 16.62-27.67 kcal/mol. Although, there is no experimental value of the activation energy for alkylation of benzene with ethylene in zeolites to compare with, our computed apparent activation energy range seems reasonable when compared with the apparent activation energies (10–18 kcal/mol) for alkylation of benzene with propylene in zeolites [4,6,46]. Because ethylene is a poorer alkylating agent than propylene, and the rate of benzene alkylation with ethylene is much slower than that with propylene and generally it requires a higher reaction temperature to obtain the same conversion level as that of the alkylation with propylene [1,4,47,53], the activation energy of the alkylation with ethylene is expected to be higher than the activation energy of the alkylation with propylene.

#### 4. Conclusion

The alkylation of benzene with ethylene over faujasite zeolite has been investigated using the ONIOM3 model. The model is shown to be accurate in predicting adsorption energies of the adsorbed reactants and product compared to experimental estimates. Two alkylation mechanisms, stepwise and concerted, are considered. For the stepwise mechanism, the alkylation starts with protonation of the adsorbed ethylene which leads to the formation of the active surface ethoxide intermediate. Benzene alkylation takes place via interactions between the ethoxide species and a benzene molecule. The rate-determining step is found to be the reaction step where concerted bond forming between the carbon of the ethyl fragment and benzene and bond breaking of a benzene proton occur. The activation energy of 38.18 kcal/mol is predicted. For the concerted mechanism, the alkylation of benzene takes place in a single reaction step of the coadsorbed reactants without prior alkoxide formation. The activation energy is calculated to be 33.41 kcal/mol.

The results derived in the present study suggest that the ONIOM approach yields an accurate and practical model

for exploring the structure, adsorption, and reaction mechanisms of zeolites.

#### Acknowledgments

This work was supported in part by grants from the Thailand Research Fund (TRF Senior Research Scholar to J.L.) and the Kasetsart University Research and Development Institute (KURDI), as well as the Ministry of University Affairs under the Science and Technology Higher Education Development Project (MUA-ADB funds). The support from the Dow Chemical Company (USA) is also acknowledged.

#### References

- T.F. Degnan Jr., C.M. Smith, C.R. Venkat, App. Catal. A 221 (2001) 283.
- [2] P.B. Venuto, L.A. Hamilton, P.S. Landis, J. Catal. 5 (1966) 484.
- [3] J. Weitkamp, Int. Sympos. in Zeolite Catalysis, Siofok, Hungary, Acta Phys. Chem. 217 (1985).
- [4] A. Corma, V. Martinez-Soria, E. Schnoeveld, J. Catal. 192 (2000) 163.
- [5] Y. Morita, H. Matsumoto, T. Kimura, F. Kato, M. Takayasu, Bull. Jpn. Pet. Inst. 15 (1) (1973) 37.
- [6] K.A. Becker, H.G. Karge, W.-D. Streubel, J. Catal. 28 (1973) 403.
- [7] P.G. Smirniotis, E. Ruckenstein, Ind. Eng. Chem. Res. 34 (1995) 1517.
- [8] W.W. Kaeling, R.E. Holland, J. Catal. 19 (1988) 212.
- [9] N.Y. Chen, W.E. Garwood, Catal. Rev.-Sci. Eng. 28 (1986) 185.
- [10] K.S.N. Reddy, B.S. Rao, U.P. Shiralkar, Appl. Catal. A 95 (1993) 53.
- [11] A. Corma, Chem. Rev. 95 (1995) 559.
- [12] R. Shab, J.D. Gale, M.C. Payne, J. Phys. Chem. B 101 (24) (1997) 4787.
- [13] Y. Jeanvoine, J.G. Angyan, G. Kresse, J. Hafner, J. Phys. Chem. B 102 (1998) 5573.
- [14] I.H. Hillier, J. Mol. Struct. (Theochem.) 463 (1999) 45.
- [15] J. Limtrakut, S. Jungsuttiwong, P. Khongpracha, J. Mol. Struct. 525 (2000) 153.
- [16] J. Sauer, M. Sierka, J. Comput. Chem. 21 (2000) 1470.
- [17] J. Sauer, P. Ugliengo, E. Garrone, V.R. Saunders, Chem. Rev. 94 (1994) 2095.
- [18] J. Sauer, Chem. Rev. 89 (1989) 199.
- [19] J. Limtrakul, Chem. Phys. 193 (1995) 79.
- [20] J. Limtrakul, P. Treesukol, C. Ebner, M. Probst, Chem. Phys. 215 (1997) 77.
- [21] P.E. Sinclair, A.H. de Vries, P. Sherwood, C.R.A. Catlow, R.A. van Santen, J. Chem. Soc., Faraday Trans. 94 (1998) 3401.
- [22] M. Brandle, J. Saucr, J. Am. Chem. Soc. 120 (1998) 1556.
- [23] S.P. Greatbanks, I.H. Hillier, N.A. Burton, P. Sherwood, J. Chem. Phys. 105 (1996) 3370.
- [24] R.Z. Khaliullin, A.T. Bell, V.B. Kazansky, J. Phys. Chem. A 105 (2001) 10,454.
- [25] J. Limtrakul, T. Nanok, P. Khongpracha, S. Jungsuttiwong, T.N. Truong, Chem. Phys. Lett. 349 (2001) 161.

- [26] A.H. de Vries, P. Sherwood, S.J. Cotlins, A.M. Rigby, M. Rigutto, G.J. Kramer, J. Phys. Chem. B 103 (1999) 6133.
- [27] M. Svensson, S. Humbel, R.D.J. Froese, T. Matsubara, S. Sieber, K. Morokuma, J. Phys. Chem. 100 (1996) 19357.
- [28] C. Raksakoon, J. Limtrakul, J. Mol. Struct. (Theochem.) 631 (2003) 147.
- [29] W. Panjan, J. Limtrakul, J. Mol. Struct. 654 (2003) 35.
- [30] S. Kasuriya, S. Namuangruk, P. Treesukol, M. Tirtowidjojo, J. Limtrakul, J. Catal. 219 (2003) 320.
- [31] K. Bobuatong, J. Limtrakul, Appl. Catal. A 253 (2003) 49.
- [32] A. Pelmenschikov, J. Leszczynski, J. Phys. Chem. B 103 (1999) 6886.
- [33] T.A. Wesolowski, O. Parisel, Y. Ellinger, J. Weber, J. Phys. Chem. A 101 (1997) 7818.
- [34] E.G. Derouane, C.D. Chang, Mesopor. Mater. 35-36 (2000) 425.
- [35] L. A. Clark, M. Sierka, J. Sauer, J. Am. Chem. Soc. 125 (2003) 2136.
- [36] A.M. Vos, X. Rozanska, R.A. Schoonheydt, R.A. van Santen, F. Hutschka, J. Hafner, J. Am. Chem. Soc. 123 (2001) 2799.
- [37] X. Rozanska, R. A van Santen, F. Hutschka, J. Hafner, J. Am. Chem. Soc. 123 (2001) 7655.
- [38] D.H. Olson, E. Dempsey, J. Catal. 13 (1969) 221.
- [39] J.R. Hill, C.M. Freeman, B. Delley, J. Phys. Chem. A 103 (1999) 3772.
- [40] A.K. Rappe, C.J. Casewit, K.S. Colwell, W.A. Goddard, W.M. Skiff, J. Am. Chem. Soc. 114 (1992) 10,024.
- [41] M.J. Frisch, G.W. Trucks, H.B. Schlegel, G.E. Scuseria, M.A. Robb, J.R. Cheeseman, V.G. Zakrzewski, J.A. Montgomery, R.E. Stratmann Jr., J.C. Burant, S. Dapprich, J.M. Millam, A.D. Daniels, K.N. Kudin, M.C. Strain, O. Farkas, J. Tornasi, V. Barone, M. Cossi, R. Cammi, B. Mennucci, C. Pomelli, C. Adamo, S. Clifford, J. Ochterski, G.A. Petersson, P.Y. Ayala, Q. Cui, K. Morokuma, P. Salvador, J.J. Dannenberg, D.K. Malick, A.D. Rabuck, K. Raghavuchari, J.B. Foresman, J. Cioslowski, J.V. Ortiz, A.G. Baboul, B.B. Stefanov, G. Liu, A. Liashenko, P. Piskorz, I. Komaromi, R. Gomperts, R.L. Martin, D.J. Fox, T. Keith, M.A. Al-Laham, C.Y. Peng, A. Nanayakkara, M. Challacombe, P.M.W. Gili, B. Johnson, W. Chen, M.W. Wong, J.L. Andres, C. Gonzalez, M. Head-Gordon, E.S. Replogle, J.A. Pople, Gaussian B. Gaussian, Pinsburgh, PA, 2001.
- [42] D. Freude, J. Klinowski, H. Hamdan, Chem. Phys. Lett. 149 (1988) 355.
- [43] N.W. Cant, W.K. Hail, J. Catal. 25 (1972) 161.
- [44] D. Barthomeuf, B.H. Ha, J. Chem. Soc., Faraday Trans. 112 (1973) 2158.
- [45] D.M. Ruthven, M. Goddard, Zeolites 6 (1978) 275.
- [46] S. Siffert, L. Gaillard, B.-L. Su, J. Mol. Catal. A 153 (2000) 267.
- [47] Y. Du, H. Wang, S. Chen, J. Mol. Catal. A 179 (2002) 253.
- [48] P.B. Venuto, P.S. Landis, Adv. Catal. 18 (1968) 259.
- [49] C. Flego, I. Kiricsi, C. Perego, G. Bellussi, Stud. Surf. Sci. Catal. 94 (1995) 405.
- [50] E.M. Evleth, E. Kassab, H. Jessri, M. Allavena, L. Montero, L.R. Sierra, J. Phys. Chem. 100 (1996) 11,368.
- [51] X. Rozanska, Th. Demuth, F. Hutschka, J. Hafner, R.A. van Santen, J. Phys. Chem. B 106 (2002) 3248.
- [52] M. Boronat, C.M. Zircovich-Wilson, P. Viruela, A. Corma, J. Phys. Chem. B 105 (2001) 11,169.
- [53] A.M. Vos, R.A. Schoonheydt, F.D. Proft, P. Geerlings, J. Phys. Chem. B 107 (2003) 2001.
- [54] B. Arstad, S. Kolboe, O. Swang, J. Phys. Chem. B 108 (2004) 2300.



#### Available online at www.sciencedirect.com





Journal of Molecular Catalysis A: Chemical 207 (2004) 137-146

www.elsevier.com/locate/molcata

## Density functional theory study of the ethylene epoxidation over Ti-substituted silicalite (TS-1)

Jumras Limtrakula, i, Chan Inntama, Thanh N. Truongb,\*

Computational & Applied Chemistry Laboratory, Physical Chemistry Division, Kasetsart University, Bangkok 10900, Thailand b Department of Chemistry, Henry Eyring Center for Theoretical Chemistry, University of Utah, 315 S 1400 E, Room 2020, Salt Lake City, UT 84112, USA

Received 2 January 2003; received in revised form 10 June 2003; accepted 10 June 2003

#### Abstract

The mechanism of ethylene epoxidation with hydrogen peroxide over Ti-substituted silicalite (TS-1) catalyst was investigated by using both the cluster and embedded cluster approaches at the B3LYP/6-31G(d) level of theory. The complete catalytic cycle was determined. The epoxidation of ethylene consists of three steps. First, the chemisorption of H<sub>2</sub>O<sub>2</sub> at the Ti active site forms the oxygen donating Ti-OOH species and then the transfer of an oxygen atom from the Ti-OOH species to the adsorbed ethylene. The final step is the dehydration of the Ti-OH species to regenerate to active center. The oxygen atom transfer step was found to be the rate-limiting step with the zero-point energy corrected barrier of 17.0 kcal/mol using the embedded cluster model at B3LYP/6-31G(d) level of theory, which is in agreement with the experimental estimate of about 16.7 kcal/mol. Regeneration of the active center by dehydration of the Ti-OOH species was found to have a rather small barrier and the overall process is exothermic. Our results also show that inclusion of the effects of the zeolite crystal framework is crucial for obtaining quantitative energetic information. For instance, the Madelung potential increases the barrier of the oxygen atom transfer step by 5.0 kcal/mol.

@ 2003 Elsevier B.V. All rights reserved.

Keywards: Density functional theory; Ethylene epoxidation; Ti-substituted silicalite

#### 1. Introduction

Ti-substituted silicalite (TS-1) has been widely used as a catalyst for several important oxidation reactions such as the olefin epoxidation, the phenol hydroxylation, cyclohexanone amoxidation, as well as the conversions of ammonia to hydroxylamine, of secondary alcohol to ketone, and of secondary amine to dialkylhydroxylamine [1-7]. In particular, its use in alkene epoxidation reactions with hydrogen peroxide as oxidant has been experimentally [4-7] and theoretically [8-15] studied. The characterization of TS-1 structure and the nature of its active site have been studied experimentally by using X-ray diffraction, IR, Raman, UV-Vis spectroscopy and EXAFS [16-21].

There have been several previous theoretical studies on the oxidation of ethylene over TS-1 catalysts using quan-

culations are often computationally demanding if it is still

feasible. The embedded cluster methodology provides a cost

tum chemistry methods. These studies provided useful information on the mechanism and energetic properties of

the reaction, though complete catalytic cycle has not been

determined and the rate determining step has not been well

understood. Furthermore, all of these studies used the clus-

ter models to represent the reactive center and thus did not include the effects of the zeolite framework. In our previous study, we found that the Madelung potential from the zeolite framework can increase the adsorption energy of ethylene in H-ZSM-5 zeolite by about 50% and bring the predicted results in much closer agreement with experimental observations [22]. This indicates that the Madelung potential could be an important factor in stabilizing the adsorption complexes and transition states for the ethylene epoxidation over TS-1 catalyst. To accurately include the effects of the extended zeolite framework on the catalytic properties, one can employ periodic electronic structure methods, such as the periodic density functional theory methodology. However, due to the large unit cells of typical zeolites, such cal-

<sup>\*</sup> Corresponding author.

E-mail addresses: [scijr]@ku.ac.th (J. Limtrakul), truong@chem.utah.edu (T.N. Truong).

<sup>&</sup>lt;sup>1</sup> Co-corresponding author.

effective computational strategy for including the effects of the zeolite framework [23–32]. In this approach, the effects of the zeolite framework can be modeled either by a classical molecular mechanic force field or by a set of point charges.

In this study, we investigated the complete catalytic cycle for the alkene oxidation over TS-1 catalysts in the presence of hydroperoxides and the influence of a zeolitic framework, particularly the Madelung potential on the structural and energetic information. The surface charge representation of the external embedded potential (SCREEP) embedded cluster methodology was used. This method has been found to be rather accurate in representing the Madelung potential for studying adsorptions and reactions in zeolites [22,26-31].

#### 2. Method

The active site of TS-1 is modeled by a five-tetrahedral (ST) cluster (OH)<sub>2</sub>Ti[OSi(OH)<sub>2</sub>OSiH<sub>3</sub>]<sub>2</sub> selected from the ZSM-5 zeolite structure where the Ti atom is located at the T12 site. To have a more accurate description of the active site, OH terminations were used for Si atoms closed to the Ti atom. The T12 site has been used as an active site of ZSM-5 in many theoretical studies since it was predicted to be among the most stable Brønsted acid sites [33,34]. It is located at the intersection of main and sinusoidal channels and is accessible to adsorbates. It should be noted that the preferred Ti-substitution sites in TS-1 are still not known for certain and thus require further detailed study. The 5T cluster used in this study (see Fig. 1) is one half of the 10T ring and is the largest cluster that has been used previously. For the embedded cluster model, (see Fig. 1), this 5T cluster is embedded in a set of point charges according to the surface charge representation of external embedded potential method [23]. Accuracy of this method for modeling adsorption processes in zeolites has already been addressed in

several previous studies [22,26-31]. These models consist of three layers. The center layer is a five-tetrahedral (5T) quantum chemical cluster. The next layer of the model is a set of explicit point charges located at the lattice positions. Their magnitudes were derived from periodic population analyses of zeolite systems. To minimize the interaction that occurs between the quantum mechanical terminating hydrogens and the neighboring point charges, the layer of explicit point charges nearest to the quantum cluster is moved out and combined with the next layer of point charges. The charge values of the moved point charges are fitted to minimize deviation from the original external electrostatic field. The outermost layer of the model is the SCREEP surface represented by a set of surface point charges to model the remaining Madelung potential from the extended zeolite crystal.

All geometry optimizations were done at the B3LYP/6-31G(d) level. The two SiH<sub>3</sub> groups and H atoms of the six OH groups bonded to the Ti and Si atoms were fixed along the Si-O crystal framework (see Fig. 2) while other atoms in the quantum cluster were allowed to relax in all geometry optimizations. Normal mode analyses were carried out to verify the transition states to have one imaginary frequency whose mode correspond to the designated reaction. All calculations were done using the Gaussian98 program [35].

#### 3. Results and discussion

For the purpose of clarity, we separate the discussion below into two sub-sections. In one sub-section we discuss only the mechanisms of ethylene epoxidation by the TS-1 zeolite using the embedded cluster model. In the other section we focus only on the effects of the Madelung potential on structural and energetic information of this reaction by comparing the differences in the results predicted by the embedded and bare cluster models.

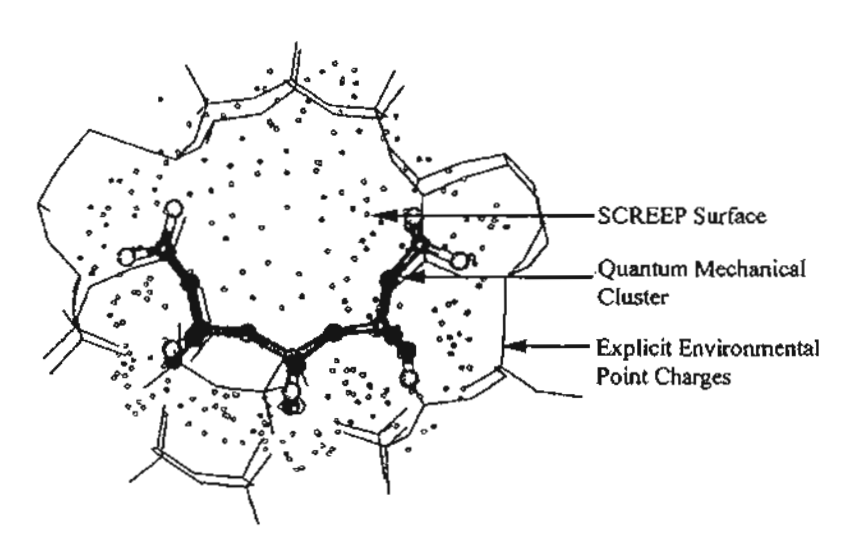


Fig. 1. SCREEP embedded cluster model for studying adsorption or reaction in zeolites.

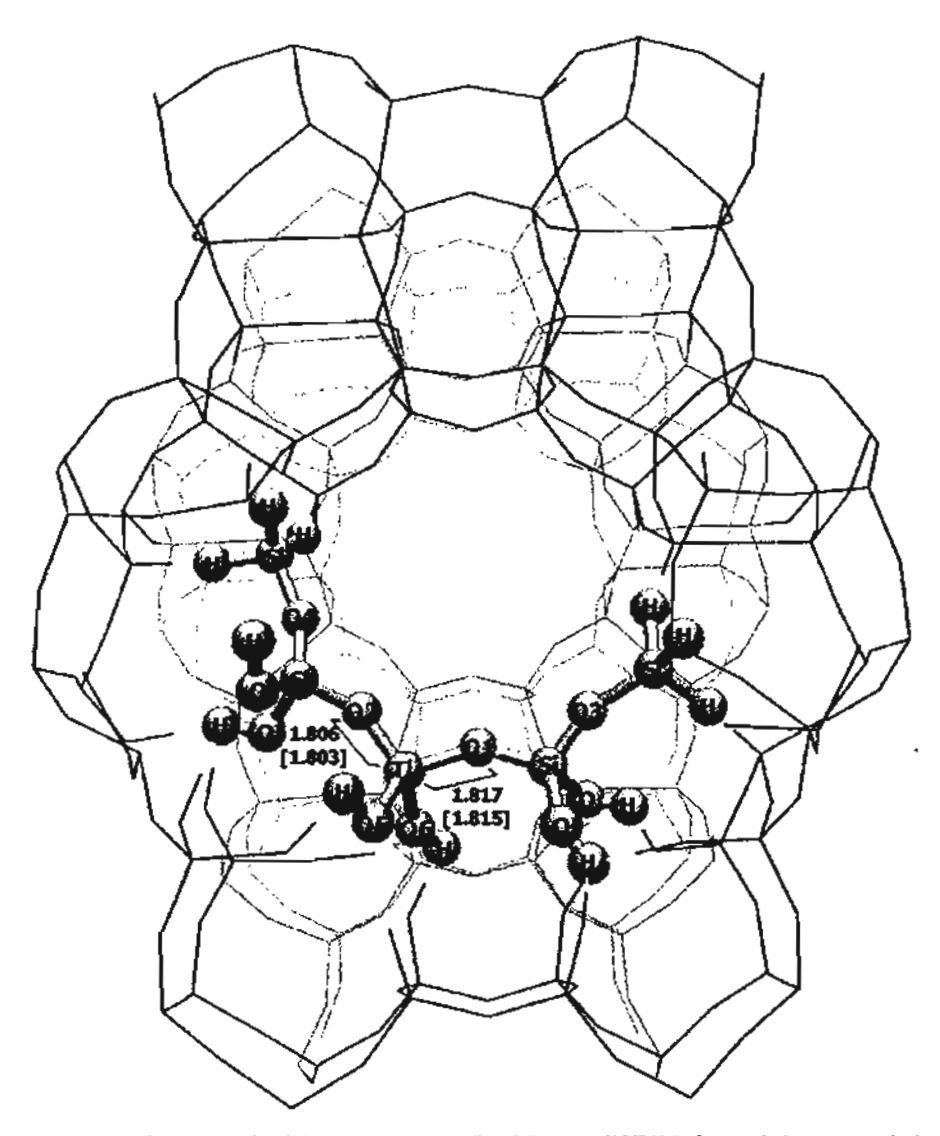


Fig. 2. Embedded ST cluster model of the active site Ti(IV) of the TS-1 zeolite. Selected B3LYP/6-31G(d) optimized geometrical parameters using both the bare cluster and embedded cluster models are also given. The values in parentheses are obtained from the cluster model.

## 3.1. Chemistry of ethylene epoxidation by TS-1 zeolite

The complete catalytic cycle of the ethylene epoxidation by hydrogen peroxide is known to consist of three steps: (1) chemisorption of hydrogen peroxide to form Ti-OOH active species; (2) epoxidation of ethylene by the Ti-OOH species and the desorption of the adsorbed ethylene epoxide; and (3) dehydration to regenerate the active center [8-15]. It is informative to first discuss the nature of the active site in comparison with known experimental data. This would provide indication on the accuracy of the computational method.

#### 3.1.1. The active site

In this study, the active site of TS-1 is modeled by a Ti(IV) atom located at the T12 site of the ZSM-5 zeolite framework as shown in Fig. 2. Selected optimized geometrical parameters are reported in Table 1, and also depicted in Fig. 2.

Table 1
Selected optimized geometrical parameters of the active site of TS-1 using both the bare cluster and embedded cluster models at the B3LYP/6-31G(d) level of theory

Bond (Å) or angle (°)	Embedded	Bare cluster	Expt.
Ti-O1	1.817	1.815	-
Ti-O2	1.806	1.803	-
Ti-O5	1.804	1.805	-
Ti-06	1.766	1.790	_
(Ti-O)	1.798	1.803	1.79°, 1.80–{.81°
Si-O1	1.630	1.642	-
\$i-O2	1.633	1.646	-
(Si-O)	1.635	1.650	_
∠Ti-O1-Si	150.7	152.4	
∠Ti-O2-\$i	140.6	144.7	
∠O1-Ti-O2	108.3	110.5	-

<sup>\*</sup> XRD data is taken from [36].

b EXAFS data are taken from [19,37,38].

The calculated average Ti-O bond lengths of 1.798 Å is in good agreement with that of 1.79 Å obtained from XRD experiments [36] and of 1.80-I.81  $\pm$  0.01 Å from EXAFS [19,37,38] experiments.

#### 3.1.2. Chemisorption of H<sub>2</sub>O<sub>7</sub>

 $H_2O_2$  chemisorbs on the Ti active site to form two possible active oxygen donor species, Ti-OOH denoted as Ti( $\eta_1$ -OOH) and Ti( $\eta_2$ -OOH). In the former, the terminal oxygen atom of the OOH group binds to the Ti atom whereas in the latter both oxygen atoms of the OOH group bind to the Ti atom resembling a bidentate configuration.

The  $Ti(\eta_2\text{-OOH})$  species was found to be more stable than the  $Ti(\eta_1\text{-OOH})$  by about 9.2 kcal/mol. This is slightly larger than that of 8.0 kcal/mol from the DFT/DNP done by Karlsen and Schoeffel [9]. For this reason, we focused only on the formation of the  $Ti(\eta_2\text{-OOH})$  species and its interaction with ethylene in the second step of the epoxidation process.

Fig. 3 shows structures of the stationary points for the dissociative chemisorption of  $H_2O_2$  on the active site of TS-1 to form the  $Ti(\eta_2\text{-OOH})$  species. Selected optimized geometrical parameters are listed in Table 2.  $H_2O_2$  first molecularly adsorbs to the active site with the  $O_a$  atom binding to the Ti atom at the distance of 2.469 Å. The corresponding adsorption energies for the  $H_2O_2/5T$  complex is -10.8 kcal/mol. This is lower than that of -7.4 kcal/mol from non-local GGA/BP DFT single-point energy calculations at the optimized local LDA/VWN geometries done by Munakata et al. [15]. The difference is partly due to the inclusion of H-bonding such as between  $H_a$ - $O_3$  in our adsorbed complex (see Fig. 3a) but not in the model used by Munakata et al. [15].

The transition structure for chemisorption of H<sub>2</sub>O<sub>2</sub> on TS-1 zeolite is shown in Fig. 3b. The chemisorption of the H<sub>2</sub>O<sub>2</sub> molecule occurs over both the Ti and O1 atoms rather than just over the Ti atom. As the adsorption complex approaches the transition state the Ti-Oa bond is shortened from 2.469 to 2.151 Å, and the Ha atom migrates to the OI atom with the Oa-Ha bond elongated from 0.976 to 1.249 Å. Due to the change in the valancy of the O1 atom as Ha migrating over, the Ti-O1 bond distance is elongated from 1.826 to 2.043 Å. Continuing trends are observed as the system moves from the transition state to form the dissociated product, Ti(n2-OOH). Note that this complex plays a major role as an oxidizing agent in the oxidation reaction of unsaturated hydrocarbons. The optimized structure of Ti(n2-OOH) is in agreement with available experimental data [10] found in the crystal structure of  $\{[(\eta_2-tert-buty|peroxo)titanatrane]_2-3-dichrolomethane\}$  $Ti-O_a = 1.97 \text{ Å}$  versus 1.91 Å,  $Ti-O_b = 2.21 \text{ Å}$  versus 2.27 Å and  $O_a$ - $O_b$  = 1.48 Å versus 1.47 Å (the latter numbers are the experimental results).

The barrier height,  $\Delta E_a^{\rm I}$ , for the chemisorption of  $H_2O_2$  is predicted to be 13.6 kcal/mol. Our finding is consistent with the previously reported barrier of 11.9 kcal/mol ob-

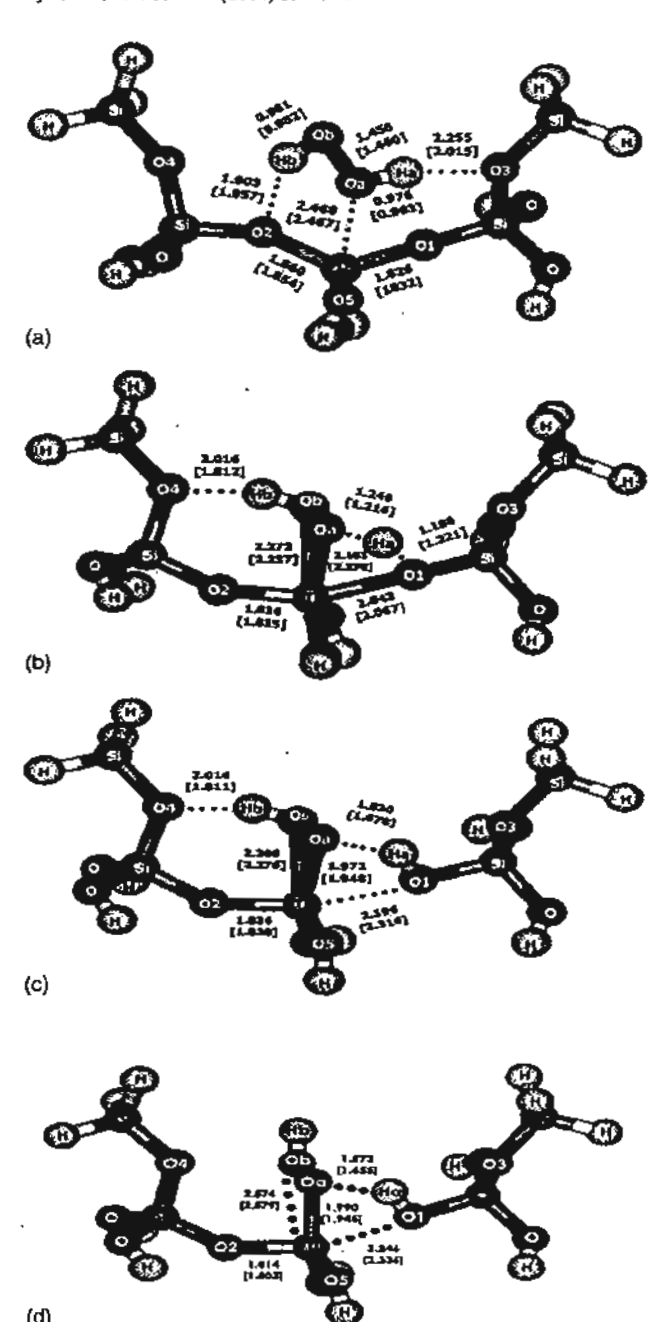


Fig. 3. Structures of the  $H_2O_2/TS-1$  complexes: (a) physisorbed complex; (b) transition state structure; (c) chemisorbed  $Ti(\eta_2\text{-OOH})$  complex; (d) chemisorbed  $Ti(\eta_1\text{-OOH})$  complex. Selected B3LYP/6-31G(d) optimized geometrical parameters using both the bare cluster and embedded cluster models are also given. The values in parentheses are obtained from the cluster model.

tained from BP86/DZVP calculations but with a smaller cluster [11]. The formation of  $Ti(\eta_2\text{-OOH})$  active species (Fig. 3c) is found to be energetically favorable with the reaction energy calculated to be -3.2 kcal/mol. Our predicted reaction energy is lower than that of Munakata et. al. [15] by 5.8 kcal/mol which may be due to the inclusion

Table 2 Selected optimized geometrical parameters for the  $H_2O_2/TS-1$  system: (3a) physisorbed complex; (3b) transition state; (3c) chemisorbed product at the B3LYP/6-31G(d) level of theory

		Physisorbed complex (Fig. 3a)		Transition state (Fig. 3b) Ti(η2-O		mplex (Fig. 3c)	Ti(η <sub>1</sub> -OOH) complex (Fig. 3d	
angic (°)	Embedded cluster	Bare cluster	Embedded cluster	Bare cluster	Embedded cluster	Bare cluster	Embedded cluster	Bare cluster
Ti-O.	2.469	2.467	2.151	2.170	1.972	1.948	1.990	1.945
11-O₀	_	-	2.272	2.237	2.208	2.276	2.574	2.579
ฑ-0เ	1.826	1.832	2.043	2.067	2.196	2.316	2.246	2.336
Ti-O2	1.860	1.854	1.836	1.835	1.836	1.820	1.814	1.803
O <sub>a</sub> -O <sub>b</sub>	1.455	1.460	1.478	1.477	1.479	1.475	1.476	1.470
O <sub>6</sub> -H <sub>6</sub>	0.981	0.982	0.983	0.992	0.983	0.990	0.974	0.972
O <sub>4</sub> -H <sub>4</sub>	0.976	0.983	1.249	1.216	1.830	1.678	1.573	1.655
OI-H.	2,543	2.495	1.188	1.222	0.987	0.999	1.015	1.000
03-H,	2.255	2.015	_	_	_	-	_	-
02~Hb	1.903	1.957	_	_	_	_		-
04-H <sub>b</sub>	2.509	2.434	2.016	2.016	2.016	1.811	3.126	3.068
∠Ti-O1-Si	157.3	155.1	138.9	154.9	137.0	177.5	171.8	178.4
∠TiO2-Si	138.6	144.3	154.4	1527	143.7	146.1	141.6	144.7
∠Ti-O₁-O₀	113.6	110.8	75.0	72.9	78.1	82.1	94.8	97.1
∠O1-Ti-O2	116.2	119.2	156.2	155.9	163.1	158.4	154.8	155.5

of additional hydrogen bonding in our physical model, as mentioned earlier.

## 3.1.3. Epoxidation of ethylene by $Ti(\eta_2\text{-}OOH)$ and desorption of ethylene epoxide

Fig. 4 shows the structures of the oxygen atom transfer from the active  $Ti(\eta_2\text{-OOH})$  species to the absorbed ethylene and of the adsorbed product ethylene epoxide. Selected optimized geometrical parameters for these two stationary points are given in the figure and are also listed in Table 3. The ethylene molecule preferably attacks the  $Ti(\eta_2\text{-OOH})$  at the  $O_a$  position yielding the product of ethylene epoxide

Table 3 Selected B3LYP/6-31G(d) optimized geometrical parameters for the  $C_2H_4/Ti(\gamma_2\text{-OOH})$  complexes

Bond (Å) or angle (°)	Transition st (Fig. 5a)	nicture	Epoxide con (Fig. 5b)	plex
	Embedded cluster	Bare cluster	Embedded cluster	Bare cluster
Ti-O <sub>a</sub>	2.037	2.053	2.314	2.461
Ti-O <sub>b</sub>	2.087	2.043	1.988	1.932
Ti-OI	2.323	2.333	2.327	2.341
Ti-O2	1.830	1.818	1.818	1.815
O <sub>4</sub> -O <sub>6</sub>	1.791	1.807	2.636	2.622
$O_b-H_b$	0.974	0.979	0.970	0.972
O4-Hb	2.300	1.993	2.679	2.320
Ob-Ha	2.227	2.204	1.483	1.590
O <sub>a</sub> -H <sub>a</sub>	1.638	1.709	2.760	2.789
OI-H.	200.1	0.997	1.038	1.013
O <sub>a</sub> Cl	2.149	2.107	1.458	1.448
O,-C2	2.265	2.152	1.458	1.450
C1-C2	1.355	1.358	1.467	1.466
∠Ti-O1-Si	173.9	<b>{71.6</b>	167.5	176.5
∠3ĭ-O2-Si	144.0	142.8	142.6	143.1
∠1ĭ-0,-C	122.8	122.8	112.8	114.2
∠O1~1ĭ~O2	160.6	161.5	162.7	162.8
∠C1~Oa~C2	60.3	60.8	35.6	52.4

(see Fig. 4a). A similar finding has also recently been reported [10]. At the transition state, the Ti-O<sub>a</sub> distance (see Fig. 4a) is elongated from 1.972 to 2.037 Å. The C1-C2 distance is calculated to be 1.355 Å which is only slightly larger than the corresponding C-C distance of the isolated C<sub>2</sub>H<sub>4</sub> (1.331 Å) and is significantly smaller than that of the isolated epoxide OC<sub>2</sub>H<sub>4</sub> species (1.430 Å). This indicates that the transition state is closer to the reactant than the product. Since the reaction is rather exothermic of 42.4 kcal/mol, this result is consistent with the Hammond postulate (Table 4).

The barrier for the ethylene epoxidation,  $\Delta E_a^{II}$ , is predicted to be 18.5 kcal/mol. As compared to the chemisorption of  $H_2O_2$  step, the ethylene epoxidation is the rate-limiting step in this catalytic process. Including the zero-point energy correction lowers this barrier to 17.0 kcal/mol. This result is particularly encouraging since it compares well with the experimental estimate for the activation barrier of 16.7 kcal/mol [39]. Fig. 4b illustrates the product,  $OC_2H_4$ , adsorbed on the Ti-OH complex. We found that O-C1 and O-C2 distances of the  $OC_2H_4$  molecule are virtually identical (1.448 Å versus 1.450 Å). These distances are slightly different from those of the isolate  $OC_2H_4$ 

Table 4
Energies (kcal/mol) of stable complexes and transition states for the ethylene epoxidation reaction relative to the separated reactants

	B3LYP/6-31G(d)		
	Embedded cluster	Bare cluster	
Physisorption complex (Fig. 3a)	~10.8	-16.3	
Transition state I (Fig. 3b)	2.8	-4.7	
Ti(η2-OOH) complex (Fig. 3c)	-3.2	-6.7	
Transition state II (Fig. 4a)	15.3	6.8	
Epoxide complex (Fig. 4b)	-45.6	-53.6	
Transition state III (Fig. 5b)	-41.6	-46.2	
Water adsorption complex (Fig. 5c)	-67.6	-64.5	

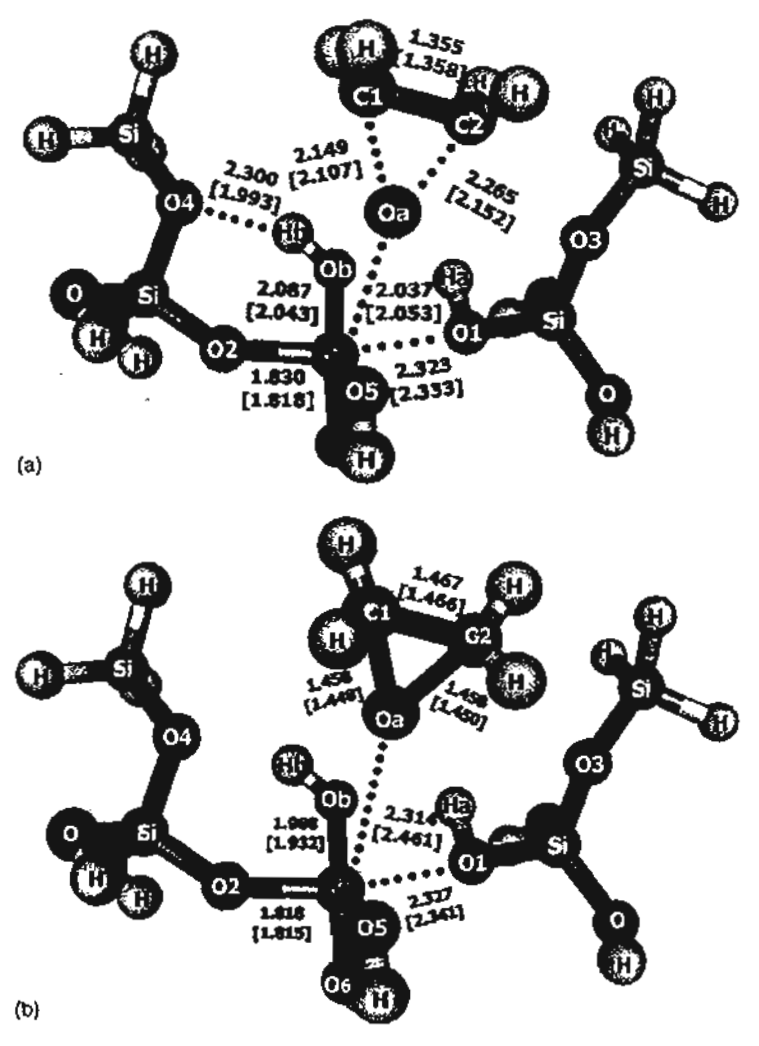


Fig. 4. Similar to Fig. 3, except for the geometries of (a) the transition state structure of the epoxidation step and (b) the adsorbed ethylene epoxide complex.

species, C-O = 1.431 Å. The reaction energy for formation of the  $OC_2H_4/TiOH$  complex is -45.6 kcal/mol with respect to the separated reactants. In addition, we found that the calculated desorption energy of  $OC_2H_4$  from the Ti-OH complex is predicted to be 3.3 kcal/mol.

## 3.1.4. Dehydration to regenerate the active site

Previous studies have not considered the regeneration the active site by dehydration of the Ti-OH species. As shown in Fig. 5a-c, we found that this step involves the migration of a hydrogen atom H1 bound to the zeolite frame-work oxygen atom O3 to the oxygen of the Ti-OH species and the strengthening of Ti-O3 bond. In particular, the Ti-O2 from 1.903 to 2.266 Å. The concerted motion of the hydrogen migration and the shortening of the Ti-O3 bond lead to a rather small barrier to dehydration step of 0.6 kcal/mol relative to the energy of the Ti-OH species. The product of this step is the adsorbed water on the Ti active site. The step is also rather exothermic with the reaction energy of -25.4 kcal/mol with respect to the Ti-OH species. Desorp-

tion of the adsorbed water to regenerate the Ti active site requires 21.1 kcal/mol.

### 3.1.5. Discussion

Figs. 6 and 7 illustrate the catalytic cycle and schematic energy profile along this cycle with respect to the overall zero of energy, namely the energies of the separated reactants. It is clear that the rate-limiting step is the oxygen migration from the Ti-OOH active species to the adsorbed ethylene. This step has the barrier of 15.3 kcal/mol relative to the overall zero and of 18.5 kcal/mol relative to the stable intermediate of adsorbed ethylene on the Ti-OOH species. The overall energy of the catalytic cycle is -46.5 kcal/mol. It is interesting to compare our present results with those from previous studies. Wu and Lai [8] reported a BLYP study using the HOOTi(OH)3 cluster model to study the epoxidation step and found the barrier height to be 10.7 kcal/mol. Karlsen and Schoffel [9] used a rather small Ti(OH)4 cluster with the B88LYP/DNP method and found the corresponding barrier height to be 22.9 kcal/mol. Hillier and co-workers

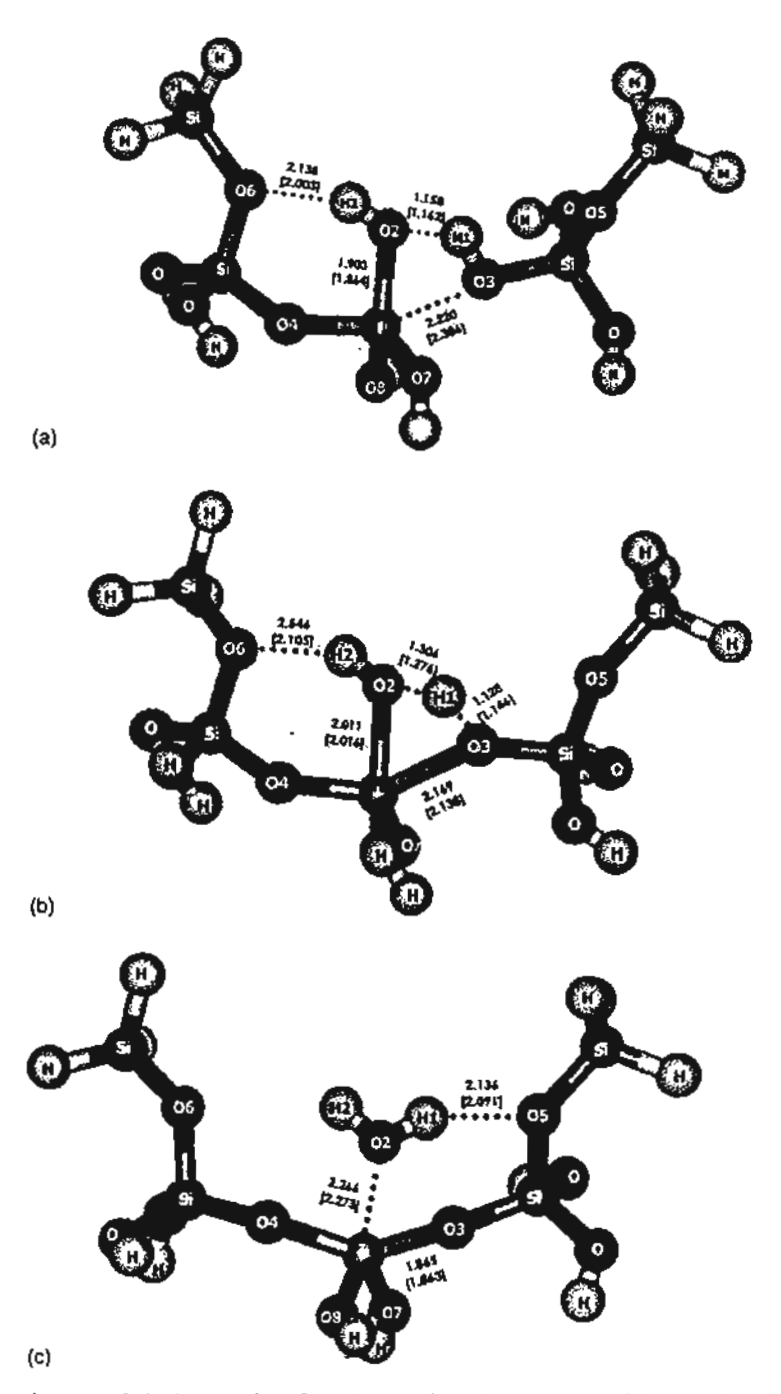


Fig. 5. Similar to Fig. 3, except for the optimized geometries of (a) the Ti-OH species; (b) the transition state for the dehydration step; and (c) the adsorbed water on the Ti active site.

[10] employed the B3LYP/3-21G(d) level of theory with the (H<sub>3</sub>SO)<sub>3</sub>Ti(IV)-O(1)O(2)H/MeOH cluster model and found that the corresponding barrier beight was estimated to be 11.9 kcal/mol. Using a different 4T cluster model with the BP86 DFT method, Sinclair and Catlow [11] found that the chemisorption of H<sub>2</sub>O<sub>2</sub> is the rate-limiting step instead of the epoxidation step with the barrier of 13.3 kcal/mol whereas the epoxidation step has a lower barrier of 10.2 kcal/mol.

Munakata et al. [15] performed BP//VWN calculations with a different 5T cluster to model the Ti active site. The authors modeled the epoxidation reaction with an additional water molecule in coordination with the adsorbates, H<sub>2</sub>O<sub>2</sub> and C<sub>2</sub>H<sub>4</sub> and found the barrier, relative to the complex [active site-H<sub>2</sub>O·C<sub>2</sub>H<sub>4</sub>], is about 18.3 kcal/mol. The estimated barrier of the epoxidation step is 15.8 kcal/mol with respect to the separated reactants. Our study does not consider such

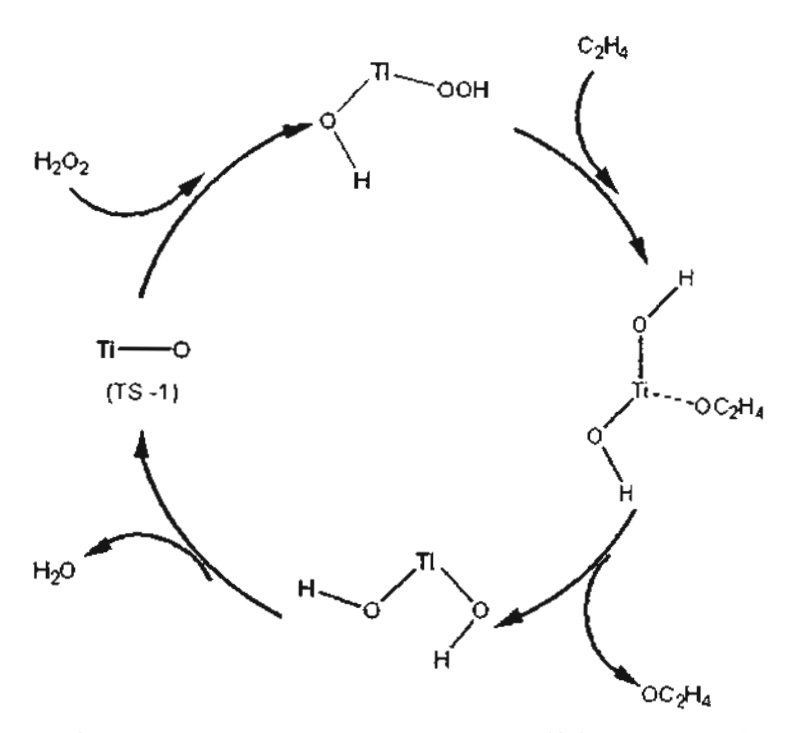


Fig. 6. Schematic diagram to illustrate the catalytic cycle for the epoxidation of ethylene by TS-1 zeolite.

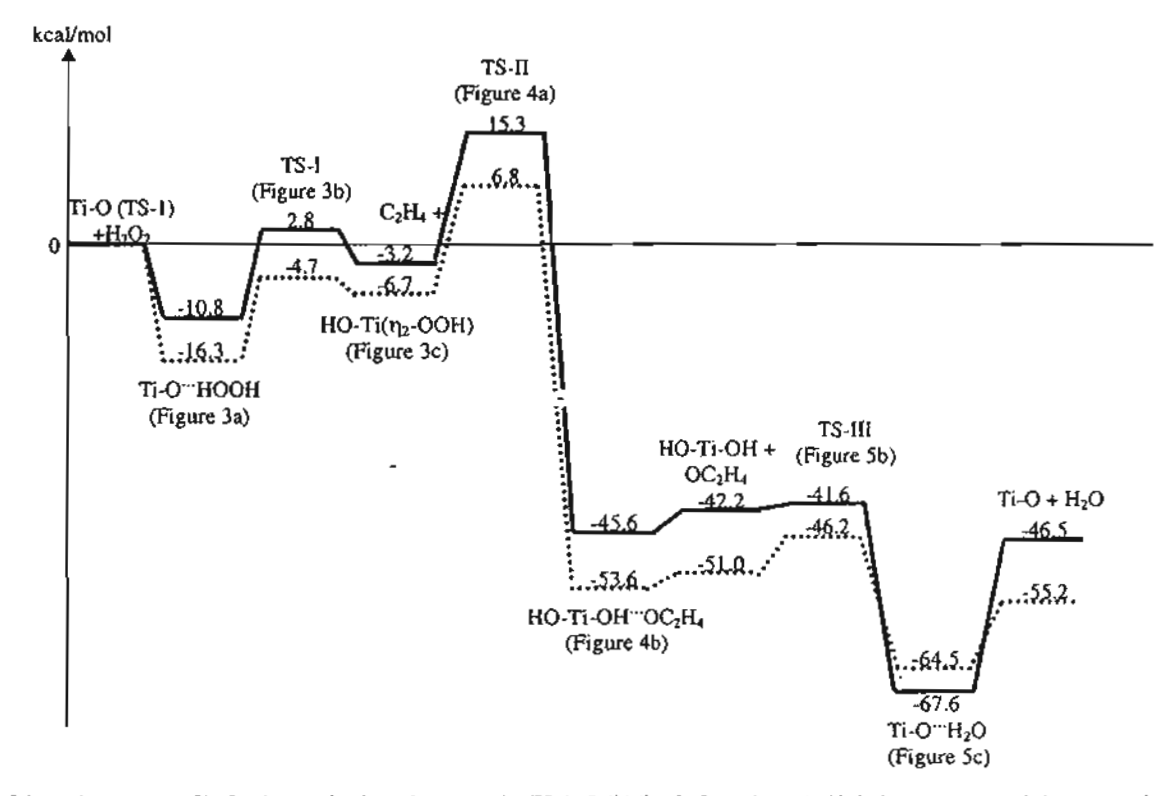


Fig. 7. Schematic energy profile for the epoxidation of ethylene by TS-1. Solid line is from the embedded cluster results and the dashed line is from the bare cluster results using the B3LYP/6-31G(d) level of theory.

additional water and our results are also consistent with available experimental data. Thus, it is not clear what are the roles of the water in overall mechanism for the ethylene epoxidation by hydrogen peroxide in TS-1 zeolite. Though water is produced in the dehydration step with the adsorption energy of -21.1 kcal/mol that is almost twice larger than the adsorption of the hydrogen peroxide on the Ti active site. However, the overall exothermicity of the catalytic cycle of -46.5 kcal/mol would have sufficient energy to regenerate the active center. More study is certainly needed to further understand the roles of water in the mechanism of this reaction.

## 3.2. Effects of the Madelung potential

We found that the local structure of the active site of the TS-1 model is not very sensitive to the inclusion of the Madelung potentials. It is noted that the Madelung potential has an effect of destabilizing  $Ti(\eta_1\text{-OOH})$  and  $Ti(\eta_2\text{-OOH})$ by about 3.5 kcal/mol for the n2 structure (Fig. 3c) and 2.1 kcal/mol for the  $\eta_1$  structure (Fig. 3d) does not change the order of relative stability of the two complexes. The Madelung potential from the zeolite framework has a significant effect on the adsorption structure, particularly the hydrogen H<sub>b</sub>-O<sub>2</sub> and H<sub>a</sub>-O<sub>3</sub> bonds where it shortens the former by 0.05 Å and elongates the latter by 0.3 Å. Consequently, it lowers the adsorption energy (or increases the binding energy) by 5.5 kcal/mol. We found that the effects of the Madelung potential on the structure increase as the reaction proceeds toward the product. In fact at the dissociated product, Ti(n2-OOH) as shown in Fig. 3c, such effects were found to be noticeably large. The Ti-O1 bond is shortened by 0.12 Å while Ti-O<sub>a</sub> is elongated by 0.03 Å. For the transition state to oxygen migration step to form ethylene epoxide, the Ti-O<sub>2</sub> bond distance is shortened by 0.16 Å. As a result, the Madelung potential increases the barrier for this rate-limiting step by 5.0 kcal/mol. The largest effect of the Madelung potential is seen in the desorption energy of water to regenerate the Ti active site. It increases the water desorption energy by 11.8 kcal/mol.

A general observation from these results and from the differences between our cluster and embedded cluster results is that the effects of the Madelung potential are rather large and thus the embedded cluster model used in this study appears to provide more quantitative information on the energetic properties as compared with experimental observation.

#### 4. Conclusion

We have carried systematic ab initio cluster and embedded cluster studies on the mechanism of the ethylene epoxidation by hydrogen peroxide over the Ti-substituted silicalite zeolite. B3LYP/6-31G(d) level of theory was employed. The active site of the TS-1 zeolite was modeled by a 5T cluster. The effects of the Madelung potential from extended zeolite framework on the structural and energetic properties of this process were investigated. The complete catalytic cycle was determined. The reaction involves three steps: (a) the chemisorption of hydrogen peroxide to form Ti-OOH active species; (b) the oxygen atom transfer from the Ti-OOH active species to the adsorbed ethylene to form the produce ethylene peroxide and Ti-OH species; and (c) the dehydration of Ti-OH species to regenerate the Ti active site. The chemisorption of the H<sub>2</sub>O<sub>2</sub> molecule on the TS-1 catalyst has the barrier of 13.6 kcal/mol to form dominantly oxygen donor species, Ti(η2-OOH) using the embedded cluster model. For the epoxide formation, the ethylene molecule interacts with the oxygen atom close to the Ti atom of the Ti(n2-OOH) complex. The epoxidation step is found to be the rate-limiting step where the oxygen atom from the Ti-OOH group transfer to the adsorbed ethylene molecule. The predicted activation energy including the zero-point energy correction for this step is 17.0 kcal/mol. Our predicted results are in agreement with the experimental estimate for the activation barrier of 16.7 kcal/mol. The dehydration of the Ti-OH species to regenerate the Ti active site has rather small barrier. We found that the Madelung effects are rather large, in particular they increase the activation energy of the rate-limiting step by 5.0 kcal/mol.

#### Acknowledgements

This work is supported by grants from the Thailand Research Fund (senior TRF research scholar), the Development and Promotion for Science and Technology Talents project (DPST), the Kasetsart University Research and Development Institute (KURDI) and the Ministry of University Affairs under the Science and Technology Higher Education Development Project (MUA-ADB funds). It is also supported in part by the ACS-PRF fund to TNT. The computer support from the University of Utah Center for High Performance Computing and Kasetsart 72 clusters is gratefully acknowledged. Our sincere thanks are due to Professor R. Ahlrichs (Karlsruhe, Germany) for his continued support of this work.

#### References

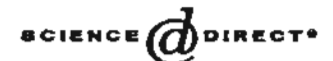
- [1] M. Taramasso, G. Perego, B. Notari, U.S. Patent 4,410,501 (1983).
- [2] B. Notari, Adv. Catal. 41 (1996) 253.
- [3] I.W.C.E. Arends, R.A. Sheldon, M. Wallau, U. Schuchardt, Angew. Chem. 36 (1997) 1144.
- [4] M.G. Clerici, P. Ingallina, J. Catal, 140 (1993) 71.
- [5] M.G. Clerici, G. Bellussi, U. Romano, J. Catal. 129 (1991) 159.
- [6] C.B. Khouw, C.B. Daru, J.A. Labinger, M.E. Davis, J. Catal. 149 (1994) 195.
- [7] G. Bellussi, A. Catari, M. Clerici, G. Maddinelli, R. Millim, J. Catal. 133 (1992) 220.
- [8] Y.D. Wu, D.K.M. Lai, J. Org. Chem. 60 (1995) 673.
- [9] E. Karlsen, K. Schoffel, Catal. Today 32 (1996) 107.

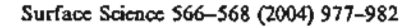
- [10] D. Tantanak, M.A. Vincent, I.H. Hillier, Chem. Commun. (1998) 1031.
- [11] P.E. Sinclair, C.R.A. Catlow, J. Phys. Chem. B 103 (1999) 1084.
- [12] P.E. Sinclair, C.R.A. Catlow, Chem. Commun. (1997) 1881.
- [13] M. Neurock, L.E. Manzer, Chem. Commun. (1996) 1133.
- [14] G.N. Vayssilov, R.A. van Santen, J. Catal. 175 (1998) 170.
- [15] H. Munakata, Y. Oumi, A. Miyamoto, J. Phys. Chem. B 105 (2001) 3493.
- [16] G. Ricchiardi, A. Damin, S. Bordiga, C. Lamberti, G. Spano, F. Rivetti, A. Zecchina, J. Am. Chem. Soc. 123 (2001) 11409.
- [17] J. Sudhakar Reddy, S. Sivasanker, P. Ratnasarny, J. Mol. Catal. 69 (1991) 383.
- [18] T. Blasco, M.A. Camblor, A. Corma, J. Perez-Pariente, J. Am. Chem. Soc. 115 (1993) 11806.
- [19] S. Bordiga, S. Collucia, C. Lamberti, L. Marchese, A. Zecchina, F. Boscherini, F. Buff, F. Genoni, G. Leofanti, G. Petrini, G. Vlaic, J. Phys. Chem. 98 (1994) 4125.
- [20] F.J. Feher, D.A. Newman, J.F. Walzner, J. Am. Chem. Soc. 111 (1989) 1741.
- [21] A. Zecchina, S. Bordiga, C. Lamberti, G. Ricchiardi, D. Scaranto, G. Petrini, G. Leofanti, M. Mantegazza, Catal. Today 32 (1996) 97.
- [22] J. Limtrakul, T. Nanok, P. Khongpracha, S. Jungsuttiwong, T.N. Truong, Chem. Phys. Lett. 349 (2001) 161.
- [23] E.V. Stefanovich, T.N. Truong, J. Phys. Chem. B 102 (1998) 3018.
- [24] S.P. Greatbanks, I.H. Hillier, N.A. Burton, P. Sherwood, J. Chem. Phys. 105 (1996) 3370.
- [25] R.Z. Khaliullin, A.T. Bell, V.B. Kazansky, J. Phys. Chem. A 105 (2001) 10454.
- [26] P. Treesukol, J. Limurakul, T.N. Truong, J. Phys. Chem. B 105 (2001) 2421.
- [27] J. Limtrakul, P. Khongpracha, S. Jungsuttiwong, T.N. Truong, J. Mol. Catal. A 153 (2000) 2469.
- [28] S. Jungsuttiwong, S. Nokbin, P. Chuichay, P. Khongpracha, T.N. Truong, J. Limtrakul, Stud. Surf. Sci. Catal. 135 (2001) 2518.
- [29] J. Limtrakul, P. Khongpracha, S. Jungsuttiwong, J. Mol. Struct. 525 (2000) 153.
- [30] J. Limtrakut, S. Nokbin, P. Chuichay, J. Mol. Struct. 560 (2001) 169.
- [31] J. Limtrakul, S. Nokbin, S. Jungsuttiwong, P. Khongpracha, T.N. Truong, Stud. Surf. Sci. Catal. 135 (2001) 2469.

- [32] (a) R. Vetrivel, C.R.A. Catlow, E.A. Colbourn, Proc. R. Soc. London A 417 (1998) 81;
  - (b) M. Allavena, K. Seiti, E. Kassab, G. Ferency, J.G. Angyan, Chem. Phys. Lett. 168 (1990) 461;
  - (c) G. Aloisi, P. Barnes, C.R.A. Catlow, R.A. Jackson, A.J. Richard, J. Phys. Chem. 93 (1990) 3573;
  - (d) J.C. White, A.C. Hess, J. Phys. Chem. 97 (1993) 8730;
  - (e) E.H. Teunisson, A.P.J. Jansen, R.A. van Santen, R. Orlando, R. Dovesi, J. Phys. Chem. 101 (1994) 5865;
  - (f) A. Kyrlidis, S.J. Cook, A.K. Chakraborty, A.T. Bell, D.N. Theodorou, J. Phys Chem. 99 (1995) 1505;
  - (g) E.H. Teunissen, A.P.J. Jansen, R.A. van Santen, J. Phys. Chem. 99 (1995) 1873;
  - (h) U. Eichler, M. Brandle, J. Sauer, J. Phys. Chem. B 99 (1997) 1873:
  - (i) M. Brandle, J. Sauer, J. Am. Chem. Soc. 120 (1998) 1556.
- [33] E.G. Derouane, J.G. Fripat, Zeolites 5 (1985) 165.
- [34] A.E. Alvaradoswaisgood, M.K. Baw, P.T. Hay, A. Redondo, J. Phys. Chem. 95 (1991) 10031.
- [35] M.J. Frisch, G.W. Trucks, H.B. Schlegel, G.E. Scuseria, M.A. Robb, J.R. Cheeseman, V.G. Zakrzewski, J.A. Montgomery, R.E. Stratmann, J.C. Burant, S. Dapprich, J.M. Millam, A.D. Daniels, K.N. Kudin, M.C. Strain, O. Parkas, J. Tomasi, V. Barone, M. Cossi, R. Cammi, B. Mennucci, C. Pomelli, C. Adamo, S. Clifford, J. Ochterski, G.A. Petersson, P.Y. Ayala, Q. Cui, K. Morokuma, P. Salvador, J.J. Dannenberg, D.K. Malick, A.D. Rabuck, K. Raghavachari, J.B. Foresman, J. Cioslowski, J.V. Ortiz, A.G. Baboul, B.B. Stefanov, G. Liu, A. Liashenko, P. Piskorz, I. Komaromi, R. Gomperts, R.L. Martin, D.J. Fox, T. Keith, M.A. Al-Laham, C.Y. Peng, A. Nanayakkara, M. Challacombe, P.M.W. Gill, B. Johnson, W. Chen, M.W. Wong, J.L. Andres, C. Gonzalez, M. Head-Gordon, E.S. Replogle, J.A. Popte, Gaussian '98, Gaussian, Inc., Pittsburgh, PA, 2001.
- [36] G. Bellussi, V. Fatore, Stud. Surf. Sci. Catal. 69 (1991) 79.
- [37] S. Pei, G.W. Zajak, J.A. Kaduck, J. Faber, B.I. Boyanov, D. Duck, D. Fazzini, T.I. Morrison, D.S. Yang, Catal. Lett. 21 (1993) 333.
- [38] R.J. Davis, Z. Liu, J.E. Tabora, W.S. Wielband, Catal. Lett. 34 (1995) 101.
- [39] A. van der Pol, J.H.C. van Hooff, Appl. Catal. A 106 (1993) 97.



#### Available online at www.sciencedirect.com







# DFT plane-wave calculations of the Rh/MgO(001) interface

Somkiat Nokbin a,b, Jumras Limtrakul b, Kersti Hermansson a,\*

Materials Chemistry, The Angström Laboratory, Box 538, SE-751 21 Uppsala, Sweden
 Laboratory for Computational and Applied Chemistry, Department of Chemistry, Kasetsart University, Bangkok 10900, Thailand
 Available online 15 June 2004

# Abstract

The Rh/MgO(001) system has been studied by periodic plane-wave density functional calculations using the VASP code and PAW potentials. Four different adsorption sites (which were reduced to three after optimization) and three different surface coverages were investigated. For the most stable site, above O, the adhesion energy was found to decrease as a function of coverage (from 2.0 to 1.1 eV as the coverage increases from 1/8 to 1 ML), while the adsorption energy was found to increase with surface coverage. Electron density difference plots were calculated to display some of the electron rearrangement responsible for the Rh-oxide adhesion energy, and the features of the Mg and O adsorption sites were compared.

© 2004 Elsevier B.V. All rights reserved.

Keywords: Density functional calculations; Magnesium oxides; Rhodium; Chemisorption; Electron density, excitation spectra calculations

# 1. Introduction

The role of the metal oxide support in metal/ oxide catalytic systems is intriguing. The activity and reactivity of metal-metal oxide catalysts depend on the nature and structure of both the metal and the metal oxide support and on their interplay. Even the very stable MgO system appears to play a decisive role in heterogeneous catalysis, and then not only as an inactive support or as a model system. The present study is concerned with the Rh/MgO system. The functionality of Rh/MgO catalysts has been studied intensively experimentally (see, for example, [1-12]). Only rather few

As for theoretical studies, to the best of our knowledge, only a small number of Rh/MgO studies have been published. Wu and Freeman [15] investigated the possible magnetism of Pd, Rh and Ru monolayers on MgO(001) using full-potential linearized augmented-plane-wave (FLAPW) periodic calculations (see [15] for details); there, five-layer MgO slabs were used with the metal atoms

E-mail address: kersti@mkem.uu.se (K. Hermansson).

studies have been directly concerned with the structural characterization of Rh/MgO systems at an atomic level. One such example is the work by Emrich et al. [13], who used EXAFS (Extended X-ray absorption fine structure spectroscopy) to investigate the structure of highly dispersed Rh particles on MgO under reduced conditions and determined the Rh-O bond length to be 1.95 Å (under these conditions). The ionic state of reduced Rh particles has also been investigated by X-ray photoelectron spectroscopy (XPS) [14].

<sup>\*</sup>Corresponding author. Tel.: +46-18-471-3767; fax: +46-18-

placed on top of every O atom on each side of the slab (i.e. the coverage was 100%, using the definition that full coverage, i.e. I ML, is when either each cation or each anion is covered by one metal atom). They found an adhesion energy (see definition later) of 0.84 eV and an optimized Rh-O distance of 2.34 Å. Periodic DFT (density functional theory) calculations with the BLYP functional and a local atom-based basis set (LCAO) were reported by Stirling et al. [16] for Rh adsorbed over two different adsorption sites (O or Mg) on one side of a one-layer MgO slab, with a surface coverage of 1/8 ML. The reactivity with NO and NO2 was also investigated. It was found that Rh prefers to bind to O rather than to Mg, with an optimized Rh-oxide interaction energy of 1.8 eV for a Rh-O distance of 2.1 A. Very recently, Bogicevic et al. [17] calculated the energy of adhesion for a number of transition metals, including Rh, on the MgO(100) surface, with and without oxygen vacancies present. These authors used periodic, plane-wave DFT calculations with the GGA (generalized gradient approximation) treatment of the exchange-correlation functional and the systems consisted of five-layer oxide slabs with the metal atom placed on one side of the slab only, and a coverage of 1/18 ML. The adhesion energy for Rh on top of O was reported to be 1.93 eV.

If we try to summarize the adsorption information resulting from the three theoretical studies just described, we arrive at the following picture: the Rh atoms prefer to reside above the oxygen atoms on MgO(001) and the adhesion energy is approximately 1.9 [17], 1.8 [16] and 0.8 [15] eV per ad-atom for a coverage of 1/18, 1/8 and 1 ML, respectively. The values display a strongly decreasing trend as a function of surface coverage, which may or may not be a consequence of the fact that different DFT methods were used in the studies compared. In the current study we present optimized geometries and interaction energies for the Rh/MgO(001) interface system for three different coverages, calculated with one and the same theoretical method, namely, plane-wave DFT calculations at the GGA level with the projector augmented-wave (PAW) method to describe the core electrons [18]. Four different adsorption sites were investigated.

#### 2. Computational details

The Rh/MgO(001) system in our calculations was described with a periodic slab model, where each slab was infinite in the x and y directions and finite along the z direction, and then repeated periodically along the z direction with a vacuum gap between nearest slab images. In the present calculations, each slab consisted of 4 MgO(001) layers with one Rh layer placed on only one side of the slab and the vacuum gap was approximately 15 A (7 Mg-O distance intervals). All Mg-O distances in the x and y directions were kept fixed at the optimized bulk value (2.125 A; the experimental value is 2.105 Å [19]) and the Rh layer was placed epitaxially on top of the oxide slab. Four different adsorption sites and three different coverages (1/8, 1/2 and 1 ML) were explored and will be further discussed in Section 3.1. A 1×1 crystallographic supercell was selected as a model for the 1/2 and 1 ML calculations, whereas a 2×2 supercell was used for the 1/8 ML case. Both the Mg-O and Rh-oxide distances along the z direction were allowed to relax, but two different relaxation schemes were used, namely either all Mg-O distances were allowed to relax in the z direction, or the bottom two oxide layers were kept fixed at the optimized bulk structure value. The two relaxation models gave virtually identical structural and energetical results and only the fully optimized (in the z direction) slab results are reported here. Moreover, test calculations with an 8layer oxide slab confirmed that a four-layer oxide slab was thick enough for our interface study.

The calculations were performed within the framework of periodic DFT using the Vienna Ab initio Simulations package (VASP) [20,24]. Here, non-spin polarized calculations are reported, since we also performed spin polarized calculations and found the effect on the calculated adsorption energy to be 0.2 eV or less. The valence electron configurations used in our calculations were Rh(4p<sup>6</sup>, 5s<sup>1</sup>, 4d<sup>8</sup>), Mg(2p<sup>6</sup>, 3s<sup>2</sup>) and O(2s<sup>2</sup>, 2p<sup>4</sup>) and the projector augmented-wave method (PAW) [18,22] was used to treat the core electrons. The GGA functional PW91 [23] was used. An energy cut-off of 500 eV and a Gaussian smearing factor with  $\sigma = 0.1$  eV were applied in all cases.

For the bulk and surface systems, respectively,  $(6 \times 6 \times 6)$  and  $(6 \times 6 \times 1)$  meshes of k-points, selected according to the Monkhorst-Pack (MP) algorithm [24], were used in the Brillouin zone sampling. All structures were optimized until the forces on all unconstrained atoms were less than 0.01 eV/ Å.

#### 3. Results and discussions

# 3.1. Rh/MgO(001) structure

As mentioned, four different adsorption sites were investigated for surface coverages of 1/8, 1/2 and 1 ML: (i) on top of O, (ii) on top of Mg, (iii) above the middle of the Mg-O bond and (iv) above a hollow site (see Fig 1a). It turned out that when Rh was placed above the middle of the Mg-O bond, the Rh atoms moved towards the O site and found the same equilibrium positions as for a starting position above the O atoms. Therefore only the results for three sites are reported in Table 1.

We find that a Rh overlayer placed over the O atoms induces an "inverse buckling" (inverse rumpling) of the oxide surface, compared to the relaxed surface structure of the isolated MgO(001) slab. Thus, with the Rh atoms present on top of the O atoms, the Mg atoms in the surface layer lie further out from the slab center than the (Rh-covered) O atoms. For the 1 ML case, this inverse rumpling is as large as 0.13 Å and smaller values of 0.02 and 0.03 are found for the 1/2 and 1/8 coverages, respectively. The optimized atomic positions reported in [15] also bear evidence of this inverse rumpling.

The optimized vertical distances between the Rh atoms and the MgO surface are reported in Table 1. As seen in the table, Rh prefers to bind to the O atom, in agreement with experimental [13] and previous theoretical [15-17] results. Our optimized Rh-O distance is 1.99 Å for 1/8 ML coverage, in good agreement with the reported low-coverage theoretical values in the literature (2.09 Å [16] and 2.01 Å [17]). We find that the distance increases with higher coverage, reaching a value of 2.10 Å for 1 ML coverage. The only experimental distance reported in the literature (see Section 1) is 1.95 Å [13].

# 3.2. Rh/MgO(001) energetics

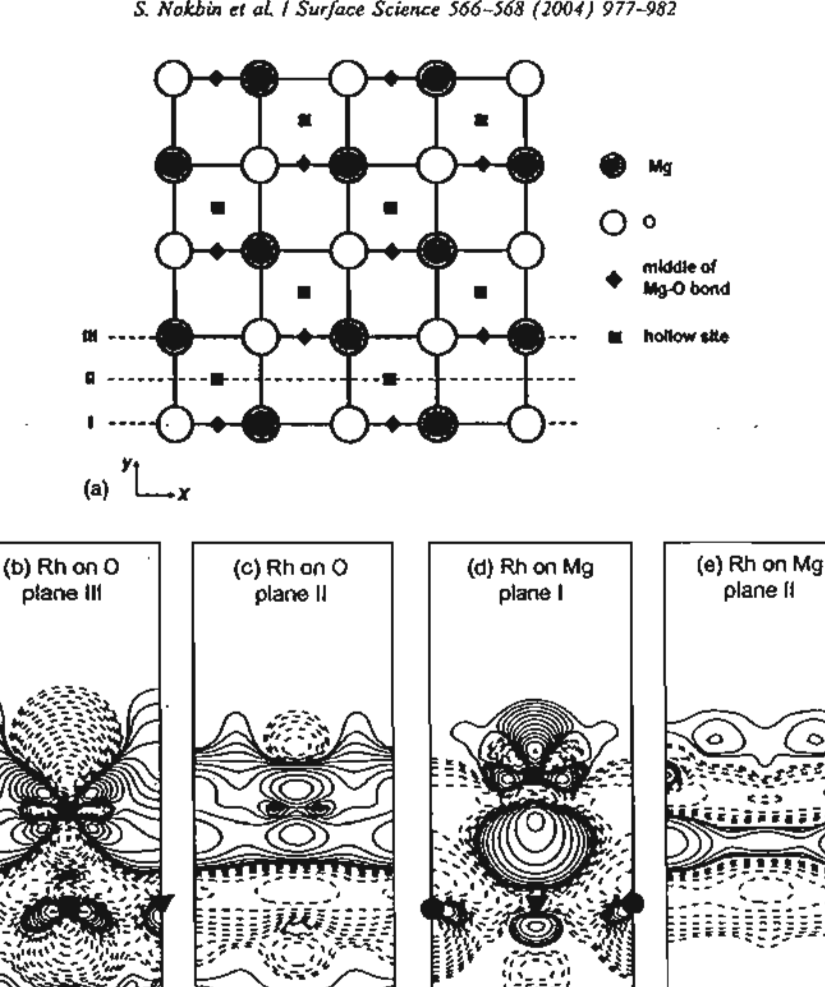
Two types of metal-metal oxide interaction energies were calculated, namely the adsorption energy  $E_{ads}$  and the adhesion energy  $E_{adh}$  defined in (2) and (3) below. The formation of the metal/oxide interface (3) can be thought of as consisting of two consecutive steps, (1) and (2), according to

- (1)  $Rh(g) \rightarrow Rh$ -layer  $\Delta E_1 = -\Delta E_{formation-of-layer}$
- (2) Rh-layer + MgO-slab  $\rightarrow$  Rh/MgO-slab  $\Delta E_2 = -E_{adh}$
- (3) Sum: Rh(g) + MgO-slab  $\rightarrow$  Rh/MgO-slab  $\Delta E_3 = \Delta E_1 + \Delta E_2 = -E_{ads}$

These definitions of  $E_{\rm ads}$  and  $E_{\rm adh}$  follow the usual convention in the literature, but also step (I) has been highlighted above, since this energy contribution becomes particularly interesting when adsorption energies at different coverages are compared.  $\Delta E_{\rm formation-of-layer}$  is thus the energy required or gained when an isolated overlayer is produced from the isolated metal atoms. All systems in the definitions above have the same atomic positions, namely those of the total (geometry-optimized) Rh/MgO interface system.

The  $E_{\rm ads}$  and  $E_{\rm adh}$  values for the optimized structures are also presented in Table 1.  $\Delta E_{\rm formation-of-layer}$  is not included in the table since it is constant for each coverage and is less than 0.001 eV for 1/8 coverage, equal to 0.55 for 1/2 ML coverage and 2.88 eV for 1 ML. The Rh layer is thus stabilized by an increased number of Rh-Rh interactions.

The adhesion energy, however, is seen to become less stabilizing for larger coverages, in agreement with the trends suggested by the existing data in the literature (see Section 1). The magnitude of  $\Delta E_{\text{formation-of-layer}}$  is larger than the magnitude of  $E_{\text{adh}}$ , however, and the combined effect of  $\Delta E_{\text{formation-of-layer}}$  and  $E_{\text{adh}}$  is that the total adsorption energy  $E_{\text{ads}}$  increases with surface coverage (see Table 1). Given the larger value of  $\Delta E_{\text{formation-of-layer}}$  compared to the  $E_{\text{adh}}$  one might expect "island formation" of Rh to be important. We have not made any attempt to study this phenomenon in the present paper.



▼ Mg ■ Rh O Fig. 1. (a) Top view of the clean MgO(001) surface, indicating the various adsorption sites as described in the text. The figure shows a 2×2 crystallographic supercell where the left and right edges are thus identical, as well as the upper and lower edges. The adsorption pattern corresponds to 1 ML coverage in each case. The labels I, II and III indicate the xz sections [(010) plane] used for the electron density plots. (b)-(e) Difference electron density,  $\Delta \rho = \rho_{Rh/MgO} - [\rho_{MgO,dub} + \rho_{Rh,layer}]$ , for the optimized interface system with four oxide layers and 1 ML Rh coverage. Rh over O in (b)-(c) and over Mg in (d)-(e). Solid contour lines denote electron excess, dashed lines electron loss. The contour levels are at ±0.0005, ±0.0008, ±0.0013, ... e/a.u. increasing by a factor of 1002 for every contour line.

Our  $E_{adh}$  result for the low coverage, 2.05 eV, shows quite similar result as compared to other low-coverage studies in the literature, i.e. 1.82 eV

[16] and 1.93 eV [17], and our 1 ML  $E_{adh}$  value of . 1.1 eV is in reasonable agreement with the highcoverage value of 0.8 eV reported in [15].

Table 1
Interaction energies (in eV) and vertical Rh-surface distance (in Å) for the optimized Rh/MgO(001) system at different coverages

Coverage	Adsorpt	ion site							
	0			Hollow			Mg		
	r	E <sub>state</sub>	$E_{ada}$	r	E <sub>adh</sub>	Eads	r	$E_{\rm adh}$	Eada
1/8 ML	1.99	2.05	2.05	1.80	1.91	1.91	2.55	0.60	0.60
1/2 ML	2.07	1.71	2.25	1.93	1.18	1.72	2.70	0.39	0.94
1 ML	2.10	1.11	3.99	2.48	0.35	3.23	2.92	0.16	3.04

The adhesion energy and adsorption energy are defined in the text.

As for the other adsorption sites, the hollow site is a fairly good one, whereas the Mg ion is not. This is reflected both by the Rh-surface distance and by  $E_{\rm ads}$ .

# 3.3. Rh/MgO(001) electronic charge density

Fig. 1b-e shows the electron density redistribution corresponding to 1 ML adsorption over the O and Mg sites (Fig. 1b-c and d-e, respectively). More exactly, the quantity plotted is  $\Delta \rho =$  $\rho_{Rh/MgO} - [\rho_{MgO slab} + \rho_{Rh layer}]$ , which is the electron redistribution occurring when an isolated Rh layer and an isolated MgO slab combine to form the interface system (all components at the optimized interface system geometry). This difference density is thus the "density-equivalent" of  $\Delta E_{*dh}$ . The difference density has been plotted in three different xz planes, defined in Fig. 1a. From Fig. 1b, for example, we see that the O ion in the topmost layer induces strong electron density rearrangements in the Rh atom lying just above it. The electron density "spills over" to the region above the Mg ions, giving a stabilizing effect. The electron density rearrangement induced by the Rhsurface interaction is seen to extend quite far down into the slab, although it of course decreases as a function of depth. Electron density maps were also presented in [15], where the authors emphasized that the electron density rearrangement was essentially confined to the Rh atoms and the outermost oxide layer, a conclusion supported by their electron density maps. As usual, however, the choice of contour levels may be crucial in steering the scientific conclusions drawn from the analysis of electron density maps. It is clear from our results that also the atoms a few layers down into the slab are significantly affected by the Rh overlayer. Fig. 1c shows that also in the region "between and below" the Rh atoms there are some effects of the Rh layer present, although relatively very small.

In Fig. 1e, no such features are visible (with the current choice of contour levels). This is one manifestation of the fact that the Rh-Mg interaction is weaker than the Rh-O interaction. Fig. 1d shows the plane containing the Rh atom and the Mg atom directly below it (plus all the other atoms in that plane). A comparison with Fig. 1b shows that, overall, the polarization features are more enhanced for Rh adsorption at the O site than at the Mg site. The fact that we obtained a much larger  $E_{\rm adh}$  value for the O site supports this conclusion, although it must be borne in mind that any interaction energy also contains components which are not visible in a difference electron density map, namely truely electrostatic contributions.

#### 4. Conclusion

The structural and energetic properties of Rh atoms on MgO(001) were studied by periodic DFT plane-wave calculations. Our results show that Rh prefers to bind to the surface O site, which exhibits both relatively large adhesion energy and a short Rh-surface distance. Also the hollow site is a rather attractive site for Rh. Our calculated adhesion energies over O are in good agreement with the scarce literature data existing. The adhesion energy is found to decrease with coverage and the adsorption energy increases with coverage. Rh adsorption at the O site introduces more electron density rearrangement in the oxide slab than adsorption at the Mg site.

#### Acknowledgements

Financial support from the Swedish Foundation for International Cooperation in Research and Higher Education (STINT) and the Swedish Research Council (VR) are gratefully acknowledged. S.N. and J.L. wish to thank the Thailand Research Fund (TRF) for a Royal Golden Jubilee Ph.D. fellowship (3.C.KU/43/A.2) and a TRF Senior Research Scholar.

#### References

- [1] D. Qin, J. Lapszewicz, Catal. Today 21 (1994) 551.
- [2] H.Y. Wang, E. Ruckenstein, J. Catal, 186 (1999) 181.
- [3] M. Baerns, O.V. Buyevskaya, L. Mieczko, D. Wolf, Stud. Surf. Sci. Catal. 107 (1997) 421.
- [4] D. Qin, J. Lapszewicz, X. Jiang, J. Catal. 159 (1996) 140.
- [5] T. Iizuka, Y. Tanaka, K. Tanabe, J. Catal. 76 (1982) 1.
- [6] J. Wang, J.A. Lercher, G.L. Haller, J. Catal. 88 (1984) 18.
- [7] F. Solymosi, A. Erdohelyi, J. Catal. 91 (1985) 327.
- [8] Y.W. Chen, J. Chin. Inst. Chem. Engrs. 19 (1988) 53.

- [9] A.M. Efstathiou, J. Mol. Catal. 69 (1991) 105.
- [10] A. Ualikhanova, A.E. Temirbulatova, Z. Prikladnoi Khimii (Sankt-Peterburg, Russian Federation) 64 (1991) 2393.
- [11] T. Lopez, J. Mendez-Vivar, R. Juarez, J. Non-Cryst. Solids 147-148 (1992) 778.
- [12] F. Solymosi, J. Cserenyi, L. Ovari, J. Catal, 171 (1997) 476.
- [13] R.J. Emrich, A.N. Mansour, D.E. Sayers, S.T. McMillan, J.R. Katzer, J. Phys. Chem. 89 (1985) 4261.
- [14] M.A. Baltanas, J.H. Onuferko, S.T. McMillan, J.R. Katzer, J. Phys. Chem. 91 (1987) 3772.
- [15] R. Wu, A.J. Freeman, Phys. Rev. B 51 (1995) 5408.
- [16] A. Stirling, I. Gunji, A. Endou, Y. Oumi, M. Kubo, A. Miyamoto, J. Chem. Soc. Faraday Trans. 93 (1997) 1175.
- [17] A. Bogicevic, D.R. Jennison, Surf. Sci. 515 (2002) L481.
- [18] P.E. Bloechl, Phys. Rev. B 50 (1994) 17953.
- [19] R.W.G. Wyckoff, Crystal Structures, 2nd ed., vol. 2, Interscience, New York, 1964.
- [20] G. Kresse, J. Hafner, Phys. Rev. B 47 (1993) 558.
- [21] G. Kresse, J. Furthmueller, Phys. Rev. B 54 (1996) 11169.
- [22] G. Kresse, D. Joubert, Phys. Rev. B 59 (1999) 1758.
- [23] J.P. Perdew, J.A. Chevary, S.H. Vosko, K.A. Jackson, M.R. Pederson, D.J. Singh, C. Fiolhais, Phys. Rev. B 46 (1992) 6671.
- [24] H.J. Monkhorst, J.D. Pack, Phys. Rev. B 13 (1976) 5188.





Journal of Molecular Structure 733 (2005) 239-246



www.elsevier.com/locate/molstruc

# The adsorption of benzene on industrially important nanostructured catalysts (H-BEA, H-ZSM-5, and H-FAU): confinement effects

Ratana Rungsirisakun, Bavornpon Jansang, Piboon Pantu, Jumras Limtrakul\*

Laboratory for Computational and Applied Chemistry, Physical Chemistry Division, Department of Chemistry, Faculty of Science,
Kasetsart University, 50 Phahonyothin Road, Lat Yao Sub., Bangkok 10900, Thailand

Received 1 June 2004; revised 26 August 2004; accepted 1 September 2004

#### Abstract

The structure of industrially important zeolitic catalysts (H-BEA, H-ZSM-5, and H-FAU) and their interactions with benzene have been investigated within the framework of our-own-N-layered integrated molecular orbital + molecular mechanics (ONIOM) approach utilizing the three-layer ONIOM scheme (B3LYP/6-31G(d,p):HF/3-21G:UFF). Inclusion of the extended zeolitic framework covering the nanocavity has an effect on adsorption properties and leads to differentiation of different types of zeolite, unlike the small cluster models which are not able to make this differentiation. The ONIOM adsorption energies of benzene on ZSM-5, BEA, and FAU zeolites are ~19.23, ~16.11, and ~15.22 kcal/mol, respectively, which agrees well with the known adsorption trend of these three zeolites. On the other hand, the small cluster models underestimate the adsorption energies and even yield an unreasonable trend of adsorption energies (~8.09, ~8.48, and ~8.93 kcal/mol for ZSM-5, BEA, and FAU, respectively). With the inclusion of basis set superposition error (BSSE) and the MP2 corrections, the ONIOM3(MP2/6-31G(d,p):HF/3-21G:UFF) adsorption energies are predicted to be ~18.96, ~16.34, and ~15.18 kcal/mol, for ZSM-5, BEA, and FAU, respectively. The last value can be compared well with the experimental data (~15.31 kcal/mol) for benzene adsorption on a FAU zeolite. The results derived in this study suggest that the ONIOM3(MP2/6-31G(d,p):HF/3-21G:UFF) scheme provides a more accurate method for investigating the adsorption of aromatic hydrocarbons on these zeolites.

© 2004 Elsevier B.V. All rights reserved.

Keywords: BEA zeolite; Faujasite zeolite; ZSM-5 zeolite; DFT-study; Benzene adsorption; ONIOM

# 1. Introduction

Zeolite is one of the most important heterogeneous catalysts for environmental and industrial applications [1,2]. Many petrochemical processes take advantage of the high activity of the protonic form of these aluminosilicates [3-12]. It has been shown that the difference in catalytic activity can be ascribed to different acid strengths of the acid sites and to the confinement effect, i.e. interactions between adsorbed molecules and the nanostructured zeolitic pores [13]. Derouane et al. [14,15] found that the confinement effects are results of van der Waals interactions which are major factors for determining the strength of interactions between the adsorbed molecule and the zeolite Brønsted

sites. The understanding and rational utilization of confinement effects will undoubtedly contribute to increase the productivity, selectivity and specificity of such chemical transformations [13–16].

Numerous theoretical models, including the periodic electronic structure methods, have been proposed to study the interactions in extended systems such as crystals or surfaces [17-24]. For nanostructured materials, such as zeolites, that have a high impact in industrial processes usually possess hundreds of atoms per unit cell. This makes the use of accurate periodic structure calculations computationally too expensive and even impractical when very large zeolites are concerned. Alternatively, hybrid methods, such as embedded cluster or combined quantum mechanics/molecular mechanics (QM/MM) [25-31] methods, as well as the more general our-own-N-layered integrated molecular orbital+molecular mechanics (ONIOM) method

Corresponding author,
 E-mail address: fscijrl@ku.ac.th (J. Limtrakul).

[32,33], have brought a larger system within reach of obtaining accurate results.

In this study we present the ONIOM method that takes advantage of the density functional theory for the accurate treatment of the interactions of adsorbed molecules with the acid site of zeolite and of the universal force fields (UFF) for rigorous presentation of the van der Waals interaction due to the confinement of the extended zeolitic structure [34-40]. This efficient scheme has been demonstrated to yield adsorption energies close to the experimental estimates [34,35,41,42], suggesting that the ONIOM approach is a sufficiently accurate and practical model in studying adsorption of unsaturated hydrocarbons on zeolites. In this study, the effects of the zeolite environments on the adsorption properties of benzene in three different zeolites. (H-BEA, H-ZSM-5, and H-FAU), are examined and compared in order to address the confinement effect in these nanostructurted materials.

#### 2. Methods

Two different strategies have been employed to model the different types of zeolites and their complexes with benzene. First, small quantum cluster (B3LYP/6-31G(d,p):HF/3-21G) of 10T H-ZSM-5, 12T H-BEA, and 12T H-FAU zeolites are modeled to represent the active sites of the H-ZSM-5, H-BEA and faujasite (H-FAU) zeolites. The second strategy employs the ONIOM3(-B3LYP/6-31G(d,p):HF/3-21G:UFF) approach for the more realistic models of 46T-H-ZSM-5, 78T-H-BEA and 84T-H-FAU zeolites.

The cluster models of H-ZSM-5, H-BEA and H-FAU were obtained from their crystal lattice structures of H-ZSM-5, H-BEA and H-FAU, respectively [10,43,44]. The 12T-BEA cluster is the 12-membered-ring representing the main gateway to the intersection of two perpendicular 12MR channel systems (Fig. 1a). The 10T-ZSM-5 cluster is the 10-membered-ring window representing the zigzag gateway of the ZSM-5 zeolite that is large enough to allow the probe molecule to move freely (Fig. 2a). The 12T-FAU cluster is the 12-membered-ring window connecting two supercages of FAU zeolite (Fig. 3a).

The effect of the extended framework structure of zeolites cannot be totally neglected if accurate results are required. Thus, realistic clusters were proposed for representing the systems of H-ZSM-5, H-BEA and H-FAU using the ONIOM scheme. In the ONIOM scheme, for computational efficiency, only the active region is treated accurately with the ab initio method, while interactions in the rest of the model is approximated by a less accurate method. As for Beta zeolite, the 78T cluster is used for representing nanocavity at the intersection of the two perpendicular 12MR channels (Fig. 1b). The ONIOM3 scheme, in which the whole model is subdivided into three layers, is adapted. The active region consisting of the 3T

cluster, H3SiOAl(OH)2O(H)SiH3, which is considered the smallest unit required to represent the acid site of zeolite, and the reactive molecules is treated with the B3LYP/6-31G(d,p) or MP2/6-31G(d,p) method. A silicon atom at a T5 position in Beta zeolite is substituted by an aluminum atom, and a proton is added to the bridging oxygen atoms bonded directly to the aluminum atom, conventionally called O5 position [10]. The extended framework environment is included using less expensive levels of theories, the Hartree-Fock, and molecular mechanics force field (UFF) methods [45]. The HF/3-21G method is used for the 9T ring fragment connecting the 3T acidic site to complete the 12T pore opening of the Beta zeolite (Fig. 1). The remainder of the 78T extended framework is treated with the UFF force field to reduce computational time and to practically represent the confinement effect of the zeolite pore structure.

In order to observe the interactions of the adsorbed molecule with different environments of the zeolite framework, comparison is made with a similar ONIOM3 scheme for H-ZSM-5 and H-FAU zeolites. We utilize the MP2 or B3LYP method for the 3T cluster of Brønsted acid site and the benzene. In the intermediate layer, the Hartree-Fock method is employed to complete the remainder of the 10T and 12T membered-ring windows of the H-ZSM-5 and H-FAU zeolites, respectively. The selected outermost layers include the extended framework up to 46T and 84T tetrahedral atoms for the H-ZSM-5 (Fig. 2b) and H-FAU (Fig. 3b) zeolites, respectively, which cover all the important frameworks—where the reaction normally takes place.

All calculations have been performed using the GAUSSIAN 98 code [46]. The 6-31G(d,p) basis set is used for the B3LYP and MP2 calculations, while the basis set for the Hartree–Fock calculations is 3-21G. During the structure optimization, only the active site region  $\{ \equiv SiO(H)Al(O)_2. OSi \equiv \}$ , and the adsorbates are allowed to relax while the remainder is fixed at the crystallographic coordinates [10,43,44].

In order to obtain more reliable interaction energies, basis sets superposition error (BSSE) corrections were also taken into account. It is known that DFT does not account for the dispersion component of the interactions. Single point MP2/6-31G(d,p) calculations for the high-level active region were carried out at the B3LYP optimized geometries to improve the energetic information between benzene and the zeolite framework.

#### 3. Results and discussion

3.1. Comparisons of small cluster with extended zeolitic cluster models

The 12T and 78T cluster models for H-BEA zeolite are shown in Fig. 1. Selected geometrical structures for all

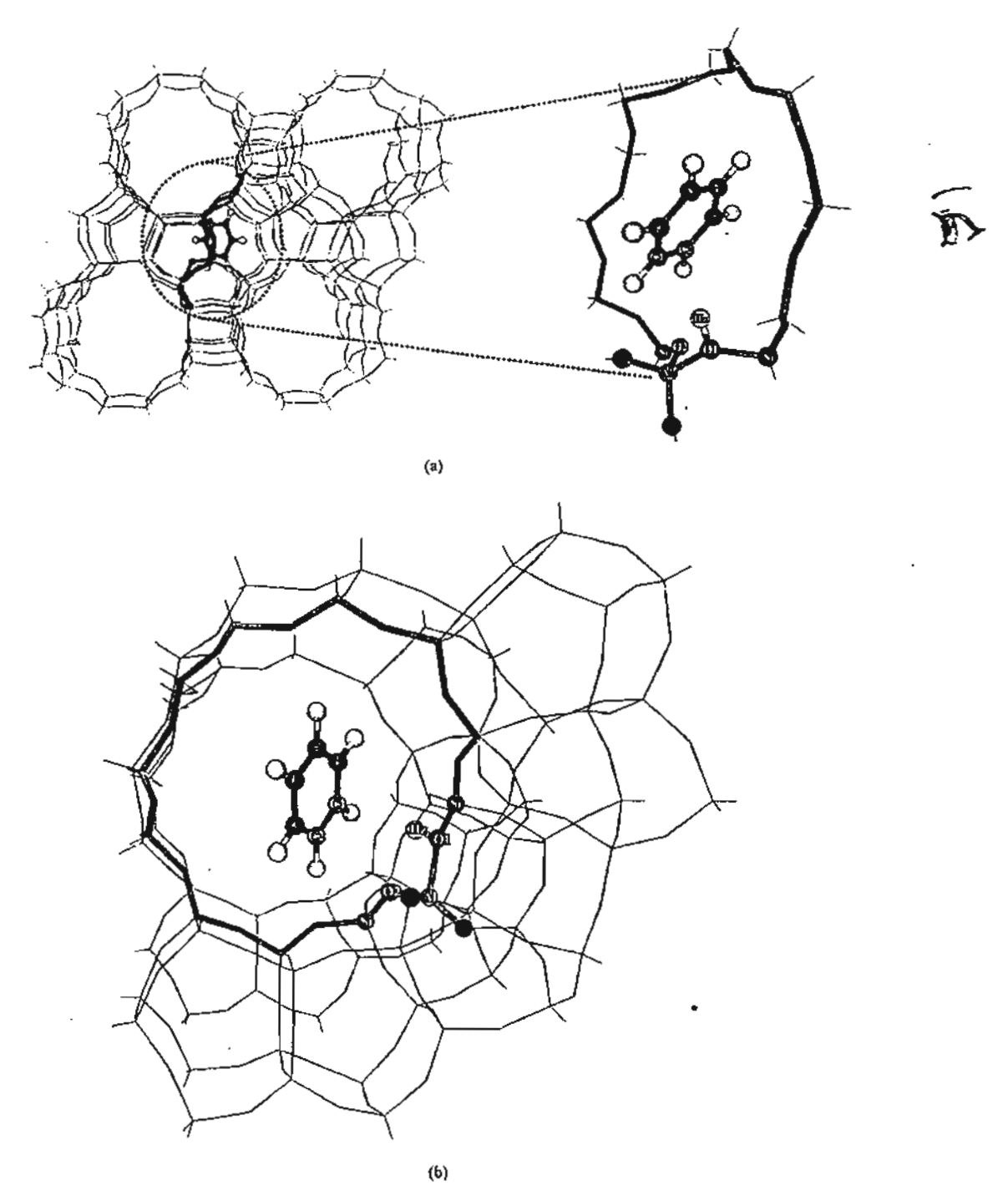


Fig. 1. The oval dashed line encloses an intersection of two perpendicular 12MR channel systems of Beta zeolite which is modeled by the 78T cluster-serving as a nanoreactor, where the benzene molecule is favorably adsorbed. (a) The 12T-BEA cluster is the 12-membered-ring representing the main gateway to the intersection of Beta zeolite and is viewed along [100] as indicated by the eye's sign. (b) The 78T cluster model viewed from the main channel. The atom belonging to the 12T quantum cluster is drawn as a sphere.

cluster models are documented in Tables 1 and 2. The extended structure included in the ONIOM3(B3LYP/6-31G(d,p):HF/3-21G:UFF) scheme was found to have a small effect on the structure of BEA zeolite. In the most realistic model of the 78T cluster model, Si-O1, Al-O1 bond

lengths decrease slightly. On the other hand, this model slightly elongates the O1-Hz bond distance (Brønsted acid site) by 0.1 pm for BEA zeolite. There is also a slight increase in the Si-O1-Al bond angle as compared to the small cluster model (131.1 vs. 135.5 pm).

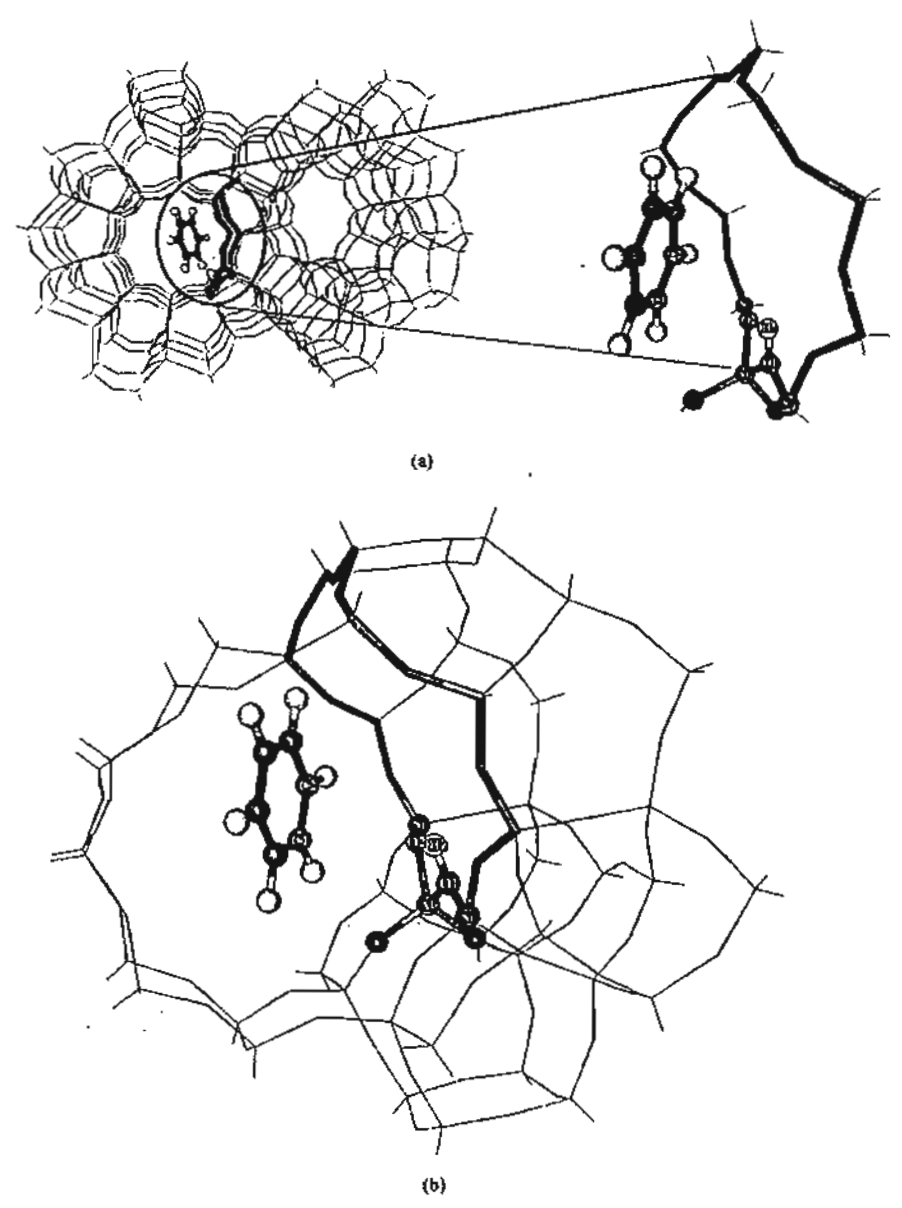


Fig. 2. Optimized structures of C<sub>6</sub>H<sub>6</sub> adsorbed on H-ZSM-5 zeolite. (a) The IOT cluster model of H-ZSM-5/C<sub>6</sub>H<sub>6</sub> complex is the IO-membered-ring window representing the zigzag gateway of the ZSM-5 zeolite. (b) The 46T cluster model of the H-ZSM-5/C<sub>6</sub>H<sub>6</sub> complex; both are viewed from the direction of the straight channel of the H-ZSM-5 zeolite. The atom belonging to the IOT quantum cluster is drawn as a sphere.

Further support for the reliability of the active site subunit,  $\equiv$ Si-OH-Al $\equiv$ , by our model calculations is given from NMR studies. Klinowski et al. have estimated the internuclear distance between the aluminum and proton nuclei in the Brønsted acid site, Al···Hz, of different zeolites [47,48] to be in the range of 234-252 pm, and our computed Al···Hz distances of the most realistic models of 78T-H-BEA, 46T-H-ZSM-5 and 84T-H-FAU zeolites are in the range of 233-245 pm.

Despite the small magnitude, the changing of distances and angles at the active region with the ONIOM model, one can expect that adsorption of probe molecules on the zeolites will be affected by the presence of the long-range interaction of the framework, and this will be discussed in the following text.

#### 3.2. The interactions of benzene with the BEA zeolite

The C-C and C-H bond lengths of a benzene molecule were ascertained experimentally to be 139.7 and 108.4 pm, respectively. The B3LYP/6-31G(d,p) level of theory predicted the bond lengths of 139.6 and 108.6 pm which are in excellent agreement with the experimental observation. For the bare 12T quantum cluster, the changes of geometrical parameters upon the adsorption of benzene are in accordance with Gutmann's rule [49,50], i.e. a lengthening of

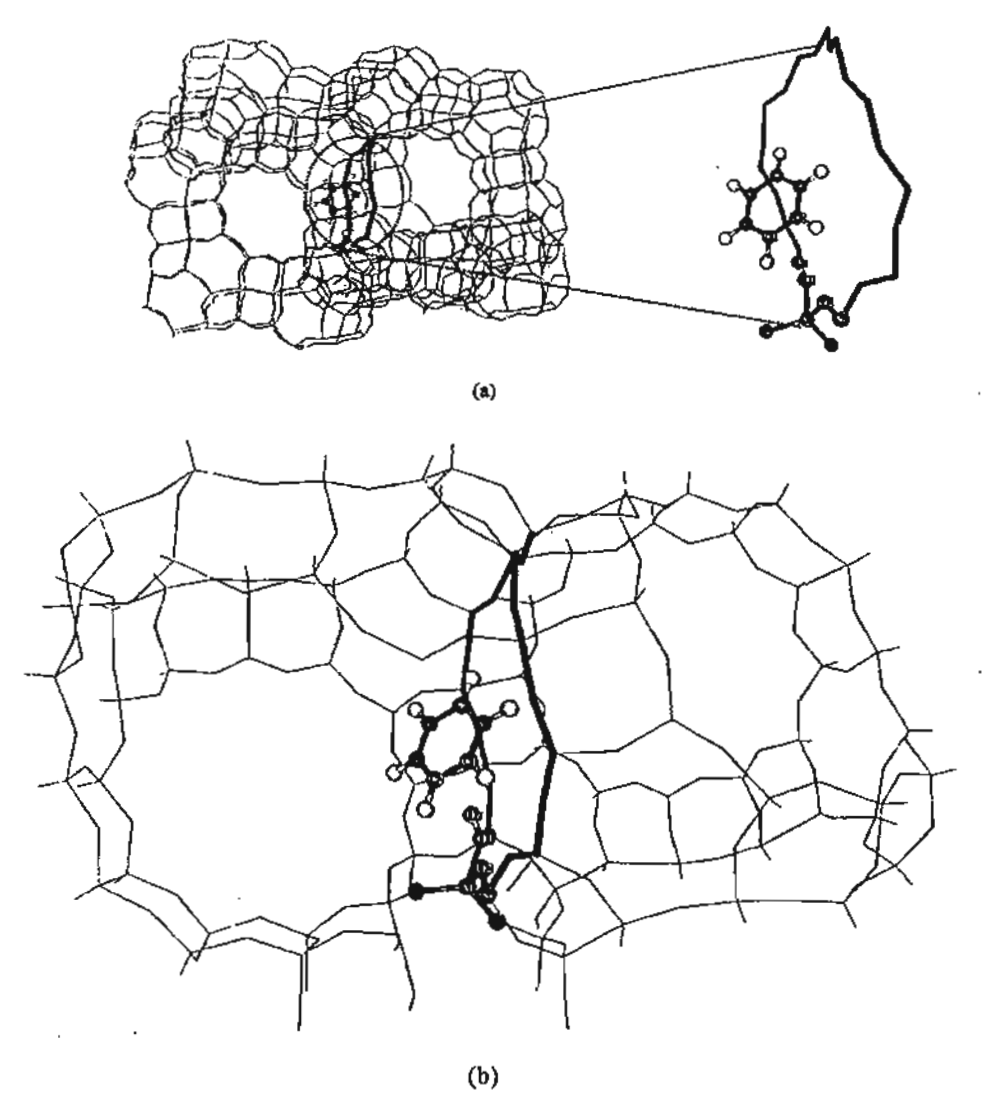


Fig. 3. Optimized structures of  $C_6H_6$  adsorbed on H-FAU zeolite. (a) The L2T-FAU cluster model of H-FAU/ $C_6H_6$  complex is the 12-membered-ring window connecting two supercages of FAU zeolite. (b) The 84T cluster model of the H-ZSM-5/ $C_6H_6$  complex, which includes two supercages. The atom belonging to the 12T quantum cluster is drawn as a sphere.

Table 1 Structure parameters for various zeolites and their complexes with  $C_6H_6$  are obtained at small clusters

Parameters	10T ZSM-5		12T BEA		12T FAU	
	Isolated	Complex	Isolated	Complex	Isolated	Complex
O1-Hz	97.2	97.5	96.9	98.4	97.1	98.5
Si-O1	1.66.1	166.2	168.3	168.2	168.6	168.4
AI-O1	183.7	183.0	187.9	187.0	190.6	189.4
AI-02	167.4	167.3	168.7	169.5	169.7	170.0
AlHz	238.8	238.7	236.2	237.3	250.6	248.8
∠Si-O1-AI	134.0	133.3	131.1	129.6	125.6	124.7
CIHz	~	300.1	_	227.7	_	233.5
C2···Hz	-	319.0	-	259.0	-	258.0
C1-C2	139.6	140.1	139.6	140.2	139.6	140.2
CI-HI	108.6	108.7	108.6	108.7	108.6	108.6

Bond lengths are in picometer and bond angles are in degree.

Table 2 Structure parameters for various zeolites and their complexes with  $C_6H_6$  are obtained at large clusters

Parameters	46T ZSM-5		78T BEA		84T FAU	
	Isolated	Complex	Isolated	Complex	Isolated	Complex
 01-Нг	97.2	97.4	97.0	'98.3	97.2	98.7
Si-O1	164.6	164.7	166.5	165.7	166.5	166.1
Al-Ol	184.3	183.6	184.9	185.6	187.1	186.1
A!-02	166.0	165.9	169.2	170.2	168.9	169.1
Al···Hz	232.6	232.8	- 234.4	234.6	245.0	243.9
∠\$i-O1-A1	135.0	134_3	135.5	135.2	123.5	123.6
C1···Hz	-	333.1	-	253.5	-	220.4
C2···Hz	-	398.4	-	300.8	-	257.6
C1-C2	139.6	139.8	139.6	139.9	139.6	140.3
CI-HI	108.6	108.7	108.6	108.6	108.6	108.7

Bond lengths are in picometer and bond angles are in degree.

the O1-Hz (96.9 vs. 98.4 pm) along with a corresponding slight decrease in Al-O1 and lengthening of Al-O2 (not adjacent to the bridging OH). The distances of Brønsted proton (Hz) and C1 and C2 atoms of benzene are calculated to be 227.6 and 259.0 pm, respectively. Benzene adsorption results in a slight elongation of the C-C bonds as compared to the isolated molecule (140.2 vs. 139.6 pm). However, no significant change is observed in the lengths of the C-H bonds. Our calculated adsorption energy from the 12T cluster models is estimated to be ~8.48 kcal/mol at B3LYP/6-31G(d,p) level, which is significantly lower than the adsorption energy of benzene obtained from the ONIOM model (-16.11 kcal/mol). After BSSE correction, the adsorption energy ( $\Delta E_{Ads}^{BSSE}$ ) predicted by the ONIOM model is -13.54 kcal/mol, which is reasonably close to the experimental estimate of -15.31 kcal/mol for related zeolite [51]. The large deviation observed in the 12T model is due to the fact that the small cluster model neglects longrange interactions of the extended framework, which is important for adsorption-desorption in zeolites [52,53].

3.3. The effect of the different types of zeolite framework (FAU, BEA and ZSM-5) on the adsorption properties of benzene

In order to demonstrate that ONIOM3 can be employed to explore the different types of zeolites, adsorption of benzene on other industrially important zeolites, FAU and ZSM-5, are also studied using the same ONIOM3 scheme. Similar trends about the adsorption energies have also been observed ( $\Delta E_{Adx}^{BSSE}$  reported in Table 3), in which the adsorption energies ( $\Delta E_{Ads}^{BSSE}$ ) for small cluster models (-5.78 and -6.46 for the H-ZSM-5 and H-FAU complexes, respectively) are significantly lower than the corresponding values obtained from the large ONIOM cluster models. Therefore, in order to keep this article short, we will discuss mainly the effect of the different pore sizes in these zeolites on adsorption properties. The structural parameters of these complexes are documented in Tables 1 and 2. A pronounced effect of the zeolite framework of H-ZSM-5 is observed in adsorption of benzene. The 10T ring

Table 3
Adsorption energies for C<sub>6</sub>H<sub>6</sub>/H-zeolites obtained from various models and methods

Zeolite ZSM-5	Mode)	Method	Adsorption energy (kcal/mol)		
			∆E <sub>Ads</sub>	ΔEBSSE.	
	10T	B3LYP/6-31G(d,p):HF/3-21G	-8.09	-5.78	
	IOT	MP2/6-31G(d,p):HF/3-21G //B3LYP/6-31G(d,p):HF/3-21G	-11.50	-8.02 (-9.31) <sup>6</sup>	
	46T	B3LYP/6-31G(d,p):HF/3-21G:UFF	-19.23	-17.24	
	46T	MP2/6-31G(d,p):HF/3-21G:UFF //B3LYP/6-31G(d,p):HF/ 3-21G:UFF	-21.88	-18.96	
BEA .	12T	B3LYP/6-31G(d.p):HF/3-21G	-8.48	5.41	
	12T	MP2/6-31G(d,p):HF/3-21G //B3LYP/6-31G(d,p):HF/3-21G	-11.64	-6.94 (−8.74)b	
	78T	B3LYP/6-31G(d,p):HF/3-21G:UFF	- 16.11	-13.54	
	78T	MP2/6-31G(d,p):HF/3-21G:UFF //B3LYP/6-31G(d,p):HF/ 3-21G:UFF	-20.36	-16.34	
FAU	12 <b>T</b>	B3LYP/6-31G(d,p):HF/3-21G	-8.93	~6.46	
	12T	MP2/6-31G(d.p):HF/3-21G //B3LYP/6-31G(d.p):HF/3-21G	- 12.06	$-8.27 (-10.34)^{b}$	
	84T	B3LYP/6-31G(d,p):HF/3-21G:UFF	-15.22	- 12.22	
	84T	MP2/6-31G(d,p):HF/3-21G:UFF //B3LYP/6-31G(d,p):HF/ 3-21G:UFF	-18.86	15.18	

 <sup>\( \</sup>Delta E^{\text{BSSE}} \) is the calculated adsorption energy with the BSSE correction.

With additional columbic interactions due to a set of point charges located on the positions of zeolite framework [23].

of H-ZSM-5 zeolite is apparently too constricted for the benzene molecule to form a complex within the 10 membered-ring. The benzene molecule is moved toward the intersection of the pore channels, which is more spacious (see Fig. 2). This finding is supported by the neutron and Xray diffraction measurement [54]. Unlike H-ZSM-5, the FAU consists of a 12 membered-ring which allows the benzene to be trapped within its window. The small cluster models significantly underestimate the adsorption energies of benzene/ZSM-5 and benzene/FAU. Inclusion of the extended framework results in higher adsorption energies, i.e. -17.24 and -12.22 kcal/mol for benzene/ZSM-5 and benzene/FAU complexes, respectively. The interaction energies of benzene adsorbed on zeolites, calculated from the ONIOM models, are much larger than from the bare quantum cluster models and better in agreement with experimental results. This difference is mainly attributed to 'non-local interactions' which are the van der Waals interactions due to confinement of the zeolite microporous structure, and the long range electrostatic interactions. The interactions of benzene with the zeolite acidic site are small as reflected by the small interaction energies obtained from the cluster calculations and minute changes in structure of adsorbed benzene. Since benzene is a non-polar molecule the long range electrostatic interactions are not expected to be significant. Indeed, by using columbic calculations with the quantum cluster directly interacted with the potential due to a set of point charges located on the positions of zeolite framework [23], we can demonstrate that for benzene adsorbed on the different types of zeolite, (ZSM-5, BEA and FAU), inclusion of the long range electrostatic interactions only increases the interaction energy by 1-2 kcal/mol compared to the quantum cluster calculations (cf. Table 3). On the other hand, the van der Waals interactions, accounted for by the UFF force field, with the zeolite pore walls should contribute significantly to the adsorption of benzene because the size of benzene molecule is comparable to the nanometer-sized zeolite pores [34, 36-40]. The results also suggest that the large extended zeolite framework covering nanocavity is needed for accurate representation of the different types of zeolite, which cannot be drawn from the typical small quantum cluster. The difference in interaction energies of benzene in the H-ZSM-5, H-BEA, and H-FAU zeolites may be due to the combination of the acidity and confinement effects of the zeolites. Due to the smaller pore size of H-ZSM-5 (540 pm) than that of H-BEA (640 pm) and H-FAU (740 pm for cage window and 1250 pm for supercage) zeolites, the confinement effect (mainly van der Waals interactions) is stronger in ZSM-5 zeolite. Since the van der Waals interactions dominate the adsorption of non-polar molecules, the adsorption energy of benzene in H-ZSM-5 is higher than those of H-BEA and H-FAU zeolites. In the ONIOM3(B3LYP:HF:UFF) scheme, the acidity of zeolite is sufficiently accounted for by the quantum cluster of the active region treated by the density functional theory

(B3LYP) and the van der Waals interaction is reasonably described by the UFF force field [45]. Therefore, the ONIOM3 scheme proposed here can provide a better estimate of adsorption energies than the typical small quantum cluster calculations.

It is known that DFT does not account for the dispersion component of the interactions. Single point MP2/6-31G(d,p) calculations for the high-level active region were carried out at the B3LYP optimized geometries to improve the energetic information between benzene and the zeolite framework. Using the MP2 in place of the B3LYP for the active region in the ONIOM3(MP2/6-31G:HF/3-21G:UFF) scheme, the models yield the adsorption energies ( $\Delta E_{AA}^{BSSE}$ ) of -18.96, -16.34, and -15.18 kcal/mol, for the H-ZSM-5. H-BEA, and H-FAU complexes, respectively. The last value is in excellent agreement with the experimental estimate of -15.31 kcal/mol obtained by Coker et al. [51], indicating that our combined approach is considered to be one of the best combinations for the ONIOM scheme. This efficient scheme provides a cost effective computational strategy for treating the effects of a large extended framework structure.

Thus, the studies of the zeolite framework structure revealed that adsorption properties of zeolite do not depend only on the acidic site center, but also on the framework structure where the acidic site is located.

# 4. Conclusion

We have carried out systematic ONIOM studies on the adsorption of benzene on industrially important H-BEA, H-ZSM-5, and H-FAU zeolites. The effects of the extended zeolite framework covering the nanocavity on the adsorption properties were investigated using ONIOM3 schemes. We found that the zeolite environ ment significantly enhances the adsorption energies of benzene on zeolites. The efficient ONIOM schemes, the ONIOM3(B3LYP/6-31G(d,p):HF/3-21G:UFF) and ONIOM3(MP2/6-31G(d,p):HF/3-21G:UFF) superbly in comparison to the known adsorption trend of these three zeolites. Conversely, the small cluster models yield very low adsorption energies for these three zeolites and even yield an unreasonable trend of adsorption energies for these zeolites/benzene complexes (-8.09; -8.48, and -8.93 kcal/mol for benzene adsorption on H-ZSM-5, H-BBA, and H-FAU zeolites, respectively). With the inclusion of basis set superposition error (BSSE) and the MP2 corrections, the ONIOM3(MP2/6-31G(d,p):HF/3-21G:UFF) adsorption energies are predicted to be -18.96, -16.34, and -15.18 kcal/mol, for benzene adsorption on H-ZSM-5, H-BEA, and H-FAU zeolites, respectively. The computed adsorption energy for benzene/H-FAU can be compared well with the experimental observation of -15.31 kcal/mol for benzene adsorption on an H-FAU zeolite. The results derived in this study suggest that the ONIOM3(MP2/6-31G(d,p):HF/3-21G:UFF) scheme provides a more accurate method for investigating the adsorption of aromatic hydrocarbons on these zeolites.

# Acknowledgements

This work was supported in part by grants from the Thailand Research Fund (TRF Senior Research Scholar to J.L.) and the Kasetsart University Research and Development Institute (KURDI), as well as the Ministry of University Affairs under the Science and Technology Higher Education Development Project (MUA-ADB funds). The support from the Dow Chemical Company (USA) is also acknowledged.

#### References

- C.R.A. Catlow, Modeling of Structure and Reactivity in Zeolites, Academic Press, San Diego, 1992.
- [2] R.A. van Santen, G.J. Kramer, Chem. Rev. 95 (1995) 637.
- [3] N.O. Gonzales, A.T. Bell, A.K. Chakraborty, J. Phys. Chem. B 101 (1997) 10058.
- [4] S. Bordiga, G. Ricchiardi, G. Spoto, D. Scarano, L. Carnelli, A. Zecchina, C.O. Arean, J. Chem. Soc. Faraday Trans. 89 (1993) 1843.
- [5] J. Sauer, P. Ugliengo, E. Garrone, V.R. Saunders, Chem. Rev. 94 (1994) 2095.
- [6] M. Sierka, J. Sauer, J. Phys. Chem. B 105 (2001) 1603.
- [7] Y. Huang, H. Wang, Langmuir 19 (2003) 9706.
- [8] J. Limtrakul, Chem. Phys. 193 (1995) 79.
- [9] W.H. Chen, A. Pradhan, S.J. Jong, T.Y. Lee, I. Wang, T.C. Tsai, S.B. Liu, J. Catal. 163 (1996) 436.
- [10] A.H. de Vries, P. Sherwood, S.J. Collins, A.M. Rigby, M. Rigutto, G.J. Krarner, Phys. Chem. B 103 (1999) 6133.
- [11] J. Pardillos, D. Brunel, B. Coq. P. Massiani, L.C. De Ménorval, F. Figueras, J. Aro. Chem. Soc. 112 (1990) 1313.
- [12] G. Bellussi, G. Pazzuconi, C. Perego, G. Girotti, G. Terzoni, J. Catal. 157 (1995) 227.
- {13} E.G. Derouane, J.M. Andre, A.A. Lucus, J. Catal, 110 (1988) 58.
- [14] E.G. Derouane, C.D. Chang, Microporous Mesoporous Mater. 35–36 (2000) 425.
- [15] E.G. Derouane, J. Mol. Catal. A 29 (1998) 134.
- [16] S.M. Babitz, B.A. Williams, J.T. Miller, R.Q. Snurr, W.O. Haag, H.H. Kung, Appl. Catal. A 179 (1999) 71.
- [17] R. Shah, J.D. Gale, M.C. Payne, Chem. Commun. 1997; 131.
- [18] Y. Jeanvoine, J.G. Angyan, G. Kresse, J. Hafner, J. Phys. Chem. B 102 (1998) 5573.
- [19] J. Limtrakul, S. Nokbin, S. Jungsuttuwong, P. Khongpracha, Stud. Surf. Sci. Catal. 135 (2001) 2469.
- [20] P. Treesukol, J. Limtrakul, T. Truong, J. Phys. Chem. B 105 (2001) 2421.
- [21] J. Sauer, M. Sierka, J. Comput. Chem. 21 (2000) 1470.
- [22] E.H. Teunissen, A.P. Jansen, R.A. van Santen, R. Orlando, R. Dovesi, J. Chem. Phys. 101 (1994) 5865.
- [23] V. Dungsrikaew, J. Limtrakul, K. Hermansson, M. Probst, Int. J. Quantum Chem. 96 (2003) 17.

- [24] S. Ketrat, J. Limtrakul, Int. J. Quantum Chem. 94 (2003) 333.
- [25] H.I. Hillier, J. Mol. Struct. (Theochem) 463 (1999) 45.
- [26] J. Limtrakul, S. Jungsuttuwong, P. Khongpracha, J. Mol. Struct. 525 (2000) 153.
- [27] P.E. Sinclair, A.H. de Vries, P. Sherwood, C.R.A. Catlow, R.A. van Santen, J. Chem. Soc. Faraday Trans. 94 (1998) 3401.
- [28] M. Brandle, J. Sauer, J. Am. Chem. Soc. 120 (1998) 1556.
- [29] S.P. Greatbanks, L.H. Hillier, N.A. Burton, P. Sherwood, J. Chem. Phys. 105 (1996) 3770.
- [30] R.Z. Khaliullin, A.T. Bell, V.B. Kazansky, J. Phys. Chem. A 105 (2001) 10454.
- [31] J. Limtrakul, T. Nanok, P. Khongpracha, S. Jungsuttiwong, T.N. Truong, Chem. Phys. Lett. 349 (2001) 161.
- [32] S. Dapprich, I. Komaromi, K.S. Byun, K. Morokuma, M.J. Frisch, J. Mol. Struct. (Theochem) 461 (1999) 1.
- [33] M. Svensson, S. Humbel, R.D.J. Froese, T. Matsubara, S. Sieber, K. Morokuma, J. Phys. Chem. 100 (1996) 19357.
- [34] S. Kasuriya, S. Namuangruk, P. Treesukol, M. Tirtowidjojo, J. Limtrakel, J. Catal. 219 (2003) 320.
- [35] K. Bobuatong, J. Limtrakul, App. Catal. A, Gen. 253 (2003) 49.
- [36] A. Pelmenschikov, J. Leszczynski, J. Phys. Chem. B 103 (1999) 6886.
- [37] T.A. Wesolowski, O. Parisel, Y. Ellinger, J. Weber, J. Phys. Chem. A 101 (1997) 7818.
- [38] L.A. Clark, M. Sierka, J. Sauer, J. Am. Chem. Soc. 125 (2003) 2136.
- [39] A.M. Vos, X. Rozanska, R.A. Schoonheydt, R.A. van Santen, F. Hutschka, J. Hafner, J. Am. Chem. Soc. 123 (2001) 2799.
- [40] X. Rozanska, R. van Santen, F. Hutschka, J. Hafner, J. Am. Chem. Soc. 123 (2001) 7655.
- [41] C. Raksakoon, J. Limtrakill, J. Mol. Struct. (Theochem) 631 (2003) 147.
- [42] W. Panjan, J. Limtrakul, J. Mol. Struct. 654 (2003) 35.
- [43] H. van Koningveld, H. van Bekkum, J.C. Jansen, Acta Crystallogr. B 43 (1987) 127.
- [44] D.H. Olson, B. Dempsey, J. Catal. 13 (1969) 221.
- [45] A.K. Rappe, C.J. Casewit, K.S. Colwell, W.A. Goddard, W.M. Skiff, J. Am. Chem. Soc. 114 (1992) 10024.
- [46] M.J. Frisch, G.W. Trucks, H.B. Schlegel, G.E. Scuseria, M.A. Robb, J.R. Cheeseman, V.G. Zakrzewski, J.A. Montgomery, R.E. Stratmann, Jr., J.C. Burant, S. Dapprich, J.M. Millam, A.D. Daniels, K.N. Kudin, M.C. Strain, O. Farkas, J. Tomasi, V. Barone, M. Cossi, R. Cammi, B. Mennucci, C. Pomelli, C. Adamo, S. Clifford, J. Ochterski, G.A. Petersson, P.Y. Ayala, Q. Cui, K. Morokuma, P. Salvador, J.J. Dannenberg, D.K. Malick, A.D. Rabuck, K. Raghavachari, J.B. Foresman, J. Cioslowski, J.V. Ortiz, A.G. Baboul, B.B. Stefanov, G. Liu, A. Liashenko, P. Piskorz, I. Komaromi, R. Gomperts, R.L. Martin, D.J. Fox, T. Keith, M.A. Al-Laham, C.Y. Peng, A. Nanayakkara, M. Challacombe, P.M.W. Gill, B. Johnson, W. Chen, M.W. Wong, J.L. Andres, C. Gonzalez, M. Head-Gordon, E.S. Replogle, J.A. Pople, Gaussian, Inc., Pittsburgh, PA, 2001.
- [47] D. Frende, J. Klinoski, H., Harnden, Chem. Phys. Lett. 149 (1988) 355.
- [48] J. Klinowski, Chem. Rev. 91 (1991) 1459.
- [49] V. Gutmann, The Donor-Acceptor Approach to Molecular Interaction, Plenum Press, New York, 1978.
- [50] V. Gutmann, G. Resch, W. Linert, Coord, Chem. Rev. 43 (1982) 133.
- [51] E.N. Coker, C. Jia, H.G. Karge, Langmuir 16 (2000) 1205.
- [52] J. Xie, M. Bousmina, G. Xu, S. Kaliaguine, J. Mol. Catal. A 135 (1998) 187.
- [53] B. Coughlan, M.A. Keane, J. Chem. Soc. Faraday Trans. 86 (1990) 3961
- [54] R. Goyal, A.N. Fitch, H. Jobic, J. Phys. Chem. B 102 (2000) 2878.

# THE INFLUENCE OF THE FRAMEWORK TO STRUCTURES AND ENERGETIC PROFILES OF THE VAPOR PHASE OF THE BECKMANN REARRANGEMENT ON DIFFERENT TYPES OF ZEOLITE

Jakkapan Sirijaraensre, and Jumras Limtrakul\*

Computational & Applied Chemistry Laboratory, Physical Chemistry Division, Kasetsart University, Bangkok, Thailand

#### Introduction

The Beckmann rearrangement<sup>1-6</sup> is an industrially important reaction for the production of -caprolactam, a raw material for the production of Nylon-6, where the market consumption was millions of tons in 1998.7 Caprolactam is produced by the Beckmann rearrangement of cyclohexanone oxime with oleum or concentrated sulfuric acid as a reaction medium. Although this procedure is convenient from the chemical standpoint, difficulties in manufacturing anticorrosion equipment and eliminating a large amount of the ammonium sulfate formed during the neutralization process make the process environmentally unacceptable. However, using a heterogeneous catalyst in this reaction, usually called the vapor phase of the Beckmann rearrangement, can solve these problems. Zeolite proves to be an excellent candidate 8-40 for taking over the catalytic function since the use of a zeolitic catalyst has the benefit not only from an economical point of view, but also from an ecological viewpoint.

The Beckmann rearrangement of oxime compound has been widely investigated, especially on solid catalysts such as H-ZSM5<sup>8-18</sup>, FAU<sup>19-20</sup>, and B-ZSM5<sup>23-26</sup> etc. Zecchina et al<sup>17</sup> studied the vapor phase of the Beckmann rearrangement in H-Faujasite, H-ZSM-5 and silicalite-1 by using IR-spectroscopy and found that: a) both internal silanols and strong acid sites in zeolite can catalyze the Beckmann rearrangement of cyclohexanone oxime; b) a stable protonated intermediate is formed on a strong acid site; c) the reaction at weak acid sites has a higher activation energy through a mechanism not involving a protonated intermediate. Rhee et al<sup>21-22</sup> studied the Beckmann rearrangement of cyclohexanone oxime over an H-beta catalyst using FT-IR spectroscopy. They suggested that the initial step of the rearrangement involved the N-protonated complex of oxime, not the O-protonated complex. Recently, Nguyen et al<sup>41-41</sup> used MP2 to investigate the

Recently, Nguyen et al. used MP2 to investigate the mechanism of the Beckmann rearrangement in the gas phase. The reaction path was proposed in two key steps. The first step is called 1,2 H-shift, which connects the N-protonated complex and the O-protonated complex. The second step, called the Beckmann rearrangement, is a migration of the alkyl group to the nitrogen atom and an elimination of water molecule, giving a nitrilium cation. The first step was found to be the rate-determining step with an energy barrier of 54 kcal/mol. It is noted that in their calculations they used a proton to model the Brønsted acid of the catalyst interacting with the oxime molecule, thus the effect of the catalytic framework was omitted.

To the best of our knowledge, no theoretical works regarding the interaction of oxime and zeolite catalysts have been published. In this work, the formaldehyde oxime was chosen as a model for simplicity (small oxime molecule). The interaction of the ZSM-5 and FAU zeolites with the N-, O-formaldehyde oxime have been carried out at both the cluster and the embedded cluster approaches with the aim of: a) investigating the mechanism of the Beckmann rearrangement on both zeolites; b) determining the effects of the zeoltic framework, particularly the effect of the Madelung potential to the reaction mechanism and the energetic profile.

#### Methods

The bare cluster and embedded cluster models were used to determine the adsorbed structure of oxime molecules on zeolite (active site) as well as their possible N-protonated and O-protonated species. For the ZSM-5 system, the 10T cluster model (Figure 1(a)) was taken from the crystal structure of ZSM-5 to model the ZSM-5 system. The Si atom at T12 position, at the intersection between the straight channel and the zigzag channel, was replaced by Al atom and the negative charge was counter balanced by a proton which is sitting on the oxygen bridging atom. 34-40 While in the FAU system, the 12T cluster model (Figure 1(b)) which is surrounded by two supercages was taken from the crystal structure of the FAU to model the FAU system.

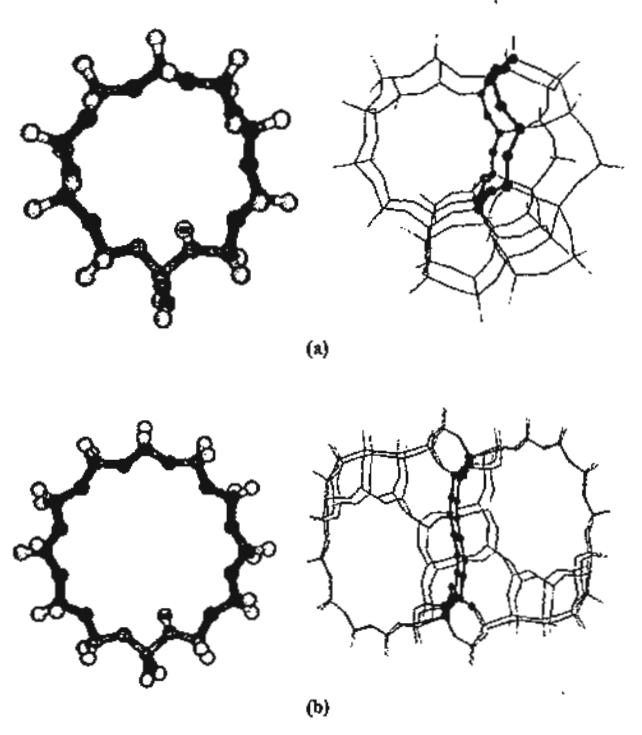


Figure 1. Presentation of the bare cluster models of zeolite. (a) 10T bare cluster model of H-ZSM-5 zeolite illustrating the zigzag gateway of the ZSM-5 zeolite (b) 12T bare cluster model of H-FAU zeolite showing the two supercages.

In the embedded cluster model, the static Madelung potential from the infinite lattice of zeolite can be mimicked by point charges surrounding the cluster. More details on this method can be found elsewhere. 44-47 With this small number of point charges, the additional computational cost is often less than 5% when compared to bare cluster calculations.

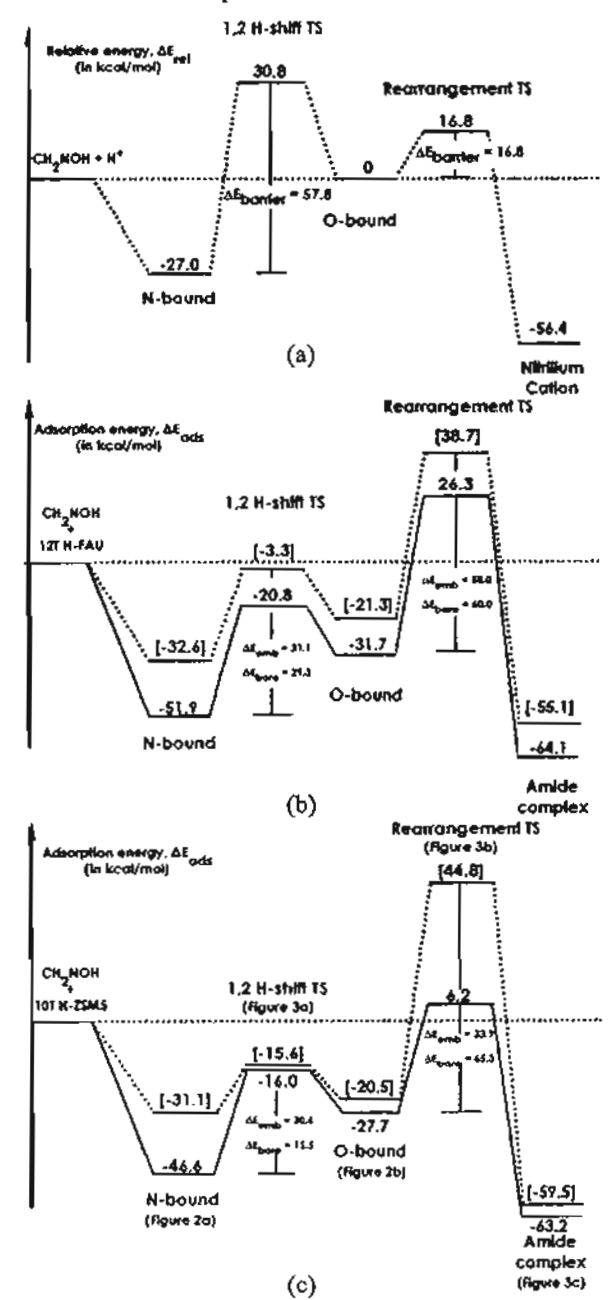


Figure 2. Comparison of the energetic profiles along the pathway of the Beckmann rearrangement of formaldehyde oxime adsorbed on different acid catalysts: gas phase model (a), H-FAU (b) and H-ZSM-5 (c) zeolites, respectively, at the B3LYP level of theory. The energetic changes for the embedded cluster (solid line) and the bare cluster (dash line) complexes are in keal/mol.

In the present work, the calculations of 10T and 12T models have been done at the B3LYP level of theory. In both models. only the active site (H2Si1OAl(OH)2O(H)Si2H2) had been treated at B3LYP/6-31G(d,p) while a lower basis set, 3-21G basis set had been applied to the rest of the cluster models. In all geometrical optimizations, the Si, Al, O bridging atoms and HI (Brønsted acid site) of the active site region of the quantum cluster were allowed to relax, while other atoms were kept fixed at the experimental structure. All calculations were performed using the Gaussian98 program. 46 The computations were performed using the computer resources at the Laboratory for Computational and Applied Chemistry (LCAC) at Kasetsart University.

#### Results and Discussion

The vapor-phase Beckmann rearrangement reaction. The vapor-phase Beckmann rearrangement is investigated on the industrial catalysts, FAU and ZSM-5 zeolites. This study is the investigation the reaction mechanism and the energetic profile of the Beckmann rearrangement at the strong acid site of both zeolites by using bare cluster and embedded cluster models. The energetic profiles of the Beckmann rearrangement on both zeolites are shown in Figure 2. The proposed reaction mechanism is divided into two steps. The first step is the 1,2 H-shift step which is the transformation from the N-bound configuration structure (interactions of formaldehyde oxime via its nitrogen-end with proton from the acid catalyst) to the O-bound configuration structure (interactions of formaldehyde oxime via its oxygen-end with proton from acid catalyst). After that, the second step is the Beckmann rearrangement step (BR) which is the transformation from the oxime compound to the amide compound by the migration of the tran-alkyl group (or hydride group) at the carbon atom of the oxime compound concurrently with the releasing of the water molecule. Next, the water molecule is released and this reacts with the nitrilium cation to form the amide compound (eq 1).

The reaction mechanism on the embedded cluster model of Faujasite and ZSM-5 zeolites. In order to take into account the long range interactions of the extended zeolite lattice beyond the bare cluster models, the embedded cluster models of 10T H-ZSM-5 and 12T H-FAU zeolites are employed. Comparing the result between the cluster and the embedded cluster models, the Madelung potential has the effect of lengthening the O1-H1 bond distance (Brønsted acid site) by about 0.7 pm and shortening the adjacent Al-O bond which is in accordance with Gutmann's rules. In addition, the Mulliken population on the H1 atom is slightly increased from 0.38 to 0.41 due to the Madelung potential effect.

The results obtained from the embedded cluster models of both zeolites still provided the reaction mechanism as found in the bare cluster model. The optimized structures are slightly changed, but the influence from the Madelung potential has a significant effect on the energetic profile, especially in the

H-ZSM-5 zeolite. In the 1,2 H-shift step, influence from Madelung potential has the effect of stabilizing the adsorption complexes, especially in both of the adsorption complexes (N-bound and O-bound complexes). The adsorption energy of the N-bound complex (Figure 3(a)) is enhanced to -51.9 and -46.6 kcal/mol for on H-FAU and H-ZSM-5 zeolites, respectively. The optimized structures in both zeolites are still in the form of a protonated complex. While in the O-bound complex (Figure 3(c)), the adsorption energy is increased to -31.7 and -27.7 kcal/mol for H-FAU and H-ZSM-5 zeolites, respectively. But the optimized structures are turned into protonated structures at the oxygen-end of oxime compound. The energy barrier of the 1, 2 H-shift step (Figure 3(b)) is calculated to be 31.1 and 30.6 kcal/mol for the H-FAU and H-ZSM-5 zeolites, respectively. The transition state structures obtained from cluster and embedded cluster calculations are quite similar. The OI-HI distance of the embedded cluster is slightly changed by about 3 pm. The transition state of the embedding calculation is more stable than that of the bare cluster. The higher energy barrier compared to the energy barrier of the bare cluster model can be explained by the fact that the N-protonated complex is effectively stabilized by the long-range electrostatic potential from the zeolite framework.

In the last step of this reaction, rearrangement step (Figure 3(d)), the activation energy is slightly changed in the case of the H-FAU zeolite, but significantly changed in H-ZSM-5 zeolite. The activation energy derived from the embedded calculation of the H-ZSM-5 zeolite was decreased from 65.3 to 33.9 kcal/mol. The difference in activation energies of H-ZSM-5 and H-FAU zeolites may be due to the combination of topology of TS structure at acid site and pore size of zeolites. Due to the smaller pore size of ZSM-5 than that of FAU zeolite, the Madelung effect is stronger in ZSM-5 zeolite and its effect is to significantly stabilize the TS structure of ZSM-5.

From these results, the embedded cluster model provides the different results to those obtained from the bare cluster model. This indicates that the influences from the zeolite lattice have an important effect on both the reaction mechanism and the energetic profile. Moreover, the embedded technique can differentiate the types of zeolite, unlike the bare cluster model which is not able to make this differentiation.

#### Conclusion

The vapor phase Beckmann rearrangement of formaldehyde oxime over both types of zeolite, FAU and ZSM-5 zeolites, have been studied by both the bare cluster and the embedded cluster methods at the B3LYP/6-31G (d,p) level of theory. The N-protonated species was obtained in both the cluster and the embedded cluster methods and was similarly found in both FAU and ZSM-5 zeolites. Regarding the interaction of zeolite with the oxygen atom of oxime (O-oxime) molecules, the cluster models yielded only hydrogen bonded adducts, while the O-protonated species were only obtained with the embedded cluster model and was the same in both zeolites. The embedded results indicate that the N-protonation of oxime is preferable to the O-protonation.

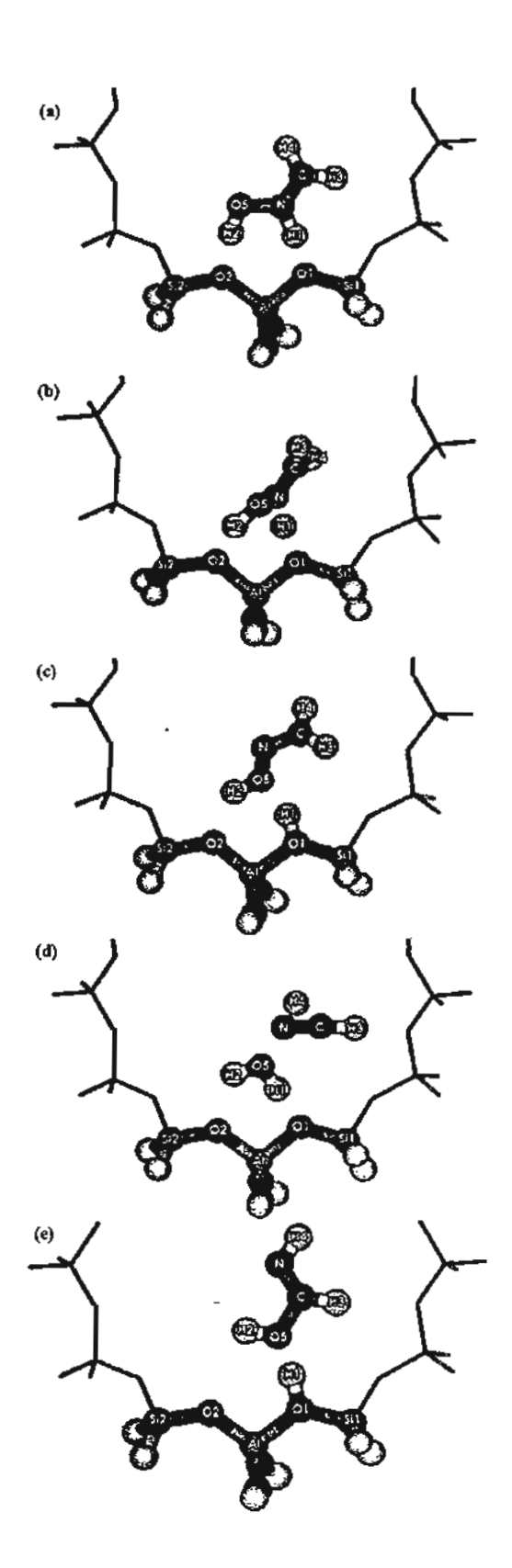


Figure 3. Presentation of the structure of each step in the Beckmann rearrangement on zeottic; (a) N-bound complex, (b) 1,2 H-shift TS, (c) O-bound complex (d) rearrangement of TS and (e) Arnide complex.

This study suggests that the initial structure of the Beckmann rearrangement reaction is not the O-protonation but the N-protonation of oxime. From the results of both types of zeolite, the energies barrier for the 1,2 H-shift connecting N, O protonated species is lower than that of the rearrangement step. Comparing the difference between the types of zeolite from the energetic profile, it is indicated that the H-ZSM5 zeolite is a better acid catalyst for the Beckmann rearrangement reaction of formaldehyde oxime than the H-FAU zeolite. Our finding may be good supporting evidence for the newly proposed mechanism for the cyclohexanone oxime interacting with zeolites and finding the suitable zeolite for this reaction. This indicates that inclusion of the effects of the zeolite crystal framework is crucial for obtaining the mechanistic aspect of the Beckmann rearrangement.

Acknowledgements. This work was supported in part by grants from the Thailand Research Fund (TRF Senior Research Scholar to JL.) and the Kasetsart University Research and Development Institute (KURDI), as well as the Ministry of University Affairs under the Science and Technology Higher Education Development Project (MUA-ADB funds). The support from the Dow Chemical Company (USA) is also acknowledged.

#### References

- (1) Beckmann, E. Chem. Ber. 1886, 89, 988.
- (2) Blatt, A.H. Chem. Rev. 1933, 12, 215.
- (3) Jones, B. Chem. Rev. 1944, 35, 335.
- (4) Heldt, W.Z. J. Org. Chem. 1961, 26, 1695.
- (5) Ungnade, H.E.; McLaren, A.D. J. Org. Chem. 1945, 10, 29.
- (6) Pearson, D.E.; Bruton, J.D. J. Org. Chem. 1954, 19, 957.
- (7) European Chemical News 1999, 18.
- (8) Takahashi, T.; Nishi, M.; Tagawa, Y.; Kai, T. Micropor. Mater. 1995. 3. 467.
- (9) Takahashi, T.; Ueno, K.; Kai, T. Micropor. Mater. 1993, 1, 323.
- (10) Heitmann, G.P.; Dahlhoff, G.; Hölderich, W.F. J. Catal. 1999, 186, 12.
- (11) Ichihashi, H.; Kitamura, M. Catal Today 2002, 73, 23.
- (12) Yashima, T.; Oka, N.; Komatsu, T. Catal Today 1997, 38, 249.
- (13) Kath, H.; Gläser, R.; Weitkamp, J. Chem. Eng. Technol. 2001, 24, 150.
- (14) Misona, M.; Inui, T. Catal. Today 1999, 51, 369.
- (15) Takahashi, T.; Nasution, M.N.A.; Kai, T. Appl. Catal. A: General 2001, 210, 339.
- (16) O'Sullivan, P.; Forni, L.; Hodnett, B. K. Ind. Eng. Chem. Res. 2001, 40, 1471.
- (17) Fois, G. A.; Ricchiardi, G.; Bordiga, S.; Busco, C.; Dalloro, L.; Spano, G.; Zecchina, A. Stud. Surf. Sci. Catal. 2001, 135, 2477.
- (18) Ichihashi, H.; Sato, H. Appl. Catal. A: General 2001, 221, 359.
- (19) Dai, L.X.; Iwaki, Y.; Koyama, K.; Tatsumi, T. Appl. Surf. Sci. 1997, 121-122, 335.
- (20) Dai, L.X.; Koyama, K.; Miyamoto, M.; Tatsumi, T. Appl. Catal. A: General 1999, 189, 237.
- (21) Rhee, H. K.; Chung, Y. M. J. Mol. Catal. A: Chemical 2000, 159, 389.
- (22) Rhee, H. K.; Chung, Y. M. J. Mol. Catal. A: Chemical 2001, 175, 249.
- (23) Hölderich, W.F. Catal. Today 2000, 62, 115.

- (24) Röseler, J.; Heitmann, G.; Hölderich, W. F. Appl. Catal. A: General 1996, 144, 319.
- (25) Heitmann, G.P.; Dahlhoff, G.; Neiderer, J.P.M.; Hölderich, W.F. J. Catal. 2000, 194, 122.
- (26) Hölderich, W. F.; Röseler, J.; Heitmann, G.P.; Liebens, A.T. Catal. Today 1997, 37, 353.
- (27) Dal Pozzo, L.; Fornasari, G.; Monti, T. Catal. Commun. 2002, 3, 369.
- (28) Paker Jr., W. O. Magn. Reson. Chem. 1999, 37, 433.
- (29) Komatsu, T.; Maeda, T.; Yashima, T. Micropor. Mesopor. Mater. 2000, 35-36, 173.
- (30) Ko, A. N.; Hung, C. C.; Chen, C. W.; Ouyang, K. H. Catal. Lett. 2001, 71, 219.
- (31) Chaudhari, K.; Bal, R.; Chandwadkar, A.J.; Sivasanker, S. J. Mol. Catal. A: Chemical 2000, 77, 247.
- (32) Shouro, D.; Ohya, Y.; Mishima, S.; Nakajima, T. Appl. Catal. A: General 2001, 214, 59.
- (33) Singh, P.S.; Bandyopadhyay, R.; Hegde, S.G.; Rao, B.S. Appl. Catal. A: General 1996, 136, 249.
- (34) Limtrakul, J.; Nanok, T.; Khongpracha, P.; Jungsuttiwong, S.; Truong, T. N. Chem. Phys. Letts. 2001, 349, 161.
- (35) Treesukol, P.; Limtrakul, J.; Truong, T. N. Phys. Chem. B 2001, 105, 2421.
- (36) Limtrakul, J.; Nokbin, S.; Chuichay, P. J. Mol. Struct. 2001, 560, 169.
- (37) Limtrakul, J.; Nokbin, S.; Jungsuttiwong, S.; Khongpracha, P.; Truong, T. N. Stud. Surf. Sci. Catal. 2001, 135, 2469.
- (38) Jungsuttiwong, S.; Nokbin, S.; Chuichay, P.; Khongpracha, P.; Truong, T. N.; Limtrakul, J. Stud. Surf. Sci. Catal. 2001, 135, 2518.
- (39) Limtrakul, J.; Khongpracha, P.; Jungsuttiwong, S. J. Mol. Struct. 2000, 525, 153.
- (40) Limtrakul, J.; Khongpracha, P.; Jungsuttiwong, S.; Truong, T. N. J. Mol. Catal. A: Chemical 2000, 153, 2469.
- (41) Nguyen, M. T.; Raspoet, G.; Vanquickenborne, L. G. J. Chem. Soc., Perkin Trans. 2 1995, 9, 1791.
- (42) Nguyen, M. T.; Raspoet, G.; Vanquickenborne, L. G. J. Am. Chem. Soc. 1997, 119, 2552.
- (43) Nguyen, M. T.; Raspoet, G.; Vanquickenborne, L. G. J. Chem. Soc., Perkin Trans. 2 1997, 4, 821.
- (44) Stefanovich, E. V.; Truong, T. N. J. Phys. Chem. B 1998, 102,
- (45) Vollmer, J. M.; Stefanovich, E. V.; Truong, T. N. J. Phys. Chem.
- B 1999, 103, 9415.
  (46) Ketrat, S.; Limtrakul, I. Int. J. Quan. Chem. 2003, 96(6), 333.
- (47) DungSrikaew, V.; Limtrakul, J.; Hermansson, K.; Probst, M. Int. J. Quan. Chem. 2004, in press.
- (48) Frisch, M. J.; Trucks, G. W.; Schlegel, H. B.; Scuseria, G. E.; Robb, M. A.; Cheeseman, J. R.; Zakrzewski, V. G.; Montgomery, J. A.; Stratmann, R. E. Jr.; Burant, J. C.; Dapprich, S.; Millam, J. M.; Daniels, A. D.; Kudin, K. N.; Strain, M. C.; Farkas, O.; Tomasi, J.; Barone, V.; Cossi, M.; Cammi, R.; Mennucci, B.; Pomelli, C.; Adamo, C.; Ctifford, S.; Ochterski, J.; Petersson, G. A.; Ayala, P. Y.; Cui, Q.; Morokuma, K.; Salvador, P.; Dannenberg, J. J.; Malick, D. K.; Rabuck, A. D.; Raghavachari, K.; Foresman, J. B.; Cioslowski, J.; Ortiz, J. V.; Baboul, A. G.; Stefanov, B. B.; Liu, G.; Liashenko, A.; Piskorz, P.; Komaromi, I.; Gomperts, R.; Martin, R. L.; Fox, D. J.; Keith, T.; Al-Laham, M. A.; Peng, C. Y.; Nanayakkara, A.; Chaltacombe, M.; Gill, P. M. W.; Johnson, B.; Chen, W.; Wong, M. W.; Andres, J. L.; Gonzalez, C.; Head-Gordon, M.; Replogle, E. S.; Pople, J. A. Gaussian 98; Gaussian, Inc.; Pittsburgh, PA, 2001.



Fuel Processing Technology 85 (2004) 1623-1634



www.elsevier.com/locate/fuproc

# Synthesis of ZSM-5 zeolite from lignite fly ash and rice husk ash

Metta Chareonpanich <sup>a,\*</sup>, Teerapong Namto <sup>a</sup>, Paisan Kongkachuichay <sup>a</sup>, Jumras Limtrakul <sup>b</sup>

<sup>a</sup>Department of Chemical Engineering, Kasetsart University, 50 Paholyothin Rd., Chatuchak,

Bangkok 10900, Thailand

bDepartment of Chemistry, Kasetsart University, Chatuchak, Bangkok 10900, Thailand

Accepted ! October 2003

#### Abstract

The lignite fly ash from the Mae-Moh power plant, Thailand, and rice husk ash were used as raw materials for ZSM-5 zeolite synthesis. Factors affecting the yield of ZSM-5 zeolite synthesized from fly ash, i.e., the SiO<sub>2</sub>/Al<sub>2</sub>O<sub>3</sub> mole ratio, the presence of tetrapropyl ammonium bromide (TPABr, the structure-directing material for ZSM-5 zeolite synthesis), the holding temperature and time, and the initial pressure were investigated. It was found that without TPABr only zeolite P could be synthesized at SiO<sub>2</sub>/Al<sub>2</sub>O<sub>3</sub> mole ratios of 2.8-200. In order to synthesize ZSM-5 zeolite, sodium silicate solution was added to adjust the SiO<sub>2</sub>/Al<sub>2</sub>O<sub>3</sub> mole ratio in raw ash. The yield of ZSM-5 zeolite was as high as 59 wt.% when following conditions were used: SiO<sub>2</sub>/Al<sub>2</sub>O<sub>3</sub> mole ratio, 40; the holding temperature, 210 °C; the holding time, 4 h and the initial pressure, 4 bar. The catalytic performance for CO<sub>2</sub> hydrogenation reaction of the ZSM-5 zeolite was preliminary tested and compared with that of commercial one. It was observed that there was no significant difference in the catalytic performance between these two catalysts.

© 2004 Elsevier B.V. All rights reserved.

Keywords: Fly ash; ZSM-5 zeolite; Rice husk ash; CO2 hydrogenation

# 1. Introduction

In Thailand, low quality lignite is found predominantly. Approximately 74% of coal produced are supplied to power station as energy source. The major problem in coal-fired power generation is that the plenty of solid waste so-called fly ash (of about 30% of raw

<sup>\*</sup> Corresponding author. Tel./fax: +662-579-2083. E-mail address: fengrate@ku.ac.th (M. Chareonpanich).

coal) is produced [1]. Previously, almost all the fly ash was disposed by landfill, which became increasingly expensive and caused an environmental problem. Therefore, fly ash utilization was considered by many investigators. Fly ash can be mainly used as building materials according to its pozzolanic properties [2-4]. However, due to the fluctuation of demand, the alternative utilization of fly ash as the raw material for zeolite synthesis was focused.

The synthesis of zeolites from fly ash can be classified into direct and non-direct synthesis. For the direct synthesis [5-13], fly ash was hydrothermally treated with an alkaline solution. At the temperature lower than 100 °C, zeolites P, X and Na-P1 were obtained with 2-4 M NaOH solution while hydroxy sodalite and zeolite Y were obtained with 4-10 M NaOH solution. At the temperature higher than 120 °C, zeolite Na-P1, hydroxy sodalite and analcime were obtained with 4-10 M NaOH solution.

For the non-direct synthesis [14,15], silica and alumina were firstly extracted from fly ash with hot alkaline solution and this resulted in the mixture of silicate and aluminate extracts. These extracts were used as the starting material for faujasite synthesis at as low a temperature as 60-90 °C and at a synthesis period of 2-5 days.

In this work, the direct synthesis of ZSM-5 zeolite using the Mae-Moh lignite fly ash as the main raw material was focused. However, the SiO<sub>2</sub>/Al<sub>2</sub>O<sub>3</sub> mole ratio in the raw fly ash is too low to synthesize ZSM-5 zeolite (SiO<sub>2</sub>/Al<sub>2</sub>O<sub>3</sub> mole ratio=2.8). In order to obtain the appropriate SiO<sub>2</sub>/Al<sub>2</sub>O<sub>3</sub> mole ratio, the sodium silicate solution was added to adjust the mole ratio of raw fly ash. From the economic point of view, the sodium silicate solution prepared from rice husk ash was used instead of the commercial ones because there is an abundant supply of rice husk in Thailand. The factors affecting the ZSM-5 zeolite yield, i.e., SiO<sub>2</sub>/Al<sub>2</sub>O<sub>3</sub> mole ratio, the presence of tetrapropyl ammonium bromide, temperature and initial pressure were investigated. In all cases, the most suitable condition that gave the maximum yield of ZSM-5 zeolite was focused.

# 2. Experimental

#### 2.1. Raw feed and reagents

Lignite fly ash obtained from the Mae-Moh electric power station, Thailand, was ground and sieved to the diameter of lower than 0.074 mm. The sample was dried at 105 °C for 1 h and kept in the desiccator before use. Chemical compositions of fly ash were examined by X-ray Fluorescence Spectroscopy (XRF: Philips, PW 1400). Physical characteristics were analyzed by X-ray Diffraction Spectroscopy (XRD: Philips, PW 1830/40, Cu-α radiation) and BET surface area analysis (Quantachrome, NOVA 1200).

Sodium silicate solution (Na<sub>2</sub>Si<sub>3</sub>O<sub>7</sub>: 4 wt.% NaOH; 27 wt.% SiO<sub>2</sub>) was used to adjust the SiO<sub>2</sub>/Al<sub>2</sub>O<sub>3</sub> ratio of fly ash mixture. First, rice husk was treated with 1 M HCl for 2.5 h. The treated rice husk was washed thoroughly with distilled water, dried at 120 °C and pyrolyzed in oxygen atmosphere at 600 °C for 1 h. The residual ash with about 99.6 wt.% silica was dissolved in NaOH solution to obtain a desired composition of sodium silicate solution.

Tetrapropyl ammonium bromide (TPABr; C<sub>12</sub>H<sub>28</sub>BrN) of 98% purity from Fluka Chemicals was used as a structure-directing substance for ZSM-5 zeolite preparation.

# 2.2. Synthesis of ZSM-5 zeolite from lignite fly ash

Batch experiments were carried out to determine effects of the SiO<sub>2</sub>/Al<sub>2</sub>O<sub>3</sub> mole ratio, the presence of TPABr, the temperature and the initial pressure on the yield of crystalline ZSM-5 zeolite. The characteristics of products were determined by XRD and Scanning Electron Microscopy (SEM: Jeol, JSM-5600 LV). The yield of ZSM-5 zeolite was obtained by converting the peak intensity of ZSM-5 zeolite from XRD analysis to weight of zeolite using of standard curved. The product yield was reported as wt.% of pure ZSM-5 zeolite in the solid product.

# 2.2.1. Effect of SiO<sub>2</sub>/Al<sub>2</sub>O<sub>3</sub> mole ratio and the presence of TPABr

In this series of experiments, 3 g of lignite fly ash was mixed with 50 cm<sup>3</sup> of 0.001 M NaOH solution and variable amounts of sodium silicate solution. The average SiO<sub>2</sub>/Al<sub>2</sub>O<sub>3</sub> mole ratio in raw fly ash was about 2.8 (data from XRF). Subsequently, the SiO<sub>2</sub>/Al<sub>2</sub>O<sub>3</sub> mole ratios were adjusted to 20, 40, 60, 80, 100 and 200 by adding the sodium silicate solution into the fly ash mixture. The TPABr (0.37 g, 20 mol% of alumina in fly ash) was added to the mixture. The 0.5 M H<sub>2</sub>SO<sub>4</sub> solution was used to adjust the pH of the mixture (fixed at 11±0.2). With fast synthesis process, the mixture was placed in the autoclave, pressurized at 3 bar by using nitrogen gas (99.99% purity) and then heated up from room temperature to 210 °C within 2 h. During this period, the pressure in the autoclave was autogeneously increased. The temperature was kept constant here for 2 h. By using this process, ZSM-5 zeolite can be synthesized in 4 h. The crude product was then separated from the solution, washed thoroughly with distilled water and dried in the oven at 110 °C for 2.5 h before analysis.

The experimental conditions in Sections 2.2.2 and 2.2.3 were the same as that of Section 2.2.1 unless otherwise indicated.

# 2.2.2. Effect of temperature

The effect of reaction temperature was examined using the same experimental conditions as those of Section 2.2.1 except the temperature and the holding time. The mixture was heated up from room temperature to 150, 180 and 210 °C with the heating rate of 1.5 °C/min and held there for 2 h. For the study of the effect of the holding time, the synthesis temperature was fixed at 210 °C and the holding time was varied from 0 to 4.0 h.

# 2.2.3. Effect of initial pressure

The optimum SiO<sub>2</sub>/Al<sub>2</sub>O<sub>3</sub> mole ratio and temperature determined in Sections 2.2.1 and 2.2.2 were used, and the initial pressures were varied from 1 to 6 bar. The detail of all experimental conditions is shown in Table 1.

# 2.3. Catalytic performance of ZSM-5 zeolite from fly ash

The catalytic performance of ZSM-5 zeolite synthesized from fly ash was examined in the hydrogenation reaction of carbon dioxide. The experiment was conducted in a catalytic packed bed reactor, made of SUS-316 (id. 7.6 mm). The reactor was 500 mm long, equipped with an infrared furnace. The ZSM-5 zeolite product (powder, 59 wt.% purity)

Table 1
Details of experimental conditions

Series of experiment	SiO <sub>2</sub> /Al <sub>2</sub> O <sub>3</sub> mole ratio <sup>6</sup>	Holding temperature (°C) <sup>b</sup>	Holding period (h) <sup>b</sup>	Initial pressure (bar)
Effect of SiO <sub>2</sub> /Al <sub>2</sub> O <sub>3</sub> mole ratio (2.2.1)	2.8, 20, 40, 60, 80, 100, 200	210	2	3
Effect of holding temperature (2.2.2)	Α .	150, 180, 210	2	3
Effect of holding period (2.2.2)	Α	В	0, 1, 2, 3, 4	3
Effect of initial pressure (2.2.3)	A	В	С	1, 2, 3, 4, 5, 6

In all experiment; 3 g of fly ash, 50 cm<sup>3</sup> of 0.001 M NaOH solution and the heating rate of 1.5 °C/min were used.

was packed in the isothermal zone of the reactor (bed length, 4 cm). The reactor was first flushed with  $N_2$  (purity>99%) and heated to reaction temperatures (200-500 °C). Reactant gases (CO<sub>2</sub> and H<sub>2</sub>) were allowed to flow at 50 ml (NTP)/min and the GHSV was approximately 16 h<sup>-1</sup>. The mole ratio of CO<sub>2</sub> to H<sub>2</sub> was 1:3 and the operating pressure was fixed at 5 bar. The amounts of CO<sub>2</sub>, CO and all hydrocarbon products were quantitatively analyzed using gas chromatography (Hewlett Packard 5890 series II) equipped with TCD and FID detectors and Porapack Q columns. The experiment was repeated three to five times in each condition.

# 3. Results and discussion

# 3.1. Chemical compositions of fly ash

The chemical compositions of fly ash analyzed by XRF are shown in Table 2, in which SiO<sub>2</sub>, Al<sub>2</sub>O<sub>3</sub>, Fe<sub>2</sub>O<sub>3</sub> and CaO are the major components. The X-ray diffraction pattern in

Table 2
The chemical composition of fly ash analyzed by XRF

Composition	Amount (wt.%)
SiO <sub>2</sub>	39.60
$Al_2O_3$ .	24,25
Fe <sub>2</sub> O <sub>3</sub>	12.60
CaO	10.66
MgO	2.80
Na <sub>2</sub> O	1.29
TiO <sub>2</sub>	0.49
P2O5	0.16
Others	8.15

<sup>&</sup>lt;sup>b</sup> A, B, and C were optimum synthesis conditions obtained from experimental Sections 2.2.1 and 2.2.2, respectively.

Fig. 1 revealed the major solid compositions in the fly ash was amorphous in nature. The BET surface area of fly ash was 5 m<sup>2</sup>/g.

# 3.2. Synthesis of ZSM-5 zeolite from lignite fly ash

# 3.2.1. Effect of SiO<sub>2</sub>/Al<sub>2</sub>O<sub>3</sub> mole ratio and the presence of TPABr

Without addition of sodium silicate solution, the  $SiO_2/Al_2O_3$  mole ratio in fly ash is 2.8. In order to obtain  $SiO_2/Al_2O_3$  mole ratios of 20, 40, 60, 80, 100 and 200, lignite fly ash was mixed with 27.4, 59.1, 90.9, 122.6, 154.4 and 313.2 cm<sup>3</sup> of sodium silicate solution, respectively. To dissolve the silica and alumina in fly ash, NaOH solution was added to the mixture while the pH of the mixture was controlled at  $11\pm0.2$ . It was found that without TPABr, at the  $SiO_2/Al_2O_3$  mole ratios of 2.8-200, only zeolite P could be synthesized. The XRD pattern of the zeolite P and amorphous solid products are shown in Fig. 2.

The effects of  $SiO_2/Al_2O_3$  mole ratio (in the range of 2.8–200) and the presence of TPABr on the yield of ZSM-5 zeolite were investigated. The yields of ZSM-5 zeolite obtained from XRD patterns are shown in Fig. 3. The results reveal that without sodium silicate solution, the ZSM-5 zeolite could not be synthesized. It is clear that the  $SiO_2/Al_2O_3$  mole ratio of 2.8 is not suitable for ZSM-5 zeolite synthesis. At the  $SiO_2/Al_2O_3$  mole ratio of 20–100, ZSM-5 zeolite can be synthesized. The maximum yield of 43 wt.% was found at the  $SiO_2/Al_2O_3$  mole ratio of 40.

The SEM photographs of the zeolitic products of various  $SiO_2/Al_2O_3$  mole ratios are shown in Fig. 4. The obtained ZSM-5 zeolite is mainly cubic crystals, accompanying with some flake-like structure. As the  $SiO_2/Al_2O_3$  mole ratio increases from 20 to 40, the cubic crystals of ZSM-5 zeolite are increased in size from 5 to 8  $\mu$ m. However, the opposite trend was observed when the  $SiO_2/Al_2O_3$  mole ratio is higher than 40. The smallest size of about 1  $\mu$ m was found at the  $SiO_2/Al_2O_3$  mole ratio of 100.

From this study, it was noticed that the fast synthesis process without TPABr, even if SiO<sub>2</sub>/Al<sub>2</sub>O<sub>3</sub> mole ratio was varied, could not produce ZSM-5 zeolite from lignite fly ash.

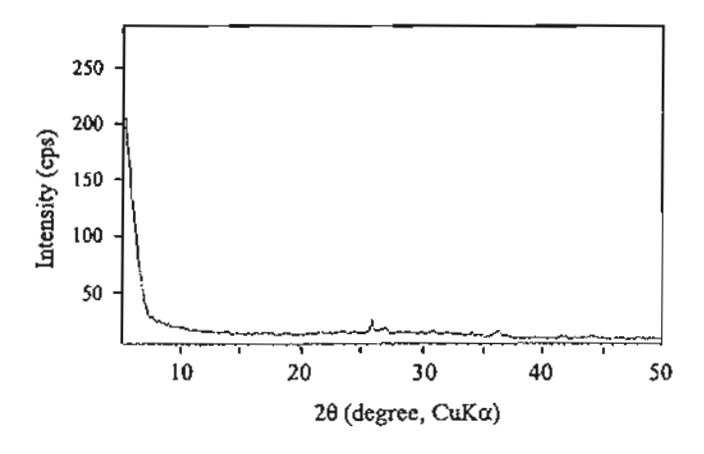


Fig. 1. XRD pattern of Mae-Moh lignite fly ash.

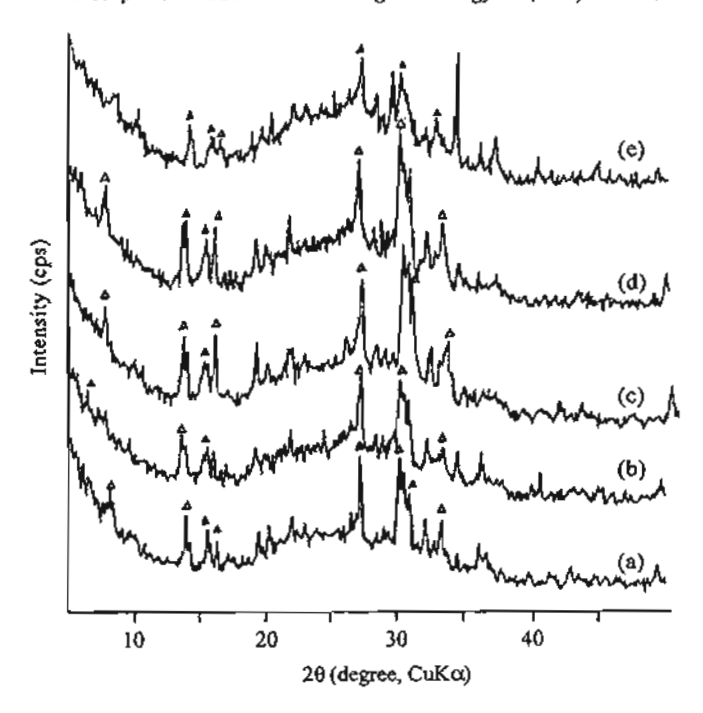


Fig. 2. XRD patterns of zeolitic products obtained from synthesis experiments without the presence of TPABr at  $SiO_2/Al_2O_3$  mole ratios of (a) 20, (b) 40, (c) 60, (d) 80, and (e) 100 ( $\Delta$ , Zeolite P; Initial pressure: 3 bar, holding temperature: 210 °C, holding period: 2 h).

In addition, irrespective of the SiO<sub>2</sub>/Al<sub>2</sub>O<sub>3</sub> mole ratio, the addition of TPABr of approximately 20 mol% of alumina in fly ash still could not promote the ZSM-5 zeolite formation.

Since the maximum yield of the ZSM-5 zeolite was obtained at a SiO<sub>2</sub>/Al<sub>2</sub>O<sub>3</sub> mole ratio of 40, this mole ratio was then used in the following experiments.

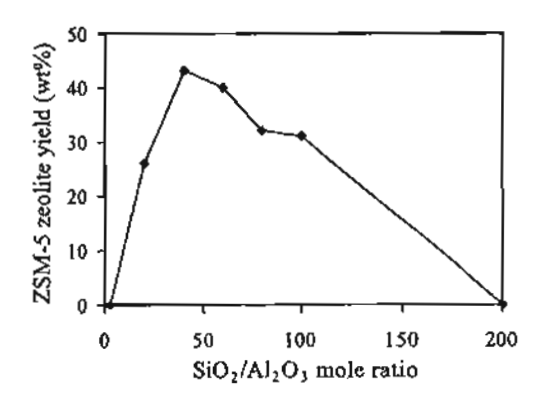


Fig. 3. Yields of ZSM-5 zeolite obtained from various SiO<sub>2</sub>/Al<sub>2</sub>O<sub>3</sub> mole ratios with TPABr (Initial pressure: 3 bar, holding temperature: 210 °C, holding period: 2 b).

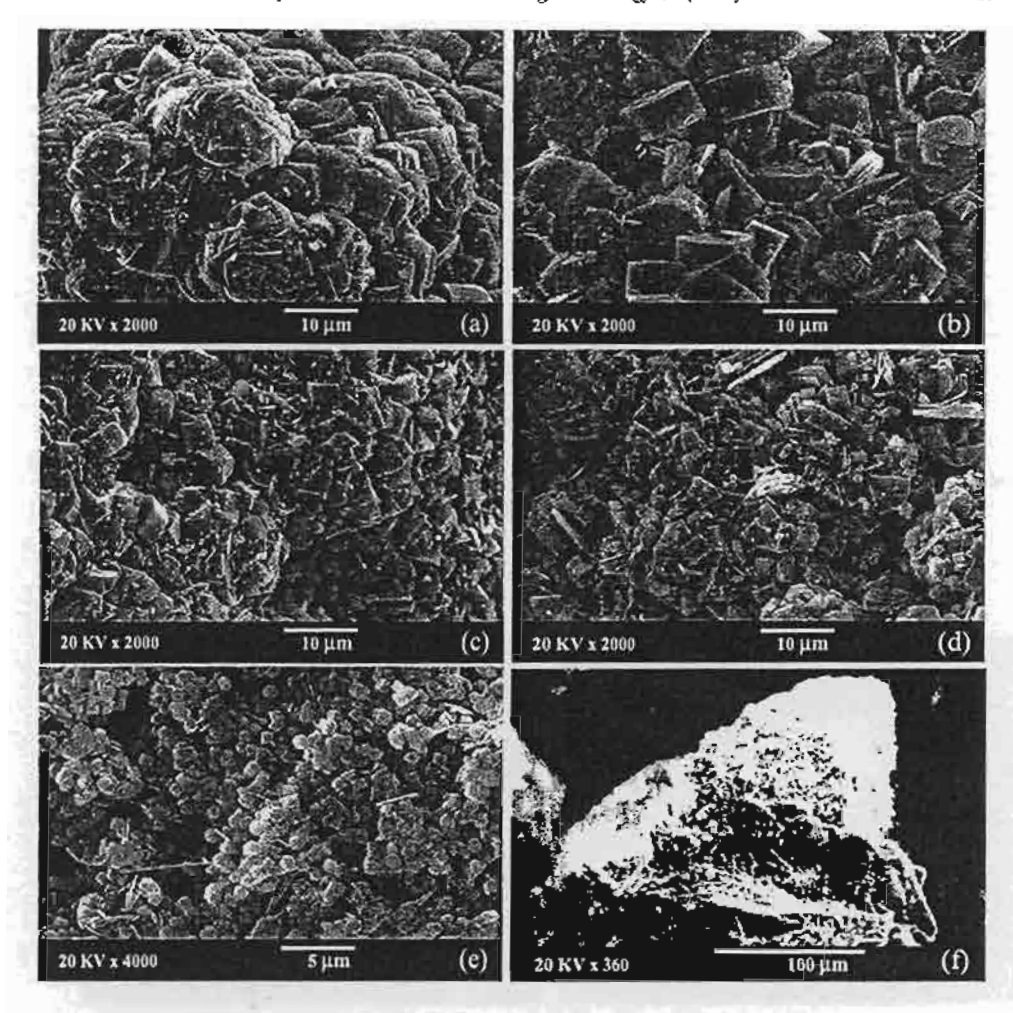


Fig. 4. SEM photographs of treated products obtained from SiO<sub>2</sub>/Al<sub>2</sub>O<sub>3</sub> mole ratios of (a) 20, (b) 40, (c) 60, (d) 80, (e) 100, and (f) 200 with TPABr (a-e=ZSM-5 zeolite, f-amorphous product; Initial pressure: 3 bar, holding temperature: 210 °C, holding period: 2 h).

# 3.2.2. Effect of temperature

The yields of the ZSM-5 zeolite obtained at temperatures ranging from 150 to 240 °C are shown in Fig. 5 and the SEM photographs of the products at 150 and 180 °C are shown in Fig. 6. At the temperature of 150 °C, the unknown amorphous solids of irregular shape and crystalline were found. It was noticed that the ZSM-5 zeolite could not be produced under this low temperature. The XRD pattern of the product obtained at 180 °C is shown in Fig. 7, which revealed that ZSM-5 zeolite (16 wt.%) and zeolite P were formed. At 210 °C, only ZSM-5 zeolite was found (43 wt.%). In accordance with the XRD result, the SEM photograph of the product at 180 °C indicates the presence of the cubic crystals of ZSM-5 zeolite and the needle-like crystals of zeolite P, while only the cubic

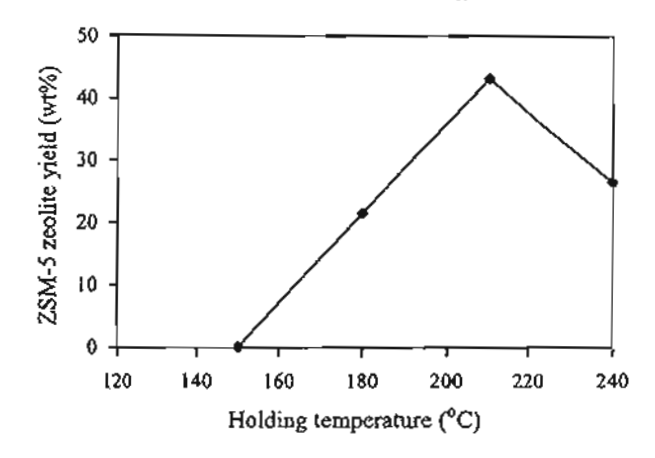


Fig. 5. Yields of ZSM-5 zeolite obtained from various holding temperatures (SiO<sub>2</sub>/Al<sub>2</sub>O<sub>3</sub> mole ratio: 40, initial pressure: 3 bar, holding period: 2 h).

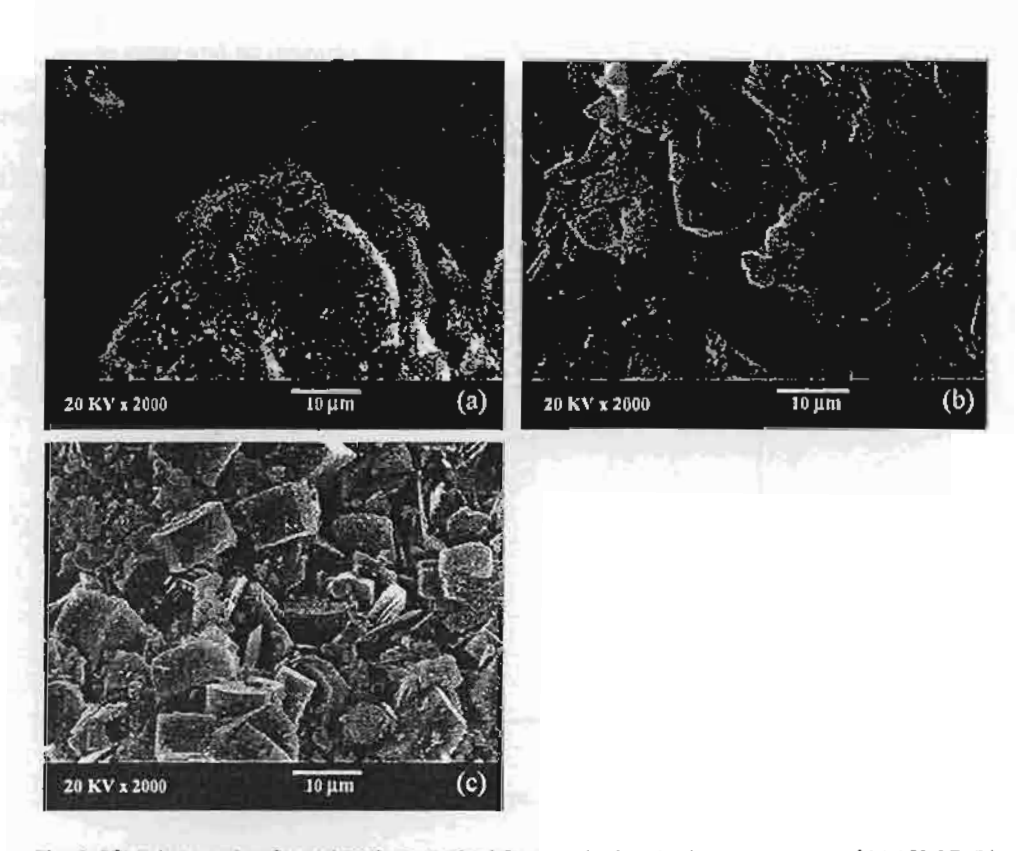


Fig. 6. SEM photographs of treated products obtained from synthesis at holding temperatures of (a) 150 °C, (b) 180 °C, and (c) 210 °C (SiO<sub>2</sub>/Al<sub>2</sub>O<sub>3</sub> mole ratio: 40, initial pressure: 3 bar, holding period: 2 h).

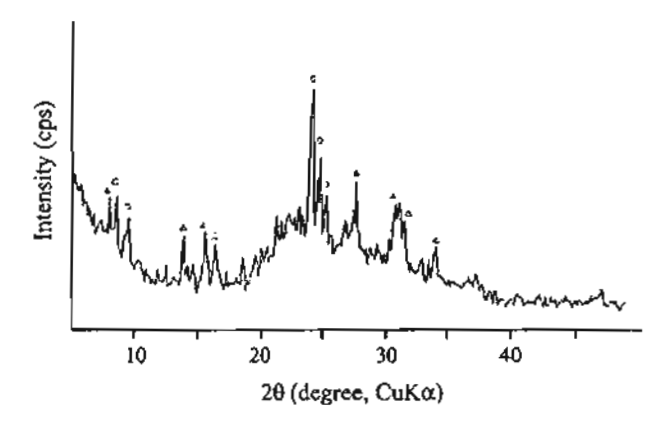


Fig. 7. XRD pattern of zeolitic products obtained from synthesis temperature of 180 °C (O=ZSM-5 zeolite,  $\Delta$ =Zeolite P) (SiO<sub>2</sub>/Al<sub>2</sub>O<sub>3</sub> mole ratio: 40, initial pressure: 3 bar, holding period: 2 h).

crystals of the ZSM-5 zeolite were found at 210 °C. The reason is that the formation of metastable phases of zeolites depend on temperature, and then the most stable phase will continue to grow and be detected finally [16]. Not only the temperature, but the holding time and the initial pressure also play an important role on the formation of the specific metastable phase of zeolite.

For the study on the effect of the holding time, the synthesis temperature was fixed at 210°C and the holding time was varied at 0, 1, 2, 3 and 4 h. The yields of the product crystals shown in Fig. 8 notify that the longer the holding time, the greater the yield of ZSM-5 crystalline zeolite. As the holding time increased, the alkaline solution could more thoroughly dissolve silica and alumina from the fly ash. These silica and alumina in the alkaline solution are the sources of precursors for ZSM-5 zeolite formation and growth.

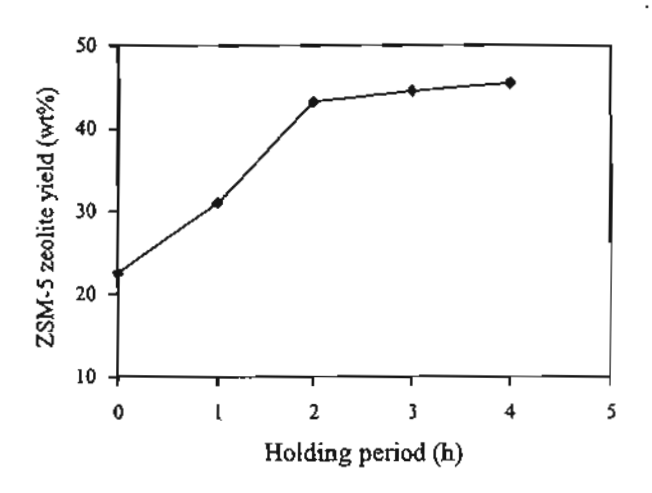


Fig. 8. Yields of ZSM-5 zeolite obtained from various holding periods (SiO<sub>2</sub>/Al<sub>2</sub>O<sub>3</sub> mole ratio: 40, initial pressure: 3 bar, holding temperature: 210 °C).

Therefore, the longer holding time used (in this study, 4 h) the higher yield of ZSM-5 zeolite could be obtained.

# 3.2.3. Effect of initial pressure

The effect of the initial pressure of inert gas on the yield of ZSM-5 zeolite was determined in the range of 1-6 bar. The yields of the ZSM-5 zeolite obtained at various initial pressures are shown in Fig. 9. It should be noted that all the XRD patterns of the products confirm the existence of only ZSM-5 zeolite. The ZSM-5 zeolite yields are gradually increased with the increase of initial pressure up to 4 bar (13 wt.% at 1 bar and 43 wt.% at 4 bar) and then decreased (31 wt.% at 5 bar and 26 wt.% at 6 bar). The initial pressure has a significant effect on the ZSM-5 zeolite synthesis. This is because the synthesis process takes place at high temperature under steam saturation condition. The increase of the initial pressure thermodynamically enhances the solubility of silica and alumina in fly ash in the alkaline solution and consequently the rate of formation of the ZSM-5 zeolite. However, at the initial pressure above 4 bar, the yield of ZSM-5 zeolite tends to decrease. This may be due to the competitive formation of different metastable phases of zeolite during the crystalline formation stage, which resulted in the formation of different phases of zeolite [16].

# 3.3. Hydrogenation of carbon dioxide over ZSM-5 zeolite from fly ash

The catalytic performance of ZSM-5 zeolite synthesized here was preliminary tested and compared with a commercial ZSM-5 zeolite (SiO<sub>2</sub>/Al<sub>2</sub>O<sub>3</sub> ratio, 40; surface area, 670 m<sup>2</sup>/g). The average results are shown in Table 3. With both catalysts, CO<sub>2</sub> conversions are gradually increased with the increase of reaction temperature (from 2-3 mol% at 200 °C to 28-30 mol% at 500 °C). In order to investigate the effect of thermal reaction, the reaction was tested under the same operating condition with an inert sand bed. It was

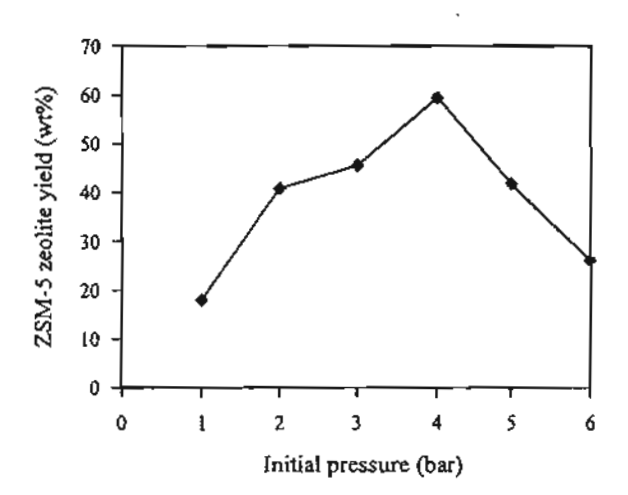


Fig. 9. Yields of ZSM-5 zeolite obtained from various initial pressures (SiO<sub>2</sub>/Al<sub>2</sub>O<sub>3</sub> mole ratio: 40, holding temperature: 210 °C, holding period: 4 h).

Table 3
Product distribution obtained from the reaction of CO<sub>2</sub> and H<sub>2</sub> over commercial ZSM-5 zeolite and ZSM-5 zeolite synthesized from fly ash and rice husk ash (in mol%)

Temperature	Commercial ZSM-5 zeolite				Synthesized ZSM-5 zeolite			
(°C)	COz	Product distribution			CO2	Product distribution		
	conversion	co	CH₄	C2-C3	conversion	со	CH₄	C2-C3
200	2	6	87	7	3	7	83	10
300	16	5	83	12	15	17	73	11
400	18	5	84	11	24	10	71	19
500	28	10	78	12	30	17	64	19

found that the conversion of CO<sub>2</sub> over the sand bed at 500 °C was lower than 5 % and methane was the major product.

The CO<sub>2</sub> conversion of the synthesized ZSM-5 zeolite and the commercial one were comparable. The products were mainly CO, methane and ethane. However, higher yields of C2-C3 were obtained with the synthesized ZSM-5 zeolite. At 500 °C, the C2-C3/CH<sub>4</sub> ratios were 0.3 with the synthesized ZSM-5 zeolite and 0.15 with the commercial one. It was suggested that metal oxide impurities remained in the synthesized ZSM-5 zeolite seem to have a little effect on the catalytic hydrogenation reaction.

#### 4. Conclusions

The alternative utilization of Mae-Moh lignite fly ash and rice husk ash as raw materials for ZSM-5 zeolite synthesis is feasible. The effects of SiO<sub>2</sub>/Al<sub>2</sub>O<sub>3</sub> mole ratio, the presence of TPABr, temperature and initial pressure on the yield of ZSM-5 zeolite have been investigated using the fast synthesis process (about 2-6 h). Without the addition of sodium silicate solution, ZSM-5 zeolite could not be synthesized. With the presence of TPABr, ZSM-5 zeolite could be synthesized in a range of the SiO<sub>2</sub>/Al<sub>2</sub>O<sub>3</sub> mole ratio of 20-100. At a holding temperature of lower than 210 °C, several types of zeolites were produced. The maximum yield of ZSM-5 zeolite, 59 wt.%, was obtained at a SiO<sub>2</sub>/Al<sub>2</sub>O<sub>3</sub> mole ratio of 40, synthesis temperature of 210 °C, holding time of 4 h and initial pressure of 4 bar.

The catalytic performance of ZSM-5 zeolite synthesized from fly ash in the hydrogenation of CO<sub>2</sub> is remarkable. The conversion of CO<sub>2</sub> was 30 mol% at 500 °C and the products were carbon monoxide, methane, ethane and propane. With ZSM-5 zeolite synthesized from fly ash, higher yield of C2-C3 was produced when compared with the commercial one.

# Acknowledgements

The Kasetsart University Research and Development Institute (KURDI) and the Senior Research Scholar Fund from Thailand Research Fund (TRF) have financially supported this research. Lignite fly ash sample was supplied by the Electricity Generating Authority of Thailand (EGAT).

#### References

- [1] V.I. Kouprianov, Fuel Process. Technol. 76 (2002) 187.
- [2] J. Majling, D.M. Roy, Am. Ceram. Soc. Bull. 72 (1993) 77.
- [3] B.E. Scheetz, R. Earle, Solid State Mater. Sci. 3 (1998) 510.
- [4] L.D. Chen, Y. Shen, J. Su, X. Wu, Cem. Concr. Res. 30 (2000) 881.
- [5] C.F. Lin, H.C. Hsi, Environ. Sci. Technol. 29 (1995) 1109.
- [6] C. Amrhein, G.H. Haghnia, T.S. Kim, P.A. Mosher, R.C. Gagajena, T. Amanios, L. Torre, Environ. Sci. Technol. 30 (1996) 735.
- [7] V. Berkgaut, A. Singer, Appl. Clay Sci. 10 (1996) 369.
- [8] E.L. Salinas, P. Salas, I. Schifter, M. Moran, S. Castillo, E. Mogica, Progress in zeolite and microporous materials, Stud. Surf. Sci. Catal. 105 (1997) 1565.
- [9] X. Querol, A. Alastuey, A. López-Soler, F. Plana, Environ. Sci. Technol. 31 (1997) 2527.
- [10] G. Steenbruggen, G.G. Hollman, J. Geochem. Explor. 62 (1998) 305.
- [11] A. Srinivasan, M.W. Grutzeck, Environ. Sci. Technol. 33 (1999) 1464.
- [12] X. Querol, J.C. Umana, F. Plana, A. Alastuey, A. Lopez-Soler, A. Medinaceli, A. Valero, M.J. Domingo, E. Garcia-Rojo, Fuel 80 (2001) 857.
- [13] X.S. Zhao, G.Q. Lu, H.Y. Zhu, J. Porous Mater, 4 (1997) 245.
- [14] H.L. Chang, W.H. Shih, Ind. Eng. Chem. Res. 37 (1998) 71.
- [15] G.G. Hollman, G. Steenbruggen, M.J. Janssen, Fuel 78 (1999) 1225.
- [16] D.W. Break, Zeolite Molecular Sieves: Structure, Chemistry and Use, Wiley, 1974.

# Partial cross sections for positive and negative ion formation following electron impact on uracil

S Feil<sup>1</sup>, K Gluch<sup>1,3</sup>, S Matt-Leubner<sup>1</sup>, P Scheier<sup>1</sup>, J Limtrakul<sup>1,4</sup>, M Probst<sup>1</sup>, H Deutsch<sup>1,5</sup>, K Becker<sup>1,6</sup>, A Stamatovic<sup>1,7</sup> and T D Märk<sup>1,2</sup>

E-mail: kbecker@stevens.edu

Received 4 May 2004 Published 20 July 2004 Online at stacks.iop.org/JPhysB/37/3013 doi:10.1088/0953-4075/37/15/001

#### Abstract

We report absolute partial cross sections for the formation of selected positive and negative ions resulting from electron interactions with uracil. Absolute calibration of the measured partial cross sections for the formation of the three most intense positive ions, the parent C<sub>4</sub>H<sub>4</sub>N<sub>2</sub>O<sub>2</sub><sup>+</sup> ion and the C<sub>3</sub>H<sub>3</sub>NO<sup>+</sup> and OCN+ fragment ions, was achieved by normalization of the total single uracil ionization cross section (obtained as the sum of all measured partial single ionization cross sections) to a calculated cross section based on the semi-classical Deutsch-Märk formalism at 100 eV. Subsequently, we used the OCN\* cross section in conjunction with the known sensitivity ratio for positive and negative ion detection in our apparatus (obtained from the well-known cross sections for SF<sub>4</sub> and SF<sub>4</sub> formation from SF<sub>6</sub>) to determine the dissociative attachment cross section for OCN- formation from uracil. This cross section was found to be roughly an order of magnitude smaller, about  $5 \times 10^{-22}$  m<sup>2</sup> at 6.5 eV, compared to our previously reported preliminary value. We attribute this discrepancy to the difficult determination of the uracil target density in the earlier work. Using a reliably calculated cross section for normalization purposes avoids this complication.

<sup>&</sup>lt;sup>1</sup> Institut für Ionenphysik, Leopold-Franzens Universität, A-6020 Innsbruck, Austria

Department of Plasma Physics, Comenius University, SK-84248 Bratislava, Slovakia

<sup>&</sup>lt;sup>3</sup> Permanent address: Institute of Mathematics, Physics and Informatics, Maria Curie-Sklodowska University, Lublin 20-031, Poland.

Permanent address: Department of Chemistry, Kasetsart University, Bangkok 10900, Thailand.

Permanent address: Institut f
ür Physik, Universit
ät Greifswald, D-17487 Greifswald, Germany.

<sup>&</sup>lt;sup>6</sup> Permanent address: Department of Physics and Center for Environmental Systems, Stevens Institute of Technology, Hoboken, NJ 07030, USA.

Permanent address: Faculty of Physics, University Beograd, PO Box 638, Yu-11001 Beograd, Serbia.

3014 S Feil et al

#### 1. Introduction

Recently, electron interactions with biologically important molecules such as amino acids and nucleotides, in particular (dissociative) electron attachment studies, have gained prominence following the pioneering work of Sanche and co-workers [1]. Electron scattering experiments with complex biomolecules in the gas phase are challenging because of the difficulties in the preparation of well-characterized pure gas targets of these molecules and the difficulties in the subsequent quantitative determination of the target densities. The RNA base uracil (see figure 1 for a schematic molecular structure diagram) and various halo-uracil compounds as well as DNA bases such as thymine, cytosine, adenine, various halo-uracil compounds and simple organic acids such as formic and acetic acid and several amino acids (glycine, deoxyribose) have been studied successfully in gas-phase electron scattering experiments [2-17]. Very recently [2], our group measured the first absolute electron attachment cross sections for the RNA base uracil ( $C_4H_4N_2O_2$ ) and reported peak values ranging from 1 to  $30 \times 10^{-21}$  m<sup>2</sup> for four fragment anions, CN<sup>-</sup>, OCN<sup>-</sup>, C<sub>3</sub>H<sub>2</sub>NO<sup>-</sup> and C<sub>4</sub>H<sub>3</sub>N<sub>2</sub>O<sub>2</sub><sup>-</sup>, at electron energies below 10 eV. The importance of anion formation via dissociative electron attachment in these molecules stems from the fact that it is the only mechanism that can cause bond cleavage at very low electron energies, which are typical for (nearly) thermalized secondary electrons produced by the interaction of high-energy radiation with the complex environments surrounding and constituting living cells. However, it has also been pointed out [10, 15, 18] that positive ion formation induced by electron impact on uracil and halo-uracil compounds is an important fragmentation mechanism for these molecules, particularly for low electron energies just above the ionization threshold.

In this paper, we report the first absolute partial and total cross sections for the electronimpact ionization of uracil. Absolute cross sections were obtained by normalizing the total
single ionization cross section of uracil (at an electron energy of 100 eV) to a calculated
total single ionization cross section using the semi-classical Deutsch-Märk (DM) formalism
[19, 20]. The DM formalism has been shown to yield reliable total single ionization cross
sections (with an accuracy ranging between 5% and 20%) for a large number of molecules,
including complex molecules [19, 21-23]. On the basis of the absolute calibration process for
positive ions in conjunction with a sensitivity ratio measurement for positive-to-negative ion
formation in our apparatus, we also revise our earlier absolute cross section for dissociative
attachment to uracil [2] downward by about an order of magnitude. We attribute this
discrepancy to difficulties in the accurate target number density determination in the earlier
experiment.

# 2. Experimental procedure and cross section normalization

The current experiments were carried out in our well-characterized double-focusing two-sector field mass spectrometer of reversed geometry described in numerous earlier publications (see, e.g., [24–26]), to which we refer the reader for further experimental details. Figure 2 shows a mass spectrum of positive ions produced by 120 eV electrons on uracil. The most intense peak at a mass-to-charge (m/z) ratio of 112 corresponds to the parent uracil  $C_4H_4N_2O_2^*$  ion (m/z=112 Thomson). Two other groups of peaks are seen around the two most abundant fragment ions,  $C_3H_3NO^+$  (m/z=69 Thomson), with adjacent weaker peaks corresponding to the loss of additional H atoms, and  $OCN^+$  (m/z=42 Thomson). The additional weaker peaks around m/z=40 correspond to ions with two carbon atoms, one nitrogen or oxygen atom and from 0-3 hydrogen atoms. We recorded relative partial ionization cross sections for the three most intense mass-selected ions in the mass spectrum

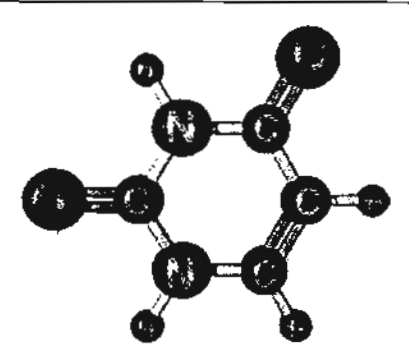


Figure 1. Schematic structure diagram of the tracil C4H4N2O2 molecule,

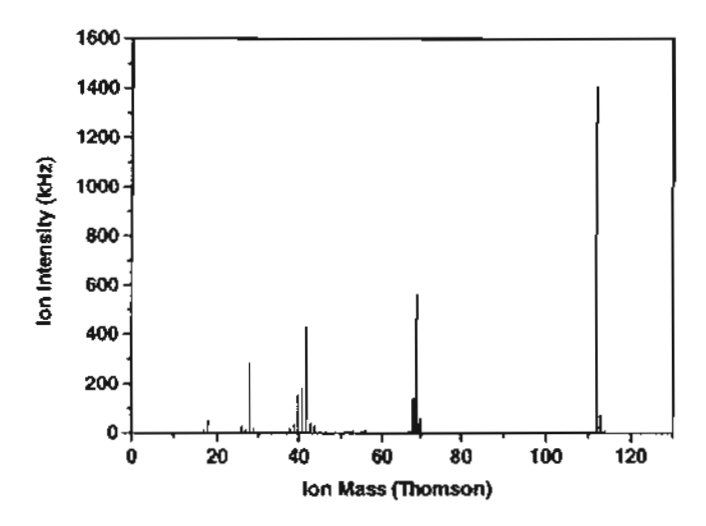


Figure 2. Mass spectrum of positive ions formed by 120 eV electron impact on uracil. The most intense peaks correspond to the parent C<sub>4</sub>H<sub>4</sub>N<sub>2</sub>O<sub>2</sub><sup>\*</sup> ion and two fragment ions C<sub>3</sub>H<sub>3</sub>NO<sup>\*</sup> and OCN<sup>\*</sup>.

shown in figure 2 for electron energies from threshold to 1000 eV. The sum of all partial ionization cross sections for the formation of singly charged product ions yields the relative total single uracil ionization cross section. We note that we did not find ion signals of appreciable intensity that correspond to the formation of doubly (or more highly) charged ions, so that the total single uracil ionization cross section is essentially identical to the total ionization cross section of this molecule. The relative total single uracil ionization cross section was put on an absolute scale by normalizing the experimentally determined cross section to a calculated total single uracil ionization cross section using the DM formalism at 100 eV,  $15.7 \times 10^{-20} \text{ m}^2$ . The DM formalism applied to molecules has been shown to yield reliable absolute total ionization cross sections with an accuracy between 5% and 20% for a large number of molecules, including complex molecules such as the silicon-organic compounds tetramethylsilane (TMS), hexamethyldisiloxane (HMDSO) and tetraethoxysilane (TEOS) [19, 21-23]. The only category of molecular targets for which the DM formula shows poor agreement with the experimental data is for fluorine-containing radicals such as  $CF_x$  and  $NF_x$  (x = 1-3) [27]. A detailed comparison between calculated DM cross sections and

3016 S Feil et al

measured data for more than 40 species has shown that the reliability of the DM calculation depends critically on the accuracy of the quantum chemical representation of the molecular orbitals in terms of the atomic orbitals of the constituent atoms [19]. The accuracy of the DM method is difficult to assess in general as its errors have different sources. For the ionization energies, accurate quantum chemical values can be derived. Concerning the atomic orbital populations, however, this is not possible in the same way. There is no unique definition of dividing up the molecular orbitals into atomic contributions, since in the limit of an infinite basis set even the basis set of a single atom can describe the wavefunction of the whole molecule. While smaller basis sets might even provide more reasonable relative atomic orbital charge contributions than bigger ones, they suffer from the poor quality of the overall wavefunction. This dilemma, which is sometimes found in the quantum chemical calculation of other properties as well, can be partially overcome by using more sophisticated schemes of charge partitioning etc, but the coefficients g and r in the DM formula are still derived from isolated atoms and cannot easily be improved upon without abandoning the general scheme. In light of these arguments, an empirical statement concerning the accuracy of the DM method seems to be most appropriate. The large number of molecules, where comparisons between experimental and cross sections calculated with the DM formula have been made, shows that the errors for molecules of not more than about 20 atoms are not larger than 20% (often significantly smaller) and comparable to the errors reported for the experimental cross sections.

The cross-calibration between the formation of positive and negative ions from the same parent molecule was first described in our earlier paper on the electron impact ionization of  $C_{60}$  [28, 29]. Briefly, the method uses the well-known absolute cross sections for formation of  $SF_4^+$  and  $SF_4^+$  ions from  $SF_6$  by electron impact and determines, under exactly identical experimental conditions, the ratio of  $SF_4^+$  ions to  $SF_4^+$  ions detected in our apparatus in an effort to determine the ratio of detection efficiencies for, respectively, negative and positive ions. This ratio in conjunction with the absolute value of the partial ionization cross section for formation of a particular positive ion then determines the absolute dissociative attachment cross section for formation of the corresponding negative ion for a gas under study. In the present case of uracil, we found that electrons incident on this molecule produce both positive OCN<sup>+</sup> and negative OCN<sup>-</sup> fragment ions and we used these ions for the cross-calibration.

The uncertainties of the absolute ionization cross sections reported here are in the range of 21–22% for positive ions and about 26% in the case of the attachment cross sections. In the case of the positive ions, we combine the uncertainty in the measurement of the relative cross section curves of 5% (which takes into account the statistical uncertainty and systematic uncertainties due to all fluctuations of the experimental parameters such as gas density, electron beam current, etc) in quadrature with a conservative estimate of a 20% uncertainty in the calculated DM cross section. For the negative ions, we add to this uncertainty in quadrature the 15% uncertainty in the SF<sub>4</sub> to SF<sub>4</sub> cross section ratio [29].

# 3. Results and discussion

Figure 3 shows the experimentally determined total single uracil ionization cross section from threshold to 1000 eV in comparison with the calculated DM cross section. The experimental data were normalized to the calculation at 100 eV. Both cross sections exhibit the typical shape with a maximum (of about  $16 \times 10^{-20}$  m²) at an energy slightly below 100 eV and a gradual decline towards higher impact energies. The agreement is very good over the entire range of impact energies. The two curves are essentially identical in the low-energy regime from threshold up to about 150 eV. At higher impact energies above about 200 eV, the

S Feil et al

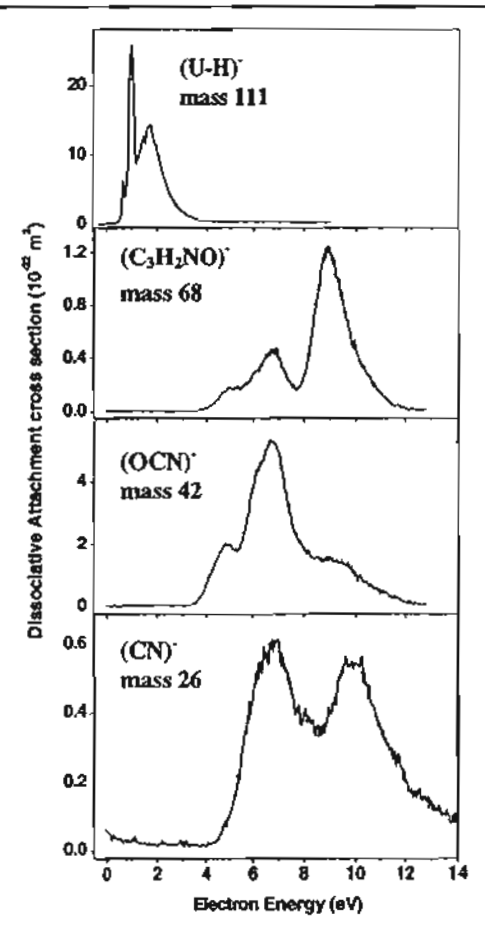


Figure 5. Absolute partial cross sections for dissociative electron attachment to uracil as a function of electron energy. (U-H)<sup>-</sup> refers to the C<sub>4</sub>H<sub>3</sub>N<sub>2</sub>O<sub>2</sub><sup>-</sup> ion.

largest peak value of about  $4.4 \times 10^{-20}$  m<sup>2</sup> (at about 100 eV) whereas the two fragment ions have cross sections that peak around  $2.2 \times 10^{-20}$  m<sup>2</sup> at a slightly higher impact energy. It is quite noteworthy for a complex molecule such as uracil that the largest partial ionization cross section is the one for parent ion formation. Many complex molecules do not have stable parent ions and their ionization is dominated by dissociative ionization channels [19, 21-23].

Lastly, figure 5 shows four absolute partial cross sections for dissociative electron attachment to uracil leading to, respectively,  $C_4H_3N_2O_2^-$ ,  $C_3H_2NO^-$ ,  $OCN^-$  and  $CN^-$  ions as a function of electron energy after cross-calibration to the absolute  $OCN^+$  ionization cross section using the relative cross sections given in [2]. (We note that the labels of the two curves corresponding to the  $C_3H_2NO^-$  and  $OCN^-$  negative ions were interchanged; figure 4 in this paper shows the correct labelling.) In all four cases, the absolute cross sections are about an order of magnitude lower compared to those reported earlier [2]. We attribute the discrepancy between the present absolute calibration of the dissociative attachment cross sections and our earlier measurement to difficulties in the determination of the target number density in the earlier experiments. In the present work, the normalization to a reliable calculated

ionization cross section in conjunction with the positive—negative ion cross-calibration avoids the potential error associated with the target number density determination.

#### 4. Conclusions

We report absolute partial cross sections for the formation of selected positive and negative ions resulting from electron interactions with uracil. Because of the difficulties associated with the preparation of well-characterized gas targets of essentially all biologically important molecules and the absolute determination of the gas target density, we obtained the absolute cross sections in our study by normalizing the total single ionization cross section of uracil (at an electron energy of 100 eV) to a calculated total single ionization cross section using the semi-classical Deutsch-Märk formalism [19, 20]. The DM formalism has been shown to yield reliable total single ionization cross sections (with an accuracy ranging between 5% and 20%) for a large number of molecules, including complex molecules [19, 21-23]. On the basis of the absolute calibration process for positive ions in conjunction with a sensitivity ratio measurement for positive-to-negative ion formation in our apparatus, we subsequently revised our earlier absolute cross section for dissociative attachment to uracil [2] downward by about an order of magnitude.

# Acknowledgments

This work was partially supported by the FWF, ÖNB and ÖAW, Vienna, Austria and the EU Commission, Brussels. We would like to acknowledge financial support from the US Department of Energy, Office of Basic Energy Sciences, Chemical Sciences, Geosciences, and Biosciences Division to KB as well as support from the Thailand Research Fund (TRF), Kasetsart University (KURDI) and the Ministry of University Affairs (MUA-ADB) to IL.

# References

- [1] Boddaiffa B, Cloutier P, Hunting D, Huels M A and Sanche L 2000 Science 287 1658
- [2] Hanel G, Gstir B, Deniff S, Scheier P, Probst M, Farizon B, Farizon M, Illenberger E and Märk T D 2003 Phys. Rev. Lett. 90 188104
- [3] Desfrançois C, Abdoul-Carime H and Schermann J P 1994 Phys. Rev. Lett. 73 2436
- [4] Desfrançois C, Abdoul-Carime H and Schermann J P 1996 J. Chem. Phys. 104 7792
- [5] Desfrançois C, Periquet V, Boutellier Y and Schermann J P 1998 J. Phys. Chem. 102 1274
- [6] Aflatoori K, Gallup G A and Burrow P D 1998 J. Phys. Chem. 102 6205
- [7] Huels M A, Hahndorf I, Illenberger E and Sanche L 1998 J. Chem. Phys. 108 1309
- [8] Abdoul-Carime H, Huels M A, Brüning F, Illenberger E and Sanche L 2000 J. Chem. Phys. 113 2517
- [9] Abdoul-Carirne H, Huels M A, Sanche L and Illenberger E 2001 J. Am. Chem. Soc. 123 5354
- [10] Coupier B et al 2002 Eur. Phys. J. D 20 459
- [11] Abdoul-Carine H, Huels M A, Illenberger E and Sanche L 2003 Int. J. Mass Spectr. 228 687
- [12] Deniff S, Prasinska S, Cingel M, Matejcik S, Scheier P and Märk T D 2003 Chem. Phys. Lett. 377 27
- [13] Abouaf R, Pommier J and Dunet H 2003 Int. J. Mass Spectrom. 226 397
- [14] Deniff S, Matejik S, Gstir B, Hanel G, Probst M, Scheier P and Märk T D 2003 J. Chem. Phys. 118 4107
- [15] Denift S, Ptasinska S, Scheier P and Mäck T D 2004 Int. J. Mass Spectrom. 232 99
- [16] Gianturco F et al 2004 Phys. Rev. Lett. at press
- [17] Deniff S, Ptasinska S, Hanel G, Gstir B, Scheier P and Märk T D 2004 J. Chem. Phys. 120 6557
- [18] Wetmore S D, Boyd R J and Eriksson L A 2000 Chem. Phys. Lett. 322 129
- [19] Deutsch H, Becker K, Man S and Märk T D 2000 Int. J. Mass Spectrom. 197 37
- [20] Deutsch H, Scheier P, Becker K and Märk T D 2004 Int. J. Mass Spectrom. 233 13
- [21] Deutsch H, Hilpert K, Becker K, Probst M and Märk T D 2001 J. Appl. Phys. 89 1915
- [22] Probst M, Deutsch H, Becker K and Märk T D 2001 Int. J. Mass Spectrom. 206 13

3020

- [23] Bernhardt P and Pareizke G H 2003 Int. J. Mass Spectrom. 223/224 599
- [24] Grill V, Walder G, Margreiter D, Rauth T, Poll H U, Scheier P and Märk T D 1993 Z. Phys. D 25 217
- [25] Poll H U, Grill V, Matt S, Abramzon N, Becker K, Scheier P and Märk T D 1998 Int. J. Mass Spectrom. Ion Proc. 177 143
- [26] Gluch K, Scheier P, Schustereder W, Tepnual T, Feketeova L, Mair C, Matt-Leubner S, Stamatovic A and Märk T D 2003 Int. J. Mass Spectrom. 228 307
- [27] Huo W M, Tarnovsky V and Becker K 2001 Chem. Phys. Lett. 358 328
- [28] Dünser B, Lezius M, Scheier P, Deutsch H and Märk T D 1995 Phys. Rev. Lett. 74 3364
- [29] Matt S, Dünser B, Lezius M, Deutsch H, Becker K, Stamatovic A, Scheier P and Märk T D 1996 J. Chem. Phys. 105 1880

# Theoretical Study of the Adsorption of Ethylene on Alkali-Exchanged Zeolites

#### SOMBAT KETRAT, JUMRAS LIMTRAKUL

Laboratory for Computational & Applied Chemistry, Physical Chemistry Division, Kasetsart University, Bangkok 10900, Thailand

Received 30 August 2002; accepted 8 May 2003

DOI 10.1002/qua.10706

ABSTRACT: The structures of alkali-exchanged faujasite (X-FAU, X = Li\* or Na\* ion) and ZSM-5 (Li-ZSM-5) zeolites and their interactions with ethylene have been investigated by means of quantum cluster and embedded cluster approaches at the B3LYP/6-31G (d, p) level of theory. Inclusion of the Madelung potential from the zeolite framework has a significant effect on the structure and interaction energies of the adsorption complexes and leads to differentiation of different types of zeolites (ZSM-5 and FAU) that cannot be drawn from a typical quantum cluster model, H<sub>3</sub>SiO(X)Al(OH)<sub>2</sub>OSiH<sub>3</sub>. The Li-ZSM-5 zeolite is predicted to have a higher Lewis acidity and thus higher ethylene adsorption energy than the Li-FAU zeolites (16.4 vs. 14.4 kcal/mol), in good agreement with the known acidity trend of these two zeolites. On the other hand, the cluster models give virtually the same adsorption energies for both zeolite complexes (8.9 vs. 9.1 kcal/mol). For the larger cation-exchanged Na-FAU complex, the adsorption energy (11.6 kcal/mol) is predicted to be lower than that of Li-FAU zeolites, which compares well with the experimental estimate of about 9.6 kcal/ mol for ethylene adsorption on a less acidic Na-X zeolite. © 2003 Wiley Periodicals, Inc. Int J Quantum Chem 94: 333-340, 2003

Key words: ZSM-5 zeolite; faujasite zeolite; DFT study; ethylene adsorption; embedded cluster

#### Introduction

地名加加加加西马克斯

eolites are of prime importance as catalysts for many industrial processes, due mainly to their shape selectivity and acid sites [1–9]. Cation-exchanged zeolites have been found to be potential catalysts for hydrocarbon reactions [10–19]. Of par-

Correspondence to: J. Limtrakul; e-mail: fscijrl@ku.ac.th

ticular interest in this area of active research is the alkene adsorption on alkali-exchanged zeolite, which is the foundation of several industrially important reactions, namely, aromatization of olefins [18], formation of ethylbenzene and styrene [19], and the production of xylene [20].

7.00

٠:.

The importance of metal-exchanged zeolites suggests that a better understanding of the structure and mechanistic properties at the molecular level of the catalyst is certainly required [21]. A review of

quantum chemical calculations applied to zeolites and their interaction with unsaturated hydrocarbon has been recently reported [22]. All early works of adsorption of C<sub>2</sub>H<sub>4</sub> on bare zeolite clusters were limited to small model fragments that are not specific to a particular zeolite but represent a generic tetrahedral subunit in an unconstrained environment [22–26]. It is known that small zeolitic clusters may inadequately reflect adsorption complexes at the active site and the cluster environment may enhance binding energy and, hence, more accurately predict the structures of reaction intermediates, transition states, and products [5, 27].

To include the effects of the zeolite framework on adsorption of C<sub>2</sub>H<sub>4</sub> in zeolites, a periodic electrostatic structure method can be utilized [28–31]. This corresponds to the high loading case and is often computationally expensive for most zeolites due to their relatively large unit cells.

Alternatively, the embedded cluster approach [5, 9] provides a more practical methodology with little additional computational cost when compared to the bare cluster calculation. To the best of our knowledge, no theoretical work regarding the metal-exchanged zeolite-ethylene complex has been carried out so far.

In this study, we examine the effects of cations and the zeolitic framework on the adsorption properties of ethylene in alkali-exchanged faujasite and ZSM-5 using the embedded cluster methodology.

#### "Methods

"Y Zeolites have elementary building units of tetrahedral SiO<sub>4</sub> and AlO<sub>4</sub> commonly called T atoms. A 3-D framework of faujasite-type zeolite is built on 24-T cubo-octahedral sodalite cages linked via their six-membered rings forming large cavities called supercages [Fig. 1(a)]. On the other hand, the ZSM-5 zeolite framework is built on connected penfasil units forming straight and sinusoidal pore systems [Fig. 1(b)].

We employed the clusters illustrated in Figures 2–4 as the models of interaction of unsaturated hydrocarbon on alkali-metal-exchanged zeolites. The models H<sub>3</sub>SiO(X)Al(OH)<sub>2</sub>OSiH<sub>3</sub>, where X = Li and Na, will hereafter be referred to as [Li-FAU], [Na-FAU], and [Li-ZSM-5], and their complexes, H<sub>3</sub>SiO(X)Al(OH)<sub>2</sub>OSiH<sub>3</sub>/[C<sub>2</sub>H<sub>4</sub>], will be referred to as [Li-FAU]/[C<sub>2</sub>H<sub>4</sub>], [Na-FAU]/[C<sub>2</sub>H<sub>4</sub>], and [Li-ZSM-5]/[C<sub>2</sub>H<sub>4</sub>]. The bare quantum clusters are specifically modeled according to crystallographic

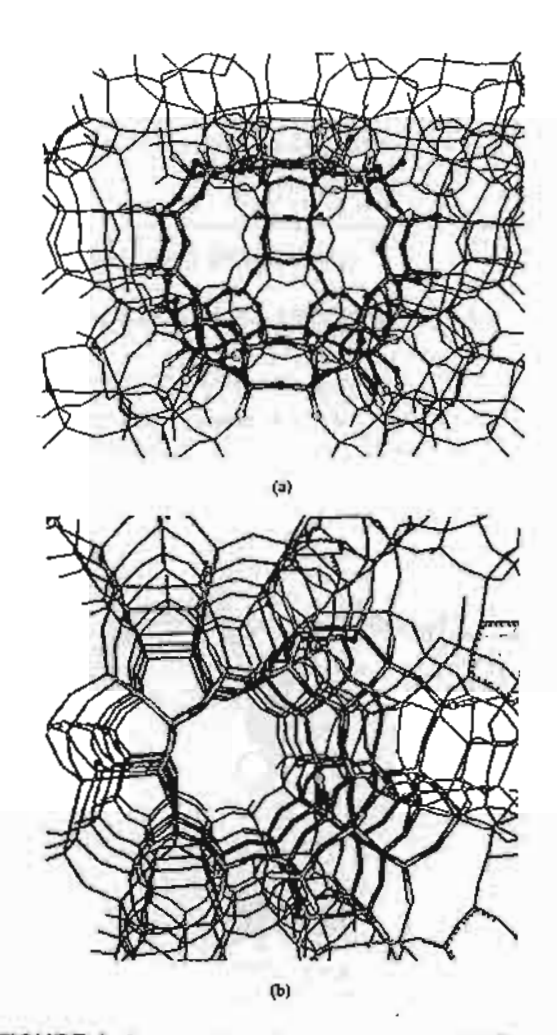


FIGURE 1. Presentation of zeolite structure. (a) Structure of faujasite showing the supercage. (b) Structure of ZSM-5 viewed from the straight direction. [Color figure can be viewed in the online issue, which is available at www.interscience.wiley.com.]

structures of active sites in faujasite [31] and ZSM-5 [32] zeolites. In these models, the dangling bonds of the Si atoms are terminated by H atoms and the Si—H bonds are aligned with the corresponding S—O bonds of the structures of zeolites, respectively. The naked alkali–cation/ $C_2H_4$  adducts, Li<sup>+</sup>/ $[C_2H_4]$  and Na<sup>+</sup>/ $[C_2H_4]$ , are also included for comparison with the effect of the negative zeolite oxygen framework surrounding the alkali cations.

In the embedded cluster model (cf. Fig. 5), the static Madelung potential due to atoms outside of the quantum cluster is represented by charges located at the zeolite lattice sites. Charges close to the

tal.

(a)

134.1

[133.8]

(a)

134.1

[133.8]

(b)

194.6

[187.3]

194.6

[187.3]

194.6

(b)

他以前がおけいた

3.

41

ch that that that that

FIGURE 2. Li-FAU zeolite structures and their interaction with ethylene optimized at 83LYP/6-31G(d, p) using embedding and cluster calculations (values in parentheses); bond distances in pm. (a) Li-FAU. (b) Li-FAU/C<sub>2</sub>H<sub>4</sub>. [Color figure can be viewed in the online issue, which is available at www.interscience.wiley.com.]

quantum cluster are treated explicitly, while the Madelung potential from the remaining charges from an infinite lattice is represented by a set of surface charges that were derived from the surface charge representation of external embedded potential (SCREEP) method. More details on our method can be found elsewhere [5, 9]. For faujasite, the total Madelung potential is represented by 288 explicit charges and 960 surface charges, whereas for ZSM-5 the potential is represented by 360 explicit charges and 240 surface charges. With this small number of point charges, the additional computational cost is often less than 5% when compared to bare cluster calculations.

Geometry optimizations were carried out at the B3LYP level using the 6-31G (d, p) basis with the Gaussian 98 program [33]. The computations were carried out on PC clusters at the KU Computing Center and a DEC alpha station 250 workstation at

the Laboratory for Computational and Applied Chemistry at Kaselsart University and a cluster of IBM RISC/6000 workstations at the Henry Eyring Center for Theoretical Chemistry, University of Utah.

#### Results and Discussion

#### METAL-EXCHANGED FAUJASITE (X-FAU)

#### Li-Zeolite (Li-FAU)

Cluster and embedded cluster models for alkalimetal-exchanged zeolites are shown in Figures

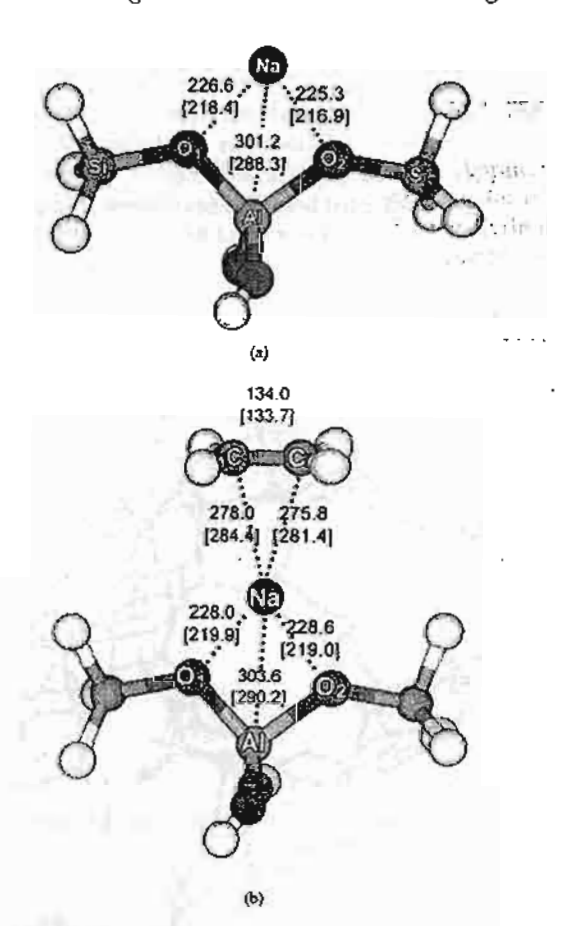


FIGURE 3. Na–FAU zeolite structures and their interaction with ethylene optimized at B3LYP/6-31G(d, ρ) using embedding and cluster calculations (values in parentheses); bond distances in pm. (a) Na–FAU. (b) Na–FAU/C<sub>2</sub>H<sub>a</sub>. [Color figure can be viewed in the online issue, which is available at www.interscience.wiley. com.]

#### KETRAT AND LIMTRAKUL

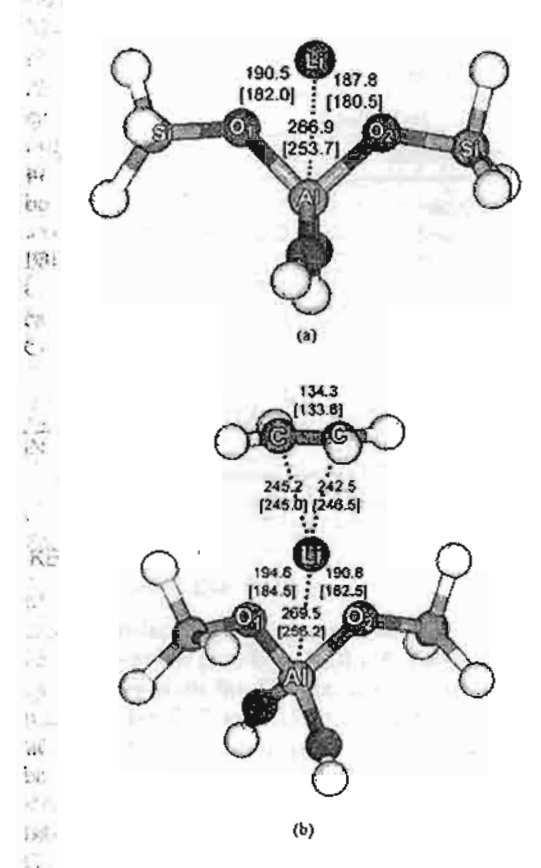


FIGURE 4. Li–ZSM-5 zeolite structures and their interaction with ethylene optimized at the B3LYP/6-31G(a, p) level using embedding and cluster calculations (values in parentheses); bond distances in pm. (a) Li–ZSM-5. (b) Li–ZSM-5/C<sub>2</sub>H<sub>4</sub>. (Color figure can be viewed in the online issue, which is available at www.interscience.wiley.com.)

2(a)-4(a). Selected optimized geometric parameters and atomic charges for bare quantum cluster and embedded cluster models are documented in Tables I and II. For the Li-FAU zeolite [see Fig. 2(a)], the alkali-metal cation does not bind with a particular bridging oxygen atom in the [AlO<sub>4</sub>] but is symmetrically bidentated to O1 and O2 of [AlO<sub>4</sub>] tetrahedron, in agreement with the previously reported ESR experiment [34]. The interaction of the cationic metal with the zeolite framework leads to substantial perturbation of the active acidic site. In particular, we found that the Al-O distances were élongated by 2.3 pm, but by only 0.9 pm for the Al-O2 and Al-O1 distances, respectively, while the Si—O bonds were shortened by 3.6 and 4.0 pm for the Si-O1 and Si-O2 bonds, respectively, but

100

10 .

bl. th da

there was no significant change for the O1—Al—O2 angle. A reciprocal effect is that the zeolite framework reduces the Li charge. The charge on Li\* cation was reduced to 0.53, and 0.63 a.u. for the bare cluster and the embedded models, respectively. The increase of charges on Li cation is clearly observed by the changes of charges on Al and Si atoms of the Li-FAU complexes as compared to the corresponding charges of their anionic framework (cf. Table II). The Madelung potential was found to have a significant effect on the structure of Li-exchanged FAU. In particular, it elongates the Li-Al by 10.7 pm. The extent of Li-O distances increased with the embedded model (Li. O1 = 185.1 pm vs. 191.4 pm and Li···O2 = 183.9 pm vs. 190.4 pm). This indicates that the Madelung field weakens the attachment of the Li cation to the zeolite framework, and thus reduces the strength of the complexes, which is reflected by lower complexation energy (-135.92 kcal/mol) of Li(1) and zeolitic anion than those obtained from the bare quantum cluster (-160.78 kcal/mol).

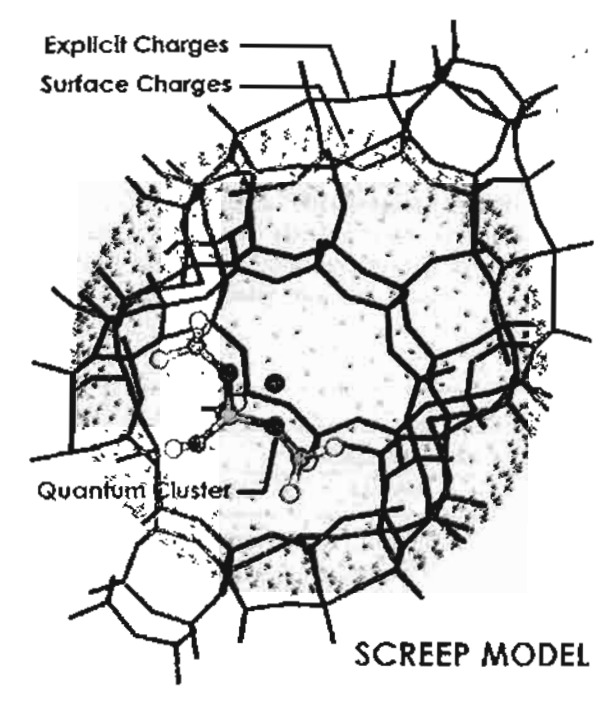


FIGURE 5. SCREEP embedded cluster model. {Color figure can be viewed in the online issue, which is available at www.interscience.wiley.com.}

VOL. 94, NO. 6

	(Li	-ZSM-5]	ון	Li-FAU]	ſv.	la-FAU]
Parameters	Bare	Embedded	Bare	Embedded	Bare	Embedded
X+—AI	253.7	266.9	249.8	260.5	288.3	301.2
X+-01	182.0	190.5	185.1	191.4	218.4	226.6
X+—O2	180.5	187.8	183.9	190.4	216.9	225.3
O1-X+-O2	88.4	83.5	92.2	88.6	76.8	73.6
AIO1	176.8	178.5	180.2	181.1	179.3	180.4
AIO2	177.1	178.3	180.8	183.1	180.0	182.3
O1-AI-O2	91.1	89.9	94.9	94.2	97.6	96.5
SIO2	164.3	160.7	166.7	162.7	165.1	161.3
SI01	164.1	160.0	166.6	163.0	164.8	161.5
qX+	0.52	0.63	0.53	0.63	0.67	0.73

Bond lengths are in pm and bond angles in degrees.

#### Na-Zeolite (Na-FAU)

A similar trend has been observed for the Na-EAU complex [see Fig. 3(a)] (cf. Tables I and II). The charges on the Na+ cation within the zeolite models are 0.67 and 0.73 for cluster and embedded cluster models, respectively. The Na. . . O distances are elongated with the embedded model (Na O1 = 218.4 pm vs. 226.6 pm and  $Na \cdot O2 = 216.9 \text{ pm vs. } 225.3 \text{ pm}$ ). The calcufated Na. Al distance of the embedded model is 12.9 pm larger than that of the bare cluster, indicating that the embedding environment weakens the attachment of the metal cation to the zeolite framework. Regarding the energetics of the Na-FAU complexes, the complexation energy of the Na cation to the zeolitic framework leads to change in the geometric structures (the O1-Al-O2 bond angles and X+-Al distances, the distance between the cation and the A1 atom of zeolite framework, are increased with the increasing cationic size). These are, as expected, smaller than those for the Li-FAU complex (cf. Table II). The complexation energies of the monovalent ions Li+ and Na+ that are bound to a zeolitic framework are -135.92 (Li-FAU) and -118.19 (Na-FAU) kcal/mol at the embedded cluster models, following the conventional electrostatic trend. We found that the extended structure decreases the complexation energy by 24.86 kcal/mol in the Li-FAU and by 17.43 kcal/mol in the Na-FAU zeolites. This implies that the complexation energy of alkali cation bound to FAU zeolites cannot be obtained accurately by small bare quantum cluster models.

TABLE II \_\_\_\_\_\_
Atomic charges of LI-FAU and Na-FAU complexes.

f.		Bare cluster		8	Embedded cluste	er :
Åtoms	Isolated	Ŀi~FAU	Na-FAU	Isolated	Li-FAU	Na-FAU
Şi1	0.67	0.74	0.74	1.34	1.23	1.23
Si2	0.69	0.73	0.73	1.27	1.25	1.23
Q1	-0.66	-0.79	-0.76	-0.61	-0.75	-0.72
02	-0.67	-0.79	-0.77	-0.61	-0.75	-0.73
AÌ '	0.80	0.99	0.89	0.76	0.90	0.83
O1 O2 Al Cation	1.00	0.53	0.67	1.00	0.63	0.73
Çòmplexation energy						
(kcal/mol)	_	-160.78	-135.62	_	135.42	-118,19

INTERNATIONAL JOURNAL OF QUANTUM CHEMISTRY

ú

:00

B3LYP/6-31G(d, p)-optimized geometric parameters of the complex of ethylene with naked Li\*, Li-ZSM-5, Li-FAU, naked Na+ and Na-FAU zeolites.

	Li⁺/C₂H₄	Li-ZS	 3M-5/C₂H₄	Li⊢F	AU/C₂H₄	Na <sup>+</sup> /C₂H₄	Na-f	FAU/C <sub>2</sub> H <sub>4</sub>
Parameters	Naked	Bare	Embedded	Bare	Embedded	Naked	Bare	Embedded
C=Ca	134.5	133.8	134.3	133.8	134.1	134.3	133.7	134.0
X*—C1	238.3	245.0	245.2	248.9	242.9	272.2	284.4	278.0
X⁺—C2	238.5	246.5	242.5	244.7	242.5	272.2	281.4	275.8
X+—(C—C) <sup>b</sup>	228.7	236.5	233.1	237.6	233.3	263.8	274.9	268.6
AlX <sup>*</sup>		256.2	269.5	252.9	263.6		290.2	303.6
X*—01		184.5	194.6	187.3	194.6		219.9	228.0
X+—O2	_	182.5	190.8	187.2	193.8		219.0	228.6
01-X+-02		87.0	82.2	90.5	86.9	_	76.0	72.7
AI01	_	176.3	177.8	179.7	180.5	_	179.0	180.0
Ái02	_	176.7	177.7	180.2	182.5	_	179.6	181.9
Q1-Al-O2	_	91.4	90.4	95.3	94.8	_	97.8	96.7
Si—O1	_	163.5	159.3	166.1	162.5	_	164.5	161.2
 \$FO2	_	163.9	160.3	166.1	161.8	_	164.8	160.8
\$IO2 qX+	0.69	0.30	0.36	0.32	0.36	0.77	0.52	0.54

Bond lengths are in pm and bond angles in degrees.

2. A The calculated B3LYP/6-31G(d, p) of C⇒C bond distance in the gas phase is 133.0 pm.

The distances between Li cation to the midpoint of the C—C bond.

#### INTERACTION OF METAL-EXCHANGED FAUJASITE (X-FAU) WITH ETHYLENE

#### interaction of Li-Zeolite (Li-FAU) with Ethylene

7. Cluster and embedded cluster models for the adsorption of ethylene on alkali metal-exchanged zeolites are illustrated in Figures 2(b)-4(b). Selected geometric parameters of the adduct complexes are listed in Table III. Adsorption energies have been évaluated by employing different models and are

given in Table IV. For the Li-FAU/ $C_2H_4$  zeolite [see Fig. 2(b)], the Optimized Li. . . C2H4 distances between Li cation to the midpoint of the C=C bond are found to be 233.3 and 237.6 pm, and the corresponding energies are 14.35 and 9.08 kcal/mol with basis set superpo-

sition error (BSSE) correction for the embedded cluster and quantum cluster, respectively. It is interesting to compare the adsorption of C2H4 on Li-FAU zeolite with the case where the zeolite framework is absent, i.e., in the naked Li-C<sub>2</sub>H<sub>4</sub> system. As expected, C2H4 binds more strongly by a factor of 2 to the Li+ cation (23.15 kcal/mol) than in the Li-PAU zeolite in the binding energy. The simple naked Li-C2H4 model obviously overestimates the interaction of C2H4 in a real Li-exchanged-FAU system due to the large electrostatic field generated by the naked Li cation. The bare cluster model causes a large reduction of the positive charge of the Li cation and, thus, possibly underestimates the interaction of C2H4 with the Li-exchanged-FAU system. The embedding environment improves the results of the bare cluster

TABLE IV Calculated adsorption energies (kcal/mol) of C2H4 on naked Li+, Na+, bare quantum cluster, and embedded cluster model of Li-ZSM-5, Li-FAU, and Na-FAU zeolites.

	ધ*/ C₂H₄	Li-Z\$	M-5/C <sub>2</sub> H <sub>4</sub>	Li–F	AU/C₂H₄	Na*/ C₂H₄	Na-FAU/C₂H₄	
	Naked	Bare	Embedded	Bare	Embedded	Naked	Bare	Embedded
<u>.</u> ΔΕ	-24.83 -23.15	-11.55 -8.94	18.98 16.41	~11,58 ~9.08	~16.87 ~14.35	-17.76 15.97	-9.42 -7.35	-13.76 -11.63
ΔE <sub>ass∈</sub>	~23.15	-8.94	-16.41	~9.08	-14.35	-15.97	<b>-7.35</b>	

VOL. 94, NO: 6

338

Ί, ÷.

٠;

model. One can see that the adsorption energy of the embedded cluster model lies between those of the bare quantum cluster model and the simple naked  $\text{Li}/\text{C}_2\text{H}_4$  system.

### interaction of Na-Zeolite (Na-FAU) with Ethylene

For the cluster model [see Fig. 3(b)], the adsorption energy of Na-FAU/C2H4 complexes is calculated to be 7.35 kcal/mol lower than that of the Li-FAU/C2H4 complex (9.08 kcal/mol); this may be attributed to its large cationic size (relative to Li+), which causes its interactions to be weaker than that of the Li complex. We found that the Madelung potential increases the adsorption energy by 5.27 kcal/mol in the Li-FAU and by 4.28 kcal/mol in the Na-FAU zeolites. With the inclusion of BSSE correction and the effects of the Madelung potential, we predict that the Li-FAU/C2H4 complex is more stable by about 2.72 kcal/mol compared to the Na-FAU/C2H4 complex. The adsorption energy is predicted to be 11.63 kcal/mol for the embedded cluster model of the Na-FAU/ C2H4, which compares well with the experimental value of 9.6 kcal/mol for the less acidic Na-X zeolite complex [35]. The lower adsorption energy in Na-X zeolite, which is an aluminum-rich faujasite zeolite with an Si/Al ratio in a range of 1-1.5, corresponds to the lower acid strength of the Na-X zeolite because the acid strength of zeolite decreases as the aluminum content increases.

### at Effect of the Zeolite Framework on the Adsorption Properties of Ethylene

Another point of interest is the comparison of the results obtained using both cluster and embedded cluster models for exploring the different types of zeolites (faujasite and ZSM-5). Faujasite is considered a large-pore-size zeolite with a pore diameter of 74 pm and spacious supercages with a diameter of 130 pm, while ZSM-5 is a middle-pore-size zeolite with a pore diameter of about 50 pm. Although the two types of zeolites have different crystal structures (see Fig. 1), the cluster models give virtually the same adsorption energies (9.08 vs. 8.94 kcal/mol) for both Li-FAU/C<sub>2</sub>H<sub>4</sub> [cf. Fig. 2(b)] and Li-ZSM-5/C<sub>2</sub>H<sub>4</sub> [cf. Fig. 4(b)] complexes as listed in Table IV.

We found that inclusion of the Madelung potential increases the adsorption energy by 7.47 and 5.27 kcal/mol for the Li-ZSM-5 and Li-FAU zeolites,

₹.

ķ.,

respectively. With the inclusion of BSSE correction and the effects of the Madelung potential, the Li-ZSM-5/C<sub>2</sub>H<sub>4</sub> complex is more stable by about 2.06 kcal/mol as compared to the Li-FAU/C<sub>2</sub>H<sub>4</sub> complex. Thus, the Madelung potential was found to reveal that adsorption properties of zeolite do not depend only on the acidic site center but also on the framework structure where the acidic site is located.

#### Conclusion

The structures of alkali-exchanged faujasite (X-FAU,  $X = Li^+$ , or  $Na^+$  ion) and ZSM-5 (Li-ZSM-5) zeolites and their interaction with ethylene have been investigated by means of both the quantum duster and embedded cluster approaches at the B3LYP/6-31G (d, p) level of theory. The effects of the Madelung potential were found to be important. The bare quantum cluster is too small to account for the extended structure and, therefore, yields almost the same binding energies (8.94 vs. 9.08 kcal/mol) for both Li-ZSM-5/C2H4 and Li-FAU/C2H4 complexes. On the other hand, the binding energy derived from the embedded model of Li-ZSM-5/C2H4 is calculated to be 16.41 kcal/ mol, which is larger than that obtained from the Li-FAU complex (14.35 kcal/mol), indicating that the metal-exchanged ZSM-5 is more acidic than the metal-exchanged FAU zeolites and leads to a better agreement with the experimental observation. The ion (X)...Al distance increases with the increase in ionic radii. The predicted adsorption energy for Na-FAU/C<sub>2</sub>H<sub>4</sub> (11.63 kcal/mol) is comparable with the experimental estimate of about 9.6 kcal/ mol for ethylene adsorbed on Na-X zeolite. The results obtained in the present study suggest that the embedded cluster approach yields a more accurate and practical model than the bare quantum cluster for exploring the zeolite framework and catalytic properties.

#### **ACKNOWLEDGMENTS**

This work was supported by the Thailand Research Fund (TRF) in supporting the TRF Senior Research Scholar to J.L., by ADB-MUA, and by the Kasetsart University Research and Development Institute (KURDI). Sincere thanks are extended to Professor R. Ahlrichs (Karlsruhe, Germany) and Professor T. N. Truong (University of Utah, Salt

#### KETRAT AND LIMTRAKUL

Lake City, UT) for their continued support of this work.

#### References

12

- Catlow, C. R. A. Modeling of Structure and Reactivity in Zeolites; Academic: San Diego, 1992.
- 2. van Santen, R. A.; Kramer, G. J. Chem Rev 1995, 95, 637.
- 3. Limtrakul, J. Chem Phys 1995, 193, 79.
- Limtrakul, J.; Treesukol, P.; Probst, M. Chem Phys 1997, 215, 77.
- Limtrakul, J.; Nanok, T.; Jungsuttiwong, S.; Khongpracha, P.; Truong, T. N. Chem Phys Lett 2001, 349, 161.
- 6. Limtrakul, J.; Tantanak, D. Chem Phys 1996, 208, 331.
- 7. Zygmunt, J. A.; Curtiss, L. A.; Iton, L. E.; Erhardt, M. K. J. Phys Chem 1996, 100, 6663.
- 8: Krossner, M.; Sauer, J. J Phys Chem 1996, 100, 6199.
- Treesukol, P.; Troung, T. N.; Limtrakul, J. J Phys Chem B
   2001, 105, 2421.
- 10. Barthomeuf, D. Catal Rev 1996, 38, 521.
- \$1. Maxwell, L. E. Adv Catal 1982, 31, 1.
- 12. Engelhardt, J.; Szani, J.; Valyon, J. J Catal 1987, 107, 29.
- 13. Hathaway, P. E.; Davis, M. E. J Catal 1989, 119, 497.
- 14. Corma, A. Mater Res Soc Symp Proc 1991, 233, 17.
- Hölderich, W. F.; Hesse, M.; Naümann, F. Angew Chem. 1988, 27, 226.
- 16. Fu, Z. H.; Ono, Y. Catal Lett 1993, 21, 43.
- 17. Sidorenko, Y. N.; Galich, P. N.; Gutyrya, V. S.; Il'in, V. G.; Neimark, I. E. Dokl Akad Nauk SSSR 1967, 173, 132.
- 18. Huang, M.; Kaliaguine, S. J Mol Catal 1993, 81, 37.
- 19. Yashima, T.; Sato, K.; Hayasaka, H. T.; Hara, N. J Catal 1972,
- 20. Kanzansky, V. B. Catal Today 1999, 51, 419.
- 21. Deka, R. C.; Hirao, K. J Mol Catal A 2002, 181, 275.
- 22. Boronat, M.; Viruela, P.; Corma, A. J Phys Chem A 1998, 102,

- 23. Kazansky, V. B. Acc Chem Res 1991, 24, 379.
- Evleth, E. M.; Kassab, E.; Jessri, H.; Allavena, M.; Montero, L.; Sierra, L. R. J Phys Chem 1996, 100, 11368.
- Ugliengo, P.; Ferrari, A. M.; Zecchina, A.; Garrone, E. J Phys Chem 1996, 100, 3632.
- 26. O'Malley, P. J.; Franworth, K. J. J Phys Chem 1998, 102, 4507.
- Greatbanks, S. P.; Hillier, I. H.; Burton, N. A.; Sherwood, P. J Chem Phys 1996, 105, 3370.
- Dovesi, R.; Saunders, V. R.; Roetti, C. Crystal 92, an ab initio Hartree-Fock LCAO Program for Periodic Systems; Theoretical Chemistry Group, University of Torino and SERC, Daresbury Laboratory: Torino, Italy, 1992.
- Campana, L.; Selloni, A.; Weber, J.; Pasquarello, A., Papai, I.;
   Goursot, A. Chem Phys Lett 1994, 226, 245.
- Teunissen, E. H.; Roetti, C.; Pisani, C.; de Man, A. J. M.; Jansen, A. P. J.; Orlando, R.; van Santen, R. A.; Dovesi, R. Model Simul Mater Sci Eng 1994, 2, 921.
- Mortier, W. J.; van der Bosche, E.; Uytherhoven, J. B. Zeolites 1984, 4, 41.
- van Koningveld, H.; van Bekkum, H.; Jansen, J. C. Acta Crystallogr B 1987, 43, 127.
- 33. Frisch, M. J.; Trucks, G. W.; Schlegel, H. B.; Scuseria, G. E.; Robb, M. A.; Cheeseman, J. R.; Zakrzewski, V. G.; Montgomery, J. A.; Stratmann, R. E. Jr.; Burant, J. C.; Dapprich, S.; Millam, J. M.; Daniels, A. D.; Kudin, K. N.; Strain, M. C.; Farkas, O.; Tomasi, J.; Barone, V.; Cossi, M.; Cammi, R.; Mennucci, B.; Pomelli, C.; Adamo, C.; Clifford, S.; Ochterski, J.; Petersson, G. A.; Ayala, P. Y.; Cui, Q.; Morokuma, K., Salvador, P.; Dannenberg, J. J.; Malick, D. K.; Rabuck, A. D.; Raghavachari, K.; Foresman, J. B.; Cioslowski, J.; Ortiz, J. V.; Baboul, A. G.; Stefanov, B. B.; Liu, G.; Liashenko, A.; Piskorz, P.; Komaromi, I.; Gomperts, R.; Martin, R. L.; Fox, D. J.; Keith, T.; Al-Laham, M. A.; Peng, C. Y.; Nanayakkara, A.; Challacombe, M.; Gill, P. M. W.; Johnson, B.; Chen, W., Wong, M. W.; Andres, J. L.; Gonzalez, C.; Head-Gordon, M., Replogle, E. S.; Pople, J. A. Gaussian 98; Gaussian, Inc.; Pittsburgh, PA, 2001.
- Hosono, H.; Kawazoe, H.; Nishii, J.; Kanazawa, J. J Non Cryst Solid 1982, 51, 217.
- Carter, J. L.; Yates, D. J. C.; Lucchesi, P. J.; Elliott, J. J.; Kevorkian, V. J Phys Chem 1996, 70, 1126.

ί.

3.

::

10



Available online at www.sciencedirect.com



Journal of Catalysis 219 (2003) 320-328

JOURNAL OF CATALYSIS

www.elsevier.com/locate/icat

## Adsorption of ethylene, benzene, and ethylbenzene over faujasite zeolites investigated by the ONIOM method

S. Kasuriya, S. Namuangruk, P. Treesukol, M. Tirtowidjojo, and J. Limtrakul a.\*

Laboratory for Computational and Applied Chemistry, Kasetsart University, Bangkok 10900, Thailand b The Dow Chemical Company, 2301 N. Brazosport Blvd, B-1226, Freeport, TX 77541-3257, USA

Received 17 January 2003; revised 11 April 2003; accepted 29 April 2003

#### Abstract

The performance of the ONIOM (Our-own-N-layered Integrated molecular Orbital + molecular Mechanics) approach utilizing 10 combinations of two-layer ONIOM2 schemes has been tested for various sizes of faujasite clusters containing up to 84T tetrahedral atoms and the complexes they form with ethylene, benzene, and ethylbenzene molecules. Interaction energies of the adsorbates with a 3T bare quantum cluster are calculated to be -8.14, -7.48, and -7.76 kcal/mol at B3LYP/6-31G(d,p) level of theory, respectively. The long-range effects of the extended structure of zeolite were found to differentiate the stability of adsorption complexes that cannot be drawn from the typical 3T quantum cluster. The interaction energies of ethylene, benzene, and ethylbenzene molecules on the more realistic cluster, 84T, using ONIOM2(B3LYP/6-311++G(d,p):UFF) scheme are predicted to be -8.75, -15.17, and -21.08 kcal/mol, respectively, which compare well with the experimental estimates of -9.1, -15.3, and -19.6 kcal/mol, respectively. This finding clearly demonstrates that the interaction between adsorbate and acidic zeolites does not depend only on the Brønsted group center but also on the lattice framework surrounding the adsorption site. The results obtained in this study suggest that the ONIOM approach, when carefully calibrated, is a computationally efficient and accurate method for studying adsorption of aromatics on zeolites.

© 2003 Elsevier Inc. All rights reserved.

Keywords: Zeolite; Faujasite; ONIOM; QM/MM; Adsorption; Benzene; Ethylbenzene

#### 1. Introduction

Ethylene, benzene, and their derivatives, including ethylbenzene and styrene, are among the most important chemicals in the chemical industry. Ethylbenzene is, commercially, the largest volume derivatives of benzene. Over 90% of the world's production of ethylbenzene is used in the manufacture of styrene, which is one of the most important industrial monomers. Other applications are paint solvents and pharmaceuticals [1]. The interaction between ethylene and benzene to ethylbenzene and the conversion of ethylbenzene to styrene are important industrial processes. The conventional processes of benzene alkylation are usually catalyzed by AlCl<sub>3</sub>. This catalyst causes a number of problems concerning handling, safety, corrosion, and waste disposal [2]. An immense endeavor has been put into de-

Zeolites are widely used in the petroleum and chemical industries as solid catalysts for a number of commercially important hydrocarbon reactions due to their outstanding properties, i.e., Brønsted and Lewis acid sites, size-shape selectivity, and thermal stability [3]. Using proton- and metalzeolites as the catalysts can increase the percentage yield of the required products and thus reduce the production cost significantly. Zeolites have been used as effective catalysts in converting many hydrocarbon materials to value-added products. The adsorptions of ethylene, benzene, and ethylbenzene on zeolites, which are the elementary steps of the catalytic processes, have been studied experimentally by using FTIR [4-7] and NMR [8,9]. The adsorption energy of ethylene on the acidic H-Y zeolite was determined to be -9.1 kcal/mol [6]. The differential enthalpies of adsorption of benzene and benzene derivatives on H-Y zeolite were

veloping alternative catalyst systems that are more environmentally friendly. Nowadays the conventional AlCl<sub>3</sub>-based processes have been progressively substituted with zeolitebased processes.

Corresponding author.
 E-mail address: fscijrl@ku.ac.th (J. Limtrakul).

found to increase in the following order: benzene < ethylbenzene < 1,4-diethylbenzene  $\approx$  1,3-diethylbenzene [10].

Numerous theoretical models, including the periodic calculations, have been proposed to study the crystalline zeolite [11-19]. Nevertheless, zeolites that have a high impact in industrial processes usually possess hundreds of atoms per unit cell. This makes the use of sophisticated methods, such as periodic ab initio calculations, computationally too expensive and even impractical sometimes when very large zeolites are concerned. Therefore, the electronic properties of zeolites are usually modeled with quantum chemical methods for relatively small clusters where only the most important part of zeolites is focused [16-19]. With such limited models, the effect of the framework which can significantly change the structure and energetics of the system, is not taken into account. The recent development of hybrid methods, such as embedded cluster or combined quantum mechanics/molecular mechanics (QM/MM) methods [13,14, 20-25], as well as the more general ONIOM method has brought a larger system within reach of obtaining accurate results [26,27].

Up to date, the ONIOM method is applied to the study of extended systems, for example, chemical reactions on surface [28–33], and in enzymes [34]. However, there are no reports of the ONIOM method on H-FAU zeolites interacted with aromatic hydrocarbons.

In this study, we present the results of using the ONIOM model to represent the complicated structure of zeolites and to study the adsorption of ethylene, benzene, and ethylbenzene, which is the first important step for a more comprehensive study of alkylation reaction. Since the Brønsted acid site is considered as the active site for the alkylation of benzene [35-38] (although the adsorbates can be adsorbed at other sites), we limit the investigation to adsorption at the Brønsted acid site. We are focusing on the systems of faujasite (H-FAU), which are of high importance in many industrial reactions. The faujasite's unit cell of 576 atoms limits the use of periodic calculation, thus we use the ONIOM method to model the active site of H-FAU, the Brønsted acid site. The adsorption of ethylene, benzene, and ethylbenzene on the H-FAU has been investigated, and the rational choice of the levels of calculations for the ONIOM scheme has been examined. The results are compared to experimental data to find efficient combinations to satisfactorily reproduce the adsorption energies of H-FAU zeolites. This should provide us with a better understanding of the role of H-FAU in catalyzing the process of producing ethylbenzene.

#### 2. Method

The cluster models were taken from the lattice structure of faujasite zeolite [39]. The 3T cluster H<sub>3</sub>SiOAl(OH)<sub>2</sub>O(H) SiH<sub>3</sub> (Fig. 1) is considered as the smallest unit required to represent the active site of zeolite. One of the silicon atoms in faujasite zeolites is substituted by an aluminum atom, and

a proton is added to one of the oxygen atoms bonded directly to the aluminum atom. There are four distinct bridging configurations; the resulting structures will be called O1-H, according to the usual convention for the oxygen atoms in faujasite [39,40]. The Si-H bonds are fixed along the Si-O bonds of the faujasite framework [39]. The effect from the framework structure of zeolite cannot be totally neglected if more accurate results are required. Thus, the larger clusters were proposed for representing the system of protonated faujasite (H-FAU). The 20T model, illustrated in Fig. 2, is the 12-membered-ring window connecting two supercages of faujasite, including eight more tetrahedral atoms at the base next to the Al atom. The largest 84T cluster, including two supercages, acts as a nanoscopic reaction vessel (Fig. 3) where the adsorbates can be trapped inside.

Due to the limitation of computational resources and time consumption, the active region is treated more accurately with the ab initio method, while interaction in the rest of the model is approximated by a less accurate method.

According to the two-layer ONIOM approach, the calculation of energies can be simplified by treating the active region (i.e., the active Brønsted acidic site of a zeolite catalyst) with a high-level quantum mechanical (ab initio or density functional) approach, and the extended framework environment with a less expensive level, the HF, semiempirical, and molecular mechanics force fields methods. The total energy of the whole system can be expressed within the framework of the ONIOM methodology developed by Morokuma and co-workers,

$$E_{\text{ONIOM2}} = E_{\text{Low}}^{\text{Real}} + \left(E_{\text{High}}^{\text{Cluster}} - E_{\text{Low}}^{\text{Cluster}}\right),$$

where the superscript Real means the whole system and the superscript Cluster means the active region, which would be treated with the higher level of calculation. Subscripts High and Low mean high- and low-level methodologies used in the ONIOM calculation. In this study, the high-level region is treated by the Hartree-Fock and the density functional theory with the hybrid functional B3LYP. The remainder is treated by molecular mechanics force fields (UFF) [41], semiempirical or the Hartree-Fock methods.

The accuracy of the QM/MM method, particularly the ONIOM method, depends significantly on the choice of the level of calculations for high- and low-level regions. Progressing through various types of quantum mechanics, semiempirical, and molecular mechanics methods, the experimental adsorption energy of the benzene/zeolite system can be used to validate the choice of methods. Using the B3LYP method for treating the quantum cluster, we varied the methods for the low-level region from the molecular mechanics force fields (UFF), semiempirical, over to the Hartree-Fock methods. Using the experimental observation as a benchmark, we found that the UFF method provides reasonable values corresponding to the experimental prediction. This is due to the explicit consideration of van der Waals contribution, which is the dominant contribution in adsorptiondesorption in zeolites [42-47]. Therefore, the UFF method

is the practical choice for the low-level methodology when the high-level region is treated by the B3LYP/6-31G(d,p) method.

All calculations have been performed by using Gaussian98 code [48]. The basis set for the Hartree–Fock calculations is 3-21G, while the basis set 6-31G(d,p) is utilized for the B3LYP calculations. During the structure optimization, only the active site region, [ $\equiv$ SiO(H)Al(O)<sub>2</sub>OSi $\equiv$ ], and the adsorbate are allowed to relax.

In order to obtain more reliable interaction energies, basis sets superposition error (BSSE) corrections were also taken into account. In addition, the common practice of running a higher level single-point energy calculation at the geometry generated by use of a cheaper method is as effective as performing all calculations at the higher level of theory. Thus, using the optimized geometries produced by the B3LYP/6-31G(d,p), we carried out the single-point energy calculations at the B3LYP/6-311±+G(d,p) level.

#### 3. Results and discussion

For the purpose of clarity, we separate the discussion below into two sections. In one section we compare the ONIOM results with experimental results. In the other section we focus mainly on the effects of the extended framework on the structural and energetic information of the interaction of ethylene, benzene, and ethylbenzene with H-FAU zeolites.

### 3.1. Comparison of ONIOM results with experimental results

Different two-layer ONIOM2 integrated schemes were performed on the ethylene, benzene, and ethylbenzene interaction with the different cluster models, as illustrated in Figs. 1-3. The faujasite zeolites were modeled by three different aluminosilicate clusters containing up to 84T tetrahedrally coordinated tetravalent atoms. Tables 1 and 2 list some

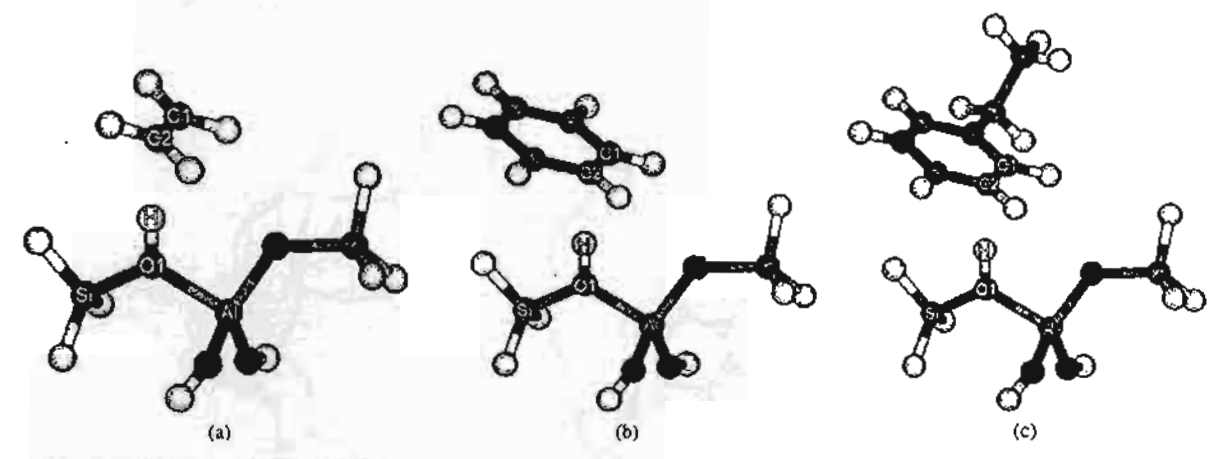


Fig. 1. Presentation of models of faujasite and interacting with adsorbates: (a) full 3T cluster model interacting with ethylene; (b) full 3T cluster model interacting with benzene; and (c) full 3T cluster model interacting with ethylbenzene.

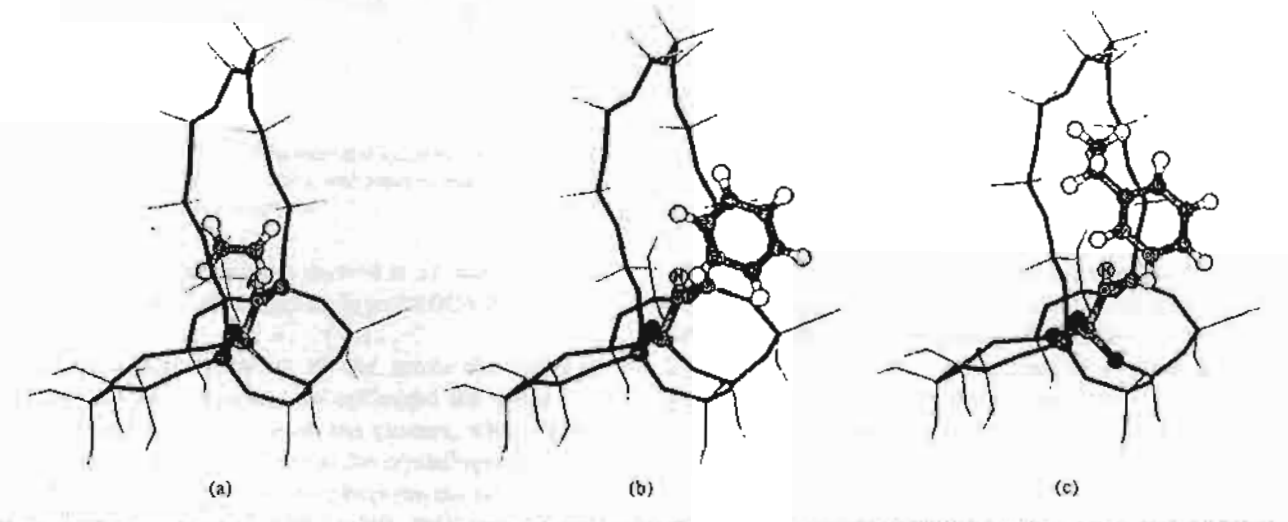


Fig. 2. Presentation of models of faujasite and interacting with adsorbates: (a) ONIOM2 layer models of 20T cluster interacting with ethylene; (b) ONIOM2 layer models of 20T cluster interacting with benzene; and (c) ONIOM2 layer models of 20T cluster interacting with ethylbenzene. Atoms belonging to the high-level regions are drawn as spheres.

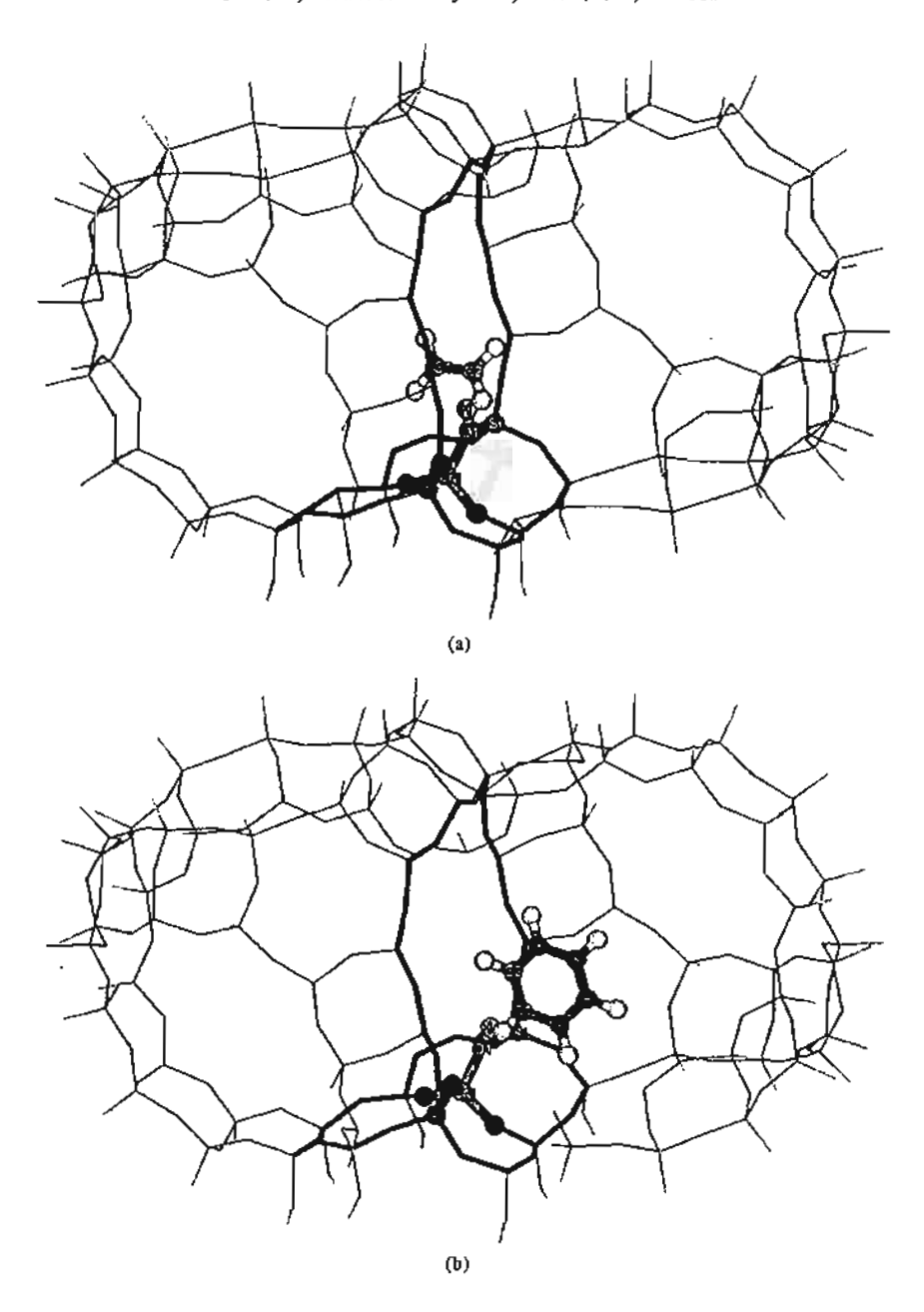


Fig. 3. Presentation of models of faujasite and interacting with adsorbates: (a) ONIOM2 layer models of 84T cluster interacting with ethylene; (b) ONIOM2 layer models of 84T cluster interacting with benzene; and (c) ONIOM2 layer models of 84T cluster interacting with ethylbenzene. Atoms belonging to the high-level regions are drawn as spheres.

selected structure parameters derived at 3T and 20T quantum clusters and the different two-layer ONIOM2 integrated schemes.

To assess the sensitivity of the active site structure with varying environments, we optimized the active site, [ $\equiv$ SiO(H)Al(O)<sub>2</sub>OSi $\equiv$ ], for all the clusters, while the remaining atoms were kept fixed at the crystallographic positions. By comparing the structure between the full quantum cluster model of 3T and 20T models, it is seen that the cluster size environment has a little effect on the structure of the active site. The extended framework has the

effect of lengthening the O1-H bond distance (Brønsted acid site) by 0.3 pm (full HF) and 0.2 pm (full B3LYP). In the ONIOM2 schemes, specifically B3LYP/6-31G(d,p):HF/3-21G and B3LYP/6-31(d,p):UFF, the O1-H bond distances are increased by 0.5 and 0.1 pm, respectively, thus enhancing the acidity of the Brønsted acid site.

Further support for the reliability of the active site subunit, [≡SiO(H)Al(O)<sub>2</sub>OSi≡], by our calculations is given from NMR studies. Klinowski and co-workers have estimated the internuclear distance between the aluminum and the proton nuclei in a Brønsted acid site, r(Al···H),

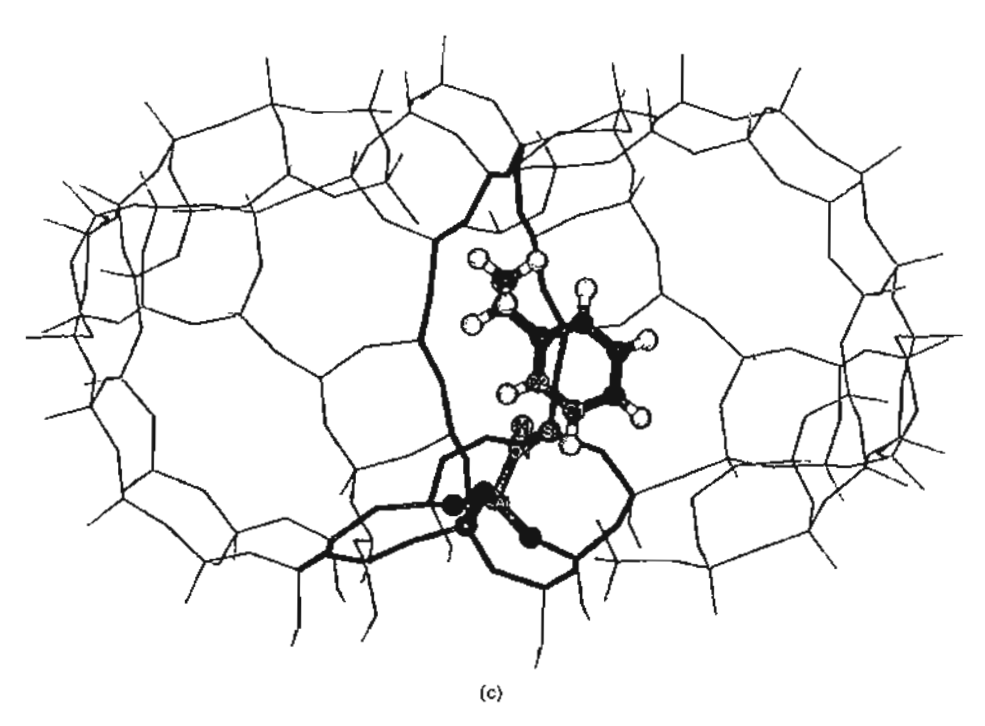


Fig. 3. Continued.

Table I
Structural parameters of faujasite obtained at full HF/3-21G and various (wo-layer ONIOM2 schemes (bond distances in pm and bond angles in degrees)

Parameters	3T			20T	<u> </u>		84T
	Full HF	Pull HF	HF:MNDO	HP:AM1	HF:PM3	HTF: UPP	HF:UFF
OI-H	96.8	97.2	96.9	97.0	96.8	96.8	96.8
AI-01	184.2	185.6	183.0	183.2	185.8	2.081	180.5
Si-OI	171.9	170.1	171.3	167.5	172.1	169.4	169.4
(AI-OI-Si	127.4	129.4	126.9	124.J	125.5	126.0	£26.0
AI-H	233.5	239.6	231.5	230.3	235.6	230.2	230.3

The HF is Hatree-Fock with 3-21G basis set.

Table 2
Structural parameters of faujasite obtained at full B3LYP/6-31G(d,p) and various ONIOM2 schemes (bond distances in pm and bond angles in degrees)

Parameters	3T	Accelerate the made as a second 20T							
	Full B3LYP	Full B3LYP	B3LYP:HF	B3LYP:MNDO	B3LYP:AM1	B3LYP:PM3	B3LYP:UFF	B3LYP:UFF	
01-11	96.7	96.9	97.2	96.8	96.8	96.7	96.8	96.8	
AI-OI	191.6	191.4	193.7	190.1	191.1	193.8	186 0	1860	
Si-Ol	170.9	170.4	168.2	170.5	166.0	170.8	168.6	168.6	
ZAI-OI-Si	126.7	128.4	129.0	126.0	122.6	123.9	125.6	125.5	
Al-H	246.0	250.8	254.3	243 4	244.6	249.6	240.0	240.2	

The B3LYP is density functional theory with 6-31G(d,p) basis set; HF is Hartree-Fock with 3-21G basis set.

of faujasite [49] to be 238.0  $\pm$  4 pm, whereas our computed  $r(Al\cdots H)$  distance of 20T cluster is evaluated to be 240.0 pm at B3LYP/6-31G(d,p). It is noted that the computed  $r(Al\cdots H)$  distances are underestimated in the cases of HF/3-21G combining with the semiempirical and molecular mechanics force fields [HF/3-21G:MNDO (231.5 pm), HF/3-21G:AM1 (230.3 pm), HF/3-21G:PM3 (235.6 pm), and HF/3-21G:UFF (230.2 pm)]. In comparison with the experimental data, the computed  $r(Al\cdots H)$  distances using the ONIOM2 scheme are well represented generally

by the B3LYP/6-31G(d,p), but not by the HF/3-21G which gives the  $r(Al\cdots H)$  too small distances, specifically at the HF/3-21G:UFF (230.2 pm) vs B3LYP/6-31G(d,p):UFF (240.0 pm). The largest model of 84T at the B3LYP/6-31G(d,p):UFF shows structure parameters consistent with those of the 20T model. This suggests that B3LYP should be employed for a high-level model. Since the ONIOM2 (B3LYP:UFF) method gives a good structural representation of the Brønsted acid site and the UFF force field is also a theoretically appropriate method for representing the ef-

Table 3
Structure parameters for adsorbate/zeolite cluster complexes, where adsorbates are ethylene, benzene, and ethylbenzene

Methods	Parameters		3T			20T	
		Ethylene	Benzene	Ethylbenzene	Ethylene	Benzene	Ethylbenzene
HOF	O1-H	97.7	97.5	97.6	98.9	98.1	98.4
	Al-O1	183.1	182.9	182.8	184.2	184.3	184.0
	\$i-O1	171.0	171.1	171.0	169. L	169.5	169.4
	∠AI-OI-Si	127.5	127.7	127.7	129.5	129.3	127.6
	C1-H	226.3	220.6	217.2	219.4	244.0	220.8
	C2-H	226.5	224.8	225.8	227.4	252.0	250.6
	C=C	132.1	138.9	138.9	132.4	138.8	139.5
	qН	0.51	0.53	0.54	0.53	0.53	0.54
	qO1(H)	-1.01	-1.01	<b>~1.01</b>	-1.03	-1.02	-1.02
	qO2	-1.10	-1.10	-1.10	-1.12	-1.12	-1.12
B3LYP	O1-H	98.5	98.0	98.2	99.3	98.4	97.9
	A1-O1	189.9	189.8	189.7	189.1	189.6	189.9
	Si-O1	170.0	170.1	170.1	169.0	169.9	170.6
	∠AI-O1-Si	126.2	126.5	126.4	128 2	127 7	127.5
	CI-H	218.6	221.4	217.7	210.8	228.0	262.8
	C2-H	219.4	224.2	224.8	217.1	255.8	273.7
	C=C	133.7	140.1	140.0	133.8	140.2	140.5
	qН	0.36	0.38	0.38	0.37	0.38	0.38
	qO1(H)	-0.66	-0.66	-0.66	-0.67	0.66	-0.66
	qO2	-0.71	-0.71	-0.71	-0.68	~0.68	-0.69

The zeolite clusters are 3T, 20T (bond distances in pm and bond angles in degrees). The B3LYP is density functional theory with 6-31G(d,p) basis set; HP is Hatree-Fock with 3-21G basis set.

fect of extended framework for this purpose (as discussed above) only the ONIOM models with the UFF force field will be discussed in detail hereafter.

### 3.2. Interactions of ethylene, benzene, and ethylbenzene with faujasite zeolites

Some structural parameters of the adsorption complexes calculated at finite clusters and at different ONIOM models (HF:UFF and B3LYP:UFF) are tabulated in Tables 3 and 4. respectively. Table 3 presents the comparison between the 3T and 20T cluster models of the adsorption complexes, indicating that adsorption does not significantly perturb structures of the adsorbed molecules or the zeolites due to the weak interactions between the hydrocarbons and the zeolite. Increasing cluster size has only a small effect on the structure of the active site, but significantly affects the orientation of the adsorbed molecules. For the small cluster models, the adsorbed molecules are Pi-bonded to the active site with almost equal bond distances between the two double-bond carbons and the Brønsted proton. For the 20T cluster models, interactions with the extended framework cause the adsorbed molecules to move farther from the acid proton and lose the symmetrical bidentated structures.

Table 4 shows structure parameters of the adsorption complexes calculated with the ONIOM2 method using 20T and 84T models showing that structures of the acid site are not affected by the increase of cluster sizes by enlarging the UFF outer layer. Similar to what was observed with the full quantum calculations at 20T, the adsorption does not significantly change the structures of the adsorbed molecules. Upon the adsorption of hydrocarbon on the acid site, the

changes in Mulliken charges on acidic proton and bridging oxygen are minute. Increasing the quantum cluster size from 3T to 20T does not have any effect on the Mulliken charges on the acidic proton and its nearby oxygen atom (cf. Table 3). The same results are also observed for the ONIOM models (cf. Table 4). This suggests that the distribution of electron in the active region is not sensitive to the size of the cluster. However, significant changes in the orientation of the adsorbed molecules compared to the full quantum calculations of 20T models at B3LYP are observed. With the 84T ONIOM model at B3YLP:UFF, the adsorbed ethylene is moved slightly farther from the acid site and symmetrically bidentated to the Brønsted proton, while the adsorbed benzene and ethylbenzene are moved significantly closer to the zeolitic proton, possibly due to the confinement effect of the pore structure represented by the UFF force field.

The adsorption energy is one of the most valuable data obtained from experimental observation which can be used to validate the theoretical data. The adsorption energies of ethylene, benzene, and ethylbenzene on H-FAU zeolites calculated from different models, as discussed above, and also those from the ONIOM models using the semiempirical and molecular mechanics force fields for the outer layer are presented in Table 5.

Using the 3T cluster model, the DFT methods predict the adsorption energies of ethylene, benzene, and ethylbenzene to be -8.14, -7.48, and -7.76 kcal/mol, respectively. This is in contradiction with the experimental results. The adsorption energy of ethylene on the acidic H-FAU zeolite was determined to be -9.1 kcal/mol [6]. The adsorption energies of benzene and ethylbenzene on H-FAU zeo-

Table 4
Structure parameters for adsorbate/zeolite cluster complexes, where adsorbates are ethylene, benzene, and ethylbenzene

Methods	Parameters		201			84T	
		Ethylene	Benzene	Ethylbenzene	Ethylene	Веплее	Ethylbenzene
HF:UFF	O1-H	97.7	97.3	97.5	97.9	97.3	97.5
	AI-OI	179.7	179.7	179.4	179.6	179.4	179.4
	Si-O1	168.7	168.9	168.8	168.7	168.9	168.9
	ZAI-O1-Si	126.2	126.4	126.3	126.2	126.5	126.4
	CI-H	218.9	225.8	220.7	223.4	222.5	226.0
	C2-H	236.0	228.3	239.8	224.7	267.4	235.7
	C=C	132.2	139.0	138.8	132.2	138.7	138.9
	qΗ	0.52	0.53	0.54	0.52	0.53	0.54
	qO1(H)	-1.02	-1.01	-1.02	-1.03	-1.01	-1.02
	qO2	-1.11	-1.11	-1.11	-1.11	-1.11	-1.11
B3LYP:UFF	O1–H	98.9	98.2	98.3	98.9	98.0	98.1
	AJ-O1	184.3	185.1	184.6	184.4	184.9	184.6
	Si-Oi	167.5	168.2	168.1	167.6	168.4	168.1
	∠Al-Ol-Si	125.3	124.9	125.0	125.3	124.9	125.2
	C1-H	214.6	217.3	215.4	214.5	219.1	229.7
	C2-H	214,7	239.7	236.1	215.2	259.4	231.0
	C=C	133.7	140.3	140.0	133.8	140.1	140.0
	qΗ	0.37	0.38	0.39	0.37	0.38	0.38
	gOI(H)	0.64	-0.63	-0.63	-0.64	-0.63	-0.63
	qO2	-0.71	-0.69	0.69	-0.71	-0.70	-0.70

The zeolite clusters are 20T, 84T (bond distances in pm and bond angles in degrees). The B3LYP is density functional theory with 6-31G(d,p) basis set; HF is Hatree-Fock with 3-21G basis set.

Table 5
Binding energy of ethylene, beazene, and ethylbeazene on the Brøasted proton of faujasite zeolites (binding energy in kcal/mol)

Methods/models		3T	_		20T			84T	
	Ethylene	Benzene	Ethylbenzene	Éthylene	Benzene	Ethylbenzene	Ethylene	Benzene	Ethylbenzene
B3LYP/6-31G(d,p)	-8.14	-7.48	-7,76	-10.93ª	-14.28ª	-15.90 <sup>a</sup>		-	_
B3LYP/6-31G(d,p):UFF	_	_	-	-10 <sub>-</sub> 78	-14.94	-18.35	~11.49	-17.15	-22.99
B3LYP/6-31G(d,p)+B\$SEd	-7.61	-6.54	-6.69	-10.25	-13.93	-17.30	-10.96	-16.15	-21.94
B3LYP/6-311++G(d,p)b	-5.39	-5.35	-5.78	-8.03	-12.23	-16,40	-8.75	-15.17	-21.08
HP/3-21G	-8.37	-9.49	-9.88	-10.90	-13.16	-17.23		-	-
HF/3-21G:UFF	-	-	-	-10.48	-16.76	-19.73	-11.43	<b>−18.33</b>	-24.09
HF/3-21G+B\$SEd	-7.85	-8.42	-8.29	-10.05	-15.74	-18.50	-10.91	-17.21	-22.84
HF/6-311++G(d,p) <sup>c</sup>	-3.28	3.47	-3.91	~6.21	10.51	11.74	-6.54	-13.69	-19.65
B3LYP/6-31G(d,p):HF/3-21G	_	-	-	-10.98	-11.40	-12,00	-	-	-
B3LYP/6-31G(d,p):MNDO	~		-	6.99	-3.37	-3.23	-	-	_
B3LYP/6-31G(d,p):AM1	-		-	-7.67	-4.49	-4.99	-	~	
B3LYP/6-31G(d,p):PM3		-	-	-5.41	-1.95	-1.13	_	-	_
HF/3-21G:MNDO	-			-7.10	-5.67	-5.65	-	-	-
HF/3-21G:AM1	-	-	-	-7.34	-6.50	-7.25	-	-	-
HF/3-21G:PM3	-	_	-	-5.63	-4.31	-4.12	-	-	-

Experimental adsorption energies of ethylene on H-FAU is -9.1 kcal/mol, taken from Ref. [6]. Experimental adsorption energies of benzene and ethylbenzene on H-FAU are -15.3! and -19.6 kcal/mol, respectively, taken from Ref. [10].

- a Mixed basis sets of 6-31G(d,p) and 3-21G.
- b Indicates single-point energy at indicated level of theory on the optimized B3LYP/6-31G(d,p): UFF structure.
- c Indicates single-point energy at indicated level of theory on optimized HF/3-21G: UFF structure.
- <sup>d</sup> Basis set superposition error corrected.

olites were experimentally measured to be  $-15.3 \pm 1$  and  $-19.6 \pm 1$  kcal/mol, respectively, indicating that the enthalpy of adsorption ( $\Delta H_{ads}$ ) of benzene is less than that of ethylbenzene [10].

Increasing the cluster size from 3T to 20T clusters, the calculated adsorption energies ( $\Delta E_{ads}$ ) of ethylene, benzene, and ethylbenzene interacted with zeolites are well differentiated (Table 5). Tests on the 20T clusters show

that the ONIOM2 schemes, only the ONIOM2(B3LYP/6-31G(d,p):UFF) but not other ONIOM2 schemes, can be compared favorably with the full HF and B3LYP levels of theory. Using semiempirical methods, i.e., AM1, PM3, and MNDO for the outer layer, the wrong trend of  $\Delta E_{\rm ads}$  is observed as compared to the experimental data. The ONIOM2 model can substantially reduce the computational expense. For example, the single-point calculation

of the 20T/ethylene complex on an SGI machine (Origin 200) requires about 5 min (computational time) for the ONIOM2(B3LYP:UFF) method whereas, the full quantum cluster requires more than 50 min. This again confirms that the cost-effective ONIOM2 strategy should be utilized to obtain an accurate description of the system.

Increasing the cluster size from 20T up to the more realistic model, 84T, by enlarging the outer layer, the differences between each adsorption energy are pronounced. The adsorption energies of ethylene, benzene, and ethylbenzene calculated from the 84T cluster using ONIOM2 (B3LYP/6-31G(d,p):UFF) are calculated to be -11.49, -17.15, and -22,99 kcal/mol, respectively. These interaction energies are somewhat overestimated as compared to the experimental results. Including the basis set correction by single-point calculations at the higher basis set, 6-311++G(d,p), the corresponding interaction energies are predicted to be of -8.75, -15.17, and -21.08 kcal/mol. The BSSE corrections were also performed and gave similar results as the single-point calculations at the high basis set (see Table 5). These results are in good agreement with the experiment [6,10]. However, one may question if the energy could change if the model becomes bigger and bigger. To ensure the convergence of the ONIOM model, the structure optimization of a larger model of 336T with ethylbenzene has been carried out at the HF:UFF level of calculation. The adsorption energy of -24.60 kcal/mol from the 336T model is almost identical to the 24.09 kcai/mol from the 84T model at the same level of calculation, indicating that the use of the 84T ONIOM model is practical and increasing the model size would not have any profound effect on the energetics of the system.

It is noted that the choices of the methods using the highand low-levels in the ONIOM scheme and also the sizes of the inner and outer regions are arbitrary. The size of the inner region employed in this study (3T cluster) is sufficient to represent the acid property of zeolites while small enough to guarantee that the van der Waals interactions between the hydrocarbon and the zeolite are well accounted for by the UFF force field, which is better than the DFT for this purpose [45-47]. Using the larger inner region, which may require the use of the MP2 level of theory in place of DFT, will be advantageous in searching for the transition state leading from ethylene and benzene to ethylbenzene. This challenging reaction is being actively pursued. From the structure and adsorption energy point of views, the B3LYP combining the UFF force fields method as a lower level is considered to be one of the best combinations for the ONIOM2 scheme. This efficient scheme provides a cost-effective computational strategy for treating the effects of a large extended framework structure.

#### 4. Conclusions

The adsorption of ethylene, benzene, and ethylbenzene on H-FAU zeolites has been investigated with three dif-

ferent cluster sizes and methods comprising various twolevel ONIOM2 schemes. The bare 3T B3LYP/6-31G(d,p) quantum cluster approach predicts the ethylene/H-FAU, benzene/H-FAU, and ethylbenzene/H-FAU complexes to have the binding energies of -8.14, -7.48, and -7.76 kcal/ mol, respectively. The effect of the zeolite framework is modeled on the ONIOM2 method. We found that the extended framework significantly enhances their adsorption energy of adsorbates to the zeolites. In particular, the final predicted adsorption energies of -8.75, -15.17, and -21.08 kcal/mol, for the ethylene/H-FAU, benzene/H-FAU, and ethylbenzene/H-FAU complexes were calculated by the ONIOM2(B3LYP/6-311++G(d,p):UFF) scheme. This efficient scheme performs superbly when compared with the experimental estimates of -9.1, -15.3, and -19.6 kcal/mol, respectively. The results obtained in the present study suggest that the ONIOM approach yields a more accurate and practical model in studying the adsorption of unsaturated hydrocarbons on zeolites.

#### Acknowledgments

This work was supported in part by grants from the Thailand Research Fund (TRF Senior Research Scholar to J.L.) and the Kasetsart University Research and Development Institute (KURDI) as well as the Ministry of University Affairs under the Science and Technology Higher Education Development Project (MUA-ADB funds). The support from the Dow Chemical Company (USA) is also acknowledged. All comments and suggestions from the reviewers are sincerely appreciated. Our sincere thanks are due to Professor R. Ahlrichs (Karlsruhe, Germany) for his continued support of this work.

#### References

- T.F. Degnan Jr., C.M. Smith, C.R. Venkat, Appl. Catal. A 221 (2001) 283.
- [2] G. Bellussi, G. Pazzuconi, C. Perego, G. Girouit, G. Terzonit, J. Catal. 157 (1995) 227.
- [3] C.R.A. Catlow, Modeling of Structure and Reactivity in Zeolite, Academic Press, San Diego, CA, 1992.
- [4] B. Kontnik-Matecka, M. Gorska, J. Eysymott, A. Salek, J. Mol. Struct. 80 (1982) 199.
- [5] B.V. Liengme, W.K. Hall, Trans. Faraday Soc. 62 (1966) 3229.
- [6] N.W. Cant, W.K. Hall, J. Catal. 25 (1972) 161.
- (7) Y. Du, H. Wang, S. Chen, J. Mol. Catal. A 179 (2002) 253.
- (8) J.L. White, L.W. Beck, J.F. Haw, J. Am. Chem. Soc. 114 (1992) 6182.
- [9] E.G. Derouane, J.B. Nagy, J.P. Gilson, Z. Gabrlica, Stud. Surf. Sci. Catal. 7 (1981) 1412.
- [10] E.N. Coker, C. Jia, H.G. Karge, Langmuir 16 (2000) 1205.
- [11] R. Shah, J.D. Gale, M.C. Payne, Chem. Commun. (1997) 131.
- [12] Y. Jeanvoine, J.G. Angyan, G. Kresse, J. Hafner, J. Phys. Chem. B 102 (1998) 5573.
- [13] H.I. Hillier, J. Mol. Struct. (Theochem.) 463 (1999) 45.
- [14] J. Limtrakul, S. Jungsuttiwong, P. Khongpracha, J. Mol. Struct. 525 (2000) 153.
- [15] J. Sauer, M. Sierka, J. Comput. Chem. 21 (2000) 1470.

- [16] J. Sauer, P. Ugliengo, E. Garrone, V.R. Saunders, Chem. Rev. 94 (1994) 2095.
- [17] J. Sauer, Chem. Rev. 89 (1989) 199.
- [18] J. Limtrakul, Chem. Phys. 193 (1995) 79.
- [19] J. Limtrakul, P. Treesukol, C. Ebner, M. Probst, Chem. Phys. 215 (1997) 77.
- [20] P.E. Sinclair, A.H. de Vries, P. Sherwood, C.R.A. Catlow, R.A. van Santen, J. Chem. Soc., Faraday Trans. 94 (1998) 3401.
- [21] M. Brandle, J. Sauer, J. Am. Chern. Soc. 120 (1998) 1556.
- [22] S.P. Greatbanks, I.H. Hillier, N.A. Burton, P. Sherwood, J. Chem. Phys. 105 (1996) 3370.
- [23] R.Z. Khaliullin, A.T. Bell, V.B. Kazansky, J. Phys. Chem. A 105 (2001) 10454.
- [24] J. Limtrakul, T. Nanok, P. Khongpracha, S. Jungsuttiwong, T.N. Truong, Chem. Phys. Lett. 349 (2001) 161.
- [25] A.H. de Vries, P. Sherwood, S.J. Collins, A.M. Rigby, M. Rigutto, G.J. Kramer, J. Phys. Chem. B 103 (1999) 6133.
- [26] M. Svensson, S. Humbel, R.D.J. Froese, T. Matsubara, S. Sieber, K. Morokuma, J. Phys. Chem. (1996) 19357.
- [27] S. Dapprich, I. Komaromi, K.S. Byun, K. Morokuma, M.J. Frisch, J. Mol. Struct. (Theochem.) 461 (1999) 1.
- [28] H.R. Tang, K.N. Fan, Chem. Phys. Lett. 330 (2000) 509.
- [29] I. Roggero, B. Civalleri, P. Ugliengo, Chem. Phys. Lett. 341 (2001) 625
- [30] K. Siliar, P. Burk, J. Mol. Struct. (Theochem.) 589 (2002) 281.
- [31] C. Raksakoon, J. Limurakul, J. Mol. Struct. (Theochem.) 2003, in press.
- [32] X. Solans-Monfort, J. Bertran, V. Branchadell, M. Sodupe, J. Phys. Chem. B 106 (2002) 10220.
- [33] A. Damin, F. Bonino, G. Ricchiardi, S. Bordiga, A. Zecchina, C. Lamberti, J. Phys. Chem. B 106 (2002) 7524.
- [34] M. Torrent, T. Vreven, D.G. Musaev, K. Morokuma, J. Am. Chem. Soc. 124 (2002) 192.

- [35] P.B. Venuto, L.A. Hamilton, P.S. Landis, J. Catal. 5 (1966) 484.
- [36] K.A. Becker, H.G. Karge, W.D. Streubel, J. Catal. 28 (1973) 403.
- [37] A. Corma, V. Martinez-Soria, E. Schnoeveld, J. Catat. 192 (2000) 163.
- [38] M. Sierka, J. Sauer, J. Phys. Chem. B 105 (2001) 1603.
- [39] D.H. Olson, E. Dempsey, J. Catal. 13 (1969) 221.
- [40] J.R. Hill, C.M. Freeman, B. Delfey, J. Phys. Chem. A 103 (1999) 3772.
- [41] A.K. Rappe, C.J. Casewit, K.S. Colwell, W.A. Goddard, W.M. Skiff, J. Arn. Chem. Soc. 114 (1992) 10024.
- [42] A. Pelmenschikov, J. Leszczynski, J. Phys. Chem. B 103 (1999) 6886.
- [43] T.A. Wesotowski, O. Parisel, Y. Ellinger, J. Weber, J. Phys. Chem. A 101 (1997) 7818.
- [44] E.G. Derouane, C.D. Chang, Micropor. Mesopor. Mater. 35-36 (2000) 425.
- [45] L.A. Clark, M. Sierka, J. Sauer, J. Am. Chem. Soc. 125 (2003) 2136.
- [46] A.M. Vos, X. Rozanska, R.A. Schoonheydt, R.A. van Santen, F. Hutschka, J. Hafner, J. Am. Chem. Soc. 123 (2001) 2799.
- [47] X. Rozanska, R.A. van Santen, F. Hutschka, J. Hafner, J. Am. Chem. Soc. 123 (2001) 7655.
- [48] M.J. Frisch, G.W. Trucks, H.B. Schlegel, O.E. Scuseria, M.A. Robb, J.R. Cheeseman, V.G. Zakrzewski, J.A. Montgomery, R.E. Stratmann Jr., J.C. Burant, S. Dapprich, J.M. Millam, A.D. Daniels, K.N. Kudin, M.C. Strain, O. Farkas, J. Tomasi, V. Barone, M. Cossi, R. Cammi, B. Mennucci, C. Pornelli, C. Adamo, S. Clifford, J. Ochterski, G.A. Petersson, P.Y. Ayala, Q. Cui, K. Morokuma, P. Salvador, J.J. Dannenberg, D.K. Malick, A.D. Rabuck, K. Raghavachari, J.B. Foresman, J. Cioslowski, J.V. Ortiz, A.G. Baboul, B.B. Stefanov, G. Liu, A. Liashenko, P. Piskorz, I. Komaromi, R. Gomperts, R.L. Martin, D.J. Fox, T. Keith, M.A. Al-Laham, C.Y. Peng, A. Nanayakkara, M. Challacombe, P.M.W. Gill, B. Johnsoo, W. Chen, M.W. Wong, J.L. Andres, C. Gonzalez, M. Head-Gordon, E.S. Replogle, J.A. Pople, Gaussian'98, Gaussian, Inc., Pittsburgh, PA, 2001.
- [49] D. Frende, J. Klinowski, H. Harndan, Chem. Phys. Lett. 149 (1988) 355.



#### Available online at www.sciencedirect.com







### Effects of the zeolite framework on the adsorption of ethylene and benzene on alkali-exchanged zeolites: an ONIOM study

#### Karan Bobuatong, Jumras Limtrakul\*

Laboratory for Computational & Applied Chemistry, Physical Chemistry Division, Department of Chemistry, Faculty of Science, Kasetsart University, Bangkok 10900, Thailand

Received 9 June 2003; received in revised form 9 June 2003; accepted 10 June 2003

#### Abstract

The density functional theory (B3LYP/6-31G(d,p)) and our-own-N-layered integrated molecular orbital + molecular mechanics (ONIOM) approach utilizing two-layer ONIOM schemes (B3LYP/6-31G(d,p): UFF) have been employed to investigate the structures of alkali-exchanged faujasite (FAU) and ZSM-5 zeolites, and their interactions with ethylene and benzene. Inclusion of the extended zeolite framework has an effect on the structure and energetics of the adsorption complexes and leads to differentiation of different types of zeolites (ZSM-5 and FAU), which cannot be drawn from typical small quantum clusters. The ONIOM binding energies of the Li-ZSM-5 and Li-FAU zeolites that are bound to an ethylene are -16.94 and -14.27 kcal/mol, respectively, and to a benzene are -28.78 and -19.46 kcal/mol, respectively, which agrees favorably with the known adsorption trend of these two zeolites. On the other hand, the quantum cluster models yield virtually the same binding energies for both zeolites/ $C_2H_4$  complexes (-12.25 kcal/mol versus -12.91 kcal/mol) and even yield an unreasonable trend of adsorption energies for zeolites/C<sub>6</sub>H<sub>6</sub> complexes (-11.91, -15.75 kcal/mol, for Li-ZSM-5 and Li-FAU, respectively). For the larger cation-exchanged Na-ZSM-5/C<sub>2</sub>H<sub>4</sub> and Na-FAU/C<sub>2</sub>H<sub>4</sub> complexes, the calculated interaction energies (-15.67 kcal/mol versus -11.83 kcal/mol) are predicted to be lower than those of smaller Li-zeolites following the conventional electrostatic trend. With the inclusion of basis set correction and the effects of the extended framework included in the ONIOM model, the interaction energy for the Na-FAU/C<sub>2</sub>H<sub>4</sub> complex is predicted to be -8.65 kcal/mol, which can be compared favorably with the experimental data (8.8-9.6 kcal/mol) for ethylene adsorption on a Na-Y zeolite. © 2003 Elsevier B.V. All rights reserved.

Keywords: ZSM-5 zeolite; Paujasite zeolite; DFT-study; Ethylene adsorption; ONIOM

#### 1. Introduction

Zeolites are of prime importance as catalysts for many industrial processes, due mainly to their shape-selectivity and acid sites [1–9]. Cation-exchanged zeolites have been found to be potential catalysts for hydrocarbon reaction [10–19]. Of particular inter-

aliphatic and aromatic hydrocarbon adsorption on alkali-exchanged zeolite that is the foundation of several industrially important reactions, namely, aromatization of olefins [18], formation of ethylbenzene and styrene [19], and the production of xylene [20].

est, in this area of active research, is the unsaturated

The importance of metal-exchanged zeolites suggests that a better understanding of structure and mechanistic properties at the molecular level of the catalyst is certainly required [21]. A review of quantum chemical calculations applied to zeolites and their

fax: 4-66-2-9428900x324.

E-mail address: fscijrl@ku.ac.th (I. Limtrakul).

<sup>\*</sup> Corresponding author. Tel.: +66-2-9428900x323;

interaction with unsaturated aliphatic and aromatic hydrocarbons has been recently reported [22–26]. All early works of adsorption of C<sub>2</sub>H<sub>4</sub> [22–26] and C<sub>6</sub>H<sub>6</sub> [27] on bare zeolite clusters were limited to the small model fragments that are not specific to a particular zeolite, but represent a generic tetrahedral subunit in an unconstrained environment [22–26,28–30]. It is known that small zeolitic clusters may inadequately reflect adsorption complexes at the active site and the cluster environment may enhance binding energy, and hence, more accurately predict the structures of reaction intermediates, transition states and products [31–41].

Numerous theoretical models, including the periodic calculations, have been proposed to study the crystalline zeolite [1-9,23-26,32-42]. Nevertheless, zeolites that have a high impact in industrial processes usually possess hundreds of atoms per unit cell. This makes the use of sophisticated methods, such as periodic ab initio calculations, computationally too expensive and impractical. Therefore, the electronic properties of zeolites are usually modeled with quantum chemical methods for relatively small clusters, where only the most important part of zeolites is focused [1-9]. With such limited models, the effect of the framework which may change the structure and energetic of the system is not taken into account. The recent development of hybrid methods, such as embedded cluster or combined quantum mechanics/molecular mechanics (QM/MM) methods [31-40], as well as the more general our-own-N-layered integrated molecular orbital + molecular mechanics (ONIOM) method has brought a larger system within reach of obtaining accurate results [43,44].

Up to the present time, the ONIOM method is applied to the study of extended systems, for example, chemical reactions on surface [45–48], and in enzymes [49]. However, there are no reports of the ONIOM method on alkali-exchanged zeolites interacted with unsaturated aliphatic and aromatic hydrocarbons.

In this study, we are focusing on the systems of ZSM-5 and faujasite (FAU), which are of high importance in many industrial reactions. The zeolites' unit cell of many atoms (FAU: 576 atoms and ZSM-5: 288 atoms) limits the use of periodic calculation, but we are able to use the ONIOM method to model the active site of these alkali-exchanged zeolites. The adsorption of ethylene on alkali-exchanged zeolites has

been investigated, and the rational choice of the levels of calculations for the ONIOM scheme have been examined. The results are compared to experimental data to find efficient combinations to satisfactorily reproduce the adsorption energies of alkali-exchanged zeolites. This should provide us with a better understanding of the role of alkali-exchanged zeolites for hydrocarbon reactions.

#### 2. Methods

Two different strategies have been employed to model the alkali-exchanged zeolites. First, two quantum clusters (B3LYP/6-31G(d,p)) of 10T-ZSM-5, and 12T-FAU models are modeled to represent the active sites of ZSM-5 and FAU zeolites, whilst the second strategy employs the ONIOM2 (B3LYP/6-31G(d,p): UFF) approach for the more realistic models of 46T-ZSM-5 and 84T-FAU.

The cluster models of ZSM-5 and FAU were obtained from their crystal lattice structures of H-ZSM-5 and FAU zeolites, respectively [50,51]. The 10T-ZSM-5 cluster is the 10-membered-ring window representing the zigzag gateway of the ZSM-5 zeolite that is large enough to allow the probe molecule to move freely (Figs. 3a, 4a and 6a). The 12T-FAU cluster is the 12-membered-ring window connecting two supercages of FAU zeolite (Figs. 1a, 2a and 5a).

The effect from the extended framework structure of zeolite cannot be totally neglected if more accurate results are required. Thus, realistic clusters were proposed for representing the systems of H-ZSM-5 and FAU using the ONIOM scheme. However, due to the limitation of computational resources and time consumption, only the active region is treated more accurately with the ab initio method, while interaction in the rest of the model is approximated by a less accurate method. As for ZSM-5 zeolite, the 46T cluster, covering the 10T active region and three different channel structures (channel intersection, the straight channel, and the zigzag channel)-where the reaction normally takes place—is selected (Figs. 3b, 4b and 6b). Regarding FAU, the 84T model containing the active region of the 12T membered-ring surrounded by two supercages, where the adsorbates can be trapped inside, is chosen (Figs. 1b, 2b and These selected models for the ZSM-5 and FAU

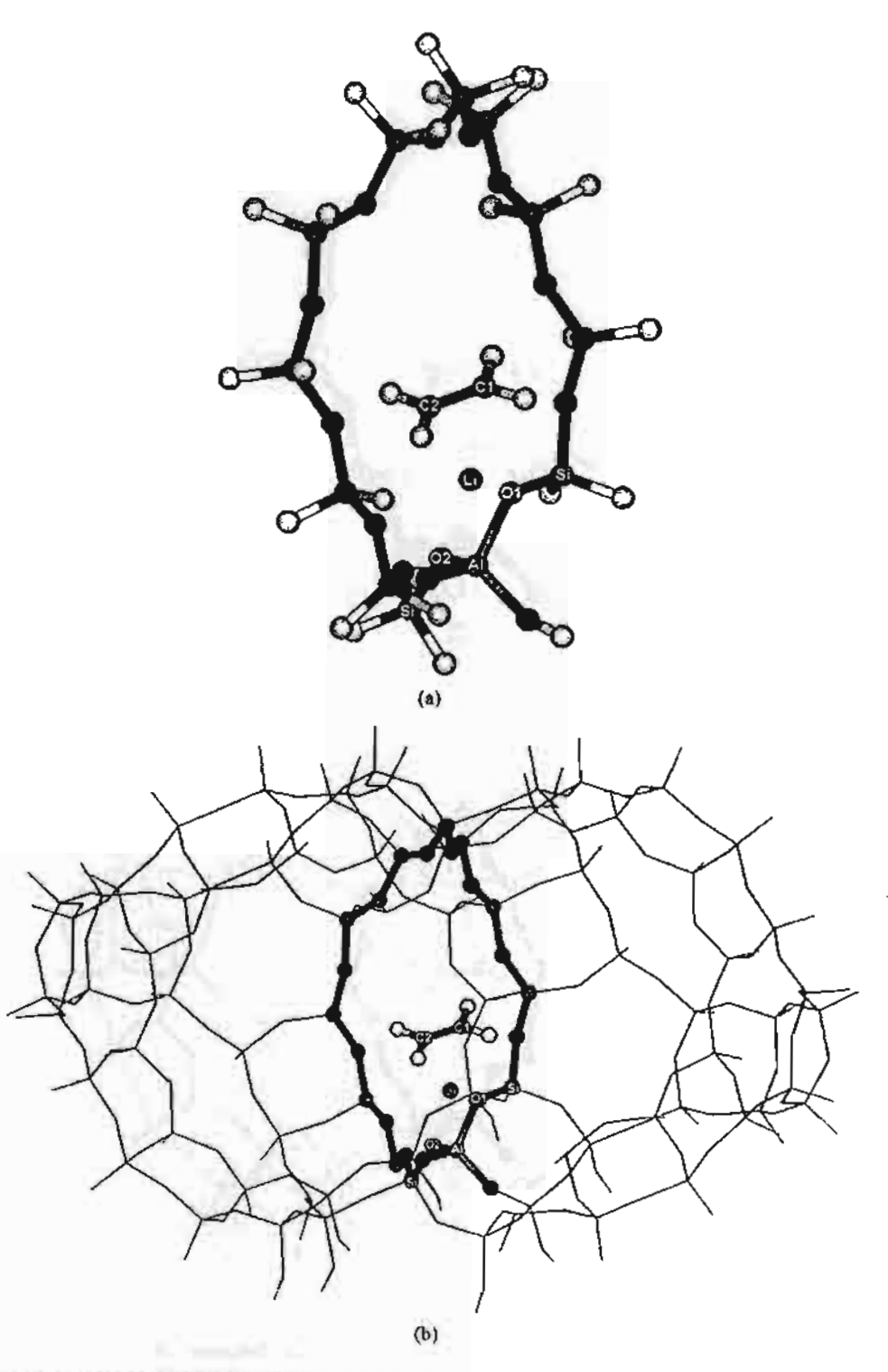


Fig. 1. Optimized structures of  $C_2H_4$  interacted with Li-FAU zeolite. (a) 12T bare quantum cluster model of the Li-FAU/ $C_2H_4$  complex. (b) 84T ONIOM model of the Li-FAU/ $C_2H_4$  complex. Atoms belonging to the 12T quantum cluster drawn as spheres.

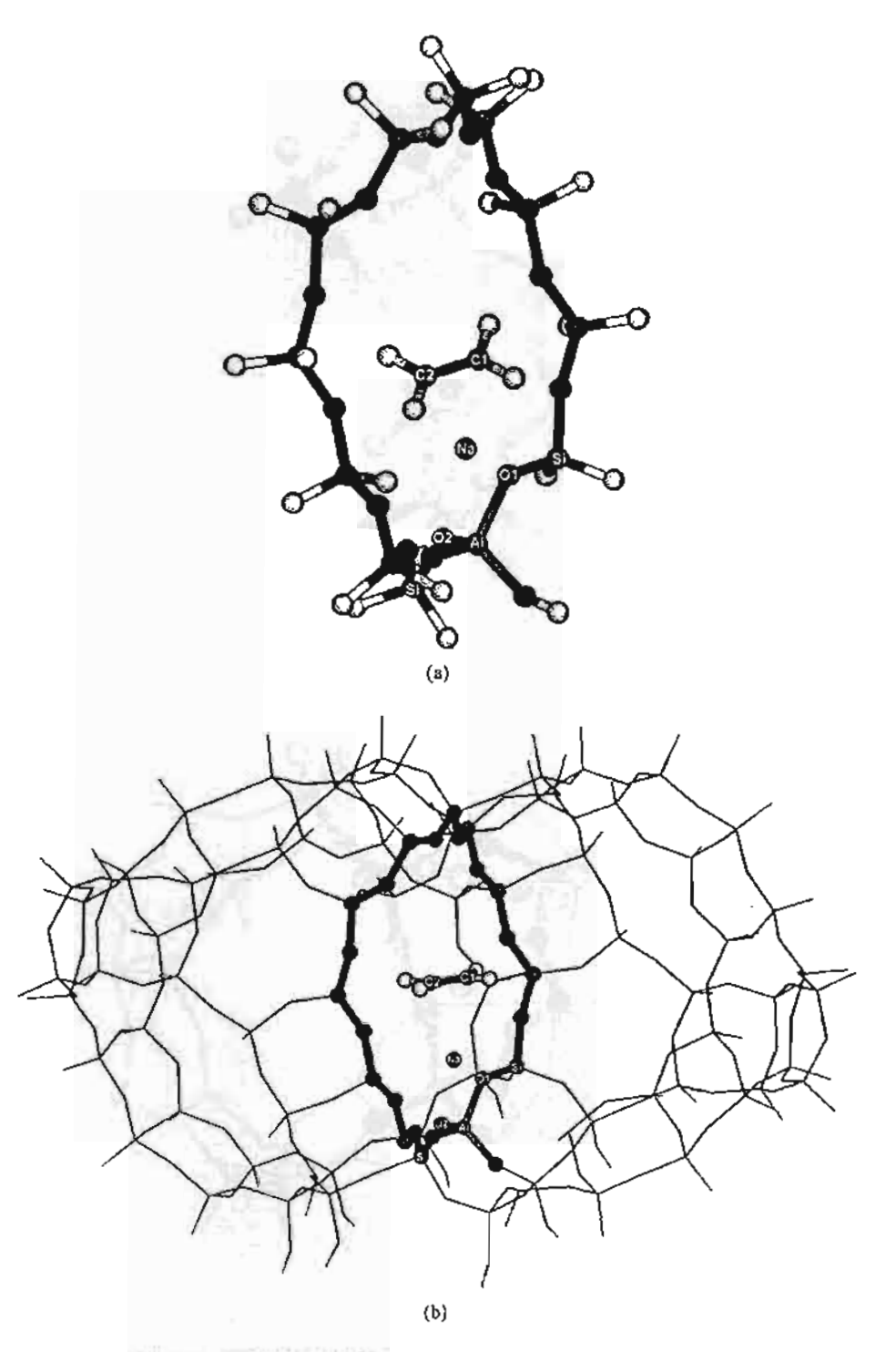


Fig. 2. Optimized structures of  $C_2H_4$  interacted with Na-FAU zeolite. (a) 12T bare quantum cluster model of the Na-FAU/ $C_2H_4$  complex. (b) 84T ONIOM model of the Na-FAU/ $C_2H_4$  complex. Atoms belonging to the 12T quantum cluster drawn as spheres.

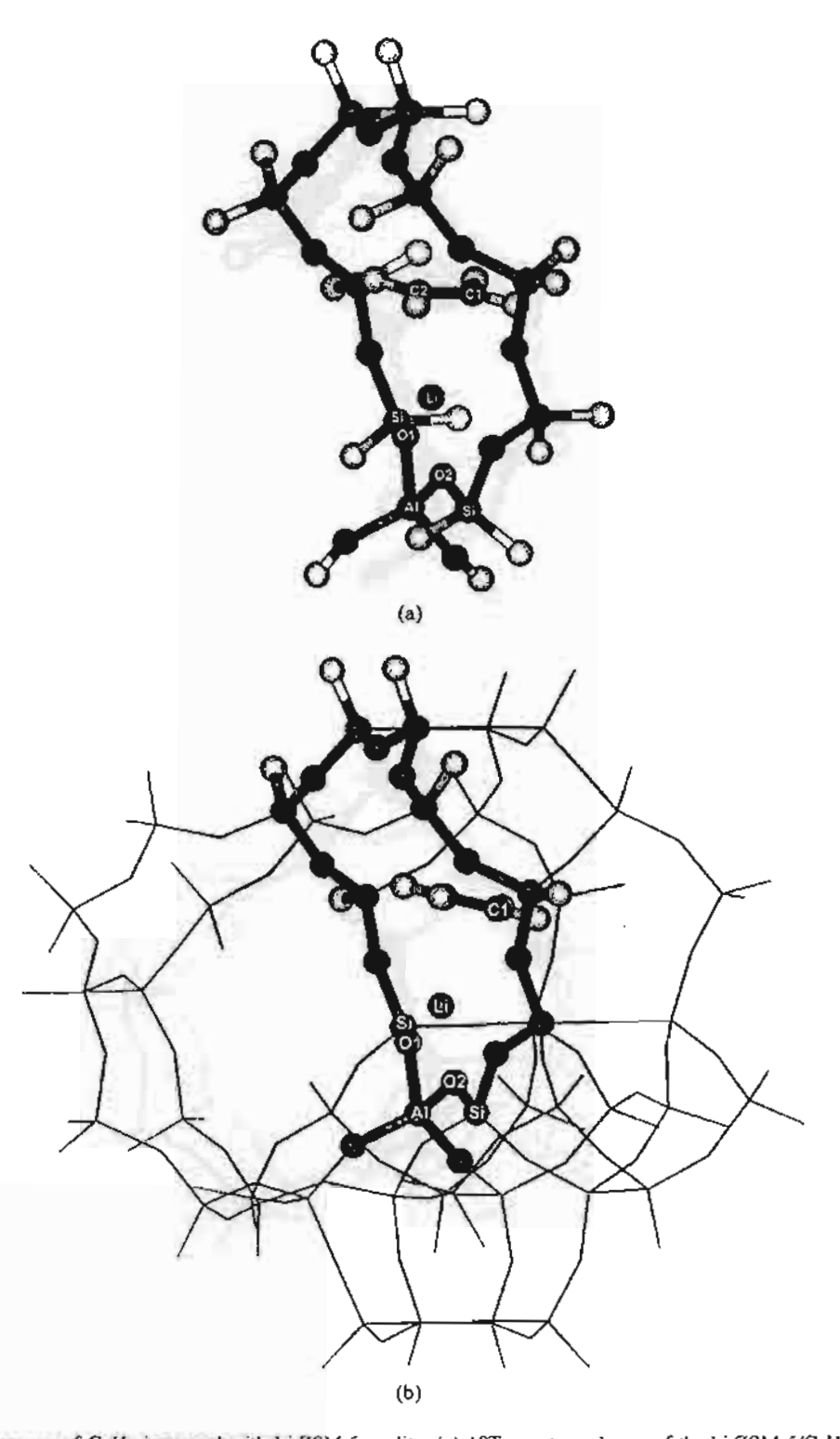


Fig. 3. Optimized structures of  $C_2H_4$  interacted with Li-ZSM-5 zeolite. (a) 10T quantum cluster of the Li-ZSM-5/ $C_2H_4$  complex. (b) 46T ONIOM model of the Li-ZSM-5/ $C_2H_4$  complex. Atoms belonging to the 10T quantum cluster drawn as spheres.

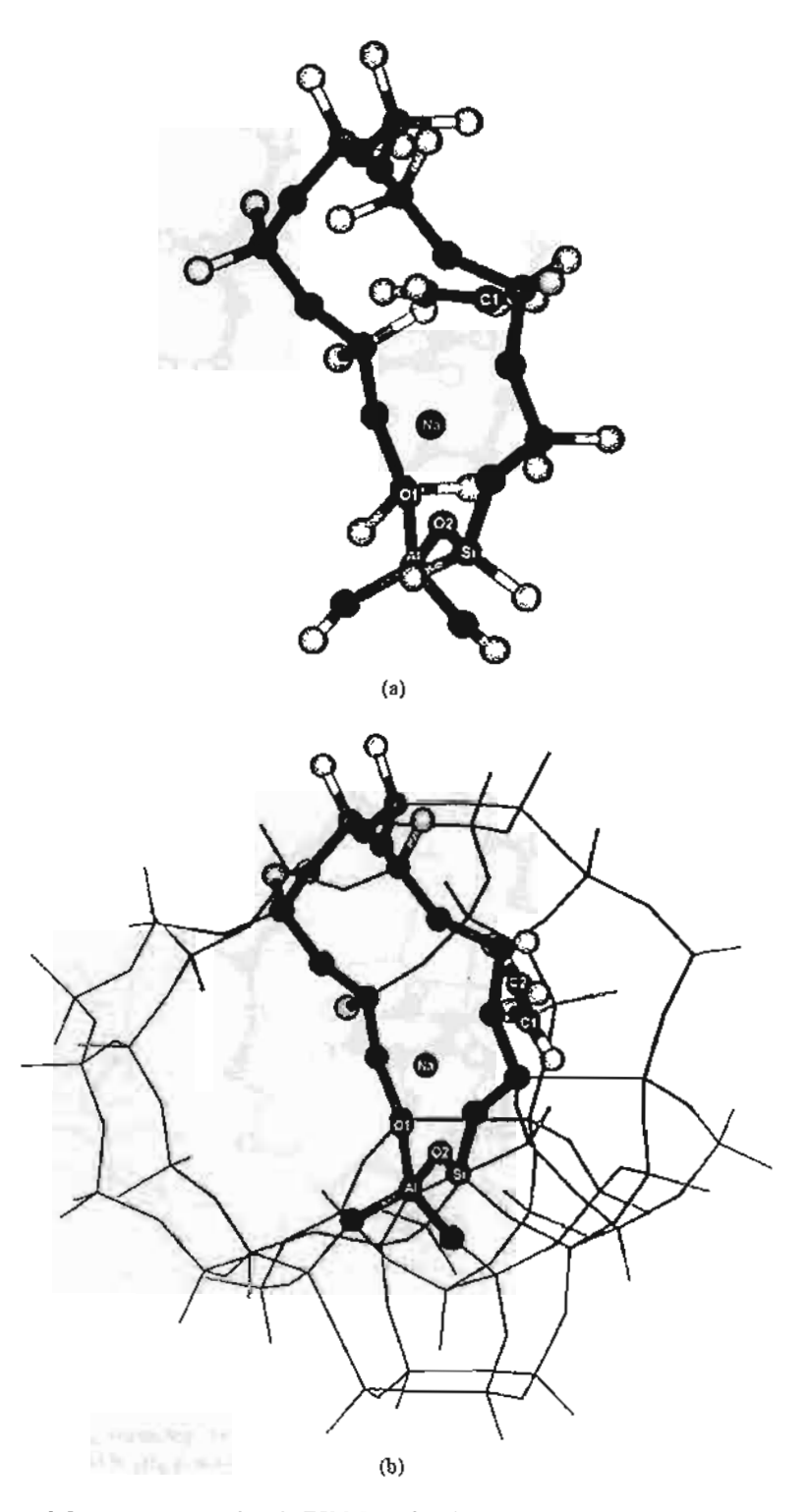


Fig. 4. Optimized structures of  $C_2H_4$  interacted with Na-ZSM-5 zeolite. (a) 10T bare quantum cluster model of the Na-ZSM-5/ $C_2H_4$  complex. (b) 46T ONIOM model of the Na-ZSM-5/ $C_2H_4$  complex. Atoms belonging to the 10T quantum cluster drawn as spheres.

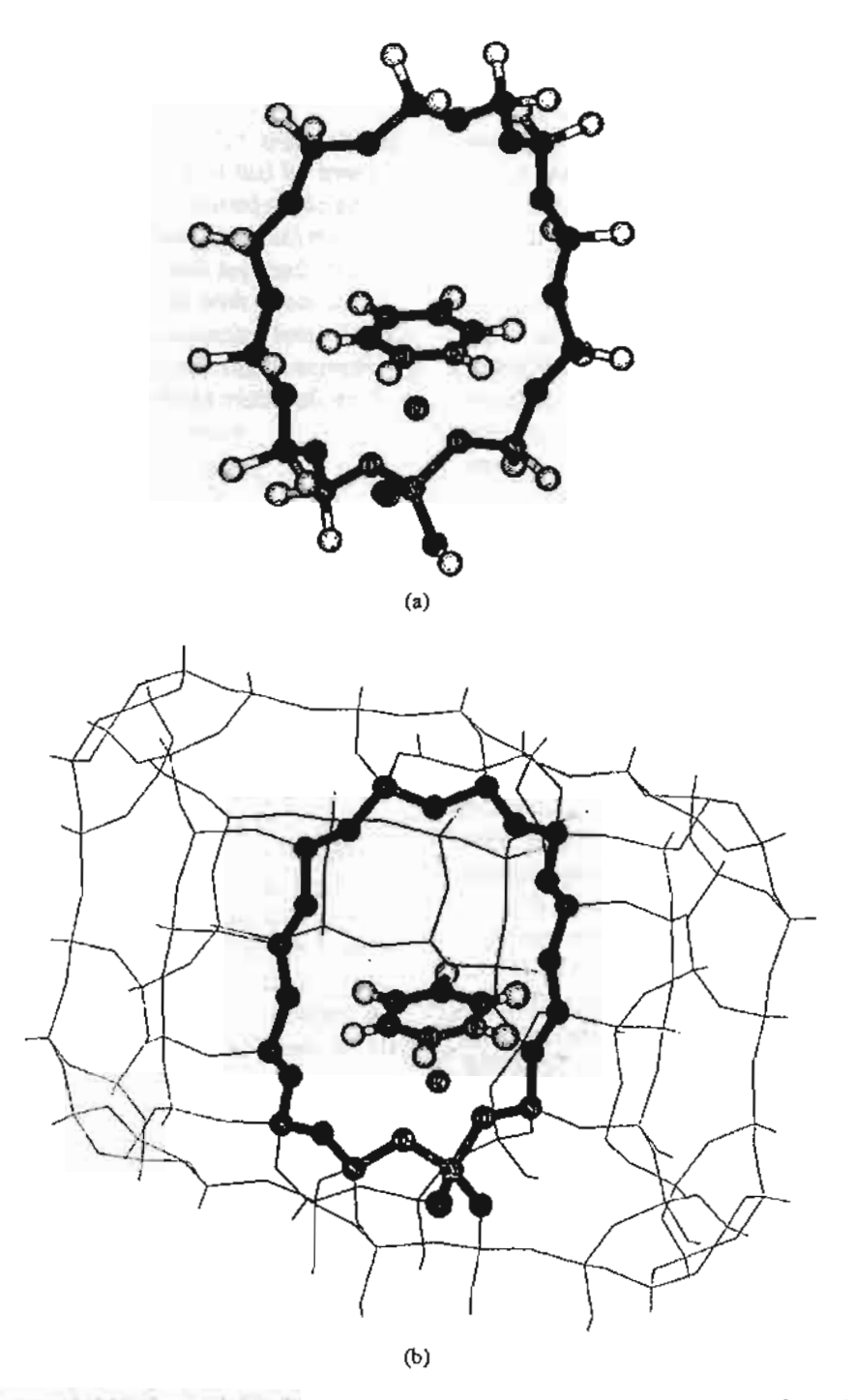


Fig. 5. Optimized structures of  $C_6H_6$  interacted with Li-FAU zeolite. (a) 12T bare quantum cluster model of the Li-FAU/ $C_6H_6$  complex. (b) 84T ONIOM model of the Li-FAU/ $C_6H_6$  complex. Atoms belonging to the 12T quantum cluster drawn as spheres.

zeolites are considered to be large enough to cover all the important framework effects acting on both the active site and on the adsorbates.

According to the two-layer ONIOM approach, the calculation of energies can be simplified by treating the active region (i.e. the active Brønsted acidic site of a zeolite catalyst), with a high-level quantum mechanical (ab initio or density functional) approach and the extended framework environment with a less expensive level, HF and molecular mechanics force fields. The total energy of the whole system can be expressed within the framework of the ONIOM methodology developed by Morokuma and co-workers

$$E_{\text{ONIOM2}} = E_{\text{Low}}^{\text{Real}} + (E_{\text{High}}^{\text{Cluster}} - E_{\text{Low}}^{\text{Cluster}})$$

where the superscript Real means the whole system and the superscript Cluster means the active region, which would be treated with the higher level of calculation. Subscripts High and Low mean high- and low-level methodologies used in the ONIOM calculation. In this study, the high-level region is treated with the density functional theory with the hybrid functional B3LYP. The rest is treated by molecular mechanics force field (UFF).

The accuracy of the QM/MM methods, particularly the ONIOM method, depends significantly on the choices of the level of calculations for high- and low-level regions. Going through various types of quantum mechanics and molecular mechanics methods, the experimental adsorption energy of the hydrocarbon/zeolite system can be used to validate the choice of methods. Using the B3LYP method for treating the quantum cluster, we varied the methods for the low-level region from the molecular force field (UFF) to the Hartree-Fock method. Using the experimental observation as a benchmark, we found that the molecular mechanics force field, particularly the UFF, method provide reasonable values corresponding to the experimental prediction (-15.17 kcal/mol versus -15.30 kcal/mol are adsorption energies for benzene adsorption on protonated FAU observed at the ONIOM2 (B3LYP/6-31G(d,p): UFF, BSSE corrected) and experimental data, respectively) [48]. This is due to the fact that the UFF force field considers van der Waals interactions explicitly [52,53]. Therefore, it can reasonably account for van der Waals interactions, which have been reported to have significant contributions to adsorption-desorption of probe molecules in zeolites [54-59]. While the Hartree-Fock method, which cannot describe accurately van der Waals contributions, poorly estimates the adsorption energy. This suggests that the UFF force field method is the practical choice for the low-level methodology when the high-level region is treated by the DFT/B3LYP method.

All calculations have been performed by using the Gaussian 98 code [60]. During the structure optimization, only the 3T portion of the active site region  $[\equiv SiO(H)Al(O)_2OSi\equiv]$ , and the adsorbate are allowed to relax while the rest is fixed at the crystallographic coordinates [50,51]. In calculations of the interaction energy,  $\Delta E$  between two systems (A, B) based on the molecular orbital method, the value of  $\Delta E$  is determined as the difference between subsystem energy  $E_{AB}$  and the sum of the subsystem energies ( $E_{A}$ ,  $E_{B}$ )

$$\Delta E \text{ (kcal/mol)} = (E_{AB} - E_{A} - E_{B})$$

where  $E_{AB}$  is the subsystem energy and  $E_A$ ,  $E_B$  are the isolated energies of subsystems A and B, respectively.

In order to obtain more reliable interaction energies, basis sets superposition error (BSSE) corrections were also taken into account. In addition, the common practice of running a higher-level single-point energy calculation at the geometry generated by use of a cheaper method is as effective as performing all calculations at the higher level of theory [61]. Thus, using the optimized geometries produced by the B3LYP/6-31G(d,p), we carried out the single-point energy calculations and BSSE corrections at the B3LYP/6-311++G(d,p) level.

#### 3. Results and discussion

#### 3.1. Structure of Li- and Na-zeolites

Bare quantum cluster and ONIOM models for alkali metal-exchanged zeolites are shown in Figs. 1-6. Selected, optimized geometrical structures for the bare quantum cluster and ONIOM models are documented in Table 1. For the Li-exchanged zeolites, the alkali-metal cation does not bind with a particular bridging oxygen atom in the [AlO<sub>4</sub>]<sup>-</sup>, but is symmetrically bidentated to O1 and O2 of [AlO<sub>4</sub>]<sup>-</sup> tetrahedron. The symmetric binding between the

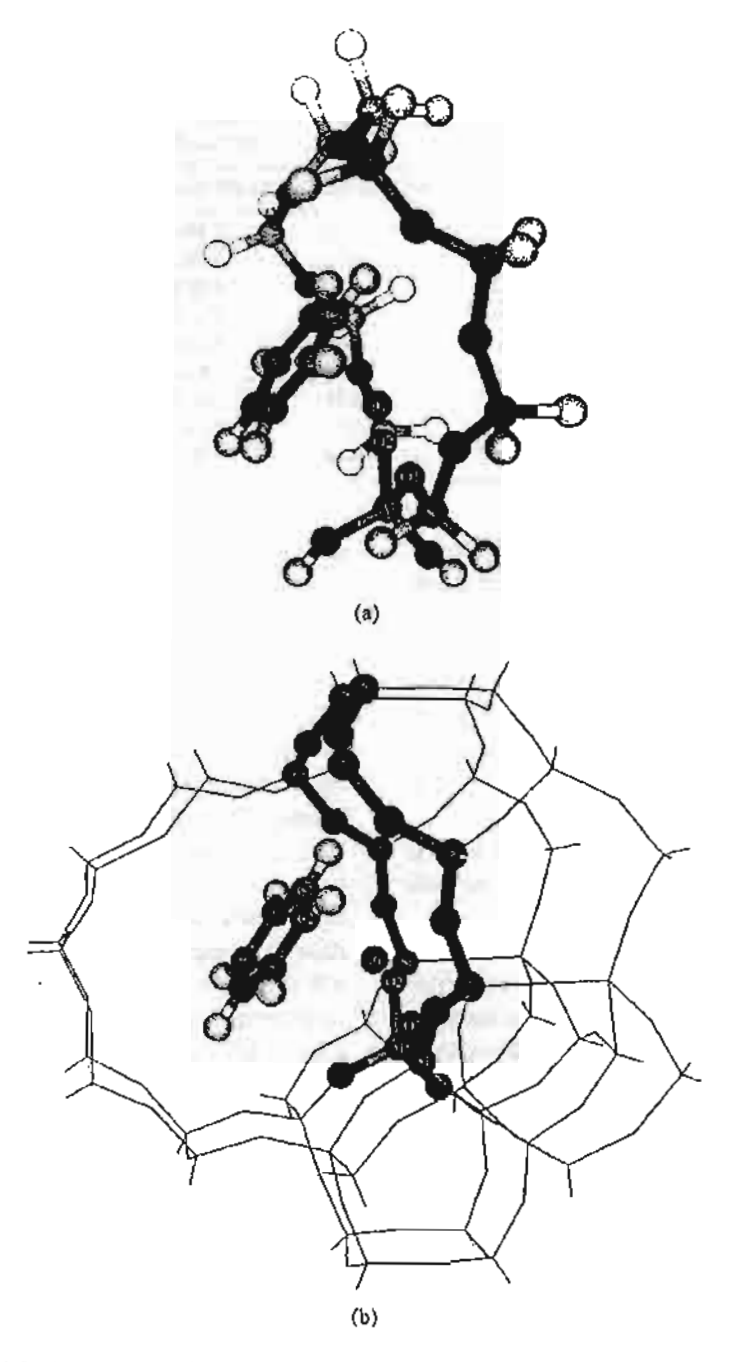


Fig. 6. Optimized structures of  $C_6H_6$  interacted with Li-ZSM-5 zeolite. (a) 10T quantum cluster of the Li-ZSM-5/ $C_6H_6$  complex. (b) 46T ONIOM model of the Li-ZSM-5/ $C_6H_6$  complex. Atoms belonging to the 10T quantum cluster drawn as spheres.

alkali-metal and [AlO<sub>4</sub>]<sup>-</sup> has been confirmed by an ESR experiment [62]. The interaction of the cationic metal with the zeolite framework leads to perturbation of the active acidic site. The extended structure

included in the ONIOM model was found to have a small effect on the structure of Li-exchanged zeolites. In the ONIOM model, Li<sup>+</sup>-O1, Li<sup>+</sup>-O2, Al-O1 and Al-O2 bond lengths decrease slightly. On the other

Table 1
Optimized geometrical parameters for Li-ZSM-5, Na-ZSM-5, Li-PAU, and Na-FAU zeolites using bare quantum cluster (B3LYP/6-31G(d,p)) and for ONIOM models (B3LYP/6-31G(d,p): UFF) (bond lengths are in pm and bond angles are in °)

Parameters	Li-Z\$M-5		Na-ZSM-5	Na-ZSM-5		Li-FAU		Na-FAU	
	IOT cluster	10T ONIOM	10T cluster	MOINO TOI	12T cluster	12T ONIOM	12T cluster	12T ONIOM	
X+Al	255.2	256.6	294.2	296.I	252.2	253.0	291.1	292.5	
X+-01	184.1	183.5	219.1	218.6	186.5	185.9	220.9	219.9	
X+-02	182.1	181.0	216.4	215.9	186.9	185.5	219.8	219.2	
Al-Ol	174.3	173.2	173.2	172.3	180.0	177.4	179.0	176.7	
A1O2	174.5	174.0	173.5	173.0	179.2	178.5	178.3	177.6	
Si-O1	161.6	159.5	160.1	158.3	164.9	163.1	163.4	161.7	
Si-O2	161.5	161.0	160.1	159.6	164.3	164.0	162.6	162.2	
O1-Al-O2	91.3	89.8	93.6	91.5	95.3	94.3	97.9	96.6	
O1-X+-O2	85.8	84.5	70.9	69.4	90.6	89.3	75.4	74.1	

hand, it elongates the Li-Al distance by 1.4, and 0.8 pm for Li-ZSM-5 and Li-FAU, respectively. There is a slight decrease in the O1-Li<sup>+</sup>-O2 and O1-Al-O2 bond angles as compared to the bare quantum model.

Regarding the structure of Na-zeolites, a similar trend has been observed (see Table 1). It is noted that the Na-Al distance is significantly longer than the Li-Al distance, in accordance to the cationic size trend (Li+: 66.0 pm, Na+: 99.0 pm), e.g. for metal-ZSM-5, the Li-Al distance is 255.2 pm whereas the Na-Al distance is 294.2 pm. It was also found that the Na-Al distance is slightly elongated with the ONIOM model (from 294.2 to 296.1 pm for the Na-ZSM-5). Despite the small magnitude, the increasing of metal-Al distance with the ONIOM model

suggests that the long-range electrostatic interaction weakened the attachment of the alkali cations to the zeolite framework.

One can expect that adsorption of probe molecules on the Li- and Na-exchanged zeolites will be affected by the presence of the long-range interaction of the framework, and this will be discussed in the following text.

### 3.2. The interaction of Li-zeolite (Li-FAU) and Na-zeolite (Na-FAU) with ethylene

Bare quantum cluster and ONIOM models for the adsorption of ethylene on alkali metal-exchanged zeolites are illustrated in Figs. 1 and 2. Selected geometrical parameters of the adduct complexes are

Table 2 Optimized geometrical parameters for Li-FAU/C<sub>2</sub>H<sub>4</sub>, and Na-FAU/C<sub>2</sub>H<sub>4</sub> zeolites using bare quantum cluster models (B3LYP/6-31G(d,p)) and for ONIOM models (B3LYP/6-31G(d,p): UFF) (bond lengths are in pm and bond angles are in  $^{\circ}$ )

Parameters	Naked Li/C2H4	Naked Na/C <sub>2</sub> H <sub>4</sub>	Li-FAU/C2H4		Na-PAU/C <sub>2</sub> H <sub>4</sub>	
			12T cluster	12T ONIOM	12T cluster	12T ONIOM
X+-AI	-	74	255.0	255.5	293.1	297.8
X+-CI	238.5	310.7	245.3	243.8	279.9	281.5
X+-C2	238.5	310.7	244.8	244.6	281.5	280.6
X+-01		<u> </u>	188.8	188.4	222.9	222.4
X+-O2	-	_	190.1	188.2	222.0	221.5
AI-OI	-	-	179.5	177.0	178.7	176.4
Al-O2	-	-	178.7	178.1	178.0	177.2
Si-Ol	-	-	164.4	162.6	163.1	161.3
Si-O2	-	_	163.8	163.5	162.2	162.0
O1-AI-O2	_		95.7	94.8	98.2	96.9
O1-X+-O2	-	-	89.0	87.9	74.6	73.2

documented in Table 2 and the corresponding adsorption energies in Table 5.

The ethylene molecule weakly interacts with the metal ion forming  $\pi$ -adsorption complex with almost symmetrical distances between  $X^+$ –C1 and  $X^+$ –C2 ( $X^+$  = Li<sup>+</sup> or Na<sup>+</sup>). In all models, the structures of Lewis acid sites and the ethylene molecule are little perturbed upon the adsorption. It was observed that the metal–Al distances are slightly lengthened when employing the ONIOM models (e.g. from 255.0 to 255.5 pm for the Li-FAU/C<sub>2</sub>H<sub>4</sub> and from 293.1 to 297.8 pm for Na-FAU/C<sub>2</sub>H<sub>4</sub>), indicating that the crystal framework embedding in the ONIOM model weakens the attachment of the alkali cations, thus enhancing the acidity of the complexes, which is reflected by higher interaction energy than that obtained from the bare quantum cluster.

It is interesting to compare the adsorption of C<sub>2</sub>H<sub>4</sub> on Li-FAU zeolite with the case where the zeolite framework is absent, i.e. in the naked Li/C<sub>2</sub>H<sub>4</sub> system. As anticipated, the C<sub>2</sub>H<sub>4</sub> binds much more strongly to the Li<sup>+</sup> cation (-24.83 kcal/mol) than in those of the Li-FAU zeolite. The simple, naked Li<sup>+</sup>/C<sub>2</sub>H<sub>4</sub> model obviously overestimated the interaction of C<sub>2</sub>H<sub>4</sub> in a real Li-exchanged zeolite system due to the large electrostatic field generated by the naked Li<sup>+</sup> cation. The extended environment embedded in the ONIOM scheme improves the results of the bare cluster model. One can see that the adsorption energy of the ONIOM cluster model (-14.27 kcal/mol) lies between those of

the bare quantum cluster model (~12.91 kcal/mol) and the simple, naked Li/C<sub>2</sub>H<sub>4</sub> system (~24.83 kcal/mol).

As for the Na-FAU, the adsorption of the ethylene molecule on the Na-FAU is significantly weaker than on the Li-FAU. The corresponding binding energies are -12.91, and -10.43 kcal/mol for Li-FAU and Na-FAU, respectively, following the conventional electrostatic trend. We found that the extended structure increases the adsorption energy by 1.36 kcal/ mol in the Li-ZSM-5 and by 1.40 kcal/mol in the Na-ZSM-5 zeolites. After correction with BSSE or single-point calculation at high basis set, the adsorption energy of ethylene on Na-FAU predicted by the ONIOM method (8.65, 8.97 kcal/mol for single-point and BSSE corrections, respectively) is in excellent agreement with the experimental value (8.8-9.6 kcal/mol), whereas, the cluster model gives significantly lower values (7.18, 7.64 kcal/mol for single-point and BSSE corrections, respectively). This implies that the binding energy of alkali-ZSM-5 bound to C<sub>2</sub>H<sub>4</sub> can be obtained more accurately by the ONIOM models than small bare quantum cluster models.

### 3.3. The interaction of Li-zeolite (Li-FAU) with benzene

The C-C and C-H bond lengths were ascertained experimentally to be 139.7 and 108.4 pm, respectively. The B3LYP/6-31G(d,p) level of theory predicted the

Table 3
Optimized geometrical parameters for Li-ZSM-5/C<sub>6</sub>H<sub>6</sub>, and Li-FAU/C<sub>6</sub>H<sub>6</sub> zeolites using bare quantum cluster models (B3LYP/6-31G(d,p)) and for ONIOM models (B3LYP/6-31G(d,p): UFF) (bond lengths are in pm and bond angles are in °)

Parameters	Naked Li/C <sub>6</sub> H <sub>6</sub>	Li-ZSM-5/C <sub>6</sub> H <sub>6</sub>		Li-FAU/C6H6	
		10T cluster	IOT ONIOM	12T cluster	12T ONIOM
Li+-Al	_	255.0	255.8	259.0	259.9
C1-C2	140.6	139.9	140.0	140.1	140.0
Li+-Ci	234.8	269.8	273.0	261.4	263.1
Li+-C2	234.8	246.5	244.7	261.7	261.0
Li+-O!	_	191.3	188.4	192.6	192.8
Li+-02	<u></u>	188.5	187.8	195.3	192.9
Al-Ol		173.5	172.1	178.3	176.6
A1-O2	_	173.8	173.5	179.0	177.6
Si-O1	_	160.9	158.7	163.8	162.2
Si-O2	-	161.0	160.1	163.5	163.2
O1-A1-O2	-	92.0	89.2	96.0	95.1
01-Li+-02	_	82.2	80.3	86.4	85.4

bond lengths of 139.6 and 108.6 pm which are in excellent agreement with the experimental observation. The benzene molecule adsorbs on the lithium cation via  $\pi$ -interaction with almost equal distances of Li+-Cl and Li+-C2 (see Table 3). Benzene adsorption results in a slight elongation of the C-C bonds as compared to the isolated molecule (the C-C bond increases by, at most, 1 pm for the naked Li model). However, no significant change is observed in the lengths of the C-H bonds. Our calculated adsorption energy from the bare cluster models is estimated to be -15.75 kcal/mol at B3LYP/6-31G(d,p) level which is significantly less than the adsorption energy of benzene obtained from the ONIOM model (-19.46 kcal/mol). After correction with single-point calculations at a higher basis set, the predicted adsorption energies are -10.99 and -14.69 kcal/mol for the cluster and ONIOM models, respectively. The adsorption energy predicted by the ONIOM model is reasonably close to the experimental estimate of  $-16 \, \text{kcal/mol}$  [63]. The large deviation observed in the cluster model is due to the fact that the cluster model neglects long-ranged interactions of the extended framework, which is important for adsorption-desorption in zeolites [63,64].

### 3.4. The effect of the zeolite framework on the adsorption properties of ethylene and benzene

Another remarkable point of interest is the comparison of the results obtained using both bare quantum

and ONIOM models for exploring the different types of zeolites (FAU and ZSM-5).

Structural parameters of adsorption complexes of ethylene in ZSM-5 are tabulated in Table 4. Similar to adsorption in FAU zeolites, the ethylene molecule forms a weak π-adsorption complex with the alkali ion (Figs. 3 and 4) and the adsorption does not significantly perturb structures of the zeolite or the adsorbed molecule. As listed in Table 5, bare quantum models, Li-ZSM-5/C2H4 and Li-FAU/C2H4 complexes have virtually the same adsorption energies (-12.25 kcal/mol versus -12.91 kcal/mol). We found that the inclusion of extended structure increases the binding energies by 4.69 and 1.36 kcal/mol for the Li-ZSM-5 and Li-FAU zeolites, respectively. For the Na-exchanged zeolite complexes, in the bare quantum cluster models, the interaction energy of Na-FAU/C2-H<sub>4</sub> is 1.37 kcal/mol which is unreasonably more stable than the Na-ZSM-5/C<sub>2</sub>H<sub>4</sub> complexes. However, when extended structures are included, the reverse trend is obtained which is in accordance with the acidity trend that the ZSM-5 zeolite is more acidic than the FAU zeolite and adsorption of non-polar molecules in ZSM-5 zeolite is stronger than in FAU zeolite [65]. The interaction energies are evaluated to be -15.67 and -11.83kcal/mol for the Na-ZSM-5 and Na-FAU complexes, respectively. These interaction energies are somewhat overestimated as compared to experimental results. Including of the basis set correction by single-point calculations at the higher basis set, 6-311++G(d,p), the corresponding interaction energies are predicted to

Table 4

Optimized geometrical parameters for Li-ZSM-5/C<sub>2</sub>H<sub>4</sub>, and Na-ZSM-5/C<sub>2</sub>H<sub>4</sub> zeolites using bare quantum cluster (B3LYP/6-31G(d,p)) and for ONIOM scheme (B3LYP/6-31G(d,p): UFF) (bond lengths are in pm and bond angles are in °)

Parameters	Naked Li/C <sub>2</sub> H <sub>4</sub>	Naked Na/C <sub>2</sub> H <sub>4</sub>	Li-ZSM-5/C2H4		Na-ZSM-5/C <sub>2</sub> H <sub>4</sub>	
			10T cluster	10T ONIOM	10T cluster	10T ONIOM
X+-Al		_	257.6	260.4	295.0	299.8
X+-C1	238.5	310.7	245.5	252.0	280.2	283.3
X+-C2	238.5	310.7	248.1	250.9	268.0	285.2
X+-01	_	_	186.2	186.2	220.6	221.1
X+-02	_	_	184.5	183.1	215.5	216.7
Al-OI	_	_	173.9	172.8	173.0	172.1
A1-O2	_	~	174.1	173.7	173.1	172.8
Si-O1	-	_	161.0	159.0	159.8	158.0
Si-O2	-	-	161.2	160.7	159.6	159.3
O1-A1-O2	_	-	91.7	90.0	93.8	91.7
O1-X+-O2	-	-	84.7	83.1	70.9	68.9

 $Adsorption \ energies \ (\Delta E_{ndn}, \ kcal/mol) \ of \ C_2H_4 \ and \ C_6H_6 \ on \ nuked \ alkali-metals \ and \ on \ alkali-metal-exchanged \ zeolites$ 

	Lt-Zoolite/Cally		Na-Zeoliśc/C <sub>3</sub> H <sub>4</sub>		Li-ZeoEte/C <sub>4</sub> H <sub>4</sub>	
	ZSM-S	FAU	ZSM-S	FAU	ZSM-3	PAU
Nakot	-24.83 (-21.54) [-23.16]		-17.76 (-1440) [-15.98]		42.56 (-38.43) [-40.20]	
Questum	-12.25 (-8.35) (-7.92)	-1291 (-931) (-1026)	-9.06 (-5.22) [-4.56]	-10.43 (~7.48) {-7.64}	-15.9t (-7.00) (-5.11)	-15.75 (-10.99) [-10.17]
ONTOM	-16.94 (-13.10) (-15.35)	-(4.27 (=10.64) [=11.19]	-15.67 (-12.18) (-12.58)	-11.83 (8.65) [-8.97]	-28.78 (-21.29) (-23.36)	-19.46 (-14.69) (-13.93)

Experiment adsorption energy of the ethylene on Ne-Y is 8.8-9.6kcal/mol from [66]. Values in perenthesis are single-point calculations at B3LYP/6-311++C(d.p)//B3LYP/6-31G(d.p) level of theory. Results of the BSSE corrected are indicated in brackets.

be of -12.18 and -8.65 kcal/mol, respectively. The BSSE corrections were also performed and gave similar results (-12.58 and -8.97 kcal/mol) as the single-point calculations with higher basis sets (see Table 5). The latter values closely agree with the results with the experimental value of 8.8-9.6 kcal/mol for the Na-Y zeolites complex [66].

A more pronounced effect of the zeolite framework is observed in adsorption of benzene. The 10T ring of ZSM-5 zeolite is apparently too constricted for the benzene molecule to form a  $\pi$ -interaction with the alkali ion. The benzene molecule is moved toward the intersection of the pore channels, which is more spacious (see Fig. 6). The quantum cluster predicts a wrong trend of adsorption energy of benzene in which Li-FAU/benzene is more stable and Li-ZSM-5/benzene by 3.84 kcal/mol. Inclusion of the extended framework also results in a correct trend of adsorption energies, i.e. -19.46 kcal/mol for Li-FAU/benzene complex and -28.78 kcal/mol for Li-ZSM-5/benzene complex. The results suggest that a large extended zeolite framework is needed for accurate representation of the different types of ZSM-5 and FAU zeolites, which cannot be drawn from the typical bare quantum cluster.

The difference in interaction energies of ethylene and benzene in the alkaline metal-exchanged ZSM-5 and FAU zeolites may be due to the combination of the acidity and confinement effects of the zeolites. Due to the smaller pore size of ZSM-5 than that of FAU zeolite, the confinement effect (mainly van der Waals interactions) is stronger in ZSM-5 zeolite. Since the van der Waals interactions dominate the adsorption of non-polar molecules, the adsorption energies of ethylene and benzene in ZSM-5 are higher than for FAU zeolite.

In the ONIOM2 (B3LYP: UFF) method, the acidity of zeolite is sufficiently accounted for by the 10T cluster of active region treated by density functional theory (B3LYP) and van der Waals interactions is reasonably described by the UFF force field [67]. Therefore, the ONIOM2 scheme proposed here can provide a better estimate of adsorption energies than the typical quantum cluster calculations. It is noted that the higher level of theories such as the MP2 method can better account for van der Waals interactions, but it would require much higher computational time to perform the calculation.

Thus, the studies of the zeolite framework structure revealed that adsorption properties of zeolite do not depend only on the acidic site center, but also on the framework structure where the acidic site is located.

#### 4. Conclusion

The structures of alkali-exchanged FAU and ZSM-5 zeolites and their interaction with ethylene and benzene have been investigated by means of both the quantum cluster and the ONIOM approaches at the B3LYP/6-31G(d,p) level of theory. It is shown that whereas the bare B3LYP/6-31G(d,p) quantum cluster cannot accurately describe characteristics of two structurally distinctive zeolites (ZSM-5 and FAU), the ONIOM2 (B3LYP: UFF) method can do much better and can differentiate the stability of adsorption complexes. The ONIOM2 adsorption energies of ethylene complexes, Li-ZSM-5/C2H4 and Li-FAU/C<sub>2</sub>H<sub>4</sub> complexes are predicted to be -16.94 and -14.27 kcal/mol, respectively. The ion (X)-Al distance increases with the increase in ionic radii. With the inclusion of basis set correction at B3LYP/6-311++G(d,p)//B3LYP/6-31G(d,p) level and the effects of the extended framework included in the ONIOM model, the energy for Na-FAU/C<sub>2</sub>H<sub>4</sub> is predicted to be -8.65 kcal/mol, which is comparable with the experimental estimate of about 8.8-9.6 kcal/mol for ethylene adsorbed on the Na-Y zeolite. With regards to unsaturated aromatic hydrocarbon, the ONIOM2 adsorption energies of benzene complexes, Li-ZSM-5/benzene and Li-FAU/benzene complexes are evaluated to be -21.29 and -14.69 kcal/mol, respectively. The results obtained in the present study suggest that the ONIOM approach yields a more accurate and practical model than the bare quantum cluster for exploring the zeolite framework and the catalytic properties.

#### Acknowledgements

This work was supported by the Thailand Research Fund (TRF) in supporting the TRF Senior Research Scholar to J.L., by ADB-MUA and by the Kasetsart University Research and Development Institute (KURDI). Our sincere thanks are due to Professor R.

Ahlrichs (Karlsruhe, Germany) for his continued support of this work.

#### References

- C.R.A. Catlow, Modeling of Structure and Reactivity in Zeolites, Academic Press, San Diego, 1992.
- [2] R.A. van Santen, G.J. Kramer, Chem. Rev. 95 (1995) 637.
- [3] J. Limtrakul, Chem. Phys. 193 (1995) 79.
- [4] J. Limtrakul, P. Treesukol, M. Probst, Chem. Phys. 215 (1997) 77
- [5] J. Limtrakul, D. Tantanak, Chem. Phys. 208 (1996) 331.
- [6] J.A. Zygmunt, L.A. Curtiss, L.E. Iton, M.K. Erhardt, J. Phys. Chem. 100 (1996) 6663.
- [7] J. Sauer, P. Ugliengo, E. Garrone, V.R. Saunders, Chem. Rev. 94 (1994) 2095.
- [8] J. Sauer, Chem. Rev. 89 (1989) 199.
- [9] M. Krossner, J. Sauer, J. Phys. Chem. 100 (1996) 6199.
- [10] D. Barthomeuf, Catal. Rev. 38 (1996) 521.
- [11] M. Hunger, J. Weitkamp, Angew. Chem. 40 (2001) 2954.
- [12] N.W. Cant, I.O.Y. Liu, Calal. Today 63 (2000) 133.
- [13] P.E. Hathaway, M.E. Davis, J. Catal. 119 (1989) 497.
- [14] A. Corma, M.J. Climent, H. Carcia, J. Primo, Appl. Catal. 59 (1990) 333.
- [15] W.P. Hölderich, M. Hesse, F. Naümann, Angew. Chem. 27 (1988) 226.
- [16] Z.H. Fu, Y. Ono, Catal. Lett. 21 (1993) 43.
- [17] E.J. Doskocil, S.V. Bordawekar, B.G. Kaye, R.J. Davis, J. Phys. Chem. B 103 (1999) 6277.
- [18] M. Huang, S. Kaliaguine, J. Mol. Catal. 81 (1993) 37.
- [19] T. Yashima, K. Sato, H.T. Hayasaka, N. Hara, J. Catal. 26 (1972) 303.
- [20] V.B. Kanzansky, Catal. Today 51 (1999) 419.
- [21] R.C. Deka, K.J. Hirao, J. Mol. Catal. A 181 (2002) 275.
- [22] M. Boronat, P. Viruela, A. Corma, J. Phys. Chem. A 102 (1998) 982.
- [23] P.J. O'Malley, K.J. Franworth, J. Phys. Chem. B 102 (1998) 4507.
- [24] L.W. Bech, T. Xu, J.B. Nicolas, J.P. Haw, J. Am. Chem. Soc. 117 (1995) 11594.
- [25] I.P. Zaragoza, J.M. Martinez-Magadan, R. Santamaria, D. Dixon, M. Castro, Int. J. Quantum Chem. 80 (2000) 125.
- [26] J.A. Ryder, A.K. Chakraborty, A.T. Bell, J. Phys. Chem. B. 104 (2000) 6998.
- [27] D.H. Barich, T. Xu, J. Zhang, J.F. Haw, Angew. Chem. Int. 18 (1998) 2530.
- [28] V.B. Kazansky, Acc. Chem. Res. 24 (1991) 379.
- [29] E.M. Evleth, E. Kassab, H. Jessri, M. Allavena, L. Montero, L.R. Sierra, J. Phys. Chem. 100 (1996) 11368.
- [30] P. Ugliengo, A.M. Ferrari, A. Zecchina, E. Garrone, J. Phys. Chem. 100 (1996) 3632.
- [31] S.P. Greatbanks, I.H. Hillier, N.A. Burton, P. Sherwood, J. Chem. Phys. 105 (1996) 3770.
- [32] I.H. Hillier, J. Mol. Struct. (Theochem.) 463 (1999) 45.
- [33] J. Limtrakul, S. Jungsuttiwong, P. Khongpracha, J. Mol Struct. 525 (2000) 153.

- [34] J. Limtrakul, T. Nanok, S. Jungsuttiwong, P. Khongpracha, T.N. Truong, Chem. Phys. Lett. 49 (2001) 161.
- [35] P. Treesukol, T.N. Troung, J. Limtrakul, J. Phys. Chem. B 105 (2001) 2421.
- [36] J. Sauer, M. Sierka, J. Comput. Chem. 21 (2000) 1470.
- [37] P.E. Sinclair, A.H. de Vries, P. Sherwood, C.R.A. Catlow, R.A. van Santen, J. Chem. Soc. Faraday Trans. 94 (1998) 3401.
- [38] M. Brandle, J. Sauer, J. Am. Chem. Soc. 120 (1998) 1556.
- [39] R.Z. Khaliullin, A.T. Bell, V.B. Kazansky, J. Phys. Chem. A 105 (2001) 10454.
- [40] A.H. de Vries, P. Sherwood, S.J. Collins, A.M. Rigby, M. Rigutto, G.J. Kramer, J. Phys. Chem. B 103 (1999) 6133.
- [41] R. Shah, J.D. Gale, M.C. Payne, Chem. Commun. (1997) 131.
- [42] Y. Jeanvoine, J.G. Angyan, G. Kresse, J. Hafner, J. Phys. Chem. B 102 (1998) 5573.
- [43] M. Svensson, S. Humbel, R.D.J. Froese, T. Matsubara, S. Sieber, K. Morokuma, J. Phys. Chem. 100 (1996) 19357.
- [44] S. Dapprich, I. Komaromi, K.S. Byun, K. Morokuma, M.J. Prisch, J. Mol. Struct. (Theochem.) 461 (1999) 1.
- [45] H.R. Tang, K.N. Fan, Chem. Phys. Lett. 330 (2000) 509.
- [46] I. Roggero, B. Civalleri, P. Ugliengo, Chem. Phys. Lett. 341 (2001) 625.
- [47] K. Sillar, P. Burk, J. Mol. Struct. (Theochem.) 589 (2002) 281.
- [48] S. Kasuriya, S. Namuangruk, P. Treesukol, M. Tirtowidjojo, J. Limtrakul, J. Catal., 2003, in press.
- [49] M. Torrent, T. Vreven, D.G. Musaev, K. Morokuma, J. Am. Chem. Soc. 124 (2002) 192.
- [50] H. van Koningveld, H. van Bekkum, J.C. Jansen, Acta Crystallogr. B 43 (1987) 127.
- [51] D.H. Olson, E. Dempsey, J. Catal. 13 (1969) 221.
- [52] X. Rozanska, R.A. van Santen, F. Hutschka, J. Hafner, J. Am. Chem. Soc. 123 (31) (2001) 7655.
- [53] L.A. Clark, M. Sierka, J. Sauer, J. Am. Chem. Soc. 125 (8) (2003) 2136.
- [54] E.G. Derouane, J. Catal. 100 (1986) 541.
- [55] E.G. Derouane, C.D. Chang, Microporous Mesoporous Mater. 35–36 (2000) 425.
- [56] A. Pelmenschikov, J. Leszczynski, J. Phys. Chem. B 103 (1999) 6886.
- [57] S.M. Babitz, B.A. Williams, J.T. Miller, R.Q. Snurr, W.O. Haag, H.H. Kung, Appl. Catal. A 179 (1999) 71.
- [58] T.A. Wesolowski, O. Parisel, Y. Ellinger, J. Weber, J. Phys. Chem. A 101 (1997) 7818.
- [59] A.M. Vos, X. Rozanska, R.A. Schoonheydt, R.A. van Santen, F. Hutschka, J. Hafner, J. Am. Chem. Soc. 123 (2001) 2799
- [60] M.J. Frisch, G.W. Trucks, H.B. Schlegel, G.E. Scuseria, M.A. Robb, J.R. Cheeseman, V.G. Zakrzewski, J.A. Montgomery, R.E. Stratmann Jr., J.C. Burant, S. Dapprich, J.M. Millam, A.D. Daniels, K.N. Kudin, M.C. Strain, O. Farkas, J. Tomasi, V. Barone, M. Cossi, R. Cammi, B. Mennucci, C. Pomelli, C. Adamo, S. Clifford, J. Ochterski, G.A. Petersson, P.Y. Ayala, Q. Cui, K. Morokuma, P. Salvador, J.J. Dannenberg, D.K. Malick, A.D. Rabuck, K. Raghavachari, J.B. Foresman, J. Ciosiowski, J.V. Ortiz, A.G. Baboul, B.B. Stefanov, G.

- Liu, A. Liashenko, P. Piskorz, I. Komaromi, R. Gomperts, R.L. Martin, D.J. Pox, T. Keith, M.A. Al-Laham, C.Y. Peng, A. Nanayakkara, M. Challacombe, P.M.W. Gill, B. Johnson, W. Chen, M.W. Wong, J.L. Andres, C. Gonzalez, M. Head-Gordon, E.S. Replogle, J.A. Pople, Gaussian Inc., Pittsburgh, PA, 2001.
- [61] J. Limtrakul, M. Baer, R. Ahlrichs, Chem. Phys. Lett. 160 (1989) 479.
- [62] H. Hosono, H. Kawazoe, J. Nishii, J. Kanazawa, J. Non-Cryst. Solid. 51 (1982) 217.
- [63] J. Xie, M. Bousmina, G. Xu, S. Kaliaguine, J. Mol. Catal. A 135 (1998) 187.
- [64] B. Coughlan, M.A. Keane, J. Chem. Soc. Faraday Trans. 86 (23) (1990) 3961.
- [65] J.A. Dunne, M. Roa, S. Sircar, R.J. Gorte, A.L. Myers, Langmuir 12 (1996) 5896.
- [66] V.R. Choudary, S. Mayadevi, A.P. Singh, J. Chem. Soc. Faraday Trans. 91 (1995) 2935.
- [67] A.K. Rappe, C.J. Casewit, K.S. Colwell, W.A. Goddard III, W.M. Skiff, J. Am. Chem. Soc. 114 (1992) 10024.



Available online at www.sciencedirect.com



Chemical Physics Letters 378 (2003) 250-256

CHEMICAL PHYSICS LETTERS

www.elsevier.com/locate/cplett

### Dissociative electron attachment to acetic acid (CH<sub>3</sub>COOH)

Wolfgang Sailer <sup>a</sup>, Andrzej Pelc <sup>a,1</sup>, Michael Probst <sup>a</sup>, Jumras Limtrakul <sup>b</sup>, Paul Scheier <sup>a</sup>, Eugen Illenberger <sup>c,\*</sup>, Tilmann D. Märk <sup>a,2</sup>

\* Institut für Ionenphysik der Universität Innsbruck, Technikerstrasse 25 A-6020 Innsbruck, Austria

\* Department of Chemistry, Kasetsart University, Bangkok 10900, Thailand

\* Department of Chemistry, Kasetsart University, Bangkok 10900, Thailand

e Physikalische und Theoretische Chemie, Freie Universität Berlin, Takustrasse 3, D-14195 Berlin, Germany

Received 3 March 2003; in final form 28 July 2003

#### Abstract

Dissociative electron attachment (DEA) to acetic acid in the energy range between about 0 and 13 eV generates as much as nine different fragment ions. The dominant products are CH<sub>3</sub>COO<sup>-</sup> and CH<sub>2</sub>O<sub>2</sub><sup>-</sup> which appear from two closely spaced low energy resonances peaking at 0.75 and 1.5 eV. In view of our ab initio calculation we assign these states as single particle shape resonances associated with the first and second virtual MO, respectively. The electronic and geometrical structure of CH<sub>2</sub>O<sub>2</sub><sup>-</sup> remains under question, the thermodynamics of the associated DEA reaction, however, predict an exceptionally high stability of this anion.

© 2003 Published by Elsevier B.V.

#### 1. Introduction

Acetic acid (CH<sub>3</sub>COOH) is, after formic acid (HCOOH), the second simplest organic acid. In a previous Letter [1], we reported on electron attachment to formic acid as part of an ongoing programme to study the effect of the interaction of low energy electrons with biologically relevant molecules under isolated conditions. Besides its

fundamental interest, the motivation for such investigations is directly related to processes in the interstellar medium and to elementary steps in biological material, e.g. in the molecular description of the primary events relevant in radiation damage. Formic acid has recently been identified as being present in the interstellar medium (ISM) [2,3] and it has therefore been suggested that it may be a key compound in the formation of more complex organic molecules in the ISM. On the other hand organic acids are components of biomolecules and hence serve as model systems for the properties of larger and more complex amino acids, or proteins, e.g., their behaviour during exposure to high energy radiation. It is well estabfished that the interaction of ionizing radiation

<sup>\*</sup>Corresponding author, Fax: +49-30-83856612.

E-mail address: iln@chemie.fu-berlin.de (E. Illenberger).

<sup>&</sup>lt;sup>1</sup> Present address: Institute of Physics, Marie Curie-Sklodowska University, Lublin 20031, Poland.

<sup>&</sup>lt;sup>2</sup> Also Adjunct Professor at Department of Plasmaphysics, Comenius University, 84248 Bratislava, Slovak Republic.

with matter generates electrons as the most abundant secondary species. It has recently been demonstrated that these ballistic electrons (3-20 eV) can efficiently induce single and double strand breaks in supercoiled DNA [4].

Electron attachment to the previously studied formic acid generated the three fragment ions HCOO-, O- and OH-. By far the most abundant species was HCOO- which is formed by ejection of a neutral hydrogen atom from the transient parent anion which itself is generated upon resonant electron attachment in the vicinity of 1.3 eV. As will be demonstrated in this study electron attachment to acetic acid generates a variety of as much as nine different negative ions as a result of dissociative electron attachment (DEA) in the energy range from about 0 to 13 eV. In the literature we find one single beam study on thermal electron attachment to acetic acid [5]. In this early paper the observation of a weak signal due to a long lived metastable parent anion with a lifetime of 330 µs was reported. While we could not measure a signal due to an undissociated anion, the previous observation may be related to the considerably higher pressure used in this early experiment.

#### 2. Experimental

The electron attachment spectrometer used here consists of a molecular beam system, a high resolution trochoidal electron monochromator (TEM) and a quadrupole mass filter with a pulse counting system for analysing and detecting the ionic products. The substantially modified TEM has recently been described in detail [6,7]. The anions produced by the electron attachment processes are extracted by a weak electric field into a quadrupole mass filter where they are mass analysed and then detected. After crossing the collision region the remaining electrons are collected and the electron current is monitored online during the experiment using a pico-ampèremeter.

Since acetic acid is a relatively weak electron scavenger (see below) the instrument was operated at an energy resolution of 120 meV as a reasonable compromise between ion intensity and energy resolution. The energy is calibrated by recording

Cl<sup>-</sup> from CCl<sub>4</sub> as well known standard for the electron energy.

Samples of 98% pure acetic acid were obtained from Sigma-Aldrich, Wien, Austria and used without further purification After proper mixing of the saturated vapour of the liquid sample of CH<sub>3</sub>COOH with vapour of CCl<sub>4</sub> (used for energy and cross-section calibration) and Ar as buffer gas (ratio 36:1:43) the mixture was expanded into the attachment region resulting in a background pressure of about 10<sup>-6</sup> mbar as measured by the gauge at one of the flanges. The entire apparatus was kept at a constant temperature of about 55 °C.

Absolute calibration of the presently measured partial DEA cross-sections (anion yields vs electron energy) was carried out by measuring the ratio of the anion current for the production of  $CH_3COO^-$  from  $CH_3COOH$  at the peak value of the 1.5 eV resonance and the anion current for the production of  $Cl^-$  from  $CCl_4$  at the peak value of the 0.8 eV resonance. Taking the ratios for the gas mixture prior to expansion (and assuming similar ratios in the ion source) and the well known cross-section for the production of  $Cl^-$  from  $CCl_4$  (5 × 10<sup>-20</sup> m<sup>2</sup> at 0.8 eV [8,9]) we can estimate the total DEA cross-section.

#### 3. Results and discussion

Figs. 1 and 2 present the energy dependences of the partial cross-section for DEA of the nine different fragment ions. The intensity is given in arbitrary units but comparable between the different fragments. From the procedure described above the absolute cross-section for the most abundant ion, CH<sub>3</sub>COO<sup>-</sup>, is estimated as  $6 \times 10^{-23}$  m<sup>2</sup> at the peak with an accuracy within one order of magnitude. This number indicates that the DEA cross-section is considerably below the geometrical cross-section of the molecule and acetic acid can, as formic acid, be considered as a weak electron scavenger.

We were not able to detect any signal due to an undissociated anion as reported in the early beam experiment [5] which was performed at an appreciably higher pressure (10<sup>-4</sup> mbar) in comparison to the present experiment. This weak signal was

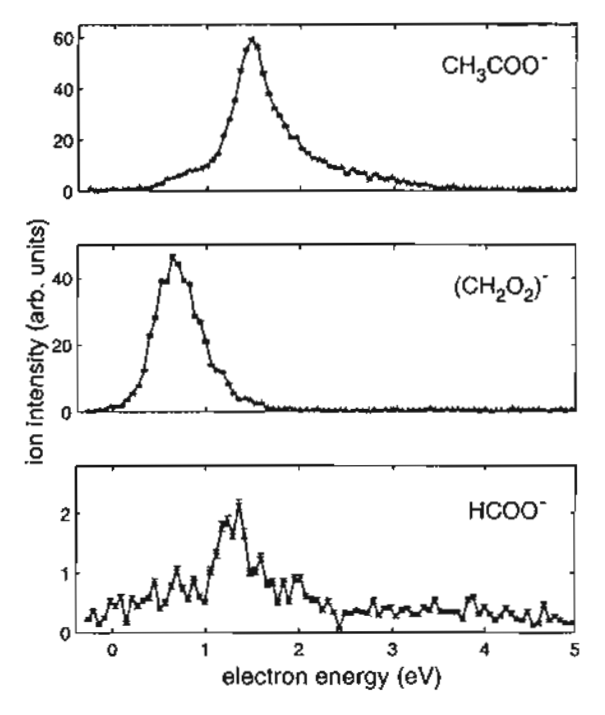


Fig. 1. Fragment ions obtained from formic acid which appear via the low energy features.

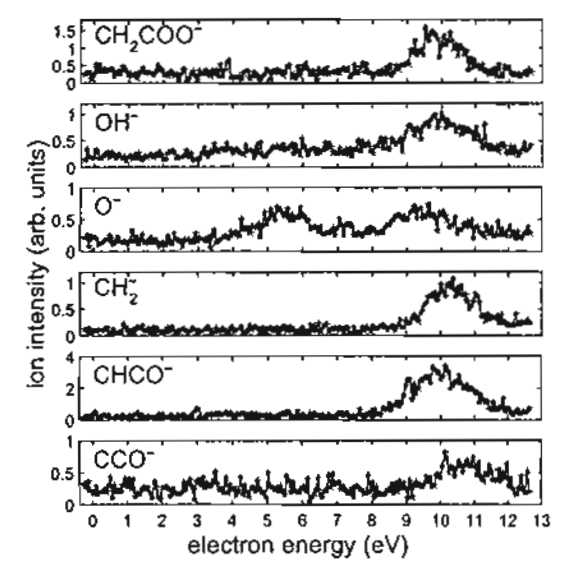


Fig. 2. Fragment ions from acetic acid which are formed from the core excited states.

interpreted as a nuclear excited Feshbach resonance (nowadays called vibrational Feshbach resonance, VFR). It is possible that secondary collisions

(which are operative to some degree at that pressure) can transform the transitory anion into a configuration where it becomes stable or metastable towards autodetachment (see discussion below and Fig. 3).

Fig. 1 shows that acetic acid exhibits two prominent, energetically overlapping features at low energy (peaking at 0.75 and 1.5 eV). These resonances are associated with the formation of CH<sub>3</sub>COO<sup>-</sup>, CH<sub>2</sub>O<sub>2</sub><sup>-</sup> and HCOO<sup>-</sup>. All other fragments (Fig. 2) appear from a comparably broader and resonant-like structure in the energy range between 9 and 11 eV. Only the O<sup>-</sup> channel is additionally visible within a very weak resonance in the electron energy range 5-6 eV.

We assign the two low energy features due to two different electronic states of the transient anion representing one particle shape resonances with the extra electron occupying the first (LUMO) and the second virtual orbital (LUMO+1), respectively (see Section 3.3). The negative ion states at higher energy can be considered as core excited resonances, i.e., transient anions with the extra electron bound to an electronically excited state of the neutral. The features in the energy range 9-11 eV are then associated to Rydberg excitations while that in the range 5-6 eV (only visible at the O<sup>-</sup> channel) is correlated to the first electronically excited state of neutral acetic acid [10].

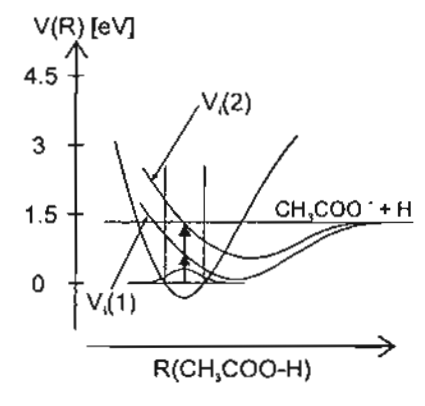


Fig. 3. Schematic potential energy diagram illustrating CH<sub>3</sub>COO<sup>-</sup> formation.  $V_1(1)$  and  $V_1(2)$  describe the potential curves associated with the shape resonances located at 0.75 and 1.5 eV, respectively (see the text).

### 3.1. DEA reactions via the low energy resonances

The most intense fragments are CH<sub>3</sub>COO<sup>-</sup> and (CH<sub>2</sub>O<sub>2</sub>)<sup>-</sup> with the first predominantly observed via the 1.5 eV feature while (CH<sub>2</sub>O<sub>2</sub>)<sup>-</sup> nearly exclusively appears from the low energy state located at 0.75 eV. In addition, a comparatively weak signal due to HCOO<sup>-</sup> is seen in the vicinity of 1.5 eV. These ions are formed via the following DEA reactions:

$$e^- + CH_3COOH \rightarrow CH_3COO^- + H$$
 (1)

$$e^- + CH_3COOH \rightarrow (CH_2O_2)^- + CH_2$$
 (2)

$$e^- + CH_3COOH \rightarrow HCOO^- + CH_3$$
 (3)

Process (1) represents a direct cleavage of the CH3COO-H bond in the transient anion with the negative charge remaining on the large fragment. In contrast to that, the low energy process (2) is due to a rather complex reaction involving hydrogen transfer in the precursor ion and cleavage of the C-C bond. Process (3) is associated with the C-C bond rupture followed by rearrangement (hydrogen transfer) in the negative fragment into the stable configuration HCOO-. Both CH3COOand HCOO- are closed shell anions with the electron delocalized on the COO group. (CH<sub>2</sub>O<sub>2</sub>) can be considered as a negative ion which is isomeric to formic acid (HCOOH) as neutral counterpart. Formic acid, however, cannot bind an additional electron [1] and we must hence assume that HCOOH and (CH2O2)" possess very different geometries.

### 3.1.1. CH3COO-

From experimental and theoretical investigations of the gas phase ion chemistry [11] the heats of formation of the compounds involved in reaction (1) are available:  $\Delta H_{\rm f}^0({\rm CH_3COOH}) = -432 \text{ kJ}$  mol<sup>-1</sup>, and  $\Delta H_{\rm f}^0({\rm CH_3COO}^-) = -505 \text{ kJ mol}^{-1}$  with an uncertainty in the range of 15 kJ mol<sup>-1</sup>. With the well established number  $\Delta H_{\rm f}^0({\rm H}) = 218 \text{ kJ}$  mol<sup>-1</sup> [13] we arrive at  $\Delta H_{\rm R}^0(1) = 1.50 \pm 0.3 \text{ eV}$  for the thermodynamic threshold (reaction enthalpy) of process (1) at room temperature. This is in good agreement with an earlier value ( $\Delta H_{\rm R}^0(1) = 1.38$  eV) obtained from gas phase acid equilibria [12].

Further quantities directly related to the above numbers are the bond dissociation energy  $D(CH_3COO-H) = 4.77$  eV and electron affinity  $EA(CH_3COO) = 3.39$  eV [11,12].

Fig. 1 indicates that the closed shell anion CH<sub>3</sub>COO<sup>-</sup> appears appreciably below the predicted threshold which cannot be explained by the finite resolution of the electron beam. In this context it should also be noted that CH<sub>3</sub>COO<sup>-</sup> is not the only anion with the stoichiometric composition C<sub>2</sub>H<sub>3</sub>O<sub>2</sub>. Gas phase ion chemistry studies report compounds with the structure CH<sub>2</sub>=C(OH)O<sup>-</sup>, HCO<sub>2</sub>CH<sub>2</sub> and CH<sub>3</sub>OCO<sup>-</sup> [13]. These anions, however, are by 1-2 eV less stable with respect to CH<sub>3</sub>COO<sup>-</sup>. We must therefore conclude that the only ion energetically accessible within the second resonance is CH<sub>3</sub>COO<sup>-</sup>.

We then assign the comparatively weak CH<sub>3</sub>COO<sup>-</sup> contribution from the low energy resonance (i.e., below the threshold) to transitions from vibrationally excited states of the neutral. Such hot band transitions are ubiquitous in DEA at low electron energies. They can be very pronounced due to the reciprocal energy dependence of the electron capture process [14–17]. Although the molecules were at room temperature in the course of the present experiments and hence the vibrational levels are only weakly populated, these activated molecules can substantially contribute to the DEA ion signal.

These hot band transitions were usually observed in exothermic DEA reactions subjected to an activation barrier and proceeding along one electronic state, repulsive in the Franck-Condon region. In the present case the situation differs since we have an endothermic process and two different transition states accessible at low energy. Fig. 3 illustrates a possible scenario in the approximation of two-dimensional potential curves. Transitions from the v = 0 level of the neutral to the upper state  $(V_i(2))$  are responsible for the dominant CH<sub>3</sub>COO<sup>-</sup> contribution at 1.5 eV while the corresponding transitions to the lower state  $(V_i(1))$  are entirely below the dissociation threshold. Only transitions from vibrationally excited states provide transitions to  $(V_i(1))$  above the dissociation exit, however, at lower electron energies.

### 3.1.2. (CH2O2)-

The appearance of a fragment ion with the composition (CH<sub>2</sub>O<sub>2</sub>)<sup>-</sup> (reaction (2)) is surprising considering the thermodynamic background. This ion cannot possess the structure of formic acid as its negative ion only exists as scattering state (negative ion resonance) [1]. The heat of formation of (CH<sub>2</sub>O<sub>2</sub>)<sup>-</sup> can be calculated using the presently observed appearance energy AE(CH<sub>2</sub>O<sub>2</sub>)<sup>-</sup> and using the relation

$$AE(CH_2O_2)^- = \Delta H_R^0(2) + E^*,$$
 (4)

where  $E^*$  is the total excess energy imparted to the fragments at the appearance energy and  $\Delta H_R^0(2)$  is the reaction enthalpy of (2) which itself can be expressed as

$$\Delta H_{R}^{0}(2) = \Delta H_{\Gamma}^{0}(CH_{2}) + \Delta H_{\Gamma}^{0}(CH_{2}O_{2})^{-} - \Delta H_{\Gamma}^{0}(CH_{3}COOH).$$
 (5)

Taking  $AE(CH_2O_2)^- = 0.3 \pm 0.1$  eV from the present experiment,  $\Delta H_c^0(CH_2) = 368 \text{ kJ mol}^{-1} [13]$ and  $\Delta H_s^0(CH_1COOH)$  from above we arrive at  $\Delta H_1^0(CH_2O_2)^- \le -790 \pm 30 \text{ kJ mol}^{-1}$  where the equality stands for the case when reaction (2) would proceed without excess energy (at the appearance energy). This number indicates a remarkable stability of (CH<sub>2</sub>O<sub>2</sub>)-: if we take the heat of formation for neutral formic acid  $(\Delta H_c^0(HCOOH) = -379 \text{ kJ mol}^{-1})$  it immediately follows that the energy of anion (CH2O2) is by more than 3 eV below the neutral counterpart HCOOH. To our knowledge an anion of that composition has not been observed and its geometric and electronic structure remains under question. For the neutral counterpart two compounds are known, formic acid and dioxirane (CH2O2). At that point we note that current experiments by our laboratory revealed that (CH2O2) is also major product from DEA to propionic acid (CH3CH2COOH) [18].

### 3.1.3. HCOO-

One can assume that the thermodynamics of reaction (3) is comparable to that of HCOOfformation from formic acid: the O-H bond dissociation energy should be approximately equal in both compounds and the C-C bond

strength is close to that of C-H. In formic acid, the thermodynamic threshold was at  $1.37 \pm 0.23$  eV [I].

### 3.2. DEA reactions via the core excited resonances

Fig. 3 collects all further product ions observed in the energy range up to 13 eV. They usually appear far above the thermodynamic limit and hence the neutral channel will usually consists of more than one particle. We shall discuss these reactions only briefly.

### 3.2.1. CH2COO-

The lowest dissociation channel is

$$e^- + CH_3COOH \rightarrow CH_2COO^- + H_2$$
 (6)

With the heat of formation for the radical anion,  $\Delta H_R^0(\mathrm{CH_2COO^-}) = -286 \text{ kJ mol}^{-1}$  [13], the reaction enthalpy becomes  $\Delta H_R^0(6) = 1.5 \text{ eV}$ . This demonstrates that the excess energy of reaction (1) is more than 7.5 eV. The question whether the neutral channel consists of  $H_2$  or H+H depends on the way how this excess energy is distributed between the fragments. Just to illustrate the complexity in assigning dissociation channels: There is a further compound of that stoichiometry, ethanedial (CHOCHO) having a positive electron affinity. With the available data [13] the threshold energy to generate this ion via (6) is near 1.6 eV.

### 3.2.2. OH", O"

For OH<sup>-</sup> we can assume an energetic threshold which is very close to that estimated in formic acid (3.48 eV [1]). While OH<sup>-</sup> can be formed by a simple bond rupture O<sup>-</sup> arises from a more complex process

$$e^- + CH_3COOH \rightarrow CH_3COH + O^-$$
 (7)

with acetaldehyde the energetically favourable neutral channel. With  $\Delta H_{\rm f}^0({\rm CH_3COH}) = -171$  kJ mol<sup>-1</sup> and  $\Delta H_{\rm f}^0({\rm O}^-) = 108$  kJ mol<sup>-1</sup> [13] we get with  $\Delta H_{\rm f}^0(7) = 3.8$  eV and hence the appearance energy ( $\approx$ 4 eV) is not far from the energy threshold.

3.2.3. CH<sub>2</sub>
The reaction

$$e^- + CH_3COOH \rightarrow HCOOH + CH_7^-$$
 (8)

is complementary to (2) with respect to the negative charge. With the heats of formation from above and  $EA(CH_2) = 0.65$  eV [13], the reaction enthalpy becomes  $\Delta H_R^0(8) = 2.8$  eV which again demonstrates that the neutral channel cannot consist of formic acid, but of dissociation products.

### 3.2.4. HCCO-, CCO-

These two ions can arise from the following reactions:

$$e^- + CH_1COOH \rightarrow HCCO^- + H_2O + H$$
 (9)

$$e^- + CH_1COOH \rightarrow CCO^- + H_2O + H_2$$
 (10)

HCCO<sup>-</sup> has the structure <sup>-</sup>HC=CO [13], with the value  $\Delta H_{\rm f}^0({\rm HCOO}^-) = -57~{\rm kJ~mol^{-1}}$  we obtain  $\Delta H_{\rm R}^0(9) = 3.6~{\rm eV}$ . Accordingly, for the reaction enthalpy of process (10) (taking  $\Delta H_{\rm f}^0({\rm CCO}^-) = -160 \pm 30~{\rm kJ~mol^{-1}}$  [13]) we get exactly the same value  $\Delta H_{\rm R}^0(9) = 3.6~{\rm eV}$ .

### 3.3. Ab initio calculations

We have carried out ab initio calculations in order to get some information on the character and energy of the lowest unoccupied molecular orbitals involved in DEA at low electron energies. The molecular geometry was optimized from MP2 calculations with the 6-31G\* [19,20] basis set. The energies of the first virtual orbitals were then calculated via Koopman's theorem [21] from Hartree Fock calculations with the D-95V basis set [22]. With the same basis set we have also calculated the vertical attachment energies (VAEs) via the outer-valence Green's Function method [23,24].

We note that in our recent work on formic acid [1] we have reported similar calculations that were, however, obtained with the aug-cc-pvTZ basis set [25]. In the meantime it has been brought to our attention [26,27] that such larger basis sets, especially ones that include diffuse functions, lead to artificially lowered vertical attachment energies

(VAEs) [28,29] and orbitals that are too extended. In contrast, the D-95V basis sets, e.g., often gives good results for transient negative ion states [26-28], provided that scaling of the orbital energies

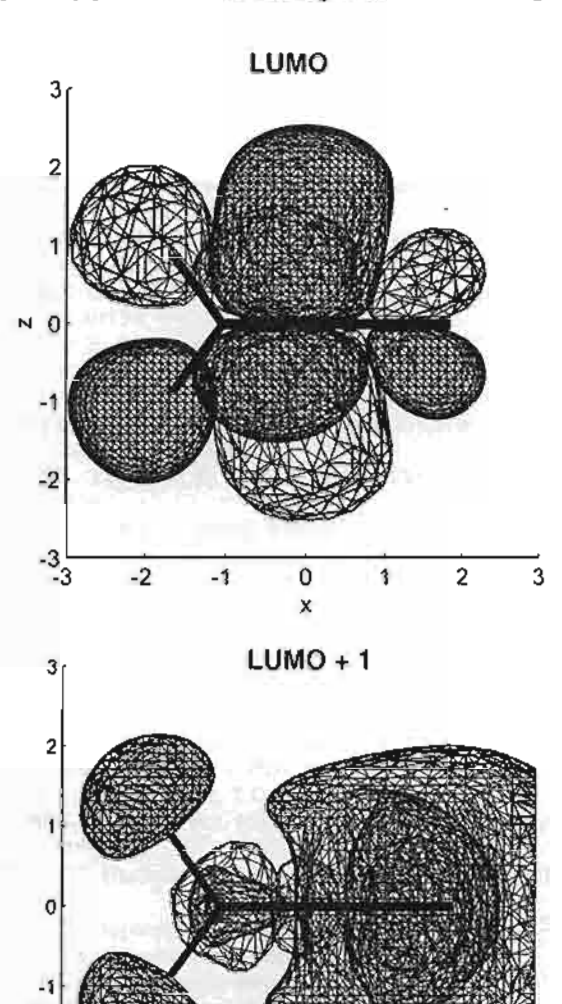


Fig. 4. LUMO and LUMO + 1 of acetic acid as calculated with the D-95V basis set. The isosurfaces are drawn at values of -0.02 a.u. (light grids) and +0.02 a.u. (denser grids). The backbone of the molecule resides in the x-y plane with the carboxylic carbon atom at the origin. In the plots, the methyl group is on the left side. It can be seen that the LUMO has a node in the symmetry plane of the molecule while LUMO + 1 has its largest densities in the molecular plane.

is performed. Scaling laws of the form VAE =  $a\varepsilon - b$ , where  $\varepsilon$  is the energy of the virtual orbital calculated from Koopman's theorem and a, b constant factors (a < 1, b < 2) have been used [27,28].

Fig. 4 shows a plot of the lowest unoccupied MO (LUMO) and second virtual (LUMO+1) in acetic acid calculated at the geometry of the neutral. The LUMO has some C-C antibonding nature and is extended to the CH<sub>1</sub> group while LUMO has large coefficients at the COOH group. We identify electron attachment into the LUMO with the resonance at 0.75 eV and attachment to LUMO+1 with the resonance at 1.5 eV. The C-C antibonding nature of the LUMO explains that CH2O2 is predominantly formed via the low energy state. This low energy state was not observed in the experiment on formic acid. According to the present calculations it is supported by the additional CH3 group in acetic acid.

The calculated VAEs from Koopman's theorem are 4.16 and 6.11 eV for the first and second virtual MO, respectively. The corresponding values with the D-95V basis set via the Green's function method are 3.30 and 5.34 eV. Adjustment to the experimental values is obtained by the scaling relation VAE =  $0.385\epsilon - 0.852$ .

### Acknowledgements

This work has been supported in part by the FWF, ÖAW, and ÖNB, Wien, Austria, the EU Commission, Brussels and the DFG, Bonn, Germany.

### References

- A. Pelc, W. Sailer, P. Scheier, M. Probst, N.J. Mason, E. Illenberger, T.D. Märk, Chem. Phys. Lett. 361 (2002) 277.
- [2] S.D. Rodgers, S. Charnley, Mon. Not. R. Astron. Soc. 320 (2001) L61.

- [3] D. Bockelee-Morvan, D.C. Lis, J.E. Wink, D. Despois, J. Crovisier, R. Bachiller, D.J. Benford, N. Biver, P. Colom, J.K. Davies, E. Gerard, B. Germain, M. Houde, D. Mehringer, R. Moreno, G. Paubert, T.G. Phillips, H. Rauer, Astron. Astrophys. 353 (2000) 1101.
- [4] B. Boudaïffa, P. Cloutier, D. Hunting, M.A. Huels, L. Sanche, Science 287 (2000) 1658.
- [5] A. Hadjiantoniou, L.G. Christophorou, J.G. Carter, J. Chem. Soc. Faraday Trans. II 69 (1973) 1704.
- [6] V. Grill, H. Drexel, W. Sailer, M. Lezius, T.D. Märk, J.Mass Spectrom. 36 (2001) 151.
- [7] V. Grill, H. Drexel, W. Sailer, M. Lezius, T.D. Märk, Int. J. Mass Spectrom. 205 (2001) 209.
- [8] S. Matejcik, G. Senn, P. Scheier, A. Kiendler, A. Stamatovic, T.D. Märk, J. Chem. Phys. 107 (1997) 8955.
- [9] D. Klar, M.-W. Ruf, H. Hotop, Int. J. Mass Spectrom. 205 (2001) 93.
- [10] M.B. Robin, in: Higher Excited States of Polyatomic Molecules, vols. I and II, Academic Press, New York, 1974
- [11] D. Yu, A. Rauk, D.A. Armstrong, J. Chem. Soc. Perkin Trans. 2 (1994) 2207.
- [12] R. Yamdagni, P. Kebarle, J. Am. Chem. Soc. 95 (1973) 4050
- [13] The NIST Chemistry WebBook. Available from <a href="http://webbook.nist.gov/chemistry">http://webbook.nist.gov/chemistry</a>.
- [14] I. Hahndorf, L. Lehr, E. Illenberger, J. Manz, Chem. Phys. Lett. 231 (1994) 460.
- [15] I. Hahndorf, E. Illenberger, Int. J. Mass Spectrom, Ion. Process, 167/168 (1997) 87.
- [16] A. Kiendler, S. Matejcik, J.D. Skalny, A. Stamatovic, T.D. Märk, J. Phys. B 29 (1996) 6217.
- [17] S. Matejcik, G. Senn, P. Scheier, A. Kiendler, A. Stamatovic, T.D. Märk, J. Phys. Chem. 107 (1997) 8955.
- [18] A. Pelc, W. Sailer, T.D. Märk, in preparation.
- [19] R. Ditchfield, W.J. Hehre, J.A. Pople, J. Chem. Phys. 54 (1971) 724.
- [20] P.C. Hariharan, J.A. Pople, Theor. Chim. Acta 28 (1973) 213.
- [21] T. Koopmans, Physica 1 (1934) 104.
- [22] T.H. Dunning Jr., J. Chem. Phys. 53 (1970) 2823.
- [23] L.S. Cederbaum, J. Phys. B 8 (1975) 290.
- [24] J.V. Ortiz, J. Chem. Phys. 89 (1988) 6348.
- [25] D.E. Woon, D.H. Dunning Jr., J. Chem. Phys. 98 (1993) 1358.
- [26] A. Modelli, H.-D. Martin, J. Phys. Chem. A 106 (2002) 7271.
- [27] K. Aflatooni, B. Hitt, A. Gallup, P.D. Burrow, J. Chem. Phys. 115 (2001) 6489.
- [28] S.S. Staley, J.T. Stnrad, J. Phys. Chem. 98 (1994) 116.
- [29] N. Heinrich, W. Koch, G. Frenking, Chem. Phys. Lett. 124 (1986) 20.

# Magnetizabilities of Ring-Structured Molecules, [8]-Cyclacene, [8]-BN-Cyclacene and [8]-Collarene, and their Effect on <sup>3</sup>He Nuclear Shielding Tensor

Somsak Tonmunphean, Atchara Wijitkosoom, Yuthana Tantirungrotechai,\*.† Narin Nuttavut,†† and Junras Limtrakul†††

Department of Chemistry, Faculty of Science, Chulalongkom University, Bangkok 10330 Thailand †Department of Chemistry, Faculty of Science, Mahidol University, Rama 6 Road, Bangkok 10400 Thailand ††Department of Physics, Faculty of Science, Mahidol University, Rama 6 Road, Bangkok 10400 Thailand †††Department of Chemistry, Faculty of Science, Kasetsart University, Bangkok 10900 Thailand

(Received Pebruary 3, 2003)

The magnetizabilities of three ring-structured molecules, [8]-cyclacene, [8]-BN-cyclacene, and [8]-collarene, were subsequently calculated at the B3LYP/6-3IG\* level with the CSGT gauge-origin treatment. The magnetizability of [8]-cyclacene shows a large diamagnetic nature in the direction parallel to the ring cylindrical axis, while the value of [8]-BN-cyclacene is nearly isotropic, and that of [8]-collarene is slightly more diamagnetic in the perpendicular direction than in the parallel direction. A large diamagnetic magnetizability in the parallel direction of [8]-cyclacene arises from the current flow around the ring circumference. The magnetic environment in the ring channel of these three molecules was investigated by calculating the nuclear shielding tensor of the <sup>3</sup>He atom when the atom moves through the ring channel. The GIAO nuclear shielding tensor changes significantly toward a prolate shape in [8]-cyclacene, but becomes a slightly oblate shape in [8]-BN-cyclacene and [8]-collarene. The changes correlate well with the magnetizabilities of the ring-structured molecules.

Cyclacenes are ring-structured molecules which consist of several benzene units forming a closed loop. It can sometimes be thought of as basic cylindrical carbon units of a zigzag nanotube. 1-4 Although a successful synthetic attempt of monomeric cyclacene has not yet been reported, there are a number of theoretical investigations of these molecules, particularly a study of the relationship between the electronic structure and the aromaticity as a function of its ring size. 1-4 Türker calculated the HOMO-LUMO energy gap of a series of Hückel and Möbius cyclacene with various ring sizes at the semiempirical MNDO level. As the ring size increases, the author found a decrease in the energy gap of the Möbius type while it is nearly constant in the Hückel type. Choi and Kim calculated the isotropic magnetic susceptibilities, the proton chemical shifts, and the energy gaps of the cyclacene ring as a function of the number of fused benzene rings.2 The authors observed an oddeven effect in most properties considered; this was discussed in terms of the aromaticity of two transulene units.3 Houk et al. re-investigated the singlet-triplet energy gap and the structural parameters of cyclacene.4

It is well known that the benzene ring has a large degree of electron delocalization. It is, therefore, interesting to investigate the electron delocalization in a system constructed from benzene subunits, such as cyclacene. In cyclacene (see Fig. 1), there are two distinguished directions for the electron delocalization; around the ring circumference and in the perpendicular direction. A difference in the degree of electron delocalization between two directions implies a large anisotropic

magnetizability, hence yielding an interesting anisotropic magnetic environment inside the ring channel.

In this work, we calculated the magnetizability of cyclacene and investigated its effect on a nuclear shielding tensor of a <sup>3</sup>He atom when the atom moves through the ring channel. The <sup>3</sup>He atom is used as a probe atom to study the magnetic field along the ring channel of cyclacene since it interacts weakly with cyclacene. Therefore, it does not significantly perturb the investigated molecule. Bühl et al. calculated the chemical shifts of an encapsulated <sup>3</sup>He atom in fullerene and fullerene derivatives.6 The authors deduced the degree of aromaticity of C60 and C70 fullerenes from this shielding information. Schleyer et al. later generalized the method of using an inert atom to probe the magnetic environment of a small ring system: the nucleus-independent chemical shift (NICS) is defined as the negative of the absolute magnetic shielding at some selected point in space, for example, at the ring center. 7,8 The NICS was used by Schleyer and co-workers as an aromaticity/antiaromaticity indicator. 7.9 It was pointed out, however, by Aihara that the NICS is the measurement of the diatropicity/paratropicity character which correlates with aromaticity/antiaromaticity only in certain case."

In addition to cyclacene, BN-cyclacene, and collarene were also included in our studies. BN-cyclacene is isoelectronic to cyclacene with B-N bonds replacing all C-C bonds (see Fig. 1). Collarene is a ring structure consisting of benzene ring units connected together by CH<sub>2</sub>-linkages (see Fig. 1). Because of the limitation in computational resources, only com-

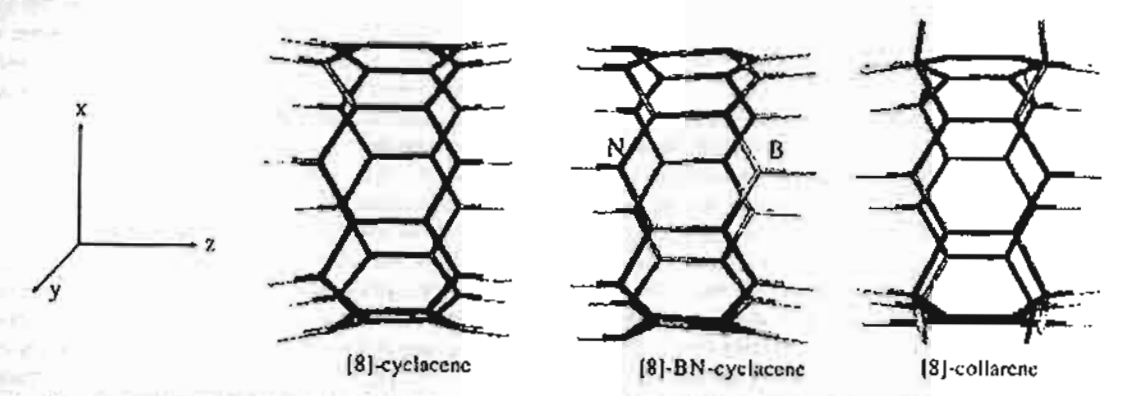


Fig. 1. The ring-structured molecules considered in this work: [8]-cyclacene, [8]-BN-cyclacene, and [8]-collarene. For [8]-BN-cyclacene, the nitrogen end is pointed toward the negative z direction. The distances between the hydrogen atoms at both ends are 9.41, 9.40, and 9.47 bohr for [8]-cyclacene, [8]-BN-cyclacene, and [8]-collarene respectively.

pounds with eight six-membered ring units ( $n \approx 8$ ), which are large enough to accommodate <sup>3</sup>He atom inside their channels, were considered.

### Computational Methods

The structures of [8]-cyclacene, [8]-BN-cyclacene, and [8]collarene were optimized at the semiempirical AM1 level using the GAMESS program. 10 The structure of [8]-cyclacene obtained at this level agrees favorably with the literature values calculated using the Density Functional Theory (DFT).24 Thus, the AM! optimized structures are adequately sufficient for our investigations and were used throughout this study. The vertical energy gaps between the lowest singlet and triplet states were calculated within the unrestricted Hartree-Fock (UHF) and DFT/6-31G\* with the B3LYP functional (B3LYP/6-31G\*) frameworks. The magnetizabilities of all molecules were computed at the B3LYP/6-31G\* level with the continuous set of gauge transformation (CSGT) method to overcome the gauge-origin dependent problem. The CSGT was chosen because it is the best method for the magnetizability currently implemented in the Gaussian 98 program.

The 3He atom was then positioned along the ring cylindrical axis (z axis in Fig. 1). The interaction energy ( $\Delta E$ ), the nuclear shielding constant ( $\tilde{\sigma} = (\sigma_{\parallel} + 2\sigma_{\perp})/3$ ), and the nuclear shielding anisotropy ( $\Delta \sigma = \sigma_{\parallel} - \sigma_{\perp}$ ), where the parallel direction is along the ring cylindrical axis, were then calculated as a function of the distance R between the 3He atom and the center of mass of a ring-structured molecule. The B3LYP/6-31G\* with the gauge-independent atomic orbitals (GIAO) method was used for the shielding tensor calculations. We note that although the DFT is the most economical way to include the electron correlation, the functionals currently used such as the B3LYP functional are not the current-density functional and, hence, do not necessarily yield the magnetic properties better than those obtained from conventional ab initio correlated methods, such as the GIAO/MP2 method.11 However, the DFT is the method of choice in our case due to the large system size considered. All ab initio calculations were performed using the Gaussian 98 program. 12

### Results and Discussion

The vertical singlet-triplet energy gaps of all compounds

Table 1. The Vertical Energy Gaps between the Lowest Singlet and Triplet States of [8]-Cyclacene, [8]-BN-Cyclacene, and [8]-Collarene at the AMI Optimized Structure. The 6-31G\* Basis Set is Used in the Calculations

	UHF/kJ mol-1	UB3LYP/kJ mol-
[8]-Cyclacene	-224.5	9.3
(8)-BN-cyclacene	923.3	562.7
[8]-Collarene	553.0	388.0

Table 2. The Magnetizabilities of [8]-Cyclacene, [8]-BN-Cyclacene, and [8]-Collarene. For the Purpose of Comparison, the Magnetic Anisotropy is Defined as  $\Delta \chi = \chi_1 - \chi_1$  where the Parallel Direction is along the Ring Cylindrical Axis. The Method of Calculation is the B3LYP/6-31G\* with the CSGT Gauge-origin Treatment

	X1/cgs	χ <sub>11</sub> /cgs	χ̄/cgs	Δ χ/cgs
[8]-Cyclacene	-274	-837	-462	-563
[8]-BN-cyclacene	-197	-174	189	23
[8]-Collarene	-274	-145	-231	129

are tabulated in Table 1. The UHF energy gap of [8]-cyclacene (-224.5 kJ/mol) indicates that at a given structure the triplet state is more stable than the singlet state. However, the UB3LYP result (9.3 kJ/mol) leads to an inverse conclusion, i.e. the singlet state is slightly more stable than the triplet state. Our result re-emphasizes the importance of the electron correlation in this type of molecule. Interesting magnetic properties of the cyclacene molecule are thought to originate from this low-lying triplet state. For [8]-BN-cyclacene and [8]-collarene, both UHF and UB3LYP predict a singlet ground state with a lesser energy gap from the UB3LYP than from the UHF.

Considering the magnetizabilities of these three molecules (see Table 2), it is clear that [8]-cyclacene has a large negative magnetizability in the parallel direction to the cylindrical axis  $(\chi_{\parallel})$ . As will be shown later, this is due to an electron delocalization around the ring circumference. The magnetizability in the perpendicular direction  $(\chi_{\perp})$  is, however, equal to that of [8]-collarene. Our  $\bar{\chi}$  of [8]-cyclacene (-462 cgs) compares well with the value of -469 cgs reported previously by Choi

and Kim;<sup>2</sup> the difference is most likely due to the use of a slightly different geometry used.

The perpendicular component of the magnetizability of [8]colfarenc is more negative than the parallel component, which is in an opposite trend to [8]-cyclacene. In other words, [8]collarene is more diamagnetic in the perpendicular direction than in the parallel direction. The magnetizabilities in the perpendicular component of [8]-collarene and [8]-cyclacene should be attributed to the  $\pi$  electron delocalization in benzene subunits; this is supported by the fact that they have the same numerical value in our calculation. Since the [8]-collarene consists of four benzene units linked together by CH2 linkages, one would expect that  $\pi$  electrons do not delocalize easily between each benzene unit, hence leading to a less negative X, of [8]-collarene. The difference between X1 of [8]-cyclacene and [8]-collarene should provide an indication of an enhanced magnetizability due to an electron delocalization around the ring circumference in the [8]-cyclacene. The [8]-BN-cyclacene, in contrast, shows a small and rather isotropic magnetizability with  $\Delta \chi$  of only 23 cgs. This seems to imply that there

is no favorable delocalization in both directions. In other words, the electron is more localized in the [8]-BN-cyclacene system than in the other two systems. This agrees with the fact that the triplet-singlet energy gap is largest in the [8]-BN-cyclacene.

An enhanced diamagnetic magnetizability in the parallel direction of [8]-cyclacene in comparison to those of other two molecules can be confirmed by examining the current density plot in the plane passing through the middle of the ring perpendicular to the axis direction (the xy plane in Fig. 1). Figures 2(a)-2(c) show the current density of [8]-cyclacene, [8]-8N-cyclacene, and [8]-collarene, respectively. The current flow in this plane leads to a magnetic field in the axis direction, which is anti-parallel to the applied external magnetic field. A large diamagnetic magnetizability in the parallel direction of [8]-cyclacene should have an origin from the complete current flow around the ring circumference, which can be observed in Fig. 2(a). This feature is missing in the cases of [8]-BN-cyclacene and [8]-collarene, which have a much less  $\chi_{\parallel}$  (see Figs. 2(b), 2(c)); both plots show only a localized cur-

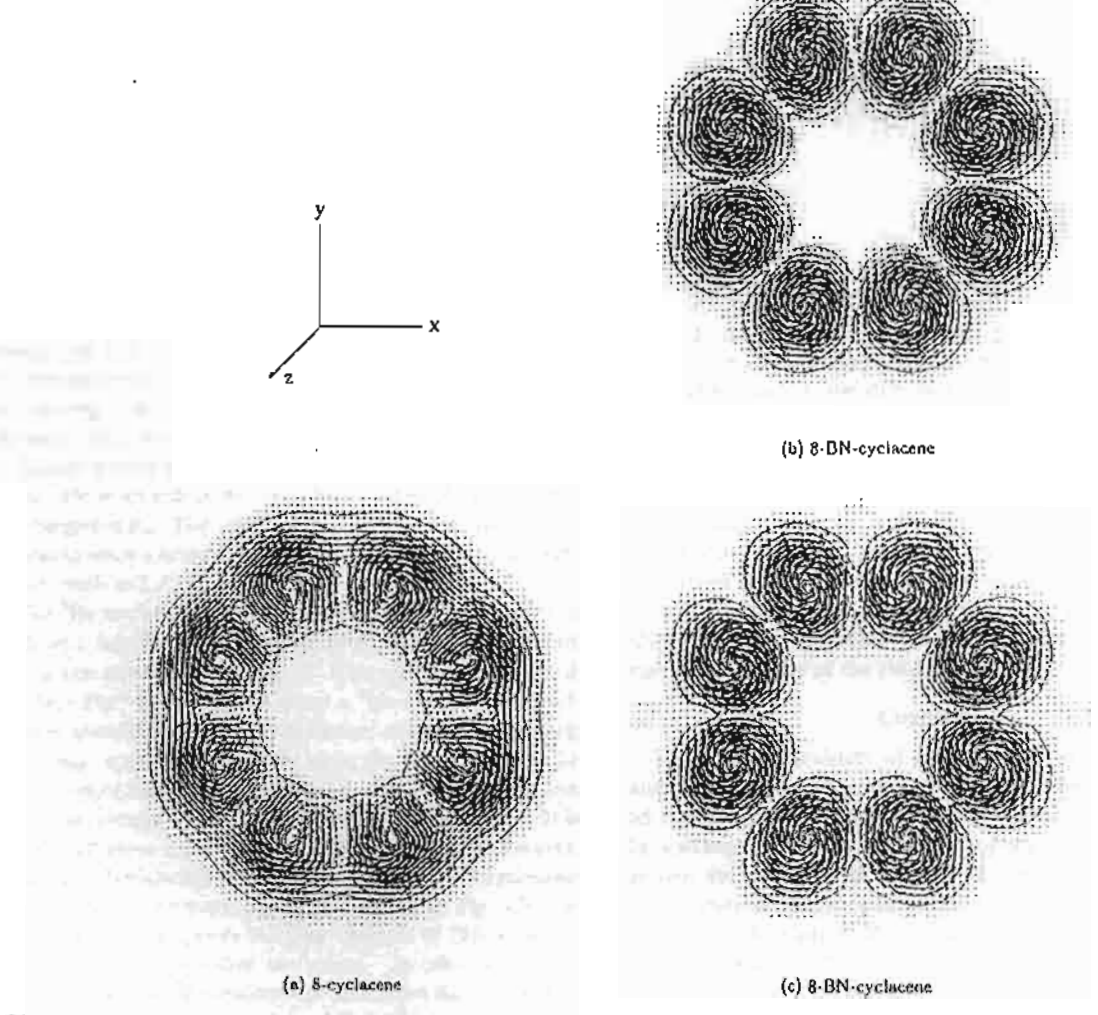


Fig. 2. The current density plots in the plane perpendicular to the cylindrical axis at the middle of the ring-structured molecule.

The current density is represented by an arrow at a given point. The contour plot of the current density magnitude is also shown.

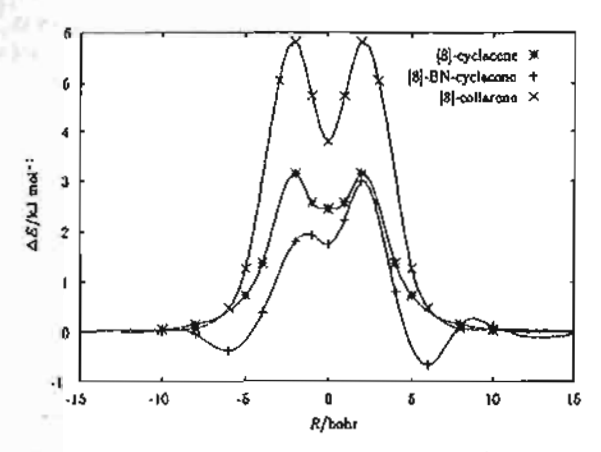


Fig. 3. The interaction energy ΔE between the <sup>3</sup>He atom and the ring-structured molecule as the <sup>3</sup>He atom moves through the ring channel along the ring cylindrical axis. The intermolecular distance R is measured from the <sup>3</sup>He atom to the center of mass of the ring-structured molecule. All lines joining calculated values were interpolated using the cubic spline method. The B3LYP/6-31G\* method was used in the calculations.

rent flow in the subunits.

Considering the insertion of 3He into a ring-structured molecule, the interaction energies ( $\Delta E$ ) between <sup>3</sup>He and each three ring-structured molecules as a function of intermolecular distance (R) are displayed in Fig. 3. We considered this term qualitatively, since it is known that the DFT method with the B3LYP functional does not describe the van der Waals interaction well. 13 The interaction energy is positive but small, less than 6 kJ/mol, in all cases. There is a local minimum at the center of the ring channel for all systems considered. Although the interaction energy is positive, it is so small that the thermal energy would overcome the positive potential barrier making it possible for the 3He atom to move through the channel. The interaction energy curve of the 3He-[8]-BNcyclacene complex is not symmetrical; the barrier is smaller if the 3He atom enters the ring channel through the nitrogen end (negative R). The insertion process becomes much more favorable when a neutral 1He atom is replaced by a small-sized cation, such as Li 1.14

The 3He nuclear shielding constant and the shielding anisotropy as a function of the intermolecular distance in all complexes are represented in Fig. 4. The shielding constant of <sup>3</sup>He (see Fig. 4(a)) increases when a <sup>3</sup>He atom moves inside the ring channel; the 3He-[8]-cyclacene complex has the largest change, approximately 50%, while the 3He-[8]-BN-cyclacene complex has the smallest change. The 3He shielding constant is maximum at the center of the ring channel (R = 0) in the [8]-cyclacene and [8]-collarene systems, whereas the maximum is shifted toward the boron-end in the [8]-BN-cyclacene. The shielding anisotropy,  $\Delta \sigma = \sigma_1 - \sigma_1$ , (see Fig. 4(b)) increases when 3He enters the ring channel of [8]-cyclacene, but decreases in the other two cases. In other words, the shielding tensor of 3He becomes prolate when the atom moves inside the [8]-cyclacene channel, while it becomes oblate when the atom moves inside the channel of the other two ring-structured molecules. The shielding tensor changes inside three

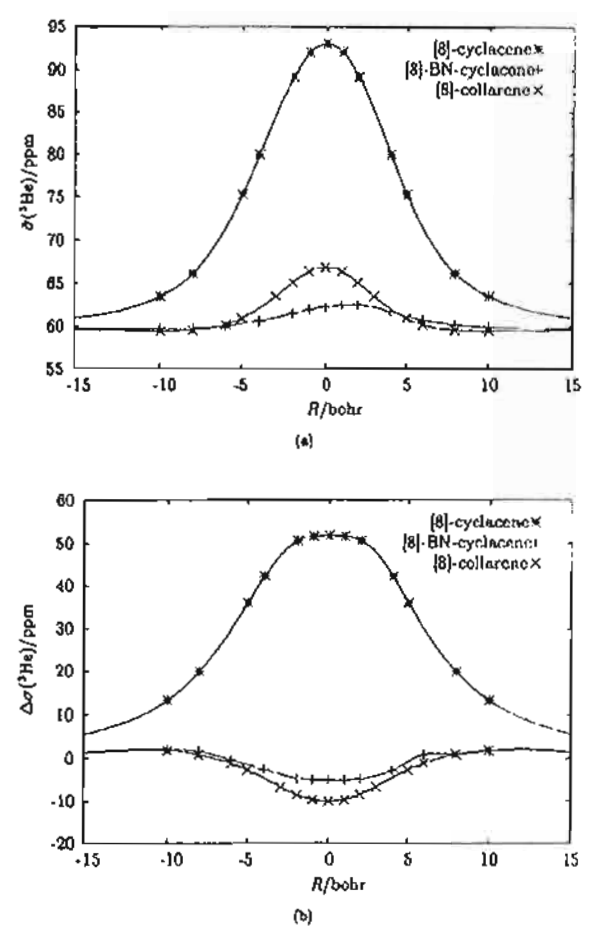


Fig. 4. The <sup>3</sup>He shielding constant  $(\bar{\sigma} = (\sigma_{\parallel} + 2\sigma_{\perp})/3)$  and the <sup>3</sup>He nuclear shielding anisotropy  $(\Delta \sigma = \sigma_{\parallel} - \sigma_{\perp})$ , where the parallel direction is along the ring cylindrical axis, as the atom moves through the ring channel along the ring cylindrical axis. For a free atom,  $\bar{\sigma}(^{3}\text{He})$  is 59.8 ppm. The B3LYP/6-31G\* with the GIAO gauge-origin treatment was used in the calculation.

ring-channels correlate well with the magnetizability tensor of the ring-structured molecules (see Table 2). Inside the channel of [8]-cyclacene, the shielding anisotropy varies slowly with the distance. Both the shielding constant and the shielding anisotropy return to the free-atom value when <sup>3</sup>He moves further out of the ring channel.

### Conclusion

The magnetizabilities of [8]-cyclacene, [8]-BN-cyclacene and [8]-collarene are reported. A large difference in the parallel component of the magnetizability of [8]-cyclacene and of [8]-collarene indicates an enhanced electron delocalization around the ring circumference. This is evidently supported by the current density plot in the plane perpendicular to the ring cylindrical axis. The perpendicular component of the magnetizability of [8]-collarene is more negative than the parallel component; this should arise mainly from the  $\pi$ -electron delocalization within the benzene subunits. The [8]-BN-cyclacene has a small and nearly isotropic magnetizability, suggesting an electron localization in this system. The different nature

of the magnetizabilities of the three ring-structured molecules leads to different behaviors of the magnetic field in the ring channel, as probed by the <sup>3</sup>He atom. A large increase in the isotropic and anisotropic parts of the <sup>3</sup>He shielding tensor, when the atom moves through the ring channel of [8]-cyclacene, indicates a anisotropic magnetic environment due to current flow around the ring circumference of the [8]-cyclacene system. The changes of the <sup>3</sup>He shielding tensor in the three complexes correlate well with the magnetizabilities of the corresponding ring-structured molecules.

S. T., and A. W. would like to thank Faculty of Science, Chulalongkorn University for computational resources, and other research facilities. Y. T. thanks the Higher education Development Project: Postgraduate Education and Research Program in Chemistry, funded by the Royal Thai Government, for support. Financial support was provided by the Thailand Research Fund (TRF) Senior Research Scholar to J. L. and Y. T. Finally the authors would like to thank the referees for very useful and constructive comments.

### References

- 1 L. Türker, J. Mol. Struct.: THEOCHEM, 454, 83 (1998).
- H. S. Choi and K. S. Kim, Angew. Chem., Int. Ed., 38, 2256 (1999).
- A. A. Fokin, H. Jiao, and P. v. R. Schleyer, J. Am. Chem. Soc., 120, 9364 (1998).
- 4 K. N. Houk, P. S. Lee, and M. Nendel, J. Org. Chem., 66, 5517 (2001).
  - 5 P. Y. Bruice, "Organic Chemistry," 3rd ed, Prentice-Hall

(2000).

- 6 M. Bühl, W. Thiel, H. Jiao, P. v. R. Schleyer, M. Saunders, and F. A. L. Anet, J. Am. Chem. Soc., 116, 7429 (1994).
- 7 P. v. R. Schleyer, C. Maerker, A. Dransfeld, H. Jiao, and N. J. R. van Eikema Hommes, J. Am. Chem. Soc., 118, 6317 (1996).
  - 8 J. Aihara, Bull. Chem. Soc. Jpn., 76, 103 (2003).
  - 9 S. Patchkovskii and W. Thiel, J. Mol. Model., 6, 67 (2000).
- 10 M. W. Schmidt, K. K. Baldridge, J. A. Boatz, S. T. Elbert, M. S. Gordon, J. H. Jensen, S. Koseki, N. Matsunaga, K. A. Nguyen, S. Su, T. L. Windus, M. Dupuis, and J. A. Montgomery, J. Comput. Chem., 14, 1347 (1993).
- 11 T. Helgaker, M. Jaszunski, and K. Ruud, Chem. Rev., 99, 293 (1999).
- 12 Gaussian 98, Revision A.I., M. J. Frisch, G. W. Trucks, R. B. Schlegel, G. E. Scuseria, M. A. Robb, J. R. Cheeseman, V. G. Zakrzewski, J. A. Montgomery, Jr., R. E. Stratmann, J. C. Burant, S. Dapprich, J. M. Millam, A. D. Daniels, K. N. Kudin, M. C. Strain, O. Farkas, J. Tomasi, V. Barone, M. Cossi, R. Cammi, B. Mennucci, C. Pomelli, C. Adamo, S. Clifford, J. Ochterski, G. A. Petersson, P. Y. Ayala, Q. Cui, K. Morokuma, D. K. Malick, A. D. Rabuck, K. Raghavachari, J. B. Foresman, J. Cioslowski, J. V. Ortiz, A. G. Baboul, B. B. Stefanov, G. Liu, A. Liushenko, P. Piskorz, I. Komaromi, R. Gomperts, R. L. Martin, D. J. Fox, T. Keith, M. A. Al-Laham, C. Y. Peng, A. Nanayakkara, C. Gonzalez, M. Challacombe, P. M. W. Gill, B. Johnson, W. Chen, M. W. Wong, J. L. Andres, C. Gonzalez, M. Head-Gordon, E. S. Replogle, and J. A. Pople, Gaussian, Inc., Pittsburgh PA, 1998.
- 13 X. Wu, M. C. Vargas, S. Nayak, V. Lotrich, and G. Scoles, J. Chem. Phys., 115, 8748 (2001).
- 14 Y. Tantirungrotechai and S. Tonmunphean, unpublished results.

### Comparison of Methods for Point-Charge Representation of Electrostatic Fields

### VIRASAK DUNGSRIKAEW,¹ JUMRAS LIMTRAKUL,¹ KERSTI HERMANSSON,² MICHAEL PROBST³

<sup>1</sup>Department of Chemistry, Kasetsart University, Bangkok 10900, Thailand

Received 25 February 2003; accepted 15 August 2003

DOI 10.1002/qua.10789

ABSTRACT: The calculation of the electrostatic potential resulting from an infinite or extended array of charges in the interior of a region of interest is a frequent task in computational chemistry. In case of a periodic potential this can, for example, be done by Ewald summation or by multipole methods. An important alternative are those methods where arrays of auxiliary point charges are optimized with respect to charge and/or position to reproduce the original electrostatic potential. In the literature different variations are reported. We compare the performance of some of these with respect to their ability to reproduce the original potential and the computational effort required. Between (1) surface charges determined by the conductor-boundary condition, (2) optimized surface charges, and (3) surface charges floating on the surface we find that (2) offers good quality with small computational costs involved. © 2003 Wiley Periodicals, Inc. Int.) Quantum Chem 96: 17-22, 2004

Key words: electrostatic potential; Ewald potential; point charges; Madelung potential; partial charges

### Introduction

n molecular modeling it is often useful to be able to represent the electrostatic potential from a large or infinite number of ions or polar molecules

Correspondence to: M. Probst; e-mail: michael.probst@uibk.ac.at or jumras@lcac.sci.ku.ac.th

by a finite set of point charges. Such an approach is in particular suitable when the actual chemical system studied is periodic and the computational method to be employed, for example some highlevel electronic structure method, is only implemented for finite systems or is too costly to apply to large systems. Another application is local defects in an otherwise periodic system: The destruction of the symmetry may call for an alternative treatment

International Journal of Quantum Chemistry, Vol 96, 17-22 (2004) © 2003 Wiley Periodicals, Inc.

<sup>&</sup>lt;sup>2</sup>Materials Chemistry, The Ångström Laboratory, University of Uppsala, Box 538, 75121 Uppsala, Sweden

<sup>&</sup>lt;sup>3</sup>Institut für Ionenphysik, Universität Innsbruck, Technikerstrasse 25, 6020 Innsbruck, Austria

### DUNGSRIKAEW ET AL

of the long-range electrostatic effects. Also in classic molecular dynamics simulations can such a long-range treatment in terms of a finite set of point charges be required. For example, if a simulated liquid is in contact with a solid (e.g., "liquids in confined spaces") it is often useful to describe the electrostatic potential of the solid in this way.

For a periodic system (either a true crystal or a periodic simulation cell) the electrostatic potential can be calculated by the Ewald summation technique [1]. An important alternative are those methods where arrays of auxiliary point charges are optimized with respect to charge and/or position to reproduce the original electrostatic potential. In the literature various methods are reported [2-4]. In this article, we compare the performance of some of these methods with respect to their ability to reproduce the original potential and with respect to the computational effort required to obtain the auxiliary point charge arrays.

### Method

### SYSTEMS

Most of the results presented in this article refer to a system consisting of a 10 × 10 × 10 point charge array, with alternative +1 and -1 charges, 2 A apart. The electrostatic potential from the entire system was calculated at all points of a dense grid within a spherical "test region" centered at the origin and with a radius of 1 Å. These potential values were compared with the potential values derived by the three sets of model charges discussed in this article (from the SCREEP method, a "least-squares charge-fitting" method and a "least-squares floating-charge fitting" method). Such a spherical test region in general deviates in size and shape from the embedded region one would typically choose in a practical computational example of interest (such as the envelope of the sum of van der Waals atoms for an embedded supermolecule). The results presented in this article are, however, applicable also to such cases.

Also, two "realistic" tests system were investigated. They consisted of a central cluster of five water molecules. In the first test system, this cluster was surrounded by 100 point-charge water molecules (SPC model, O: -0.83 e, H: +0.415 e) and the solvation energy of the five-water cluster was calculated at the Hartree–Fock (HF)/3-21G level as the energy of the total system minus the self-energy of

the 300 point charges. In the second test system, the water cluster was embedded in 459 water molecules (corresponding to a box with a side length of 25 Å) and the solvation energy was determined at the HF level with the 6-311G\* basis set. For each of these two systems, the solvation energy was compared with the solvation energies computed with the three model point-charge methods.

### Calculation of Embedding Charges

### SURFACE CHARGES DETERMINED BY THE CONDUCTOR-BOUNDARY CONDITION

The conductor-boundary condition has a well-known physical background: Because there exists no electric field inside a metallic conductor, any such field outside the conductor will be compensated by an (induced) charge density at the surface of the conductor. This means that (even if it is not generated by induction, in the case of nonmetallic conductors) a 2-D charge distribution on the surface of an arbitrary volume can exactly cancel—or reproduce—any electric field inside this volume. The external field can, for example, be generated by a finite or infinite 3-D distribution of point charges. The basic equation is

$$V_{el}(\mathbf{r}) = \int_{c} \frac{\sigma(\mathbf{r}')}{|\mathbf{r} - \mathbf{r}'|} d^{2}\mathbf{r}'. \tag{1}$$

 $V_{cl}(\mathbf{r})$  is the external potential,  $\mathbf{r}$  is a point inside the volume,  $\sigma(\mathbf{r}')$  is the charge density on the surface, and  $\mathbf{r}'$  is a point on the surface. This equation can be written in matrix form [5] if the surface S is discretized into small surface elements with the charges in their centers:

$$V - A \cdot q = 0. \tag{2}$$

V is a vector containing the values of the external potential at the (centers of) n surface elements, q is the vector of the charges of the surface elements and A is a matrix describing the surface. According to [5], the diagonal terms of this matrix are given by

$$A_{ij} = 1.07(4\pi/S_i)^{1/2}, (3)$$

where  $S_j$  is the size of the surface element j and the off-diagonal terms are simply the reciprocal dis-

18 VOL 96, NO. 1

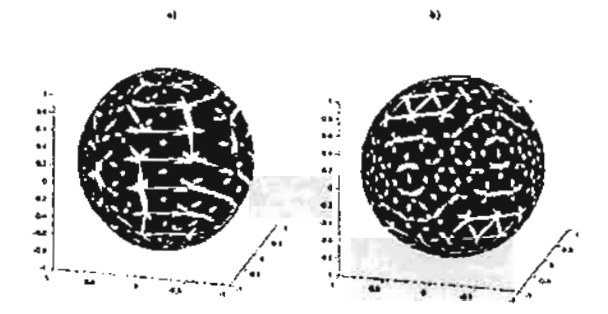


FIGURE 1. Surfaces created by triangulating a sphere: (a) "globe"; (b) "triangulated polyhedron." For better visualization, each triangle has been reduced by 50%. See text for explanations.

tances between (the centers of) two surface elements:

$$A_{ij} = |r_i - r_i|^{-1}. (4)$$

Equation (2) can be solved directly by matrix division of V by A but other methods like Gauss elimination are often numerically more efficient. This way of employing the conductor-boundary condition was proposed by Stefanovich and Truong [3] and called "surface charge representation of electrostatic embedding potential" (SCREEP). Surface charges determined in this way have, for example, been applied in studies of some important catalytic properties of zeolites [6, 7].

For the calculation of the (initial) positions of the surface charges, we used two ways of triangulation: In the first method these positions were taken to be the intersections of circles of longitude and circles of altitude and a further charge is placed at the middle of each rectangular patch (i.e., not on the poles where the patches are triangles). This allows for an easy control of the desired number of surface charges but they are not equidistant on the surface. In the second method the faces of a regular dodecahedron were triangulated and then the new triangles again, up to the desired level. That method allows for nearly equidistant positions on the sphere. However, because the depth of triangulation is the only parameter, the number of surface charges can be varied only in increasingly large steps. Figure 1 shows the triangulated spheres. The first method was used for the results presented in this article.

### SURFACE CHARGES DETERMINED BY FITTING

Auxiliary charges (not necessarily situated on a surface) that reproduce a given electrostatic potential can also be derived by fitting. Due to Coulomb's law the electrostatic potential is, at any point in space, proportional to the magnitude of the generating charges. Therefore, only a system of equations that are linear in the charges must be solved when minimizing the deviation  $\Delta^2$  between the external potential V and the fitted potential between the external potential  $V^{\text{aux}}$  in the least-square sense:

$$\Delta^2 = \iiint (V - V^{\text{aux}})^2 dx dy dz.$$
 (5)

In matrix notation, the equation

$$\mathbf{q} \cdot \mathbf{R} = \mathbf{V} \tag{6}$$

is solved to obtain q in the least-square sense. q is a vector containing the magnitudes of the auxiliary charges, R is a matrix whose elements are  $1/r_{ij}$ , the reciprocal distances between q and a vector of test points inside the volume, and V is the external electrostatic potential at these test points. In the present work all the fitted point charges reside on the spherical surface. A similar approach, although with the point charges placed in a region around the central cluster, was introduced by Almlöf et al. [2] and has, for example, since been applied in embedded-cluster simulations of crystalline hydrates [8, 9].

### FITTED CHARGES FLOATING ON THE SURFACE

If the positions of the charges are allowed to be optimized as well, the fitting equations become nonlinear and have to be solved iteratively. This is computationally more demanding than if only the magnitudes of the charges are variable, but it is interesting to find out how much quality can be gained by the additional degrees of freedom. Here, we used a Marquart-Levenberg algorithm to determine all parameters simultaneously. We restricted the charges to the surface of the sphere by optimizing their positions in polar coordinates and projecting out the distance to the center of the sphere from the gradient of the least-square deviation. For arbi-

No. of surface		r-boundary dition	Optlmize	d charges	Floating, optimized charges		
charges	$\Delta V_{\rm rms}$	$\Delta V_{ m abs}$	$\Delta V_{\rm rms}$	ΔV <sub>abs</sub>	$\Delta V_{rms}$	$\Delta V_{\rm abs}$	
24	0.155408	1.671769	0.133368	1.295595	0.007414	0.067692	
60	0.063992	0.690267	0.007715	0.063390	0.000058	0.000466	
112	0.053577	0.737572	0.001651	0.012386	0.000027	0.000250	
180	0.021238	0.272141	0.000187	0.001414	0.000009	0.000086	
240	0.003767	0.050634	0.000004	0.000039	0.000002	0.000016	
420	0.020834	0.296894	0.000059	0.000519	0.000006	0.000049	
760	0.017824	0.255184	0.000037	0.000289	0.000026	0.000223	
960	0.000329	0.004114	0.000038	0.000315	0.000028	0.000264	

trary surfaces, the same result can be achieved by optimizing via Lagrange parameters or simply by including a suitably chosen penalty function in the expression to be minimized.

### Results and Discussion

### $10 \times 10 \times 10$ POINT CHARGE SYSTEM

Table I and Figure 2 show the deviation between the original and the reproduced electrostatic potential for the three methods outlined above as a function of the number of surface elements (surface charges) used in the calculation. Two measures  $\Delta V_{\rm rms}$  and  $\Delta V_{\rm abs}$  were used and calculated according to

$$\Delta V_{cons} = \sqrt{\frac{1}{N} \sum_{k=1}^{N} [V(r_k) - V_E(r_k)]^2}$$
 (7)

$$\Delta V_{\text{abs}} = \frac{1}{N} \sum_{k=1}^{N} \{ V(r_k) - V_{\xi}(r_k) |.$$
 (8)

Equation (7) gives as the standard error the quantity minimized in the fitting process while (8) is the average deviation. The SCREEP-derived potential always gives the largest deviation and this deviation decreases less quickly with the number of surface charges than for the other two methods. Already the optimization by linear regression shows considerably better results than the SCREEP

method. These two methods require about the same, rather low, computational effort.

For the SCREEP method, q in Eq. (2) is obtained as the solution of a system of n linear equations for the n charges of the surface elements. The second method, the linear fitting, is a standard regression calculation: For each of the m test positions inside the sphere the square of the deviation is given by an expression containing the n fitting parameters. Derivation of the total sum with respect to these parameters leads to n expressions that must be zero at the error minimum and this system of equations is, as well, solved via Gaussian elimination. The values for the third method are obtained when the charges, in addition to optimizing their values, are allowed to relocate themselves ("float") on the surface. It can be seen that the deviations are again considerably reduced, the improvement being roughly equivalent to doubling the number of surface charges for the second method. The iterative algorithm used in this case is about two orders of magnitude slower than the linear fitting if allowed to converge, but most of the improvement already occurs in the first 5-10 cycles. Therefore, this method is not impractical but offers only a real advantage in situations where only a small number of auxiliary charges can be incorporated (as might be the case in some embedded cluster/quantum chemical calculation).

The somewhat increased error in the case of the SCREEP method for 420 surface charges compared to 240 is a numerical artifact due to the nonoptimal placement of the surface charges and the finite number of test charges.

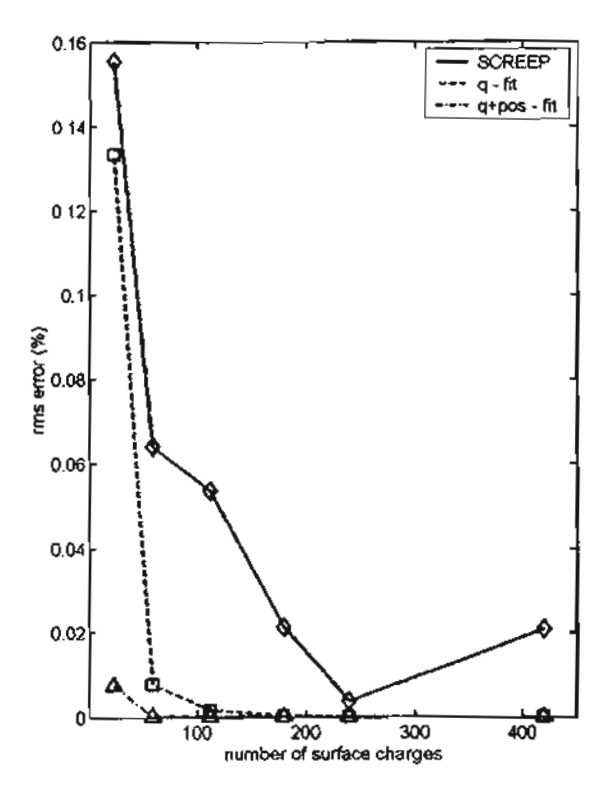


FIGURE 2. Root mean square deviations for the SCREEP method (diamonds, solid line), the fitted surface charges (squares, broken line), and the fully optimized surface charges (triangles, broken-dotted line) from the reference potential as a function of the number of surface charges.

The factor 1.07 used for deriving the diagonal matrix elements in Eq. (3) is somewhat empirical. We calculated the deviation between the SCREEP potential and the true potential as a function of this factor. As seen from Figure 3, a value of 1.05 performs slightly better than the original value. However, this might depend also on details of the potential and of the surface and was not investigated further.

### WATER CLUSTER EMBEDDED IN 300 POINT CHARGES

For our second test case, a quantum chemical calculation of a hydrated 5-water supermolecule (atomic coordinates given in Table II), the 100 SPC water molecules,\* represented by point charges, gave a hydration energy of -2.71 kcal/mol. The

"The coordinates of the various point charge arrays are available upon request (michael.probst@uibk.ac.at).

electrical field from these 300 external point charges was then approximated by 144 point charges, placed on a spherical surface with a distance of at least 1 A to each atom of the supermolecule inside. The SCREEP method gave a hydration energy of -2.92 kcal/mol, the least-squares fit gave -2.66 kcal/mol, and the complete optimization resulted in a hydration energy of -2.70 kcal/mol. Those calculations were performed at the HF/3-21G level. The same trand as in test case 1, although less dramatic, can therefore be seen in this quantum chemical application. It so happens that, in this example, the number of charges to describe the potential is only reduced by a factor of 2, but our conclusion would hold for an arbitrarily large number of original charges: To reach the same accuracy of about 0.2 kcal/mol, 144 surface charges are sufficient.

### WATER CLUSTER EMBEDDED IN 1377 POINT CHARGES

For this last test case, the same hydrated 5-water supermolecule was surrounded by the point charges of 459 SPC water molecules (taken from a simulation box with a side length of 25 Å). A solvation energy of -0.649 kcal/mol was ob-

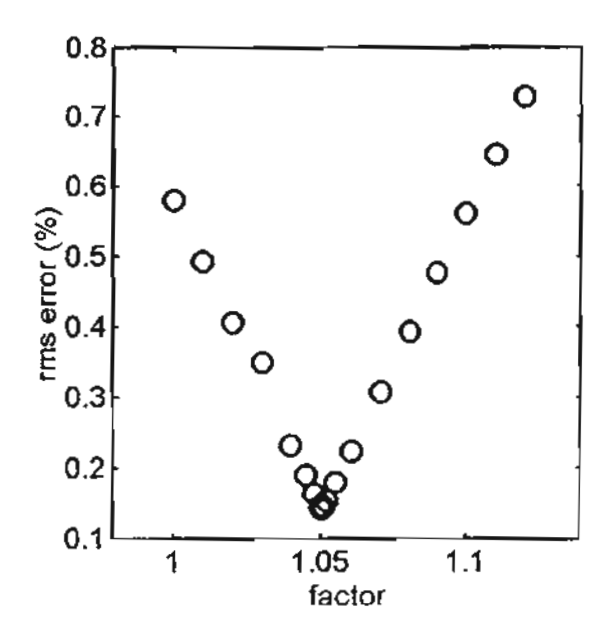


FIGURE 3. Quality (=deviation from the original potential) for the SCREEP method as a function of the factor in Eq. (3).

		0			н		н			
	x	у	Z	×	у	Z	х	У	z	
1	-0.649	-1.678	-1.041	-0.591	-1.382	-0.133	-0.384	0.918	-1.559	
2	-1.287	-0.442	1.400	-1.878	0.309	1.368	-1.865	-1.199	1.493	
3	-1,549	1.132	-1.541	1.899	0.555	-0.863	-0.909	1.678	-1.085	
4	1.316	-0.047	-2.956	1.899	0.689	-2.767	1.872	-0.821	-2.874	
5	1.150	0.200	2.956	0.288	0.074	2,560	1.474	1.014	2.570	

tained at the 6-311G\* level. We calculated the solvation energy for the SCREEP and the least-square-fitting methods as a function of the number of point charges. The full optimization was only performed for 84 point charges. Figure 4 shows the solvation energies. It can be seen that for an intermediate number of point charges the least-square-fitting performs again better; for more charges both methods perform similarly. The error for the full optimization with 84 point charges is approximately half of those obtained with the two other methods.

Conclusions

Our investigation shows that a standard linear optimization of an array of auxiliary charges

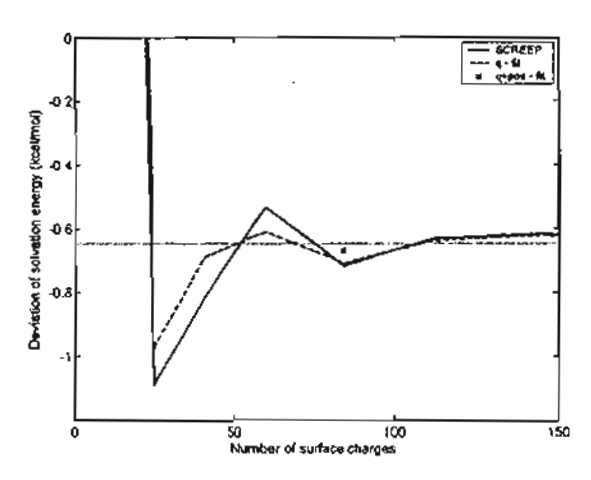


FIGURE 4. Solvation energy for the SCREEP method (solid line) and for the fitted surface charges (broken line) for the system with 459 point-charge water molecules. Cross marker: Value for 84 fully optimized surface charges.

yields a closer agreement to an original electrostatic potential than the conductor-boundary condition method. The merits of the conductorboundary condition method therefore is its simplicity as well as the proof that it is sufficient to consider surface charges instead of (complicated) 3-D arrays of charges. Especially when only a small number of charges are used, optimization of their positions improves the agreement further but it will depend on the problem under consideration if the increased computational expense is justified. The first two methods require virtually zero CPU time.

### ACKNOWLEDGMENTS

This work was supported by EU Project HPRN-CT-2000-19, the Thailand Research Fund (TRF Senior Research Scholar to J.L.), and the Ministry of University Affairs under the Science and Technology Higher Education Development Project (MUA-ADB).

### References

- 1. Ewald, P. Ann Phy Leipzig 1921, 64, 253.
- 2. Almiöf, J.; Lindgren, J.; Tegenfeldt, J. J Mol Struct 1972, 14, 427.
- 3. Stefanovich, E.; Truong, T. J Phys Chem B 1998, 102, 3018.
- Derenzo, S.; Klintenberg, M.; Weber, M. J Chem Phys 2000, 112, 2074; Klintenberg, M.; Derenzo, S.; Weber, M. Comp Phys Commun 2000, 131, 120.
- Klamt, A.; Schüürmann, G. J Chem Soc Perkin Trans 1993, 2, 799
- Limirakul, J.; Khongpracha, P.; Jungsuttiwong, S.; Truong, T. N. J Mol Catal A 2000, 153, 155.
- Limtrakul, J.; Nokbin, S.; Jungsuttiwong, S.; Chuichay, P.; Jungsuttiwong, S.; Khongpracha, P.; Jungsuttiwong, S.; Truong, T. Stud Surf Sci Catal 2001, 135, 2469.
- 8. Hermansson, K.; Lunell, S. Acta Crystallogr B 1982, 38, 2563.
- 9. Ojamãe, L.; Hermansson, K. J Phys Chem 1992, 96, 9035.

22 VOL. 96, NO. 1



Available online at www.sciencedirect.com



Chemical Physics Letters 381 (2003) 216-222

## CHEMICAL PHYSICS LETTERS

www.elsevier.com/locate/cplett

### Low energy electron attachment to CH<sub>3</sub>CN

W. Sailer, A. Pelc<sup>1</sup>, P. Limão-Vieira<sup>2,3</sup>, N.J. Mason<sup>2,4</sup>, J. Limtrakul<sup>5</sup>, P. Scheier, M. Probst, T.D. Märk<sup>\*,6</sup>

Institut für Ionenphysik, Leopold Franzens Universität, Technikerstrasse 25, A-6020 Innsbruck, Austria
Received 8 June 2003; in final form 15 September 2003

### Abstract

Low energy electron attachment cross sections for acetonitrile (CH<sub>3</sub>CN) are reported in the energy range from about 0 up to 10 eV determined with an energy resolution of 140 meV. Electron attachment is shown to be a purely dissociative process with the production of the five anionic fragments: CH<sub>2</sub>CN<sup>-</sup>, CHCN<sup>-</sup>, CCN<sup>-</sup>, CN<sup>-</sup> and CH<sub>3</sub> observed in two energy regions, the first between 1 and 4 eV, the second in excess of 6 eV. Quantum chemical and trajectory calculations have been carried out to complement the experimental results.

© 2003 Elsevier B.V. All rights reserved.

### 1. Introduction

Acetonitrile CH<sub>3</sub>CN (also known as cyanomethane or methyl cyanide) is an important atmospheric and astrophysical molecule. In the terrestrial atmosphere acetonitrile has recently been shown to be a useful gaseous tracer of biomass burning [1] since simultaneous CO and acetonitrile measurements may be used to characterize the ratio of biomass burning to fossil fuel combustion - a key issue for current global warming studies. Acetonitrile is also an important molecular species observed in gas clouds of the interstellar medium [2] where it is believed to be synthesized by heterogeneous chemistry on interstellar dust grains. Acetonitrile is therefore recognized as a fundamental building block of the amino acids and thus an important precursor molecule in the study of the origins of life [3]. Hence it is important to study those mechanisms by which acetonitrile may be dissociated through the interactions with photons [4], electrons [5] and surfaces [6].

To date there appear to have been only a few studies of electron attachment to this molecule,

0009-2614/\$ - see front matter © 2003 Elsevier B.V. All rights reserved. doi:10.1016/j.cplett.2003.09.118

<sup>\*</sup>Corresponding author.

E-mail address: tilmann.maerk@uibk.ac.at (T.D. Märk).

<sup>&</sup>lt;sup>1</sup> Permanent address: Institute of Physics, Maria Curie -Skłodowska University, 20031 Lublin, Poland.

<sup>&</sup>lt;sup>2</sup> Previous address: Department of Physics and Astronomy, University College London, Gower Street, London WC1E 6BT,

<sup>&</sup>lt;sup>3</sup> Permanent address: Departamento de Física, FCT – Universidade Nova de Lisboa, P-2829-516 Caparica and Centro de Física Molecular, Complexo I, IST, Av. Rovisco Pais, P-1049-001 Lisboa, Portugal.

<sup>&</sup>lt;sup>4</sup> Permanent address: Department of Physics and Astronomy, Centre for Molecular and Optical Science, The Open University, Walton Hall, Milton Keynes Mk7 6AA, UK.

<sup>&</sup>lt;sup>5</sup> Permanent address: Department of Chemistry, Kasetsart University, Bangkok, 10900 Thailand.

<sup>&</sup>lt;sup>6</sup> Also: Department of Plasmaphysics, Comenius University, 84248 Bratislava, Slovak Republic.

we are only aware of the early work of Tsuda et al. [7] and Stockdale et al. [8] in a study of a series of molecules containing methyl groups. Tsuda et al. [7] reported for three different electron energies (80, 40 and 9.5 eV) using a standard experimental set-up (with no means to reduce the electron energy distribution from the hot rhenium filament) relative anion abundances, at the energy of 9.5 eV which is of interest in the present study they observed only the presence of CN-. Stockdale et al. [8] using a RPD electron gun (with an energy resolution of about 500 meV) in conjunction with a time of flight mass spectrometer reported relative attachment efficiency curves in the energy range from about 0 to 30 eV for the CH2CN- and the CN- ions. The position of the CH2CN peak at 4 eV is in agreement with an earlier observation and a mass 41 peak at the same energy can be accounted for in terms of the expected abundance of CH2CN- containing one <sup>13</sup>C atom. Stockdale et al. also show that the mass 41 signal observed in the region above about 8 eV is to freat to be accounted for in terms of CH2CN- containing one 13C atom and arrive at the conclusion that in this energy regime also the parent anion is being produced. A more comprehensive study of halogenic-nitrile compounds using a crossed beam arrangement with an energy resolution of 200 meV was reported by Heni and Illenberger [9] including relative attachment efficiency curves for acetonitrile up to 16 eV for five anions CH2CN-, CN-, CHCN-, C2N- and CH3. The work in [9] showed that anions formed in electron impact with acetonitrile have virtually no kinetic energy (<0.1 eV) and may therefore be detected with high efficiency with modest extraction fields. This fact should make it possible (see below) to obtain measures for the absolute anion formation cross sections without kinetic energy discrimination.

In this Letter we report a comprehensive study of the dissociation patterns of acetonitrile by low energy electrons (up to 10 eV) using a high resolution crossed beam apparatus. The first absolute cross sections are reported and mechanisms for the formation of electron scattering resonances are discussed for CH<sub>2</sub>CN<sup>-</sup>, CN<sup>-</sup>, CHCN<sup>-</sup>, C<sub>2</sub>N<sup>-</sup> and CH<sub>2</sub> fragment ions. In agreement with the work of

Illenberger and co-workers [9] the negative parent ion, CH<sub>3</sub>CN<sup>-</sup>, has not been detected under the low pressure crossed beam conditions and in the energy range studied.

### 2. Experimental

The current experiments have been performed using a high resolution trochoidal electron monochromator (TEM) in tandem with a quadrupole mass filter and channeltron secondary electron multiplier for ion analysis and detection. The TEM has been described in detail in earlier publications [10,11] and recent modifications to improve the energy resolution at high impact energies are discussed in [12,13]. With the improved monochromator an energy resolution of about 30 meV independent of incident electron energy can be obtained however, due to the low cross sections of some fragmentation processes, larger electron currents, 45 nA (and hence lower resolutions, 140 meV) were used in some of the present experiments. The electron beam was crossed at right angles with an effusive gas beam emanating from an orifice 20 µm in diameter.

In the present studies gaseous samples of acetonitrile were prepared from liquid samples supplied by Sigma Aldrich with a quoted purity in excess of 99%. Acetonitrile has a vapour pressure of 99 mbar at room temperature (20 °C) thus, after some freeze/thaw distillation to remove any dissolved gases in the liquid sample, pure vapour samples were mixed with CCl4 in a mixing ratio of 10:1. Cl<sup>-</sup> production from electron impact of CCl<sub>4</sub> shows s-wave dissociative electron attachment (DEA; a strong resonance at zero electron energy) and therefore may be used to calibrate the electron energy scale in our experiment [14]. Pressures of the two admixtures were recorded on an absolute capacitance pressure gauge. The pressure in the experimental chamber was limited to a range from 1.0 to  $2.0 \times 10^{-6}$  mbar to ensure that there were only negligible intermolecular collisions and hence reduce the probability of secondary molecular interactions occurring.

As mentioned above, the anions formed by electron impact with acetonitrile have a kinetic

energy of less than 0.1 eV and may therefore be detected with high efficiency using modest extraction fields, such that it should be possible to measure absolute anion formation cross sections. Therefore only a modest symmetric extraction field (applying at maximum ±1 V) was used in the interaction region to collect the anionic fragments and draw them into the quadrupole optics. The intensity of the anionic yields from acetonitrile was measured as a function of incident electron energy and compared with the Cl- yield from CCl4 under the same experimental conditions (taking into account the pressure ratios). The production cross section of Cl- from CCL exhibits a second resonance at 0.8 eV the magnitude of which has been accurately determined to be  $5 \times 10^{-20}$  m<sup>2</sup> [15,16] and may therefore be used to derive a measure for the cross section for the formation of each of the fragment anions produced by low energy electron impact of acetonitrile. In the present experiment we assumed constant transmission efficiency for each anion through the quadrupole optics and that the counting efficiency of the ion detector is mass independent.

### 3. Results and discussion

Electron attachment is shown to be in the present case a purely dissociative process with the production of the five anionic fragments CH<sub>2</sub>CN<sup>-</sup>, CHCN-, CCN-, CN- and CH<sub>3</sub> (see Fig. 1). It is interesting to note that Hashemi and Illenberger reported the formation of the parent CH<sub>3</sub>CN<sup>-</sup> as a result of resonant attachment of free electrons to acetonitrile clusters [17]. This result is also in line with a study of the collisions between rare gas atoms in highly excited Rydberg states giving evidence for the existence of stable CH<sub>3</sub>CN<sup>-</sup> parent anions [8], this (i.e., the reaction sequence CH3CN+ CH3CN → CH3CN-) has also been invoked as a likely explanation for the observation of the CH<sub>3</sub>CN<sup>-</sup> parent anion by Stockdale et al. [8] by electron impact above an energy of about 8 eV. As discussed by Illenberger and co-workers [9] the production in the case of the parent anion can be rationalized via the production of a dipole bound state where the extra electron is extremely weakly

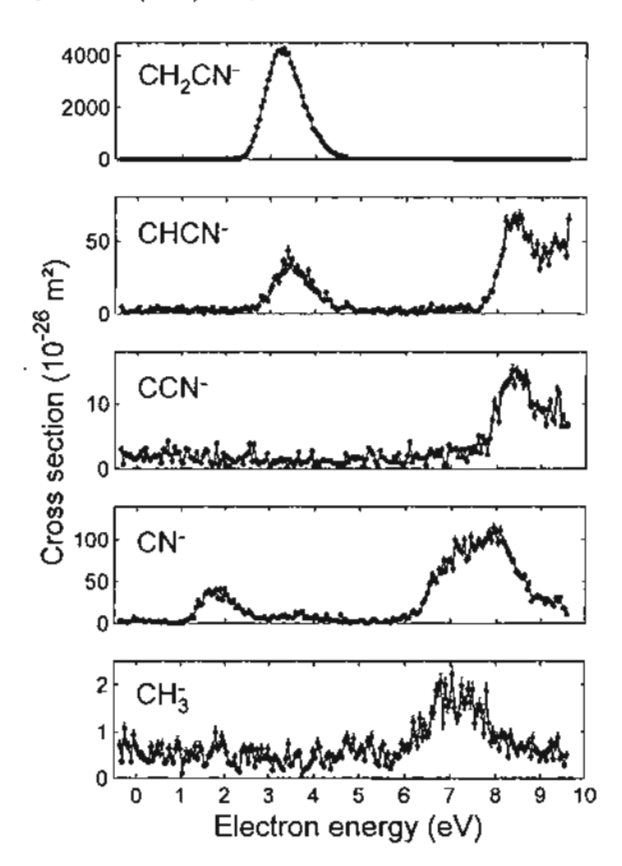


Fig. 1. Dissociative electron attachment cross sections for anions produced by electron impact on acetonitrile.

bound in the field of the  $CH_3CN$  dipole. In the cluster case it seems that the cluster coupled bound state tends to stabilize this anion, allowing for the accommodation of an extra electron. In the case of the monomer however Heni and Illenberger [9] proposed a DEA process that is common to all nitriles namely electron capture into a  $\pi_{CN}^c$  molecular orbital followed by a  $\sigma$  bond cleavage.

3.1. Dissociative electron attachment at energies <5 eV

The energetics of a DEA process to a molecule M can be described as

$$AE(M-X)^{-} = D((M-X)-X) - EA(M-X) + \Delta E$$
(1)

where AE is the appearance energy for the fragment anion (M-X), D the bond dissociation energy, EA the electron affinity for the fragment (M-X) and  $\Delta E$  the excess energy of the process.

The most intense fragment ion formed in DEA of acetonitrile is  $CH_2CN^-$  formed from the fragmentation of the parent anion by the loss of a single hydrogen atom. Assuming that the electron affinity  $EA(CH_2CN^-) = 1.560 \pm 0.006$  eV [18] and the bond dissociation energy  $D(H-CH_2CN) \sim 4$  eV [19], an appearance energy  $AE(CH_2CN^-/CH_3CN) = 2.44 \pm 0.2$  eV is predicted which is in good agreement with the experimental value of  $2.35 \pm 0.1$  eV. The maximum cross section for production of  $CH_2CN^-$  is  $\approx 4 \times 10^{-23}$  m<sup>2</sup> at 3.2 eV.

An identical appearance energy and cross section profile is observed in the yield of CHCN-formed by the abstraction of an H<sub>2</sub> molecule from the parent anion albeit with a cross section value two orders of magnitude lower than for CH<sub>2</sub>CN<sup>-</sup>.

The cross section profiles for  $CH_2CN^-$  and  $CHCN^-$  are characteristic of those arising from the capture of the incident electron into the unoccupied molecular orbital of the target to form a temporary negative ion (TNI). Assuming  $EA(CHCN) \approx 0.8 \pm 0.4$  eV [9],  $AE(CHCN^-) = 2D[(H-CH_2CN)] - D(H-H) - EA(CHCN)$  [19,20], the threshold for the AE of CHCN<sup>-</sup> is estimated to be  $2.3 \pm 0.6$  eV which is in relatively good agreement with the value of  $2.9 \pm 0.1$  eV obtained from our experiment.

Calculations have shown that the highest occupied molecular orbital (HOMO) of radical anions of the nitriles is  $\pi^*$  antibonding with virtually all the additional charge localized at the CN group, leading to a reduction in the C=N bond dissociation energy [9]. The formation of CN<sup>-</sup> is therefore associated with energy transfer from the C≡N bond to the CH3-CN bond. Dissociation into CN- and CH3 radicals in their electronic ground state is symmetry forbidden (this is only true as long as no distortions are occurring) and can only occur through pre-dissociation of the parent anion, thus the cross section for formation of CN- is small at low energies peaking at  $\approx\!\!4\times10^{-25}~m^2$  at 1.8 eV with an appearance energy of 1.10 ± 0.1 eV. Assuming the H<sub>3</sub>C-CN bond dissociation energy is 5.36 ± 0.03 eV [19] and the electron affinity of the cyano radical is 3.82 eV [21], the threshold for the appearance energy of CN<sup>-</sup>

becomes  $1.54 \pm 0.03$  eV, close to the experimentally observed value of  $1.10 \pm 0.1$  eV. In the work reported for acetonitrile by Illenberger and coworkers [9], the low energy resonance for CNseems to be slightly energy shifted compared with the present experimental data showing an appearance energy of about 2.7 eV, in contrast the data by Stockdale et al. [8] supports the present appearance energy. It is interesting to note that we have observed similar low energy patterns for CNproduction in other CN containing compounds such as CH<sub>1</sub>NO<sub>2</sub> [22]. It is however possible that such yields may arise from the excitation of vibrationally excited CH3CN and future studies of anion yield as a function of temperature of the target are planned.

### 3.2. Dissociative electron attachment at energies >6 eV

At higher impact energies several anion fragments are observed, including the first yield of the bare backbone CCN<sup>-</sup>. The formation of CCN<sup>-</sup> requires the largest number of bonds in the parent to be broken, all three C-H bonds having to be severed. Consequently, there is a high appearance energy for CCN<sup>-</sup>, around 7.8 eV. In contrast to the observation of the CCN<sup>-</sup> ion at these high energies there is no evidence for the formation of the simplest dissociation product CH<sub>2</sub>CN<sup>-</sup>.

The profiles of CHCN-, CCN-, CN- and CH; cross sections above 6 eV suggest that these fragment ions may arise from a series of overlapping resonances. The data of Illenberger and co-workers [9] suggests (in accordance with the present data) that the high energy yield of CHCN- and CCN is a composite of two resonance features peaking at 8.3 and at 10 eV. The production mechanism for the CHCN- anion could proceed through an excited state of the TNI and may be associated with the formation of two separated hydrogen atoms (multi-fragmentation) rather than with the formation of a hydrogen molecule. The similarity of the cross section profiles of CHCNand CCN- at these higher energies suggest that simple H abstraction from CHCN- may occur and that these two processes share common parent TNIs.

The complementary molecule-ion pair  $CN^- + CH_3$  or  $CN + CH_3^-$  arises from cleavage of the central C-C bond. The appearance energy of  $CH_3^-$  is obtained as  $5.28 \pm 0.03$  eV since the methyl radical  $CH_3^-$  possesses an electron affinity of 0.08 eV [23]. Both ion yields therefore have about the same appearance energy, 6.2 and 5.8 eV respectively, and peak at about the same position of 7 eV. The  $CN^-$  yield resonance is composed of three overlapping peaks, one at about 7 eV, one at about 8 eV, and one centred about 9.2 eV. For the two higher resonances a multi-fragmentation pattern with formation of  $CH_2$  and H is probable since there is no corresponding peak in the  $CH_3^-$  yield.

### 3.3. Quantum chemical and trajectory calculations

In order to get information on the electronic structure and especially about the higher-lying molecular orbitals of acetonitrile that might be involved in the formation of the TNI (see also a useful reference in this context discussing temporary anion states in this and related molecules [24] based on electron transmission spectroscopy locating the  $\pi^*$  resonance at 2.84 eV), we have calculated the vertical electron affinities by means of a outer-valence Greens' function method [25,26] (a more accurate alternative to Koopmans' theorem) together with the D-95 V basis set [27]. It is known [28-30] that only such medium-sized basis sets reproduce semi-quantitatively the energies of transient negative ion states. Normally it is found that the first attachment energy is overemphasized by such calculations but that the differences within the first few attachment energies are qualitatively correct. Trends between similar molecules are well reproduced, as is discussed in detail in [30]. All calculations were performed with the GAUSSIAN 98 and 03 set of programs [31] and the corresponding results are given in Table 1. One sees that the medium-sized basis set indeed avoids the continuum of unbound electron states. All EAs are negative, indicating that there is no thermodynamically stable anion state.

We further tried to obtain qualitative insight into the fragmentation processes by performing a limited set of trajectory calculations. In these calculations, the CH<sub>3</sub>CN molecule was described

Table 1 Calculated vertical electron affinities (see text) for attachment into the LUMO and the five next higher orbitals of CH<sub>2</sub>CN

The state of the s
Energy (eV)
-4.81
-6.00
-6.80
-8.50
-8.24

quantum chemically by the B3LYP [32] density functional and the 6-31G\* [33] basis set and the dynamics was generated by the atom centred density matrix propagation (ADMP) method [34,35].

An encounter between one CH3CN molecule and one electron was then simulated in the following way: (a) The electron was attached to the LUMO of CH3CN in the equilibrium geometry of the neutral molecule. (b) Boltzmann-distributed velocities were assigned to the atoms of the CH<sub>2</sub>CN<sup>-</sup> anion with a total kinetic energy equivalent to the energy of the incoming electron (1 eV corresponds to a temperature of 1938 K). The individual velocity components were created by appropriate scaling of random numbers. (c) This process was repeated and five trajectories each for kinetic energies of 0, 1, 2, 4, 8 and 10 eV were calculated. (d) Each trajectory was propagated for about 500 time-steps of 0.1 fs each. This trajectory calculation differs from the experimental situation mostly in the respect that the kinetic energy of the electron is thermally distributed over the molecule whereas in reality it will excite only certain vibrational modes that might lead to dissociation before an equilibration takes place. Further, five trajectories of 50 fs each obviously do not allow goodquality statistical sampling but it must be kept in mind that the computational expense of the abinitio molecular dynamics calculations is still very high, even with the modest 6-31G\* basis set.

Despite these limitations, it is interesting to compare the simulated decomposition and the experimentally observed fragments since the former ones represent the limiting case of the anion in thermal equilibrium. An analysis of the individual trajectories revealed the following pattern: The abstraction of hydrogen is always the first step and takes place very quickly within the first femtosec-

ond, sometimes even at energies <1 eV. At slightly larger energy, it is likely reaction is that a second hydrogen is lost as well but in some cases this H later recombines again with the CHCN fragment. The breaking of the C-C bond is much slower and occurs only at higher energies. We observed it first in one of the trajectories at 8 eV after about 30 fs elapsed time.

Therefore, despite of the thermalized anion, the fragmentation pattern agrees qualitatively with the experimental findings. This should be not unexpected for a small molecule where energy fluctuations after a few vibrational cycles lead to local concentrations of the kinetic energy.

#### 4. Conclusions

In the present study DEA to acetonitrile has been investigated from about 0 to 10 eV. Intensity ratios of the product ions: CH<sub>2</sub>CN<sup>-</sup>, CHCN<sup>-</sup>, CCN<sup>-</sup>, CN<sup>-</sup> and CH<sub>3</sub> are 2000:35:7:50:1, these have been converted to absolute cross sections by comparison with the known standard cross section for the production of Cl<sup>-</sup> from CCl<sub>4</sub>. With the exception of CH<sub>2</sub>CN<sup>-</sup> all anion cross sections are quite small. In fact, CH<sub>3</sub> exhibits the smallest cross section ever measured with this instrument, 200 barn.

It is clear that DEA occurs via accommodation of an extra electron into a  $\pi_{CN}^*$  character orbital. The most energetically favourable channel,  $CH_3^* + CN^-$  is the result of a transition to the low-lying excited states having repulsive adiabatic potential surfaces crossing with the electronic ground state above the dissociation limit leading to pre-dissociation of the bond. The result is a low  $CN^-$  cross section at  $\sim 2$  eV and an inter- and intramolecular energy transfer (or re-distribution) with virtually no kinetic energy release.

### Acknowledgements

This work was partially supported by the FWF and ÖNB, Wien Austria and the EU Commission, Brussels. NJM and PLV also wish to recognise the support of the EPSRC in the UK. The work was also supported in part by grants from the Thailand Research Fund (TRF Senior Research Scholar to

J.L.), the Kasetsart University Research and Development Institute (KURDI) as well as by the Ministry of University Affairs (MUA-ADB).

#### References

- A.J.T. de Laat, J.A. de Gouw, J. Lelieveld, A. Hansel, J. Geophys. Res. 106 (2001) 28469.
- [2] R.J. Habing, G.H. Macdonald, Astron. Astrophys. 252 (1991) 705.
- [3] A. Brack, Molecular Origins of Life, Cambridge University Press, Cambridge, MA, 2000.
- [4] F. Edard, M. Tronc, J. Phys. B 20 (1987) L265.
- [5] M. Suto, L.C. Lee, J. Geophys, Res. 90 (1985) 13037.
- [6] C. Mair, Z. Herman, J. Fedor, H. Lezius, Z. Herman, T.D. Märk, J. Chem. Phys. 118 (2003) 1479.
- [7] S. Tsuda, A. Yokohata, T. Umba, Bull. Chem. Soc. Jpn. 43 (1970) 3383.
- [8] J.A. Stockdale, F.J. Davis, R.N. Compton, C.E. Klots, J. Chem. Phys. 60 (1973) 4279.
- [9] M. Heni, E. Illenberger, Int. J. Mass Spectrom. Ion Proc. 73 (1986) 127.
- [10] S. Matejcik, A. Kiendler, P. Stampfli, A. Stamatovic, T.D. Märk, Phys. Rev. Lett. 77 (1996) 3771.
- [11] S. Matejcik, G. Senn, P. Scheier, A. Kiendler, A. Stamatovic, T.D. Märk, J. Chem. Phys. 107 (1997) 8955.
- [12] V. Grill, H. Drexel, W. Sailer, M. Lezius, T.D. Mārk, Int. J. Mass Spectrom. 205 (2001) 209.
- [13] V. Grill, H. Drexel, W. Sailer, M. Lezius, T.D. Märk, J. Mass Spectrom. 36 (2001) 151.
- [14] D. Klar, M.W. Ruf, H. Hotop, Chem. Phys. Lett. 189 (1992) 448.
- [15] K. Aflatooni, P.D. Burrow, J. Chem. Phys. 113 (2000) 1455.
- [16] S.C. Chu, P.D. Burrow, Chem. Phys. Lett. 172 (1990) 17.
- [17] R. Hashemi, E. Illenberger, J. Phys. Chem. 95 (1991) 6402.
- [18] J. Marks, D.M. Wetzel, P.B. Comita, J.I. Brauman, J. Chem. Phys. 7 (1975) 837.
- [19] M.N.R. Ashfold, S.P. Simons, J. Chem. Soc. Faraday Trans. II 74 (1978) 1263.
- [20] A. Pelc, W. Sailer, P. Scheier, M. Probst, N. Mason, E. Illenberger, T.D. Märk, Chem. Phys. Lett. 361 (2002) 277.
- [21] R. Klein, R.P. McGinnis, S.R. Leone, Chem. Phys. Lett. 100 (1983) 475.
- [22] W. Sailer, A. Pelc, S. Matejcik, E. Illenberger, P. Scheier, T.D. Märk, J. Chem. Phys. 117 (2002) 7989.
- [23] G.B. Ellison, P.C. Engelking, W.C. Lineberger, J. Am. Chem. Soc. 100 (1978) 2556.
- [24] P.D. Burrow, A.E. Howard, A.R. Johnston, K.D. Jordan, J. Phys. Chem. 96 (1992) 7570.
- [25] J.V. Ortiz, J. Chem. Phys. 89 (1988) 6348.
- [26] L.S. Cederbaum, J. Phys. B 8 (1975) 290.
- [27] T.H. Dunning Jr., J. Chem. Phys. 53 (1970) 2823.
- [28] A. Modelli, H.-D. Martin, J. Phys. Chem. A 106 (2002)

- [29] K. Aflatooni, B. Hitt, A. Gallup, P.D. Burrow, J. Chem. Phys. 115 (2001) 6489.
- [30] S.S. Staley, J.T. Strnad, J. Phys. Chem. 98 (1994) 116.
- [31] Gaussian 03 and Gaussian 98, Gaussian, Inc., Pittsburgh PA, 2003.
- [32] A.D. Becke, Phys. Rev. A 38 (1988) 3098; J. Chem. Phys. 98 (1993) 1372, 5648.
- [33] R. Ditchfield, W.J. Hehre, J.A. Pople, J. Chem. Phys. 54 (1971) 724.
- [34] H.B. Schlegel, S.S. Iyengar, X. Li, J.M. Millam, G.A. Voth, G.E. Scuseria, M.J. Frisch, J. Chem. Phys. 117 (2002) 8694.
- [35] S. Iyengar, H.B. Schlegel, J.M. Millam, G.A. Voth, G.E. Scuseria, M.J. Frisch, J. Chem. Phys. 115 (2001) 10291.



Available online at www.sciencedirect.com

Journal of Molecular Structure 654 (2003) 35-45

Journal of MOLECULAR STRUCTURE

www.elsevier.com/locate/molstruc

## The influence of the framework on adsorption properties of ethylene/H-ZSM-5 system: an ONIOM study

Wasinee Panjan, Jumras Limtrakul\*

Laboratory for Computational and Applied Chemistry, Chemistry Department, Kasetsart University, Bangkok 10900, Thailand
Received 10 December 2002; revised 11 February 2003; accepted 11 February 2003

Abstract

We changes) approaches have been carried out on different aluminosilicate clusters representing H-ZSM-5 zeolitic catalysts containing up to 46 tetrahedrally coordinated tetravalent atoms and their interaction with ethylene. When carefully calibrated, by using the experimental observation, the ONIOM2(B3LYP/6-311++G(d,p):HF/3-21G) scheme, in which an inner part of the system containing the active site is treated at the B3LYP/6-311++G(d,p) level, and the rest—using the HF/3-21G—has been found to provide reliable information for calculating the effects of the extended zeolite framework on the structural and energetic properties of the  $C_2H_4/H$ -ZSM-5 system. The predicted adsorption energy for this ONIOM2 scheme is -9.14 kcal/mol, which corresponds well with the experimental estimate of -9 kcal/mol. © 2003 Elsevier Science B.V. All rights reserved.

Keywords: Zeolites; Aluminosilicate clusters; Ethylene

### 1. Introduction

Nowadays, ZSM-5 zeolite is one of the important nanostructured catalysts for many industrial processes owing to its unique characteristics, i.e. shape-thand size-selectivity, active sites, thermal stability and ion-exchange [1]. The adsorption and subsequent reactions of hydrocarbons on zeolites have been carried out for a number of experimental [2-5] and theoretical methods [6-12]. Of particular interest in this area of active research is the alkene adsorption on zeolites that is the foundation

of several industrially important reactions, namely, the polymerization and hydrocarbon cracking processes [9,10].

The adsorption of ethylene on zeolites has been studied experimentally by using Fourier transform IR spectroscopy (FTIR) [13], proton and carbon-13 solid-state NMR spectroscopy [14,15]. The observed shifts in the spectral peaks provide information on the strength of the interaction between the Brønsted acid site and ethylene. Theoretical studies using accurate quantum mechanical methods can provide, in addition to the energetic properties, details on the adsorption structure. For the purpose of this study, we focus mainly on the adsorption of ethylene on zeolites as a starting point for a more comprehensive study on hydrocarbon cracking and ethylene epoxidation

0022-2860/03/5 - see front matter © 2003 Elsevier Science B.V. All rights reserved. doi:10.1016/S0022-2860(03)00154-6

<sup>\*</sup> Corresponding author Tel.: +66-2-942-8900x323; fax: +66-2-942-8900x324.

E-mail address: fseijrl@ku.ac.th (1. Limtrakul).

10 30,50 in the parts Sec. 3. C. Liker 11.00

1 1 1

reactions in zeolites. There have been several previous theoretical studies on the adsorption of ethylene on zeolites using both ab initio [6-11] and semiempirical [12] electronic structure methods. All of these studies, however, used the cluster models representing a generic tetrahedral sub-unit in an unconstrained environment and thus cannot make any reference on the effects of the zeolite framework. The predicted adsorption energy of ethylene (-4 to -7 kcal/mol) [6-11] so far is noticeably smaller compared to the experimental adsorption energy of ethylene on the acidic H-Y zeolite (-9 kcal/mol) [5]. Such deviation indicates that the long range electrostatic of the extended framework could be an important factor in stabilizing the adsorption complex. This raises the need for a better understanding of the effects of extended framework in the adsorption of unsaturated hydrocarbons. To accurately include the effects of the extended zeolite framework on the adsorption properties, one can employ the periodic electronic structure methods such as the periodic density functional theory methodology. However, due to the large computational demand, such calculations are limited to rather small unit-cell zeolites that often are not used in the actual industrial processes. Combined quantum mechanical and molecular mechanical (QM/MM) methods have been proven to be powerful tools for treatment of large molecular systems [16-29]. This embedded methodology provides a cost effective computational strategy for including the effects of extended structure.

One such method is the original 'ONIOM (Ourown N-layered Integrated molecular Orbital + molecular Mechanics)' approach, which has been developed by Morokuma and co-workers [30-36] and extended to the regime of large chemical and biological systems. To date, this method is mostly applied to large biomolecules, organometallic complexes. To our knowledge, no theoretical work on unsaturated hydrocarbon interacted with zeolite has been reported by using the ONIOM methodology. In this study, the applicability and reliability of the ONIOM method will be tested to investigate the effect of the zeolitic framework structure on adsorption properties. The various two-level ONIOM2 schemes are optimized to find an efficient scheme by using the experimental data as a benchmark.

### 2. Method

Two different strategies have been employed to model the H-ZSM-5. First, different aluminosilicate clusters are modeled to represent the active sites, whilst the second strategy employs the ONIOM2 approach. The cluster models were obtained from the lattice structure of H-ZSM-5 zeolite [37]. The 3T cluster H<sub>3</sub>SiO(H)Al(OH)<sub>2</sub>OSiH<sub>3</sub> (Fig. 1) is considered as the smallest unit that is required to represent the active site of zeolite. The effect from the framework structure of zeolite cannot be totally neglected if more accurate results are required. Thus, the larger clusters were proposed for representing the system of H-ZSM-5. The six cluster structures of increasing size considered in this work were: 3T:AlSi<sub>2</sub>O<sub>4</sub>H<sub>9</sub>, 10T:AlSi<sub>9</sub>O<sub>12</sub>H<sub>21</sub>, 14T:AlSi<sub>13</sub>O<sub>16</sub>H<sub>27</sub>, 18T:AlSi<sub>17</sub>O<sub>22</sub>H<sub>29</sub>, 28T:AlSi<sub>27</sub>. O40H33, 46T:AlSi45 O68H49. These cluster models are shown in Figs. 1-6. The labels on the models refer to the number of tetrahedrally coordinated atoms, T atoms, that is Si and Al atoms in each model. All of the models have  $C_1$  symmetry with the maximum Si:Al ratio of 45:1, corresponding approximately to a zeolite composition with 2 Al atoms per unit cell. Model 18T has small rings of 4T, 5T and 6T atoms and a larger ring of 10T atoms (see Fig. 4). The 10T atom ring encloses an entrance

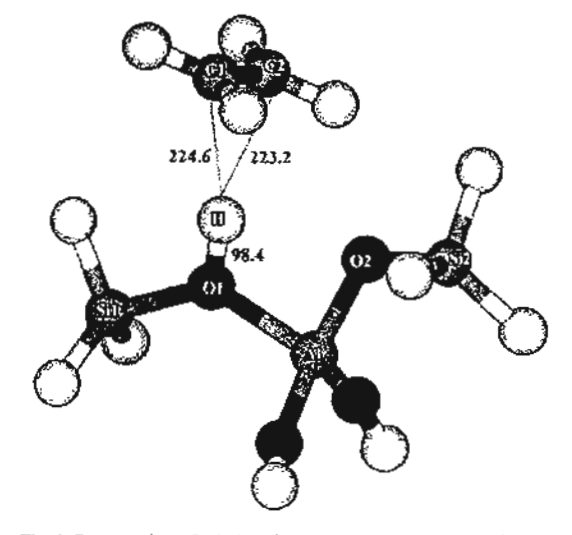


Fig. 1. Presentation of ethylene interaction with the model of the H-ZSM-5 zeolite cluster, 3T:AISi2O4Ha.

the Control 1000 . 64.55 has 3 \$500 A . . .

Charles S. 115000

30 10 10

ALL TOTAL STATE OF THE PROPERTY OF THE PROPERT

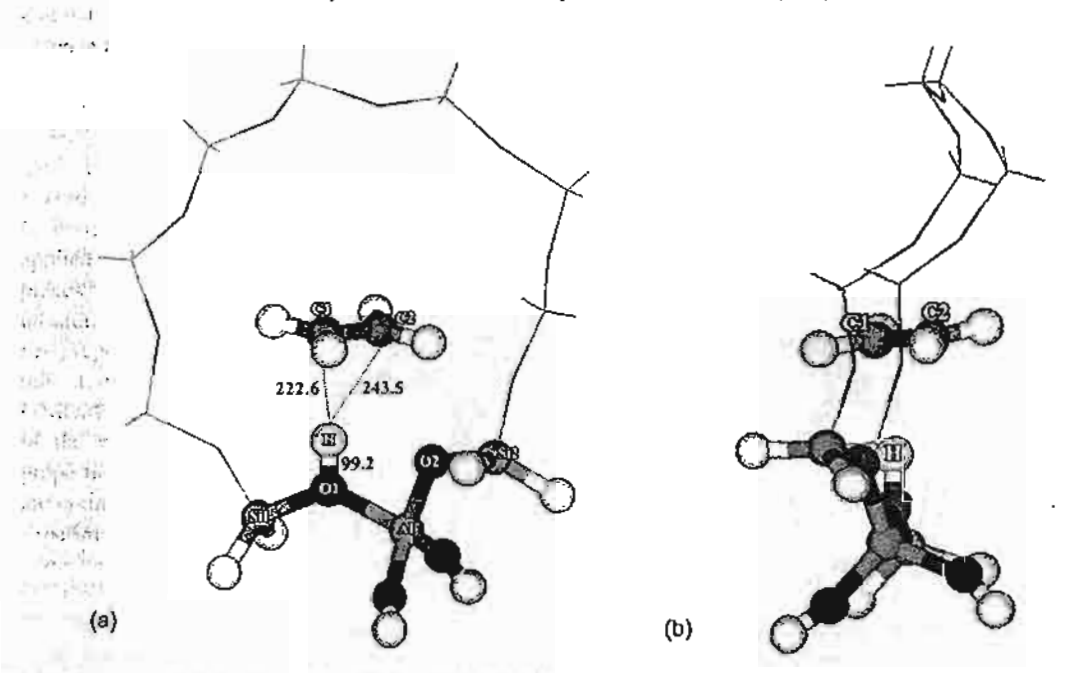


Fig. 2. Presentation of ethylene interaction with the model of the H-ZSM-5 zeolite cluster, 10T:AlSi<sub>2</sub>O<sub>12</sub>H<sub>21</sub>. (a) The model is viewed from the zigzag direction, while figure (b) is viewed from the direction of the straight channel. Atoms belonging to the active region drown as sphere.

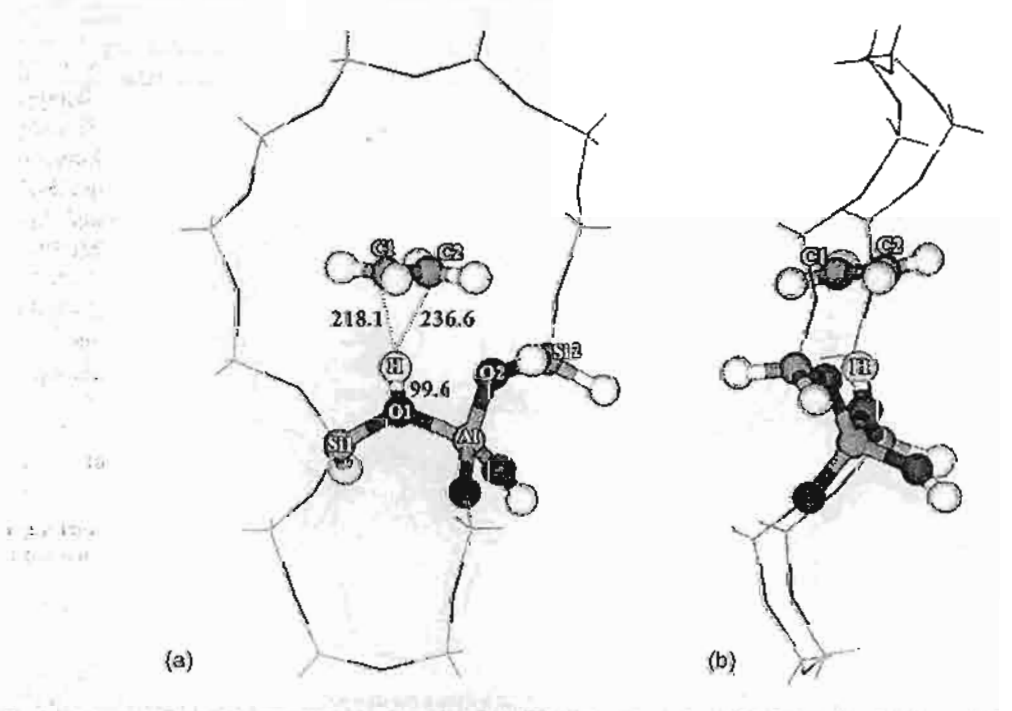


Fig. 3. Presentation of ethylene interaction with the model of the H-ZSM-5 zeolite cluster, 14T:AlSil<sub>3</sub>O<sub>16</sub>H<sub>27</sub>. (a) The model is viewed from the zigzag direction, while figure (b) is viewed from the direction of the straight channel. Atoms belonging to the active region drown as sphere.

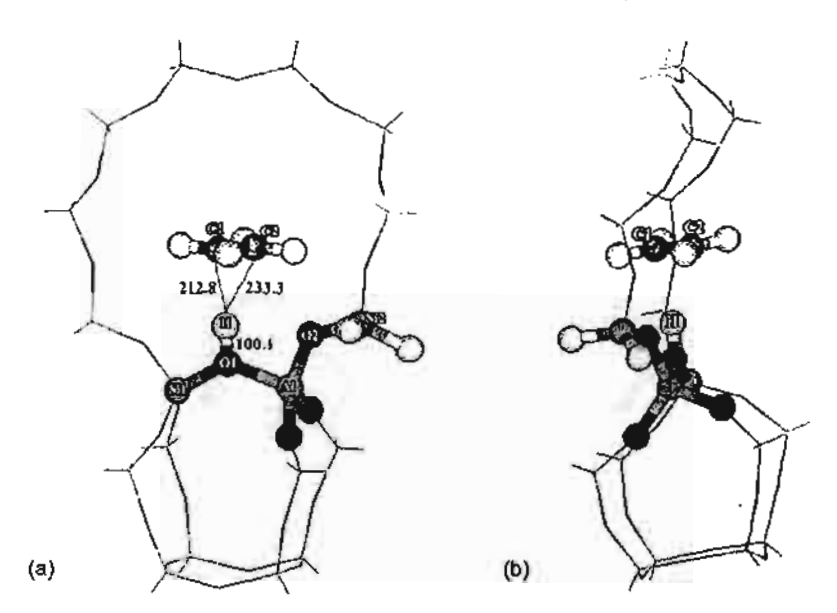


Fig. 4. Presentation of ethylene interaction with the model of the H-ZSM-5 zeolite cluster, 18T:AlSi<sub>17</sub>O<sub>22</sub>H<sub>29</sub>. (a) The model is viewed from the zigzag direction, while figure (b) is viewed from the direction of the straight channel. Atoms belonging to the active region drown as sphere.

of the sinusoidal channel into the straight channel at the channel intersection. Model 28T is built from 18T by the addition of a second 10T atom ring on the sinusoidal channel. Finally, the largest model created for this study is 46T, which is considered to be large enough to cover all important framework effect acts on both the active site and the adsorbate. Due to the limitation of computational resources and

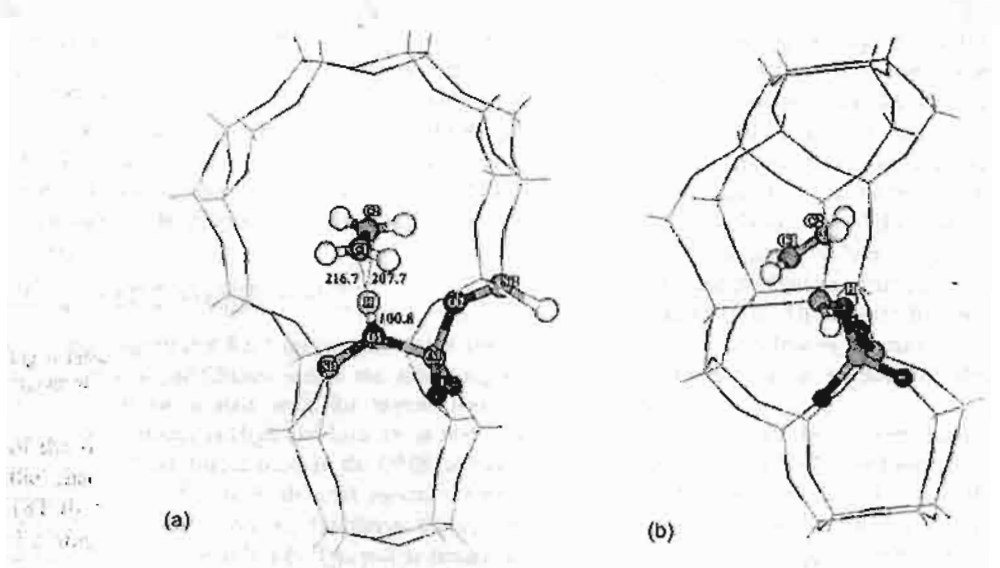


Fig. 5. Presentation of ethylene interaction with the model of the H-ZSM-5 zeolite cluster, 28T:AlSi<sub>27</sub>O<sub>40</sub>H<sub>33</sub>. (a) The model is viewed from the zigzag direction, while figure (b) is viewed from the direction of the straight channel. Atoms belonging to the active region drown as sphere.

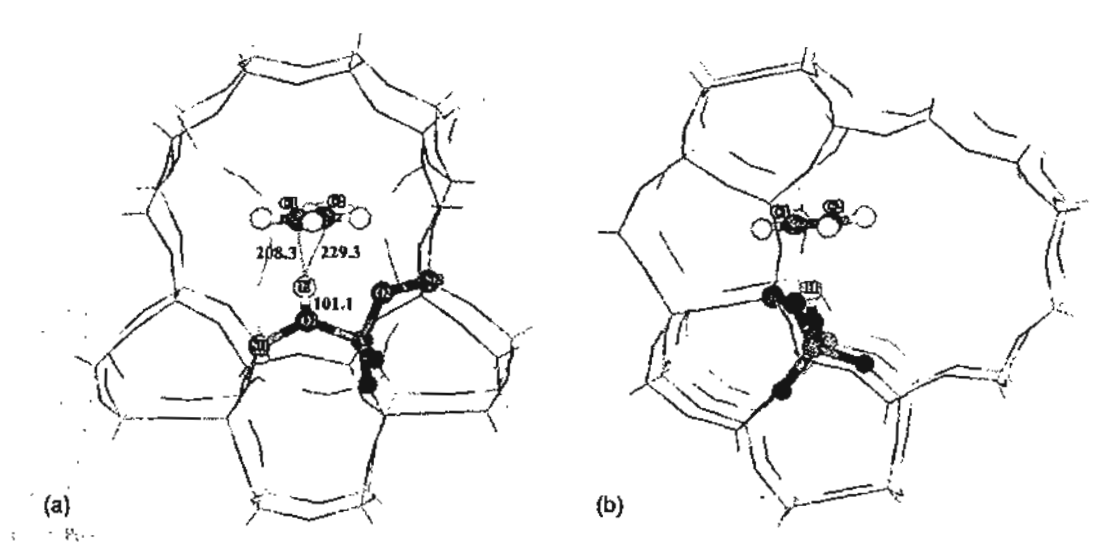


Fig.: 6. Presentation of ethylene interaction with the model of the H-ZSM-5 zeolite cluster, 46T:AlSi<sub>45</sub>O<sub>68</sub>H<sub>49</sub>. (a) The model is viewed from the zigzag direction, while figure (b) is viewed from the direction of the straight channel. Atoms belonging to the active region drown as sphere.

time consumption, the active region is treated more accurately with the ab initio method, while interaction in the rest of the model is approximated by a less accurate method.

According to the two-layer ONIOM approach, the calculation of energies can be simplified by treating the active region (i.e. the active BrØnsted acidic site of a zeolite catalyst) with a high-level quantum mechanical (ab initio or density functional) approach and the extended framework environment with a less expensive level, HF and molecular mechanics force field. The total energy of the whole system can be expressed within the framework of the ONIOM methodology developed by Morokuma and coworkers

$$E_{\text{ONJOM2}} = E_{\text{Low}}^{\text{Real}} + (E_{\text{High}}^{\text{Cluster}} - E_{\text{Low}}^{\text{Cluster}})$$

where the superscript Real means the whole system and the superscript Cluster means the active region, which would be treated with the higher level of calculation. Subscripts High and Low mean high- and low-level methodologies used in the ONIOM calculation. In this study, the high-level region is treated with Hartree-Fock or density functional theory with the hybrid functional B3LYP. The rest is treated by molecular mechanics force field (UFF) or the Hartree-Fock method.

The accuracy of the OM/MM method, particularly the ONIOM method, depends significantly on the choices of the level of calculations for highand low-level regions. Going through various types of quantum mechanics and molecular mechanics methods, the experimental adsorption energy of the ethylene/zeolite system can be used to validate the choice of methods. Using the B3LYP method for treating the quantum cluster, we varied the methods for low-level region from the molecular mechanics force field (UFF) to the Hartree-Fock method. Using the experimental observation as a benchmark, we found that the molecular mechanics force field, particularly the UFF, and HF methods provide reasonable values corresponding to the experimental prediction. This suggests that the UFF force field and HF methods are the practical choices for the low-level methodology when the high-level region is treated by the DFT/B3LYP method.

All calculations have been performed by using GAUSSIAN98 code [38]. The basis set for the Hartree-Fock calculations is 3-21G, while the basis set 6-31G(d,p) is utilized for the B3LYP calculations. The basis set error is approximated by a single point calculation at the higher basis set, 6-311++G(d,p). During the structure optimization, only the active site

street and in some of the second seco

### 3. Results and discussion

: :

The state of the Themson is a state of the s

For the purpose of clarity, we separate the discussion below into two sections. In one section we compare the cluster models and ONIOM results with experimental results. In the other section we focus mainly on the effects of extended framework on structural and energetic information of the interaction of ethylene with H-ZSM-5 zeolite.

3.1. Comparison of cluster models and ONIOM results with experimental results

Different two-layer ONIOM2 integrated schemes (B3LYP/6-311++G(d,p):HF/3-21G, B3LYP/6-31G(d,p):UFF, and HF/3-21G:UFF) were performed on six structures of ethylene/H-ZSM-5 adsorption complexes, as shown in Figs. 1-6. The H-ZSM-5 zeolites were modeled by

six different aluminosilicate clusters containing up to 46 tetrahedrally coordinated tetravalent atoms.

Three H-ZSM-5 zeolite containing 3, 10 up to 14 tetrahedrally coordinated tetravalent atoms clusters calculated at the full HF/3-21G and B3LYP/6-31G(d,p) levels of theory are documented in Table 1 and Tables 2-4 list some selected structure parameters derived at different two-layer ONIOM2 integrated schemes mentioned earlier.

Cluster results. The comparison of the geometry of the smaller zeolitic cluster (see Table 1) between the full B3LYP/6-31G(d,p) and the full HF/3-21G results agrees with 1 pm for Si-O and O1-H, while the weaker Al-O bond lengths agree with 2-7 pm, depending on cluster size models. The Si1-O1-A1 and Si2-O2-A1 parameters are in good agreement with HF. The more flexible Si2-O2-Al angle is well represented by B3LYP but not by HF, the latter giving an angle 9° larger than the former. This suggests that B3LYP should be employed for a high-level model. It is also seen that the O1-H bond lengths are increased as the size of the clusters are increased from 3T to 14T for both methods. The A1-O and Si-O bonds of

Table 1

HP/3-21G and B3LYP/6-31G(d,p) optimized geometrical parameters computed for 3T/C<sub>2</sub>H<sub>4</sub>, 10T/C<sub>2</sub>H<sub>4</sub> and 14T/C<sub>2</sub>H<sub>4</sub> systems (bond lengths in ptn and bond angles in degree)

Parameters	HF/3-21	G	_				B3LYP/6-31G(d,p)					
region in a	3T		101		14T		<b>3T</b>		107		14T	
otenijski gradij <u>ska —</u>	Isolated	Complex	isolated	Complex	Isolated	Complex	Isolated	Complex	Isolated	Complex	Isolated	Complex
01-H	97.1	97.6	97.2	98.3	97.3	98.6	96.8	98.4	97.0	98.6	97.1	99.0
AL÷OŁ.	179.0	178.4	176.6	176.2	176.4	175.8	186.6	185.4	184.2	183.3	183.0	182.0
\$11-01	169.6	169.2	167.0	166.7	166.0	165.6	169.3	168.7	167.3	166.9	166.8	166.3
A)-02	167.4	167.6	165.3	165.2	164.9	164.7	169.6	169.8	168.1	168.0	167.5	167.5
Si2-O2	162.8	162.6	159.7	159.2	159.8	159.2	162.6	162.1	160.4	159.7	160.6	159.9
LSi1:-OL-A)	132.4	132.4	132.1	131.4	131.2	130.6	134.3	133.4	134.3	132.7	133.5	132.1
∠Si202-AI	131.0	131.8	132.4	134.0	134.3	136.0	122.5	123.9	122.9	124.8	124.7	126.7
Al···H	221.9	227.0	225.9	229.2	226.8	229.9	232.8	238.5	234.6	238.3	234.3	238.1
С1-Н С2-Н	-	233.7	-	230.7	-	226.L	-	224.6	-	233.0	-	227.2
C2-H	_	230.2	-	242.9	_	239.1	-	223.2	-	231.9	-	226.4
C=C <sup>t</sup> land	-	132.1	-	132.2	-	132.2	-	133.7	-	133.7	-	133.7
ZH II	-	222 3	-	227.5	-	223.1	-	213.7	-	222.6	-	216.7

<sup>1.</sup> The calculated HF/3-21G and B3LYP/6-31G(d,p) gas phase C≈C bond distances are 131.5 and 133.0 pm, respectively.

b Bond distance of protonic zeolite with the mid point of the C=C bond.

Table 2 The ONIOM2(B3LYP/6-31G(d,p):HF/3-21G) optimized geometrical parameters of the H-ZSM-5 and H-ZSM-5/C<sub>2</sub>H<sub>4</sub> adsorption complex (bond lengths in pm and bond angles in degree)

Parameters .	Model									
	101		4T		1 <b>8T</b>	18 <b>T</b>			46T	
<u> </u>	Isolated	Complex	Isolated	Сощрісх	Isolated	Complex	Isolated	Complex	Isolated	Complex
O1-H	97.2	99.2	97.3	99.6	97.0	100.1	97.4	100.8	97.6	101.1
A1-01	183.7	182.6	182.8	181.6	181.7	180.4	180.9	179.3	181.0	179.5
Síl-Oi	166.1	165.7	164.9	164.5	163.4	163.0	163.4	162.6	163.2	162.5
Al-O2	167.4	167.3	167.0	166.9	166.5	166.3	166.1	166.1	165.9	165.8
Si2-O2	159.3	158.5	159.5	158.6	159.6	158.6	158.1	157.1	156.7	155.8
∠Sil-Ol-Al	133.9	132.1	132.6	131.1	1320	130.4	131.2	130.2	131.6	130.0
∠Si2-Q2-Al	123.4	125.8	125.4	128.1	126.4	129.3	126.9	129.6	127.8	130.4
Ale iH	238.8	240.5	239.2	241.0	239.0	240.1	238.7	240.9	238.1	239.3
C1~H. ₹	-	222.6	_	218.1	-	212.8	-	216.7	-	208.3
C2-H	-	243.5	-	236.წ	_	233.3	_	207.7	_	229.3
CTC*: C	-	133.7	_	133.8	-	133.9	-	134.0	-	134.0
C,	-	223.5	-	217.4	-	213.0	-	201.4	-	208.5
ZH···lĭ										
Less C										

The calculated B3LYP/6-31G(d,p) gas phase C=C bond distance is 133.0 pm.

Bond-distance of protonic zeolite with the mid point of the C=C bond.

, \* p 432

Parks.

Table 3 The ONIOM2(B3LYP/6-31G(d,p):UFF) optimized geometrical parameters of the H-ZSM-5 and H-ZSM-5/C2H4 adsorption complex (bond lengths in pm and bond angles in degree)

Parameters	Model									
No 632	101		14T		18T		28T		46T	
5 ( 160 3 ( 140	Isolated	Complex	[solated	Complex	Isolated	Complex	Isolated	Complex	Isolated	Complex
ot∸iț <sub>i</sub>	97.1	98.3	97.1	98.2	97.0	98.0	97.0	98.1	97.1	98.0
ม−0¦	182.9	181.7	185.7	184.1	188.4	186.6	185.4	184.0	184.1	182.8
ii-Öl	169.2	168.7	168.9	168.3	168.1	167.7	168.3	167.2	167.5	167.2
1-02	166.7	166.7	166.0	166.0	. 165.6	165.5	165.7	165.4	165.8	165.9
i2-02 .	162.3	161.8	162.1	161.5	161.7	161.1	160.8	160.2	159.8	159.3
Si1-01-Al	139.9	139.0	139.1	138.3	139.6	138.6	139.2	137.3	139.2	138.3
Si2-02-Al	125.7	127.6	124.7	126.5	123.7	125.7	120.5	122.7	120.3	121.8
.~-H <sup>:</sup> /	224.0	228.7	226.9	231.7	228.8	233.7	226.3	231.7	223.9	228.6
-H-36	-	234.2	-	233.5	<b>-</b>	235.6	_	238.2	-	242.5
ર=Hન્ત્રને લ	-	234.4	_	234.1	-	236.0	_	238.4	_	243.0
=Cr	-	133.6	-	133.6	_	133.6	-	133.6	~	133.6
رمه	-	224.5	-	224.1	_	226.1	-	228.7	~	233.4
ZH···II :	-	224.3	•	224.1	-	220.1	-	220.1	-	233.4

<sup>\*</sup> The calculated B3LYP/6-31G(d,p) gas phase C=C bond distance is 133.0 pm.

1 - 11 - 5 . .4

Francisco de

<sup>&</sup>lt;sup>b</sup> Bond distance of protonic zeolite with the mid point of the C=C bond. · x - 00.31

..!. والمنتقد والمراجون A Perch J. Garage

Table 4 The ONIOM2(HF/3-21G:UFF) optimized geometrical parameters of the H-ZSM-5 and H-ZSM-5/C2H4 adsorption complex (bond lengths in pm and bond angles in degree)

•										
	101	10T		14T		18T			46T	
·	Isolated	Complex	Isolated	Complex	Isolated	Complex	Isolated	Complex	[solated	Complex
OI-H	97.2	97.8	97.2	97.7	97.2	97.7	97.3	97.7	97.4	97.6
Al-Oi	176.2	175.6	177.4	176.8	178.E	177.4	176.8	176.2	176.0	175.5
Sil-Ol	169.6	169.2	169.3	168.8	168.6	168.2	168.7	168.3	167.9	167.6
AI=02	165.0	165.2	164.4	164.6	164.2	164.4	164.7	164.9	165.0	165.1
Si2-O2	162.5	162.3	162.1	162.0	161.9	161.7	161.2	161.0	160.4	160.2
∠Sil-Ol~AL	136.3	136.3	135.4	135.4	135.0	135.0	135.3	135.3	135.4	135.5
∠Si2-O2-AI	134.0	135.է	134.1	135.0	134.0	135.0	130.3	131.1	129.4	(30.0
Al · · H	218.0	221.5	219.0	222.8	218.7	222.9	217.1	221.3	214.6	218.8
СГ-Н С2-Н, " С=С"	-	237.7	-	237.5	_	242.3	-	246.2	~	248.7
C2-H, "	-	235.0	. –	233.7	_	235.5	_	238.6	-	243.6
C=C, c	-	132,1	-	132.1	_	132.0		132.0	-	132.0
C <sub>p</sub>	-	226.9	_	226.2	-	229.6	_	233.3	-	237.1
ZH····lĭ ·Ç										

A The calculated HP/3-21G gas phase C=C bond distance is 131.5 pm.

-8 Bond distance of protonic zeolite with the mid point of the C=C bond.

the bridging hydroxyl groups are evaluated as being too long in 3T clusters as compared to the 14T cluster model for both levels of theory. It is noted that the OI-H bond lengths calculated at the HF/3-2TG level are longer than that of the B3LYP/6-31G(d,p) as expected, which can be reflected by the corresponding higher adsorption energies (-7.35 vs. - 8.98 kcal/mol, cf. Table 5).

ONIOM results. To assess the sensitivity of the active site structure with varying environments, we optimized the active site, =SiO(H)Al(O)2OSi=, for all the clusters, the remaining atoms were kept fixed at the crystallographic positions. The hydrogen atoms at the terminal position are fixed. By comparing the structure between the full B3LYP/6-31G(d,p) quantum cluster models and those ONIOM2 schemes, it is seen that the cluster environment imposed in the ONIOM2 scheme has small effect on the structure of the active site in the ONIOM2 schemes, specifically B3LYP/6-31G(d,p):HF/3-21G (cf. Table 2), the extended framework has the effect of lengthening the OI-H bond distance (BrØnsted acid site) by 0.4 pm, and thus enhancing the acidity of the Bronsted acid site. 1300

Further support for the reliability of the active site subunit, =Si-OH-Al=, by our calculations is given from NMR studies. Klinowski et al. have estimated the internuclear distance between aluminum and proton nuclei in a Bronsted acid site, r(Al···H), of H-Faujasite [39] and H-ZSM-5 [40] to be 238.0  $\pm$  4 and 248.0 ± 4 pm, respectively, whereas our computed  $r(Al \cdot \cdot H)$  distances of the most realistic model of 46T cluster are 238.1, 223.9, and 214.6 pm for the B3LYP/6-31G(d,p):HF/3-21G, B3LYP/6-31G(d,p):UFF, HF/3-21G:UFF, respectively. As can be seen from the experimental data, the computed  $r(Al \cdots H)$  distance in the ONIOM2 is well represented by the B3LYP/6-31G(d,p):HF/3-21G scheme, but not by the two schemes: B3LYP/6-31G(d,p):UFF, HF/3-21G:UFF, these schemes giving the  $r(AI \cdots H)$  distance 14.2 and 23.5 smaller than the B3LYP/6-31G(d,p):HF/3-21G scheme. This again suggests that B3LYP should be employed for a high-level model. Therefore, in order to keep this article short, we will discuss mainly the more accurate ONIOM2 results. However, the structural parameters of the other ONIOM2 schemes: (B3LYP/6-31G(d,p):UFF, and HF/3-21G:UFF) are documented in Tables 3 and 4.

. - 13×  $\{\cdot,\cdot,\cdot\}$ N. 1-1 36 CHANGE. 1.00

42° C.3

Table 5 .

The interaction energy (kcal/mol) of ethylene molecule with different aluminosilicate clusters representin gH-ZSM-5 zeolites containing up to 46T cluster model

Method	Model					
	3T	10T	14T	18T	28T	46T
Full HF/3-21G	- 6.66	8.33	-8.98		_	
Part B3LYP/6-31G(d,p)	6.57	6.84	-7.35	_	-	_
ONIOM2(HE/3-21G:UFF)	_	-10.76	- 10.84	10.68	- 14.40	- 14.46
ONIOM2(B3LYP/6-31G(d,p):UFF)	_	- 10.09	-10.22	-9.95	- 14.28	-14.18
ONIOM2(B3LYP/6-31G(d.p):HF/3-21G)	_	-8.24	-9.02	- 9.83	-11.00	-11.67
ONIOM2(B3LYP/6-311++G(d,p):HF/3-21G)	-	- 5.95	-6.67	-7.40	- 8.60	<b>-9.14</b>

3.2. The interaction of ethylene with H-ZSM-5 zeolite

1.00

And the control of th

BUSSET

Charlest with the same and subject of the feet of the

Cluster results. The changes in the structural parameters of the C2H4 and 3T cluster model of zeolite upon complexation are small. However, the changes are in accordance with Gutmann's rules [41], i.e. a lengthening of the O1-H (96.8 vs. 98.4 pm) and C#Cibonds (133.0 vs. 133.7 pm) and shortening of the Si-O and Al-O bonds. Our calculated ethylene adsorption energy from the bare 3T cluster models is estimated to be -4.25 kcal/mol at B3LYP/6-3TT++G(d,p) level, which is in the lower end of the predicted range from -4 to -7 kcal/mol from previous theoretical studies [9-11]. In this case, one can expect the extended structure included in the ONIOM model would enhance the binding energy of ethylenesion zeolites. Variation of the calculated adsorption energies,  $\Delta E$ , are at about 2.32 kcal/mol at the full HF/3-21G and about 0.78 kcal/mol at the full B3LYP/6-31G(d,p) level of theory. It is observed that the  $\Delta E$  for the 14T cluster model obtained with 6-31G(d.p) basis set is 2.35 kcal/mol larger than that derived with the 6-311++G(d.p). Such a difference, about 30% of  $\Delta E$ , is not negligible. In order to obtain a more reliable  $\Delta E$ , single point calculation using a larger basis set, B3LYP/6-311++G(d,p) has to be evaluated at the B3LYP/6-31G(d,p) structure.

the NIGM results. Increasing the cluster size from the pare: 3T quantum cluster to 46T in the ONIOM2 integrated scheme, B3LYP/6-31Q(d,p):HF/3-21G, shortens the adsorption distance (i.e. the distance between the Brønsted proton and the mid-point of the C=C bond) by about 5.2 pm; while it elongates the C=C slightly and

O1-H bond distance by about 0.3 and 2.7 pm, respectively. Similar findings are also obtained from the less accurate ONIOM2 results (see Tables 2-4).

Regarding smaller clusters, the use of the HF method for the low level overestimates the adsorption energy by about 1.40 and 1.67 kcal/mol for the 10T and 14T, respectively, which is relative to the corresponding full B3LYP/6-31G(d,p) level of theory. Similar trends are also observed for the UFF when used as a low-level theory. The adsorption energy is found to depend on the cluster employed, suggesting that structural differences beyond the active sites may play an important role in determining adsorption energies due to the long-range electrostatic effects.

As for the results of the ONIOM2 scheme, in going from the bare 3T quantum cluster model up to the more realistic 46T cluster model, we found that the extended framework of zeolite has a large effect on the adsorption energetics. Specifically, it decreases the adsorption energy of ethylene on H-ZSM-5 by -7.61 kcal/mol (3T cluster result at full B3LYP/6-31G(d,p) level vs. 46T cluster result at ONIOM2(B3LYP/6-31G(d,p):UFF) level). When the HF/3-21G is employed instead of UFF-molecular mechanics force field-method for the low level, it decreases the adsorption energy by --5.10 kcal/mol (3T cluster result at full B3LYP/6-31G(d,p) level vs. 46T cluster result at ONIOM2(-B3LYP/6-31G(d,p):HF/3-21G) level) for the [C<sub>2</sub>H<sub>4</sub>]/H-ZSM-5 system. Finally, in order to obtain a more reliable  $\Delta E$ , single point calculation using a larger basis set, B3LYP/6-311++G(d,p), was evaluated at the B3LYP/6-31G(d,p) structure,

which yields the adsorption energy complex of -9.14 kcal/mol. Our predicted value for the [C<sub>2</sub>H<sub>4</sub>]/H-ZSM-5 system is in excellent agreement with the experimental estimate of -9 kcal/mol obtained by Cant and Hall [5].

### 4. Conclusion

The second secon

The adsorption of ethylene on H-ZSM-5 zeolites , has been investigated with six different cluster sizes ; and methods comprising various two-level ONIOM2 B3LYP/6-311++G(d,p):HF/3-21G, : schemes: -B3LYP/6-31G(d,p):HF/3-21G, B3LYP/6-31G(d,p):UFF, and HF/3-21G:UFF. The bare 3T quantum cluster approach predicts the [C2H4]/H-ZSM-5 complexes to have the binding energies of - 4.25 kcal/mol. The effect of the zeolite framework is modeled by the ONIOM2 method. We found that the extended framework significantly enhances the adsorption energy of ethylene to the zeolites. In particular, the final predicted adsorption energy of 5.9.14 kcal/mol for the [C<sub>2</sub>H<sub>4</sub>]/H-ZSM-5 complexes was calculated by the ONIOM2(B3LYP/6-311++G(d,p):HF/3-21G) method. This efficient scheme performs superbly as compared with the experimental estimate of -9 kcal/mol. The results obtained in the present study suggest that the ONIOM approach yields a more accurate and practical model in studying adsorption of unsaturated hydrocarbons on zeolites. Selection (

### Acknowledgements

A 18 . 1

affi can Village to Sa

E. Oak

This work was supported in part by grants from the Thailand Research Fund (TRF Senior Research Scholar to JL) and the Kasetsart University Research and Development Institute (KURDI) as well as the Ministry of University Affairs under the Science and Technology Higher Education Development Project (MUA-ADB funds). The support from the Dow Chemical Company (USA) is also acknowledged. Our sincere thanks are due to Professor R. Ahlrichs (Karlsruhe, Germany) for his continued support of this work.

#### References

- C.R.A. Catlow (Eds.), Modeling of Structure and Reactivity in Zeolites, Academic Press, San Diego, 1992.
- [2] C. Pereira, G.T. Kokotailo, R.J. Gorte, J. Phys. Chem. 95 (1991) 705.
- [3] S. Bordiga, G. Ricchiardi, G. Spoto, D. Scarano, L. Carnelli, A. Zecchina, C.O. Arean, J. Chem. Soc., Faraday Trans. 89 (1993) 1843.
- [4] B.V. Liongme, W.K. Hall, Trans. Faraday Soc. 62 (1966) 3229.
- [5] N.W. Cant, W.K. Hall, J. Catal, 25 (1972) 161.
- [6] V.B. Kazansky, Catal. Today 51 (1999) 419.
- [7] M. Boronat, P. Viruela, A. Corma, J. Phys. Chem. A 102 (1998) 982.
- [8] V.B. Kazansky, Acc. Chem. Res. 24 (1991) 379.
- [9] E.M. Evleth, E. Kassab, H. Jessri, M. Aliavena, L. Montero, L.R. Sierra, J. Phys. Chem. 100 (1996) 11368.
- [10] P. Ugliengo, A.M. Ferrari, A. Zecchina, E. Garrone, J. Phys. Chem. 100 (1996) 3632.
- [11] P.J. O'Malley, K.J. Franworth, J. Phys. Chem. B 102 (1998) 4507
- [12] S. Beran, J. Mol. Catal. 30 (1985) 95.
- [13] B. Kontnik-Matecka, M. Gorska, J. Eysymontt, A. Salek, J. Mol. Struct. 80 (1982) 199.
- [14] J.L. White, L.W. Beck, J.P. Haw, J. Am. Chem. Soc. 114 (1992) 6182.
- [15] E.G. Derouane, J.B. Nagy, J.P. Gilson, Z. Gabrlica, Stud. Surf. Sci. Catal. 7 (1981) 1412.
- [16] J. Gao, in: K.B. Lipkowitz, D.B. Boyd (Eds.), Reviews in Computational Chemistry, vol. 7, VCH, New York, 1995, p. 119
- [17] M.J. Field, P.A. Bash, M. Karplus, J. Comput. Chem. 11 (1990) 700.
- [18] U.C. Sighn, P.A. Kollman, J. Comput. Chem. 7 (1996) 718.
- [19] E.V. Stefanovich, T.N. Truong, J. Phys. Chem. B 102 (1998) 3018.
- [20] S.P. Greatbanks, J.H. Hillier, N.A. Burton, P. Sherwood, J. Chem. Phys. 105 (1996) 3370.
- [21] R.Z. Khaliullin, A.T. Bell, V.B. Kazansky, J. Phys. Chem. A 105 (2001) 10454.
- [22] J. Limtrakul, T. Nanok, P. Khongpracha, S. Jungsuttiwong, T.N. Truong, Chem. Phys. Lett. 349 (2001) 161.
- [23] P. Treesukol, J. Limtrakul, T.N. Truong, J. Phys. Chem. B 305 (2001) 2421.
- [24] J. Limtrakel, P. Khongpracha, S. Jungsuttiwong, T.N. Truong, J. Mol. Catal. A 153 (2000) 2469.
- [25] S. Jungsuttiwong, S. Nokbin, P. Chuichay, P. Khongpracha, T.N. Truong, J. Limtrakui, Stud. Surf. Sci. Catal. 135 (2001) 2518.
- [26] J. Limtrakul, P. Khongpracha, S. Jungsuttiwong, I. Mol. Struct. 525 (2000) 153.
- [27] J. Limtrakul, S. Nokbin, P. Chuichay, J. Mol. Struct. 560 (2001) 169.
- [28] J. Limtrakul, S. Nokbin, S. Jungsuttiwong, P. Khongpracha, T.N. Truong, Stud. Surf. Sci. Catal. 135 (2001) 2469
- [29] R. Vetrivel, C.R.A. Catlow, E.A. Colboum, Proc. R. Soc. Lond. A 417 (1998) 81 (b) M. Allavena, K. Sciti, E. Kassab,

G. Ferenczy, J.G. Angyan, Chem. Phys. Lett. 168 (1990) 461. (c) G. Aloisi, P. Barnes, C.R.A. Catlow, R.A. Jackson, A.J. Richard, J. Phys. Chem. 93 (1990) 3573. (d) J.C. White, A.C. Hess, J. Phys. Chem. 97 (1993) 8730. (e) E. Teunisson, A.P.J. Jansen, R.A. van Santen, R. Orlando, R. Dovesi, J. Phys. Chem. 101 (1994) 5865. (f) A. Kyrlidis, S.J. Cook, A.K. Chakraborty, A.T. Bell, D.N. Theodorou, J. Phys. Chem. 99 (1995) 1505. (g) E.H. Teunissen, A.P.J. Jansen, R.A. van Santen, J. Phys. Chem. 99 (1995) 1873. (h) U. Eichier, M. Brändle, J. Sauer, J. Phys. Chem. 8 99 (1997) 1873. (i) M. Brandle, J. Sauer, J. Am. Chem. Soc. 120 (1998) 1556.

· . · . .

A COMMENT OF THE PARTY OF THE P

1:120 ... ( 85.04 1120 -124 (1) Chen 1 400 1000 State Best 341.15 Luit W. 124 1 10 5 V 5 V 5 V 2 . . ..... . : 18. 3

- [30] F. Mascras, K. Morokuma, J. Comput. Chem. 16 (1995) 1170.
   [31] T. Matsubara, S. Sieber, K. Morokuma, Int. J. Quantum Chem. 60 (1996) 1101.
- [32] S. Humbel, S. Sieber, K. Morokuma, J. Chem. Phys. 105 (1996) 1959.
- [33] M.:Svensson, S. Humbel, K. Morokuma, J. Chem. Phys. 105 (1996) 3654.
- [34] M. Svensson, S. Humbel, R.D.J. Froese, T. Matsubara, K. Morokuma, J. Phys. Chem. 100 (1996) 19357.
- [35] S. Dapprich, I. Komaromi, K.S. Byun, K. Morokuma, M.J. Frisch, J. Mol. Struct. (Theochem) 461 (1999) 1.
- [36] T. Vreven, K. Morokuma, J. Comput. Chem. 21 (2000) 1419.

- [37] H. van Koningveld, H. van Bekkum, J.C. Jansen, Acta Crystallogr. B 43 (1987) 127.
- [38] M.J. Frisch, G.W. Trucks, H.B. Schlegel, G.E. Scuseria, M.A. Robb, J.R. Cheeseman, V.G. Zakrzewski, J.A. Montgomery, Jr., R.E. Stratmann, J.C. Burant, S. Dapprich, J.M. Millam, A.D. Daniels, K.N. Kudin, M.C. Strain, O. Farkas, J. Tomasi, V. Barone, M. Cossi, R. Cammi, B. Mennucci, C. Pomelli, C. Adamo, S. Clifford, J. Ochterski, G.A. Petersson, P.Y. Ayala, Q. Cui, K. Morokuma, P. Salvador, J.J. Dannenberg, D.K. Malick, A.D. Rabuck, K. Raghavachari, J.B. Foresman, J. Cioslowski, J.V. Ortiz, A.G. Baboul, B.B. Stefanov, G. Liu, A. Liashenko, P. Piskorz, I. Komaromi, R. Gomperts, R.L. Martin, D.J. Fox, T. Keith, M.A. Al-Laham, C.Y. Peng, A. Nanayakkara, M. Challacombe, P.M.W. Gill, B. Johnson, W. Chen, M.W. Wong, J.L. Andres, C. Gonzalez, M. Head-Gordon, E.S. Replogle, J.A. Pople, GAUSSIAN98, Gaussian, Inc., Pittsburgh PA, 2001
- [39] R.L. Stevenson, J. Catal. 21 (1971) 113. (b) D. Frende, J. Klinowski, H. Hamdan, Chem. Phys. Lett. 149 (1988) 355.
- [40] J. Klinowski, Chem. Rev. 91 (1991) 1459.
- [41] V. Gutmann, The Donor-Acceptor Approach to Molecular Interaction, Plenum Press, New York, 1978.



6

80

THEO CHEM

Journal of Molecular Structure (Theochem) 631 (2003) 147-156

www.elsevier.com/locate/theochem

## Adsorption of aromatic hydrocarbon onto H-ZSM-5 zeolite investigated by ONIOM study

Chadchalerm Raksakoon, Jumras Limtrakul\*

Taboratory for Computational and Applied Chemistry, Chemistry Department, Kasetsart University, Bangkok 10900, Thailand
Received 13 December 2002; accepted 17 March 2003

ONIOM (Our-own-N-layer Integrated molecular Orbital + molecular Mechanics) approach utilizing two-layer ONIOM2 schemes—ONIOM2(MP2/6-31G(d,p):HF/3-21), ONIOM2(B3LYP/6-31G(d,p):HF/3-21), ONIOM2(B3LYP/6-31G(d,p):HF/3-21), ONIOM2(B3LYP/6-31G(d,p):HF/3-21), ONIOM2(B3LYP/6-31G(d,p):HF/3-21), ONIOM2(B3LYP/6-31G(d,p):HF/3-21), ONIOM2(B3LYP/6-31G(d,p):HF/3-21), ONIOM2(B3LYP/6-31G(d,p):HF/3-21), ONIOM2(B3LYP/6-31G(d,p):HF/3-21), ONIOM2(B3LYP/6-31G(d,p):HF/3-21), oniomatical states of the control of straight and sinusoidal channels, which is supported by the recent power neutron and synchrotron X-ray-diffraction techniques. The predicted adsorption energy for the ONIOM2(MP2/6-31G(d,p):HF/3-21) scheme is 13.75 kcal/mol, which corresponds well with the experimental estimate of 14.0 kcal/mol.

Keywords: H-ZSM-5 zeolite; Our-own-N-layer Integrated molecular Orbital; Synchrotron X-ray diffraction

### I. Introduction

Zeolites are crystalline solids having an 'open' porous internal surface whose framework is built by SiO<sub>4</sub> and AlO<sub>4</sub> tetrahedra connected via oxygen bridges. The dimensions of the pores and channels are of the order of a nanometer (1 nm = 10 Å). In some cases, the channels of the internal surface form intersections that is considerably larger than their channels. For example, the diameter of the roughly dylindrical pores and channels of zeolites having the MFF topology as ZSM-5 are about 5 Å (cf. Fig. 1), but the diameter of the roughly spherical intersection

\* Corresponding author Tel.: +66-2-942-8900x323; fax: +66-2-942-8900x324.

E-mail address: fscijrl@ku.ac.th (J. Limtrakul).

is about 9 Å which act as nanoscopic catalytic reactors.

At the present time, ZSM-5 zeolite is one of the important nanostructured catalysts for modern petrochemical and hydrocarbon processing owing to its unique characteristics, i.e. shape- and size-selectivity, active sites, thermal stability and ion-exchanged [1]. The adsorption and subsequent reactions of hydrocarbons on zeolites have been carried out for a number of experimental [2-13] and theoretical methods [14-20]. Of particular interest in this area of active research is the aromatic hydrocarbon adsorption on zeolites that is the foundation of several industrially important reactions, namely, the processing of BTX (benzene, toluene, xylene); e.g. toluene disproportionation, adsorptive separation of the xylene isomers and benzene alkylation [6]. The adsorption of benzene

0166-1280/03/\$ - see front matter © 2003 Elsevier B.V. All rights reserved.doi:10.1016/S0166-1280(03)00240-9

ी. देशहेंचर्च

Zeoist

C. Raksakoon, J. Limtrakul / Journal of Molecular Structure (Theochem) 631 (2003) 147-156

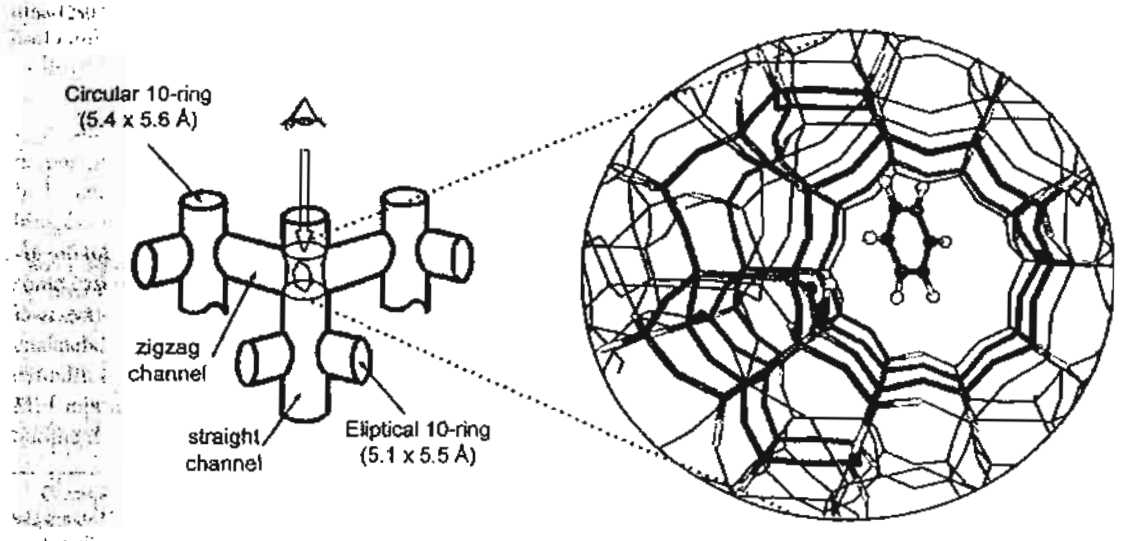


Fig. 1. The structure of H-ZSM-5 showing three different channel structures: channel interaction, the straight channel, and the zigzag channels. The large circle (linset) represents an intersection channel—modeled by the 46T cluster—serving as a nanoscopic reactor where the benzene molecule is favorably adsorbed. The inset is viewed from the top view of the straight channel direction as indicated by the eye's sign.

in zeolites has been studied experimentally by using Fourier Transform Raman spectroscopy [7], 29Si and <sup>2</sup>H NMR spectroscopy [8-11], power neutron and synchrotron X-ray diffraction [12] and calorimetric studies [13]. Although this system has been examined using several techniques, the exact structures of benezene/H-ZSM-5 complexes are still unsolved since there is no single-crystal XRD data available to date. One of the questions remaining unsolved is the controversy of the location of benzene molecules inside the ZSM-5 framework. 2H NMR studies [8-11] indicated that at low loadings, the benzene molecules reside in the midsection of the straight channels, while the power XRD result [12], on the other hand, indicated the benzene first adsorbed in the intersection channel. A sorption kinetic study [21] indicated that the initial adsorption of benzene occurs in the straight channels and at the channel intersections, until the loading level reaches four molecules perjunit; cell. Very recently the FT-Raman technique indicated that at low loadings all of the guest molecules reside at the intersection of the zeolitic framework [7].

strategy and the purpose of this study, we focus mainly on

the adsorption of benzene on zeolites as a starting point for a more comprehensive study on the reaction of industrial alkylation aromatic hydrocarbons and benzene derivatives in zeolites. There have been several previous theoretical studies on the adsorption of benzene in zeolites using ab initio electronic structure methods [14-17]. All of these studies, however, used the small cluster models and thus the effects of the zeolite framework are not taken into account. The predicted adsorption energy of benzene (-4 to -6 kcal/mol) [14] so far is noticeably lower compared to the experimental adsorption energy of benzene on the acidic H-Y zeolite (-14 kcal/mol) [22]. Such deviation indicates that the long-range interactions of the extended framework could be an important factor in stabilizing the adsorption complex. This raises the need for a better understanding of the effects of the extended framework in the adsorption of aromatic hydrocarbons.

To accurately include the effects of the extended zeolite framework on the adsorption properties, one can employ the periodic electronic structure methods such as the periodic density functional theory methodology. However, due to the large computational demand, such calculations are limited to rather small unit-cell zeolites that often are not used in the actual industrial processes. Combined quantum

to date. I the cope thirds t in fill moleculacultatella

other has

alande promatin ambolica

story lie story case interpolation. Will top. hid top y mechanical and molecular mechanical (QM/MM) methods have been proven to be powerful tools for treatment of large molecular systems [23-36]. This embedded methodology provides a cost effective computational strategy for including the effects of extended structure.

One such method is the original 'Our-own-N-layer Integrated molecular Orbital + molecular Mechanics (ONIOM)' approach, which has been developed by Morokuma and co-workers [37-43] and extended to the regime of large chemical and biological systems. To date, this method is applied mostly to large biomolecules, organometallic complexes. To our knowledge, no theoretical work on aromatic hydrocarbons interacted with zeolite has been reported by using the ONIOM methodology. In this study, the applicability and reliability of the ONIOM method will be tested to investigate the effect of the zeolitic framework structure on adsorption properties. The various two-level ONIOM2 schemes are optimized to find an efficient scheme by using the experimental data as a benchmark.

embedda computar

so the stants on the stants on the stants on the stants of the stants of

Day Fo.

# 2. Method

One st

IntTwo.different strategies have been employed to model the H-ZSM-5. First, different aluminosilicate olusters, are modeled to represent the active sites, whereas the second strategy employs the ONIOM2 approach. The cluster models were obtained from the tattice; structure of H-ZSM-5 zeolite [44]. The 3T cluster H3SiOAI(OH)2O(H)SiH3 which is considered as the smallest unit that is required to represent the active site of zeolite. The effect from the framework structure of zeolite cannot be totally neglected if more accurate results are required. Thus, the larger clusters were proposed for representing the system of H-ZSM-5. The five cluster structures of increasing size considered in this work were: 3T:AlSi2O4H9,  $10T_{c}AlSi_{9}O_{12}H_{21}$ ,  $14T_{c}AlSi_{13}O_{16}H_{27}$ ,  $18T_{c}AlSi_{17}O_{22}$ . H<sub>29</sub>, 46T:AlSi<sub>45</sub>O<sub>68</sub>H<sub>49</sub>. These cluster models are illustrated in Figs. 2-6. The labels on the models refer to the number of tetrahedrally coordinated atoms, T atoms, that is Si and Al atoms in each model. All of the models have C1 symmetry with the maximum Si/ Al ratio of 45:1, corresponding approximately to a zeolite composition with two Al atoms per unit cell.

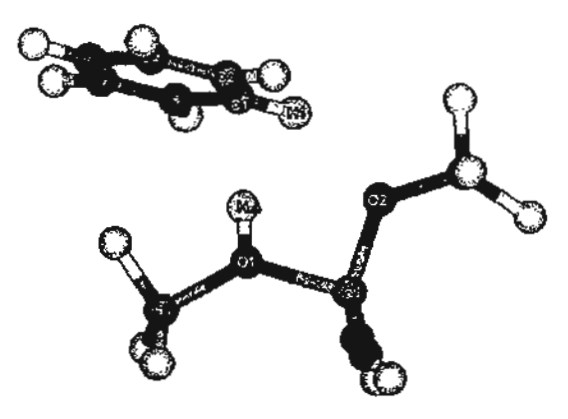


Fig. 2. Presentation of benzene interaction with the model of the H-ZSM-5 zeolite cluster, 3T:AlSi<sub>2</sub>O<sub>4</sub>H<sub>9</sub>.

The largest model created for this study is 46T, which is considered to be large enough to cover all important framework effect acts on both the active site and the adsorbate. Fig. 1 shows the three different channel structures of the H-ZSM-5: channel intersection, the straight channels are near-circular, having dimensions of  $5.4 \times 5.6$  Å, while the zigzag channels are elliptical and have dimensions of  $5.1 \times 5.5$  Å. The intersection channels, whose spatial dimensions are of about 9 Å which is modeled by the 46T cluster, where the benzene molecule is favorably located is illustrated in the inset. The inset is viewed from the top view of the straight channel direction.

Due to the limitation of computational resources and time consumption, the active region is treated more accurately with the ab initio method, while interaction in the rest of the model is approximated by a less accurate method.

According to the two-layer ONIOM approach, the calculation of energies can be simplified by treating the active region (i.e. the active Brønsted acidic site of a zeolite catalyst) with a high-level quantum mechanical (ab initio or density functional) approach and the extended framework environment with a less expensive level, the HF and molecular mechanics force fields. The total energy of the whole system can be expressed within the framework of the ONIOM methodology developed by Morokuma and coworkers

$$\mathcal{E}_{\text{ONIOM2}} = \mathcal{E}_{\text{Low}}^{\text{Real}} + (\mathcal{E}_{\text{Bigh}}^{\text{Cluster}} - \mathcal{E}_{\text{Low}}^{\text{Cluster}})$$

Altergravitation and the state of the state

C. Raksakoon, J. Limtrakul / Journal of Molecular Structure (Theochem) 631 (2003) 147-156

Distriction of the control of the co

1000 1000 1000 1000

350 000

FT ANSA

4,100

1 (184 1 (186 1 (186 1 (186 1 (186 1 (186 1 (186 1 (186 1 (186)))

4.

2 - 4 9.5 2 - 1 - 19. 1 - 10 - 64 - 5 - 64 - 5 - 64 - 6 - 65

> Cig. A. Pan 19 A Miliga

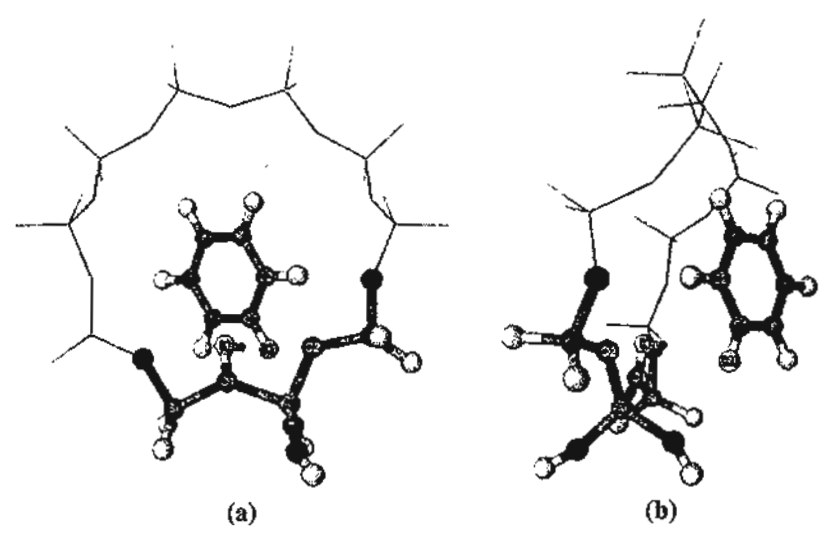


Fig. 3. Presentation of benzene interaction with the model of the H-ZSM-5 zeolite cluster, 10T:AlSi<sub>2</sub>O<sub>12</sub>H<sub>21</sub>. (a) The model is viewed from the 21grag; direction, while (b) is viewed from the direction of the straight channel. Atoms belonging to the active region drawn as sphere.

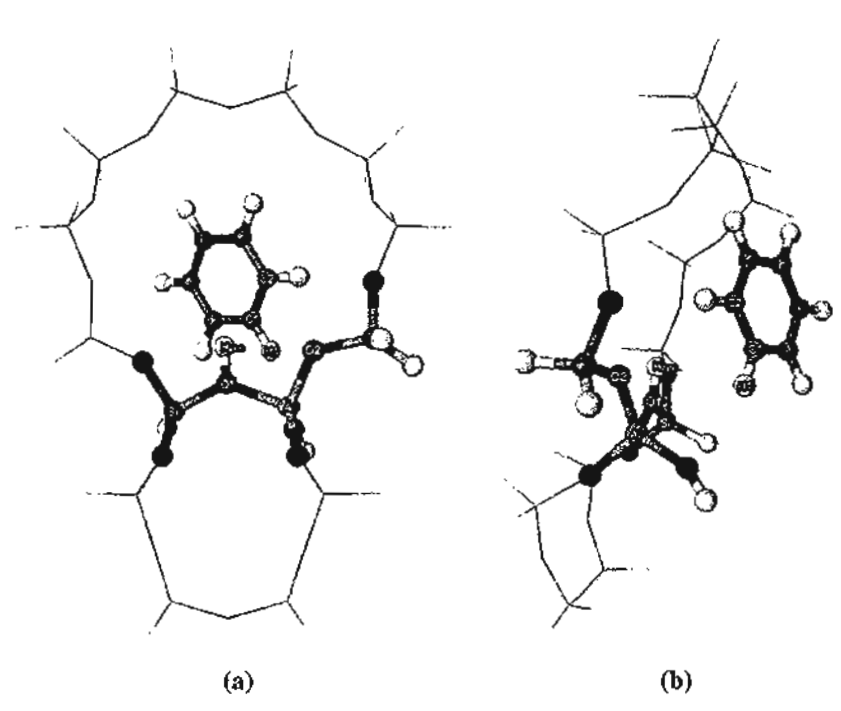


Fig. 4. Presentation of benzene interaction with the model of the H-ZSM-5 zerolite cluster, 14T:AlSi<sub>33</sub>O<sub>16</sub>H<sub>27</sub>. (a) The model is viewed from the zigzag direction, while (b) is viewed from the direction of the straight channel. Atoms belonging to the active region drawn as sphere.

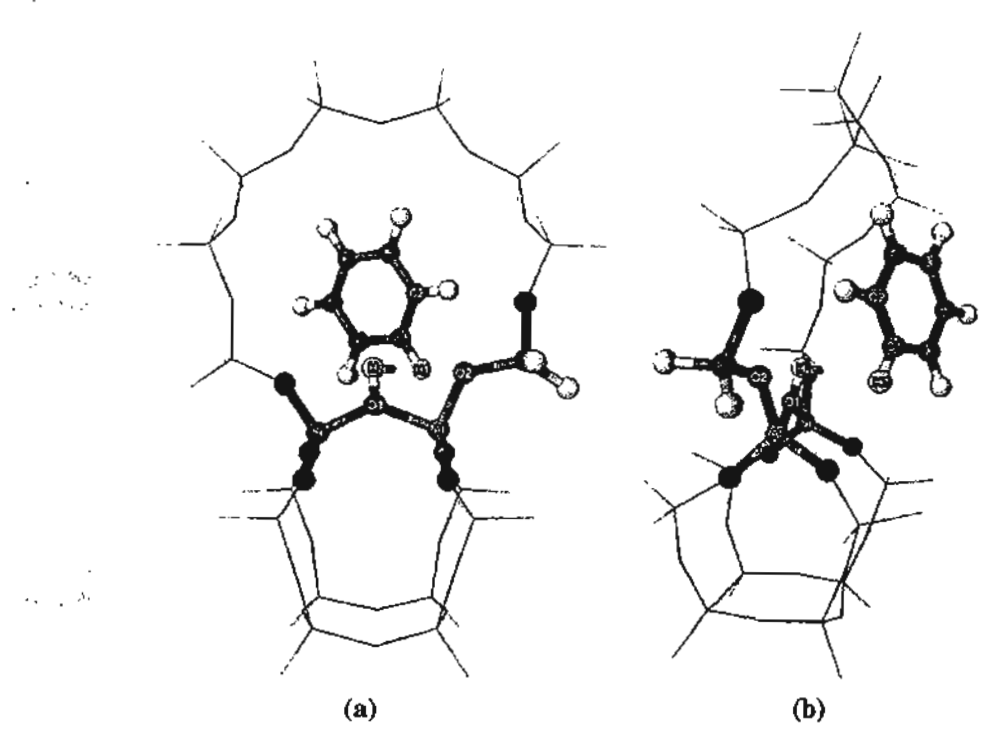


Fig. 5. Presentation of benzene interaction with the model of the H-ZSM-5 zeolite cluster, 18T:AlSi<sub>17</sub>O<sub>22</sub>H<sub>29</sub>. (a) The model is viewed from the zigzag direction, while (b) is viewed from the direction of the straight channel. Atoms belonging to the active region drawn as sphere.

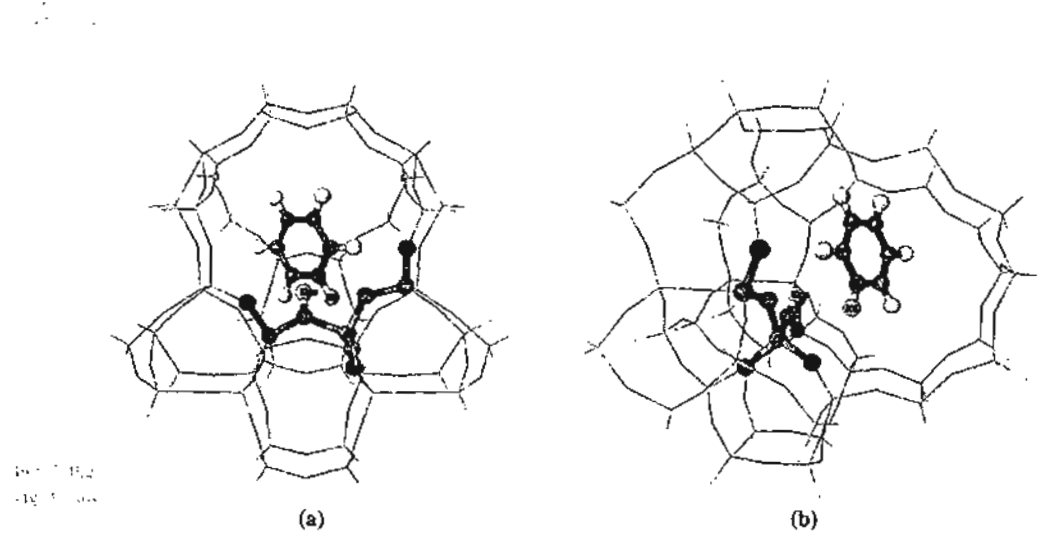


Fig. 6. Presentation of benzene asteraction with the model of the H-ZSM-5 zeolite cluster, 46T:AlSitsOceH49. (a) The model is viewed from the zigzag direction, while (b) is viewed from the direction of the straight channel. Atoms belonging to the active region drawn as sphere.

where the superscript Real means the whole system and the superscript Cluster means the active region, which would be treated with the higher level of calculation. Subscripts High and Low mean high- and low- level methodologies used in the ONIOM calculation. In this study, the high-level region is treated by the Hartree-Fock and density functional theory with the hybrid functional B3LYP. The rest is treated by molecular mechanics force field (UFF) or the Hartree-Fock method.

The accuracy of the QM/MM method, particularly the ONIOM method, depends significantly on the choices of the level of calculations for high- and lowlevel regions. Going through various types of QM/MM methods, the experimental adsorption energy of the benzene/zeolite system can be used to validate the choice of methods. Using the B3LYP method for treating the quantum cluster, we varied the methods for the low-level region from the molecular force field (UFF) to the Hartree-Fock method, Using the experimental observation as a benchmark, we found that the HF method provides reasonable values corresponding to the experimental prediction. This suggests that the HF method is the practical choice for the low-level methodology when the high-level region is treated by the B3LYP/6-31G(d,p) method.

theAll calculations have been performed by using GAUSSIAN98 code [45]. The basis set for the Hartree-Focks calculations is 3-21G, while the basis set 6-31G(d,p) is utilized for the B3LYP calculations. It is known that DFT does not account for the dispersion component of the interactions, single point MP2/6-31G(d,p) calculations were carried out at the B3LYP optimized geometries to improve the energetic information between benezene and the zeolite framework. During the structure optimization, only the active isite region [=SiOHAl(O)2OSi=], and the adsorbate are allowed to relax.

Ancs L. that orga

# 3. Results and discussion

For the purpose of clarity, we separate the discussion below into two sections. In one section we compare the ONIOM results with experimental results. In the other section we focus mainly on the effects of extended framework on structural and energetic information of the interaction of benzene with H-ZSM-5 zeolite.

# 3.1. Comparison of ONIOM results with experimental results

Different two-layer ONIOM2 integrated schemes (B3LYP/6-31G(d,p):HF/3-21G, B3LYP/6-31G(d,p): UFF, and HF/3-21G:UFF) were performed on four structures of benzene/H-ZSM-5 adsorption complexes, as illustrated in Figs. 3-6. The H-ZSM-5 zeolites were modeled by four different aluminosilicate clusters containing up to 46 tetrahedrally coordinated tetravalent atoms. Tables 1-2 list some selected structure parameters derived at full 3T quantum cluster and the different two-layer ONIOM2 integrated schemes mentioned earlier.

To assess the sensitivity of the active site structure with varying environments, we optimized the active site, [=SiOHAl(O)2OSi=], for all the clusters, whilst the remaining atoms were kept fixed at the crystallographic positions. By comparing the structure between the full B3LYP/6-31G(d,p) quantum cluster model of 3T and the ONIOM2 schemes, it is seen that the cluster environment imposed in the ONIOM2 scheme has small effect on the structure of the active site. In the ONIOM2 scheme, specifically B3LYP/6-31G(d,p):HF/3-21G (cf. Table 2), the extended framework has the effect of lengthening the O1-Hzen bond distance (Brønsted acid site) by 0.4 pm, and thus enhancing the acidity of the Brønsted acid site.

HF/3-21G and B3LYP/6-31G(d,p) optimized geometrical parameters of the C<sub>6</sub>H<sub>6</sub>/H-ZSM-5 adsorption coraplexes

Bond (pm) and angle (degree)	HF/3-210	i 	B3LYP/6-31G(d,p)		
(degree)	Isolated	Complex	Isolated	Complex	
Si-QI	169.6	169.3	169.3	169.1	
AI-OI	179.0	178.2	186.5	185.4	
A1-O2	167.4	162.7	169.6	169.8	
OI-Hzeo	97.1	97.4	96.8	97.8	
Si-01-Al	132.4	132.7	134.3	133.6	
ClH <sub>zeo</sub>	-	232.0	~	232.0	
C2···H <sub>260</sub>	-	229.4	-	230.0	
C1-C2	138.5	138.9	139.6	140.1	
CI-H3	107.2	107.1	108.6	108.6	

to Main 2- 4-1-62 LOSGIO OFIA 410 Page C. St. 1885

talohain 

Table ? ... Structure parameters for the C<sub>b</sub>H<sub>6</sub>/H-ZSM-5 adsorption complexes (located in the intersection) are obtained at various ONIOM2 Scheme

Model	Bond (pm) and angle (degree)			B3LYP/6-31	B3LYP/6-31G(d,p):UFF		B3LYP/6-31G(d,p):HF/3- 21G	
		Isolated	Complex	fsolated	Complex	Isolated	Comple	
10T% fr	Si-O1	169.7	169.8	169.2	169.2	166.1	166.2	
1110	A]-Q]	176.2	175.8	182.9	182.3	183.7	183.0	
11. 11.44	Al-O2	165.0	165.1	166.7	166.6	167.4	167.3	
	OI-Hzeo	97.2	97.2	97.1	97.2	97.2	97.5	
-	\$i-01-A}	136.3	136.5	139.9	140.0	134.0	133.3	
5. RP 668	C1···H <sub>2e0</sub>	_	3!1.6	-	309.4	_	300.1	
1, 10P 01.8	C2···H <sub>200</sub>	_	284.1	_	290.3	-	319.0	
•	C1-C2	138.5	138.8	139.6	139.9	139.6	140.1	
J	C1-H1	107.2	107.4	108.6	108.7	108.6	108.7	
All roots								
14T	Si-O1	169.3	169.4	168.9	168.9	164.9	164.9	
	AI-01	177.4	177.0	185.6	184.8	182.8	181.9	
the series of	Al-02	164.4	164.4	166.0	165.8	167.0	167.0	
	O1 - H <sub>zeo</sub>	97.2	97.1	97.0	97.1	97.3	97.5	
	Si-O1-Al	135.3	135.6	139.2	139.2	132.7	132.3	
	C1···H <sub>zeo</sub>	-	299.7	_	297.4	-	305.1	
Little 2	C2···H <sub>zeo</sub>	-	273.0	-	278.7	-	322.2	
stockpale bec	C1-C2	138.5	138.9	139.6	140.0	139.6	140.0	
Model	C1-B1	107.2	107.4	108-6	108.7	108.6	108.7	
18T	\$i-01	168.6	168.7	168.1	168.2	163.4	163.5	
101	AJ-Ol	178.1	177.6	188-4	187.5	181.6	180.9	
	AI-02	164.3	164.2	165.6	165.2	166.5	166.4	
· · - · · · ·	01-H <sub>200</sub>	97.2	97.2	97.0	97.1	97.3	97.8	
.27E	Si-Ol-Al	135.0	135.2	139.6	139.5	132.0	131.3	
	C1···H <sub>zeo</sub>	-	307.1	-	300.0	-	342.9	
	C2···H <sub>zeo</sub>	_	280.3	_	290.5	-	280.1	
	C1-C2	138.5	138.9	139.6	140.0	139.6	139.9	
	CI-HI	107 2	107.3	108.6	108.7	108.6	108.6	
46T	Si-Ol	167 0	168.1	167.5	167.8	163.2	163.2	
701	Al-OI	175.9	175.6	184.1	182.6	181.0	180.2	
	Al-Q2	164.8	165.0	165.8	165.6	165.9	165.8	
	O1-H <sub>200</sub>	97.4	97.3	97.0	97.2	97.6	98.3	
,43	Si-OI-Al	134.7	135.6	139.3	138.5	131.6	130.9	
	Cl···H <sub>zeo</sub>	-	328.0	-	324.6	-	278.6	
	C2···H <sub>zeo</sub>	-	296.5	_	317.9	_	295.9	
-	C1-C2	138.5	138.9	139.6	140.0	139.6	140.1	
	C1=C2 C1=H1	107.2	107.3	108.6	108.7	108.6	108.7	

Further support for the reliability of the active site subunit,  $\equiv Si-OH-Al \equiv$ , by our calculations is given from NMR studies. Klinowski et al. have estimated the internuclear distance between the aluminum and proton nuclei in a Brønsted acid site, r(Al-H), of H-Faujasite [46] and H-ZSM-5 [47] to be 238.0  $\pm$  4 and 248.0  $\pm$  4 pm, respectively, whereas our

Production of the control of the con

3. Resides

The land

reach le Vicili

computed  $r(Al\cdots H_{zeo})$  distances of the most realistic model of the 46T cluster are 238.1, 223.9, and 214.6 pm for the B3LYP/6-31G(d,p):HF/3-21G, B3LYP/6-31G(d,p):UFF, HF/3-21G:UFF, respectively. As can be seen from the experimental data, the computed  $r(Al\cdots H_{zeo})$  distance in the ONION2 is well represented by the B3LYP/

Franke official, and NA facilities, protein on Taggorie on, 119, 154

C. Raksakoon, J. Limsrakul / Journal of Molecular Structure (Theochem) 631 (2003) 147-156

Table 3
The interaction energies (kcal/mol) for the C<sub>6</sub>H<sub>6</sub>/H-ZSM-5 systems are obtained at various ONIOM2 methods

Model	HF/3-21G:UFF		B3LYP/6-31C	G(d,p):UFF	B3LYP/6-31G(d,p):HF/3-21G	
	Zigzag	Intersection	Zigzag	Intersection	Zigzag	Intersection
10T	- 13.98	- 14.30	- 11.50	-10.47	- 6.20	- 8.09
14T	- 14,37	14.68	-11.93	- 10.78	- 6.45	- 8.23
187	- 14.35	- 16.00	-11.90	- 12.02	- 6.48	- 8.35
46T	-	~ 22.46	-	- 17.27	-	- 10.61

6-31G(d,p):HF/3-21G scheme, but not by the two schemes: B3LYP/6-31G(d,p):UFF, HF/3-21G:UFF, which gives the r(Al··H<sub>200</sub>) distance 14.2 and 23.5 pm smaller than the B3LYP/6-31G(d,p):HF/3-21G scheme. This again suggests that B3LYP should be employed for a high-level model. Therefore, in order to keep this article short, we will discuss mainly the more accurate ONIOM2 results. However, the structural parameters of the other ONIOM2 schemes: (B3LYP/6-31G (d,p):UFF), and (HF/3-21G:UFF) are decembered in Table 2.

Model

# 3.2. The interaction of benzene with H-ZSM-5 zeolite

in The calculation results of B3LYP/6-31G(d,p) on free benzene are documented in Table 1. The C-C and C-H bond lengths were ascertained experimentally to be 139.7 and 108.4 pm, respectively. The B3LYP/6-31G(d,p) level of theory predicted bond lengths of 139.6 and 108.6 pm are virtually the same as the experimental observation.

As for the bare 3T quantum cluster results, the changes in the structural parameters of the benzene and bare 3T quantum cluster model of zeolite upon complexation are small. However, the changes are in accordance with Gutmann's rules [48], i.e. a lengthening of the O1-Hzeo (96.8 vs 98.4 pm) along With a corresponding slight decrease in the Si-O and AI-O bonds. Our calculated benzene adsorption energy from the bare 3T cluster models is estimated to be -5.99 kcal/mol at B3LYP/6-31G(d,p) level, which is at the higher end of the predicted range from -4-to -6 kcal/mol from previous theoretical studies [14].hThe predicted 3T adsorption energy so far is naticeably less compared to the experimental adsorption energy of benzene on the acidic H-Y zeolite (-14 kcal/mol) [22]. Such deviation indicates that long-range electrostatic interactions of the extended framework could be an important factor in stabilizing the adsorption complex. In this case, one can expect that the surrounding lattice included in the ONIOM model would enhance the binding energy.

One of the important findings regarding the adsorption properties of benzene using the advantages of ONIOM methodology is the probing of the location of benzene inside the H-ZSM-5 framework. From Table 3, one can see that the ONIOM2 schemes predict that benzene is favorably located in the intersection channel. It is clearly seen that enlarging the size of the cluster from 10T up to the most realistic model of 46T cluster, the benzene molecule is favorably observed in the intersection of straight and sinusoidal channels. This finding is supported by the neutron and X-ray diffraction measurement [12].

We now focus mainly on the adsorption properties of benzene located in the intersection channel. Increasing the cluster size from the 10T up to 46T in the ONIOM2 integrated scheme, specifically, for 46T at B3LYP/6-31G(d,p):HF/3-21G level of theory, shortens the adsorption distance (i.e. the distance between the Brønsted proton and C1 and C2 of the C1=C2 bond) by about 21.5 and 23.0 pm, while it elongates the O1-Hzeo bond distance slightly by about 0.8 pm as compared to the smaller 10T ONIOM2 scheme (see Table 2). We found that the O1-Hzee distances are increased as the cluster sizes are increased. Similar findings are observed in the results taken from the less accurate ONIOM2 schemes, (HF/6-31G(d,p):UFF, and B3LYP/6-31G(d,p):UFF) (see Table 2).

Variation of the calculated adsorption energies from the smaller 10T to the more reliable 46T cluster model,  $\Delta E$ , are about 8.16, 6.80, and 2.52 kcal/mol for the ONIOM2(HF/3-21G:UFF),

(TETTA KO

ONIOM2(B3LYP/6-31G(d,p):UFF), and ONIOM2(B3LYP/6-31G(d,p):HF/3-21G) levels of theory, respectively. The adsorption energy is found to depend on the cluster size employed, suggesting that extended structure beyond the active sites may play an important role in determining adsorption energies due to the long range electrostatic effects.

Manager and the state of the st

Comparing the B3LYP/6-31G(d,p):HF/3-21G and B3LYP/6-31G(d,p):UFF methods, the latter scheme overestimates the adsorption energy by about 2.38, 2.55, 3.67 and 6.66 kcal/mol for 10T, 14T, 18T, and 46T, respectively, relative to the former scheme. This is due mainly to the use of UFF-molecular mechanics force fields for the low-level region.

As for the results of the ONIOM2 scheme, in going from the bare 3T quantum cluster model up to the more realistic 46T cluster model, we found that the extended framework of zeolite has a large effect on the adsorption energetics. Specifically, it decreases noticeably the adsorption energy of benzene on H-ZSM-S, by - 11.28 kcal/mol (3T cluster result at full B3LYP/6-31G(d,p) level, -5.99 kcal/mol, vs the 46T cluster; cesult at ONIOM2(B3LYP/6-31G(d,p):UFF) level icit 17.27 kcal/mol). When the HF/3-21G is employed instead of the UFF-molecular mechanics force field-method for the low level, i.e. ONIOM2(B3LYP/6-31G(d,p):HF/3-21G) schemes, it decreases the adsorption energy by -4.62 kcal/mol (or, 77%, of the full B3LYP/6-31G(d,p) of the 3T model) for the (C6H6)/H-ZSM-5 system.

it is known that DFT does not account for the dispersion component of the interactions, single point MP2/6-31G(d,p) calculations for the high-level active region were carried out at the B3LYP optimized geometries to improve the energetic information between benzene and the zeolite framework. This yields the adsorption energy complex of -13.75 kcal/mol at ONIOM2(MP2/6-31G(d,p):HF/3-21G). Our predicted value for the [GaH6]/H-ZSM-5 system is in excellent agreement with the experimental estimate of -14.0 kcal/mol obtained by Coker et al. [22].

# 4. Conclusions

080 080

destruction in the second seco

i.... .. ...

The adsorption of benzene on H-ZSM-5 zeolites has been investigated with four different cluster sizes

and methods comprising various two-level ONIOM2 schemes: B3LYP/6-31G(d,p):HF/3-21G, B3LYP/6-31G(d,p):UFF, and HF/3-21G:UFF. The bare 3T quantum cluster approach predicts the [C<sub>6</sub>H<sub>6</sub>]/H-ZSM-5 complexes to have the binding energies of - 5.99 kcal/mol. The effect of the zeolite framework is modeled on the ONIOM2 method. We found that the extended framework significantly enhances the adsorption energy of benezene to the zeolites. In particular, the final predicted adsorption energy of - 13.75 kcal/mol for the [C<sub>6</sub>H<sub>6</sub>]/H-ZSM-5 complexes calculated by the ONIOM2(MP2/6-31G(d,p):HF/3-21G) scheme. This efficient scheme performs superbly as compared with the experimental estimate of - 14.0 kcal/mol. The results obtained in the present study suggest that the ONIOM approach yields a more accurate and practical model in studying adsorption of unsaturated hydrocarbons on zeolites.

# Acknowledgements

This work was supported in part by grants from the Thailand Research Fund (TRF Senior Research Scholar to JL) and the Kasetsart University Research and Development Institute (KURDI) as well as the Ministry of University Affairs under the Science and Technology Higher Education Development Project (MUA-ADB funds). The support from the Dow Chemical Company (USA) is also acknowledged. Our sincere thanks are due to Professor R. Ahlrichs (Karlsruhe, Germany) for his continued support of this work.

# References

- C.R.A. Catlow (Eds.), Modeling of Structure and Reactivity in Zeolites. Academic Press. San Diego, 1992.
- [2] C. Pereira, G.T. Kokotailo, R.J. Gorte, J. Phys. Chem. 95 (1991) 705.
- [3] S. Bordiga, G. Ricchiardi, G. Spoto, D. Scarano, L. Carnelli, A. Zecchina, C.O. Arean, J. Chem. Soc., Faraday Trans. 89 (1993) 1843.
- [4] B.V. Liengme, W.K. Hall, Trans. Faraday Soc. 62 (1966) 3229.
- [5] N.W. Cant, W.K. Hall, J. Catal. 25 (1972) 161.
- [6] L. Song, Z.L. Sun, L.C. Rees, Micropor. Mesopor. Mat. 55 (2002) 31.
- [7] Y. Huang, E.A. Havenga, J. Phys. Chem. B 104 (2000) 5084.

A - - 1 - -. . . . . Maday J. 18. 14 V. 3 C. 3 62 120 27.10

4. 3. 5. 5. 5.

. . . (1) S. 49 1156 - 11

V 1875 15

C. Raksakoon, J. Limirakul / Journal of Molecular Structure (Theochem) 631 (2003) 147-156

- [8] G.W. West, Aust J. Chem. 37 (1984) 457.
- [9] I. Kustanovich, H.M. Vieth, Z. Luz, S. Vega, J. Phys. Chem. 93 (1989) 7427.
- [10] R.L. Portmouth, M.J. Duer, L.F. Gardden, J. Chem. Soc., Faraday Trans. 91 (1995) 559.
- [11] B. Zibrowius, J. Caro, J. Chem. Soc., Faraday Trans. 84 (1988) 2357.
- [12] R. Goyal, A.N. Fitch, H. Jobic, J. Phys. Chem. B 104 (2000) 2878.
- [13] H. Thamm, J. Phys. Chem. 91 (1987) 8.
- 2 [14] P.J. O'Malley, K.J. Franworth, J. Phys. Chem. B 102 (1998)
- [15] L.W. Bech, T. Xu, J.B. Nicholas, J.F. Haw, J. Am. Chem. Soc. 117 (1995) 11594.
- [16] T.P. Zaragoza, J.M. Martinez-Magadan, R. Santamaria, D. Dixon, M. Castro, Int. J. Quant. Chem. 80 (2000) 125.
- [17] J.A. Ryder, A.K. Chakraborty, A.T. Bell, J. Phys. Chem. B 104 (2000) 6998.
- [18] E. Klemm, J. Wang, G. Emig, Micropor. Mesopor. Mater. 26
- (1998) 11. [19] R.Q. Saurt, A.T. Bell, D.N. Theodorou, J. Phys. Chem. 97 (1993) 13742.
- [20] F. Vigne-Maeder, H. Jobic, Chem. Phys. Lett. 169 (1990)
- 18: 31M [21] D.B. Shah, C.-J. Guo, D.T. Hayhurst, J. Chem. Soc., Faraday
- Trans. 91 (1995) 1143. [22] R.N. Coker, C. Jia, H.G. Karge, Langmuir 16 (2000)
- 1205.
- [23] L.Gao, in: K.B. Lipkowitz, D.B. Boyd (Eds.), Reviews in Computational Chemistry, vol. 7, VCH, New York, 1995, p. 1313 139.7
- [24] Mil Field, P.A. Bash, M. Karplus, J. Comput. Chem. 11 :; 1 (1990) 700.
- [25] U.C. Sighn, P.A. Kollman, J. Comput. Chem. 7 (1996) 218
- [26] E.V. Stefanovich, T.N. Truong, J. Phys. Chem. B 102 (1998) 3018.
- [27] S.P. Greatbanks, I.H. Hillier, N.A. Burton, P. Sherwood, J. Chem. Phys. 105 (1996) 3770.
- [28] R.Z. Khaliullin, A.T. Bell, V.B. Kazansky, J. Phys. Chem. A .105 (2001) 10454.
- [29] J. Limtrakul, T. Nanok, P. Khongpracha, S. Jungsuttiwong, T.N. Truong, Chem. Phys. Lett. 349 (2001) 161.
- [30] P. Treesukol, J. Limtrakul, T.N. Truong, J. Phys. Chem. B 105 (2001) 2421.
- [31] J. Limtrakul, P. Khongpracha, S. Jungsuttiwong, T.N. Truong, J: (Mo). Cat. A 153 (2000) 2469.
- [32] S. Jungsuttiwong, S. Nokbin, P. Chuichay, P. Khongpracha, T.N.: Truong, J. Limtrakul, Stud. Surf. Sci. Catal. 135 (2001) 2518.
- [33] L.: Limtrakul, P. Khongpracha, S. Jungsuttiwong, J. Mol. Struct 525 (2000) 153.
- [34] J. Limtrakul, S. Nokbin, P. Chuichay, J. Mol. Struct. 560 (2001) 169. LS; M.C.

rimi 194 E. 715 \$ : 200 01

- [35] J. Limtrakul, S. Nokbin, S. Jungsuttiwong, P. Khongpracha, T.N. Truong, Stud. Surf. Sci. Catal. 135 (2001) 2469.
- [36] (a) R. Vetrivel, C.R.A. Catlow, E.A. Colbourn, Proc. R. Soc. Lond, A 417 (1998) 81.
  - (b) M. Allavena, K. Seiti, E. Kassab, G. Ferency, J.G. Angyan, Chem. Phys. Lett. 168 (1990) 461.
  - (c) G. Aloisi, P. Barnes, C.R.A. Catlow, R.A. Jackson, A.J. Richard, J. Phys. Chem. 93 (1990) 3573.
  - (d) J.C. White, A.C. Hess, J. Phys. Chem. 97 (1993) 8730.
  - (e) E. Teupisson, A.P.J. Jansen, R.A. van Santen, R. Orlando. R. Dovesi, J. Phys. Chem. 101 (1994) 5865.
  - (f) A. Kyrlidis, S.J. Cook, A.K. Chakraborty, A.T. Bell, D.N. Theodorou, J. Phys. Chem. 99 (1995) 1505.
  - (g) E.H. Teunissen, A.P.J. Jansen, R.A. van Santen, J. Phys. Chem. 99 (1995) 1873.
  - (h) U. Eichler, M. Brandle, J. Sauer, J. Phys. Chem. B 99 (1997) 1873.
  - M. Brandle, J. Saver, J. Am. Chem. Soc. 120 (1998) 1556.
- [37] P. Maseras, K. Morokuma, J. Comput. Chem. 16 (1995) 1170.
- [38] T. Matsubara, S. Sieber, K. Morokuma, Int. J. Quant. Chem. 60 (1996) 1101.
- [39] S. Humbel, S. Sieber, K. Morokuma, J. Chem. Phys. 105 (1996) 1959.
- [40] M. Svensson, S. Humbel, K. Morokuma, J. Chem. Phys. 105 (1996) 3654.
- [41] M. Svensson, S. Humbel, R.D.J. Froese, T. Matsubara, K. Morokuma, J. Phys. Chem. 100 (1996) 19357.
- [42] S. Dapprich, E. Komaromi, K.S. Byun, K. Morokuma, M.J. Frisch, J. Mol. Struct. (Theochem) 461 (1999) 1.
- [43] T. Vreven, K. Morokuma, J. Comput. Chem. 21 (2000) 1419.
- [44] H. van Koningveld, H. van Bekkum, J.C. Jansen, Acta Crystallogr. B 43 (1987) 127.
- [45] M.J. Frisch, G.W. Trucks, H.B. Schlegel, G.E. Scuseria, M.A. Robb, J.R. Cheeseman, V.G. Zakrzewski, J.A. Montgomery, Jr., R.E. Stratmann, J.C. Burant, S. Dapprich, J.M. Millam, A.D. Daniels, K.N. Kudin, M.C. Strain, O. Farkas, J. Tomasi, V. Barone, M. Cossi, R. Cammi, B. Mennucci, C. Pomelli, C. Adamo, S. Clifford, J. Ochterski, G.A. Petersson, P.Y. Ayala, Q. Cui, K. Morokuma, P. Salvador, J.J. Dannenberg, D.K. Malick, A.D. Rabuck, K. Raghavachari, J.B. Foresman, J. Cioslowski, J.V. Ortiz, A.G. Baboul, B.B. Stefanov, G. Liu, A. Liashenko, P. Piskorz, I. Komaromi, R. Gomperts, R.L. Martin, D.J. Fox, T. Keith, M.A. Al-Laham, C.Y. Peng, A. Nanayakkara, M. Challacombe, P.M.W. Gill, B. Johnson, W. Chen, M.W. Wong, J.L. Andres, C. Gonzalez, M. Head-Gordon, E.S. Replogle, J.A. Pople, Gaussian, Inc., Pittsburgh PA, 2001.
- [46] R.L. Stevenson, J. Catal. 21 (1971) 113. D. Frende, J. Klinowski, H. Hamdan, Chem. Phys. Lett. 149 (1988) 355.
- [47] J. Klinowski, Chem. Rev. 91 (1991) 1459.
- [48] V. Gutmann, The Donor-Acceptor Approach to Molecular Interaction, Plenum Press, New York, 1978.



# A QUANTUM CHEMICAL STUDY OF THE INTERACTION OF CARBONYLS WITH H-ZSM-5 ZEOLITE

Boekfa, B., Sirijareansre, J., Pantu, P., and Limtrakul, J.

Laboratory for Computational & Applied Chemistry, Chemistry Department, Kasetsart University, Bangkok 10900, THAILAND

# ABSTRACT

The quantum cluster, ONIOM and embedded ONIOM models have been used to investigate adsorption properties of carbonyls in H-ZSM-5 zeolites. The active site has been modeled with realistic cluster sizes up to 46 tetrahedra. The predicted adsorption energies of ZSM-5/carbonyls complexes for the embedded ONIOM2(MP2/6-311G(d,p):UFF) scheme are -119.0 and -139.0 kJ/mol for acetaldehyde and acetone, respectively, the latter value compared well with the experimental estimated of  $130 \pm 4$  kJ/mol, whereas the conventional quantum cluster yields an underestimate value of -68.2 kJ/mol. The results obtained in this study suggest that the new embedded ONIOM scheme provides a more accurate method of studying the interaction of carbonyls with zeolites.

# INTRODUCTION

Aldol condensation of acetone and acetaldehyde is an important reaction in organic synthesis because it leads to C-C bond formation. This reaction can be catalyzed by acid and base catalysts such as NaOH, H<sub>2</sub>SO<sub>4</sub> etc. However, these corrosive catalysts cause a number of problems concerning handling, safety, corrosion, and waste disposal. Therefore, the conventional liquid-acid catalysts are progressively replaced by heterogeneous catalysts. Many types of catalysts have been used for this reaction such as various oxides [1-3] and various zeolites [4-14]. The zeolite catalysts also offer the advantage of high selectivity toward the desired product due to the shape selective properties of their microcrystalline pore structures. Several types of zeolites have been reported to have high activity for aldol condensation such as H-ZSM-5, HY, HX, etc. (refs) Numerous experiments have focused on investigating the interaction of acetaldehyde and acetone on H-ZSM5 zeolite by using different techniques such as NMR [15], FT-IR [16], <sup>13</sup>C-NMR [7-8, 14, 17-18], etc. From experimental data, it is indicated that the stoichiometric of adsorption of acetaldehyde and acetone on H-ZSM5 zeolite is 1:1 adsorption complex. The adsorption complex is in the form of a hydrogen-bonded complex which is the interaction between the carbonyl group and the Brønsted acid site of zeolite. Sepa et al. [17] found that the heat of adsorption energy of acetone on H-ZSM5 zeolite is 130 ± 4 kJ/mol.

There have been several theoretical studies on the adsorption of acetone in zeolite using quantum cluster calculations [16-17, 19]. These studies provided useful information on the mechanism and energetic properties of the reaction. However, none of these studies included the effects of the zeolite framework and, as a result, the predicted adsorption energies of acetone on H-ZSM-5 in a range of -55 to -64 kJ/mol were significantly lower than the experimental adsorption energy of acetone on the acidic H-ZSM-5 zeolite (-130 ± 4 kJ/mol). Such a large deviation indicates an important effect of the extended framework in stabilizing the adsorption complex. To accurately include the effects of the extended zeolite framework on the catalytic properties, one can employ the periodic electronic structure methods such as the periodic density functional theory methodology. However, due to the large unit cells of typical zeolites, such calculations are often computationally unfeasible. The hybrid methods, such as the embedded cluster or combined quantum mechanics/molecular mechanics (QM/MM) methods, as well as the more general ONIOM (Our-own-N-layer Integrated molecular Orbital + molecular Mechanics) provide a cost effective computational strategy for including the effects of the zeolite framework [20-23].

In this study, the interactions between carbonyl compounds, acetaldehyde and acetone, with different models of H-ZSM5 have been studied with the aims of investigating; a) the effects of the zeolite framework on the interaction between carbonyl compounds with H-ZSM5 zeolite; b) efficient schemes of the ONIOM method. The models consist of an inner layer of active region, modeled by a small cluster using the density functional theory to account for interactions of the adsorbates with the acid site of zeolite, and a large outer layer of the zeolite framework, represented by a molecular mechanics force field, to account for the van der Waals interactions arising from confinement of the pore structure. Due to the large dipole moments of the adsorbates, the long-range electrostatic

interactions are expected to contribute significantly to the adsorption process. Therefore, the electrostatic effect of the whole zeolite crystal lattice is additionally included using an electronic embedded method. This is the first time that the ONIOM method and long-range interacting method are being used in combination and, thus, we call it "embedded ONIOM."

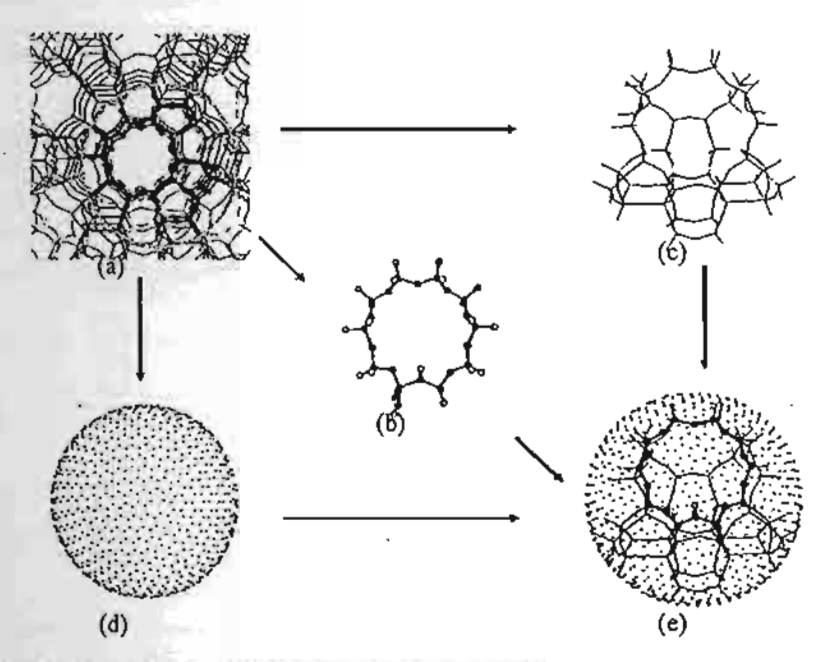


Figure 1. Schematic diagram of embedded ONIOM method: periodic structure of ZSM-5 framework (a) was subdivided into three parts: the innermost is the QM region (b); the next layer is UFF part (c) and the outermost is a set of point charges (d); complete model of embedded ONIOM (e).

# METHODS

Three different models have been employed to model the H-ZSM5 zeolite and their complexes with the adsorbed carbonyl compounds. First, bare cluster models, 3T and 10T (Figures 2-3), were taken from the crystal structure of ZSM-5 lattice [24] to model the ZSM-5 system by using B3LYP/6-31G(d,p) level of theory for calculation. Second, a larger cluster of the 46T model were proposed for representing the system of H-ZSM5 treated by using the ONIOM (B3LYP/6-31G(d,p): UFF) approach. In the ONIOM2 (B3LYP/6-31G(d,p): UFF) scheme, the active Brønsted acid site of the zeolite is treated quantum chemically at the B3LYP/6-31G(d,p) and MP2/6-31IG(d,p) level of theory, and the other extended framework, up to 46T, is treated at the UFF.

In order to take into account the long-range interactions of the zeolite lattice beyond the 46T, the third model, called "embedded ONIOM2", calculations of the zeolite framework are developed. The embedded ONIOM2 models consist of three layers. The center layer is a ten-tetrahedral (10T) quantum chemical cluster. The next layer is the UFF force fields. The outermost layer of the model is a set of optimized point charges located to model the remaining Madelung potential from the extended zeolite crystal. Accuracy of the method for modeling the adsorption process has been compared to the experimental observation [17].

All calculations have been performed by using the Gaussian 98 code [25]. The basis set 6-31G(d,p) is utilized for the B3LYP calculations. It is known that DFT does not account for the dispersion component of the interactions. Single point MP2/6-311G(d,p) calculations for the high-level active region were carried out at the B3LYP optimized geometries to improve the energetic information between benzene and the zeolite framework. During the structure optimization, only the active site region [=SiOHAI(O)<sub>2</sub>OSi=], and the adsorbate are allowed to relax.

# RESULTS AND DISCUSSION

# Comparisons of quantum cluster with ONIOM models

All cluster models of H-ZSM-5 of zeolite are illustrated in Figures 2-5 and their corresponding selected structure parameters are tabulated in Tables 1-2. Three different aluminosilicate clusters containing up to 46 tetrahedrally coordinated tetravalent atoms modeled the H-ZSM-5 zeolites. The more realistic 46T model covers the cavity at the intersection of the straight channel, and the zigzag channels, where the adsorbate is favorably adsorbed.

Table 1. Optimized geometries of the isolated model and adsorption complex of acetaldehyde on H-ZSM5 zeolite. (Bond lengths are in pm and angles in degrees)

Parameters			λ	<u>le</u> thod		
	3T		1	0T	46 T	
	isolated	Complex	Isolated	Complex	Isolated	Complex
Si1-QI	169.3	168.0	167.3	165.7	165.8	164.1
OI-Al	186.5	183.4	184.1	180.8	185.5	180.8
Al-O2	169.6	170.6	168.1	168.9	166.9	167.5
O2-Si2	165.6	161.7	160.4	159.3	158.4	157.3
O1-H1	96.B	101.4	97.0	103.0	97.1	102.7
Al-Hi	232.9	242.0	234.6	240.8	230.8	239.5
H1-O3	_	158.4	-	152.3	-	151.6
O3-C1	•	122.7	-	122.7	-	122.7
C1-H2	-	110.1	-	110.0	•	110.0
H2-O2		221.9	•	236.7	_	238.4
∠Si1-O1-Al	134.3	132.1	134.2	131.7	135.6	133.3
∠AJ-Q2-Si2	122.5	125.2	122.9	126.1	118.9	122.0
∠Al-O1-H1	106.2	113.2	109.2	113.3	105.2	112.3
∠OI-HI-03	-	171.0	-	176.3	-	173.1

To assess the sensitivity of the active site structure with varying environments, we optimized the active site, [=SiO(H)Al(O)<sub>2</sub>OSi=], for all the clusters, whilst the remaining atoms were kept fixed at the crystallographic positions. By comparing the structure between the full quantum cluster model of 3T and 10T models, it is seen that the cluster size environment has a little effect on the structure of the active site. The extended framework has the effect of lengthening the O1-H bond distance (Brønsted acid site) by 0.2 pm (full B3LYP). In the ONIOM2 schemes, specifically B3LYP/6-31(d,p):UFF, the O1-H bond distances are increased by 0.3 pm, thus enhancing the acidity of the Brønsted acid site. While the other bond distances of the active site region such as Al-O, Si-O (to O1 and O2) are affected by the increasing cluster size as shown in Tables 1-2.

# The interactions of acetone and acetaldehyde with the H-ZSM5 zeolite

The structure of acetone and acetaldehyde adsorbed on different models of H-ZSM5 zeolite are shown in Figures 2a-4a. Acetaldehyde is adsorbed on the BrØnsted acid site by forming a strong hydrogen bonding interaction between the carbonyl oxygen (O3), acidic proton (H1), and a weak hydrogen bonding interaction between the aldehyde hydrogen (H3) and the adjacent framework oxygen (O2) of the zeolite. Increasing the cluster sizes increases the interactions between the acetaldehyde and the zeolite as evidenced by the decrease of the H1-O3 bond distance from 158.4 to 152.3 and to 151.6 pm concurrently with the increase of the acidic O1-H1 bond distance from 96.8-97.1 pm for isolated acidic O1-H1 to 101.4, 103.0, and 102.7 pm as the cluster size is progressively increased. On the other hand, acetone is adsorbed by forming only one strong hydrogen bonding interaction between the carbonyl oxygen and the acidic proton. Increasing the cluster size has a more subtle effect on the adsorbed acetone.

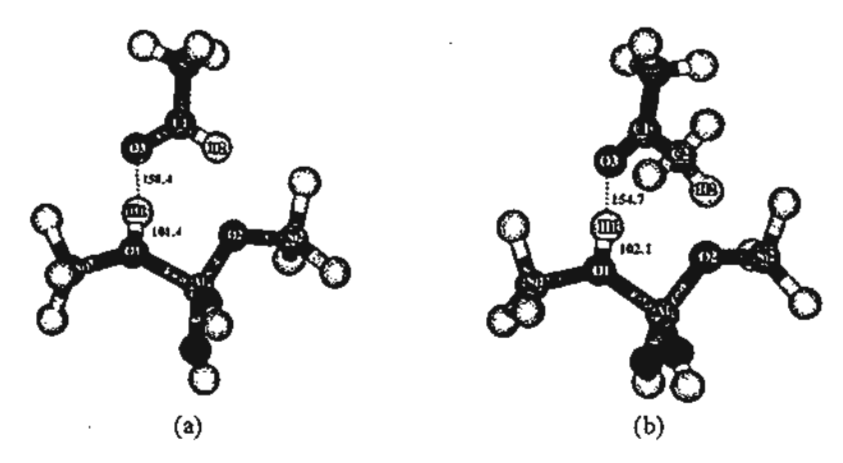


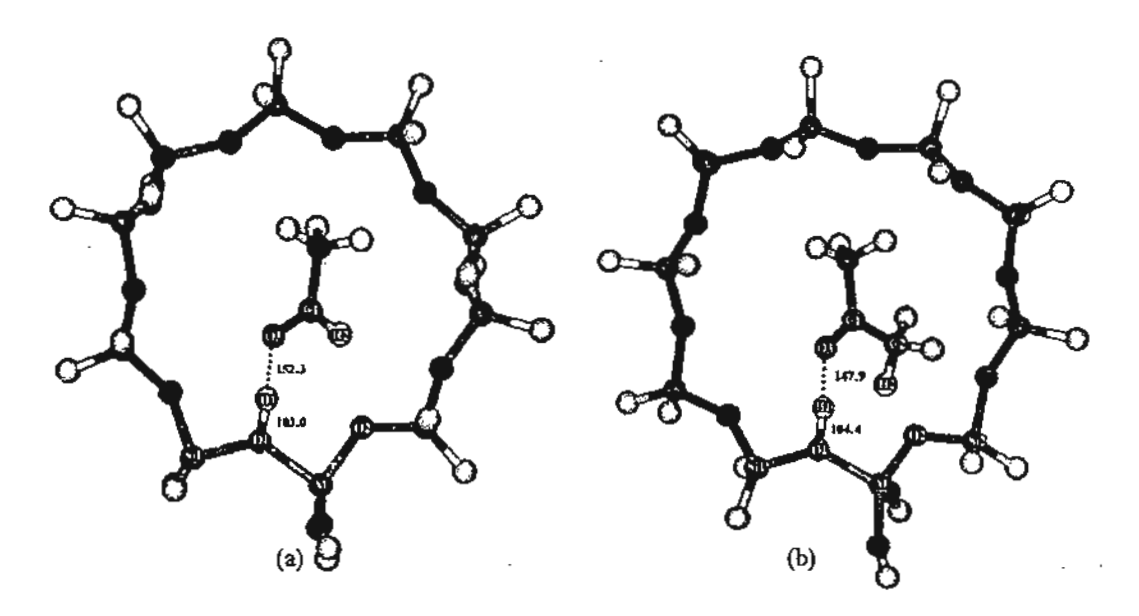
Figure 2. The interaction of carbonyls with the 3T bare cluster model of H-ZSM-5 zeolite: (a) acetaldehyde; (b) acetone.

Due to the increase in steric interactions between the methyl groups of the acetone and the zeolite framework as the cluster size increases, the adsorbed acetone is moved toward the intersection cavity, where it can be further stabilized. In all cases, the structure of the zeolite structure was not significantly changed by the adsorption of the adsorbates.

Table 2. Optimized geometries of the isolated model and their adsorption complexes of acctone on H-ZSM5 zeolite (Bond lengths are in pm and angles in degrees).

Parameters	Method							
	3	T	1	0Т	10T / 46T			
	Isolated	Complex	Isolated	Complex	Isolated	Complex		
Sil-Ol	169.3	167.8	167.3	165,4	165.8	164.5		
OI-AI	186.5	183.3	184.1	180.3	185.5	9.081		
AI-O2	169.6	170.4	168.1	168.4	166.9	166.9		
O2-Si2	165.6	161.6	160.4	159.0	158.4	157.1		
01-H1	96.8	102.1	97.0	104.4	97.1	102.9		
Al-H!	232.9	243.1	234.6	238.7	230.8	233.9		
H1-O3		154,7	-	147.9	-	154.4		
O3-C1	-	123.2	-	123.4	-	123.2		
C1-C2	-	150.5	-	150.3	-	150.6		
H2-O2	-	224.7	-	268.3	-	282.3		
∠Si1-O1-Al	134.3	132.0	134.2	132.0	135.6	133.2		
∠AJ-O2-Si2	122.5	125.5	122.9	126.5	118.9	122.1		
∠AJ-O1-H1	106.2	113.8	109.2	111.2	105.2	107.8		
∠O1-H1-O3		173.7	-	173.0	-	169.6		

The adsorption energy is one of the most valuable data obtained from experimental observation which can be used to validate the theoretical data. The adsorption energies of acetone and acetaldehyde on H-ZSM-5 zeolite calculated from different models, as discussed above, and also those from the ONIOM models using the molecular mechanics force fields for the outer layer are documented in Table 3.



Pigure 3. Presentation of carbonyl compounds interacted with the 10T bare cluster model of H-ZSM-5 zeolite; (a) acetaldehyde; (b) acetone.

Using the 3T cluster model, the DFT methods predict the adsorption energies of acetaldehyde and acetone to be -66.7 and -68.2 kJ/mol, respectively. These energy values are significantly lower than those of the experimental results. The adsorption energy of acetone on the acidic H-ZSM-5 zeolite was determined to be -130 kJ/mol [17]. Increasing the cluster size from 3T to 10T clusters, the calculated adsorption energies ( $\Delta E_{ads}$ ) of acetaldehyde and acetone interacted with zeolites is still well below the observation value, but somewhat differentiable (Table 3).

Table 3. Comparison of the adsorption energy,  $\Delta E_{ads}$  (in kJ/mol) along the adsorption of acetaldehyde and acetone on H-ZSM5 zeolite in different models and methods.

Methods/models		3T		TOT	ΙΟΤ		46T	
	٠.	Acetaldehyde	Acetone	Acetaldehyde	Acetone	Acetaldehyde	Acetone	
B3LYP/6-31G(d,p)		-66.7	-68.2	-67.7	-71.1	-	-	
B3LYP/6-31G(d,p):UFF		-	-	•	-	-83.0	-90.6	
B3LYP/6-31G(d,p):UFF+charges	•	-	-	-	-	-103.3 6	-125.6 <sup>b</sup>	
MP2/6-311G(d,p):UFF+charges*		-	-	-	-	-119.0°	-139.0 <sup>b</sup>	

Experimental adsorption energy of acetone on H-ZSM5 zeolite is 130 ± 4 kJ/mol from Ref. [17]

Increasing the cluster size from 10T up to the more realistic model, 46T, by enlarging the outer layer, the differences between each adsorption energy are pronounced. The adsorption energies of acetaldehyde and acetone calculated from the 46T cluster using ONIOM2 (B3LYP/6-31(d,p):UFF) are calculated to be -83.0 and -90.6 LJ/mol, respectively. These interaction energies are still underestimated as compared to the experimental results.

<sup>\*</sup> Set of point charges surrounding the 46T model

Indicates single-point energy at indicated level of theory on the optimized B3LYP/6-31G(d,p):UFF structure

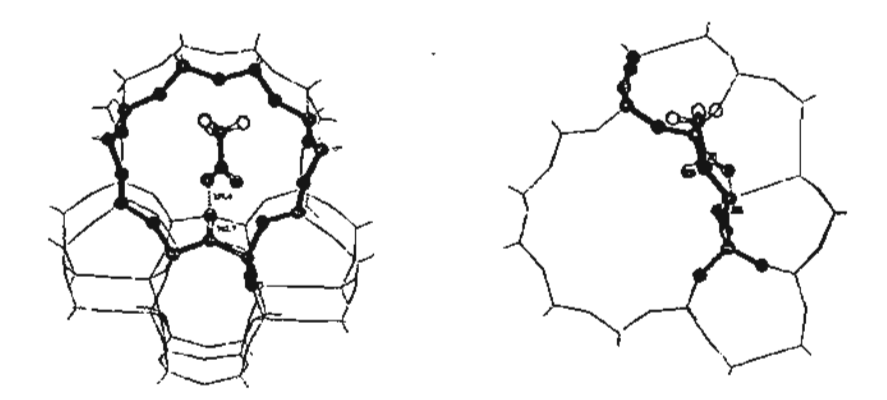


Figure 4. Presentation of acetaldehyde interacted with the 46T ONIOM model of H-ZSM-5 zeolite: viewed from the zigzag channel (a) and the straight channel (b).

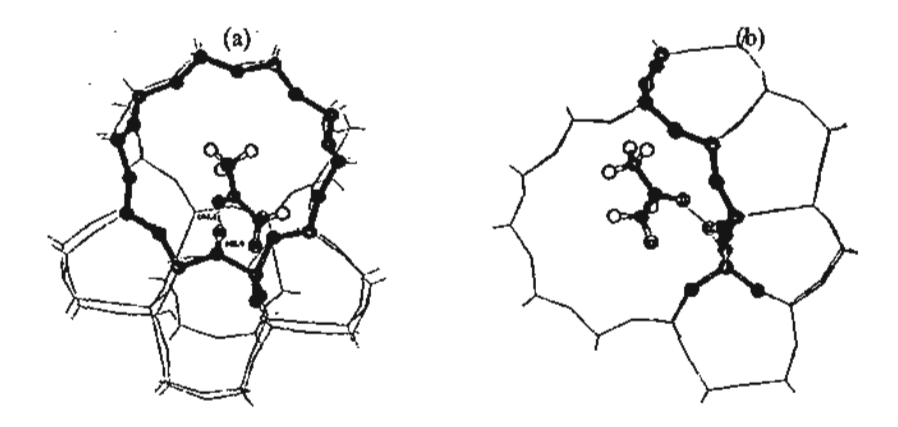


Figure 5. Presentation of acctone interaction with the 46T ONIOM model of H-ZSM-5 zeolite: viewed from the zigzag channel (a) and the straight channel (b).

It is known that DFT does not account for the dispersion component of the interactions. Single point MP2/6-311G(d,p) calculations for the high-level active region were carried out at the B3LY[b] ptimized geometries to improve the energetic information between benzene and the zeolite framework. And in order to take into account the long range interactions of the zeolite lattice beyond the 46T, the "embedded ONIOM2" calculations of the zeolite framework is employed. This yields the adsorption energies of -119.0 and -139.0 kJ/mol for acetaldehyde and acetone, respectively. Our predicted value for the latter system is in excellent agreement with the experimental estimate of -130  $\pm$  4 kJ/mol obtained by Sepa et al., [17], indicating that the MP2 combining the UFF force fields method as a lower level is considered to be one of the best combinations for the ONIOM2 scheme. This efficient scheme provides a cost effective computational strategy for treating the effects of a large extended framework structure.

# CONCLUSIONS

The adsorption of acetaldehyde and acetone on H-ZSM5 zeolite has been investigated with three different cluster sizes and methods. The bare cluster models,3T and 10T, (B3LYP/6-31G(d,p) quantum cluster approach predicts to have the adsorption energies of -66.7 (3T) vs. -68.2 (10T) kJ/mol for acetaldehyde/H-ZSM5 and -68.2

(3T) vs. -71.1 (10T) kJ/mol for acetone/H-ZSM5. The effect of zeolite framework is modeled on the ONIOM2 and e-ONIOM method. We found that the extended framework significantly enhances their adsorption energy of adsorbate molecules to the zeolite. The most accurate model, embedded ONIOM predicts the adsorption energy to be -119.0 and -139.0 kJ/mol for acetaldehyde and acetone, respectively. The calculated adsorption of acetone/H-ZSM5 complex using the e-ONIOM approach is in good agreement with the experimental data. The results obtained in this study indicate that the embedded ONIOM approach yields a more accurate model for studying adsorption properties on periodic systems.

# **ACKNOWLEDGMENTS**

This work was supported in part by grants from the Thailand Research Fund (TRF Senior Research Scholar to JL.) and the Kasetsart University Research and Development Institute (KURDI) as well as the Ministry of University Affairs under the Science and Technology Higher Education Development Project (MUA-ADB funds).

# REFERENCES

- 1. Ai, M., Bull. Chem. Soc. Jpn., 64 (1991), 1342.
- Malinowski, S., Jedrzejewska, H., Basniski, S. and Benebek, S., Chim. Ind. Genie Chim., 85 (1961), 885.
- Malinowski, S., React. Kinet. Catal., 1 (1974), 73.
- 4. Dumitriu, E., Hulea, V., Bilba, N., Carge, G. and Azzouz, A., J. Mol. Catal., 79 (1993), 175.
- Dumitriu, E., Bilba, N., Lupascu, M., Azzouz, A., Hulca, V., Carge, G. and Nibou, D., J. Catal., 174 (1994), 133
- 6. Dumitriu, E., Azzouz, A., Hulea, V., Lutic, D. and Kessler, H., Micropor. Mater., 10 (1997), 12.
- 7. Biaglow, A. I., Sepa, J., Gorte, R. J. and White, D., J. Catal., 151 (1995), 373.
- 8. Xu, T., Munson, E. J. and Haw, J. F., J. Am. Chem. Soc., 116 (1994), 1962.
- Dumitriu, E., Hulea, V., Fechete, I., Auroux, A., Lacaze, J.-F. and Guimon, C., MICROPOR. MESOPOR. MAT., 43 (2001), 341.
- 10. Panov, A. G. and Fripiat, J. J., J. Catal., 178 (1998), 188.
- 11. Kubelkaova, L., Cejka, J. and Novakova, J., Zeolites, 11 (1991), 822.
- 12. Kubelkaova, L. and Novakova, J., Zeolites, 11 (1991), 48.
- 13. Bell, V. A. and Gold, H. S., J. Catal., 79 (1983), 286.
- 14. Biaglow, A. I., Gorte, R. J., Kokotailo, G. T. and White, D., J. Catal., 148 (1994), 779.
- 15. Bohlmann, W. and Michel, D., J. Catal., 202 (2001), 421.
- 16. Florian, J. and Kubelkava, L., J. Phys. Chem., 98 (1994), 8734.
- Sepa, J., Lee, C., Gorte, R. J., White, D., Kassab, E., Evleth, E. M., Jessri, H. and Allavena, M., J. Phys. Chem., 100 (1996), 18515.
- Lee, S.-O., Kitchin, S. J., Harris, K. D. M., Sanker, G., Dugal, M. and Thomas, J. M., J. Phys. Chem. B, 106 (2002), 1322.
- 19. Kassab, E., Jessri, H., Allavena, M. and White, D., J. Phys. Chem. A, 103 (1999), 2766.
- 20. Bobuatong, K. and Limtrakul, J., Appl. Catal. A, (2003), in press.
- 21. Panjan, W. and Limtrakul, J., J. Mol. Struct., 654 (2003), 35.
- 22. Raksakoon, C. and Limtrakul, J., THEOCHEM, 631 (2003), 147.
- 23. Kasuriya, S., Namuangruk, S., Treesukol, P., Tirtowidjojo, M. and Limtrakul, J., J. Catal., (2003), in press.
- 24. Koningveld, H. v., Bekkum, H. v. and Jansen, J. C., Acta Crystallogr. B, 43 (1987), 127.
- 25. Frisch, M. J., Trucks, G. W., Schlegel, H. B., Scuseria, G. E., Robb, M. A., Cheeseman, J. R., Zakrzewski, V. G., Montgomery, J. A., Stratmann, Jr. R. E., Burant, J. C., Dapprich, S., Millam, J. M., Daniels, A. D., Kudin, K. N., Strain, M. C., Farkas, O., Tomasi, J., Barone, V., Cossi, M., Cammi, R., Mennucci, B., Pomelli, C., Adamo, C., Clifford, S., Ochterski, J., Petersson, G. A., Ayala, P. Y., Cui, Q., Morokuma, K., Salvador, P., Dannenberg, J. J., Malick, D. K., Rabuck, A. D., Raghavachari, K., Foresman, J. B., Cioslowski, J., Ortiz, J. V., Baboul, A. G., Stefanov, B. B., Liu, G., Liashenko, A., Piskorz, P., Komaromi, I., Gomperts, R., Martin, R. L., Fox, D. J., Keith, T., Al-Laharn, M. A., Peng, C. Y., Nanayakkara, A., Challacombe, M., Gill, P. M. W., Johnson, B., Chen, W., Wong, M. W., Andres, J. L., Gonzalez, C., Head-Gordon, M., Replogle, E. S., and Pople, J. A., Gaussian, Inc., Pittsburgh PA, 2001.



# ADSORPTION OF TOLUENE OVER FAUJASITE ZEOLITE INVESTIGATED BY THE COMBINED QUANTUM MECHANICS/MOLECULAR MECHANICS METHOD

Wongthong, P., Soonthornpalin, C., Pantu, P., and Limtrakul, J.

Laboratory for Computational & Applied Chemistry, Chemistry Department, Kasetsart University, Bangkok 10900, THAILAND

#### ABSTRACT

The ONIOM (Our-own-N-layered Integrated molecular Orbital + molecular Mechanics) approach utilizing two-layer ONIOM2 schemes - ONIOM2(MP2/6-31G(d,p):HF/3-21G), ONIOM2(B3LYP/6-31G(d,p):HF/3-21G), ONIOM2(B3LYP/6-31G(d,p):HF/3-21G), ONIOM2(B3LYP/6-31G(d,p):UFF), and ONIOM2(HF/3-21G:UFF) - have been used to investigate adsorption properties of aromatics in faujasite zeolites (H-FAU). The active site has been modeled with realistic clusters sizes up to 84 tetrahedra. The predicted adsorption energy of H-FAU/toluene complexes for the ONIOM2(B3LYP/6-311+G(d,p):UFF) scheme is -81.34 kJ/mol, which is in line with the experimental values of -58.5 and -85.3 kJ/mol for H-FAU/benzene and H-FAU/ethylbenzene, respectively. Where the conventional 3T quantum cluster yields an underestimated value of -32.52 kJ/mol. This finding clearly demonstrates that acidity does not depend only on the Brønsted group center but also on the lattice framework surrounding the Brønsted site. The results obtained in this study suggest that the ONIOM2 approach yields a more accurate for studying the adsorption of aromatics on zeolites.

# INTRODUCTION

Zeolites are widely used in petroleum and chemical industries as solid catalysts for a number of commercially important reactions due to their outstanding properties, i.e., Brønsted and Lewis acid sites, size-shape selectivity. Nowadays the many conventional acid-catalyzed processes have been progressively substituted with zeolite-based processes for the advantages of handling, safety, and environmental benign. Electrophilic aromatic substitution is one of the most industrially important processes that can be efficiently catalyzed by many zeolite catalysts, e.g., FAU, ZSM-5, beta [1]. For the alkylation of toluene with methanol catalyzed by zeolites, a variety of important petrochemical products can be obtained. The product selectivity is governed by many factors, such as the intrinsic reaction rate and steric constraint imposed by specific pore size and adsorption-desorption and diffusion of reactants and products. Therefore details of molecular interactions are needed to fully understand the reaction mechanism and product selectivity.

Since it is known that a significant fraction of energetics of aromatics in zeolites is derived from van der Waals interactions with the constricted zeolite pores, the effect of the extended zeolite framework is essential in accurately investigating interactions of aromatics in zeolites. Numerous theoretical models have been proposed to study the crystalline zeolite [2-3]. Nevertheless, zeolites that have a high impact in industrial processes usually possess hundreds of atoms per unit cell. This makes the use of sophisticated methods, such as periodic ab initio calculations, computationally too expensive and even impractical sometimes when very large zeolites are concerned. The recent development of hybrid methods, such as the embedded cluster or the combined quantum mechanics/molecular mechanics (QM/MM) methods, as well as the more general ONIOM (Our-own-N-layered Integrated molecular Orbital + molecular Mechanics) method has brought a larger system within reach of obtaining accurate results. Up to date, the ONIOM method is applied to the study of extended systems, for example, chemical reactions on surface [4-12], and in enzymes [13].

In this report, we present the results of using the ONIOM model to represent the complicated structure of zeolites and to study the adsorption of benzene, and toluene, which is the first important step for a more comprehensive study of alkylation reaction. We are focusing on the systems of faujasite (H-FAU), which are of high importance in many industrial reactions. The faujasite's unit cell of 576 atoms limits the use of periodic calculation, thus we manage to use the ONIOM method to model the active site of H-FAU, the Brønsted acid site. The rational choice of the levels of calculations for the ONIOM scheme has been examined. The results are

compared to experimental data to find efficient combinations to satisfactorily reproduce the adsorption energies of H-FAU zeolite. This should provide us with a better understanding of the role of H-FAU in the process of catalyzing reactions of aromatic hydrocarbons.

#### METHOD

Two different strategies have been employed to model the faujasite. First, the 3T cluster H<sub>3</sub>SiOAl(OH)<sub>2</sub>O(H)SiH<sub>3</sub> (see Figure 1a) which is considered as the smallest unit that is required to represent the active site of zeolite. The cluster models were obtained from the lattice structure of faujasite zeolite [14]. The effect from the framework structure of zeolite cannot be totally neglected if more accurate results are required. The more realistic cluster model created for this study is 84T (see Figure 1b) which includes two supercages that can act as a nanoscopic reaction vessel.

The accuracy of the QM/MM method, particularly the ONIOM method, depends significantly on the choice of the level of calculations for high- and low-level regions [15]. Using the B3LYP method for treating the quantum cluster, we varied the methods for the low-level region from the molecular mechanics force fields (UFF), semiempirical, over to the Hartree-Fock methods. Using the experimental observation as a benchmark, we found that the UFF method provides reasonable values corresponding to the experimental prediction [7-10]. This is due to the explicit consideration of van der Waals contribution, which is the dominant contribution in adsorption-desorption in zeolites [16-21]. Therefore, the UFF method is the practical choice for the tow-level methodology when the high-level region is treated by the B3LYP/6-31G(d,p) method. All calculations have been performed by using the Gaussian98 code [22]. The basis set 6-31G(d,p) is utilized for the B3LYP calculations. During the structure optimization, only the active site region [=SiO(H)Al(O)<sub>2</sub>OSi=], and the adsorbate are allowed to relax. In order to obtain more reliable interaction energies, a single-point energy calculation at the ONIOM2(B3LYP/6-311++G(d,p)/B3LYP/6-31G(d,p):UFF) level of theory and basis sets superposition error (BSSE) corrections were also taken into account.

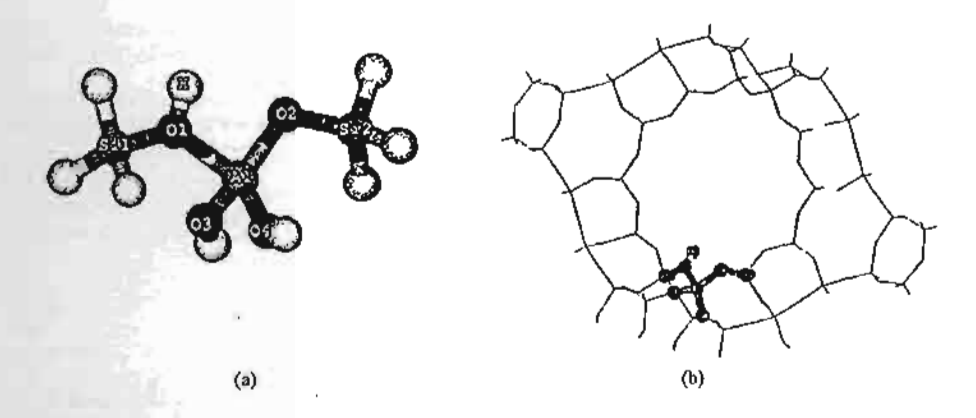


Figure 1: Presentation of cluster used to model the faujasite zeolite: (a) full 3T cluster model; (b) ONIOM2 model. The darker atoms in cluster 84T are treated at the higher level in the ONIOM2 approach.

# RESULTS AND DISCUSSION

# Structures of faujasite zeolite models

The faujasite zeolites were modeled by two different aluminosilicate clusters containing 3T and 84T tetrahedrally coordinated tetravalent atoms (see Figures 2-3). Table 1 lists some selected structural parameters derived at 3T quantum clusters and the ONIOM2 integrated schemes. By comparing the structure between the 3T

quantum cluster and the 84T ONIOM2 models, it is seen that the cluster size environment has little effect on the structure of the active site. The extended framework slightly lengthens the O1-H bond distance (Brønsted acid site) from 96.7 pm in the 3T model to 96.8 pm in the 84T model. The bond distance between the aluminum and the proton nuclei in a Brønsted acid site,  $r(A1^{-}H)$ , of faujasite was computed to be 246.0 pm and 240.2 pm for the 3T cluster and 84T ONIOM2 models, respectively compared well with the experimental measurement value of 238.0  $\pm$  4 pm reported in a literature [23]. Since the ONIOM2(B3LYP:UFF) method gives a good structural representation of the Brønsted acid site and the UFF force field is also a theoretically appropriate method for representing the effect of extended framework for this purpose (as discussed above) only the ONIOM models with the UFF force field will be discussed in detail hereafter.

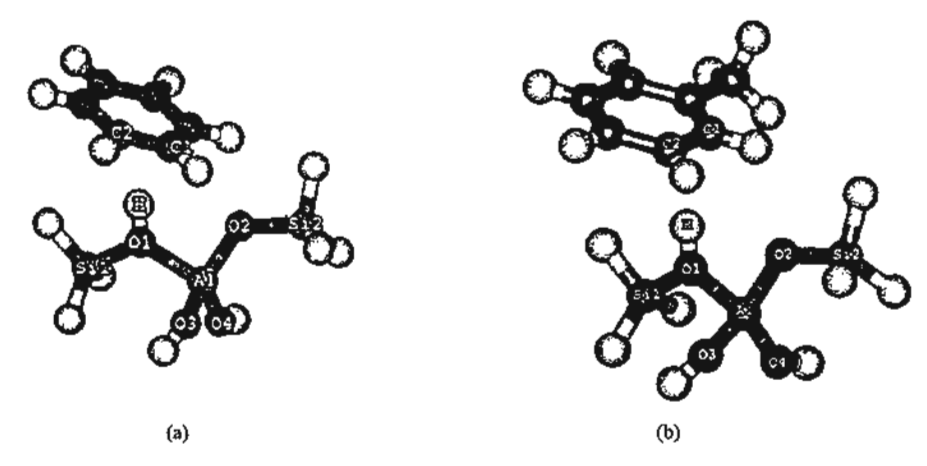


Figure 2: Presentation of models of faujasite and interacting with adsorbates: (a) full 3T cluster model interacting with benzene; (b) full 3T cluster model interacting with toluene.

Table 1: Structural parameters of faujasite obtained at full HF/3-21G, full B3LYP/6-31G(d,p) and various two-layer ONIOM2 schemes (bond distances in pm and bond angles in degrees).

Parameters	3Т		84	Т
	Full HF	Full B3LYP	HF:UFF	B3LYP:UFF
01-н	96.8	96.7	96.8	96.8
AI-01	184.2	191.7	180.5	186.0
Si1-Ol	171.9	170.9	169.4	168.6
Al-H	233,5	246.0	230.3	240.2
∠AI-O1-Si)	127.4	126.7	126.0	125.5

The HF is Hatree-Fock with 3-21G basis set.

The B3LYP is density functional theory with 6-31G(d,p) basis set.

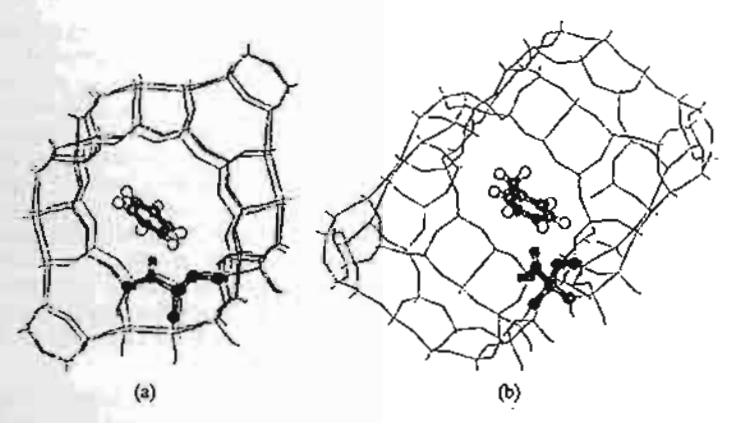


Figure 3: Presentation of models of faujasite and interacting with adsorbates: (a) ONIOM2 layer models of 84T cluster interacting with benzene; and (b) ONIOM2 layer models of 84T cluster interacting with toluene. Atoms belonging to the high-level regions are drawn as spheres.

# Interactions of toluene with faujasite zeolites

Some structural parameters of the adsorption complexes calculated at finite clusters and at different ONIOM models (HF:UFF and B3LYP:UFF) are tabulated in Table 2. Table 2 presents the comparison between the 3T and 84T cluster models of the adsorption complexes indicating that adsorption does not significantly perturb structures of the adsorbed molecules or the zeolites due to the weak interactions between the hydrocarbons and the zeolite, Increasing of cluster size has only a small effect on the structure of the active site, but significantly affects the orientation of the adsorbed molecules. For the small cluster models, the adsorbed molecules are Pi-bonded to the active site with almost equal bond distances between the two double-bond carbons and the Brønsted proton. For the 84T cluster models, interactions with the extended framework cause the adsorbed molecules to move farther from the acid proton and lose the symmetrical bidentated structures.

Table 2: Structural parameters for adsorbate/zeolite cluster complexes, where adsorbates are benzene, and toluene.

Methods	Parameters	-	3T		84T		
		Benzene	Toluene	Benzene	Tolueno		
HF	О1-Н	97.5	97.6	97.3	97.2		
	AI-01	182.9	182.8	179.4	197.4		
	Si1-O1	171.1	171.0	168.9	168.9		
	C1-H	220.8	218.3	222.5	226.0		
	C2-H	224.3	225.1	267.4	270.5		
	C=C	138.9	139.0	138.7	138.9		
	∠Al-O1-SiT	127.7	127.7	126.5	126.4		
B3LYP	O1-FI	98.0	98.2	98.0	98.2		
	Al-01	139.8	189.7	184.9	184.5		
	Si1-O1	171.0	170.1	168.4	167.9		
	C1-H	221.4	218.0	1.912	289.8		
	C2-H	224.1	224.8	259.4	211.6		
	C=C	140.1	140.0	140.1	140.0		
	∠Al-O1-Sit	126.5	1265	124.9	125.1		

The zeolite clusters are 3T, 84T (bond distances in pm and bond angles in degrees). The B3LYP is density functional theory with 6-31G(d,p) basis set; HF is Hattee-Fock with 3-21G basis set.

The adsorption energies of benzene and ethylbenzene on H-Y zeolite were experimental measured to be -58.5 and -85.3 kJ/mol, respectively. Although the adsorption energy of toluene in faujasite zeolite is not available, it is expected to be between the values of the benzene and ethylbenzene adsorption. In the 3T cluster model, the DFT calculations predict the adsorption energies of benzene and toluene to be -31.21 and -32.52 kJ/mol, respectively which are considerably lower than the experimental measurements. Moreover, the small cluster calculations incorrectly predict comparable interaction energies of the zeolite with benzene and toluene molecules mistakenly indicating no shape selectivity between these two molecules. The erroneous results are due to the fact that the quantum cluster calculations omit the effect of the zeolite crystal structure.

In the more realistic 84T ONIOM2 model, the adsorption energies of benzene and toluene are calculated to be – 71.69 and -88.66 kJ/mol, respectively. These interaction energies are somewhat overestimated as compared to the experimental results. After including the basis set correction by single point calculations at the higher basis set, 6-311++G(d,p), the corresponding interaction energies are computed to be of -63.41 and -81.34 kJ/mol. The BSSE corrections were also performed and gave similar results as the single point calculations at the high basis set (see Table 3).

It is noted that the choices of the methods using the high- and low-levels in the ONIOM scheme and also the sizes of the inner and outer regions are arbitrary. The size of the inner region employed in this study (3T cluster) is sufficient to represent the acid property of zeolites whilst small enough to guarantee that the van der Waals interactions between the hydrocarbon and the zeolite are well accounted for by the UFF force field, which is better than the DFT for this purpose [19-21]. From the structure and adsorption energy point of views, the B3LYP combining the UFF force fields method as a lower level is considered to be one of the best combinations for the ONIOM2 scheme. This efficient scheme provides a cost effective computational strategy for treating the effects of a large extended framework structure.

Table 3: Binding energy of benzene, and toluene on the Brønsted proton of faujasite zeolites (binding energy in kJ/mol)

Methods/Models	31	84T		
	Benzene	Toluene	Benzene	Toluene
HF/3-21G	-39.67	-41.07	-	
B3LYP/6-31G(d,p)	-31.27	-32.52	-	-
HF/3-21G:UFF		-	-76.62	-91. <del>9</del> 6
B3LYP/6-31G(d,p):UFF	-	+	- 71.69	-88.66
B3LYP/6-31G(d,p):UFF+BSSE*		-	-67.51	-78.75
B3LYP/6-311++G(d,p):UFF*	-	-	~63.41	-81.34
MP2/6-311++G(d,p):UFF°		-		-106.00
MP2/6-311++G(d,p):UFF+BSSE*		-	-	-89.54

Adsorption energies of benzene and ethylbenzene on H-FAU zeolites are experimentally observed to be -58.5 and - 85.3 kJ/mol, respectively [24,25].

# CONCLUSIONS

The extended framework significantly enhances the adsorption energy of toluene to the zeolites. With the ONIOM2(B3LYP/6-311++G(d,p):UFF) scheme, the adsorption energy of -81.34 kJ/mol for the H-FAU/toluene complexes was predicted. The results obtained in the present study suggest that the ONIOM approach yields a more accurate and practical model in studying adsorption of aromatics on zeolites.

# **ACKNOWLEDGMENTS**

This work was supported in part by grants from the Thailand Research Fund (TRF Senior Research Scholar to JL) and the Kasetsart University Research and Development Institute (KURDI) as well as the Ministry of University Affairs under the Science and Technology Higher Education Development Project (MUA-ADB funds). The support from the Dow Chemical Company (USA) is also acknowledged.

Basis set superposition error corrected.

Indicates single-point energy with B3LYP/6-311++G(d,p)/B3LYP/6-31G(d,p)

<sup>&</sup>quot;Indicates single-point energy with MP2/6-311++G(d,p)//B3LYP/6-31G(d,p)

# REFERENCES

- [1] Perego, C., Ingallina, P., Catal. Today, 73 (2002), 3-22.
- [2] Rozanska, X., Hutschka, F., van Santen, R.A., Saintigny, X., J. Catal., 202 (2001), 141-155.
- [3] Hutschka, F., van Santen, R.A., Rozanska, X., Hafner, J., J. Am. Soc., 123 (2001), 7655-7667.
- [4] Tang, H.R., Fan, K.N., Chem. Phys. Lett., 330 (2000), 509-514.
- [5] Roggero, I., Civalleri, B., Ugliengo, P., Chem. Phys. Lett., 341 (2001), 625-632.
- [6] Sillar, K., Burk, P., J. Mol. Struct. (Theochem.), 589 (2002), 281-290.
- [7] Raksakoon, C., Limtrakul, J., J. Mol. Struct. (Theochem), 631 (2003), 147-156.
- [8] Panjan, W., Limtrakul, J., J. Mol. Struct., 654 (2003), 35-45.
- [9] Kasuriya, S., Namuangruk, S., Treesukol, P., Tirtowidjojo, M., Limtrakul, J., J. Catal., 2003, in press.
- [10] Bobuatong, K., Limtrakul, J., Appl. Catal. A, 2003, in press.
- [11] Solans-Monfort, X., Bertran, J., Branchadell, V., Sodupe, M., J. Phys. Chem. B, 106 (2002), 10220-10266.
- [12] Damin, A., Bonino, F., Ricchiardi, G., Bordiga, S., Zecchina, A., Lamberti, C., J. Phys. Chem. B, 106 (2002), 7524-7526.
- [13] Torrent, M., Vreven, T., Musaev, D.G., Morokuma, K., J. Am. Chem. Soc., 124 (2002), 192-193.
- [14] van Koningveld, H., van Bekkum, H., Jansen, J.C., Acta Crystallogr. B, 43 (1987), 127-132.
- [15] Dapprich, S., Komarmi, I., Byun, K.S., Morokuma, K., Frish, M.J., J. Mol. Struct (Theochem), 461 (1999), 1-21.
- [16] Pelmenschikov, A., Leszczynski, J., J. Phys. Chem. B, 103 (1999), 6886-6890.
- [17] Wesolowski, T.A., Pariset, O., Ellinger, Y., Weber, J. J. Phys. Chem. A, 101 (1997), 7818-7825.
- [18] Derouane, E.G., Chang, C.D., Microporous Mesoporous. Mater., 425 (2000), 35-36.
- [19] Clark, L.A., Sicrka, M., Sauer, J., J. Am. Chem. Soc., 125 (2003), 2136-2141.
- [20] Vos, A.M., Rozanska, X., Schoonheydt, R.A., van Santen, R.A., Hutschka, F., Hafner, J., J. Am. Chem. Soc., 123 (2001), 2799-2809.
- [21] Rozanska, X., van Santen, R.A., Hutschka, F., Hafiner, J., J. Am. Chem. Soc., 123 (2001), 7655-7667.
- [22] Frisch, M.J., Trucks, G.W., Schlegel, H.B., Scuseria, G.E., Robb, M.A., Cheeseman, J.R., Zakrzewski, V.G., Montgomery, J.A., Stratmann, Jr. R.E., Burant, J.C., Dapprich, S., Millam, J.M., Daniels, A.D., Kudin, K.N., Strain, M.C., Farkas, O., Tomasi, J., Barone, V., Cossi, M., Cammi, R., Mennucci, B., Pomelli, C., Adamo, C., Clifford, S., Ochterski, J., Petersson, G.A., Ayala, P.Y., Cui, Q., Morokuma, K., Salvador, P., Dannenberg, J.J., Malick, D.K., Rabuck, A.D., Raghavachari, K., Foresman, J.B., Cioslowski, J., Ortiz, J.V., Baboul, A.G., Stefanov, B.B., Liu, G., Liashenko, A., Piskorz, P., Komaromi, I., Gomperts, R., Martin, R.L., Fox, D.J., Keith, T., Al-Laham, M.A., Peng, C.Y., Nanayakkara, A., Challacombe, M., Gill, P.M.W., Johnson, B., Chen, W., Wong, M.W., Andres, J.L., Gonzalez, C., Head-Gordon, M., Replogle, E.S., and Pople, J.A., Gaussian, Inc., Pittsburgh PA, 2001.
- [23] Frende, D., Klinowski, J., Hamdan, H., Chem. Phys. Lett., 149 (1988), 355-362.
- [24] O'Malley, P.J., Farnworth, K., J. Phys. Chem. B, 102 (1998), 4507-4515.
- [25] Dixit, L., Prasada Rao, T.S.R., J. Chem. Inf. Comput. Sci., 39 (1999), 218-223.



# STRUCTURE AND ENERGETICS OF NITROUS OXIDE AND METHANE ADSORPTION ON THE Fe-ZSM-5 ZEOLITE: ONIOM AND DENSITY FUNCTIONAL STUDIES

Pabchanda, S.1, Pantu, P.1, Tantanak, D.2 and Limtrakul, J.1

<sup>1</sup>Laboratory for Computational and Applied Chemistry, Chemistry Department, Kasetsart University, Bangkok 10900, Thailand; e-mail address; fscijrl@ku.ac.th

Chemistry Department, Faculty of Science, King Mongkut's Institute of Technology Ladkrabang, Ladkrabang, Bangkok 10520, Thailand.

# **ABSTRACT**

The quantum cluster and ONIOM methods have been used to investigate interactions between adsorbed nitrous oxide and methane on the active iron center in Fe-ZSM-5, prior to its catalytic oxidation to methanol. A model of mononuclear iron complex as an active site of the highly dispersed state of Fe-ZSM-5 was adopted in cluster models of 5T quantum cluster and 46T ONIOM2. The extended crystal framework included in the ONIOM model significantly enhances the interactions of both adsorbates with the active site. The adsorption energy of N<sub>2</sub>O on Fe-ZSM-5 calculated by the 5T quantum cluster is only ~41.2 kJ/mol, whereas, the 46T ONIOM model gives the adsorption energy of ~57.3 kJ/mol, which is comparable to the experimental estimate of ~67 kJ/mol. After correction with single point calculation at MP2/6-31G\*\*:UFF/B3LYP/6-3IG\*\*:UFF, the adsorption energy is calculated to be 66.9 kJ/mol, which is apparently identical to the experimental estimate. The ONIOM2 model also predicts the adsorption energy of ~30.5 kJ/mol for the [CH4]/Fe-ZSM-5 complexes. These results demonstrate that the adsorption properties of Fe-ZSM-5 depend significantly on the specific environment of the zeolite crystal lattice.

# INTRODUCTION

The intracrystalline nanostructured pore network of zeolites has an astonishing ability to stabilize small metal complexes leading to extraordinary catalytic activities. Small iron complexes in ZSM-5 (Fe-ZSM-5), for example, have remarkable redox behaviours [1-5] and recently have been received great attention. The Fe-ZSM-5 can catalyze selective reduction of NOx and selective hydroxylation of various organic compounds using nitrous oxide as an oxidant. An example of catalytic activity of Fe-ZSM-5 that is of the high industrial interest is the selective oxidation of benzene to phenol. However, the most fascinating catalytic activity of Fe-ZSM-5 is that it can selectively oxidize methane to methanol at room temperature.

The highly active and selective catalytic site in the Fe-ZSM-5 is commonly known as an  $\alpha$ -site whose structure, though, having been extensively studied [6-10], is still not clearly understood. An interesting point to note is that the Fe-ZSM-5 has some characteristics in common with the enzyme methane monoexygenase (MMO), found in methanotropic bacteria whose active site contains binuclear iron cluster [11,12]. The active iron atoms in Fe-ZSM-5 are found to be highly dispersed in the zeolite matrix and could be in the form of isolated ions, or dinuclear complexes, or small aggregate of iron atoms [10-14]. According to Mössbauer studies, iron atoms at the  $\alpha$ -site are in a divalent state (Fe<sup>2+</sup>) and after the decomposition of nitrous oxide, the iron atoms are changed to a trivalent state (Fe<sup>3+</sup>). With the knowledge gained from experimental studies, quantum chemical models of the  $\alpha$ -site structures have been proposed in literatures [15-17]. However, those quantum chemical studies did not include the effects of the zeolite framework which is known to have significant effects on structures and energetics of guest molecules in zeolite structures [18-20].

We herein report the results of our theoretical study on interactions of nitrous oxide and methane with Fe-ZSM-5 using a DFT method with the aims of investigating the effects of the extended zeolitic framework on the structure and function of the Fe-ZSM-5 complex. This is the first case we know of where the explicit zeolite environment is included in calculations for this zeolite catalyst.

# **METHODS**

Structures of cluster models were taken from the crystal structure of a ZSM-5 lattice with one aluminium atom substituted with a silicon atom at the T12 position and the negative charge of the cluster was balanced by either FeO<sup>+</sup> or FeO<sub>2</sub><sup>+</sup> ion to form the active centre. In this study, the Fe-ZSM-5 structure was represented by a 5T quantum cluster (Fig. 1a, 1c) and a 46T ONIOM2 model [21,22] (Fig 1b, 1d). In the ONIOM2 model the 5T active centre is treated quantum chemically at the B3LYP/6-31G(d,p) level of theory, and the rest of the extended framework, up to 46T, is treated at the UFF.

All calculations have been performed by using the Gaussian98 code [23]. The basis set 6-31G(d,p) is utilized for the B3LYP calculations. During the structure optimization, only the portion of the active site region and the adsorbate are allowed to relax. In order to obtain more reliable interaction energies, the single-point energy calculations at the ONIOM2-46T(MP2/6-31G\*\*:UFF/B3LYP/6-31G\*\*:UFF) level were carried out.

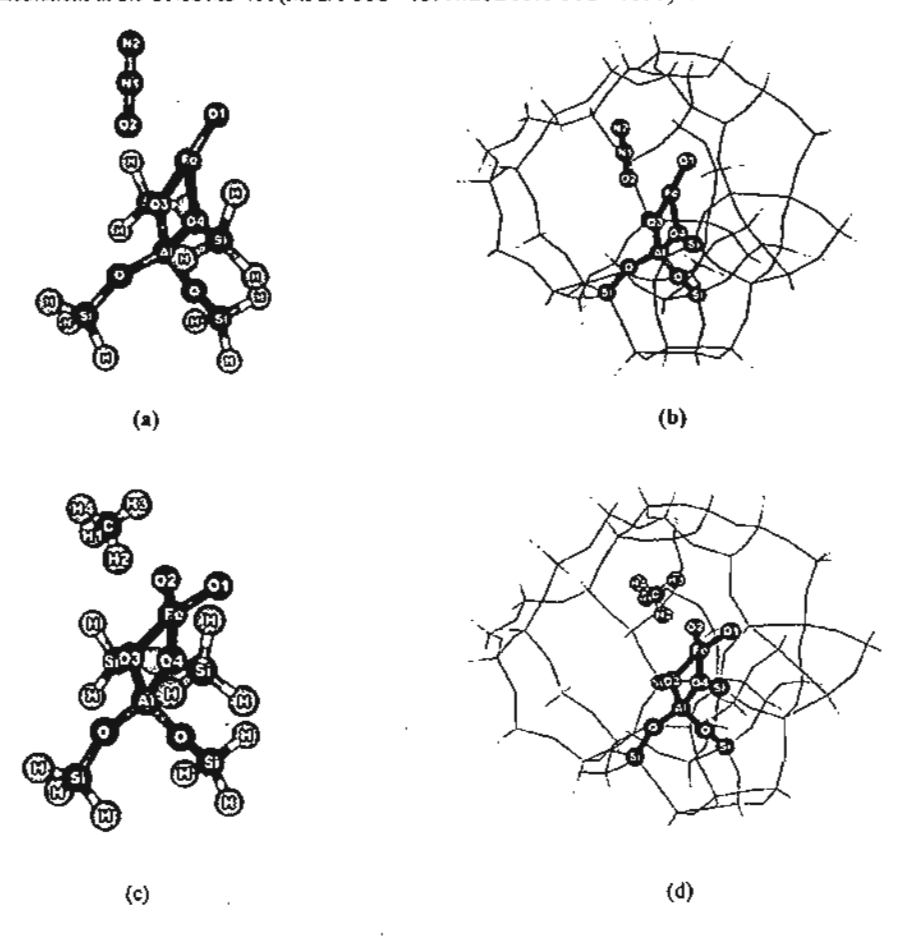


Figure 1 N<sub>2</sub>O/FeO-ZSM-5 and CH<sub>2</sub>/FeO<sub>2</sub>-ZSM-5 clusters, atoms belonging to the active region drawn as sphere, (a) 5T cluster of N<sub>2</sub>O/FeO-ZSM-5, (b) 46T ONIOM model of N<sub>2</sub>O/FeO-ZSM-5, (c) 5T cluster of CH<sub>2</sub>/FeO<sub>2</sub>-ZSM-5, (d) 46T ONIOM model of CH<sub>2</sub>/FeO<sub>2</sub>-ZSM-5.

# RESULTS AND DISCUSSION

It has been found that with low iron content in Fe-ZSM-5, iron atoms are highly dispersed in the zeolite pores and present primarily in a form of isolated mononuclear iron oxide ion at the ion-exchange sites of the ZSM-5 [24]. Therefore, the α-site can be modeled as a divalent mononuclear Fe(II)O\*/ZSM-5° and after N<sub>2</sub>O decomposition, the α-oxygen loaded active site can be modeled as Fe(II)O<sub>2</sub>\*/ZSM-5° [15]. In this work, two cluster sizes, 5T and 46T, were used to represent the Fe-ZSM-5 zeolite. In the 46T ONIOM2 model, the extended structure was included to cover the cavity at the intersection of the straight and zigzag channels where adsorbates are favorably adsorbed.

# Structures of the a-site [Fe(II)O\*/ZSM-57]

At the active site, an iron ion (FeO') is coordinated by the two bridging oxygen atoms in zeolite which act as Lewis bases via the formation of bidentate interactions (Fig 1a, 1b). These interactions are found to be approximately symmetric, with almost equal Fe-O2 and Fe-O3 bond lengths about 202 pm (Table 1). The iron atom is bound more tightly to its covalent oxygen ligand (O1) with a bond distance of about 164 pm. The Fe-O1 bond is aligned with the plane of the 10T windows of the zigzag pore channel. Increasing the cluster sizes causes the FeO+ to move farther from the zeolite framework and the distance Fe-A1 was increased from 281.3 pm to 287.1 pm and the Fe-O1 bond distance was also slightly increased from 163.9 pm to 164.4 pm.

# Structures of the \alpha-oxygen loaded site [Fe(III)O2\*/ZSM-5]

Selected structure parameters of Fe(III)O<sub>2</sub>\*/ZSM-5° model and its adsorption complex with methane are tabulated in Table 2. In the  $\alpha$ -oxygen loaded active site, the bond distances between the iron atom and the two oxygen atoms are virtually the same (Fe-OI= 166.6 pm and Fe-O2 = 166.7 pm). However, the  $\alpha$ -oxygen (O2) is pointed toward the free space in the intersection cavity and, therefore, it is more accessible by adsorbates (Fig 1c, 1d).

Table 1. Optimized geometries of isolated model and adsorption complex of nitrous oxide on FeO-ZSM-5 zeolite.

	ST(B3LYP	/6-31G(d,p))	46T(B3LYP/6	31G(d,p):UFF)
	Isolated	Complex	isolated	Complex
Fe-O1	165.1	166,4	164,9	166.2
Fe-O2		230.1		229.5
Fe-O3	202.7	203.4	202.7	203.9
Fe-O4	201.2	202.7	201.7	203.0
Fe-Al	282.5	282.8	283.1	283.3
Fe-N1	-	303.4		305.7
Fe-N2		394.8	•	398,8
N1-02	•	120.6		121.0
N1-N2	_	112.9	_	112.5

N-O of N<sub>2</sub>O = 119.2 pm N-N of N<sub>2</sub>O = 113.4 pm

# Adsorption of nitrous oxide on the a-site

It is known that a nitrous oxide molecule can be adsorbed on the FeO+ site via either the nitrogen-end or the oxygen-end of the molecule. In this study, we, however, only look at the case where adsorption takes place via the oxygen-end of the N<sub>2</sub>O molecule, since we are interested in studying interactions of N<sub>2</sub>O with the α-site (FeO<sup>+</sup>) that leads to the formation of the α-oxygen loaded site (FeO<sub>2</sub><sup>+</sup>). The N<sub>2</sub>O molecule adsorbs on the active site by having its oxygen atom pointing to the iron center and the nitrogen end pointing to the free space in the intersection cavity. In the 5T cluster calculation, the N-O bond distance is slightly increased from 119.2 to 120.6 pm while the N-N bond distance is contracted from 113.4 to 112.9 pm (see Table 1). Inclusion of the extended framework structure significantly enhances interactions between the adsorbed nitrous oxide and the active site. The adsorption energy is markedly increased from 41.2 kJ/mol to 57.3 kJ/mol, which is very close to an experimental estimate of 67 kJ/mol [21]. After correction with single point energy calculations at the high level of theory and the high basis set, MP2/6-31G\*\*:UFF/B3LYP/6-31G\*\*:UFF, the adsorption energy is calculated to be 66.9 kJ/mol, which is apparently identical to the experimental estimate (see Table 3). The result indicates that the extended framework

included by the UFF force field is sufficient to correct the absence of the framework effect in the DFT cluster calculation and, therefore, makes it possible to calculate accurate adsorption energy by using the ONIOM model.

Table 2. Optimized geometries of isolated model and adsorption complex of methane on FeO2-ZSM-5 zeolite.

	ST(B3LYF	/6-31G(d,p))	46T(B3LYP/6	-31G(d,p):UFF)
	Isolated	Complex	Isolated	Complex
Fe-O1	166.7	166.7	166.6	166.6
Fe-O2	166.6	166.6	166.5	166.5
Fe-O3	197.9	197.5	198.0	198.2
Fe-O4	197.5	198.7	197.8	199.1
01-02	228.1	227.4	228.2	227.0
Fc-Al	281.5	277.4	279.8	278.7
Fe-C	-	343.7	•	342,6
Fe-H1	-	338.1		337.8
Fe-H2	-	282.1	-	281.1
Fe-H3	-	357.8	-	357.1
Fe-H4	-	444.1		443.7
O2-H1	-	295.3	-	294.8
O2-H2	-	328.1		327.7
O2-H3	-	331,8	-	331.2
O2-H4	-	444.0	-	443.6
C-H1	-	109.1	,	109.1
C-H2	-	109,5	-	109.7
C-H3	•	109.1		109,1
C-H4	-	109.2	-	109.2

C-H of CH4 = 109.2 pm

# Adsorption of methane on the \alpha-oxygen loaded site

Methane adsorbs on the α-oxygen loaded site by having one hydrogen atom (H1) pointing toward the iron atom and another hydrogen atom (H2) pointing toward the α-oxygen atom (O2). In the 5T quantum cluster, the distance between Fe-H1 is evaluated to be 282.1 pm and that of O2-H1 is 295.3 pm. The weak interactions between the adsorbed methane and the active site do not significantly disturb the structure of the active site. On the other hand, the adsorbed methane molecule is partially activated by the adsorption as the C-H2 bond distance is slightly clongated from 109.2 to 109.5 pm. Including the extended framework increases interactions between adsorbed methane and the active center. The adsorption energy is increased from 15.5 kJ/mol to 27.2 kJ/mol and adsorbed methane is getting closer to the active iron site as reflected by decreasing in distance between Fe-C and Fe-H2 and O2-H1 (see Table 2) and also the increase of the C-H2 bond distance of the methane molecule from 109.5 to 109.7 pm. After correction with the single point energy calculations, the adsorption energy of methane on the active iron site in ZSM-5 is predicted to be -30.5 kJ/mol (see Table 3)

Table 3. The adsorption energies (kJ/mol) for the N2O/FeO-ZSM-5 and CHJ/FeO-ZSM-5 systems

Method	Adsorption energies (kJ/mol)			
•	N <sub>2</sub> O/FeO+ZSM-5	CH_/FeO-ZSM-5		
Full ST(B3LYP/6-31G(d,p))	-41.2	-15.5		
ONIOM2-46T(B3LYP/6-31G(d,p); UFF)	-57.3	-27.2		
ONIOM2-46T(MP2/6-31G(d,p): UFF// B3LYP/6-31G(d,p): UFF)	-66.9	-30.5		
Experiment	-66.9	•		

# CONCLUSIONS

The extended framework significantly enhances the adsorption energy of methane to the zeolites. With the ONIOM2(B3LYP/6-31G(d,p):UFF) scheme, the adsorption energy of N<sub>2</sub>O on Fe-ZSM-5 was accurately calculated to be -66.9 kJ/mol, the adsorption energy of -30.5 kJ/mol for the [CH<sub>4</sub>]/Fe-ZSM-5 complexes was predicted. From the structure and adsorption energy point of views, the B3LYP or MP2 combining with the UFF force fields method as a lower level is considered to be one of the best combinations for the ONIOM2 scheme. This efficient

scheme provides a cost effective computational stategy for treating the effects of a large extended framework structure. The results obtained in the present study suggest that the ONIOM approach yields a more accurate and practical model in studying adsorption of hydrocarbons on zeolites and also in studying the mechanisms of oxidation of methane to methanol using N<sub>2</sub>O as oxidant. This challenging reaction is being actively pursued.

#### ACKNOWLEDGMENTS

This work was supported in part by grants from the Thailand Research Fund (TRF Senior Research Scholar to JL.) and the Kasetsart University Research and Development Institute (KURDI) as well as the Ministry of University Affairs under the Science and Technology Higher Education Development Project (MUA-ADB funds).

#### REFERENCES

- [1] Panov, G. I., Kharitonov, A. S., Sobolev, V. I., Appl. Catal. A, 98 (1993), 1-20.
- [2] Panov, G. I., Sobolev, V. I., Dubkov, K. A., Parmon, V. N., Ovanesyan, N. S., Shilov, A. E., Shteinman, A. A., React. Kinet. Catal. Lett., 61 (1997), 251-258.
- [3] Sobolev V. I., Panov G. I., Kharitonov A. S., Romannikov V. N., Volodin A. M., Ione K. G., J. Catal., 139 (1993), 435-443.
- [4] Perez-Ramirez, J., Kapteijn, F., Mul, G., Moulijn, J. A., Chem. Commun., (2001), 693-694.
- [5] El-Malki, E.-M., van Santen, R. A., Sachtler, W. M. H., J. Catal., 196 (2000), 212-223.
- [6] Chen, H.-Y., El-Malki, E.-M., Wang, X., van Santen, R. A., Sachtler, W. M. H., J. Mol. Catal. A, 162 (2000), 159-
- [7] Spoto, G., Zecchina, A., Berlier, G., Bordiga, S., Clerici, M. G., Basini, L., J. Mol. Catal. A, 158 (2000), 107-114.
- [8] Pannov, G. I., Sobolev, V. I., Kharitonov, A. S., J. Mol. Catal., 61 (1990), 85-97.
- [9] Zhidomirov, G. M., Yakovlev, A. L., Milov, M. A., Kachurovskaya, N. A., Yudanov, I. V., Catal. Today, 51 (1999), 397-410.
- [10] Dubkov, K. A., Ovanesyan, N. S., Shteinman, A. A., Starokon, E. V., Panov, G. I., J. Catal., 207 (2002), 341-352.
- [11] Panov, G. 1., Sobolev, V. I., Dubkov, K. A., Parmon, V. N., Ovanesyan, N. S., Shilov, A. E., Shteinman, A. A., React. Kinet. Catal, Lett., 61 (1997), 251-258.
- [12] Marturano, P., Drozdova, L., Kogelbauer, A., and Prins, R., J. Catal. 192(2000), 236-247.
- [13] Berlier, G., Spoto, G., Bordiga, S., Ricchiardi, G., Fisicaro, P., Zecchina, A., Rossetti, I., Selli, E., Fomi, L., Giamello, E., Lamberti, C., J. Catal., 208 (2002), 64-82.
- [14] Lobree, L.J., Hwang, I., Reimer, J.A. and Bell, A.T., J. Catal. 186(1999), 242-253.
- [15] Ryder, J. A., Chakraborty, A. K., Bell, A. T., J. Phys. Chem. B. 106(2002), 7059-7064.
- [16] Knops-Gerrits, P. P. Goddard, W. A., J. Mol. Catal. A, 166 (2001), 135-145.
- [17] Yoshizawa, K., Shiota, Y., Yumura, T. and Yamabe, T., J. Phys. Chem. B 104(2000), 734-740.
- [18] Pelmenschikov, A., Leszczynski, J., J. Phys. Chem. B, 103 (1999) 6886.
- [19] Raksakoon, C. and Limtrakul, J., J. Mol. Struct. (Theochem), 631 (2003), 147.
- [20] Kasuriya, S., Namuangruk, S., Treesukol, P., Tirtowidjojo, M. and Limtrakul, J., J. Catal., (2003), in press.
- [21] Basch, H., Musaev, D. G. and Morokuma, K., J. Phys. Chem. B 105(2001), 8452-8460.
- [22] Basch, H., Mogi, K., Musaev, D. G. and Morokuma, K., J. Am. Chem. Soc. 121(1999), 7249-7256.
- [23] Frisch, M.J., Trucks, G.W., Schlegel, H.B., Scuseria, G.E., Robb, M.A., Cheeseman, J.R., Zakrzewski, V.G., Montgomery, J.A., Stratmann, Jr.R.E., Burant, J.C., Dapprich, S., Millam, J.M., Daniels, A.D., Kudin, K.N., Strain, M.C., Farkas, O., Tomasi, J., Barone, V., Cossi, M., Cammi, R., Mennucci, B. Pomelli, C., Adamo, C., Clifford, S., Ochterski, J., Petersson, G.A., Ayala, P.Y., Cui, Q., Morokuma, K., Salvador, P., Dannenberg, J.J., Malick, D.K., Rabuck, A.D., Raghavachari, K., Foresman, J.B., Cioslowski, J., Ortiz, J.V., Baboul, A.G., Stefanov, B.B., Liu, G., Liashenko, A., Piskorz, P., Komaromi, I., Gomperts, R., Martin, R.L., Fox, D.J., Keith, T., Al-Laham, M.A., Peng, C.Y., Nanayakkara, A., Challacombe, M., Gill, P.M.W., Johnson, B., Chen, W., Wong, M.W., Andres, J.L., Gonzalez, C., Head-Gordon, M., Replogle, E.S., Pople, J.A. Gaussian, Inc., Pittsburgh PA, 2001.
- [24] Wood, B. R., Reimer, J. A., Bell, A. T., J. Catal. 209(2002), 151-158.

# Theoretical Study of Modes of Adsorption of Water Dimer on H-ZSM-5 and H-Faujasite Zeolites

Siriporn Jungsuttiwong, t.: Jumras Limtrakul, \*.: and Thanh N. Truong \*.t

Henry Eyring Center for Theoretical Chemistry, Chemistry Department, University of Utah, 315 S 1400 E, Room 2020, Salt Lake City, Utah 84112, and Laboratory for computational and applied chemistry, Chemistry Department, Kasetsart University, Bangkok 10900, Thailand

Received: November 1, 2004; In Final Form: April 26, 2005

Modes of adsorption of water dimer on H-ZSM-5 and H-Faujasite (H-FAU) zeolites have been investigated by a quantum embedded cluster approach, using the hybrid B3LYP density functional theory. The results indicate that there are two possible adsorption pathways, namely the stepwise process where only one water binds strongly to the (-O)<sub>3</sub>-Al-O(H) tetrahedral unit while the other weakly binds to the zeolite framework and the concerted process where both water molecules form a large ring of hydrogen-bonding network with the Brønsted proton and an oxygen framework. With inclusion of the effects of the Madelung potential from the extended zeolite framework, for adsorption on H-ZSM-5 zeolite, both the neutral and ion-pair complexes exist with adsorption energies of -15.13 and -14.73 kcal/mol, respectively. For adsorption on the H-FAU, only the ion-pair complex exists with the adsorption energy of -14.63 kcal/mol. Our results indicate that adsorption properties depend not only on the acidity of the Brønsted acidic site but also on the topology of the zeolite framework, such as on the spatial confinement effects which lead to very different adsorption structures for the ion-pair complexes in H-ZSM-5 and H-FAU, even though their adsorption energies are quite similar. Our calculated vibrational spectra for these ion-pair complexes support previous experimental IR interpretations.

# Introduction

Zeolite Brønsted acid sites have been known to catalyze many industrially important processes such as hydrocarbon conversions and production of fine chemicals. Protonation of substrate molecules by Brønsted protons has been suggested, and in fact is well-accepted as the initial step of these processes. For this reason, understanding whether substrate molecules are protonated upon adsorption on a Brønsted acid site is of great fundamental and technological importance. However, adsorption of a weak base such as water presents a challenge for experimental identification of its mode of adsorption. Two possible structures have been suggested when H2O is adsorbed at the Brønsted acid site: a hydrogen-bonded or a protonated complex. The preferred equilibrium structure has been a heavily debated issue. There are challenges in both experimental and theoretical investigations making the task of resolving this controversial issue more difficult. 1-12

Adsorption of an isolated water molecule on a Brønsted acidic site has been well-accepted and confirmed to form a neutral hydrogen-bonded complex. The remaining controversial issue is the number of water molecules needed to stabilize the protonated species. In previous experimental results, mostly obtained by IR spectroscopy, Jentys et al. 4 reported that protonation was observed by further adsorption of H<sub>2</sub>O to the 1:1 hydrogen-bonded structure on H-ZSM-5 to form dimeric H<sub>2</sub>O<sub>2</sub>+ and polymeric H<sub>2</sub>O<sub>2</sub>+ n(H<sub>2</sub>O)<sub>n</sub> species. In another IR

Theoretical results obtained by Zygmunt et al. 17 using a 5T (five tetrahedral sites) cluster model found that the neutral complex is more stable than the ion-pair structure by 2.9 kcal/ mol; this finding is consistent with those of Gale et al., 18 Bell et al.,19 and Limtrakul et al.12.20 On the other hand, the results obtained by Krossner et al.21 using exactly the same 5T model as Zygmunt at a different level of theory (BP for the former versus the B3LYP for the latter) found the ion-pair complex is more stable by about 3.6 kcal/mol. These studies agree that both neutral hydrogen bonded and ion-pair complexes exist. However, the predicted adsorption structures and their relative stabilities vary greatly. The differences could be due to several different sources such as differences in the level of theory and the physical model of the zeolite active site used. It is interesting to point out that the effects of the Madelung potential from the extended zeolite structure were not included in any of these studies. Such effects have been known to stabilize the ion-pair complexes<sup>22,23</sup> and thus, one would expect they play a significant

study, Kondo et al. <sup>13</sup> also indicated that the IR spectra of the dimeric H<sub>5</sub>O<sub>2</sub><sup>+</sup> species were clearly observed. In yet a different IR study, Zecchina and co-workers suggested that H<sup>+</sup>(H<sub>2</sub>O)<sub>n</sub> ionic species are formed at a high dosage of two or more water molecules per site. <sup>14</sup> However, Jobic et al. <sup>15,16</sup> using the Inelastic Neutron Scattering technique to also study adsorption of water at different concentrations in H-ZSM-5 did not observe the formation of hydroxonium ions. These studies pointed out the difficulty in interpreting the experimental spectra, particularly at higher loading levels, due to the possibility of interferences from the channel walls, the coexistence of both the hydrogenbonded and protonated species in equilibrium condition, and the multiple possible structures of a species for a given cluster size.

Address correspondence to these authors. E-mail: truong@chemistry.utah.edu (Thanh N. Truong) and fscijrl@ku.ac.th (Jumras Linstrakul).

<sup>\*</sup> University of Utah.

Kasetsart University.

role in determining the adsorption structures of water dimer on zeolites. Furthermore, the most recent theoretical study done by Zygmunt et al.<sup>17</sup> concluded that the 3T and 5T cluster models used so far are not adequate for studying adsorption of water dimer due to the possibility for water dimer to interact with the "capped" hydrogen atoms.

The importance of a fundamental understanding of factors that can affect the mode of adsorption, the lack of conclusive evidence in experimental data, and the shortcomings of previous theoretical studies have motivated us to perform a more systematic theoretical investigation on the adsorption of water dimer on zeolites. In particular, in this study, in addition to taking into account the effects of electron correlation, of large basis set, and of the zero-point energy motions, the effects of the long-range Madelung potential from the extended zeolite framework are also included in the determinations of both adsorption structures and the relative stability of the two forms of adsorption complexes by using an embedded cluster model. With such a model, it allows theoretical investigation on the effects of different zeolite structures on the adsorption properties. Particularly, we considered the adsorption on H-ZSM-5 and H-FAU zeolites. ZSM-5 has the channel cross section of 5.6 A, whereas FAU has a 7.4 Å cross section. How the differences in the ZSM-5 and FAU zeolite structures affect the adsorption mode is a question that has not been addressed previously. Our results also indicated that formation of the water dimer complex adsorbed on a Brønsted acid site can originate from two separate pathways, which yield two different adsorption structures. In one pathway, the dimer adsorption complex is formed by adsorbing one water molecule at a time on the adsorption site in a stepwise process. In this case, the first water molecule binds to the O<sub>3</sub>-Al-O(H) tetrahedral unit more strongly while the second water molecule binds to the first water molecule and the zeolite framework. In the other pathway, the dimer adsorption complex is formed by adsorption of water dimer on the adsorption site in a concerted process. In this case, both water molecules form a larger ring with the Brønsted acid site and a nearby oxygen of the zeolite framework. Addressing the question of how these pathways manifest in the mode of adsorption of water dimer on zeolite is also part of this study. Furthermore, comparisons between the calculated and experimental IR spectra allow verifications on the experimental suggested fingerprints for the ion-pair complex species.

# Computational Details

In this study, to avoid unphysical interactions between adsorbates and capped hydrogen atoms, quantum clusters consisting of seven tetrahedrally coordinated atoms (Si, Al) from the crystal structures24 were selected to represent the Brønsted acidic sites of these zeolites which are parts of the 12-membered ring of FAU or the 10-membered ring of ZSM-5 zeolites. These rings are at the intersections of the channels and are accessible to the adsorbates. Hydrogen atoms were used to cap the dangling bonds. These capped hydrogen atoms are located along the direction of corresponding Si-O bonds. The resulting TI clusters, Si<sub>6</sub>AlO<sub>10</sub>H<sub>16</sub>, have a total of 34 atoms. For ZSM-5 zeolite, the T12 site was selected to represent the active site because it was found to be among the most stable sites for Al substitution, 25,26 and this site provides sufficient space and can be accessed easily by small adsorbates. Most previous theoretical works have also chosen the T12 site as the Al substitution site for ZSM-5 zeolite. For FAU, all of the T sites (Al or Si tetrahedral sites) are equivalent by symmetry.

In the embedded cluster models, the 7T clusters are embedded in an array of point charges that represent the static Madelung

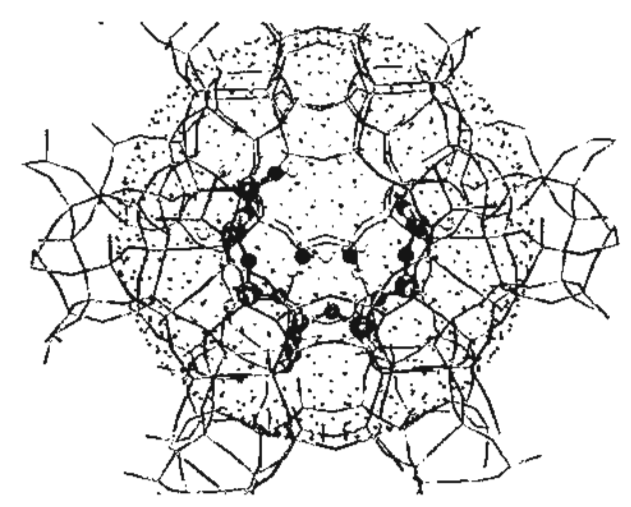


Figure 1. Illustration of the SCREEP embedded cluster model. The Madelung potential from periodic framework is represented by two sets of point charges, i.e., surface charges and explicit charges.

potential due to atoms outside the quantum cluster. Our previous study<sup>27</sup> indicated that the embedded 7T cluster model would be sufficient for studying adsorption of molecules with binding energies less than 40 kcal/mol; that is the case here as discussed below. Using the Surface Charge Representation of External Embedded Potential (SCREEP) method developed by Stefanovich and Truong,28 the Madelung potential owing to the extended zeolite structure is represented by two sets of point charges. For atoms located within the unit cell of the quantum cluster, they are represented explicitly by point charges located at the lattice positions. The magnitudes of these point charges are taken from periodic population analyses of zeolite systems. To minimize the interaction that occurs between the quantum mechanical terminating hydrogen atoms and the neighboring point charges, the first layer of explicit point charges nearest to the quantum cluster were removed and these charges are redistributed among the second shell (the next layer) explicit point charges. Specifically, the charges on the second shell are fitted to reproduce the original potential in the active center due to both the first and second shells. The Madelung potential from the remaining charges of an infinite lattice is represented by a set of surface charges that were derived from the SCREEP method (see Figure 1). More details on this method can be found elsewhere. 29,30 For H-FAU (see Figure 2), the total Madelung potential is represented by 441 explicit charges and 1311 surface charges, whereas for the H-ZSM-5 (see Figure 3), 564 explicit charges and 978 surface charges are employed. Note that pure SiO<sub>2</sub> FAU and ZSM-5 crystal structures were used in calculating the static Madelung potential therefore Si/Al ratio effects are not included in this study.

The hybrid B3LYP density functional theory was used in this study. In all structural determinations, geometries of the 3T cluster surrounding the active site (Si-O1H-Al-O2-Si) and of the water dimer are fully optimized while the remaining part of the 7T quantum cluster is fixed in their lattice positions. For these calculations, a mixed basis set was used. In particular, the 6-31G(d,p) basis set was used for all atoms in the small 3T cluster containing the active center and the water dimer mentioned above, whereas the 3-21G basis set was used for the remaining atoms of the larger 7T cluster. Single-point B3LYP calculations at a larger basis set were also done. Similarly, a mixed-basis set was used in this case where the larger 6-311+G(3df,2p) basis set was used for the smaller 3T

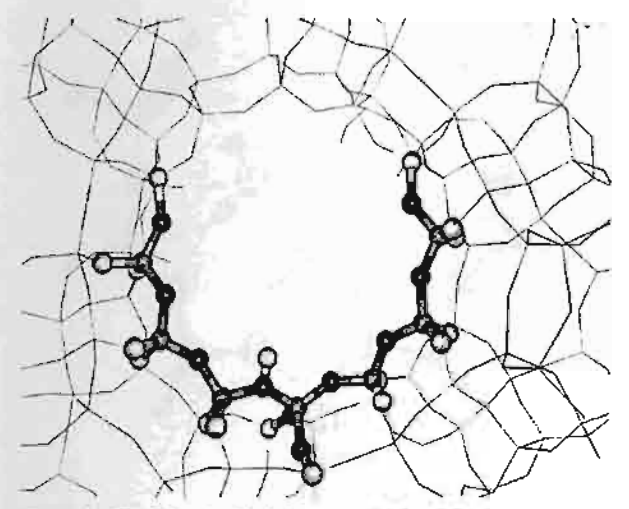


Figure 2. The 7T embedded cluster model for H-Faujasite.

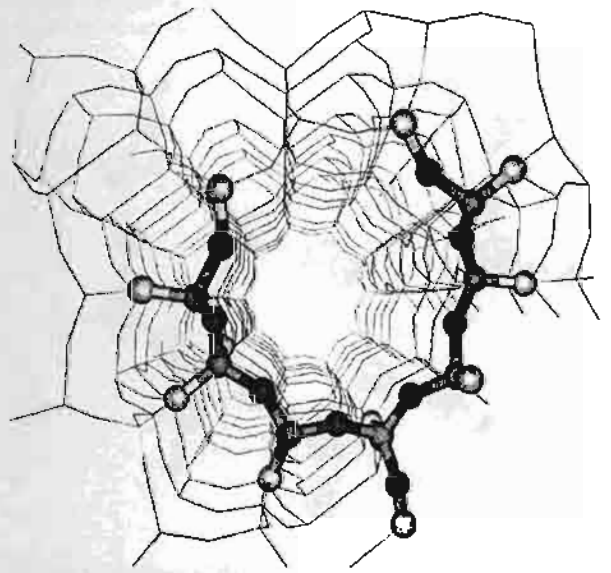


Figure 3. The 7T embedded cluster model for H-ZSM-5.

cluster and the water dimer instead of the 6-31G(d,p) one. Note that the 6-311+G(3df,2p) basis set used in the G2 theory for the effects of large basis set was also used previously by Zygmunt et al. for studying the same system, but with a smaller cluster. Normal-mode analyses using the embedded cluster model were also carried out to verify the nature of the adsorbed complexes and their IR spectra. All calculations were done with the GAUSSIAN 98 program.

# Results

In this study, we focus only on the possible modes of adsorption of water dimer on two different zeolites, namely FAU and ZSM-5. Previous theoretical studies have reported two different ways for calculating the "adsorption energy" of water dimer, specifically:

$$\Delta E_{\text{ads}} = E(\text{complex}) - E(\text{free zeolite}) - E(\text{water})_n$$
 (1)

$$\Delta E_{ads} = E(\text{complex}) - E(\text{free zeofite}) - nE(\text{water})$$
 (2)

In eq.1,20 the adsorption energy is referenced to the energy of the infinite separation of water dimer and zeolite, whereas in eq  $2^{21}$  it is referenced to the energy of infinite separation of zeolite and two isolated water molecules. The latter is closer to the definition of the formation energy of water dimer on zeolite. In this study, we used eq 1 for calculating adsorption energies. To compare with the results that came from the use of eq 2, the binding energy of water dimer,  $E_b(H_2O)_2 = E(\text{water})_n - nE(\text{water})_s$ , should be added. The binding energy of water dimer calculated at the B3LYP/6-311++G(3df,2p)/B3LYP/6-31G-(d,p) level is 3.23 kcal/mol.

There are two possible modes of adsorption of water dimer on zeolites, namely the neutral and ion-pair complexes, denoted as NC and IP complexes, respectively, in this study. The NC complex is where water dimer is stabilized by forming hydrogen bonds with the Brønsted acid site and the framework oxygen atom. In the IP complex, the Brønsted acidic proton transferred to the water dimer to form an H<sub>5</sub>O<sub>2</sub>\* hydronium ion, which is stabilized by forming strong hydrogen bonds with the deprotonated zeolite framework. Both such complexes can coexist and be stabilized by the zeolite framework. If so, there would be a transition state connecting these two stable structures. Zygmunt et al.17 found that such a transition state has a rather low barrier and thus one can expect that these two complexes, if both existed, would be in rapid thermal equilibrium. For this reason, in this study, we only focus on the stable adsorption structures. Our results indicate that there are two possible adsorption pathways for each adsorption mode. One pathway leads to the adsorption structure that has one water molecule of the dimer forming two strong hydrogen bonds to the (-O)3-Al-OH tetrahedral unit to yield a 6-membered ring structure similar to that of the adsorption of a single water molecule, while the other water molecule does not have any direct interaction with the (-O)3-Al-OH tetrahedral unit, but binds to the other water and the zeolite framework. This water dimer adsorption complex can be thought to be formed by a stepwise adsorption process, i.e., adsorption of a single water molecule at a time on the adsorption site. The other pathway yields the adsorption structure that has both water molecules forming a larger ring where one of the two water molecules makes only one hydrogen bond to the acidic proton while the other water molecule forms a hydrogen bond with the oxygen atom of the nearby tetrahedral unit of the cross section. This complex can be thought to be formed by a concerted adsorption process of water dimer on the adsorption site. These adsorption structures are somewhat different from those reported by Krossner and Sauer21 and Zygmunt et al., 17 where both water molecules form hydrogen bonds with only oxygen atoms of the (-O)3-Al-O(H) tetrahedral unit. This is because the cluster model used in these studies has only these four oxygen atoms of the (-0)3-Al-O(H) tetrahedral unit for forming hydrogen bonds with the water dimer, thus it would not be able to predict the adsorbed structures found here. In addition, in the actual ZSM-5 and FAU zcolite framework, two of the oxygen atoms of the (-O)3-Al-O(H) tetrahedral unit that are not on the zeolite cross section (the two OH groups in Figures 2 and 3) have their lone pairs pointing away and thus would not make a strong hydrogen bond with the water dimer. Such adsorption structure may still exist at a weaker birding energy; however, accurate determination of its structure would require larger quantum clusters than those used in this study and thus is beyond our current computing capability. Note that under experimental conditions, conversion between these possible adsorption complexes is possible due to thermal fluctuations. Further discussion on these structures is given below. It is important to point out that since we employed both the cluster and embedded cluster models and

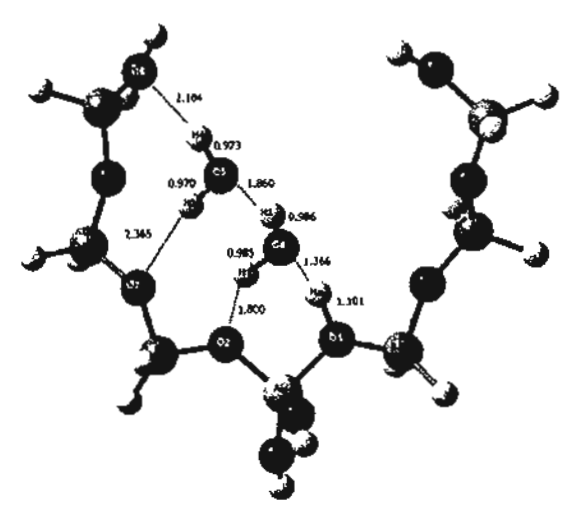


Figure 4. Structure of the neutral complex of the (H<sub>2</sub>O)<sub>2</sub>/H-ZSM-5 system optimized at the B3LYP/6-31G(d,p) level, using the cluster model (bond distances are in Å).

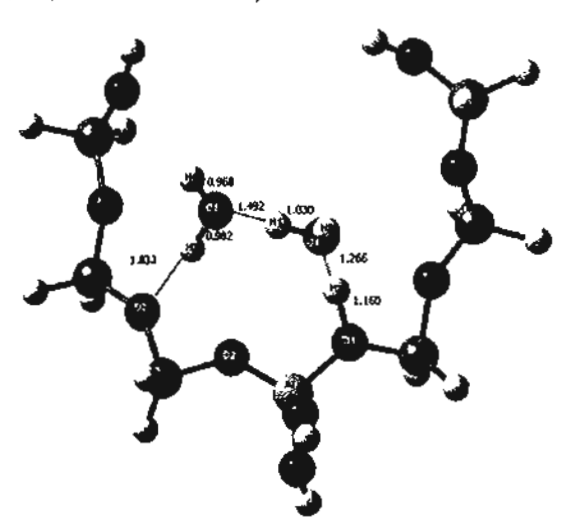


Figure 5. Structure of the neutral complex of the  $(H_2O)_2/H$ -ZSM-5 system optimized at the B3LYP/6-31G(d,p) level, using the embedded cluster model (bond distances are in Å).

the latter model is more accurate, thus, results from the cluster model are only used to illustrate the importance of the Madelung field effects. To make comparisons with experimental observations, results from the embedded cluster model are used.

Adsorption of Water Dimer on H-ZSM-5. Optimized adsorption structures of water dimer on H-ZSM-5 are shown in Figure 4, using the cluster model, and Figures 5 and 6, using the embedded cluster model. Selected bond distances are also given in the figures. Additional selected optimized geometrical parameters and calculated adsorption energies are listed in Tables 1 and 2, respectively.

To include the effect of the large basis set, our calculated adsorption energies are carried out at B3LYP/6-311+G(3df,-2p)//B3LYP/6-31G(d,p). The cluster model predicts adsorption of water dimer on H-ZSM-5 in only the NC form with the zeropoint energy (ZPE) corrected adsorption energy of -14.57 kcal/mol, whereas the embedded cluster model predicts both forms, NC and JP, existing in nearly equal population with the ZPE-corrected adsorption energies of -15.13 and -14.73 kcal/mol, respectively. Since results from previous cluster models do not include the effects of the zeolite crystal framework, they can

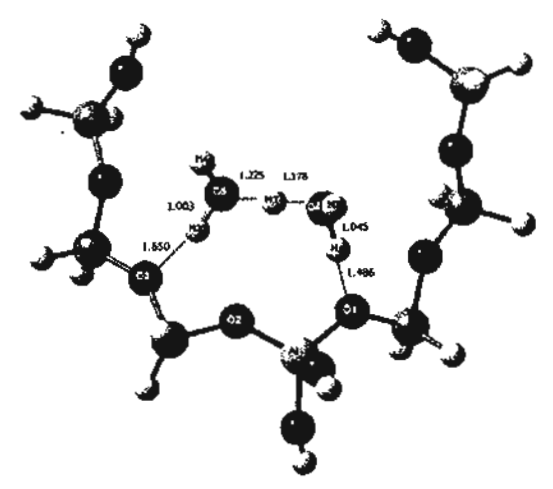


Figure 6. Structure of the ion-pair complex of the  $(H_2O)_7/H$ -ZSM-5 system optimized at the B3LYP/6-31G(d,p) level, using the embedded cluster model (bond distances are in Å).

TABLE 1: Selected Optimized Geometrical Parameters (bond lengths in Å and angles in deg) and Adsorption Energies (kcal/mol per water molecule) for Water Dimer Adsorption on ZSM-5, Using Both the Cluster and Embedded Cluster Models

NC (Figure 4)  1.49  0.4Hz  1.49  0.9-N  1.83  0.9-N  1.83  0.9-N  1.83  0.9-N  1.68  0.9-N  1.68  0.9-N  1.68  NC (Figure 4)  1.49  1.49  0.9-N  1.49  NC (NC (Figure 4)  1.49  NC (NC (NC (NC (NC (NC (NC (NC (NC (NC	cluster
O₁-Hz         1.10         O₁-Hz         1.16           O₄Hz         1.37         O₄Hz         1.27           O₂H₁         1.80         O₄-H₁         1.93           O₄-H₁         0.98         O₃H₁         1.49           O₄-H₂         0.99         O₃-H₃         0.98           O₃H₂         1.86         O₃H₃         1.83           O₃H₃         0.97         O₃-Si₁         1.68           O₃H₃         2.36         Si₁-O₂         1.65           O₃H₃         2.10         O₂-Aἰ         1.65           O₁-Al         1.78         O₁-Al         1.70           O₁-Al         1.78         O₁-Al         1.70           O₁-Al         1.70         ∠O₁AlO₂         106.4           ∠O₁AlO₂         93.7         ∠AlO₂Si₁         32.5           ∠H₁O₂Al         113.7         ∠O₂Si₁O₃         90.2           ∠H₂O₄H₁O₂         138.9         ∠Si₁O₃H₃         111.0           ∠O₄H₂O₄H₁         91.0         ∠O₃H₃O₃         167.4           ∠O₄H₂O₃         150.8         ∠O₃H₃O₃         167.4           ∠O₄H₂O₃         150.8         ∠O₃H₃O₃         177.9	qí
$ \begin{array}{cccccccccccccccccccccccccccccccccccc$	5) (Figure 6)
$\begin{array}{cccccccccccccccccccccccccccccccccccc$	1.49
$ \begin{array}{cccccccccccccccccccccccccccccccccccc$	1.04
O₄-H₂         0.99         O₅-H₃         0.98           O₅⋅H₂         1.86         O₃⋅H₃         1.83           O₅⋅H₃         0.97         O₃-Si₁         1.68           O₃⋅H₃         0.97         O₃-Si₁         1.68           O₃⋅H₃         0.97         O₃-Si₁         1.68           O₃⋅H₃         2.36         Si₁-O₂         1.65           O₁-Al         1.78         O₁-Al         1.70           O₂-Al         1.70         ∠O₁AlO₂         106.4           ∠O₁AlO₂         93.7         ∠AlO₂Si₁         32.5           ∠H₁O₂Al         113.7         ∠O₂Si₁O₃         90.2           ∠H₂O₄H₁O₂         138.9         ∠Si₁O₃H₃         111.0           ∠H₂O₄H₁O₂         138.9         ∠Si₁O₃H₃         111.0           ∠O₃H₂O₄         162.3         ∠H₃O₃H₃         111.0           ∠O₃H₂O₃         150.8         ∠O₃H₃O₃         177.9           ∠O₃H₃O₃H₂         93.8         ∠H₁O₄Hz         155.5           ∠O₃H₃O₃         158.8         ∠O₄H₂O₃         173.8           ∠O₃H₄O₃         166.8         ∠H₂O₁AlO₂         114.4           H₂O₄AlO₂         7.6         H₂O₃AlO₂         7.2 </td <td>1.18</td>	1.18
O5H₂         1.86         O3H₃         1.83           O5-H₃         0.97         O3-Si₁         1.68           O3H₃         2.36         Si₁-O₂         1.65           O6H₄         2.10         O2-Ai         1.65           O1-Al         1.78         O1-Al         1.70           O2-Al         1.70         ∠O₁AlO₂         106.4           ∠O₁AlO₂         93.7         ∠AlO₂Si₁         32.5           ∠H₁O₂Al         113.7         ∠O₂Si₁O₃         90.2           ∠H₂O₄H₁         91.0         ∠O₃H₃O₃         111.0           ∠H₂O₄H₁         91.0         ∠O₃H₃O₃         167.4           ∠H₂O₄H₂O₃         150.8         ∠O₃H₃O₃         177.9           ∠H₃O₃H₂O₃         150.8         ∠O₃H₃O₃H₁         111.0           ∠O₃H₃O₃         150.8         ∠O₃H₃O₃         173.8           ∠O₃H₃O₃         158.8         ∠O₄H₂O₁         173.8           ∠O₃H₄O₃         166.8         ∠H₂O₁AlO₂         114.4           H₂O₄AlO₂         7.6         H₂O₁AlO₂         26.9           H₁O₃AlO₂         1.0         H₃O₃Si₁O₂         30.1           H₂O₄AlO₁         6.2         O₄O₁AlO₂         30.1	1.22
O₃-H₃         0.97         O₃-Si₁         1.68           O₃H₃         2.36         Si₁-O₂         1.65           O₆H₃         2.10         O₂-A¹         1.65           O₁-Al         1.78         O₁-Al         1.70           O₂-Al         1.65         O₁-Al         1.70           O₂-Al         1.65         O₁-Al         1.70           ∠O₁AlO₂         106.4         ∠O₁AlO₂         106.4           ∠O₁AlO₂         93.7         ∠AlO₂Si₁O₃         90.2           ∠O₄H₁O₂         138.9         ∠Si₁O₃H₃         111.0           ∠O₄H₂O₂         138.9         ∠Si₁O₃H₃         111.0           ∠O₄H₂O₃         162.3         ∠H₃O₃H₃         111.0           ∠O₄H₂O₃         150.8         ∠O₃H₃O₃         167.4           ∠O₄H₂O₃         150.8         ∠O₃H₃O₃H₁         115.5           ∠O₃H₃O₃         158.8         ∠O₄H₂O₁         173.8           ∠O₃H₄O₃         166.8         ∠H₂O₁AlO₁         114.4           HzO₁AlO₂         7.6         HzO₁AlO₂         26.9           H₀O₃AlO₂         1.0         H₃O₃Si₁O₂         30.1           H₀O₄O₂AlO₁         16.2         O₄O₁AlO₂         30.1 <td>1.00</td>	1.00
$ \begin{array}{cccccccccccccccccccccccccccccccccccc$	1.65
O6H4         2.10         O2-AI         1.65           O₁-AI         1.78         O₁-AI         1.70           O₂-AI         1.70         ∠O₁AIO₂         106.4           ∠O₁AIO₂         93.7         ∠AIO₂Si₁         332.5           ∠H₁O₂AI         113.7         ∠O₂Si₁O₃         90.2           ∠H₂O₄H₁O₂         138.9         ∠Si₁O₃H₃         111.0           ∠O₁H₂O₃         162.3         ∠H₃O₃H₃         111.0           ∠O₁H₂O₃         162.3         ∠H₃O₃H₁         111.0           ∠O₄H₂O₃         150.8         ∠O₃H₁O₄         177.9           ∠H₃O₃H₂         93.8         ∠H₁O₄Hz         115.5           ∠O₃H₃O₃         158.8         ∠O₄H2O₁         173.8           ∠O₃H₄O₄         166.8         ∠H2O₁AI         114.4           H2O₁AIO₂         7.6         HzO₁AIO₂         26.9           AO₁AIO₂         1.0         H₃O₃Si₁O₂         -32.6           H1OᢋAIO₁         6.2         O₄O₁AIO₂         30.1           H2O₄O₂AI         -120.6         O₃O₃Si₁O₂         -30.8	1.70
O₁-Al         1.78         O₁-Al         1.70           O₂-Al         1.70         ∠O₁AlO₂         106.4           ∠O₁AlO₂         93.7         ∠AlO₂Si₁         32.5           ∠H₁O₂Al         113.7         ∠O₂Si₁O₃         90.2           ∠H₂O₄H₁O₂         138.9         ∠Si₁O₃H₃         111.0           ∠H₂O₄H₁         91.0         ∠O₃H₃O₃         167.4           ∠O₁H₂O₄         162.3         ∠H₃O₃H₁         111.0           ∠O₄H₂O₃         150.8         ∠O₃H₃O₄         177.9           ∠H₃O₃H₂         93.8         ∠H₁O₄Hz         115.5           ∠O₃H₃O₃         158.8         ∠O₄H₂O₃         173.8           ∠O₃H₄O₃         166.8         ∠H₂O₁Al         114.4           H₂O₄AlO₂         1.0         H₃O₃Si₁O₂         232.6           H₁OᢋAlO₂         1.0         H₃O₃Si₁O₂         30.1           H₂O₄O₂Al         -120.6         O₃O₃Si₁O₂         30.1	1.65
O₂-Al         1.70         ∠O₁AlO₂         106.4           ∠O₁AlO₂         93.7         ∠AlO₂Si₁         32.5           ∠H₁O₂Al         113.7         ∠O₂Si₁O₃         90.2           ∠H₂O₂Al         138.9         ∠Si₁O₃H₃         111.0           ∠H₂O₄H₁         91.0         ∠O₃H₃O₃         167.4           ∠O₁H₂O₃         150.8         ∠O₃H₃O₃H₁         111.0           ∠O₄H₂O₃         150.8         ∠O₃H₃O₃H₁         117.9           ∠O₃H₃O₃         150.8         ∠O₃H₃O₄         177.9           ∠O₃H₃O₃         158.8         ∠O₄H₂O₃         173.8           ∠O₃H₄O₃         166.8         ∠H₂O₁Al         114.4           H₂O₄AlO₂         7.6         H₂O₁AlO₂         26.9           H₂O₁AlO₂         1.0         H₃O₃Si₁O₂         30.1           H₂O₄O₂Al         -120.6         O₃O₃Si₁O₂         30.1           H₂O₄O₂Al         -120.6         O₃O₃Si₁O₂         -30.8	1.65
2O₁AłO₂         93.7         ∠AlO₂Sl₂         332.5           ∠H₁O₂Al         113.7         ∠O₂Si₁O₃         90.2           ∠O₄H₁O₂         138.9         ∠Si₁O₃H₃         111.0           ∠H₂O₄H₁         91.0         ∠O₃H₃O₃         167.4           ∠O₁H₂O₄         162.3         ∠H₃O₃H₁         111.0           ∠O₄H₂O₃         150.8         ∠O₃H₃O₃         177.9           ∠H₃O₃H₂         93.8         ∠H₁O₄Hz         115.5           ∠O₃H₃O₃         158.8         ∠O₄H₂O₁         173.8           ∠O₃H₄O₃         166.8         ∠H₂O₁Al         114.4           HzO₁AlO₂         7.6         HzO₁AlO₂         26.9           H₂O₄AlO₂         1.0         H₃O₃Si₁O₂         30.1           H₂O₄O₂Al         -120.6         O₃O₃Si₁O₂         30.1	1.67
∠H₁O₂AI         113.7         ∠O₂Si₁O₃         90.2           ∠O₄H₁O₂         138.9         ∠Si₁O₃H₃         111.0           ∠H₂O₄H₁         91.0         ∠O₃H₃O₅         167.4           ∠O₁H₂O₃         162.3         ∠H₃O₃H₁         111.0           ∠O₄H₂O₃         150.8         ∠O₅H₃O₄         177.9           ∠H₃O₃H₂         93.8         ∠H₁O₄H₂         115.5           ∠O₃H₃O₃         158.8         ∠O₄H₂O₃         173.8           ∠O₃H₄O₄         166.8         ∠H₂O₁AI         114.4           H₂O₁AIO₂         7.6         H₂O₁AIO₂         26.9           O₄O₁AIO₂         1.0         H₂O₃Si₁O₂         -32.6           H₁O₂AIO₁         6.2         O₄O₁AIO₂         30.1           H₂O₄O₂AI         -120.6         O₃O₃Si₁O₂         -30.8	108.6
∠O <sub>4</sub> H <sub>1</sub> O <sub>2</sub> 138.9 ∠Si <sub>1</sub> O <sub>3</sub> H <sub>3</sub> 111.0 ∠HzO <sub>4</sub> H <sub>1</sub> 91.0 ∠O <sub>3</sub> H <sub>3</sub> O <sub>5</sub> 167.4 ∠O <sub>1</sub> HzO <sub>4</sub> 162.3 ∠H <sub>3</sub> O <sub>5</sub> H <sub>1</sub> 111.0 ∠O <sub>4</sub> H <sub>2</sub> O <sub>5</sub> 150.8 ∠O <sub>5</sub> H <sub>1</sub> O <sub>4</sub> 177.9 ∠H <sub>3</sub> O <sub>5</sub> H <sub>2</sub> 93.8 ∠H <sub>1</sub> O <sub>4</sub> Hz 115.5 ∠O <sub>3</sub> H <sub>3</sub> O <sub>5</sub> 158.8 ∠O <sub>4</sub> HzO <sub>1</sub> 173.8 ∠O <sub>5</sub> H <sub>4</sub> O <sub>4</sub> 166.8 ∠HzO <sub>1</sub> AlO <sub>2</sub> 26.9 ∠O <sub>5</sub> H <sub>4</sub> O <sub>4</sub> 1.0 H <sub>2</sub> O <sub>3</sub> Si <sub>1</sub> O <sub>2</sub> −32.6 H <sub>1</sub> O <sub>4</sub> AlO <sub>2</sub> 1.0 H <sub>2</sub> O <sub>3</sub> Si <sub>1</sub> O <sub>2</sub> −32.6 H <sub>1</sub> O <sub>4</sub> AlO <sub>1</sub> 6.2 O <sub>4</sub> O <sub>1</sub> AlO <sub>2</sub> 30.1 H <sub>2</sub> O <sub>4</sub> O <sub>2</sub> Al −120.6 O <sub>5</sub> O <sub>3</sub> Si <sub>1</sub> O <sub>2</sub> −30.8	132.8
∠HzO₁H₁ 91.0 ∠O₃H₃O₅ 167.4 ∠O₁H2O₄ 162.3 ∠H₃O₃H₁ 111.0 ∠O₄H2O₅ 150.8 ∠O₅H₁O₄ 177.9 ∠H₃O₃H₂ 93.8 ∠H₁O₄Hz 115.5 ∠O₃H₃O₃ 158.8 ∠O₄H2O₃ 173.8 ∠O₃H₄O₄ 166.8 ∠HzO₁A 114.4 ∠O₃H₄O₄ 166.8 ∠HzO₁A 114.4 HzO₁AlO₂ 26.9 O₄O₃AlO₂ 1.0 H₃O₃Si₁O₂ −32.6 H₁O₃AlO₁ 6.2 O₄O₃AlO₂ 30.1 H₂O₄O₂Al −120.6 O₅O₃Si₁O₂ −30.8	89.3
∠O₁H2O₄ 162.3 ∠H₃O₅H₁ 111.0 ∠O₄H₂O₃ 150.8 ∠O₃H₁O₄ 177.9 ∠H₃O₃H₂ 93.8 ∠H₁O₄Hz 115.5 ∠O₃H₃O₃ 158.8 ∠O₄H2O₃ 173.8 ∠O₃H₄O₄ 166.8 ∠H2O₁A1 114.4 H2O₄AIO₂ 7.6 HzO₁AIO₂ 26.9 O₄O₃AIO₂ 1.0 H₃O₃Si₁O₂ −32.6 H₁O₃AIO₁ 6.2 O₄O₁AIO₂ 30.1 H₂O₄O₂AI −120.6 O₃O₃Si₁O₂ −30.8	107.1
∠O₄H₂O₂         150.8         ∠O₃H₂O₄         177.9           ∠H₃O₃H₂         93.8         ∠H₁O₄H₂         115.5           ∠O₃H₃O₂         158.8         ∠O₄H₂O₃         173.8           ∠O₃H₄O₄         166.8         ∠ H₂O₁Al         114.4           H₂O₄AlO₂         7.6         H₂O₁AlO₂         26.9           O₄O₁AlO₂         1.0         H₃O₃Si₁O₂         32.6           H₁O₃AlO₁         6.2         O₄O₁AlO₂         30.1           H₂O₄O₂Al         −120.6         O₃O₃Si₁O₂         −30.8	165.8
$ \begin{array}{cccccccccccccccccccccccccccccccccccc$	114.6
$ \begin{array}{c ccccccccccccccccccccccccccccccccccc$	177.4
$ \begin{array}{c ccccccccccccccccccccccccccccccccccc$	112.3
$\begin{array}{llllllllllllllllllllllllllllllllllll$	167.6
$\begin{array}{ccccc} O_4 O_1 A I O_2 & 1.0 & H_1 O_3 S i_1 O_2 & -32.6 \\ H_1 O_2 A I O_1 & 6.2 & O_4 O_1 A I O_2 & 30.1 \\ H_2 O_4 O_2 A I & -120.6 & O_5 O_3 S i_1 O_2 & -30.6 \\ \end{array}$	112.8
$\begin{array}{llllllllllllllllllllllllllllllllllll$	26.7
$H_2O_4O_2A$ 1 -120.6 $O_5O_3Si_1O_2$ -30.8	5 -29.3
	30.3
	3 -29.6
$O_5O_4O_7A$ ) $-133.3 O_5O_4O_1O_2 -18.2$	2 -21.39
O <sub>5</sub> O <sub>4</sub> O <sub>2</sub> O <sub>3</sub> 44.8 H <sub>1</sub> O <sub>4</sub> O <sub>1</sub> Al -36.4	4 - 37.3
$H_3O_5O_4O_2$ $-28.0$ $H_2O_4O_7AI$ 83.0	78.9
$H_4O_5O_4O_2$ -129.0 $H_4O_5O_3Si_1$ -123	.2 -121.0
ads energy $(E_{sd})$	
6-31G(d,p) ~16.09 -15.7	79 -15.75
6-311+G(3df,2p)// -14.57 -15.1	

be compared to our results for either H-ZSM-5 or H-FAU, and thus we defer such detailed comparisons on the energetics to the discussion section below. We only make comparisons on the adsorption structures where appropriate.

It is interesting to note that the preferred adsorption structures are quite different from both the cluster and embedded models. The optimized structure of the adsorbed neutral water dimer complex with use of the cluster model is shown in Figure 4. In this structure, one water molecule binds strongly to the (-O)<sub>3</sub>-

TABLE 2: Selected Optimized Geometrical Parameters (bond lengths in Å and angles in deg) and Calculated Adsorption Energy (kcal/mol per water molecule) for Adsorption of Water Dimer on Faujasite, Using Both the Cluster and Embedded Cluster Models

cluster model	embedded cluster		
19		NC	1P
(Figure 7)	1	(Figure 8)	(Figure 9)
O <sub>1</sub> Hz 1.32	O3-H2	1.10	1.38
$Q_2H_1$ 1.81	O3- • -H3	2.13	1.91
O <sub>3</sub> -Hz (.1)	Ó4H2	3.41	1.07
O <sub>3</sub> -H <sub>1</sub> 1.00	O5H1	1.58	1.45
O <sub>3</sub> -H <sub>2</sub> 1.00	$O_1 - AI$	1 84	1.85
O <sub>4</sub> H <sub>2</sub> 1.67	$O_2-A1$	1.73	1.79
O <sub>4</sub> H <sub>3</sub> 0.97	$O_2 - Si_2$	1.60	1.56
O <sub>5</sub> H <sub>3</sub> 2.16	∠O₁A1O₂	98.8	94.6
O <sub>1</sub> -A) 1.81	$\angle A10_2Si_2$	130.2	128.0
O <sub>2</sub> -Al 1.77	∠O <sub>2</sub> Si <sub>2</sub> O <sub>3</sub>	101.2	103,6
∠O₁AlO₂ 98.3	$\angle Si_2O_3H_3$	106.}	103.2
∠AlO <sub>2</sub> H <sub>1</sub> 108.3	∠03H305	169.3	166.4
∠O <sub>2</sub> H <sub>1</sub> O <sub>3</sub> 137.5	∠H₃O₃H₁	109.3	116.8
∠H <sub>1</sub> O <sub>3</sub> Hz 99.0	∠O <sub>5</sub> H <sub>1</sub> O <sub>4</sub>	177.7	175.7
∠O <sub>3</sub> HzO <sub>3</sub> 165.5	∠H₁Q₄H2	114.9	110.7
∠O <sub>3</sub> H <sub>2</sub> O <sub>4</sub> 164.4	$\angle O_4H2O_1$	177.2	173.9
∠H <sub>2</sub> O <sub>4</sub> H <sub>3</sub> 116.2	∠HzQ₁AI	117.5	108.8
∠O <sub>4</sub> H <sub>3</sub> O <sub>5</sub> 162.9	HzQ <sub>1</sub> A3O <sub>2</sub>	-2.0	-39.2
H2O1AIO2 18.4	O <sub>4</sub> O <sub>1</sub> Al O <sub>2</sub>	-1.7	-39.6
$H_2O_2AIO_1$ $-2.4$	IA₁O₄O₁H	-9.8	66.5
O <sub>2</sub> O <sub>1</sub> AlO <sub>2</sub> 16.1	H₂Q₄O₁AT	-131.3	-50.0
H <sub>2</sub> O <sub>3</sub> O <sub>1</sub> Al -138.8	H <sub>3</sub> O <sub>3</sub> Si <sub>2</sub> O <sub>2</sub>	18.1	14.3
$O_1O_3O_4O_3$ -38.6	H4O5O3Si2	-173.0	-161.7
$O_1O_3O_4H_3$ -49.7	O <sub>5</sub> Q <sub>4</sub> O <sub>1</sub> A1	-11.2	64.2
H <sub>4</sub> O <sub>4</sub> O <sub>3</sub> O <sub>1</sub> 73.9	O <sub>5</sub> O <sub>3</sub> Si <sub>2</sub> O <sub>2</sub>	18.0	19.0
ads energy (E <sub>14</sub> )			
6-31G(d,p)11.35		-13.82	-17.65
6-311+G(3df,2p)// -8.46		-11.64	-14.63

Al-O(H) tetrahedral unit by forming two hydrogen bonds H1---O2 and Hz - - O4 with the bond distances of 1.80 and 1.37 Å, respectively, while the other binds to the first water with the hydrogen bond distance of 1.86 Å, and has some attractions from its hydrogen atom with the zeolite framework oxygen atoms O3 and O6 with distances larger than 2.10 Å. A similar NC structure was found by Krossner and Sauer with the corresponding hydrogen bonds (similar to H1- - - O2 and Hz- - -O4) of the first water to be 1.92 and 1.37 Å, respectively. However, using a 3T cluster, Zygmunt et al.32 found this adsorption configuration protonated, but when they repeated the study using a larger cluster model, a different adsorption structure was obtained, as discussed below. This abovementioned structure indicates that the adsorbed complex is formed by the stepwise adsorption process. With the TT cluster model, we were not able to find the structure corresponding to the other concerted adsorption pathway. However, using the same 5T cluster model, Zygmunt et al.17 and Krossner and Sauer<sup>21</sup> found adsorption structures that corresponded to the concerted pathway where both water molecules bind to the zeolite framework to form a large ring configuration. However, their 5T cluster model consists of four H<sub>3</sub>SiO groups tetrahedrally coordinated to the centered Al atom, thus water molecules are restricted to form hydrogen bonds with only four O atoms surrounding the Al atom. Both studies found the IP complex exists for adsorption of water dimer. The results obtained by Zygmunt et al. 17 show the NC is 2.91 more stable than IP. Using the same ST cluster but with OH termination groups, Rice et al. 19 found only the NC complex, although having a different adsorption structure where the two water molecules also form a single large ring with the zeolite framework, but one is hydrogen bonded to the OH termination group. Such hydrogen

bonding does not exist in the 5T model used by Zygmunt et al.<sup>17</sup> and Krossner and Sauer.<sup>21</sup> The differences in these results indicate that the 5T cluster model is not sufficient due to large boundary effects. The 7T cluster model used in this study attempted to remove much of these effects so that there is no restriction on the hydrogen-bond configuration of water dimer with the Brønsted acid site and zeolite framework.

When the Madulung potential is included, both NC (Figure 5) and IP (Figure 6) are observed with similar structures where the two water molecules form a single large 7-membered ring-like structure (counting only heavy atoms) with the zeolite framework. There are three hydrogen bonds in this adsorption configuration in which the two water molecules form a hydrogen bond between each other and each water molecule forms one hydrogen bond with the zeolite framework. This adsorption configuration supports the concerted adsorption pathway as seen in previous studies by Zygmunt et al., <sup>17</sup> Krossner and Sauer, <sup>21</sup> and Rice et al. <sup>19</sup>

Taking a closer look at the NC and IP adsorption structures from the embedded cluster calculations as shown in Figures 5 and 6, respectively, we found that these structures are quite similar to the NC structure obtained by Rice et al. For the NC complex, the first hydrogen bond arises from the interaction of the oxygen atom of one of the two water molecules and the acidic proton (O4- - -Hz), which is calculated to be 1.27 Å. This value is comparable with 1.26 Å from Rice et al.'s structure but is noticeably shorter than the value of 1.49 Å determined by Zygmunt et al. The second hydrogen bond is formed between two water molecules, which are considered as the adsorbateadsorbate interaction, with the distance of 1.49 Å. This is slightly shorter than the value of 1.55 Å from Rice et al., but is also significantly shorter than the value of 1.70 Å from Zygmunt et al. The third hydrogen bond is from the hydrogen atom of the other water molecule, H3, and the oxygen O3 of the zeolite framework with the distance of 1.83 Å. This value is slightly longer than the value of 1.72 Å from Rice et al.'s structure and is comparable with 1.78 Å from Zygmunt et al.'s structure. However, as mentioned earlier in Zygmunt et al.'s structure, the two water molecules are restricted to form hydrogen bonds with four oxygen atoms bonded to the Al atom only (see Figure 1 in ref 17).

The IP adsorption complex has a similar overall structure with the NC complex, except that the Brønsted proton is transferred to the water (specifically to the O4 atom in Figure 6). Consequently, it changes the hydrogen bond pattern and distances. Particularly, the first hydrogen bond arises from the interaction of the oxygen atom O1 of ZSM-5 and the acidic proton (O1---Hz), which is calculated to be 1.49 Å. This value is more or less the same as the IP determined by Zygmunt et al. The water-water hydrogen bond (O5---H1) distance of 1.22 A is significantly shorter than any previously calculated values, which are above 1.50 Å. The remaining hydrogen bond between the H3 hydrogen atom in the second water and the O3 atom of zeolite framework is calculated to be 1.65 Å. This is in the range from 1.50 to 1.78 Å of previously reported values. It is interesting to note that the protonated H<sub>5</sub>O<sub>2</sub>+ ion has the angle O4H1O5 of 177.4°, the H1O5 and H1O4 distances of 1.22 and 1.18 Å, respectively, and the relative orientation of the two water molecules (see Figure 6). This configuration is closer to the configuration of H5O2+ ion, where the proton is equally shared between the two water molecules, than the H<sub>3</sub>O<sup>+</sup>---H<sub>2</sub>O configuration.

A number of experiments have been done with the FTIR technique to characterize and distinguish the IP water-zeolite

TABLE 3: Comparisons of Calculated Adsorption Energies of (H2O)2/Zeolite with Previous Theoretical and Experimental Results

level of theory	cluster	model	mode	$\Delta E$	rcf
H-ZSM-5					
B3LYP/'big'//	7T	cluster	NC	-14.57	b
B3LYP/'big'//	7 <b>T</b>	embedded	NC	-15.13	b
B3LYP/'big'//	7 <b>T</b>	embedded	1P	-14.73	b
B3LYP/6-31G(d,p)	5T	clusier	NC	-11.8	23
BP/DZP (H, Si, Al)	5T (generic)	cluster	[P	-14.28	24
TZP (O)					
B3LYP/6-31+G(d.p)	5T	cluster	NC-IP	(2.31) <sup>a</sup>	25
experiment				-8.2	26
Faujasite					
B3LYP/'big'//	7 <b>T</b>	cluster	NC	-11.64	b
B3LYP/'big'//	7T	cluster	ΙP	-8.46	b
B3LYP/'big'//	7T	embedded	IP .	-14.63	b
BP/DZP (H, Si, AI)	5T (generic)	cluster	JP .	-14.28	24
TZP (O)	•				

<sup>&</sup>quot;Relative energy. "This work.

complexes from the neutral ones. 4.13,14,33 However, interpretation of IR spectra of water in zeolites with different loading levels has been rather difficult and not without ambiguity. The reason can be best illustrated by Zecchina et al.'s remark "all the arguments developed so far for the basic IR spectroscopy of the (OH- - -B) groups also hold for the (O-- - - +HB) species and that a clear cut between the two cases is not straightforward".14 For adsorption of a single water molecule (corresponding to 10<sup>-5</sup>-10<sup>-4</sup> mbar of vapor pressure), both experimental and theoretical studies strongly support the neutral species. Even so, there are features on their IR spectra, such as the broad continuum band covering the 3000 to 1300 cm<sup>-1</sup> range and the strong peak in the region of 1860-1650 cm<sup>-1</sup>, that cannot be explained by existing arguments. For higher loading levels, i.e.,  $(H_2O)_n$  in H-ZSM-5 zeolite with n > 1, although the interpretation of the experimental IR spectra is even more difficult, there has been some consensus that dimeric H5O2+ species were observed, thus our present results are consistent with the previous IR results. In this study, we have further calculated the IR spectra for the IP and neutral water dimer complexes in H-ZSM-5 using the embedded cluster model, then compared the results with the experimental spectra.

FTIR spectra for water in H-ZSM-5 under an equilibrium pressure between 10<sup>-3</sup> to 10<sup>-2</sup> mbar done by Jentys et al.<sup>4</sup> show a strong increase in the four bands at 3695, 2885, 2457, and 1630 cm<sup>-1</sup>. The authors suggested that these four bands are characteristics of the hydroxonium H<sub>5</sub>O<sub>2</sub>+ species adsorbed on the negative charge ZSM-5 zeolite framework. In particular, the band at 3695 cm<sup>-1</sup> is due to the free OH group pointing away from the zeolite framework; the two broad bands at 2885 and 2457 cm<sup>-1</sup> are of the O- -- H<sup>+</sup>--- O part; and the band around 1630 cm<sup>-1</sup> is due to deformation of the H<sub>3</sub>O<sup>+</sup> component. Zecchina et al.,14 on the other hand, suggested the two main fingerprints for hydroxonium H+(H2O), species on IR spectra of water in H-ZSM-5 zeolite are an adsorption in the 1860-1650 cm<sup>-3</sup> range, accompanied by a partner around 1455 cm-1, in addition to the broad "continuum" band from 1300 to 3000 cm<sup>-1</sup> due to different H+(H2O), species pointed out in their earlier study.33 However, experimental spectra alone cannot precisely determine the number of H2O molecules solvating the acidic proton. Kondo et ai. later added another feature for the dimeric H<sub>5</sub>O<sub>2</sub>+ species that is the band at 3207 cm<sup>-1</sup>.

The main features of our calculated IR spectra for water dimer adsorption in H-ZSM-5 zeolite for both the NC and IP complexes are listed in Table 4. The calculated frequencies were not scaled. The characteristic vibrational modes of the bridged

TABLE 4: Calculated Unscaled Vibrational Frequencies v (cm-1) and Intensities I (KM/mol) for the NC and IP Complexes on H-ZSM-5

neutral complex		ion-pair complex		
mode	$\nu$ and $(I)$	mode	v and (1)	
ν(O4H2)	3864 (54)	v(O4H2)	3849 (89)	
v(H 3O5H4) asym	3845 (776)	ν(O5H4)	3824 (151)	
ν(O5H4)	3841 (1862)	ν(O5H3)	3179 (948)	
ν(Q5H3)	3552 (665)	(H)O4Hz) sym	2507 (1488)	
$\nu(OHz) + \nu(O4H1)$	2726 (1571)	ð(H₃O+)	1675 (417)	
δ(H1Q4H2)	1722 (251)	δ(H <sub>3</sub> O <sup>+</sup> )	1760 (92)	
ð(H3O5H4)	1669 (41)	ð(H3Q5H4)	1707 (224)	
δ (OHz)	1521 (87)	$\delta(H_3O^+)$ umb	1350 (420)	
y(OHz)	1472 (690)	,	` '	
ν(OHz)	1313 (773)			

hydroxyl group are assigned as in Figure 10. We first discuss features of the H<sub>5</sub>O<sub>2</sub>+ IP complex. The calculated vibrational frequencies at 3849 cm<sup>-1</sup> correspond to the  $\nu(OH)$  of the free OH bond of the adsorbed H<sub>5</sub>O<sub>2</sub>+ (see Figure 6), with the O4H2 is pointing away from the zeolite framework, which is in reasonable agreement with experimental observation4 at 3700 cm<sup>-1</sup>. The peaks at 3824 and 3179 cm<sup>-1</sup> are of the second H<sub>2</sub>O moiety, which are close to the calculated frequency results of 3884 and 3275 cm<sup>-1</sup> obtained by Zygmunt et al.<sup>17</sup> The former is assigned to the v(O5H4) of the free OH group, The latter belongs to the  $\nu(O5H3)$ , the frequencies shift due to one hydrogen atom being bonded to the zeolite framework (H3). The latter peak is in good agreement with the fingerprint at 3207 cm<sup>-1</sup> suggested by Kondo et al. 13 The calculated peaks at 1760 and 1675 cm<sup>-1</sup> are assigned to be the bending mode of the hydroxonium species,  $\delta(H_3O^+)$ , which is comparable to the frequency range of 1860-1650 cm-1, the fingerprints of protonated H+(H2O), species obtained by Zecchina et al., 14 and are also consistent with the experimental observation band at 1630 cm<sup>-1</sup> by Jentys et al.4 The frequency at 2507 cm<sup>-1</sup> belongs to symmetric stretch modes, v(HzO4H1), of the two hydrogen bonds of the hydroxonium ion, O4Hz and O4H1, respectively (see Figure 6), which is comparable to the peak of symmetric  $\nu(H_2O^+)$  at 2911 cm<sup>-1</sup> from Zygmunt et al. The 1350 cm<sup>-1</sup> corresponds to the umbrella mode, the characteristic of the protonated water clusters, as pointed out by Zecchina et al.

For the neutral water dimer complex, we found that the peak at 2726 cm<sup>-1</sup> belongs to the OH stretching mode of the acidic site, v(O1Hz), being very intense because it overtones with the  $\nu(O4H1)$  mode (see Figure 5). This is in good agreement with the experimental result of the  $\nu(OH---O)$  mode of group a at 2680 cm<sup>-1</sup> for a neutral complex of a single water adsorption on H-ZSM-5 (see Scheme 6 in ref 14). The peak at 1472 cm-1 assigned to the  $\gamma(OH---O)$  mode is in agreement with the frequency peak at 1415 cm<sup>-1</sup> from Zygmunt et al. The peak at 1521 cm<sup>-1</sup> is the δ(O1Hz), the bending mode of the acidic OH group. The peaks at 1722 and 1669 cm<sup>-1</sup> belong to  $\delta$ (HOH), the bending mode of the first water and the second water, respectively. The lower frequency peak is comparable to the peak at 1684 cm<sup>-1</sup> calculated by Zygmunt et al. Unfortunately, we cannot make a direct comparison between our calculated IR spectrums for the NC of water dimer adsorption on H-ZSM-5 with that of Zecchina et al. since the latter was interpreted for a single water molecule adsorption. Our result for the structure of the neutral dimer complex is quite different from those known for the neutral monomer complex.17,21

Since our results suggested both the neutral and IP complexes can exist in equilibrium in H-ZSM-5, we merge the IR features of both complexes so as to predict fingerprints for these species. Results from Table 4 confirmed the difficulty in interpreting

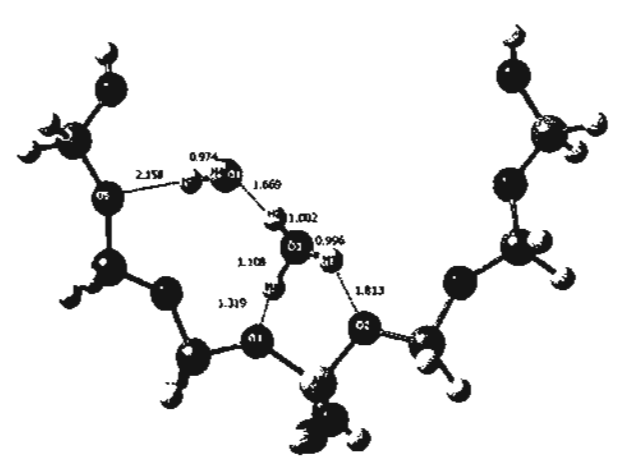


Figure 7. Structure of the ion-pair complex of the  $(H_2O)_2/H$ -Faujasite system optimized at the B3LYP/6-31G(d,p) level, using the cluster model (bond distances are in Å).

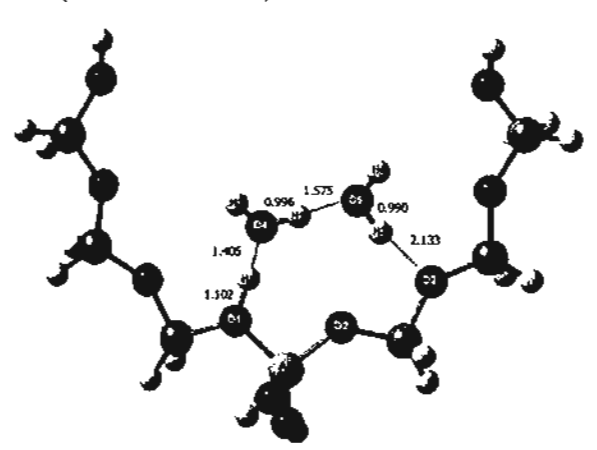


Figure 8. Structure of the neutral complex of the (H<sub>2</sub>O)<sub>2</sub>/H-Faujasite system optimized at the B3LYP/6-31G(d,p) level, using the cluster model (bond distances are in Å).

experimental IR spectra. Most bands for the water dimer in the neutral and IP complex forms overlap with consideration of broadening due to different possible configurations of these species. There is one band peaking at 3179 cm<sup>-1</sup> in the IP complex that appeared to be the most distinct fingerprint for the dimeric H<sub>5</sub>O<sub>2</sub><sup>+</sup> species, and this is in excellent agreement with that suggested by Kondo et al. By examining the relative intensities, our results also support the adsorption in the region 1865-1650 cm<sup>-1</sup> suggested by Zecchina et al. and Jentys et al. as another fingerprint for the protonated H<sup>+</sup>(H<sub>2</sub>O)<sub>n</sub> species.

Adsorption of Water Dimer on H-FAU. Optimized adsorption structures of water dimer on H-FAU are shown in Figures 7 and 8 using the cluster model, and Figure 9 using the embedded cluster model. Selected bond distances are also given in these figures. Additional selected optimized geometrical parameters and calculated adsorption energies are listed in Tables 2 and 3, respectively. The cluster model predicts that both the NC and IP complexes exist with the NC being more stable with the ZPE corrected adsorption energy of -11.64 kcal/ mol as compared to that of -8.46 kcal/mol for the IP complex. However, when the Madelung field is included, only the IP complex was found with the ZPE-corrected adsorption energy of -14.63 kcal/mol. This is very different when compared to the results for adsorption of water dimer on H-ZSM5 zeolite, where the cluster model predicts only the NC complex, while the embedded cluster model yields both the NC and IP

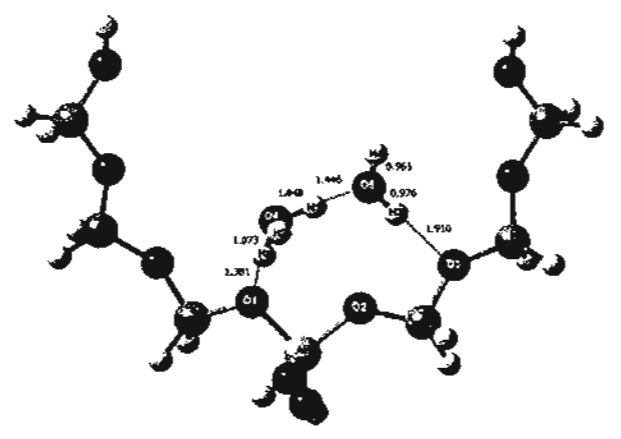


Figure 9. Structure of the ion-pair complex of the (H<sub>2</sub>O)<sub>2</sub>/R-Faujasite system optimized at the B3LYP/6-31G(d,p) level, using the embedded cluster model (bond distances are in Å).

Figure 10. The characteristic vibrational modes of the bridged hydroxyl group.

complexes. It is interesting to note that although the cluster models for both H-ZSM-5 and H-FAU have the same 7T sites, they were cut out from the actual cross section of the crystal structures of these zeolites, thus they have different 3D structures. Therefore, we observed different results for adsorption on H-ZSM-5 and H-FAU zeolites, even using only the cluster model. Previous studies 17,21 used generic cluster models to represent the Brønsted acidic site and thus did not include any effects of the crystal framework. Similar to the adsorption on H-ZSM5, both the cluster and embedded cluster models predict different results on the adsorption structures.

Optimized adsorption structures for the IP and NC complexes with the 7T cluster model are shown in Figures 7 and 8, respectively. Since we have already provided more detailed comparisons between the adsorption structures of water dimer on H-ZSM-5 with results from previous generic cluster models in the previous subsection, it is more informative here to also provide some discussion on the differences on adsorption structures of water dimer on H-ZSM-5 and H-FAU zeolites.

The IP adsorption structure from the cluster model (Figure 7) has the protonated form: the water molecule binds strongly to the two oxygen atoms of the (-O)3-Al-OH tetrahedral unit while the other water binds weakly to the zeolite framework. This structure supports the stepwise adsorption pathway. In particular, this complex has a total of four hydrogen bonds. The first two hydrogen bonds arise from interactions of the two Hz and HI of the protonated water with O1 and O2 atoms of the acidic site with bond distances of 1.32 and 1.81 Å, respectively. The other H of H<sub>3</sub>O+, namely H2, bonds to the O4 atom of the second water with the bond length of 1.67 Å. Finally, the fourth hydrogen bond is between the H3 atom of the second water and the O5 atom of extended zeolite. This structure is similar to the NC complex in H-ZSM-5 using the cluster model, except in this case the water dimer is protonated. The more stable NC complex from the cluster model, on the other hand, has the water dimer forming two hydrogen bonds with the acidic site in a single 7-member ring-like structure as mentioned earlier for the

TABLE 5: Comparisons between Calculated Unscaled Vibrational Frequencies v (cm<sup>-1</sup>) and Intensities I (KM/mol) of the lon-Pair Complexes in H-Faujasite and H-ZSM-5

ion-paiт on Fau		ion-pair on ZSM-5	
mode	ν and (/)	mode	y and (I)
ν(O 4H2)	3782 (135)	ν(O4H2)	3849 (89)
r(H3O5H4) sym	3662 (375)	ν(O5H4)	3824 (151)
v(H3O5H4) asym	3889 (139)	v(OSH3)	3179 (948)
v(H2O4H1) sym	2516 (1598)	(H1O4Hz) sym	2507 (1488)
v(HzO4H1) asym	2025 (3389)	δ(H <sub>3</sub> Q <sup>+</sup> )	1675 (417)
$\delta(H3O5H4) + \delta(H_3O^4)$	1627 (48)	$\delta(H_3Q^+)$	1760 (92)
δ(H <sub>1</sub> O <sup>+</sup> )	2726 (1571)	δ(H3O5H4)	1707 (224)
∂(H₃O*) umb	1391 (480)	$\delta(H_1O^4)$ umb	1350 (420)

concerted adsorption pathway. One hydrogen bond is between the Brønsted proton and the O4 atom of one of the two water molecules with the distance of 1.41 Å and the other is between the H3 atom of the other water molecule with the O3 atom of the zeolite framework with the distance of 2.13 Å. The hydrogen bond between the two water molecules has the distance of 1.58 A. This structure is quite similar to that observed for adsorption on H-ZSM-5 with the embedded cluster model (Figure 5), except that all hydrogen bonds in this case are noticeably longer by 0.09 to 0.18 Å.

When the effect of lattice framework is taken into account, only the protonated species (Figure 9) is observed with the ZPEcorrected adsorption energy of -14.63 kcal/mol. The structure is similar to those from the concerted adsorption pathway that has three hydrogen bonds stabilizing the ionic species. The two hydrogen bonds between the hydrogen atoms of the H5O2+ species and the oxygen atoms of the zeolite framework, namely the Hz- -- O1 and H3- -- O3, have bond distances of 1.38 and 1.91 Å, respectively. The hydrogen bond between the two water molecules, H1- - - O5, has the distance of 1.45 Å. On closer look at the structure of the protonated H<sub>5</sub>O<sub>2</sub>\* species, we find that in addition to the H1- - - O5 distance of 1.45 Å, the O4H1, O4Hz, and O4H2 bond distances of 1.05, 1.07, and 1.00 Å, respectively, and the angle O4H1O5 of 175.7° indicate the protonated H<sub>5</sub>O<sub>2</sub>+ has the configuration of H<sub>3</sub>O<sup>+</sup>---H<sub>2</sub>O. This is very different from that observed for the adsorption of water dimer on H-ZSM-5 zeolites (Figure 6), which has the configuration of H2O- -- H+- -- OH2, where the proton is shared between two water molecules. A possible explanation for such differences is given below in the discussion section.

Since the experimental IR spectrum is not available for water adsorption in H-Faujasite, in this subsection we present our calculated IR spectra for the H<sub>5</sub>O<sub>2</sub>+ IP complex using the embedded cluster model and compare the results with those for the water in the H-ZSM-5 zeolite system. Calculated observable bands due to the water dimer component in the IP complex for adsorption in both H-FAU and H-ZSM-5 are listed in Table 5. Similarly, the calculated frequencies were not scaled. The frequency of 3782 cm<sup>-1</sup> corresponds to the v(O4H2) stretch mode of the free OH group, which is lower than the 3849 cm<sup>-1</sup> frequency of H-ZSM-5 (see Figure 9). This is due to the free O4H2 bond distance for the protonated species in H-FAU being slightly longer.

The second water in H<sub>3</sub>O+---H<sub>2</sub>O in H-FAU can be considered as an outer water layer, which is quite different compared to that of the H2O---H4---OH2 complex in H-ZSM-5 where it shares the proton with the other water molecule. Therefore, we were able to observe the clear H2O moiety in the H-FAU channel: two OH stretching frequencies in the 3200-3900 cm<sup>-1</sup>, one at 3889 cm<sup>-1</sup> belonging to the antisymmetric OH stretch, v(H4O5H3), and the peak at 3662 cm<sup>-1</sup>

corresponding to the symmetric OH stretching mode, whereas in H-ZSM-5 we obtain two separated OH stretching modes of the second water, namely  $\nu(O5H4)$  and  $\nu(O5H3)$ . It is interesting to note that we found there are both the symmetric and antisymmetric OH stretching modes involving the two hydrogenbonded hydrogen atoms of the H<sub>3</sub>O+ moiety,  $\nu$ (HzO4H1), that have a relatively high intensity at 2516 and 2025 cm<sup>-1</sup>, while in H-ZSM-5 only the symmetric stretching mode, v(HzO4H1), at 2507 cm<sup>-1</sup>, was observed. In addition, the umbrella mode, which is a characteristic of the H<sub>3</sub>O+ moiety, at 1391 cm<sup>-1</sup> is in a higher region and more intense than that of 1350 cm<sup>-1</sup> in H-ZSM-5 due to the protonated species in H-FAU having more characteristics of H<sub>3</sub>O+ than that of H-ZSM-5.

#### Discussion

In our present study for adsorption of water dimer, we found that both the neutral and ion-pair complexes can coexist in H-ZSM-5 and only ion-pair complex is predicted in H-FAU zeolites. Furthermore, we also found that these adsorption complexes can be formed from two different pathways, namely the stepwise and concerted adsorption pathways. The cluster model predicts adsorption of water dimer on H-ZSM-5 resulting only in the neutral complex. However, including the effects of the zeolite lattice framework by using the embedded cluster model, we found that the ion-pair complexes are stable in both the H-ZSM-5 and H-Faujasite systems from only the concerted adsorption pathway. This indicates that the Madelung potential has the effect of stabilizing the protonated species. However, these protonated species have significantly different configurations. The IP for water dimer in H-ZSM-5 has the H2O---H+---H<sub>2</sub>O configuration where the proton is shared between the two water molecules, whereas the IP for water dimer in H-FAU has the H<sub>3</sub>O+- - - H<sub>2</sub>O configuration where the proton is associated with only one particular water molecule. This is due to the fact that ZSM-5 has the smaller 10-membered ring pore size of 5.6 Å as compared to the 12-membered ring pore size of 7.4 Å in FAU. To understand how the pore size affects the adsorption structure of water dimer, let us examine the potential surface of the isolated H<sub>3</sub>O<sub>2</sub><sup>+</sup> system.<sup>34-37</sup> The isolated H<sub>5</sub>O<sub>2</sub><sup>+</sup> system has a double-well potential energy surface (PES) with the H<sub>3</sub>O<sup>+</sup>---H<sub>2</sub>O configuration where the proton is associated with one or the other water molecules and is a stable equilibrium structure while the H2O- - - H+- - - OH2 configuration where the proton is equally shared between the two water molecules is the transition state for proton transfer between these two stable configurations. As the O-O distance decreases, the double-well PES is transformed into a single-well where the transition state configuration becomes the stable equilibrium structure. Since the ZSM-5 zeolite has a noticeably smaller pore size than that of FAU, it forces the two water molecules closer together as indicated by the O-O distance of 2.40 Å in the IP complex as compared to that of the 2.49 Å in the IP complex FAU. Since the barrier for proton transfer in the dimer H<sub>3</sub>O<sub>2</sub>+ complex is only about 0.6 kcal/mol, 17 the decrease in the O-O bond distance by 0.09 Å can lead to the PES of the H<sub>5</sub>O<sub>2</sub>+ moiety becoming a single-well, and thus the H2O---H+---H<sub>2</sub>O configuration is stabilized in ZSM-5 rather than a doublewell as in the FAU. These results show that the spatial confinement effects are rather important in understanding adsorption properties in zeolite.

The predicted adsorption energy of ion-pair complexes at the B3LYP/6-311+G(3df,2p) level of theory with inclusion of the zero-point energy corrections is -14.73 kcal/mol for H-ZSM-5 and -14.63 kcal/mol for H-Faujasite, which are considered as more or less the same adsorption energies. The neutral water dimer complex only exists in the H-ZSM-5 zeolite with the adsorption energy of -15.13 kcal/mol. This can be compared to the experimental adsorption energy of 8.2 kcal/mol per two water molecules per cation obtained by Gorte et al.,2 which was derived by measuring the equilibrium infrared spectra as a function of vapor pressure and temperature. Since it has been known that H-ZSM-5 is more acidic than H-FAU, one would expect that protonation of water dimer is easier and adsorption energy of water dimer in H-ZSM-5 would also be larger as compared to those of the H-FAU zeolite. Our results indicate that the adsorption properties depend not only on the acid strength of zeolites but also on the topologies of those zeolites. Note that in comparison with previous theoretical studies as listed in Table 3, Zygmunt et al. found that the neutral complex is more stable compared to the protonated dimer complex by 2.9 kcal/mol while the barrier for the deprotonation step (the reverse direction) is very small. Krossner and Sauer found that both NC and IP structures are minima on the potential energy surface; the NC complex is less stable compared to the IP complex by 3.6 kcal/mol. These two results are conflicting in order of stabilities. Our results indicate that, particularly for the H-ZSM-5 zeolite, both NC and IP are present as local energy minima on the potential energy surface with a small energy difference of 0.40 kcal/mol, thus they can be in thermal equilibrium and almost equal in population.

Comparisons between calculated IR spectra of the NC and IP complexes on H-ZSM-5 zeolites suggest several distinct bands for the protonated species which are consistent with experimental interpretations, namely the free OH stretch band at 3179 cm<sup>-1</sup> and the band corresponding to the bending mode of hydroxonium in the region 1675-1760 cm<sup>-1</sup>. These bands do not exist for the protonated H<sub>3</sub>O<sup>+</sup>- - - H<sub>2</sub>O species in H-FAU due to the differences in the adsorption structure. It should be noted that in the actual experimental condition of a given vapor pressure, there can be a wide range of adsorbed water clusters of different sizes existing. Even for clusters of the same size, they can be very different in their structures due to their relative orientations in the zeolite framework. For this reason, the experimental IR spectra tend to have broad bands and are difficult to interpret. Our calculations here provide molecularlevel insights into the interpretations of these spectra.

# Conclusion

We have performed a systematic theoretical study on the modes of adsorption of water diract on H-ZSM-5 and H-FAU zeolites using an embedded cluster approach with the hybrid B3LYP density functional method. Our results indicate that there are two possible adsorption pathways: a stepwise and a concerted adsorption process. The stepwise process involves adsorption of one water at a time and results in a complex where the first water binds more strongly to the (-0)3-Al-OH tetrahedral unit making a 6-membered ring structure similar to that of the adsorption of a single water molecule and the second water molecule does not have any direct interaction with the adsorption site but binds to the other water and the zeolite framework. The concerted adsorption pathway yields the adsorption structure that has both water molecules binding to the adsorption site forming a single larger ring where one of the two water molecules makes only one hydrogen bond to the Brønsted site and the other water forms a hydrogen bond with the oxygen atom of the nearby tetrahedral unit. We found that for adsorption on H-ZSM-5 zeolite, both the neutral and ionpair complexes can exist with adsorption energies of -15.13

and -14.73 kcal/mol, respectively. The relatively small difference in the adsorption energy indicates that both forms of complexes can exist in experimental conditions that are almost equal in population. For adsorption on the H-Faujasite, only the ion-pair complex exists with the adsorption energy of -14.63 kcal/mol. Our results indicate that adsorption properties depend not only on the acidity of the Brønsted acidic site but also on the topology of the zeolite framework, such as on the spatial confinement effects noted in this study. Such spatial confinement effects have led to different structures for the ion-pair complexes on H-ZSM-5 and H-FAU zeolites despite their adsorption energies being quite similar. In particular, the smaller channel cross section of the H-ZSM-5 zeolite results in the H<sub>5</sub>O<sub>2</sub>+ species having the proton almost equally shared between the two water molecules that resembles the transition state configuration H<sub>2</sub>O---H<sup>+</sup>---H<sub>2</sub>O on the isolated H<sub>5</sub>O<sub>2</sub>+ potential energy surface, whereas the larger channel cross section H-FAU yields the ion-pair complex, where the proton is associated with one particular water molecule, i.e., H<sub>3</sub>O<sup>+</sup>- - -H<sub>2</sub>O. The differences in these ion-pair complexes have led to distinct differences in their IR spectra. Our calculated IR spectra confirm several fingerprints for the ion-pair complexes on zeolites as suggested in previous experimental IR studies.

Acknowledgment. This work was supported in part by grants from the Thailand Research Fund (TRF Senior Research Scholar to J.L.), the Kasetsart University Research and Development Institute (KURDI), the Ministry of University Affairs under the Science and Technology Higher Education Development Project (MUA-ADB funds), as well as the ACS PRF grant to T.N.T., The support from the Dow Chemical Company (U.S.A.) and the computer resources provided by the University of Utah Center for High Performance Computing are also acknowledged.

# References and Notes

- (1) Greatbanks, S. P.; Hillier, I. H.; Burton, N. A.; Sherwood, P. J. Chem Phys 1996, 105, 3770.
  - (2) Ison, A.; Gorte, R. J. J. Catal. 1984, 89, 150.
- (3) Mirth, G.; Lercher, J. A.; Anderson, M. W.; Klinowski, J. J. Chem. Soc., Faraday Trans. 1990, 86, 3039.
- (4) Jentys, A.: Warecka, G.; Derewinski, M.; Lercher, J. A. J. Phys. Chem. 1989, 93, 4837.
  - (5) Haase, F.; Sauer, J. J. Am. Chem. Soc. 1995, 117, 3780.
  - (6) Bates, S.; Dwyer, J. THEOCHEM 1994, 112, 57.
- (7) Pelmenschikov, A. G.; van Santen, R. A. J. Phys. Chem. 1993, 97, 10678.
- (8) Marchese, L.; Chen, J.; Wright, P. A.; Thomas, J. M. J. Phys. Chem. 1993, 97, 8109.
  - (9) Limtrakul, J. Chem. Phys. 1995, 193, 79
- (10) Nusterer, E.; Bloechl, P. E.; Schwarz, K. Angew. Chem., Int. Ed. Engl. 1996, 35, 175.
- (11) Kogelbauer, A.; Nikolopoulos, A. A.; Goodwin, J. G.; Marcelin, G. J. Catal. 1995, 152, 122.
- (12) Limtrakul, J.; Treesukol, P.; Ebner, C.; Sansone, R.; Probst, M. Chem. Phys. 1997, 215, 77.
- (13) Kondo, J. N.; lizuka, M.; Domen, K.: Wakabayashi, F. Langmur
- (14) Zecchina, A.; Geobaldo, F.; Spoto, G.; Bordiga, S.; Ricchiardi, G.; Buzzoni, R.; Petrini, G. J. Phys. Chem. 1996, 100, 16584. (15) Jobic, H.; Tuel, A.; Krossner, M.; Sauer, J. J. Phys. Chem. 1996,
- 100, 19545. (16) Termath, V.; Haase, F.; Sauer, J.; Hutter, J.; Parrinello, M. J. Am.
- Chem. Soc. 1998, 120, 8512.
- (17) Zygmunt, S. A.; Curtiss, L. A.; Iton, L. E. J. Phys. Chem. B 2001. 105, 3034.
- (18) Gale, J. D. Top. Catal. 1996, 3, 169.
- (19) Rice, M. J.; Chakraborty, A. K.; Bell, A. T. J. Phys. Chem. A 1998, 102, 7498.
- (20) Limtrakul, J.; Nokbin, S.; Chuichay, P.; Khongpracha, P.; Jungsuttiwong, S.; Truong, T. N. Stud. Surf. Sci. Catal. 2001, 135, 2469.
   (21) Krossner, M.; Sauer, J. J. Phys. Chem. 1996, 100, 6199.

- (22) Zygmunt, S. A.; Curtiss, L. A.; Iron, L. E.; Erhatdt, M. K. J. Phys. Chem. 1996, 100, 6663.
- (23) Zygmuni, S. A.; Curtiss, L. A.; Zapol, P., Jion, L. E. J. Phys. Chem. B 2000, 104, 1944.
- (24) Mortier, W. 3; Van den Bossche, E; Uytterhoeven, J. B. Zeolites 1984, 4, 41.
- (25) Alvarado-Swaisgood, A. E.; Barr, M. K.; Hay, P. J.; Redondo, A. J. Phys. Chem. 1991, 95, 10031.
  (26) Derouane, E. G.; Fripiat, J. G. Zeolites 1985, 5, 165.
- (27) Treesukol, P.; Limirakul, J.; Truong, T. N. J. Phys. Chem. B 2001, 105, 2421.
- (28) Stefanovich, E. V., Truong, T. N. J. Phys. Chem. B 1998, 102, 3018.
- (29) Limtrakul, 3.; Jungsuttiwong, S.; Khongpracha, P. J. Mol. Struct. 2000, 525, 153.
- (30) Limtrakul, J.; Khongpracha, P.; Jungsuttiwong, S.; Truong, T. N.
- J. Mol. Catal. A 2000, 153, 155.

  (31) Frisch, M. J.; Trucks, G. W.; Schlegel, H. B.; Scuseria, G. E., Robb, M. A.; Cheeseman, J. R.; Zakrzewski, V. G.; Montgomery, J. A., Jr.; Stratmann, R. E.; Burant, J. C.; Dapprich, S.; Millam, J. M.; Daniels, A. D.; Kudin, K. N.; Strain, M. C.; Farkas, O.; Tomasi, J.; Barone, V.; Cossi,
- M.; Cammi, R.; Mennacci, B.; Pomelli, C.; Adamo, C.; Clifford, S.; Ochterski, J.; Petersson, G. A., Ayala, P. Y.; Cui, Q.; Morokunia, K.; Malick, D. K.; Rabuck, A. D.; Raghavachari, K.; Foresman, J. B.; Cioslowski, J.; Ortiz, J. V.; Stefanov, B. B.; Liu, G.; Liasbenko, A., Piskorz, P.; Komaromi, L; Gomperts, R.; Martin, R. L.; Fox, D. J.; Keith, T.; Al-Laham, M. A.; Peng, C. Y.; Nanayakkara, A.; Gonzalez, C.; Challacombe, M.; Gill. P. M. W.; Johnson, B. G.; Chen, W.; Wong, M. W.; Andres, J. L.; Head-Gordon, M.; Replogle, E. S.; Pople, J. A. Gaussian 98, revision A.7; Gaussian, Inc.: Pittsburgh, PA, 1998.
- (32) Zygmunt, S. A.; Curtiss, L. A.; Iton, L. E.; Erhardt, M. K. J. Phys. Chem. 1996, 100, 6663.
- (33) Buzzoni, R.; Bordiga, S.; Ricchiardi, G.; Spoto, G.; Zecchina, A. J. Phys. Chem. 1995, 99, 11937.
- (34) Kim, Y.-H.; Lee, I.-H.; Martin, R. M. AIP Conf. Proc. 2000, 501, 366.
  - (35) Lami, A.; Villani, G. THEOCHEM 1995, 330, 307.
- (36) Krokidis, X.; Vuilleumier, R.; Borgis, D.; Silvi, B. Mol. Phys. 1999,
- (37) Ojamae, L.; Shavitt, I.; Singer, S. J. Int. J. Quantum Chem., Quantum Chem. Symp. 1995, 29, 657.

# Density Functional Study of the Mechanism of the Beckmann Rearrangement Catalyzed by H-ZSM-5: A Cluster and Embedded Cluster Study

Jakkapan Sirijaraensre,† Thanh N. Truong,\*.; and Jumras Limtrakul\*,†

Computational and Applied Chemistry Laboratory, Physical Chemistry Division, Kasetsart University, Bangkok 10900, Thailand, and Henry Eyring Center for Theoretical Chemistry, Department of Chemistry, University of Utah. 315 \$ 1400 E, Room 2020, Salt Lake City, Utah 84112

Received: October 26, 2004; In Final Form: April 27, 2005

The mechanism of the Beckmann rearrangement (BR) catalyzed by the ZSM-5 zeolite has been investigated by both the quantum cluster and embedded cluster approaches at the B3LYP level of theory using the 6-31G-(d,p) basis set. Single-point calculations were carried out at the MP2/6-311G(d,p) level of theory to improve energetic properties. The embedded cluster model suggests that the initial step of the Beckmann rearrangement is not the O-protonated oxime but the N-protonated oxime. The energy barriers derived from the proton shuttle of the N-bound to the O-bound isomer are determined to be ~99 and ~40 kJ/mol for the embedded cluster and quantum cluster approaches, respectively. The difference in the activation energy is due mainly to the effect of the Madelung potential from the zeolite framework. The next step is the rearrangement step, which is the transformation of the O-protonated oxime to be an enol-formed amide compound, formimidic acid. The activation energy, at the rearrangement step, is calculated to be ~125 and ~270 kJ/mol for the embedded cluster and quantum cluster approaches, respectively. The final step is the tautomerization step which transforms the enol-form to the keto-form, formamide compound. The energy barrier for tautomerization is calculated to be 123 and 151 kJ/mol for the embedded cluster and quantum cluster approaches, respectively. These calculated results suggest that the rate-determining step of the vapor phase of the Beckmann rearrangement on H-ZSM-5 is the rearrangement or tautomerization step.

#### 1. Introduction

The Beckmann rearrangement 1-6 is an industrially important reaction for the production of  $\epsilon$ -caprolactam, a raw material for the production of Nylon-6, for which the market of consumption was 1 million tons in 1998.7 Caprolactam is produced by the Вескталь rearrangement of cyclohexanone oxime with oleum, or concentrated sulfuric acid as a reaction medium. Although this procedure is convenient from a chemical standpoint, difficulties in manufacturing anticorrosion equipment and eliminating a large amount of the ammonium sulfate formed during the neutralization process make the process environmentally unacceptable. However, using a heterogeneous catalyst in this reaction, usually called the vapor phase of the Beckmann rearrangement, can circumvent these problems. Zeolite proves to be an excellent candidate8-42 for taking over the catalytic function; thus, their use has benefits not only from an economical point of view but also from an ecological point of view.

The Beckmann rearrangement of the oxime compound has been widely investigated, especially on solid catalysts such as H-ZSM-5, <sup>8-20</sup> FAU, <sup>21,22</sup> B-ZSM-5, <sup>23-28</sup> etc. Fois et al. <sup>17</sup> studied the vapor phase of the Beckmann rearrangement in H-Faujasite, H-ZSM-5, and silicalite-1 by using IR spectroscopy and found that (a) both internal silanols and strong acid sites in zeolite can catalyze the Beckmann rearrangement of cyclohexanone oxime, (b) a stable protonated intermediate is formed on a strong acid site, and (c) the reaction at weak acid sites has a higher

Several theoretical studies on the mechanism of the Beckmann rearrangement in the gas phase have been reported. 17,43-47 Nguyen et al.43-45 employed rather high levels of molecular orbital theories to examine the rearrangement of CH3-CH= N-OH oxime catalyzed by a proton, as a model of the BR under a strong acid condition. The Beckmann rearrangement was found to consist of two steps. The first step is 1,2-H-shift which connects the N-protonated complex and the O-protonated complex. The second step, denoted as the rearrangement step, is the concerted migration of the alkyl group to the nitrogen atom and climination of a water molecule to produce a nitrilium cation. The first step was found to be the rate-determining step. Similar results were obtained by Fois et al. for the rearrangement of protonated cyclohexanone oxime. The latter study17 also pointed out that, when a more realistic model for acidic condition was used, namely, a HCl molecule instead of H+, a totally different mechanism was found. In fact, structures along the reaction coordinate were very different, and the rate-limiting step is the rearrangement step instead. The authors also modeled the BR catalyzed by silicalite by using a silanol molecule H<sub>3</sub>-SiOH as a model. It was found that silanol cannot protonate the oxime; however, the rearrangement step is similar to that of the HCl-oxime complex and is also the rate-limiting step.

activation energy through a mechanism not involving a protonated intermediate. Ichihashi et al. 18 found that ZSM-5 was highly active for the Beckmann rearrangement when it had an Si/Al ratio of  $\geq$ 500. Rhee et al. 23,24 studied the Beckmann rearrangement of cyclohexanone oxime over an H- $\beta$  catalyst using FT-IR spectroscopy. They suggested that the initial step of the rearrangement involved the N-protonated complex of oxime, not the O-protonated complex.

To whom correspondence should be addressed. E-mail: fscijrl@ku.ac.th (J.L.) or truong@chem.utah.edu (T.N.T.).

<sup>\*</sup> Kasetsart University.
\* University of Utah.

A conclusion by the authors is that the BR can follow different mechanisms on zeolites depending on the acidity of the Brønsted acid proton and silanol active centers. To the best of our knowledge, there has not been any theoretical study on the mechanism of the BR in a real zeolite framework. Such a study would be fundamentally important in providing more insight into the mechanism of the BR catalyzed by zeolites.

In this study, we performed a systematic theoretical investigation on the mechanism of the gas phase Beckmann rearrangement in ZSM-5 zeolite. The formaldehyde oxime was chosen as a model. Our objectives are (1) to understand the nature of the adsorption of formaldehyde oxime on H-ZSM-5 (i.e., can the Brønsted proton protonate the oxime, and if so, which form, N-protonated or O-protonated, would be more stable?), (2) to determine structures and energetic properties along the reaction pathway for the rearrangement, and thus the rate-limiting step of the reaction, and (3) to investigate the effects of the zeolite framework, particularly the effect of the Madelung potential, on the mode of adsorption of oxime and the mechanism of the BR process. To do so, we have employed both the bare cluster and embedded cluster approaches within the density functional theory.

#### 2. Methods

ZSM-5 has 12 unique tetrahedral (T) sites where an aluminum atom can substitute for the Si atom in the framework to form a Brønsted acid site. In this study, the active site is assumed to be the T12 site since it was predicted to be among the most stable Al substitution sites, 36-42 and has been used to model the active site of ZSM-5 in many theoretical studies. In addition, it is located at the intersection of the main and sinusoidal channels, and thus, it is accessible to adsorbates. In our recent study,37 we have tested model dependency on similar embedded cluster models of the ZSM-5 zeolite and found that there are two main factors that can affect the accuracy of the results. namely, the size of the QM cluster and the representation of the Madelung potential. However, it is difficult to separate the effects of these two factors. As the size of the QM cluster increases, it includes the short-range electrostatic, repulsiondispersion, and polarization contributions from the local region of the active site in its full quantum mechanical treatment. Therefore, in principle, the larger model would provide the more accurate results, although the very large model would have limited use because of its computational demand. We found that the embedded 10T cluster model, in which the quantum 10T cluster represents a complete 10-membered ring of the main channel of ZSM-5, enclosing an active site and adsorbates, is sufficient for studying adsorption of molecules with binding energies of less than 60 kcal/mol; thus, it would be adequate for the systems considered here. The hybrid density functional theory B3LYP level was used. Because of the size of the cluster, we used a mixed basis set to represent the whole system. In particular, the 6-31G(d,p) basis set was used for the active site region [H2Si1OAl(OH)2O(H)Si2H2] and the adsorbate while a smaller 3-21G basis set was used for the remaining part of the cluster. In an attempt to improve the energetic properties, singlepoint energy calculations were carried out at the MP2 level of theory using the 6-311G(d,p) basis set for the whole system.

To include the effects of the static Madelung potential from the remaining infinite lattice of zeolite (excluding the 10T quantum cluster), we employed the embedded cluster model<sup>48</sup> known as the surface charge representation of external electrostatic potential (SCREEP) method proposed by Stefanovich and Truong.<sup>49,50</sup> In this model, such an external Madelung potential

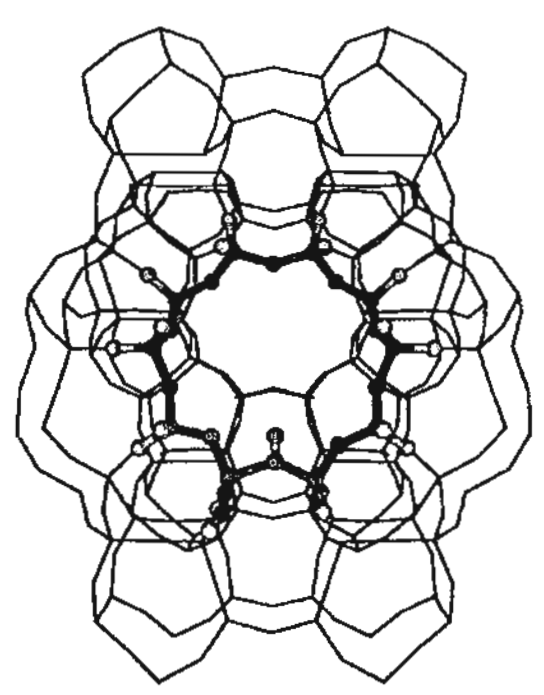


Figure 1. Optimized structures of the 10T cluster and embedded cluster of H-ZSM-5 zeolite at the B3LYP/6-31G(d,p) level of theory (values in parentheses are taken from the bare cluster).

can be represented by two sets of point charges. The potential from the unit cells that are closest to the quantum cluster is represented by point charges located at the lattice sites, while the remaining component is represented by a set of surface charges determined from the SCREEP method. Previous studies found the calculated adsorption properties agree well with experimental estimates, 36,37 suggesting that the SCREEP embedded approach is a sufficiently accurate and practical model for studying reaction mechanisms on zeolites.

In this work, in all geometrical optimizations, only the capping hydrogen atoms are fixed to be along the lattice Si-O bonds. Normal-mode analyses were performed to verify that the optimized transition state does connect the intended reactant and product. All calculations were performed using Gaussian98.<sup>51</sup> Calculations were done using computer resources at the Laboratory for Computational and Applied Chemistry (LCAC) at Kasetsart University.

#### 3. Results and Discussion

3.1. Bronsted Acidic Site. Selected optimized bond lengths in the active site region are displayed in Figure 1. Values in parentheses are from the bare cluster calculations. When the results from the cluster and embedded cluster models are compared, the Madelung potential has the effect of lengthening the O1-H1 bond distance (Brønsted acid site) from 97.0 to 97.7 pm and shortening the adjacent Al-O bond, which is in accordance with Gutmann's rules.52 In addition, the Mulliken population on the H1 atom is slightly increased from 0.38 to 0.41, indicating that the Brønsted proton is more acidic due to the Madelung potential effect. From our previous calculations on smaller clusters, we found that the structure of the Brønsted site is not very sensitive to cluster size. However, in this study, the 10T cluster is needed to accurately describe short-range electrostatic, repulsion-dispersion, and polarization interactions between the local region surrounding the active site and the adsorbate.

_	N co	mplexes	Осо	mplexes
parameter	10T cluster	10T embedded	10T cluster	10T embedded
OI-HI	354.2	177.1	101.2	139.6
N-HI	109.0	104.8	_	-
N-OI	262.0	279.2	_	-
O5-H1	-	_	!64.8	108.1
05-01		_	261.5	245.7
O2-H2	153.2	170.3	173.2	189.8
H2-O5	98.6	99.7	98.6	99.2
02-05	254.0	268.1	257.4	266.4
N-05	134.)	134.6	140.8	151.1
N-C	127.7	127.5	127.3	126.9
∠01-H1-N	168.9	163.7	-	-
∠O2-H2O5	165.7	165.7		
∠01-H1-O5	_	-	158.0	165.3
∠O2-H2-O5	_		143.0	131.8
∠01-02-05-N	165.8	165.8	133.0	98.2
$\Delta E_{\rm ads}$	-135	195	-86	-116
	-138"	-202ª	-103°	~125ª
	-1146	-176b	-85*	(13 <sup>b</sup>

"Obtained at the MP2//83LYP level of theory. Obtained at the MP2/6-311G(d,p)//83LYP level of theory.

3.2. Adsorption Complexes of Formaldehyde Oxime. There are two possible configurations of the adsorbed formaldehyde oxime (CH<sub>2</sub>NOH) for interacting with the Brønsted proton (H1). One is where H1 forms a hydrogen bond with the nitrogen atom of the oxime in what is termed the N-bound configuration, and the other is one in which H1 forms a hydrogen bond with the OH group to form the O-bound configuration. The key issue is whether the Brønsted site is able to protonate the adsorbed formaldehyde oxime.

Selected optimized geometrical parameters and adsorption energies for the N-bound complex calculated using both the bare and embedded cluster models are listed in Table 1. For simplicity in the discussion below, all energetic information is determined at the MP2/6-311G(d,p)//B3LYP level of theory, unless otherwise specified. Selected bond lengths are also shown in Figure 2a to facilitate the discussion. Both models predict that the N-bound complex is protonated. The adsorbed protonated complex forms two hydrogen bonds (O1...H1 and O2... ·H2) in a seven-membered ring configuration where the oximes are nearly in the same plane with the 10T ring (the O1-O2-O5-N dihedral angle is 166°; see also Figure 2a). The adsorption energy is predicted to be -176 kJ/mol from the embedded cluster model. Note that it is much larger than the value of -114 kJ/mol from the bare cluster model. This indicates that the effects of the Madelung potential are significant. In fact, the N-protonated oxime appears to be more ionic, as indicated by the total Mulliken population on the protonated [CH2NHOH]+ subunit of 0.76 from the embedded cluster model as compared to that of 0.67 from the bare cluster model. It is interesting to note that the Madelung potential further separates the protonated oxime moiety from the zeolite framework as the O1-H1 and O2-H2 bond distances were elongated by ~20 pm. This effect is similar to the solvation of an ion pair complex. Similarly, the results for the O-bound complex are also shown in Table 1 and Figure 2b. Here we observed even larger effects of the Madelung potential from the zeolite framework. In fact, it promotes protonation of the O-bound complex. This is evident in the fact that only a molecular adsorbed state was found using the bare cluster model, whereas only the protonated complex

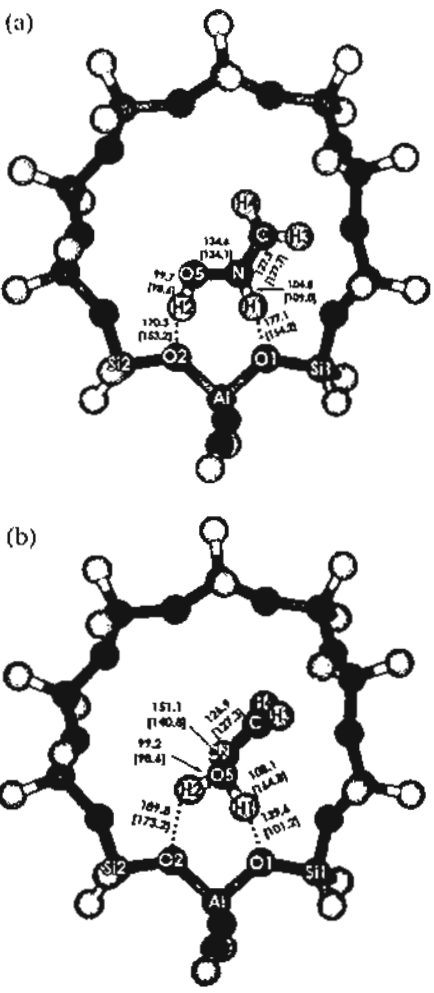


Figure 2. Optimized adsorption complexes on the 10T cluster and embedded cluster of H-ZSM-5 zeolite at the B3LYP/6-31G(d,p) level of theory: (a) N-bound complexes and (b) O-bound complexes (values in parentheses are taken from the bare cluster).

was found using the embedded cluster model. The adsorbed protonated O-bound complex also forms two hydrogen bonds with the two bridging oxygen atoms, O1 and O2, of the zeolite framework, but in a six-membered ring configuration, where the oxime fragment is almost perpendicular to the plane of the 10T ring (the O1-O2-O5-N dihedral angle is 98°; see also Figure 2b). The adsorption energy of the protonated O-bound complex is -113 kJ/mol. Despite the Madelung potential inducing changes in the adsorption mode of the O-bound complex, it has a smaller increase in adsorption energy (28 kJ/mol) as compared to the value of 62 kJ/mol observed for the N-bound complex.

The protonated N-bound complex is much more stable than the protonated O-bound species by 63 kJ/mol as determined with the embedded model, which can be compared to the value of 77 kJ/mol in the isolated protonated formaldehyde oxime system. This result suggests that the initial structure of the Beckmann rearrangement is the protonated N-bound oxime. This finding is consistent with experimental observations by Fois et al. 17 and Chung and Rhee. 23.24 The bare cluster model also predicts the N-protonated complex is more stable than the O-bound complex but only by 29 kJ/mol. This indicates that the Madelung potential has a larger degree of stabilization for the N-bound complex. However, as pointed out in previous

TABLE 2: Optimized Geometries and Adsorption Energies,  $\Delta E_{ads}$  (kilojoules per mole), for the 1,2-H-Shift Transition State in the 10T Bare Cluster and Embedded Cluster at the B3LYP/6-31G(d,p) Level of Theory (distances in picometers and angles in degrees)

parameter	10T cluster	10T embedded
01-111	98.2	100.3
N-H3	220.6	193.4
O5-H1	216.0	202.6
05-01	308.4	298.8
N-01	306.8	283.7
H2-05	98.5	97.6
112~02	180.0	202.7
02-05	272.6	288.3
N-O5	140.9	143.0
N-C	127.3	127.3
∠01-H1-N	145.7	148.4
∠01-H1-O5	156.1	160.0
∠O2−H2−O5	155.2	145.3
∠01-02-05-N	58.9	60.2
$\Delta \mathcal{E}_{ads}$	-65	-67
	-84"	-82°
	$-74^{b}$	-778

"Obtained at the MP2//B3LYP level of theory. b Obtained at the MP2/6-31] G(d,p)//B3LYP level of theory.

theoretical studies, the N-bound complex does not lead directly to the Beckmann rearrangement. It must first transform to the O-bound complex. The mechanism for such a process is discussed below.

3.3. Mechanism of the Beckmann Rearrangement. The mechanism of the Beckmann rearrangement of formaldehyde oxime on H-ZSM-5 zeolite consists of three steps. The first step is the 1,2-H-shift, which is the transformation from the N-bound configuration structure to the O-bound configuration structure. The second step is the rearrangement of the O-bound oxime complex to the amide complex, in which a hydrogen atom is transferred from the CH2 group to the nitrogen atom and a water molecule is displaced. The next step is the water binding to the carbon atom, and then transferring a hydrogen atom to the NH group to form the intermediate product. The last step is tautomerization from the intermediate product to the amide product. The general feature of the potential energy surface for the first two steps is similar to the results obtained by Nguyen et al. for the protonated formaldehyde oxime system; however, there are distinct differences as discussed below. The schematic energy profile reported by Fois et al. also consists of three steps. Unfortunately, no structural information along the reaction path was reported, thus making more detailed comparisons difficult.

For the first step, the 1,2-hydrogen shift, the optimized structure of the transition state is illustrated in Figure 3a, and selected geometrical parameters and relative energies with the reference point being the infinitely separated oxime and zeolite are given in Table 2. The nature of the 1,2-H-shift for isomerization between the N-protonated oxime and the Oprotonated oxime in ZSM-5 is very different when compared to that in the isolated protonated oxime system. In the isolated protonated oxime system, as studied by Nguyen et al., the transition state for the 1,2-H-shift has a rather tight structure where the active N-H and O-H bonds are less than 125 pm in length, whereas the transition state in the ZSM-5 zeolite has a rather loose structure where these active bonds are longer than 193.4 pm. In fact, at the transition state, the formaldehyde oxime is not protonated by ZSM-5 since the O1-H1 bond is only ~100.3 pm in length. Thus, the zeolite framework assists the 1,2-H-shift step by forming a neutral hydrogen bond complex

TABLE 3: Optimized Geometries and Adsorption Energies,  $\Delta E_{\rm ads}$  (kilojoules per mole), for the Rearrangement Step in the 10T Bare Cluster and Embedded Cluster at the B3LYP/6-31G(d,p) Level of Theory (distances in picometers and angles in degrees)

		angement tion state		mimic complex
parameter	10T cluster	10T cmbedded	10T cluster	10T embedded
01-B1	193.6	232.4	101.3	113.6
O5~H1	98.5	97.4	157.5	129.7
O2-H2	176.4	205.4	196.6	209.3
O5-H2	99.3	97.6	98.5	98.0
05-01	275.6	309.9	256.6	242.2
05-02	270.2	293.0	265.1	269.1
N-05	217.9	228.3	_	_
N-O2	400.0	475.4	428.1	427.4
N-H4	117.9	129.2	102.0	102.0
N-C	120.0	119.3	126.0	125.0
C-B3	111.4	110.5	109.3	108.9
C-H4	136.5	128.3	_	
C-O5	-	-	136.4	139.7
∠C-N-O5	108.3	100.8	_	_
∠N-C-O5	_	_	120.6	117.9
∠01-H1-05	139.0	136.0	164.6	168.9
∠O2-H2-O5	156.1	148.4	124.4	117.6
$\Delta E_{ads}$	187	26	-249	- 264
	168"	0"	-276°	-2894
	185 <sup>b</sup>	128	-260 <sup>8</sup>	-276°

<sup>a</sup> Obtained at the MP2//B3LYP level of theory. <sup>b</sup> Obtained at the MP2/6-311G(d,p)//B3LYP level of theory.

rather than the ion pair complex, thus relieving most of the structural constraints seen in the tight transition state of the isolated protonated case. Consequently, the barrier for this step in ZSM-5 is only 99 kJ/mol from the embedded model as compared to 225 kJ/mol in the isolated protonated system reported by Nguyen et al. The barc cluster model predicts the barrier for this step to be only 40 kJ/mol. This indicates that the Madelung potential from the zeolite framework has a much larger degree of stabilization of the N-bound protonate oxime than at the transition state.

The optimized geometry of the transition state for the rearrangement step is shown in Figure 3b, with selected geometrical parameters and relative energies given in Table 3, along with the information for the intermediate, HNCH-OH···HZ complex. The optimized geometry of the adsorbed formimidic acid complex is also given in Figure 3c. The rearrangement step consists of a concerted 1,2-H-shift from the CH2 group to the nitrogen atom accompanied by the release of a water molecule from the cleavage of the N-O bond. The transition state geometry qualitatively resembles that from the previous study on the protonated formaldehyde oxime. However, quantitatively there are differences; namely, the transition state for the reaction in zeolite is closer to the product side than that in the isolated system. In particular, for the reaction in zeolite the migrating hydrogen atom, H4, is at the midway point between the C and N atoms (C-H4 and N-H4 bond distances are 128.3 and 129.2 pm, respectively), whereas it is still much closer to the reactant side for the isolated protonated oxime system (C-H and N-H active bond distances are 119.2 and 142.4 pm, respectively). The breaking N-O bond is also longer for the reaction in zeolite (228.3 vs 205.6 pm). The calculated barrier for this step is 125 kJ/mol from the embedded model, which is almost 80 kJ/mol higher than the previously reported value of 44 kJ/mol for the isolated protonated oxime system. Comparing results between the embedded and bare cluster models, we found that the Madelung potential noticeably shifts

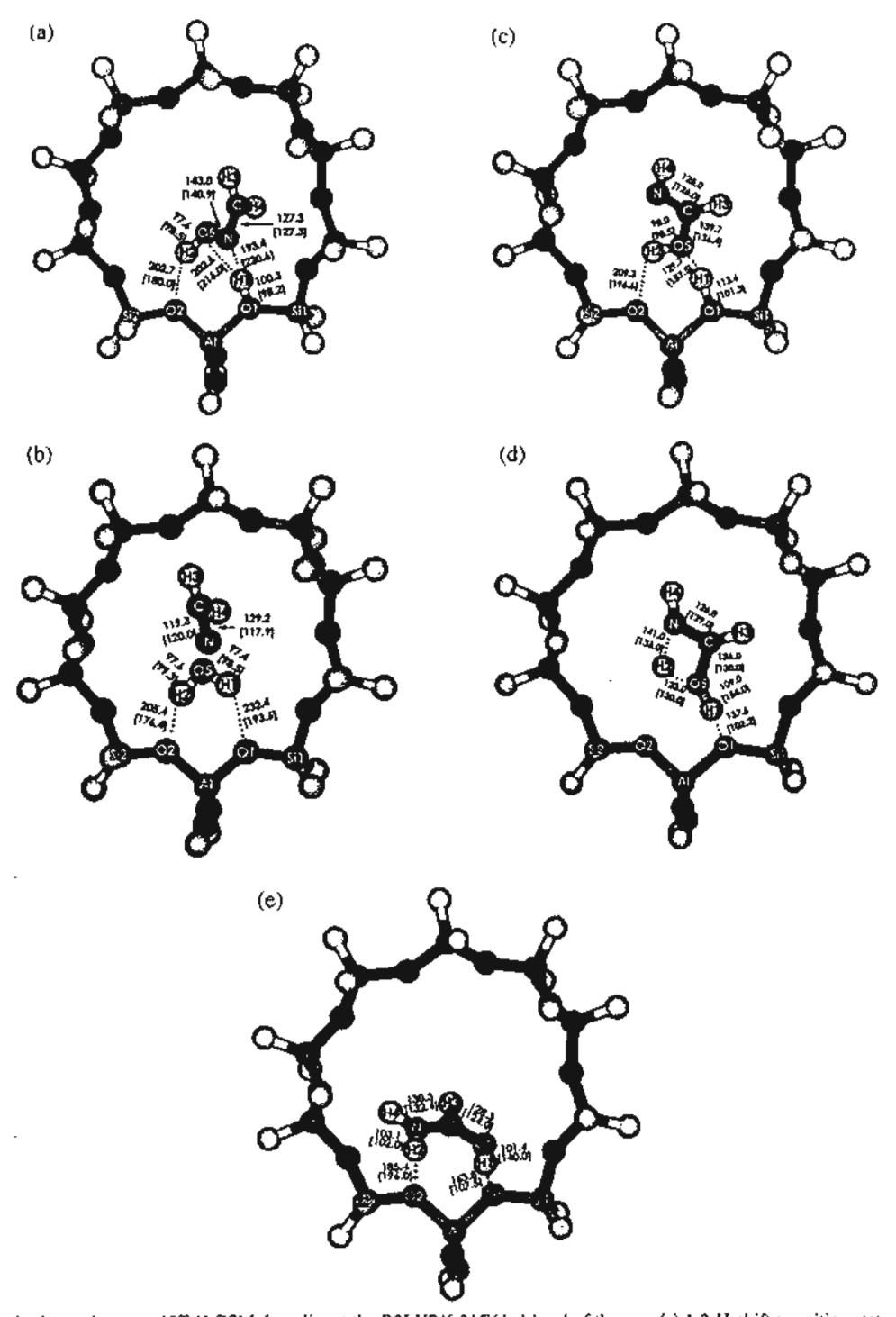


Figure 3. Optimized complexes on 10T H-ZSM-5 zeolite at the B3LYP/6-31G(d,p) level of theory: (a) 1,2-H-shift transition state complexes, (b) Beckmann rearrangement transition state complexes, (c) formimidic acid complexes, (d) tautomerization transition state complexes, and (e) formamide complexes (values in parentheses are taken from the bare cluster).

the transition state toward the primary product. The effect of the Madelung potential on the barrier height of this step, however, is much stronger. In particular, it lowers the activation energy by 145 kJ/mol.

However, the final product of the Beckmann rearrangement reaction of formaldehyde oxime is not formimidic acid (HNCHOH), which is the primary product obtained from the rearrangement step, but formamide (H2NCHO). The final step is the tautomerization of the primary product, the formimidic

acid complex (HNCHOH···HZ complex), to the more stable product, the formamide complex (H<sub>2</sub>NCHO···HZ complex), by migrating the hydrogen atom (H2) from the oxygen atom (O5) to the nitrogen atom (N). The optimization geometry of the transition state for the tautomerization step is shown in Figure 3d, and selected geometrical parameters are given in Table 4. The transferring proton (H2) is at the midway point between the O5 and N atoms (N-H2 and O2-H2 bond distances of 141.0 and 123.0 pm, respectively), which happens simulta-

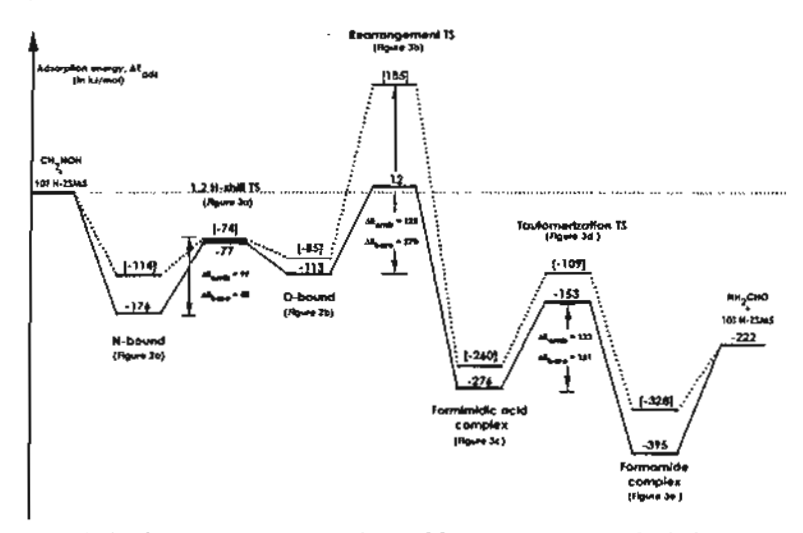


Figure 4. Energetic profile along the Beckmann rearrangement pathway of formaldehyde oxime adsorbed on 10T H-ZSM-5 zeolite at the MP2/6-313G(d,p)//B3LYP level of theory. The energetic changes for the embedded cluster (solid line) and the bare cluster (dotted line) complexes are in kilojoules per mole.

TABLE 4: Optimized Geometries and Adsorption Energies,  $\Delta E_{sds}$  (kilojoules per mole), for the Tautomerization Step in the 10T Bare Cluster and Embedded Cluster at the B3LYP/6-31G(d,p) Level of Theory (distances in picometers and angles in degrees)

		nerization ition state	formamide complex		
parameter	10T cluster	10T embedded	10T cluster	10T embedded	
01-HI 05-HI 02-H2 05-H2 05-O1 05-O2 N-O2 N-H4 N-H2 N-C C-H3 C-O5 ∠N-C-O5	102.2 154.0 - 130.0 256.7 287.2 428.3 101.0 136.0 129.0 108.0 130.0 106.8	137.6 109.0 - 123.0 245.3 288.2 403.1 101.0 141.0 126.0 108.0 136.0	107.5 140.0 196.0 — 247.0 343.4 294.9 100.0 102.0 132.4 109.0 124.0 125.5	163.8 101.4 185.4  264.6 368.7 286.7 101.2 103.1 130.3 108.9 128.3 124.7	
∠01-H1-05 ∠05-H2-N ∠01-02-N-05 ∆E <sub>ads</sub>	174.2 103.0 - -108 -130° -109°	167.4 102.8 - +169 -174 <sup>a</sup> -153 <sup>b</sup>	168.6 62.2 6.1 -327 -346° -328 <sup>b</sup>	171.5 61,8 13.7 -393 -408° -395 <sup>b</sup>	

Obtained at the MP2//B3LYP level of theory. Obtained at the MP2/6-311G(d,p)//B3LYP level of theory.

neously with the slight shortening of the C-O5 bond and the elongating of the N-C bond for shifting to the amide compound.

However, comparing the tautomerized transition state structure between both models, we found that the protonation occurred concurrently during tautomerization in the embedded cluster model. The O1-H1 bond was elongated by ~35 pm to form an O-H single bond. The energy barrier for this step is predicted to be 123 kJ/mol by using the embedded cluster model. The effect of the Madelung potential from the zeolite framework slightly lowers the activation energy as compared to that obtained from the bare cluster model. The results agree well with previous studies which have investigated in the same reaction for other different molecules such as N-nitrobenzene sulfonamides,53 isocyanates,54 β-lactams,55 carbodiimine,56 and acetamide.<sup>57</sup> The activation energy for the tautomerization step of these molecules is ~105-125 kJ/mol. Compared to the activation energy for the previous rearrangement step, it is slightly lower, and thus, both of these rearrangement steps could be the rate-limiting step for the whole mechanism.

Finally, the final product of the reaction is formamide. The optimized geometry of the adsorbed formamide complex is given in Figure 3e. From the embedded cluster model, the adsorbed protonated formamide, [H<sub>2</sub>NC(OH)H]<sup>+</sup>, forms two strong hydrogen bonds to both C=O<sup>+</sup>-H and NH<sub>2</sub> groups which interact with the two bridging oxygen atoms, O1 and O2, of the zeolite framework in the six-membered ring configuration, whereas only the neutral formed complex was found using the bare cluster model. Both adsorption complexes that are obtained correspond with their transition state structures in the tautomerization step. The adsorption energy of protonated formamide is calculated to be -395 kJ/mol using the embedded

TABLE 5: Comparison of the Adsorption Energies,  $\Delta E_{\rm ads}$  (kilojoules per mole), along the Beckmann Rearrangement of Formaldehyde Oxime on 10T H-ZSM-5 Zeolite in Bare Cluster and Embedded Cluster Models by Different Methods<sup>a</sup>

		$\Delta E_{tds}$	
	B3LYP	MP2//B3LYP	MP2/6-311G(d,p)//B3LYE
N-bound complex	-195 [-135]	-202 [-138]	-176 [-114]
1,2-H-shift transition state complex	-67 [-65]	-82 [-84]	-77 [-74]
O-bound complex	-116 [-86]	-125 [-103]	-113 (-85)
rearrangement transition state	26 [187]	0[168]	12 [185]
enol-amide complex	264 [249]	-289 [-276]	-276 [-260]
tautomerization transition state	-169 [-108]	-174 [-130]	-153 [-109]
keto-amide complex	-393 [-327]	408 [-346]	-395 [-328]

<sup>&</sup>lt;sup>4</sup> Values in brackets were obtained with the bare cluster model.

cluster model. In a comparison of the optimized structure which was obtained from both models with the isolated formamide, the structure of adsorbed formamide provides the lengthening of the C-O bond distance (by 2.4 and 6.7 pm for the bare and embedded clusters, respectively) and shortening of the C-N bond distance (by 4.1 and 5.8 pm for the bare and embedded clusters, respectively). The C-O bond length presents singlebond character, while the C-N bond length shows double-bond character, similar to that observed by Cho et al.58 Changing of the C+O and C+N bond lengths is due mainly to the mesomeric effects resulting from the donation of the lone pair of electrons from the nitrogen atom that pass through the  $\pi$ -bond of the C=O bond to give a different resonance of formamide. In this study, it seems that the framework effect which is represented by the Madelung potential plays an important role in the stabilization of the protonated N.O-formaldehyde oxime and formamide configurations, which is the crucial step in allowing the Beckmann rearrangement to occur.

The effects of the Madelung potential of the extended zeolite framework on the energetic and mechanism of this reaction can also be seen from Figure 4. In particular, the Madelung potential tends to stabilize the stable intermediates by 16-67 kJ/mol. It also lowers the activation energies for all steps involved in this mechanism. The largest effect is at the rearrangement step from the O-bound oxime to the formimidic acid (Figure 2b and Figure 3c), where the Madelung potential lowers the activation energy by 145 kJ/mol. Consequently, it makes this rearrangement step have an activation energy comparable with that of the tautomization from formimidic to formamide (Figure 3c,e); thus, either could be the rate-limiting step.

#### 4. Conclusions

The vapor phase of the Beckmann rearrangement of formaldehyde oxime over the zeolite ZSM-5 catalyst has been studied by both the bare cluster and embedded cluster methods at the B3LYP/6-31G(d,p) level of theory. The N-protonated species was obtained in both the cluster and embedded cluster methods. Using the cluster model (10T), the complex obtained by the latter method is more stable than that from the former by ~60 kJ/mol. For the interaction of zeolite with the oxygen atom of oxime (O-oxime) molecules, the cluster models yielded only hydrogen-bonded adducts, while the O-protonated species was only obtained with the 10T embedded method. This embedded result indicates that the N-protonation of oxime is preferable to the O-protonation. This study suggests that the initial structure of the Beckmann rearrangement reaction is not the O-protonation but the N-protonation of oxime. The energy barrier for the 1,2-H-shift connecting N- and O-protonated species is lower than that of the rearrangement and tautomerization steps. From the calculations, one can conclude that the rate-determining step of the reaction is either the rearrangement or tautomerization step which has an energy barrier of ~125 kJ/mol. Furthermore, we found that the extended framework significantly affects the results of protonation of the formamide molecule. Our finding may be good supporting evidence for the newly proposed mechanism for the cyclohexanone oxime that interacts with zeolites and finding the suitable zeolite for this reaction. This indicates that inclusion of the effects of the zeolite crystal framework is crucial for obtaining the mechanistic aspect of the Beckmann rearrangement.

Acknowledgment. This research has been supported in part by a TRF Senior Research Scholar from the Thailand Research Fund, The Ministry of University Affairs under the Science and

Technology Higher Education Development Project (MUA-ADB funds), the Kasctsart University Research and Development Institute (KURDI), a Grant-in-Aid for Thesis from the Graduate School, Kasetsart University, to J.S. and an ACS Petroleum Research Fund grant to T.N.T.

#### References and Notes

- (1) Beckmann, E. Chem. Ber. 1886, 89, 988.
- (2) Blatt, A. H. Chem Rev. 1933, 12, 215.
- (3) Jones. B. Chem. Rev. 1944, 35, 335.
- (4) Heldt, W. Z. J. Org. Chem. 1961, 26, 1695.
- (5) Ungnade, H. E.; McLaren, A. D. J. Org. Chem 1945, 10, 29.
- (6) Pearson, D. E.; Bruton, J. D. J. Org. Chem. 1954, 19, 957.
- (7) European Chemical News; Hnywards: Heath, U.K., 1999; Vol. 18.
- (8) Takahashi, T.; Nishi, M.; Tagawa, Y.; Kai, T. Microporous Moter 1995, 3, 467,
  - (9) Takahashi, T.; Ueno, K.; Kai, T. Microporous Mater 1993, J. 323,
- (10) Heitmann, G. P.; Dahlhoff, G.; Hölderich, W. F. J. Catal. 1999. 186, 12
  - (11) Ichihashi, H.; Kitamura, M. Catal. Today 2002, 73, 23.
  - (12) Yashima, T.; Oka, N.; Komaisu, T. Catal. Today 1997, 38, 249.
- (13) Kath, H.: Gläser, R.; Weitkamp, J. Chem. Eng. Technol. 2001, 24.
  - (14) Misona, M.; Inni, T. Catal. Today 1999, 51, 369.
- (15) Takahashi, T.; Nasution, M. N. A.; Kai, T. Appl. Cotol., A 2001, 210, 339.
- (16) O'Sullivan, P.; Form, L.; Hodnett, B. K. Ind. Eng. Chem. Res. 2001, 40, 1471.
- (17) Fois, G. A.; Ricchiardi, G.; Bordiga, S.; Busco, C.; Dalloro, L.; Spano, G.; Zeochina, A. Stud. Surf. Sci. Catal. 2001, 135, 2477
  - (18) Ichihashi, H.; Sato, H. Appl. Catal.. A 2001, 221, 359.
- (19) Takahashi, T.; Kai, T.; Nakao, E. Appl. Catal. 2004, 262, 137. (20) Forni, L.: Fornasari, G.; Giordano, G.; Lucarelli, C.; Katovic, A.; Triffiro, F.; Perri, C.; Nagy, J. B. Phys. Chem. Chem. Phys. 2004, 6, 1842.
- (21) Dai, L. X.; Iwaki, Y.; Koyama, K.; Tatsumi, T. Appl. Surf. Sci. 1997, 121-122, 335.
- (22) Dai, L. X.; Koyama, K.; Miyamoto, M.; Tatsumi, T. Appl. Catal. A 1999, 189, 237.
- (23) Rhee, H. K.; Chong, Y. M. J. Mol. Cotal. A: Chem. 2000, 159, 389
- (24) Rhee, H. K.; Chung, Y. M. J. Mol. Catal A: Chem. 2001, 175,
  - (25) Hölderich, W. F. Catal. Today 2009, 62, 115.
- (26) Röseler, J.; Heitmann, G., Hölderich, W. F. Appl. Catal., A 1996, 144, 319,
- (27) Heitmann, G. P.; Dahlhoff, G.; Neiderer, J. P. M.; Hölderich, W. F. J. Catal. 2000, 194, 122.
- (28) Hölderich, W. F.: Röseler, J.; Heitmann, G. P.; Liebens, A. T. Catal. Today 1997, 37, 353.
- (29) Dal Pozzo, L.; Fornasari, G.; Monti, T. Catal, Commun. 2002, 3, 369
  - (30) Paker, W. O., Jr. Mogn. Reson. Chem. 1999, 37, 433.
- (31) Komatsu, T.; Macda, T.; Yashima, T. Microporous Mesoporous Maier. 2000. 35-36, 173.
- (32) Ko, A. N.; Hung, C. C.; Chen, C. W.; Ouyang, K. H. Catal. Lett. 2001, 71, 219,
- (33) Chaudhari, K.; Bal, R.; Chandwadkar, A. J.; Sivasanker, S. J. Mol. Catal. A: Chem. 2000, 77, 247.
- (34) Shouro, D.; Ohya, Y.; Mishima, S.; Nakajima, T. Appl. Cotol., A 2001, 214, 59.
- (35) Singh, P. S.; Bandyopadhyay, R.; Hegde, S. G.; Rao, B. S. Appl. Calal., A 1996, 136, 249.
- (36) Limitakul, J.; Nanok, T.; Khongpracha, P.; Jungsuttiwong, S.; Troong, T. N. Chem. Phys. Lett. 2001, 349, 161.
- (37) Treesukol, P.; Limtrakul, J.; Truong, T. N. J. Phys. Chem. B 2001, 105, 2421,
- (38) Limtrakul, J.; Nokbin, S.; Chuichay, P. J. Mol. Struct. 2001, 560.
- (39) Limtrakul, J.; Nokbin, S.; Jungsuttiwong, S.; Khengpracha, P.;
  Truong, T. N. Snid. Surf. Sci. Catal. 2001, 133, 2469.
  (40) Jungsuttiwong, S.; Nokbin, S.; Chuichay, P.; Khongpracha, P.;
  Truong, T. N.; Limtrakul, J. Stud. Surf. Sci. Catal. 2001, 135, 2518.
- (41) Limtrakul, J.; Khongpracha, P.; Jungsuttiwong, S. J. Mol. Struct
- 2000, 525, 153, (42) Luntrakul, J.; Khongpracha, P.: Jungsuttiwong, S.; Truong, T. N.
- J. Mol. Catal. A: Chem. 2000, 153, 2469. (43) Nguyen, M. T.; Raspoet, G.; Vanquickenborne, L. G. J. Chem. Soc., Perkin Trans 2 1995, 9, 1791.
- (44) Nguyen, M. T.; Raspoet, G.; Vanquickenborne, L. G. J. Am. Chem. Soc. 1997, 119, 2552.

- (45) Nguyen, M. T.; Raspoet, G.; Vanquickenborne, L. G. J. Chem. Soc.. Perkin Trans. 2 1997, 4, 821.
- (46) Gomez, B.; Fuentcalba, P.; Contreras, R. Theor. Chem. Acc. 2003.
- (47) Ishida, M.; Suzuki, T.; Ichihashi, H.; Shiga, A. Catal. Today 2003, 87, 187.
- (48) Vetrivet, R.; Catlow, C. R. A.; Colbourn, E. A. Proc. R. Soc. London, Ser. A 1988, 417, 81. (b) Aloist, G.; Barnes, P.; Catlow, C. R. A.; Jackson, R. A.; Richard, A. J. J. Chem. Phys. 1990, 93, 3573. (c) Brandle, M.; Sauer, J. J. Am. Chem. Soc. 1998, 120, 1556. (d) Eichler, U.; Brandle, M.; Sanet, J. J. Phys. Chem. B 1997, 101, 10035. (e) Kyrlidis, A.; Cook. S. J.; Chakraborty, A. K.; Bell, A. T.; Theodorou, D. N. J. Phys. Chem. 1995, 99, 1505. (f) Teunissen, E. H.; Jansen, A. P. J.; van Santen, R. A. J. Phys. Chem. 1995, 99, 1873. (g) Teunisson, E. H.; Jansen, A. P. J.; van Santen, R. A.; Orlando, R.; Dovesi, R. J. Chem. Phys. 1994, 101, 5865. (h) White, J. C.; Hess, A. C. J. Phys. Chem. 1993, 97, 8730.
- (49) Stefanovich, E. V., Truong, T. N. J. Phys. Chem. B 1998, 102, 3018
- (50) Vollmer, J. M.; Stefanovich, E. V.; Truong, T. N. J. Phys. Chem. B 1999, 103, 9415.
- (51) Frisch, M. J.; Trucks, G. W.; Schlegel, H. B.; Scuseria, G. E.; Robb, M. A.; Cheeseman, J. R.; Zakrzewski, V. G.; Montgomery, J. A.; Stratmann, R. E., Jr.: Burant, J. C.; Dapprich, S.; Millam, J. M.; Daniels, A. D.; Kudin,
- K. N.; Strain, M. C.: Farkas, O.; Tomasi, J.; Barone, V.; Cossi, M.; Cammi, R; Mennucci, B.; Pomelli, C.; Adamo, C.; Clifford, S.; Ochterski, J.; Petersson, G. A.; Ayala, P. Y.; Cui, Q.; Morokuma, K.; Salvador, P.; Dannenberg, J. J.; Malick, D. K.; Rabuck, A. D.; Raghavachari, K.; Foresman, J. B.; Cioslowski, J.; Ortiz, J. V.; Baboul, A. G.; Stefanov, B. B.; Liu, G.; Liashenko, A.; Piskotz, P.; Komaromi, I.; Gomperts, R.; Martin, R. L.; Fox, D. J.; Keith, T.; Al-Laham, M. A.; Peng, C. Y.; Nanayakkara, A.; Challacombe, M.; Gill, P. M. W.; Johnson, B.; Chen, W.; Wong, M. W.; Andres, J. L.; Gonzalez, C.; Head-Gordon, M.; Replogle, E. S.; Pople, J. A. Gaussian '98; Gaussian, Inc.: Pittsburgh, PA, 200).
- (52) Guimann, V. The donor-acceptor approach to molecule interacilons; Plenum Press: New York, 1978.
  - (53) Cox. R. A. J. Chem. Soc., Perkin Trans. 1997, 2, 1743.
- (S4) Raspoet, G.; Nguyen, M. T.; McGarraghy, M.; Hegarry, A. F. J. Org. Chem. 1998, 63, 6867.
- (55) Pitarch, J.; Ruiz-Lopez, M. F.; Silla, E.; Pauscual-Ahnir, J. L.; Tunon, I. J. Am. Chem. Soc. 1998, 120, 2146.
  - (56) Lewis, M.; Glaser, R. J. Am. Chem. Soc. 1998, 120, 8541.
- (57) Barbosal, L. A. M. M.; van Santen, R. A. J. Catal 2000, 191, 200
- (58) Cho, S. J.; Cui, C.; Lee, J. Y.; Park, J. K.; Suh, S. B.; Park, J.; Kim, B. H.; Kim, K. S. *J. Org. Chem.* 1997, 62, 4068.

#### Nature of the Metal-Support Interaction in Bifunctional Catalytic Pt/H-ZSM-5 Zeolite

#### Piti Trecsukol, \*\* Kanokthip Srisuk, \* Jumras Limtrakul, \*\* and Thanh N. Truong \*.\*

Henry Eyring Center for Theoretical Chemistry, University of Utah, Salt Lake City, Utah, 84112, Faculty of Liberal Arts and Science, Kasetsart University, Kampaeng Saen Campus, Nakornpathom, Thailand 70320, and Laboratory for Computation and Applied Chemistry, Kasetsart University, Bangkok, Thailand 10900.

Received: March 4, 2005; In Final Form: April 25, 2005

The metal—support interaction of a dispersed Pt atom on H-ZSM-5 zeolite has been investigated by using an embedded cluster and cluster models with the density functional theory/B3LYP functional method. We found that the Pt atom interacts with a Brønsted proton and a nearby framework oxygen. Interaction with the framework oxygen causes electron transfer from the zeolite to the Pt atom. Concurrently, a Brønsted proton stabilizes the Pt atom on the zeolite surface by withdrawing excess electron density from the Pt atom. These charge transfers result in a zero net charge on the Pt atom while changing its orbital occupation. The binding energy of Pt on the Brønsted acid was 15 kcal/mol. Inclusion of the Madelung potential by Surface Charge Representation of the Electrostatic Embedded Potential method (SCREEP) had small effects on structure and charge density of Pt/H-ZSM-5 but it shifted the stretching mode of CO toward a higher frequency by almost 40 cm<sup>-1</sup>. The frequency shift of absorbed CO calculated with embedded cluster models was from 8 to 11 cm<sup>-1</sup> red shift, compared to 20 cm<sup>-1</sup> red shift from experiment. This implies that not only the electronic state of the Pt atom but also the Madelung potential of the support is responsible for the observed small red shift of CO on the Pt-H-ZSM-5.

#### 1. Introduction

Supported platinum particles on oxide surfaces, such as SiO<sub>2</sub>, Zr<sub>2</sub>O<sub>3</sub>, Ti<sub>2</sub>O<sub>3</sub>, or zeolite, have outstanding catalytic activity in many processes, e.g., (de)hydrogenation, <sup>1,2</sup> isomerization, <sup>3</sup> oxidation, <sup>4-6</sup> aromatization, <sup>7,8</sup> and automotive exhaust catalysis. <sup>9</sup> Basically, the main purpose of using support materials is to maintain the dispersion of metal particles, but experimental studies have revealed that the supports can also modify the catalytic properties of metal particles significantly. The catalytic reactivity of the supported metal can be tuned as desired if the metal—support interaction is well understood. Nevertheless, the nature of the metal—support interaction is still elusive. <sup>10-14</sup>

Transition metals supported on zeolite have been found to be active catalysts for many processes. 3,8,15~17 The performance and selectivity of the catalyzed processes depend on the nature of the metals and of the zeolite acidic sites. Much attention has been focused on the zeolite-supported platinum, which is a very active and very stable catalyst for hydrocracking, hydroisomerization, and reforming of hydrocarbons.17-23 The acid site of zeolite is suggested, not only to alter the catalytic property of the metal cluster, but also to have a key role in the catalytic process. Two active centers of the Pt/H-ZSM-5 (the metal particle and the acid site) may work collaboratively as the bifunctional catalyst. A model to explain the mechanism of bifunctional catalysts has been proposed: the (de)hydrogenation and ring opening occur on the metal particle while the isomerization through the carbonium ion intermediates occurs on the acid site.24-26 Nevertheless, there is no explanation for

Particle size, location, and the electronic state of supported Pt and the metal/support interaction are important factors that can affect the catalytic activity of Pt/zeolite. Studies on the Pt/ zeolite-catalyzed dehydrogenation reaction have shown that a small size of the platinum particle correlates with a high turnover frequency (TOF).27 The size of Pt clusters can be controlled by the preparation conditions and the acidity of the support. 8,17,28-31 From the fact that high acidic zeolites favor smaller Pt clusters, the metal/acid-site interaction is believed to have an important role in stabilizing dispersed metals. The differences in catalytic properties between bulk platinum and diffused Pt particles and the confined space within the zeolite framework suggest that the active Pt species in acidic zeolite must be very small to fit inside the zeolite framework. 11,32,33 Pt clusters ranging from 25 atoms in size to monatomic species have been identified, depending on the acidity and cavity size of the zeolite.28,32,34-39 The most stable sites for isolated Pt atoms in zeolite were determined to be in sodalite cages for faujasite zeolite and in side pockets for mordenite zeolite. 36,38,39 These species are inaccessible for most guest molecules. For H-ZSM-5, Pt clusters are localized in the main channels, which are catalytically active and easily accessible for guest molecules.37

One of the most controversial issues regarding zeolite supported Pt is how the zeolite framework affects the electronic property of supported platinum. Explanations have been deduced mainly based on the CO-adsorption studies, in which a small red shift of CO has been observed. Many suggested that Pt clusters are in electron-deficient states and that they give rise to the remarkable catalytic property observed. 31,38,40-42 Whether the apparent electron deficiency of Pt particles stems from intrinsic properties of the small metal particles is still debatable. 11,31,43 Electron transfer from the metal particle to the

the synergistic effect of the metal cluster and acidic support that is observed in many hydroconversion reactions.

<sup>\*</sup> Address correspondence to these authors: T. N. Truong (e-mail: truong@chem.utah.edu) and J. Limtrakul (e-mail: fscijrl@ku.ac.th).

University of Utah.

Faculty of Liberal Arts and Science, Kasetsart University,

Laboratory for Computation and Applied Chemistry, Kasetsart University.

Brønsted proton is a straightforward explanation for the electrondeficient states of PL<sup>11,12,44,45</sup> However, alternative explanations exist. 27,34,43,46,47 For instance, Miller et al. 43 reported that the valence band of Pt on LTL zeolites, with a different acidity, showed no sign of electron transfer between Pt particles and zcolite. The interaction between the metal and support leads to a shift in the energy of the metal valence orbitals, which can stabilize the bonding between Pt and the adsorbate.48

Only a small number of theoretical studies on the systems of Pt/zeolite have been reported to date. The main purpose of those works was to look for structures of the Pt particles inside zeolites and a possible explanation for the observed CO red shift, Structures of the active centers of monatomic Pt in H-Mordenite were investigated by molecular mechanics and density functional methods.49,50 Yakolev et al. used DFT/LDA with small zeolite cluster models (2T and 4T) to investigate the adsorption of CO on a supported Pt atom in the side pocket of H-Mordenite assuming specific Pt-acidic proton configurations. 50 The red shift of adsorbed CO (40-80 cm<sup>-1</sup>) was interpreted as a consequence of an electron-deficient state of the Pt atom. Grillo and de Agudelo studied the structure of Pt/H-Mor and its interactions with hydrocarbons by molecular mechanics and molecular dynamics. 49.51 However, questions such as how metal-support interaction affects the electronic structure and properties of the metal particles upon adsorption have not been addressed so far. Previous calculations on the systems of small molecules on Pt/ supports show the sensitivity of the vibrational frequencies of adsorbates not only on the electronic property of the adsorption site, but also on the support environments.52-54 In this case. the environmental effect can complicate the interpretation of the CO frequency shift and the frequency shift may not be used as direct evidence for the deficient states of Pt clusters.

In this study, our objective is to understand metal-support interaction and how it affects the electronic structures and properties of the metal particles upon adsorption. We employed the monatomic Pt on H-ZSM-5 zeolite as a model for simplicity in our theoretical efforts but it also corresponds with the high TOF case.27 The effect of the extended framework was examined by using an embedded cluster model. The adsorption of CO was investigated to examine the nature of the electronic state of the supported Pt. Other factors that can affect the results, such as the Pt particle size and the location of the Brønsted acid site, will be discussed in the future.

#### 2. Methodology

The three different-sized cluster models (3T, 5T, and 10T, where T is Si or Al atom) shown in Figure 1a-c were used to represent the active site of the H-ZSM-5 zeolite framework. These models were taken from the crystallographic structure of the ZSM-5 zeolite and were optimized at the DFT/B3LYP level of calculation.55 The clusters were parts of the 10T ring at the intersection of the zigzag and main channels, which is the most accessible region for guest molecules. One proton was added to each of the clusters to counterbalance the negative charge upon Al substitution on the T12-site Si tetrahedral in the framework. The T12 site has been found to be among the most stable Brønsted acidic sites in H-ZSM-5 zeolite.56-58 All clusters were terminated at the boundary by hydrogen atoms aligning along the broken Si-O bond direction at a distance of 1.47 Å. The Brønsted acid site (Si-O(H)-Al-O-Si) was optimized while the rest was fixed to mimic the framework constraints. A Pt atom was added to the optimized H-ZSM-5 models. The adsorbed Pt atom of 5d%s1 electronic configuration and the active site of H-ZSM-5 were reoptimized.

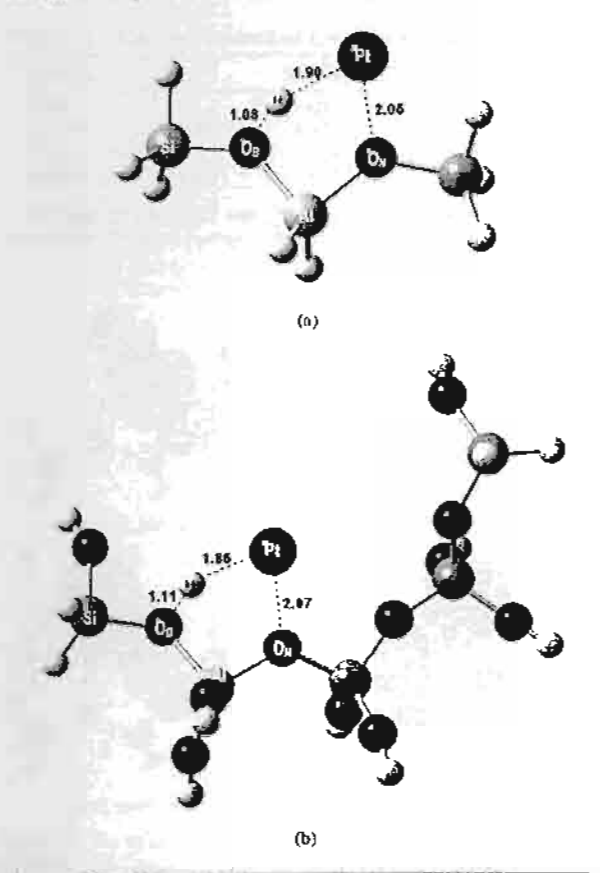
Comparison between the 3T and 5T models was made to determine the effect of the size of the zeolite model. The effect of the extended framework of zeolite was examined by means of an embedded cluster model, in which the Madelung potential from the infinite lattice is accounted for by using a set of point charges. The 5T cluster was embedded in two sets of point charges derived from the Surface Charge Representation of the Electrostatic Embedding Potential (SCREEP) method. 55,59-63

Structures of CO adsorbed on Pt/H-ZSM-5 were obtained by partial optimization where the active site and the adsorbate were relaxed. Only the adsorption with a C-bound configuration will be discussed here because it has been found to be much more stable than the one with O-bound. Vibrational modes of the carbonyl complexes were calculated and compared to experimental data. The effects of the cluster size on the binding energy and vibrational frequency of CO adsorption were determined by performing both bare cluster and embedded 10T cluster calculations where the optimized structures from the 5T cluster model were used while the remaining quantum atoms of the 10T cluster were fixed at the experimental ZSM-5 lattice positions. The embedded 10T cluster model is shown in Figure 1c. The wireframe structure and pink dots surrounding the 10T quantum cluster represent two different sets of point charges, i.e., explicit charges and surface charges, of the SCREEP embedded model.

All calculations were carried out at the DFT/B3LYP level of calculation, which is well-known for its consistency and reliability for zeolite systems. The relativistic effect was considered to be significant for the Pt atom and it was accounted for by the use of the Hay-Wadt VDZ(n+1) basis set with the effective core potential for the Pt atom. 62 The 6-31G(d,p) basis set was used for all other atoms, except for the terminating hydrogens and two silanol groups at two ends of the cluster that were treated with the 3-21G basis sct. The basis set superposition error (BSSE) was accounted for by the counterpoise method<sup>63,64</sup> where the BSSE corrected binding energy is approximated by  $E_{\text{binding}}^{CP} = E_{\text{Super}} + \sum_{i=1,n} (E_{mi} - E_{mi/*}) - \sum_{i=1,n} E_{m_{opt}}$ . In this equation,  $E_{\text{Super}}$  is the total energy of the adsorption complex.  $E_{m'}$ 's represent the energies of the individual species with the subscripts "opt" and "f" denoting individually optimized monomers and the monomers frozen in their adsorption complex geometries, with the superscript "\*" representing monomers calculated with ghost orbitals. Partial charges and population analysis were determined by Natural Atomic Orbital (NAO) and Natural Bond Orbital (NBO) methods.65 All calculations were done with the Gaussian 03 program.66

#### 3. Results and Discussion

3.1. Structure of the Pt-H-ZSM-5 Active Center. The optimized structures of the active center with 3T and 5T clusters are shown in Figure 1a,b. Selected parameters of Pt/HZSM-5 systems are tabulated in Table 1. In all cases the Pt atom was located next to a Brønsted proton of the zeolite. We found that the choice of cluster model to represent the active site of H-ZSM-5 is crucial. In particular, using small clusters such as H<sub>3</sub>SiO(H)AlH<sub>3</sub><sup>67</sup> caused fictitious interaction between the Pt atom and terminating hydrogen atoms and predicted that the Pt atom would bind only to the Brønsted proton. With use of the larger 5T cluster model, the calculated P1-O<sub>N</sub> distance of 2.07 (Pt atom and the nearest bridging oxygen) and Pt-O8 distance of 2.86 Å (Pt atom and Brønsted oxygen) agreed very well with the XANES and EXAFS finding of 2.18 and 2.7-2.9 Å for supported Pt on LTL zeolite. 31.32.43.47 The negligible changes in SiO bonds surrounding the acid site demonstrated that the Pt atom perturbed the zeolite structure only locally.



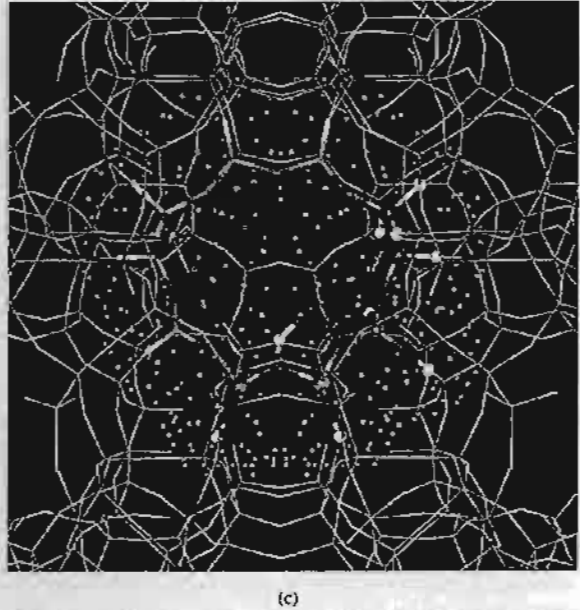


Figure 1. Optimized structures of monatomic Pt on H-ZSM-5 (a) 3T and (b) 5T cluster models (selected bond distances are in Å); (c) the embedded 10T cluster model where the structure of the ball and stick part is taken from the optimized 5T cluster model while the structure of the stick part is fixed to the experimental lattice positions.

It is interesting to note that without an acid site, the PI atom bound very weakly on the zeolite surface ( $E_{\rm B} \leq 1$  kcab'mol). The BSSE corrected binding energies between PI atom and II-ZSM-5 framework were predicted to be 18.9 and 15.0 kcab' mol from 3T and 5T cluster calculations, respectively. This result suggests that the Bronsted proton is necessary for binding a PI

atom to the zeolite framework and can be thought of as a nucleation center for Pt particles. However, the relatively small magnitude of the binding energy also suggests that at higher temperatures agglomeration of Pt atoms is possible. These results agree with experimental findings that large-size Pt clusters occur at high temperatures or in neutral or basic zeolite environments. 68-70

NBO analysis shows bonding characteristics between the d-orbital of Pt and the Brønsted proton and between the sd-orbital of Pt and the framework oxygen (Figure 2). The LUMO is an antibonding orbital between the Pt atom and framework oxygen. We also found that the interaction between supported Pt and the Brønsted proton creates a Pt-H antibonding orbital above the Fermi level of Pt/H-ZSM-5 as is also suggested by XANES studies.<sup>22,34</sup> The energy difference between the antibonding orbital and the Fermi level has been suggested to increase with increasing acidity of the support, correlating with the TOF for hydrogenolysis and isomerization processes.<sup>27</sup>

The charge densities calculated by Mulliken and by NAO population analysis display the same trend. The electronic configurations and partial charges calculated by NAO analysis are presented in Table 2. Our results show electron transfer between the Pt atom and the Brønsted acid site and the framework oxygen of H-ZSM-5 through bonding. An increase of electron density in s- and d-orbitals of Pt due to interaction with the framework oxygen and a decrease of electron density in other d-orbitals of Pt due to interaction with the Brønsted proton were observed from both Mulliken and NAO population analysis. The electron transfer from the framework oxygen strengthened the Pt-O<sub>N</sub> bonding but the Pt atom was less stable in a negative oxidation state. The Brønsted proton can stabilize the Pt atom by withdrawing excess electron density from the Pt atom. This can explain why the aggregation of Pt atoms is likely for dispersed Pt on basic or neutral supports.

The 5T cluster model had more electron density localized at the acid site, consistent with a previous observation that a larger cluster can provide more electron density to the acid site.55 The lower binding energy of PVH-ZSM-5 predicted by the 5T cluster model was probably due to more Coulombic repulsion between the Pt atom and the zeolite framework. The effect of an extended zeolitic framework on the structural and energetic properties of the active site of PVH-ZSM-5 has been examined. The effect of the Madelung potential on the active region of the Pt/H-ZSM-5 system was examined by using an SCREEP embedded cluster. We found that the external field from the extended framework has small effects on structure and charge density. The magnitudes of structural changes were on the order of hundredths of angstroms. The binding energy between Pt and zeolite was decreased by less than 1 kcal/mol. The differences are pronounced if the smaller cluster is employed.55 This implies that the 5T cluster used in this study is sufficient to model the active site of Pt/H-ZSM-5.

3.2. Adsorption of CO. The configurations of CO adsorption on supported Pt systems are shown in Figure 3. Selected optimized parameters of CO adsorptions are reported in Tables 3 and 4. A previous DFT calculation utilized cluster models to represent a Pt atom stabilized in H-Mordenite by one or two Bronsted OH's and provided the Pt-C bond length of 1.76-1.77 Å, the Pt-H distance of 2.00 Å, and the adsorbed CO bond length of about 1.15-1.16 Å. The authors also observed a linear CO adsorption on Pt atom with a C-Pt-H angle of 85°. The same adsorption configuration was found here. Carbon monoxide adsorbed linearly on the Pt atom (Pt-C-O ~ 180°). The C-Pt-H angle was almost 90°, while the C-Pt-Oy angle

TABLE 1: Selected Optimized Geometrical Parameters (Å) and Binding Energies EB (kcal/mol) of Pt/Support Systems

systems	$E_{\rm B}{}^{h}$	R(SiO <sub>8</sub> )	R(A10 <sub>8</sub> )	$R(O_8H)$	$R(AlO_N)$	R(SiO <sub>N</sub> )	R(Pt···H)	R(P(···O <sub>y</sub> )
11Z3		1.694	1.880	0.970	1.706	1.628		
PtHZ3	18.89	1.673	1.804	1.078	1.783	1.676	1.890	2.062
HZ5		1.704	1.850	0.971	1.681	1.599		
PtHZ5	15.00	1.677	1.776	1.108	1.749	1.641	1.858	2.074

"Z3 and Z5 denote 3T and 5T cluster models, respectively; O<sub>B</sub> denotes the Brønsted oxygen; O<sub>B</sub> denotes the neighboring bridging oxygen; H denotes the Brønsted proton b BSSE corrected binding energy.

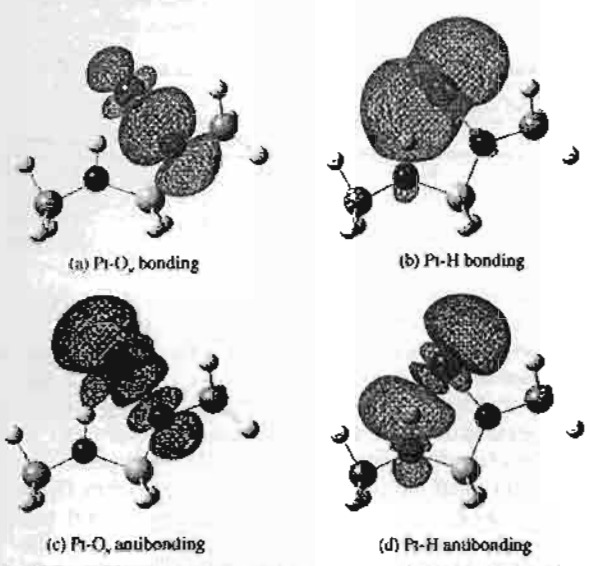


Figure 2. The natural bonding orbitals (NBO) plots of the Pt/H-ZSM-5 system.

electronic configuration

TABLE 2: Partial Charges (au) and Electronic Configurations of Pt/H-ZSM-5

partial charge (NAO)

	OH	H	$O_N$	Pı	O <sub>N</sub>	Pt
Pt(t)				0.00		6s(1.08)5d(8.92)
HZ3	-1.12	0.57	-1.27		2s(1.76)2p(5.50)	
PtHZ3	-1.18	0.43	-1.16	0.02	2s(1.75)2p(5.40)	6s(0.71)5d(9.27)
1125	-1.12	0.57	-1.29		2s(1.78)2p(5.49)	
PtHZ5	-1.19	0.41	-1.20	0.05	2s(1.76)2p(5.43)	6s(0.66)5d(9.27)
of CO. As seer distance	The Pu from es (0.1)	the la A), in I sign	listance engther teractio iificant	es for ning on bet ly up	Brensted proton all systems we of Pt-H (~0.2 ween the Pt aton on the adsorption	re about 1.8 Å. Å) and Pt—O <sub>N</sub> 1 and H-ZSM-5

The binding energy between CO and PI-H-ZSM-5 (84.5 kcal/mol) was much larger than the binding energy between PtCO adduct and H-ZSM-5 (34.9 kcal/mol). The Pt-CO interaction is probably strong enough to cleave PI atoms off of the PI clusters, as is also suggested by CO-FTIR studies showing that neutral Pt/carbonyl complexes were formed in Pt/LTL zeolite<sup>33</sup> and that metal cluster size decreases upon adsorption of

is probably due to differences in type and acidity of zeolites.

The stretching mode of the Brønsted OH is shifted significantly from 1665 to 2795 cm<sup>-1</sup>, corresponding to a shorter OH bond.

The adsorption on the Pt atom can liberate the Brønsted proton

and make the proton available for the consecutive catalyzed

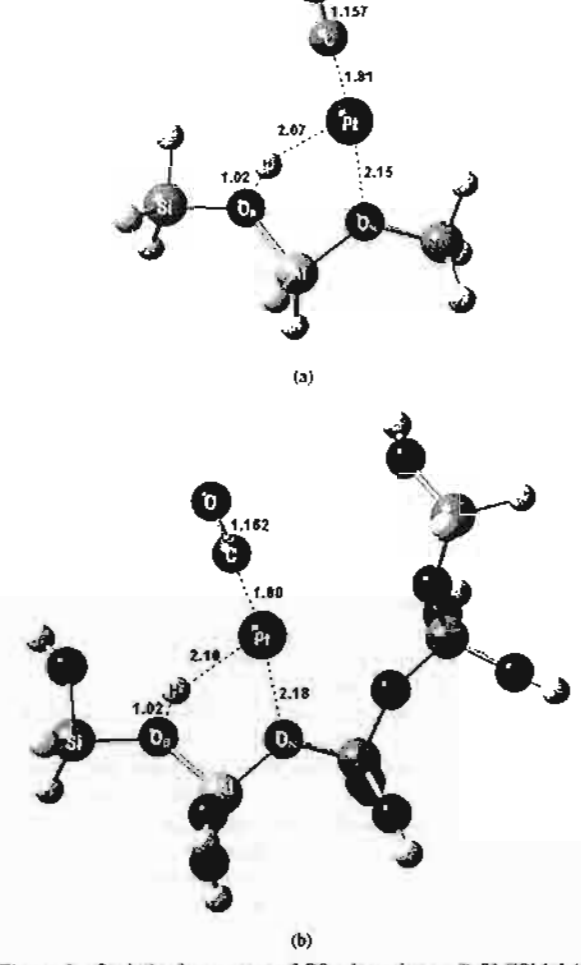


Figure 3. Optimized structures of CO adsorption on Pt/H-ZSM-5 (a) 3T and (b) 5T cluster models (selected bond distances are in Å).

CO.<sup>27,32,38,71</sup> The increased size of the zeolite model (from 3T to 5T) stabilized the adsorption of CO by 4.8 kcal/mol although it had little effect on the geometry. The difference between the binding energies predicted from 5T and 3T cluster models emphasizes the need of a realistic model to represent the zeolite framework since this can stabilize the adsorption complex. Again, the changes in structural and energetic properties of CO adsorption on Pt/H-ZSM-5 due to the inclusion of Madelung potential were minor. The binding energy between CO and Pt/H-ZSM-5 was increased by only 0.5 kcal/mol. However, this is not true for all cases. For example, in the case of H<sub>2</sub> adsorption on Pt/H-ZSM-5, the Madelung potential had a more pronounced effect of decreasing the binding energy by as much as 5 kcal/mol.<sup>67</sup>

The interaction between CO and supported PI can be examined by using NBO analysis. The bonding orbitals were formed between an occupied CO orbital and an unoccupied Pi-

TABLE 3: Selected Optimized Geometrical Parameters (Å) and Binding Energies  $E_B$  (kcal/mol) of Adsorptions of CO on Pt/Support

systems	$E_{\rm R}^{\alpha}$	$R(AIO_B)$	$R(O_{\theta}H)$	$R(AlO_N)$	$R(Pt\cdots H)$	$R(Pt\cdots O_N)$	R(Pt···C)	R(CO)h	$\Delta \nu (CO)^c$
Pil1Z3-CO	79.46	1.834	1.020	1.766	2,073	2.146	1.807	1,157	-20.7
Pil1Z5-CO	84.24	1.806	1.023	1.733	2.096	2.179	1.794	1.162	-47.9
									$(-11.0)^{n}$
PiHZ10-CO	82.65								-41.0
									$(-8.1)^d$

"BSSE correction included (4-8 kcal/mol). \*\*Calculated isolated CO bond length = 1.138 Å. \*\*Compared to experimentally isolated CO (2143 cm \*\*). \*\*Embedded cluster model. \*\*Embedded 10T cluster calculation using the optimized 5T cluster structure.

TABLE 4: Partial Charges (au) and Electronic Configurations of Adsorptions of CO on Pt/Support

			partial char	ge (NAO)		electronic configuration		
systems	O <sub>B</sub>	H	O,v	Pt	С	CO	O <sub>N</sub>	Pt
HZ3-CO	-1.14	0.54	-1.14		0.51	0.06	2s(1.76)2p(5.50)	
PillZ3-CO	-1.15	0.51	-1.25	-0.08	0.53	0.07	2s(1.75)2p(5.49)	6s(0.99)5d(9.09)
HZ5-CO	-1.14	0.54	-1.29		0.52	0.06	2s(1.78)2p(5.49)	
PillZ5-CO	-1.16	0.51	-1.28	-0.04	0.51	0,01	2s(1.77)2p(5.50)	6s(0.97)5d(9.06)

On orbital and between occupied Pt d-orbitals and the unoeccupied  $2\pi^*$ -orbital of CO (Figure 4). This interaction is comparable to the classical mechanism known as the  $\pi$ -backbonding mechanism:  $^{72}\sigma$ -donation from  $5\sigma$  of CO to sd-hybrid orbitals of Pt and  $\pi$ -back-donation from d-orbitals of Pt to  $2\pi^*$  of CO. The  $\pi$ -back-donation weakens the CO bond because of the antibonding nature of  $2\pi^*$  orbitals. Although the net charge of the CO molecule was slightly positive, the latter process (bonding between occupied Pt d-orbitals and the unoccupied  $2\pi^*$ -orbital of CO or the analogous  $\pi$ -back-donation) is very important, as can be seen from the significant increase of electron density in  $\pi^*$ -orbitals of CO and the lengthening of the CO bond. The CO bond was lengthened by as much as 0.025 Å when adsorbed on Pt-HZSM-5, corresponding to the red-shifted stretching frequency.

As mentioned earlier, the frequency shift of adsorbed CO has been used to determine the electronic state of Pt clusters and to validate the computational models. An experiment has reported that the band at 2123 cm<sup>-1</sup> assigned to CO adsorption on monatomic Pt is very stable and still remains in the spectra even after desorption at 623 K.<sup>37</sup> The stretching frequency of adsorbed CO calculated from the bare ST cluster model was 2095.1 cm<sup>-1</sup>. This 49 cm<sup>-1</sup> red shift is somewhat larger than the observed 20 cm<sup>-1</sup> red shift from experiment. Although the stretching mode of 2123 cm<sup>-1</sup> determined from the 3T cluster matches perfectly with the experimental finding, it can be considered the result of fortunate error-cancellation for this model. Our previous study of CO adsorptions on Cu-ZSM-5<sup>55</sup> showed that the stretching mode of CO is very sensitive to its environment, especially to the Madelung potential from the

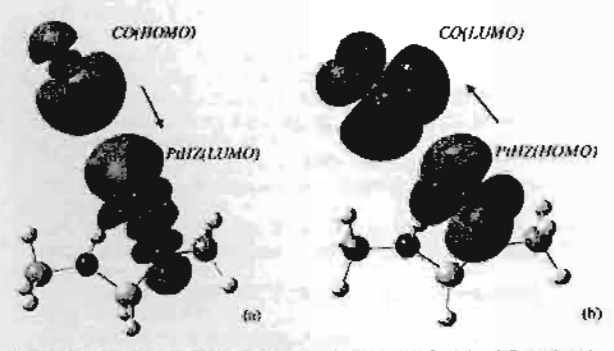


Figure 4. The interaction between the Pt/H-ZSM-5 and a CO molecule can be explained by the  $\pi$ -back-bonding processes: (a)  $\sigma$  donation and (b)  $\pi$ -back-donation. The arrows show the directions of electron transfer.

zeolite framework, Inclusion of the Madelung potential by using the SCREEP embedding scheme brought  $\nu_{\rm CO}$  to 2132.0 cm<sup>-1</sup> (11 cm<sup>-1</sup> red shift), agreeing with the experimental finding. This emphasizes the importance of the long-range effect of the framework on the vibrational modes of the adsorbates.

The effects of the cluster size were investigated by performing both cluster and embedded cluster calculations with the 10T cluster as shown in Figure 1c. In these calculations, the optimized 5T structures were used while the remaining quantum atoms of the 10T cluster were fixed in their experimental lattice positions. The binding energy of CO to Pt/II-ZSM-5 with this model was decreased by only 1.6 kcal compared to that of the embedded 5T model (see Table 3). Despite the large differences between the results from the CO adsorptions on 3T and 5T clusters, we found that frequencies of adsorbed CO calculated from the embedded 5T and 10T clusters are only 2.9 cm<sup>-1</sup> different. These results confirm that the embedded ST cluster would provide a cost-effective model for studying adsorption of small molecules in the Pt/H-ZSM-5 system. The same conclusion had been made in our previous study of CO adsorption on Cu-ZSM-5.55

The H-ZSM-5 support not only withdraws electron density from the Pt atom to the acidic proton, but it also provides electron density to the Pt atom through the framework oxygen. Thus the electron transfer from Pt atom to the proton seems not to have a considerable effect on the  $\pi$ -back-donation and the electron deficient state may not be the key reason for the notably small red shift. We suggest that the change in electronic properties of Pt is due to its interaction with the acid site and the Madelung potential from the zeolite framework. The shift of CO may not directly reflect the local properties of a Pt atom in H-ZSM-5 because the Madelung potential also has an influence on the stretching frequency of CO.

#### 4. Conclusion

The interaction between platinum atom and H-ZSM-5 has been examined by using the DFT/B3LYP level of calculation with mixed basis sets. The choice of models representing the active site of the zeolite is critical to explain the interaction between Pt and H-ZSM-5 correctly. We found that a Pt atom interacts with a Brønsted proton and with a nearby bridging framework oxygen. The binding energy of Pt on the Brønsted acid is 15 kcal/mol. The electron transfer between Pt atom and H-ZSM-s results in an electron redistribution in the Pt atom, with more electron density in the s-orbital and less in the

d-orbital. A shift of Pt's d-orbitals due to interaction with the zeolite surface was observed. These results suggest that without the Brønsted acid site the Pt atom is not stable in H-ZSM-5 and so agglomeration of Pt atoms to form a larger particle is expected. The effect of the H-ZSM-5 support is not only to withdraw electron density from the Pt atom to the acidic proton, but also to provide electron density to the Pt atom through the framework oxygen.

The adsorption of carbon monoxide was also investigated. With use of the embedded cluster model, our model predicted an 8-11 cm<sup>-1</sup> red shift of adsorbed CO on PvH-ZSM-5, matching well with the experimental 20 cm<sup>-1</sup> red shift. The frequency shift of adsorbed CO on the zeolite surface reflects not only the electronic structure of supported Pt but also the extended zeolite framework environment. The Madelung potential was found to be necessary to obtain the accurate vibrational frequency and binding energy. The  $\pi$ -back-donation between CO and PvH-ZSM-5 was significant, as is seen from the increase of electron density in  $\pi$ \*-orbitals of CO.

Acknowledgment. This work was supported in part by the Thailand Research Fund (TRF), the University of Utah, and the National Science Foundation. Computer support from the Center for High Performance Computing at the University of Utah is gratefully acknowledged

#### References and Notes

- (1) Bandiera, J.; Naccache, C.; Imelik, B. J. Chim. Phys. Phys. -Chim. Biol. 1978, 75, 406.
- (2) Chupin, J.; Gnep, N. S.; Lacombe, S.; Guisnet, M. Appl. Catal., A 2001, 206, 43.
- (3) Biomsma, E.; Martens, J. A.; Jacobs, P. A. Stud. Surf. Sci. Catal. B 1997, 105, 909.
- (4) Watanabe, M.; Uchida, H.; Igarashi, H.; Suzoki, M. Chem. Len. 1995, 21.
- (5) Iwamoto, M.; Hernandez, A. M.; Zengyo, T. Chem. Commun. (Cambridge) 1997, 37.
- (6) Benvenutti, E. V.; Franken, L.; Moro, C. C.; Davanzo, C. U. Langmuir 1999, 15, 8140.
  - (7) Davis, R. J. Heterog. Chem. Rev. 1994, 1, 41.
  - (8) Dong, J.-L.; Zhu, J.-H.; Xu, Q.-H. Appl. Catal., A 1994, 112, 105.
  - (9) Cho, B. K.; Yie, J. E. Appl. Catal., B 1996, 10, 263.
  - (10) Gallezot, P. Mol. Sieves 2002, 3, 257.
  - (11) Samant, M. G.; Boudart, M. J. Phys. Chem. 1991, 95, 4070.
  - (12) Sachtler, W. M. H. Acc. Chem. Res. 1993, 26, 383.
  - (13) Stakheev, A. Y.; Kustov, L. M. Appl. Catal., A 1999, 188, 3.
- (14) Zhidomirov, G. M.; Yakovlev, A. L.; Milov, M. A.; et al. Caral. Taday 1999, 51, 397.
- (15) Bandiera, J. J. Chim. Phys. Phys.-Chim. Biol. 1980, 77, 303.
- (16) Silva, J. M.; Ribeiro, M. F.; Ramoa Ribeiro, F.; et al. Appl. Catal., A 1995, 125, 1.
- (17) Galperin, L. B.; Bricker, J. C.; Holmgren, J. R. Appl. Catal., A 2003, 239, 297.
- (38) Sugioka, M.; Tochiyama, C.; Matsumoto, Y.; Sado, F. Stud. Surf. Sci. Catal. 1995, 94, 544.
- (19) Kurosaka, T.; Sugioka, M.; Matsuhashi, H. Bull. Chem. Soc. Jpn. 2001, 74, 757.
- (20) Vasina, T. V.; Masloboishchikova, O. V.; Khelkovskaya-Sergeeva, E. G.; et al. Stud. Surf. Sci. Catal. 2001, 135, 4207.
  - (21) Arribas, M. A.; Martinez, A. Appl. Catal., A 2002, 230, 203.
- (22) Noordhoek, N. J.; Schuring, D.; de Gauw, F. J. M. M.; et al. Ind. Eng. Chem. Res. 2002, 41, 1973.
- (23) Kuznetsov, P. N. J. Catal. 2003, 218, 12.
- (24) Mills, G. A.; Heinemann, H.; Milliken, T. H.; Oblad, A. G. Ind. Eng. Chem. 1953, 45, 134.
- (25) Weisz, P. B.; Swegler, E. W. Science 1957, 126, 31.
- (26) Kuhlmann, A.; Roessner, F.; Schwieger, W.; et al. Cutal. Today 2004, 97, 303.
- (27) Mojet, B. L.; Miller, J. T.; Ramaker, D. E.: Koningsberger, D. C. J. Catal. 1999, 186, 373.
- (28) Gallezot, P.; Alarcon-Diaz, A.; Dalmon, J. A.; et al. J. Catal. 1975, 39, 334.
- (29) Lane, G. S.; Miller, J. T.; Modica, F. S.; Barr, M. K. J. Catal. 1993, 141, 465.

- (30) Sharma, S. B.; Miller, J. T.; Dumesic, J. A. J. Catal. 1994, 148, 198.
- (31) Vaarkamp, M.; Miller, J. T.; Modica, F. S., et al. Stud. Surf. Sci. Catal 1993, 75, 809.
- (32) Mojet, B. L.; Miller, J. T.; Komngsberger, D. C. J. Phys. Chem., B 1999, 103, 2724.
- (33) Khodakov, A.; Barbouth, N.; Berthier, Y.; et al. J. Chem. Soc., Faraday Trans. 1995, 91, 569.
- (34) Boyanov, B. I.; Morrison, T. I. J. Phys. Chem. 1996, 100, 16318.
- (35) Cho, S. J.; Ahn, W.-S.; Hong, S. B.; Ryoo, R. J. Phys. Chem. 1996, 100, 4996.
- (36) Lerner, B. A.; Carvill, B. T.; Sachtler, W. M. H. J. Mol. Catal. 1992, 77, 99.
- (37) Stakheev, A. Y.; Shpiro, E. S.; Tkachenko, O. P.; et al. J. Cotal. 1997, 169, 382.
- (38) Zholobenko, V. L.; Lei, G. D.; Carvill, B. T.; et al. J. Chem. Soc., Furaday Trans. 1994, 90, 233.
- (39) Tzou, M. S.; Sachtler, W. M. H. Stud. Surf. Sci. Catal. 1988, 38, 233.
- (40) Dalla Betta, R. A.; Boudart, M. Catal., Proc. Int. Congr., 5th 1973, 2, 1329.
- (41) Datka, J.; Gallezot, P.; Massardier, J.; Imelik, B. Rev. Port. Quim. 1977, 19, 297.
- (42) Weber, R. S.; Boudart, M.; Gallezot, P. Stud. Surf. Sci. Cotal. 1980, 4, 415.
- (43) Miller, J. T.; Mojet, B. L.; Ramaker, D. E.; Koningsberger, D. C. Catal. Today 2009, 62, 101.
- (44) Vedrine, J. C.; Dufaux, M.; Naccache, C.; Imelik, B. Proc. Int. Vac. Congr., 7th 1977, 1, 481.
  - (45) Sachtler, W. M. H.; Zhang, Z. Adv. Cotal. 1993, 39, 129.
- (46) Graenert, W.; Muhler, M.; Schroeder, K.-P.; et al. J. Phys. Chem. 1994, 98, 10920.
- (47) Mojet, B. L.; Kappers, M. J.; Miller, J. T.; Koningsberger, D. C. Stud. Surf. Sci. Catal. 1996, 101, 1165.
  - (48) Hammer, B.; Norskov, J. K. Nature (London) 1995, 376, 238.
- (49) Grillo, M. E.; Ramirez de Agudelo, M. M. J. Mal. Model. 1996, 2, 183.
- (50) Yakovlev, A. L.; Neyman, K. M.; Zhidomirov, G. M.; Roesch, N. J. Phys. Chem. 1996, 100, 3482.
- (51) Grillo, M. E.: Ramirez de Agudelo, M. M. J. Mol. Catal., A 1997, 179, 105.
- 779, 105.
  (52) Warwe, R. M.; Spiewak, B. E.; Corright, R. D.; Dumesic, J. A.
- Catal. Lett. 1998, 51, 139.
  (53) Curulla, D.; Clotel, A.; Ricarl, J. M.; Illas, F. J. Phys. Chem., B
  1999, 103, 5246.
- (\$4) Ramaker, D. E.; de Graaf, J.; van Veen, J. A. R.; Koningsberger, D. C. J. Catal. 2001, 203, 7.
- (55) Treesukol, P.: Limtrakul, J.; Truong, T. N. J. Phys. Chem. B 2001, 105, 2421.
  - (56) Derouane, E. G.; Fripiat, J. G. Zeolites 1985, 5, 165.
- (57) Alvarado-Swaisgood, A. E.; Barr, M. K.; Hay, P. J.; Redondo, A. J. Phys. Chem. 1991, 95, 10031.
- (58) Schroeder, K. P.; Sauer, J.; Leslie, M.; Callow, C. R. A. Zeolites 1992, 12, 20.
- (59) Stefanovich, E. V.; Truong, T. N. J. Phys. Chem. B 1998, 102, 3018.
- (60) Vollmer, J. M.; Stefanovich, E. V.; Truong, T. N. J. Phys. Chem. B 1999, 103, 9415.
- (61) Limtrakul, J.; Khongpracha, P.; Jungsuttiwong, S.; Truong, T. N. J. Mol. Catal. A: Chem. 2000, 153, 155.
  - (62) Hay, P. J.; Wadt, W. R. J. Chem. Phys. 1985, 82, 299.
  - (63) Boys, S. F.; Bernadi, F. Mol. Phys. 1970, 19, 553.
- (64) Simon, S.; Duran, M.; Dannenberg, J. J. J. Chem. Phys. 1996, 105. 1024.
- (65) Reed, A. E.; Weinhold, F.; Curtiss, L. A.; Pochatko, D. J. J. Chem. Phys. 1986, 84, 5687.
- (66) Frisch, M. J.; Trucks, G. W.; Schlegel, H. B.; et al. Gaussian 93, Revision A.1; Gaussian, Inc. Pittsburgh, PA, 2003.
- (67) Treesukol, P.; Tritong, T. N. Unpublished results.
- (68) Gallezot, P.; Bergeret, G. Stud. Surf. Sci Catal. 1982, 12, 167.
- (69) Sachtler, W. M. H.; Tzou, M. S.; Jiang, H. J. Solid State lonics 1988, 26, 71.
- (70) Kampers, F. W. H.; Engelen, C. W. R.; Van Hooff, J. H. C.; Koningsberger, D. C. J. Phys. Chem. 1990, 94, 8574.
- (71) Stakheev, A. Y.; Shpiro, E. S.; Jaeger, N. I.; Schulz-Ekloff, G. Catal. Lett. 1995, 34, 293.
  - (72) Blyholder, G. J. Phys. Chem. 1964, 68, 2772.



Available online at www.sciencedirect.com

BCIENCE DIRECT.

Journal of Molecular Structure 748 (2005) 119-127

Journal of MOLECULAR STRUCTURE

www.elsevier.com/locate/niolsiruc

# Computational study of the carbonyl-ene reaction of encapsulated formaldehyde in Na-FAU zeolite

Winyoo Sangthonga, Michael Probstb, Jumras Limtrakuja.\*

\*Laboratory for Computational and Applied Chemistry, Department of Chemistry, Kasetsort University, 50 Phahonyothin Road, Bangkok 10900, Thailand

\*Institut für Ionenphysik, Universität Innsbruck, Technikerstraße 25, 6020 Innsbruck, Austria

Received 26 January 2005; revised 2 March 2005; accepted 4 March 2005

#### Abstract

Density-functional theory (B3LYP/6-31G(d,p)) and the ONIOM (Our-own-N-layer Integrated molecular Orbital + molecular Mechanics) approach utilizing two-layer ONIOM schemes (B3LYP/6-31G(d,p):UFF) have been employed to investigate structures of Na-exchanged zeolite-encapsulated formaldehyde (HCHO@Na-zeolite) and their interactions with propylene. The carbonyl-ene reaction of propylene and formaldehyde was studied on three model systems: (1) formaldehyde in Na-exchanged zeolite: HCHO@Na-zeolite/CH<sub>3</sub>CH=CH<sub>2</sub>; (2) naked Na(I) as catalyst: Na(I)/HCHO/CH<sub>3</sub>CH=CH<sub>2</sub>; (3) a bare model where only the reactants are present: HCHO/CH<sub>3</sub>CH=CH<sub>2</sub>. It is found that inclusion of the extended zeolite framework has an effect on the structure and energetics of the adsorption complexes and leads to a lower energy barrier (25.1 kcal/mol) of the reaction as compared to the bare model system (34.4 kcal/mol). If the naked Na(I) interacts with the HCHO/CH<sub>3</sub>CH=CH<sub>2</sub> complex the energy barrier of the system is even lower than HCHO@Na-zeolite/CH<sub>3</sub>CH=CH<sub>2</sub>, due to the large electrostatic field generated by the naked Na(I) cation (17.5 kcal/mol). The carbonyl-ene reaction of propylene using HCHO@Na-faujasite takes place in a single concerted reaction step.

Keywords: Carbonyl-ene reaction; Alkali exchanged zeolite; Encapsulated formaldehyde; Electrostatic field; ONIOM

#### 1. Introduction

Carbonyl-ene reactions are a common path of hydrocarbon rearrangement [1,2] and an increasingly useful tool in synthesis [3-5]. Conventionally, carbonyl-ene reactions proceed according to a concerted mechanism in the presence of Lewis acids as catalysts.

In the field of organic chemistry, formaldehyde is well-known as one of the most versatile carbon electrophiles. However, its application is often limited by its intractability due to a low boiling point of -19.5 °C. Moreover, it rapidly tends to polymerize to solid paraformaldehyde and trioxane. Therefore, in order to obtain formaldehyde monomer, thermal or Lewis acid treatment is used to depolymerize paraformaldehyde or trioxane, just prior to use. However,

these corrosive catalysts cause a number of problems concerning safety, corrosion, handling and waste disposal.

An immense endeavor has been put into developing alternative, more environmentally friendly catalytic systems such as zeolites. Zeolite catalysts also have the advantage of high selectivity towards the desired product due to the shape-selective properties of their acid sites and their microcrystal pore structure.

More recently, the successful storage of formaldehyde using zeolite was reported [6]. It enables the suppression of the decomposition and self-polymerization without losing the reactivity of formaldehyde toward nucleophiles. Na-faujasite type zeolites can now be used to encapsulate formaldehyde. As a result, the carbonyl-ene reaction between formaldehyde and olefins has progressively moved toward zeolite-based processes.

To clearly envision the formaldehyde/zeolite system, a theoretical study can provide insight into reaction mechanisms on a molecular level, thus complementing experimental investigations by obtaining information about properties that are not directly accessible by experimental investigations.

0022-2869/\$ - see front matter @ 2005 Elsevier B.V. All rights reserved. doi:10.1016/j.molstruc.2005.03.020

<sup>\*</sup> Corresponding author. Tel.: +66 2942 8900x323; fax: +66 2942 8900x324.

E-muit address: fscijel@ku.ac.th (J. Limtrakul).

Numerous theoretical models have been proposed to study crystalline zeolite. The electronic properties of zeolites are usually modeled using quantum chemical methods and relatively small clusters that focus only on the most important part of zeolites [7-10]. The disadvantage of such small models is that they do not take into account the effects of the framework, which play an important role to change the structure and energetics of the system significantly. The recent development of hybrid methods such as embedded cluster or combined

quantum mechanics/molecular mechanics (QM/MM) method [11-18], as well as the ONIOM [17,18] scheme has brought accurate results on a larger system within reach.

The ONIOM (Our-own-N-layer Integrated molecular Orbital+molecular Mechanics) method [17,18] is often applied to study extended systems [19-23], and has also successfully been applied to zeolites in studies of the adsorption of ethylene, benzene and ethylbenzene over acidic and alkaline faujasite and ZSM-5 zeolites [22,24-26].

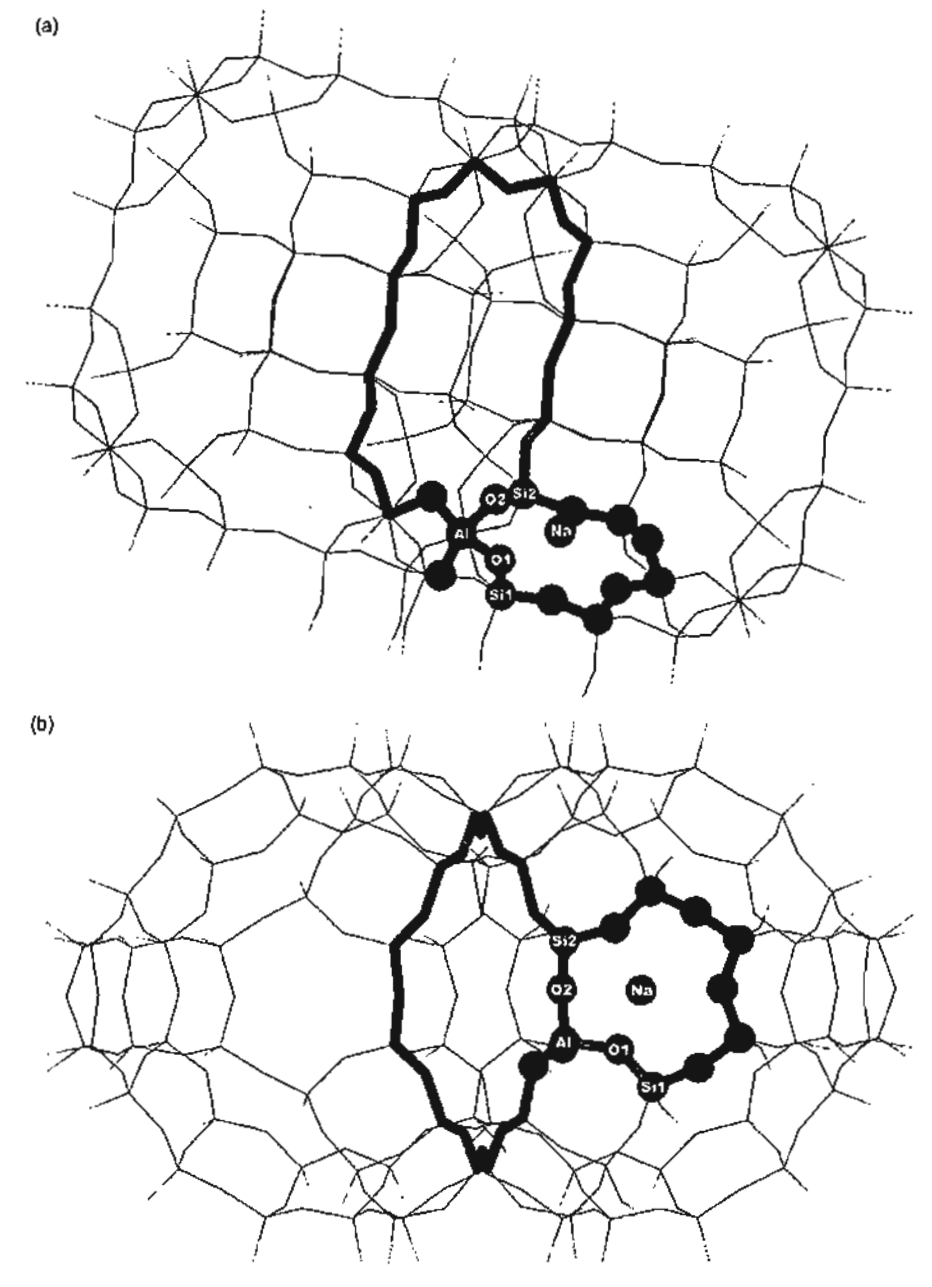


Fig. 1. ONIOM2 model of the 84T cluster. The 6-ring quantum cluster is drawn as bond and stick model and the 12T ring window is drawn with sticks; (a) side view; (b) upper view.

This efficient scheme yielded adsorption energies close to the experimental estimates and could elucidate the reaction mechanisms of benzene alkylation with ethylene on acidic faujasite zeolite [27].

#### 2. Method

In the ONIOM model, the system is separated into at least two parts. The inner layer consists of the active region, typically modeled by a small cluster using density-functional theory, to account for the interactions of adsorbates with the acid site of zeolite. The outer layer represents the zeolite framework and is described by a molecular mechanics force field to account for the van der Waals interactions due to confinement of the microporous structure [22,26–33].

In the present study, we have employed the ONIOM method to model the active site of alkaline-exchanged zeolites. Specifically, we study the reaction mechanism of the carbonyl-ene reaction between an encapsulated formal-dehyde molecule and alkene on Na-exchanged faujasite. We choose propylene to represent an alkene molecule because it is the smallest one with the required basic structure. We also study the carbonyl-ene reaction without the zeolite oxygen framework surrounding the alkaline cation in order to understand the role of alkaline-exchanged zeolites in the carbonyl-ene reaction.

This system described by three models of different sophistication:

(1) The ONIOM2 (B3LYP/6-31G(d,p):UFF) approach is applied to a model of 84T faujasite. The 84T cluster includes two supercages serving as a nanometer-size chemical reactor where the adsorbates can be trapped

inside. Its geometry is taken from the lattice structure of faujasite zeolite [34]. For Na-exchanged faujasite, the alkaline-metal cation does not bind with a particular bridging oxygen atom of [AlO<sub>4</sub>]<sup>-</sup> but sits in front of the 6-ring inside the supercage [35] (Fig. 1). The interaction of the cationic metal with the zeolite framework leads to perturbation of the active acidic site.

The active region consists of the 6-ring inside the supercage (Fig. 1), which can be considered as the smallest unit required to represent the acidic site of zeolite and that of the reactive molecules. It is treated with the B3LYP density-functional and the 6-31G(d,p) basis set. The extended framework environment is included on the molecular mechanics level with the universal force field (UFF).

(2) Density-functional calculations with the same method and basis set but without the zeolite, i.e. on Na(I)/HCHO/CH<sub>3</sub>CH=CH<sub>2</sub> and (3) on the two reactants alone, i.e. on HCHO/CH<sub>3</sub>CH=CH<sub>2</sub>, were also performed.

All the computational work has been performed by using the Gaussian 98 code [36]. In the ONIOM2 method, only the 6-ring quantum cluster (NaSi5AlO8, see Fig. 1) and the adsorbates (HCHO and CH3CH=CH2) were fully optimized. Normal mode analyses were carried out to verify the transition states to have one imaginary frequency whose mode correspond to the designated reaction. In (2) and (3) all atomic positions are optimized. For all three models, additional single-point energy calculations with the 6-311++G(d,p) and 6-311++G(d,p) basis sets have also been carried out, and the basis set superposition errors (BSSE) was estimated by the counterpoise (CP) method. The charge distribution in the complexes has been analyzed via the natural population analysis (NPA) [37-41] partitioning scheme applied to the B3LYP/6-31G(d,p) densities.

Table 1

Optimized geometric parameters of reactants, transition state and products of the carbonyl-ene reaction between formaldehyde and propylene on Na-faujasite using the ONIOM2 (B3LYP/6-31G(d,p):UFF) method (bond lengths are in pm and bond angles are in degrees)

Parameters	Naked Na-FAU	Formaldehyde adsorption	Coadsorption complex	Transition state	Product
Distances			_		
C-O	_	122.2	122.2	131.7	144.2
C1-C3	<b>-</b>	-	133.6	141.1	150.7
C2-C3	_	-	150.3	141.8	133.7
C3-H	-	~	109.8	122.0	270.6
C-C1	_	-	348.5	180.9	153.5
O-H	-	_	408.7	152.6	97.2
Na-O	-	233.1	232.1	225.4	231.1
Na-Al	315.9	315.t	319.7	323.A	314.6
Na-01	216.5	220.5	221.6	216.3	221.0
Na-O2	262.7	263.7	272.1	276.5	263.1
AJO1	180.0	179.1	179.1	180.0	179.1
Al-O2	174.9	174,7	174.3	174.9	174.6
\$i1~O1	160.7	161.1	161.1	160,7	160.7
\$i2-O2	158.1	158.5	158.4	158.1	158.4
Angles					
O1-AIO2	97.6	99.4	100.1	97.6	99.5
Si1-01-A?	138.1	138.3	138.2	1.881	138.7
Si2-O2-A1	146.3	145.5	145.3	146.3	145.3

#### 3. Results and discussion

We separate the discussion into Sections 3.1-3.3. In Section 3.1, we discuss the structure of the Na-exchanged faujasite zeolite, and then we demonstrate the existence of encapsulated formaldehyde in Na-exchanged faujasite zeolite (HCHO@Na-faujasite) in order to study the reactivity of this species, and finally we report the study of their interactions with propylene using

the ONIOM model. A symbol (M@S) is interpreted to signify that a molecule M is adsorbed on an active site S of zeolite

#### 3.1. Na-exchanged faujasite zeolite

Recent studies [24-33] have shown that the van der Waals interactions between hydrocarbons, or aromatic adsorbates and a zeolitic framework contribute

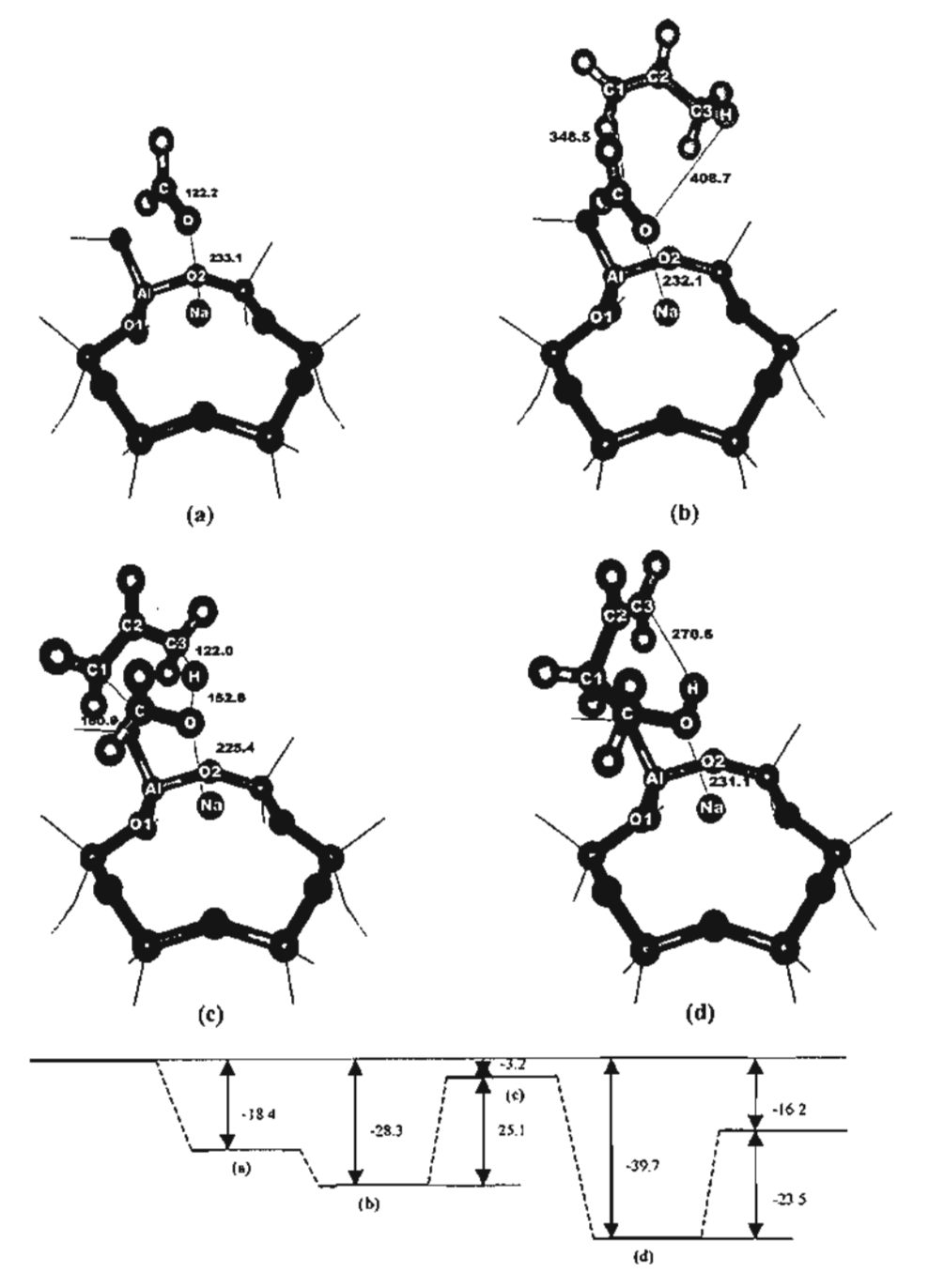


Fig. 2. Structures and calculated energy profile (kcal/mol) of the HCHO@Na-faujasite/CH<sub>3</sub>CH=CH<sub>2</sub> complexes: (a) HCHO@Na-faujasite complex; (b) coadsorption complex; (c) transition state structure; and (d) product structure.

significantly to the structural and energetic features of the adsorption-desorption processes in zeolites. Thus, hybrid methods such as QM/MM and ONIOM should be able (and necessary) to describe these interactions with the zeolite framework reasonably well. In our case, we

employed the ONIOM method to the system HCHO@Na-faujasite/CH<sub>3</sub>CH=CH<sub>2</sub>.

The structure of Na-exchanged faujasite is shown in Fig. 1 and the optimized geometrical parameters are documented in Table 1. The charge of Na in the zeolite

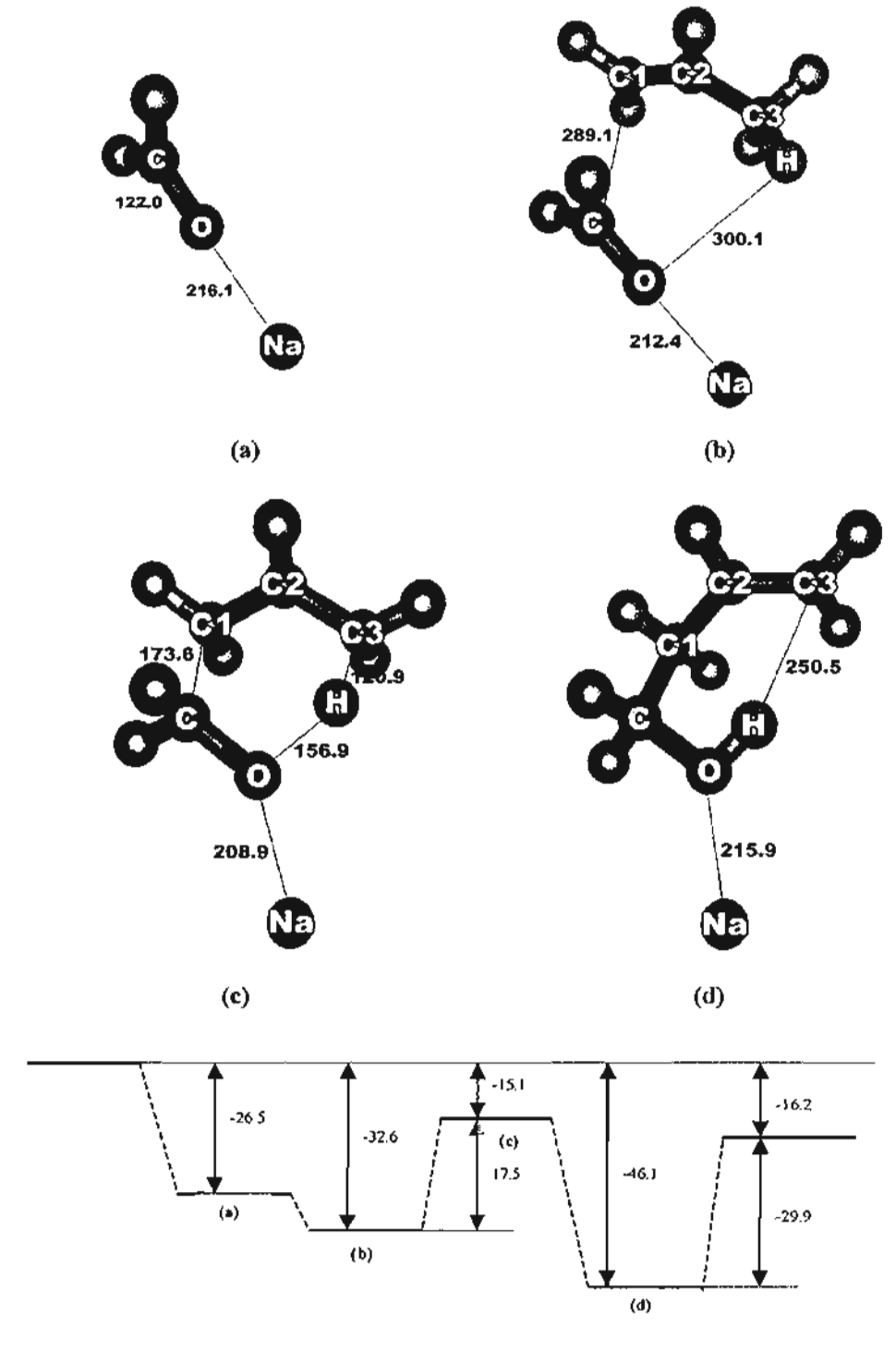


Fig. 3. Structures and calculated energy profile (kcal/mol) of the HCHO@Na(I)/CH<sub>3</sub>CH=CH<sub>2</sub> complexes: (a) HCHO@Na(I) complex; (b) coadsorption complex; (c) transition state structure; and (d) product structure.

Table 2
Atomic charge distribution calculated from the natural population analysis (NPA)

	Isolated Bare system			Naked Na ion system			Na-FAU	Na-FAU zeolite system				
	molecule	Coads.*	TS	Product	Form. ads.b	Coads *	TS	Product	Form. ads.6	Coads."	T\$	Product
q(Na)	1.00	-		-	0.98	0.98	0.96	0.97	0.91	0.91	0.91	0.92
q(O)	-0.49	-0.51	-0.66	-0.76	-0.67	-0.71	-0.88	-0.89	-0.61	-0.61	~0.79	-0.84
g(C)	0.23	0.22	-0.02	-0.09	0.31	0.27	-0.04	-0.10	0.26	0.26	-0.02	-0.10
q(C1)	-0.44	-0.46	-0.53	-0.53	_	-0.45	-0.55	0.53	-	-0.47	-0.55	-0.54
q(C2)	-0.22	-0.21	-0.09	-0.23	_	-0.20	0.07	-0.25	_	-0.22	0.01	-0.25
q(C3)	-0.73	-0.72	-0.73	-0.45	-	-0.72	-0.75	-0.43	_	-0.72	-0.74	0.44
q(H)	0.25	0.26	0.38	0.48	-	0.23	0.35	0.52	_	0.24	0.36	0.51

<sup>\*</sup> Coadsorption complex of formaldehyde and propylene.

supercage is calculated (NPA) to be 0.93. It is compensated by the surrounding oxygen atoms in the 6-ring inside the supercage.

## 3.2. Na-exchanged faujasite encapsulated formaldehyde (HCHO@Na-faujasite)

Fig. 2a displays the structure of formaldehyde as stabilized in the zeolite framework. Selected optimized geometrical parameters are listed in Table 1. Formaldehyde first interacts with the active Lewis acid site by its lone electron pair. This leads only to small changes in the zeolite structure (less than 2 pm and 2° for changes in bond distances and bond angles, respectively). The carbonoxygen bond of formaldehyde is elongated from 120.7 to 122.2 pm. The distance between the formaldehyde oxygen and the Na atom of zeolite is 233.1 pm and the corresponding adsorption energy for the HCHO@Nafaujasite complex is 18.4 kcal/mol due to the interaction between the hydrogen atoms of formaldehyde and the oxygen atoms of the framework. The C-O···Na(I) angle is 124.1°, in contrast to the model system without faujasite (2) where it is linear and the sodium cation in HCHO@Na(I) interacts directly with the oxygen atom of formaldehyde (Fig. 3a). In system (2), the C-O bond of formaldehyde bond is elongated from 120.7 to 122.0 pm

due to the presence of Na(I) and the Na-O distance is 216.1 pm. The binding energy of this complex is  $-26.5 \, \text{kcal/mol}$ . A test calculation at QCISD(T) level of theory with 6-311G(d,p) basis set gave  $-25.8 \, \text{kcal/mol}$  [42]. The results of the NPA analysis (Table 2) correspond to the trends in the binding energies: The NPA-charge of Na(I) in HCHO@Na(I) is  $+0.98 \, \text{while}$  it is  $+0.91 \, \text{in}$  the zeolite system and the charges of the oxygen atom of formaldehyde are -0.67 (system (2)) and -0.61 (system (3)), respectively.

# 3.3. Carbonyl-ene reaction between Na-exchanged faujasite encapsulated formaldehyde and propylene (HCHO@Na-faujasite/CH<sub>3</sub>CH=CH<sub>2</sub>)

The carbonyl-ene reaction can proceed via concerted interaction in the coadsorption complex of the Na-exchanged faujasite zeolite-encapsulated formaldehyde with the propylene without any intermediate. The reaction steps can be written as follow:

$$\rightarrow$$
 CH<sub>2</sub>=CHCH<sub>2</sub>CH<sub>2</sub>OH@Na-faujasite (2)

Table 3

Optimized geometric parameters of the carbonyl-ene reaction between formaldehyde and propylene for the bare system and the naked Na ion system from B3LYP/6-31G(d,p) calculations (bond lengths are in pm and bond angles are in degrees)

Parameters	isolated mol- ecule	Bare system			Naked Na(I) ion system			
		Coads.	TS	Product	Form. ads.b	Coads.*	TS	Product
Distances								
C-O	120.7	120.9	128.7	141.6	122.0	122.7	133.7	147.7
C1-C2	133.3	133.5	139.5	150.4	-	134.1	142.0	150.7
C2-C3	151.2	150.0	141.6	133.5	-	149.8	141.9	133.8
C3H	109.6	109.7	128.2	280.5	_	110.0	120.9	250.5
C-C1	_	340.5	197.0	154.0	•	289.1	173.6	153.3
OH	-	266.6	135.4	96.9	_	300.1	157.0	97.7
NaO	-	-	-	-	216.1	212.4	208.9	235.9

<sup>\*</sup> Coadsorption complex of formaldehyde and propylene.

b Formaldehyde adsorption.

Formaldehyde adsorption.

CH2 = CHCH2CH2OH@Na-faujasite

$$\rightarrow$$
 CH<sub>2</sub> = CHCH<sub>2</sub>CH<sub>2</sub>OH + Na-faujasite (3)

Step (1) is the adsorption of formaldehyde onto the Lewis acid site of the zeolite. Step (2) involves the interaction of the encapsulated formaldehyde with propylene, resulting in the adsorbed product (3-buten-1-ol), which is desorbed in the final Step (3). The selected optimized geometrical parameters of the carbonyl-ene reaction between propylene and encapsulated formaldehyde in Na-faujasite zeolite are listed in Table 1 and the same parameters of the naked Na(1) ion system and the system without sodium cation are given in Table 3. Under typical reaction temperatures, formal-dehyde readily adsorbs on the Lewis acid site via lone pair electron interaction, but propylene interacts only weakly with the Lewis acid site via a π-interaction.

The entire reaction energy profile is presented in Fig. 2. The reaction is initiated by coadsorption of propylene on the encapsulated formaldehyde at the active site of the zeolite (Fig. 2b). The propylene molecule diffuses over the adsorbed formaldehyde on the Na-exchanged faujasite zeolite with a coadsorption energy of 28.3 kcal/mol. In the naked Na(I) ion system, the coadsorption of the propylene stabilizes the adsorption complex by -32.6 kcal/mol. The distance between formaldehyde carbon (C) and propylene carbon (C1) is calculated to be 289.1 pm. Due to the larger electrostatic field generated by the naked Na(I) ion, this distance is shorter than in system (1) (348.5 pm). In system (3), however, the coadsorption energy (Fig. 4a) is only -3.3 kcal/mol and the distance between the formaldehyde carbon (C) and the carbon atom of propylene (C1) is 340.5 pm. This indicates that the carbon of the formaldehyde carbonyl group is more electrophilic if it is coordinated to the naked Na(I) than in the bare system (3).

The carbonyl-ene reaction involves concerted bond forming between the carbon atom of formaldehyde (C) and the propylene carbon (C1) and the breaking of a propylene proton (H) giving the proton to the formaldehyde oxygen (O). At the transition state, the complex exhibits one imaginary frequency (Fig. 2c). The corresponding vibrational motion shows the concerted mechanism of the carbonyl-ene reaction: A carbon-carbon bond is formed between encapsulated formaldehyde and propylene and, simultaneously, a propylene proton leaves toward the formaldehyde oxygen atom. At the transition state, the Lewis acid slightly changes its position on the zeolite (by less than 5 pm, concerning changes in distance between Na and atoms Al, Ol, O2 of the zeolite framework) and the distance between formaldehyde oxygen and Na atom becomes 225.4 pm. The propylene C3-H bond distance is lengthened from 109.8 to 122.0 pm and the distance between propylene proton (H) and formaldehyde oxygen (O) becomes 152.6 pm while the C-O double bond of the formaldehyde is elongated from 122.2 to 131.7 pm, whereas the distance between the propylene carbon (C1) and

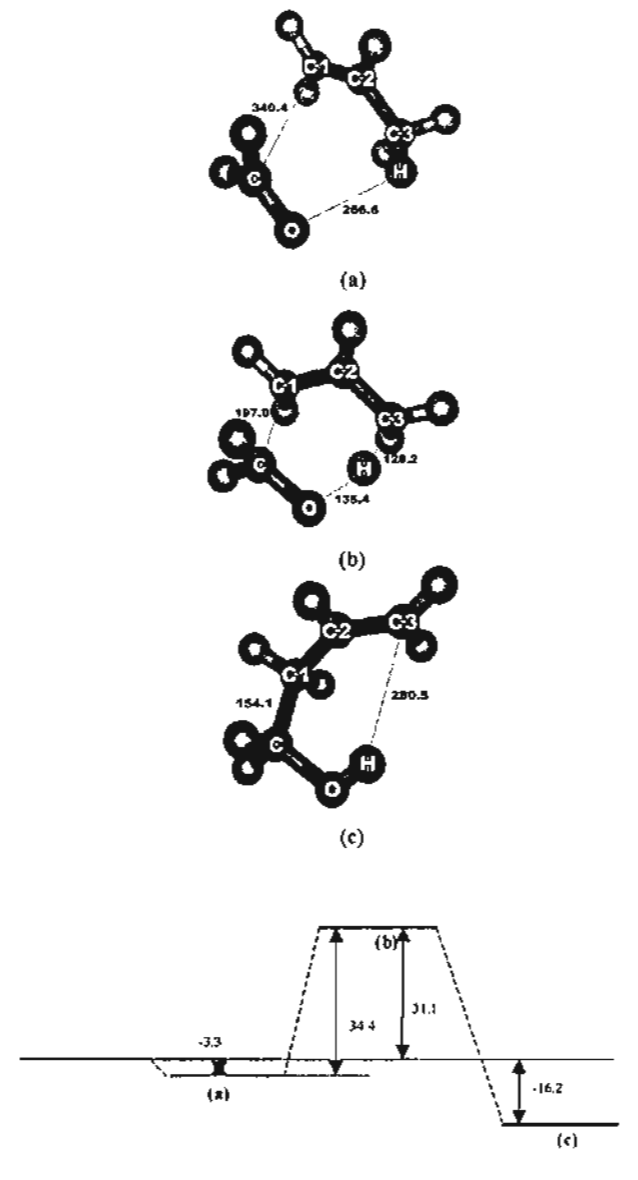


Fig. 4. Structures and calculated energy profile (kcal/mol) of the HCHO/CH<sub>2</sub>CH=CH<sub>2</sub> complexes: (a) coadsorption complex; (b) transition state structure; and (c) product structure.

formaldehyde carbon (C) becomes 180.9 pm. The C1-C2 and C2-C3 bond length change from 133.6 and 150.3 to 141.1 and 141.8 pm, respectively. The activation energy for this transition state is 25.8 kcal/mol. In the case of naked Na(I) ion system (2), the distance between the propylene carbon (C1) and formaldehyde carbon (C) is contracted from 289.3 to 173.6 pm and the C1-C2 and C2-C3 bond lengths change from 134.1 and 149.82 to 142.0 and 141.9 pm, respectively, whereas the propylene C3-H bond distance is significantly lengthened from 110.0 to 120.9 pm and the distance between propylene proton (H) and formaldehyde oxygen (O) becomes 157.0 pm while the C-O double bond of formaldehyde is elongated from 122.7 to 133.7 pm. The activation energy is 17.5 kcal/mol and

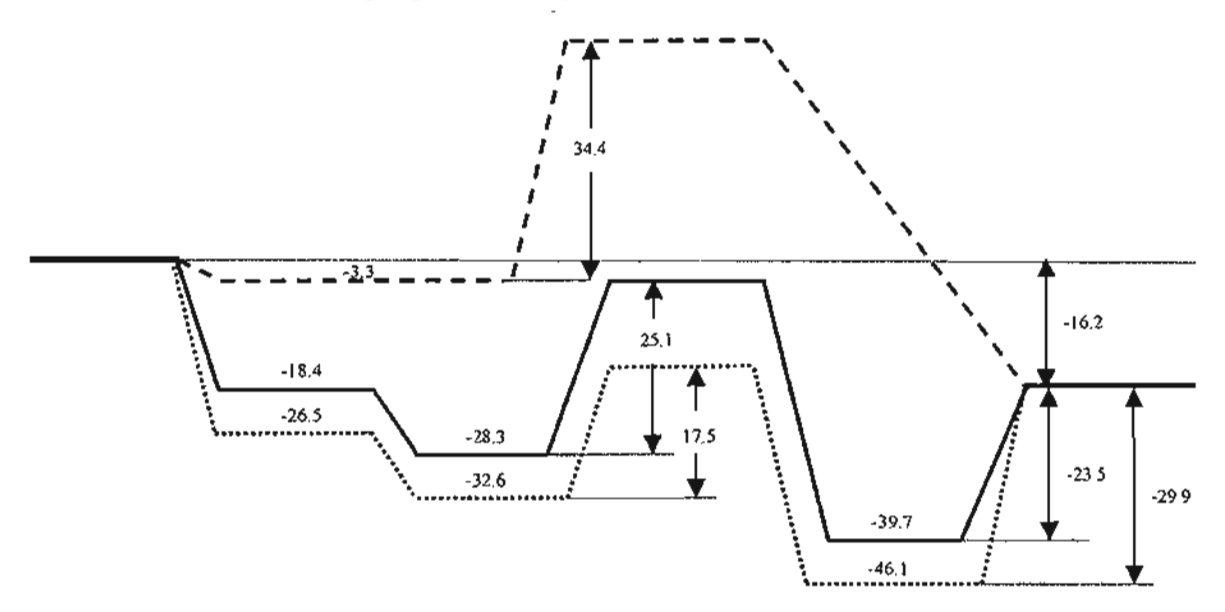


Fig. S. Calculated energetic profiles (kcal/mol) for the carbonyl-one reaction between HCHO and CH<sub>2</sub>CH=CH<sub>2</sub> in the Na-faujasite zeolite system (solid line), the naked Na(1) system (dotted line) and the bare system (dashed line).

the apparent activation energy is -15.1 kcal/mol. These results demonstrated that the electrostatic contribution from the naked Na<sup>+</sup> ion stabilizes the transition state structure. Therefore, the activation energy barrier of this system (2) is lower than in the HCHO@Na-faujasite system (1).

In the bare system (3) (Fig. 4b) the C-C1 bond distance is contracted from 340.5 to 197.0 pm. The distance between propylene proton (H) is elongated from 109.7 to 128.2 pm while the distance between formaldehyde oxygen (O) and propylene proton (H) becomes 135.4 pm. The length of the C1-C2 and C2-C3 bonds in propylene change from 134.11 and 149.82 to 142.04 and 141.87 pm, respectively. The reaction coordinate (the normal mode that has an imaginary frequency) indicates again the concerted mechanism of carbonyl-ene reaction. The activation energy is 34.4 kcal/mol and the reaction energy is -16.2 kcal/mol. This can be compared to the experimental data reported by Benson et al. (43), which are 26.4 and -13.5 kcal/mol, respectively.

The product state (Fig. 2d), in which the C-C1 bond is formed involves a proton transfer from the carbon atom of propylene to the formaldehyde oxygen. The adsorbed 3-buten-1-ol product is subsequently desorbed endothermically, requiring 23.5 kcal/mol. In the naked Na(I) ion system, the product oxygen interacts with the Na(I) ion via electrostatic interaction to the lone electron pair of the product. With a binding energy of -29.9 kcal/mol, the interaction of Na(I) with the product is stronger than that in the case of formaldehyde. The distances between the product oxygen and the Na(I) ion in both systems (the naked Na(I) ion system (2) and the Na-faujasite system (1)) are calculated to be 215.9 and 231.1 pm, respectively. The NPA analysis shows that the charge of Na(I) in system

(2) is larger (+0.97) than in the Na@faujasite (3) system (+0.92).

The energy diagrams of the three systems (1)-(3) are put into one plot in Fig. 5. For the Na-exchanged faujasite zeolite (3), the activation energy of the reaction is 25.1 kcal/mol, which lies between the activation barriers of the bare system (3) (34.4 kcal/mol) and the naked Na(I) system (2) (17.5 kcal/mol). This is due to the electrostatic field generated by the Na(I) ion and the destabilizing role of the oxygen atom in the zeolite lattice surrounding the cation. These results indicate that alkaline-exchanged faujasite zeolite can be used as a catalyst in carbonyl-ene reaction and that they stabilize all species in the carbonyl-ene reaction systems. Na-exchanged faujasite especially can preserve formaldehyde in a monomeric form and can also activate it sufficiently to promote its reaction with various olefins.

#### 4. Conclusions

The carbonyl-ene reaction between formaldehyde and propylene has been investigated theoretically. Three different models were employed to model the carbonyl-ene reaction system: (1) Na-exchanged faujasite zeolite, (2) the naked Na(I) ion system, and (3) the bare system. The reaction occurs via a concerted mechanism without an intermediate and involves a proton transfer from propylene to formaldehyde and a carbon-carbon bond formation which occur simultaneously at the transition state. The interaction between Na-exchanged faujasite zeolite and formaldehyde leads to a structure in which formaldehyde is stabilized in the zeolite framework. The energy barrier for this system is calculated to be 25.1 kcal/mol and

the apparent activation energy is -3.2 kcal/mol. It is well established that carbonyl-ene reactions are catalyzed by Lewis acids. In order to gain some insight into the mechanism by which a Lewis acid can catalyze this reaction, we employed Na(I) as a Lewis acid in order to compare these results (2) with the results from the Naexchanged zeolite system (1). The activation barrier in system (2) is even lower (17.5 kcal/mol), due to the electrostatic interaction between the naked Na(I) ion and the complex. In the bare system (3) where no zeolite framework or electrostatic field from Na(I) are present, the structure of the transition state is a 6-membered ring and its energy barrier is 34.4 kcal/mol. The results indicate that Naexchanged faujasite can preserve formaldehyde in a monomeric form and can also act as a Lewis acid which can catalyze the carbonyl-ene reaction of formaldehyde with olefins without the presence of potentially harmful acidic chemicals.

#### Acknowledgements

This work was supported in part by grants from the Thailand Research Fund (TRF Senior Research Scholar to JL) and the Kasetsart University Research and Development Institute (KURDI), as well as the Ministry of University Affairs under the Science and Technology Higher Education Development Project (MUA-ADB funds). Support from the National Nanotechnology Center under the National Science and Technology Development Agency is also acknowledged.

#### References

- [1] B.B. Snider, Acc. Chem. Res. 13 (1980) 426.
- [2] H.M.R. Hoffmann, Angew. Chem. Int. Ed. Engl. 8 (1969) 556.
- [3] W. Oppolzer, Angew. Chem. Int. Ed. Engl. 23 (1984) 876.
- [4] W. Oppolzer, V. Snieckus, Angew. Chem. Int. Ed. Engl. 17 (1978) 476.
- [5] M. Vandewalle, P. De Clercq, Tetrahedral 41 (1985) 1767.
- [6] T. Okachi, M. Onaka, J. Am. Chem. Soc. 126 (2004) 2306-2307.
- [7] J. Sauer, P. Ugliengo, E. Garrone, V.R. Saunders, Chem. Rev. 94 (1994) 2095.
- [8] J. Sauer, P. Ugliengo, E. Garrone, V.R. Saunders, Chem. Rev. 89 (1989) 199.
- [9] J. Limtrakul, Chem. Phys. 193 (1995) 79-87.
- [10] J. Limtrakul, P. Treesukol, C. Ebner, R. Sansone, M. Probst, Chem. Phys. 215 (1997) 77-87.
- [11] J. Limtrakul, S. Jungsuttiwong, P. Khongpracha, J. Mol. Struct. 525 (2000) 153-162.
- [12] P.E. Sinclair, A. de Vries, P. Sherwood, C.R.A. Catlow, R.A. van Santen, J. Chem. Soc. Faraday Trans. 94 (1998) 3401-3408.
- [13] M. Braeadle, J. Sauer, J. Am. Chem. Soc. 120 (1998) 1556-1570.
- [14] S.P. Greatbanks, I.H. Hillier, N.A. Burton, P. Sherwood, J. Chem. Phys. 105 (1996) 3770-3776.

- [15] R.Z. Khaliullin, A.T. Bell, V.B. Kazansky, J. Phys. Chem. A 105 (2001) 10454-10461.
- [16] J. Limtrakul, T. Nanok, S. Jungsuttiwong, P. Khongpracha, T.N. Truong, Chem. Phys. Lett. 349 (2001) 161-166.
- [17] A.H. de Vries, P. Sherwood, S.J. Collins, A.M. Rigby, M. Rigutto, G.J. Kramer, J. Phys. Chem. B 103 (1999) 6133-6141.
- [18] M. Svensson, S. Humbel, R.D.J. Froese, T. Matsubara, S. Sieber, K. Morokuma, J. Phys. Chem. 100 (1996) 19357-19363.
- [19] H.R. Tang, K.N. Fan, Chem. Phys. Lett. 330 (2000) 509-514.
- [20] I. Roggero, B. Civalleri, P. Ugliengo, Chem. Phys. Lett. 341 (2001) 625-632.
- [21] K. Sillar, P. Burk, J. Mol. Struct. (Theochem) 589-590 (2002) 281-290.
- [22] S. Kasuriya, S. Namuangruk, P. Treesukol, M. Tirtowidjojo, J. Limtrakul, J. Catal. 219 (2003) 320-328.
- [23] M. Torrent, T. Vreven, D.G. Musaev, K. Morokuma, O. Farkas, H.B. Schlegel, J. Am. Chem. Soc. 124 (2002) 192-193.
- [24] C. Raksakoon, J. Limtrakul, J. Mol. Struct. (Theochem) 631 (2003) 147-156.
- [25] W. Panjan, J. Limtrakul, J. Mol. Struct. 654 (2003) 35-45.
- [26] K. Bobuatong, J. Limtrakul, Appl. Catal. A: Gen. 253 (2003) 49-64.
- [27] S. Namuangruk, P. Pantu, J. Limtrakul, J. Catal. 225 (2004) 523-530.
- [28] A. Pelmenschikov, J. Leszczynski, J. Phys. Chem. B 103 (1999) 6886-6890.
- [29] T.A. Wesolowski, O. Parisel, Y. Ellinger, J. Weber, J. Phys. Chem. A 101 (1997) 7818-7825.
- [30] E.G. Derouane, C.D. Chang, Micropor. Mesopor. Mater. 35-36 (2000) 425-433.
- [31] L.A. Clark, M. Sierka, J. Sauer, J. Am. Chem. Soc. 125 (2003) 2136– 2141.
- [32] A.M. Vos, X. Rozanska, R.A. Schoonheydt, R.A. van Santen, F. Hutschka, J. Hafner, J. Am. Chem. Soc. 123 (2001) 2799-2809.
- [33] X. Rozanska, R.A. van Santen, F. Hutschka, J. Hafner, J. Am. Chem. Soc. 123 (2001) 7655-7667.
- [34] D.H. Olson, E. Dempsey, J. Catal. 13 (1969) 221.
- [35] C. Beauvais, X. Guerrault, F.-X. Coudert, A. Boutin, A.H. Puchs, J. Phys. Chem. B 108 (2004) 399-404.
- [36] M.J. Frisch, G.W. Trucks, H.B. Schlegel, G.E. Scuseria, M.A. Robb, J.R. Cheeseman, V.G. Zaktzewski, J.A. Montgomery, R.E. Stratmann Jr., J.C. Burant, S. Dapprich, J.M. Millam, A.D. Daniels, K.N. Kudin, M.C. Strain, O. Farkas, J. Tomasi, V. Barone, M. Cossi, R. Cammi, B. Mennucci, C. Pomelli, C. Adamo, S. Clifford, J. Ochterski, G.A. Petersson, P.Y. Ayala, Q. Cui, K. Morokuma, P. Salvador, J.J. Dannenberg, D.K. Malick, A.D. Rabuck, K. Raghavachari, J.B. Foresman, J. Cioslowski, J.V. Ortiz, A.G. Baboul, B.B. Stefanov, G. Liu, A. Liashenko, P. Piskorz, I. Komaromi, R. Gomperts, R.L. Martin, D.J. Fox, T. Keith, M.A. Al-Laham, C.Y. Peng, A. Nanayakkara, M. Challacombe, P.M.W. Gill, B. Johnson, W. Chen, M.W. Wong, J.L. Andres, C. Gonzalez, M. Head-Gordon, E.S. Replogle, J.A. Pople, Gaussian 98, 2001.
- [37] A.E. Reed, L.A. Curtiss, F. Weinhold, Chem. Rev. 88 (1988) 899.
- [38] J.E. Carpenter, F. Weinhold, J. Mol. Struct. (Theochem) 169 (1988)
- [39] J.P. Foster, F. Weinhold, J. Am. Chem. Soc. 102 (1980) 7211.
- [40] A.E. Reed, F. Weinhold, J. Chem. Phys. 78 (1983) 4066.
- [41] A.E. Reed, R.B. Weinstock, F. Weinhold, J. Chem. Phys. 83 (1985) 735.
- [42] M. Remko, Chem. Phys. Lett. 270 (1997) 369-375.
- [43] S.W. Benson, H.E. O'Neal, Kinetic Data on Gas Phase Unimolecular Reactions; National Standard and Reference Data Series, 1970.



Acta Crystallographica Section E
Structure Reports
Online
USSN 1600-5368
Editors: W. Clegg and D. G. Watson

### Ethane-1,2-diaminium hexaaquazinc(II) sulfate Apinpus Rujiwatra and Jumras Limtrakul

Copyright O International Union of Crystallography

Author(s) of this paper may foad this reprint on their own web site provided that this cover page is retained. Republication of this article or its storage in electronic databases or the like is not permitted without prior permission in writing from the IUCr.

Acta Cryst. (2005). E61, m1403-m1404

Apinpus and Jumras . (C2H10N2)|Zn(H2O)6)(SO4)2

Received 17 May 2005 Accepted 21 June 2005

Online 24 June 2005

Acta Crystallographica Section & Structure Reports Online ISSN 1600-5368

# Apinpus Rujiwatra\* and Jumras

Department of Chemistry, Faculty of Science, Chiane Mai University, Chiang Mai 50700. Thailand, and Department of Chemistry, Faculty of Science, Kasetsart University, 8angkok 10900, Thadland

Correspondence e-mail: apinpus@chiangmai.ac.th

Limtrakul<sup>b</sup>

Single-crystal X-ray study 7 = 293 K

Key indicators

Mean σ(C-C) = 0 003 Å R factor = 0.024

wR (actor = 0.054 Data-to-parameter ratio = 13.9

for details of how these key indicators were automatically derived from the article, see http://journals.iucr.org/e.

#### Ethane-1,2-diaminium hexaaquazinc(II) sulfate

The crystal structure of the title compound, (C<sub>2</sub>H<sub>10</sub>N<sub>2</sub>)-[Zn(H2O)6]>(SO4)2, comprises Zn31 complex cations, sulfate anions and diprotonated ethane-1,2-diamine (DAE). The Zn<sup>II</sup> atom is located on an inversion centre and is coordinated by six water molecules in an octahedral geometry. The DAE dication is located on another inversion centre. Hydrogen bonding occurs between anions and cations but not between DAE and Zn11 complex cations.

$$\begin{bmatrix} H_{2}O \\ H_{2}O_{H_{1}} \\ H_{2}O \end{bmatrix} \xrightarrow{\text{Re}} \begin{bmatrix} H_{2}O \\ H_{2}O \end{bmatrix} = \begin{bmatrix} H_{3}N \\ H_{2}O \end{bmatrix} \cdot 2 \text{ SO}_{4}^{2}$$
(I)

#### **Experimental**

The reaction mixture was prepared by dissolving ZnSO4.7H2O (RDH 98%) in ethanol (Merck 95%), into which ethylenediamine, en (Carlo Erba 98%), was added while stirring vigorously. A white precipitate with a compositional molar ratio of ZnSO4-7H2O:en:C2H5OH 1:0.1:100 was formed. The mixture was refluxed at 353 K for 6 h before allowing it to cool to room temperature. The white precipitate did not dissolve and was separated from the clear solution, into which an equivalent volume of deionized water was added. On storing at room temperature, single crystals of (I) were obtained from the solution after 24 h. Due to the acidic properties of the starting reagent, ZnSO4-7H2O and ethanol, protonation of en was assumed and confirmed from Fourier-transform IT spectroscopy (FT-IR) using a Nicolet 510 F T-IR spectrophotometer over the range 4000-400 cm<sup>-1</sup>. Samples were prepared as KBr pellets. The FT-IR spectrum showed a deformation band characteristic of NH<sub>3</sub><sup>+</sup> at 2100 cm<sup>-1</sup> and a shoulder centred at 2800 cm<sup>-1</sup> corresponding to NH stretching shifted to a lower wavenumber due to protonation of the amino group.

Crystal data

 $D_s = 1.895 \text{ Mg m}^{-3}$  $(C_2H_{10}N_2)[Zn(H_2O)_6](SO_4)_2$  $M_r = 427.71$ Mo Kα radiation Monoclinic, P2,/n Cell parameters from 1676 a = 8.1827 (6) A reflections b = 7.0914 (5) Å $\theta = 1.6-28.2^{\circ}$  $\mu = 1.99 \text{ mm}^{-1}$ c = 13.1674 (9) Å $T \approx 293 (2) \text{ K}$  $\beta = 101.154 (1)^{\circ}$  $V = 749.63 (9) \text{ Å}^3$ Needle, colourless Z = 2 $0.17 \times 0.05 \times 0.03 \text{ mm}$ 

Data collection

 $R_{\rm int} = 0.023$ Nonius KappaCCD diffractometer  $\theta_{\text{max}} = 25.2^{\circ}$ φ and ω scans  $h = -9 \rightarrow 9$ Absorption correction: none  $k = -8 \rightarrow 5$ 3753 measured reflections  $I = -15 \rightarrow 15$ 1352 independent reflections 1308 reflections with  $I > 2\sigma(I)$ 

© 2005 International Union of Crystallography Printed in Great Britain - all rights reserved

> m1403 doi:10.1107/\$1600\$36805019604 Apinpus and Jumras . (Caltin Nation (H2O), 1(5O4)2 electronic repaint

#### metal-organic papers

Refinement

Refinement on  $F^2$   $R[F^2 > 2\sigma(F^2)] = 0.024$   $wR(F^2) = 0.064$  S = 1.141352 reflections

97 parameters H-atom parameters constrained  $w = 1/(\sigma^{2}(F_{o}^{2}) + (0.0267P)^{2} + 0.7365P)$   $where P = (F_{o}^{2} + 2F_{c}^{2})/3$   $(\Delta/\sigma)_{max} = 0.001$   $\Delta\rho_{max} = 0.55 \text{ e Å}^{-3}$   $\Delta\rho_{mn0} = -0.42 \text{ e Å}^{-3}$ 

$D-H\cdots A$	D - H	$H \cdot \cdot \cdot A$	$D \cdots A$	$D - H \cdots A$
Q1-H3Q5	0.93	1.82	2.7335 (19)	167
O1-H4O4"	0.90	1.84	2.7466 (19)	178
Q2-H5···O7 <sup>id</sup>	0.87	1.98	2.8052 (19)	159
O2-H6O6	0.90	1.80	2.701 (2)	173
O3−H7···O7 <sup>#4</sup>	0.82	2.14	2.8312 (19)	143
O3-H8···O5**	0.87	1.87	2.7322 (19)	167
N1-H1AO6	0.87	2.04	2.856 (2)	156
N1-H1AO5'	0.87	2.50	3.214 (2)	140
N1-H18O7	0.91	1.91	2.820 (2)	173
N1-H1C04	0.80	2.03	2.826 (2)	168

Symmetry codes: (i)  $-x + \frac{1}{2}, y + \frac{1}{2}, -z + \frac{3}{2}$  (ii) x + 1, y, z; (iii) -x, -y, -z + 1; (iv)  $x + \frac{1}{2}, -y + \frac{1}{2}, z - \frac{1}{2}$ ; (v) x, y + 1, z.

H atoms on the N and O atoms were located in a difference Fourier map and were refined as riding in their as-found relative positions to carrier atoms. Methylene H atoms were placed in calculated positions, with C-H=0.97 Å, and included in the final cycles of refinement in the riding model, with  $U_{iso}(H)=1.5U_{eq}(C)$ .

Data collection: COLLECT (Nonius, 1998); cell refinement: SCALEPACK (Otwinowski & Minor, 1997); data reduction: SCALEPACK and DENZO (Otwinowski & Minor, 1997); program(s) used to solve structure: SHELXS97 (Sheldrick, 1997); program(s) used to refine structure: SHELXL97 (Sheldrick, 1997); molecular graphics: ORTEP3 for Windows (Farrugia, 1997); software used to prepare material for publication: WinGX (Farrugia, 1999).

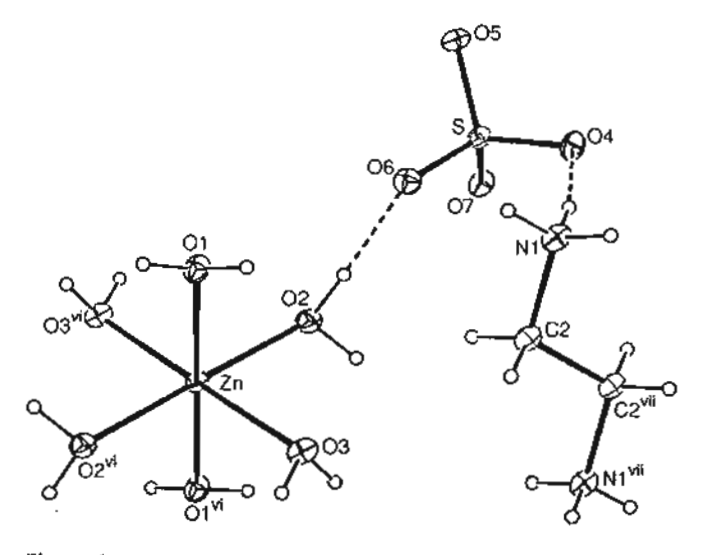


Figure 1 The molecular structure of (1) with 30% probability displacement ellipsoids (arbitrary spheres for H atoms). Dashed lines indicate hydrogen bonds. [Symmetry codes: (vi) 1-x, -y, 1-z; (vii) -x, 1-y, 1-z.]

The authors thank the Thailand Research Fund for research funding.

#### References

Farrugia, L. J. (1997). J. Appl. Cryst. 30, 565.

Farrugia, L. J. (1999). J. Appl. Cryst. 32, 837-838.

Nonius (1998). COLLECT. Nonius BV, Delft, The Netherlands.

Otwinowski, Z. & Minor, W. (1997). Methods in Enzymology, Vol. 276, Macromolecular Crystallography, Part A, edited by C. W. Carter Jr & R. M. Sweet, pp. 307-326. New York: Academic Press.

Sheldrick, G. M. (1997). SHELXS97 and SHELXL97. University of Göttingen, Germany.

# ภาคผนวก ข.

สรุปผลงาน ในการประชุมนานาชาติ

### ภาคผนวก ข.1

ผลงานในการประชุมนานาชาติ
"American Chemical Society National
Meeting ครั้งที่ 225"
จำนวน 4 เรื่อง



#### Paper #626279

# Effects of the zeolite framework on the structure and energetics of the active site of H-ZSM-5/C<sub>2</sub>H<sub>4</sub> complexes: An ONIOM method

Jumras Limtrakul<sup>1</sup>, Max Tirtowidjojo<sup>2</sup>, and Wasinee Panjan<sup>1</sup>. (1)
Department of Chemistry, Kasetsart University, Department of Chemistry,
Faculty of Science, Kasetsart University, Phaholyothin Rd., Ladyao, Jatujak,
Bangkok 10900, Thailand, Fax: 066-02-5793955, fscijrl@nontri.ku.ac.tb, (2)
Reaction Engineering, Engineering Sciences, The Dow Chemical Company

The applicability and reliability of the two-layer ONIOM2 (Our-own-N-layer Integrated molecular Orbital+ molecular Mechanics) approaches have been carried out on different aluminosilicate clusters representing H-ZSM-5 zeolitic catalysts containing up to 46 tetrahedrally coordinated tetravalent atoms and their interaction with ethylene. When carefully calibrated, by using the experimental observation, the ONIOM2 (B3LYP/6-311++G(d,p):HF/3-21) scheme, in which an inner part of the system containing the active site is treated at the B3LYP/6-311++G(d,p) level, and the rest - using the HF/3-21G - has been found to provide reliable information for calculating the effects of the extended zeolite framework on the structural and energetic properties of the C2H4/H-ZSM-5 system. The predicted adsorption energy for this ONIOM2 scheme is -9.14 kcai/mol, which corresponds well with the experimental estimate of -9 kcal/mol.

#### **ACCEPTED**

**Abstract ID#:** 626279 **Password:** 884806

**Program Selection:** Division of Inorganic Chemistry

Topic Selection: Catalysis: Poster Session

Title: Effects of the zeolite framework on the structure and energetics of the

active site of H-ZSM-5/C2H4 complexes: An ONIOM method

Invited: N

Presentation Format: Poster Only

Consider for Sci-Mix: Y Conforms to Bylaw 6: Y

**First Author** 

**Presenting**Jumras Limtrakul
Department of Chemistry

Kasetsart University
Department of Chemistry, Faculty of Science, Kasetsart University
Phanolyothin Rd., Ladyao, Jatujak

Bangkok, 10900

Thalland

Phone Number: 066-02-9407070 Fax Number: 066-02-5793955

Publishable Email: fscijrl@nontrl.ku.ac.th

#### Second Author

Max Tirtowidjojo
Reaction Engineering, Engineering Sciences
The Dow Chemical Company
2301 Brazosport Blvd., B-1226
Freeport, TX 77541-3257

Phone Number: 979-238-4109 Fax Number: 979-238-0140

Publishable Emall: maxt@dow.com

#### **Third Author**

Wasinee Panjan
Department of Chemistry
Kasetsart University
Department of Chemistry, Faculty of Science, Kasetsart University
Phaholyothin Rd., Ladyao, Jatujak
Bangkok, 10900
Thailand

Publishable Email: g4464032@ku.ac.th

Thalland

Publishable Email: dakojung@hotrmail.com

#### Fifth Author

Piti Treesukol
Department of Chemistry
Kasetsart University
Department of Chemistry, Faculty of Science, Kasetsart University
Phaholyothin Rd., Ladyao, Jatujak
Bangkok, 10900
Thalland

Publishable Email: ptreesukol@hotmall.com



#### Paper #629738

Effects of the zeolite framework on the structure and energetics of active site of H-ZSM-5/C<sub>6</sub>H<sub>6</sub> complexes: A QM/MM method

Chadchalerm Raksakoon, and Jumras Limtrakul, Department of Chemistry, Kasetsart University, Department of Chemistry, Faculty of Science, Kasetsart University, Phaholyothin Rd., Ladyao, Jatujak, Bangkok 10900, Thailand, chadchalerm@hotmail.com

The adsorption of benzene on H-ZSM-5 zeolites has been investigated with four different cluster sizes and methods comprising various two-level ONIOM2 schemes: B3LYP/6-31G(d,p):HF/3-21G, B3LYP/6-31G(d,p):UFF, and HF/3-21G:UFF. The bare 3T quantum cluster approach predicts the [C6H6]/H-ZSM-5 complexes to have the binding energies of -5.99 kcal/mol. The effect of the zeolite framework is modeled on the ONIOM2 method. We found that the extended framework significantly enhances the adsorption energy of benezene to the zeolites. In particular, the final predicted adsorption energy of -13.75 kcal/mol for the [C6H6]/H-ZSM-5 complexes was calculated by the ONIOM2(MP2/6-31G(d,p):HF/3-21G) scheme. This efficient scheme performs superbly as compared with the experimental estimate of -14.0 kcal/mol. The results obtained in the present study suggest that the ONIOM approach yields a more accurate and practical model in studying adsorption of unsaturated hydrocarbons on zeolites.

#### ACCEPTED

**Abstract ID#:** 629738 **Password:** 759156

**Program Selection:** Division of Petroleum Chemistry

**Topic Selection:** General Papers

Title: Effects of the zeolite framework on the structure and energetics of

active site of H-ZSM-5/C6H6 complexes: A QM/MM method

Invited: N

Presentation Format: Oral Consider for Sci-Mix: N Conforms to Bylaw 6: Y Preprint submitted: YES!

#### First Author

Presenting

Chadchalerm Raksakoon

Department of Chemistry
Kasetsart University
Department of Chemistry, Faculty of Science, Kasetsart University
Phaholyothin Rd., Ladyao, Jatujak
Bangkok, 10900
Thalland

Phone Number: 410-531-4205

Publishable Email: chadchalerm@hotmail.com

\* ACS Member

#### **Second Author**

Jumras Limtrakul
Department of Chemistry
Kasetsart University
Department of Chemistry, Faculty of Science, Kasetsart University
Phaholyothin Rd., Ladyao, Jatujak
Bangkok, 10900
Thailand

Phone Number: 066-02-9407070 Fax Number: 066-02-5793955

Publishable Email: fscijri@nontri.ku.ac.th



## Paper #626277

# Adsorption of aromatic hydrocarbon onto H-ZSM-5 zeolite investigated by ONIOM study

Jumras Limtrakul, and Chadchalerm Raksakoon, Department of Chemistry, Kasetsart University, Department of Chemistry, Faculty of Science, Kasetsart University, Phaholyothin Rd., Ladyao, Jatujak, Bangkok 10900, Thailand, Fax: 066-02-5793955, fscljrl@nontri.ku.ac.th

The ONIOM (Our-own-N-layer Integrated molecular Orbital+ molecular Mechanics) approach utilizing two-layer ONIOM2 schemes - ONIOM2(MP2/6-31G(d,p):HF/3-21), ONIOM2(B3LYP/6-31G(d,p):HF/3-21), ONIOM2(B3LYP/6-31G(d,p):UFF), and ONIOM2 (HF/3-21:UFF) - have been used to investigate adsorption properties of benzene in zeolites. The active site has been modeled with different cluster sizes up to 46 tetrahedra. Our results predict that benzene is favorably located in the Intersection of straight and sinusoidal channels which is supported by the recent power neutron and synchrotron X-ray diffraction techniques. The predicted adsorption energy for the ONIOM2(MP2/6-31G (d,p):HF/3-21) scheme is -13.75 kcal/mol, which corresponds well with the experimental estimate of -14.0 kcal/mol.

#### ACCEPTED

Abstract ID#: 626277 Password: 822662

Frogram Selection: Division of Inorganic Chemistry

Topic Selection: Catalysis: Poster Session

Title: Adsorption of aromatic hydrocarbon onto H-ZSM-5 zeolite investigated by ONIOM

study

Invited: N

**Presentation Format: Poster Only** 

Consider for Sci-Mix: Y Conforms to Bylaw 6: Y

First Author

#### Presenting

Jumras Limtrakul

Department of Chemistry

Kasetsart University

Department of Chemistry, Faculty of Science, Kasetsart University

Phaholyothin Rd., Ladyao, Jatujak

Bangkok, 10900

Thalland

Phone Number: 066-02-9407070 Fax Number: 066-02-5793955

Publishable Email: fscijri@nontri.ku.ac.th

#### **Second Author**

32.

::

:5

Chadchalerm Raksakoon
Department of Chemistry
Kasetsart University
Department of Chemistry, Faculty of Science, Kasetsart University
Phaholyothin Rd., Ladyao, Jatujak
Bangkok, 10900
Thailand

Publishable Emall: chadchalerm@hotmail.com



## Paper #626279

## Effects of the zeolite framework on the structure and energetics of the active site of H-ZSM-5/C2H4 complexes: An ONIOM method

Jumras Limtrakul<sup>1</sup>, Max Tirtowidjojo<sup>2</sup>, and Wasinee Panjan<sup>1</sup>. (1) Department of Chemistry, Kasetsart University, Department of Chemistry, Faculty of Science, Kasetsart University, Phaholyothin Rd., Ladyao, Jatujak, Bangkok 10900, Thalland, Fax: 066-02-5793955, fscijri@nontri.ku.ac.th, (2) Reaction Engineering, Engineering Sciences, The Dow Chemical Company

The applicability and reliability of the two-layer ONIOM2 (Our-own-N-layer Integrated molecular Orbital+ molecular Mechanics) approaches have been carried out on different aluminosilicate clusters representing H-ZSM-5 zeolitic catalysts containing up to 46 tetrahedrally coordinated tetravalent atoms and their Interaction with ethylene. When carefully calibrated, by using the experimental observation, the ONIOM2 (B3LYP/6-311++G(d,p):HF/3-21) scheme, in which an inner part of the system containing the active site is treated at the B3LYP/6-311++G(d,p) level, and the rest - using the HF/3-21G - has been found to provide reliable information for calculating the effects of the extended zeolite framework on the structural and energetic properties of the C2H4/H-ZSM-5 system. The predicted adsorption energy for this ONIOM2 scheme is -9.14 kcal/mol, which corresponds well with the experimental estimate of -9 kcal/mol.

#### **ACCEPTED**

**Abstract ID#:** 626279 Password: 884806

Program Selection: Division of Inorganic Chemistry

Topic Selection: Catalysis: Poster Session

Title: Effects of the zeolite framework on the structure and energetics of the

active site of H-ZSM-5/C<sub>2</sub>H<sub>4</sub> complexes: An ONIOM method

Invited: N

Presentation Format: Poster Only

Consider for Sci-Mix: Y Conforms to Bylaw 6: Y

First Author

#### Presenting

Jumras Limtrakul Department of Chemistry Kasetsart University

Department of Chemistry, Faculty of Science, Kasetsart University

Phaholyothin Rd., Ladyao, Jatujak

Bangkok, 10900

Thailand

Phone Number: 066-02-9407070 Fax Number: 066-02-5793955

Publishable Email: fscijrl@nontri.ku.ac.th

#### **Second Author**

Max Tirtowidjojo Reaction Engineering, Engineering Sciences The Dow Chemical Company 2301 Brazosport Blvd., B-1226 Freeport, TX 77541-3257

Phone Number: 979-238-4109 Fax Number: 979-238-0140

Publishable Email: maxt@dow.com

Publishable Email: g4464032@ku.ac.th

#### Third Author

Wasinee Panjan
Department of Chemistry
Kasetsart University
Department of Chemistry, Faculty of Science, Kasetsart University
Phaholyothin Rd., Ladyao, Jatujak
Bangkok, 10900
Thailand

### ภาคผนวก ข.2

ผลงานในการประชุมนานาชาติ

"Advances in Petrochemicals and
Polymers in the New Millennium ครั้งที่ 1"
จำนวน 4 เรื่อง

#### An International Conference on Advances in Petrochemicals and Polymers in the New Millennium July 22-25,2003 Bangkok, Thailand

## INTERACTIONS OF METHANE WITH NANOSTRUCTURED CATALYST: A MOLECULAR MODELLING STUDY

S. Pabchanda, P. Pantu, D. Tantanak, and J. Limtrakul\*
Laboratory for Computational & Applied Chemistry, Physical Chemistry Division, Kasetsart University,
Bangkok 10900, THAILAND

\*Corresponding Author E- mail address: fscijrl@ku.ac.th

#### INTRODUCTION

Owing to the nanocrystalline framework, zeolites can uniquely stabilize metal ions producing interesting catalytic characteristics. Iron exchanged ZSM-5 zeolite (Fe-ZSM-5) exhibits remarkable redox behaviors, e.g., selective oxidation of benzene to phenol and methane to methanol. The structures of such an extraordinary redox site, called  $\alpha$ -site, have been recently investigated experimentally and theoretically but are still not conclusive. Adsorption of N<sub>2</sub>O and CH<sub>4</sub> on the Fe-ZSM-5 is considered the initial step for the gas-solid catalytic reaction. However experimental studies are often lacking due to the time intensive and expensive measurement procedure. The adsorption of Fe-ZSM-5 can, alternatively, be investigated using quantum mechanics. In this work, the interactions of N<sub>2</sub>O with FeO-ZSM-5 and CH<sub>4</sub> with FeO<sub>2</sub>-ZSM-5 have been studied for the first time using an ONIOM2 method with the aim of investigating the effects of the extended zeolitic framework on the structure and function of the N<sub>2</sub>O/FeO-ZSM-5 and CH<sub>4</sub>/FeO<sub>2</sub>-ZSM-5 complexes.

#### METHOD

9) (4) (8)

His Co Po-Red Sith

The 5T small clusters are treated quantum chemically (QM = B3LYP, MP2) to represent the active region where chemical reaction taken place. The next layer enclosing the quantum region is carried out at the efficient universal force field (UFF) to explicitly cover dispersive forces. These contributions account for confinement effects in zeolite nanocavities which have been found to play a major role in stabilizing the van der Waals hydrocarbon/zeolite adduct.

#### RESULTS AND DICUSSION

The previous full quantum calculations have reported the adsorption energy of -6.6 kcal/mol for N<sub>2</sub>O adsorption on Fè-ZSM-5 using 5T cluster model [2]. The calculated energy is significantly lower than the experimental value of -16 kcal/mol[1]. The discrepancy is due to the fact that the cluster calculation, basically, neglect the confinement effect arising from the zeolite pore structure which has been found to important for adsorption-desorption and reaction in real zeolites. To practically account for the effect of extended framework of zeolite, the ONIOM2 (B3LYP/6-31G\*\*:UFF) was employed to study adsorption of N<sub>2</sub>O and CH<sub>4</sub> in Fe-ZSM-5. The corrected adsorption energy at the MP2 level of calculation by ONIOM2 (MP2/6-31G\*\*:UFF//B3LYP/6-31G\*\*:UFF) is -16.0 kcal/mol. Indicating that the extended framework significantly enhances, the adsorption of N<sub>2</sub>O and with a proper energy correction method the ONIOM2 model can yield accurate adsorption energy. This efficient scheme has also been proven to give reliable information for adsorption energy of related systems, e.g., the energy for CH<sub>4</sub>/H-ZSM-5 -5.5 kcal/mol compared well with experimental value (-5.0 kcal/mol) [3]. With the ONIOM2 (B3LYP/6-31G\*\*:UFF) scheme, the adsorption energy of -6.5 kcal/mol for [(CH<sub>4</sub>)(FeO<sub>2</sub>)]\*[ZSM-5]\* complexes was predicted. Thus, the predicted adsorption energy should correspond well with the experimental estimate, if available.

Table 1. The adsorption energies (kcal/mol) for the  $N_2O/FeO-ZSM-5$  and  $CH_4/FeO_2-ZSM-5$  systems.

Method	Adsorption energies (kcal/mol)			
r	N2O/FeO-ZSM-5	CH <sub>4</sub> /FeO <sub>2</sub> -ZSM-5		
Full ST(B3LYP/6-31G**)	-6.8	-3.7		
ONIOM2-46T(B3LYP/6-31G**:UFF)	-13.7	-6.5		
ONIOM2-46T(MP2/6-31G**:UFF//B3LYP/6-31G**:UFF)	-16.0	-7.3		
Experiment	-16.0[1]	-		

#### An International Conference on Advances in Petrochemicals and Polymers in the New Millennium July 22-25,2003 \*Bangkok, Thailand

#### CONCLUSION

M

15

() (i) (ii)

rit Lis

RE

The extended framework significantly enhances the adsorption energy of methane to the zeolites. With ONIOM2 (B3LYP/6-31G\*\*:UFF) scheme, the adsorption energy of N<sub>2</sub>O on Fe-ZSM-5 was accurately calculated to be -16.0 kcal/mol, the adsorption energy of -7.3 kcal/mol for the [CH<sub>4</sub>]/Fe-ZSM-5 complexes was predicted. The results obtained in the present study suggest that the ONIOM approach yields a more accurate and practical model in studying adsorption of hydrocarbons on zeolites and also studying mechanisms of oxidation of methane to methanol using N<sub>2</sub>O as oxidant.

#### REFERENCES

- [1] Wood, B.R., Reimer, J.A., and Bell, A.T. (2002), "Studies of N<sub>2</sub>O Adsorption and Decomposition on Fe-ZSM-5," J. Catal., 209, pp 151-158.
- [2] Ryder, J.A., Chakraborty, A.K., and Bell, A.T. (2002), "Density Functional Theory Study of Nitrous Oxide Decomposition over Fe and Co-ZSM-5," J. Phys. Chem. B, 106, pp 7059-7064.
- [3] Khaliullin, R.Z., and Bell, A.T. (2001), "An Experimental and Density Functional Theory Study of the Interactions of CH<sub>4</sub> with H-ZSM-5," J. Phys. Chem. A, 105, pp 10454-10461.

## An International Conference on Advances in Petrochemicals and Polymers in the New Millennium July 22-25,2003 •Bangkok, Thailand

## REATION MECHANISM OF FORMALDEHYDE OXIME ON H-FAU ZEOLITE: ROLE OF EMBEDDED CLUSTER MODEL

J. Sirijaraensre and J. Limtrakul\*

Laboratory for Computational & Applied Chemistry, Physical Chemistry Division, Kasetsart University,

Bangkok 10900, Thailand

\* Corresponding Author E-mail: fscijrl@ku.ac.th

#### INTRODUCTION

The Beckmann rearrangement is an industrially important reaction for production of  $\varepsilon$ -caprolactam, a raw material for the production of Nylon-6. The reaction is conventionally catalyzed by oleum or concentrated sulfuric acid, thus causing serious problems of waste disposal and reactor corrosion. The use of solid acid catalysts can markedly lessen the problems. Therefore, the vapor phase Beckmann rearrangement in large-pore zeolites has received serious attention as an alternative.

#### **EXPERIMENTAL**

In this work, we study the interactions between formaldehyde oxime with faujasite zeolite (H-FAU), the simplest model reaction of the Beckmann rearrangement. The 12T cluster model is used to represent the FAU zeolite and the effect of zeolite framework is included using ab initio embedded method. The Beckmann rearrangement reaction of formaldehyde oxime with the active site of zeolite has been investigated using the bare cluster, embedded cluster [1].

#### RESULTS AND DICUSSION

The mechanism of the Beckmann rearrangement on H-FAU zeolite is composed of two key steps. The first step is the 1,2 H-shift, which is the transformation from the N-bound configuration structure (interactions of formaldehyde oxime via its nitrogen-end with H-FAU zeolite) to the O-bound configuration structure (interactions of formaldehyde oxime via its oxygen-end with H-FAU zeolite). The adsorption energies of N-bound configuration structure is calculated to be -32.6 and -51.9 kcal/mol for bare cluster and embedded cluster models, respectively. While the adsorption energy of O-bound configuration is calculated to be -21.3 and -31.7 kcal/mol for bare cluster and embedded cluster models, respectively. The stronger adsorption energies (more exothermic) of the nitrogen-end adsorption suggest that the first step of the Beckmann rearrangement is the interaction between the nitrogen atom of formaldehyde oxime and the acid site in agreement with previously reported experimental data [2]. The next step is the rearrangement of the oxime compound to the amide compound. The migration of the hydride group from C-H4 bond eliminates the water molecule. The lone pair electrons of oxygen atom (O5) of the leaving water molecule attach to the carbon atom of [HNC\*H], giving the proton (H1) back to the zeolite framework. The final complex is an adsorption of enol formed amide compound adsorbed on H-FAU zeolite.

**Table 1.** Comparison the adsorption energy,  $\Delta E_{ads}$  (in kcal/mol) along the Beckmann rearrangement of formaldehyde oxime on different models of zeolite.

<u>cti</u>			
Geometry/method	12T Bare cluster	12T Embedded cluster	10T Embedded cluster
	of FAU zeolite	of FAU zeolite	of ZSM5 zeolite
k:	$\Delta E_{ads}$	$\Delta E_{ads}$	$\Delta E_{ads}$
N-bound complex (fig. 1(a))	-32.6	-51.9	-46.6
11,2 H-shift TS complex (fig. 1(b))	-3.3	-20.8	-16.0
·O-bound complex (fig. 1(c))	-21.3	-31.7	-27.7
Rearrangement TS (fig. 1(d))	38.7	26.3	6.2
Amide complex (fig. l(e))	~55.1 <u></u>	-64.1	-63.2

#### CONCLUSION

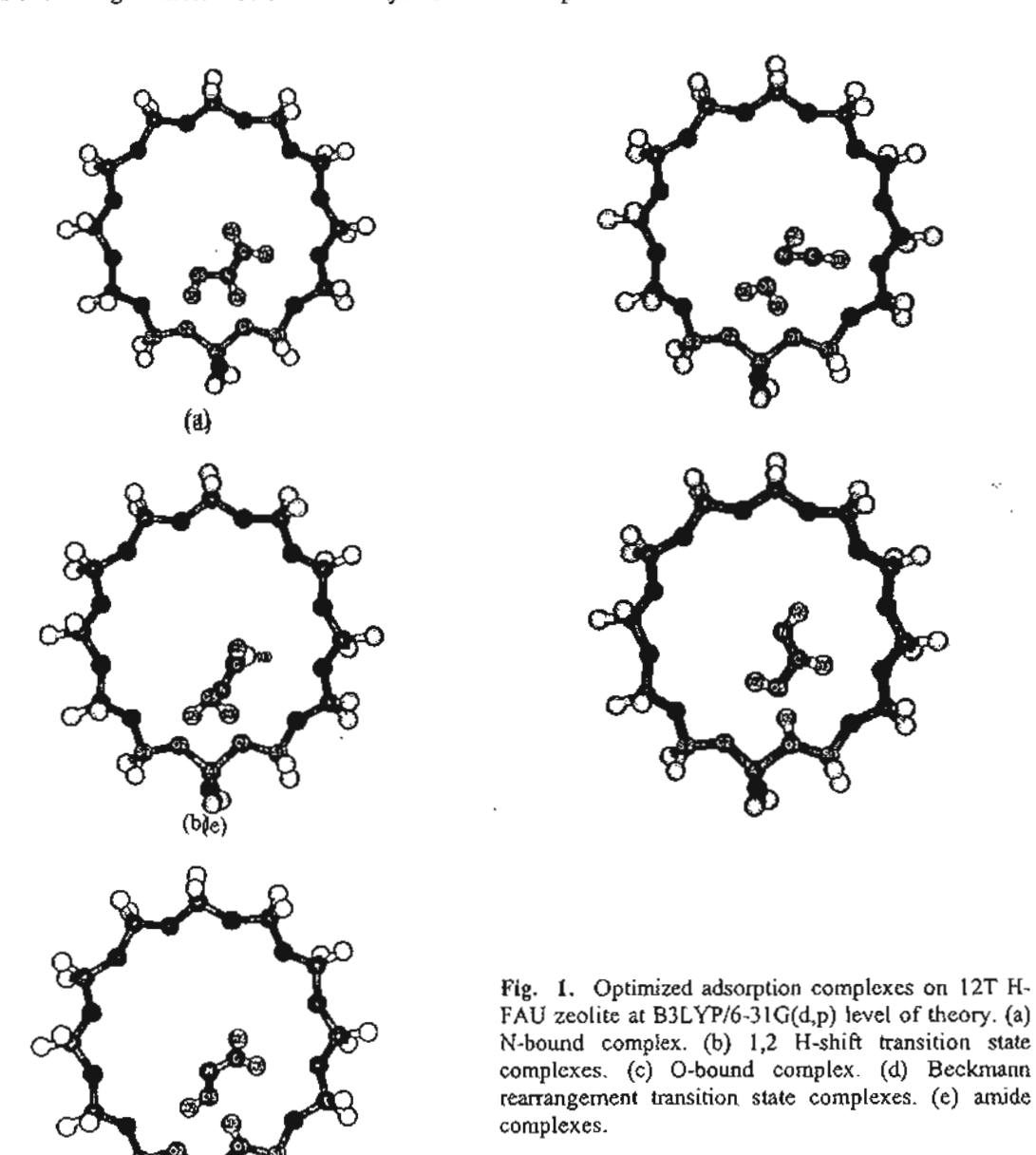
20

i in ka

These results indicate that the rate determining step of the Beckmann reaction is the rearrangement step. The prediction contrasts with the investigation of the gas phase system of Nguyen et al [3] that pointed out the rate determining step is the 1,2 H-shift step. Our results indicate that the influences from the zeolite framework have a

## An International Conference on Advances in Petrochemicals and Polymers in the New Millennium July 22-25,2003 •Bangkok, Thailand

significant effect on reaction mechanism and energetic profile. When compared the energetic profile between Hr-FAU and H-ZSM5 zeolite from Table 1, we found that the H-ZSM5 zeolite is a candidate acid catalyst for the Beckmann rearrangement reaction of formaldehyde oxime as compared to the H-FAU zeolite.



#### REFERENCES

17.

si; }}.

- [1] Limtrakul, J.; Nanok, T.; Khongpracha, P.; Jungsuttiwong, S.; Truong, T. N. (2001), 'Adsorption of unsaturated hydrocarbons on zeolites: the effects of the zeolite framework on adsorption properties of ethylene' *Chem. Phys. Letts.* 349, 161.
- [2] Chung, M. C.; Rhee, H. K. (2000), 'Solvent effects in the liquid phase Beckmann rearrangement of

An International Conference on Advances in Petrochemicals and Polymers in the New Millennium July 22-25,2003 Bangkok, Thailand

1007

 $\{\vec{\omega}\}$ 

4-hydroxyacetophenone oxime over H-Beta catalyst' J. Mol. Catal. A 159, pp 389-396.

[3] Nguyen, M. T.; Raspoet, G.; Vanquickenborne, L. G. (1997), 'A new look at the classical Beckmann rearrangement, a strong condition relief of the condition rearrangement: a strong case of active solvent effect' J. Am. Chem. Soc. 119, pp 2552-2562.

#### A QM/MM Study of Adsorption of Aromatics over Faujasite Zeolite

P. Wongthong, C. Soonthornpalin, P. Pantu and J.Limtrakul\*
\*Laboratory for Computational & Applied Chemistry, Chemistry Department, Kasetsart University,
Bangkok 10900, THAILAND \* Corresponding Author E-mail: fscijrl@ku.ac.th

#### INTRODUCTION

÷į.

H-FAU zeolite exhibits an extremely high catalytic selectivity for the alkylation of toluene and methanol to ethylbenzene, the largest commercial volume of benzene derivatives, mostly for the manufacture of styrene and polystyrene. Due to the large unit cell of faujasite (576 atoms/uc), the use of periodic calculation for accurate theoretical study is limited. In the present paper, we adopt a hybrid QM/MM (ONIOM2) to overcome the computational limitation for investigating the interactions of toluene with H-FAU, with the aim of investigating the effects of the extended zeolitic framework on the structure and function of the H-FAU/toluene complex.

#### EXPERIMENTAL SECTION

A realistic model of 84 tetrahedra cluster, including two supercages, is used to model the structure of faujasite zeolite. A hybrid QM/MM [ONIOM2(B3LYP/6-31G(d,p):UFF)] approach is employed to study the interaction of toluene with H-FAU. During the struture optimization, only the active site region [=SiOHAl(O)<sub>2</sub>OSi=], and the adsorbate are allowed to relax. Single point calculations at 6-311++G(d,p) are carried out on the optimized structures to obtain more reliable energies.

#### RESULTS AND DISCUSSION

The ONIOM2 model has been shown to give reliable adsorption energies for closely related systems, giving the values of -15.17 and -21.08 kcal/mol for H-FAU/benzene and H-FAU/ethylbenzene, respectively compared well with the experimental values (-14.0 and -20.4 kcal/mol). The confinement effect of the zeolite pore stucture which is principally arising from van der Waals interactions is efficiently accounted for by the UFF force field. Therefore, the ONIOM2 model can calculate adsorption energies and interactions of adsorbate molecules in zeolite with far better accuracy than the typical quantum cluster calculations.

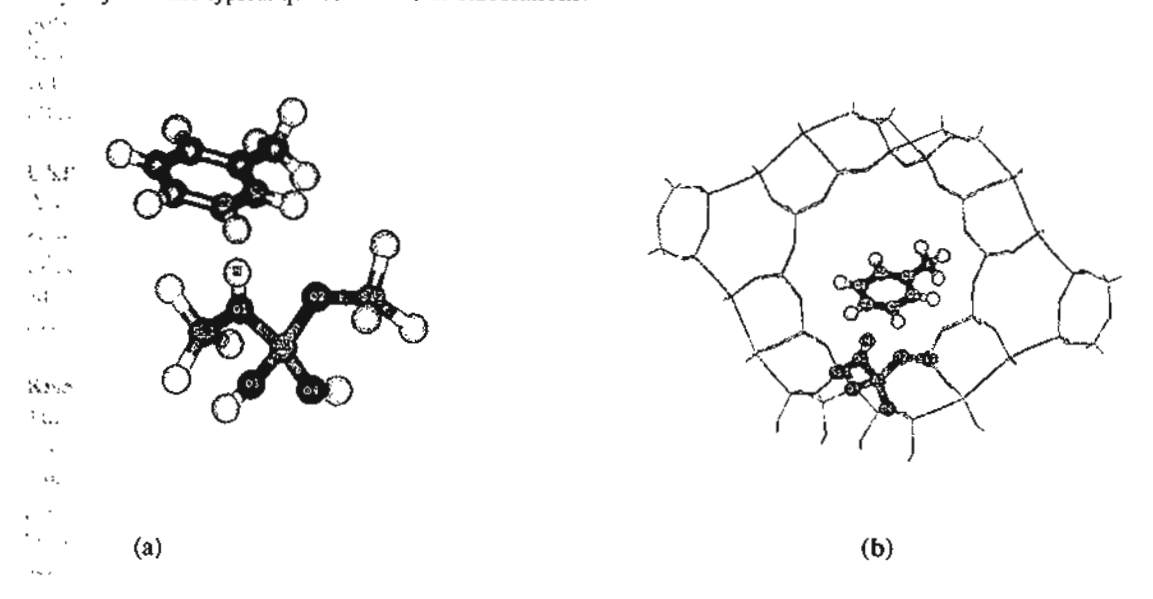


Fig. 1. The structure of faujasite zeolite showing small 3T quantum (Fig. 1a) and ONIOM2 (Fig.1b) clusters. The realistic model of two supercages – modeled by the 84 T cluster – serving as a nanoscopic reactor where the toluene molecule is favorably adsorbed. Atoms belonging to the active region drawn as a sphere.

For H-FAU/toluene, the calculations of the 84T model show a slight lengthening of the bridged O-H bond when compared to that of the 3T quantum cluster, indicating the force field environment enchancing the acidity of zeolite. The calibrated ONIOM2 scheme predicts adsorption energy of -19.46 kcal/mol in line with the experimental estimates of H-FAU/benzene, H-FAU/ethylbenzene system, whereas the 3T cluster gives an underestimated value of -7.78 kcal/mol.

Table 1. Binding energies of benzene and toluene on the Brönsted acid of faujasite zeolites. (binding energies are in kcal/mol)

Methods/Models	3	3T	84	4T
	Benzene	Toluene	Benzene	Toluene
HF/3-21G	-9.49	-9.82	-	
HF/6-31G(d,p)	-5.84	-6.01	-	-
B3LYP/6-31G(d,p)	-7.84	-7.78	-	-
HF/3-21G:UFF	-	-	-18.33	-22.00
HF/6-31G(d,p):UFF	-	-	-16.57	-19.81
B3LYP/6-31G(d,p):UFF	-	-	-17.15	-21.21
B3LYP/6-31G(d,p):UFF+BSSE a	-	-	-16.15	-18.84
$B3LYP/6-311++G(d,p):UFF^b$	-	-	-15.17	-19.46
MP2/6-311++G(d,p):UFF <sup>c</sup>	-	-	•	-25.36
MP2/6-311++G(d,p):UFF+BSSE <sup>a</sup>	-	-	-	-21.42

Adsorption energies of benzene and ethylbenzene on H-FAU zeolites are experimentally observed to be -14.0 [1] and -20.4 [3] kcal/mol, respectively. \* Basis set superposition error corrected.

#### CONCLUSION

The extended framework significantly enhances the adsorption energy of toluene to the zeolites. With the ONIOM2(B3LYP/6-311++G(d,p):UFF) scheme, the adsorption energy of -19.46 kcal/mol for the H-FAU/toluene complexes was predicted. The results obtained in the present study suggest that the ONIOM approach yields a more accurate and practical model in studying adsorption of aromatics on zeolites.

#### REFERENCES

٠.

. . .

31.

- [1] O'Malley, P.J., and Farnworth, K. (1998), 'Density Functional Studies of Weak Base Interactions with Hydroxy Group: Models for Adsorption Complexes of Weak Bases in Microporous Materials' J. Phys. Chem. B, 102, pp 4507-4515.
- [2] Kasuriya, S., Namuangruk S., Treesukol P., Tirtowidjojo M., and Limtrakul J. (2003) 'Adsorption of ethylene, benzene, and ethylbenzene over faujasite zeolites investigated by the ONIOM method', J. Catal. in
- [3] Dixit, L., and Prasada Rao, T.S.R. (1999), 'Heats of Adsorption of Hydrocarbons on Zeolite Surfaces: A Mathematical Approach' J. Chem. Inf. Comput. Sci., 39, pp218-223.

h Indicates single-point energy with B3LYP/6-311++G(d,p)//B3LYP/6-31G(d,p)

c Indicates single-point energy with MP2/6-311++G(d,p)// B3LYP/6-31G(d,p)

#### Studies of Nitrous Oxide Decomposition on Fe-ZSM5 Zeolite Catalyst

N. Peamaroon, P. Prompinit and P. Pantu\*

Laboratory for Computational and Applied Chemistry, Department of Chemistry,

Kasetsart University, Bangkhen, Bangkok 10900, THAILAND

\*Corresponding Author E-mail: fscipbp@ku.ac.th

#### Introduction

Nitrous Oxide (N<sub>2</sub>O) has been identified as a greenhouse gas that contribute to the ozone depletion and global warming. One of the major sources of N<sub>2</sub>O comes from the industrial production especially adipic acid production, nitric acid manufacture, fossil fuels, and biomass combustion [1].

Catalytic decomposition of  $N_2O$  is the effective method for the reduction of  $N_2O$  emission from the industrial exhaust gas because the reaction can be occurred at relatively low temperature (300-600 °C) [1,2]. Especially, the Fe-ZSM5 catalyst has high catalytic activity on  $N_2O$  decomposition reaction and high resistance to the presence of  $SO_x$ ,  $NO_x$  and  $H_2O$  in the feed gas [3].

In this work, the catalytic reaction of N<sub>2</sub>O decomposition is studied by using Fe-ZSM5 as catalyst. The performance of the catalysts have been tested in the plug flow reactor (PFR) and the N<sub>2</sub>O conversion dependence on the catalyst pretreatment condition is discussed.

#### Results and Discussion

Fe-ZSM5 catalysts were prepared by convention ion-exchange method [4]. The parent ZSM5 (Si/Al = 13.5) zeolite obtained from ALSI-PENTA was exchanged with Fe(NO<sub>3</sub>)<sub>3</sub> solution and the sample was then subjected to the elemental analysis using X-ray fluorescence spectrometry (XRF). Before testing the catalytic activity on N<sub>2</sub>O decomposition, the catalysts were pretreated in the various conditions and cooled down to the starting temperature (about 400 °C).

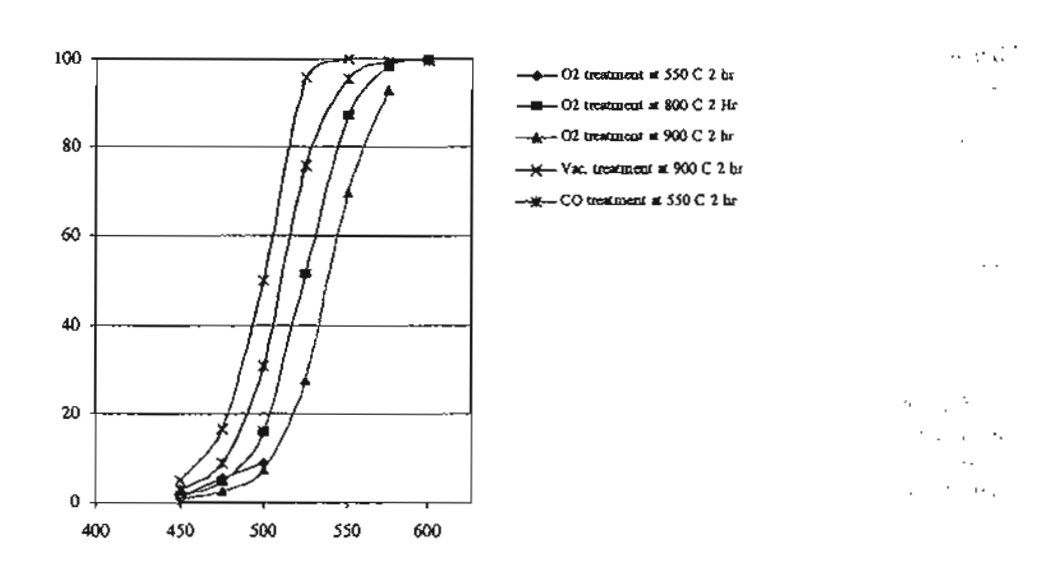


Fig. 1. N<sub>2</sub>O conversion as function of temperature over Fe-ZSM5 0.52%Fe wt. at the various pretreatment conditions using 0.05 g catalyst. Feed condition: 7% mole of N<sub>2</sub>O balance in Ar, total flow 68 ml/min.

Fig. 1. shows the  $\%N_2O$  conversion versus reaction temperature of the different pretreatment conditions of Fe-ZSM5. From the results, the vacuum treated sample showed the highest catalytic activity.

The results of the temperature program reduction (TPR) using  $H_2$  as a reducing gas show that the exchanged Fe-ZSM5 formed the active structure as small cluster of iron oxide [5] with the oxidation state Fe<sup>3+</sup> ( $H_2$ /Fe-1.5). After vacuum treatment, the results of TPR indicate the formation of Fe<sup>2+</sup> ( $H_2$ /Fe-1) that is the most active species for  $N_2$ O decomposition reaction [6]. It was also noted that the oxidation state of iron was changed back from Fe<sup>2+</sup> to Fe<sup>3+</sup> during the  $N_2$ O decomposition reaction.

#### Conclusion

Fe-ZSM5 shows high catalytic activity for  $N_2O$  decomposition reaction stoichiometrically to  $N_2$  and  $O_2$ . After vacuum treatment the most active small cluster of iron oxide with the oxidation state Fe<sup>2+</sup> is formed to react with  $N_2O$  and change the oxidation state to Fe<sup>3+</sup> after reaction.

#### References

- [1] Kapteijn, F., Rodriguez-Murasol, J., and Moulijn, J.A. (1996), "Review Heterogeneous Catalyic Decomposition of Nitrous Oxide," Appl. Catal. B, 9, pp 25-64.
- [2] Panov, G.I., Sobolev, V.I., and Kharitonov, A.S. (1990), "The Role of Iron in N<sub>2</sub>O Decomposition on ZSM-5 Zeolite and Reactivity of the Surface Oxygen Formed," J Mol. Catal. 61, pp 85-97.
- [3] Perez-Ramirez, J., Kapteijn, F., Mul, G., and Moulijn, J.A. (2001) "Superior Performance of Ex-Framework Fe-ZSM5 in Direct N<sub>2</sub>O Decomposition in Tail-Gases from Nitric Acid Plant," Chem. Comm., 8, pp 693-694.
- [4] Sang, C., and Lund C.R.F. (2000) "Isothermal light-off During Catalytic N<sub>2</sub>O Decomposition over Fe-ZSM5," Catal. Lett. 70, pp 165-173.
- [5] Van Den Brink, R.W., Booneveld, S., Pels, J.R., and Bakker, D. F. (2001) "Catalytic Removal of N<sub>2</sub>O in Model Flue Gas of a Nitric Acid Plant Using a Promoted Fe Zeolite," Appl. Catal. B, 32, pp 73-81.
- [6] Dubkov, K.A., Ovanesyan, N.S., Shteinman, A.A., Starokon, E.V., and Panov G.I. (2002) "Evolution of Iron States and Formation of α-Sites upon Activation of Fe-ZSM5 Zeolites," J. Catal., 207, pp 341-352.

### ภาคผนวก ข.3

ผลงานในการประชุมนานาชาติ
"American Chemical Society National
Meeting ครั้งที่ 227"
จำนวน 5 เรื่อง

Program Selection: Division of Petroleum Chemistry

Topic Selection: General Papers

The influence of the framework to structures and energetic

profiles of the vapor phase of the Beckmann rearrangement on

different types of zeolite

Jakkapan Sirijaraensre, and Jumras Limtrakul

The heterogeneous catalytic Beckmann rearrangement (BR) on FAU and ZSM-5 catalysts has been investigated by both the quantum cluster and embedded cluster approaches at the B3LYP level of theory using the 6-31G (d,p) basis set. The embedded cluster model of H-FAU zeolite suggests that the initial step of the Beckmann rearrangement is not the O-protonated oxime but the N-protonated oxime, the same as that obtained from the investigation of the BR on H-ZSM5 zeolite. The energy barriers derived from the proton shuttle of the N-bound to the O-bound isomer are evaluated to be about 31.1 and 23.8 kcal/mol for the embedded cluster of H-FAU and H-ZSM-5 zeolites, respectively. The difference in the activation energy is due mainly to the effect of the Madelung potential from the zeolite framework. The overall activation energy, at the rearrangement step, is calculated to be about 58.0 and 30.1 kcal/mol for the embedded cluster of H-FAU and H-ZSM-5 zeolites, respectively. These calculated results suggest that the rate-determining step of the vapor phase of the Beckmann rearrangement on both zeolites is the rearrangement step. The catalytic performance from different frameworks of both zeolites can be significantly distinguished by using the embedded technique. In comparing the energetic profile with that obtained from H-ZSM5 zeolite, we found that the H-ZSM5 zeolite is a better acid catalyst for the Beckmann rearrangement reaction of

į

formaldehyde oxime than the H-FAU zeolite.

**Topic Selection:** Catalysis (Posters)

Alkylation of benzene with ethylene over faujasite zeolte:

Structures and reaction mechanism

Supawadee Namuangruk, and Jumras Limtrakul,

The reaction mechanism of alkylation of benzene with ethylene over faujasite zeolite was investigated using the ONIOM (Our-own-N-layer Investigated molecular Orbital + molecular Mechanics) approach with an 84T cluster of faujasite zeolite modeled by the ONIOM3(MP2/6-31G(d,p):HF/3-21G:UFF) method. The model was validated to give reasonable structures and accurate adsorption energies after corrected with basis set superposition error (BSSE). The adsorption energies of ethylene, benzene and ethylbenzene on the catalyst were predicted to be -9.86, -15.51, and -22.76 kcal/mol, respectively compared well with experimental estimates of -9.1, -15.31, and -20.4 kcal/mol, respectively. The Eley-Rideal type mechanism of benzene alkylation was investigated. Formation of the surface ethoxide intermediate was occurred after protonation of the adsorbed ethylene by an acidic zeolite proton. The apparent activation energy for the ethoxide formation was calculated to be 17.95 kcal/mol comparable to the activation energy measured by Cant and Hall for protonation of deuterium exchanged ethylene on a Y zeolite of 16 kcal/mol. The reaction, subsequently, proceeded via interactions between the surface ethoxide intermediate and gaseous benzene molecule which was also found to be a rate determining step. The ONIOM3 model yielded the activation energy of 40.72 kcal/mol and apparent activation energy of 26.40 kcal/mol.

ŧ,

Topic Selection: Nanoscience (Posters)

The adsorption of aromatic hydrocarbons on industrially important nanocatalysts, ZSM-5, BEA and FAU: Confinement effects

Ratana Rungsirisakun, Bavornpon Jansang, and Jumras Limtrakul

The structures of three industrially important catalysts, ZSM-5, BEA, and FAU, and their interactions with benzene have been investigated within the framework of the density functional theory (B3LYP/6-31(d,p)) and our-own-N-layered integrated molecular orbital + molecular mechanics (ONIOM) approach utilizing three-layer ONIOM schemes (B3LYP/6-31G (d,p): HF/3-21G: UFF). Inclusion of the extended framework has an effect on adsorption properties and leads to differentiation of different types of zeolite, unlike the quantum cluster which is not able make this differentiation. The ONIOM adsorption energies of ZSM-5, BEA, and FAU zeolites that interacted with benzene are -19.50, -17.08 and -15.51 kcal/mol, respectively, which agrees favourably with the known adsorption trend of these three zeolites. On the other hand, the quantum cluster models yield very low adsorption energies for these three zeolites and even yield an unreasonable trend of adsorption energies for these zeolites/C6H6 complexes (-8.09, -8.48, and -6.78 kcal/mol). With the inclusion of basis set superposition error (BSSE) and the MP2 corrections, the ONIOM3(MP2/6-31G(d,p):HF/3-21G:UFF) adsorption energies are predicted to be -21.01, -19.36, and -15.41 kcal/mol, the latter can be compared well with the experimental data (-15.31 kcal/mol) for benzene adsorption on a FAU zeolite. The results derived in this study suggest that the ONIOM3(MP2/6-31G(d,p):HF/3-21G:UFF) scheme provides a more accurate method for investigating the adsorption of aromatic hydrocarbons on these zeolites.

Topic Selection: Computational (Posters)

QM/MM investigation of adsorption of benzene and toluene over alkali-exchanged Faujasite zeolite

Nutcha Injan, and Jumras Limtrakul

The ONIOM (Our-own-N-layered Integrated molecular Orbital + molecular Mechanics) approach utilizing two-layer ONIOM2 schemes - ONIOM2(MP2/6-311++G(d,p):UFF), ONIOM2(B3LYP/6-311++G(d,p):UFF), and ONIOM2(B3LYP/6-31G(d,p):UFF) - have been used to study the adsorption of aromatic hydrocarbons in faujasite zeolites (Na-FAU). The realistic 84 tetrahedra cluster has been modelled as an active site. The calculated adsorption energies of Na-FAU/benzene and Na-FAU/toluene complexes for the ONIOM2(B3LYP/6-311++G(d,p):UFF) scheme are -18.65 kcal/mol and -21.69 kcal/mol which are in good agreement with the experimental values of -18.0 and -19.6 kcal/mol for Na-FAU/benzene and Na-FAU/toluene, respectively. The results suggest that the ONIOM2 approach gives a more accurate result in studying the adsorption of aromatics on zeolites.

ó

Topic Selection: Catalysis (Posters)

Interaction of CH<sub>3</sub>CN with H-FAU, MFI zeolites: A combined

QM/MM study

Boonruen Sunpetch, and Jumras Limtrakul

The influence of zeolite frameworks on the acetonitrile (CH<sub>3</sub>CN) adsorption and their complexes with H-FAU and MFI zeolites have been studied by using 5T quantum

clusters and the ONIOM (Our-own-N-layered Integrated molecular Orbital + molecular

Mechanics) approach utilizing two-layer ONIOM schemes (B3LYP/6-31G(d,p):UFF).

The ONIOM2 adsorption energies for CH3CN/HFAU and CH3CN/MFI complexes are

predicted to be -18.69 and -24.13 kcal/mol, respectively, these values can be compared

favourably with the experimental estimate of -19.14 and -26.32 kcal/mol, respectively,

whereas the conventional quantum cluster yields an underestimated values of -13.64

kcal/mol. The results obtained in this study suggest that the ONIOM scheme provides a

more accurate method of studying the interaction of acetonitrile with zeolites.

## ภาคผนวก ข.4

ผลงานในการประชุมนานาชาติ
"International Zeolite Conference
ครั้งที่ 14"
จำนวน 3 เรื่อง

## STRUCTURE AND ENERGETICS OF NITROUS OXIDE AND METHANE ADSORPTION ON THE Fe-ZSM-5 ZEOLITE: ONIOM AND DENSITY FUNCTIONAL STUDIES

Suwat Pabchanda<sup>1</sup>, Piboon Pantu<sup>1</sup>, Duangkamol Tantanak<sup>2</sup>, and Jumras Limtrakul<sup>1</sup>

<sup>1</sup>Laboratory for Computational and Applied Chemistry, Chemistry Department, Kasetsart University, Bangkok 10900, Thailand; e-mail address: fscijrl@ku.ac.th

<sup>2</sup>Chemistry Department, Faculty of Science, King Mongkut's Institute of Technology Ladkrabang, Ladkrabang, Bangkok 10520, Thailand.

#### **ABSTRACT**

The quantum cluster and ONIOM methods have been used to investigate interactions between adsorbed nitrous oxide and methane on the active iron center in Fe-ZSM-5, prior to its catalytic oxidation to methanol. A model of mononuclear iron complex as an active site of the highly dispersed state of Fe-ZSM-5 was adopted in cluster models of 5T quantum cluster and 46T ONIOM2. The extended crystal framework included in the ONIOM model significantly enhances the interactions of both adsorbates with the active site. The adsorption energy of N<sub>2</sub>O on Fe-ZSM-5 calculated by the 5T quantum cluster is only -41.2 kJ/mol, whereas, the 46T ONIOM model gives the adsorption energy of -57.3 kJ/mol, which is comparable to the experimental estimate of -67 kJ/mol. After correction with single point calculation at MP2/6-31G\*\*:UFF//B3LYP/6-31G\*\*:UFF, the adsorption energy is calculated to be 66.9 kJ/mol, which is apparently identical to the experimental estimate. The ONIOM2 model also predicts the adsorption energy of -30.5 kJ/mol for the [CH4]/Fe-ZSM-5 complexes. These results demonstrate that the adsorption properties of Fe-ZSM-5 depend significantly on the specific environment of the zeolite crystal lattice.

#### INTRODUCTION

The intracrystalline nanostructured pore network of zeolites has an astonishing ability to stabilize small metal complexes leading to extraordinary catalytic activities. Small iron complexes in ZSM-5 (Fe-ZSM-5), for example, have remarkable redox behaviours [1-5] and recently have been received great attention. The Fe-ZSM-5 can catalyze selective reduction of NOx and selective hydroxylation of various organic compounds using nitrous oxide as an oxidant. An example of catalytic activity of Fe-ZSM-5 that is of the high industrial interest is the selective oxidation of benzene to phenol. However, the most fascinating catalytic activity of Fe-ZSM-5 is that it can selectively oxidize methane to methanol at room temperature.

The highly active and selective catalytic site in the Fe-ZSM-5 is commonly known as an  $\alpha$ -site whose structure, though, having been extensively studied [6-10], is still not clearly understood. An interesting point to note is that the Fe-ZSM-5 has some characteristics in common with the enzyme methane monooxygenase (MMO), found in methanotropic bacteria whose active site contains binuclear iron cluster [11,12]. The active iron atoms in Fe-ZSM-5 are found to be highly dispersed in the zeolite matrix and could be in the form of isolated ions, or dinuclear complexes, or small aggregate of iron atoms [10-14]. According to Mössbauer studies, iron atoms at the  $\alpha$ -site are in a divalent state (Fe<sup>2+</sup>) and after the decomposition of nitrous oxide, the iron atoms are changed to a trivalent state (Fe<sup>3+</sup>). With the knowledge gained from experimental studies, quantum chemical models of the  $\alpha$ -site structures have been proposed in literatures [15-17]. However, those quantum chemical studies did not include the effects of the zeolite framework which is known to have significant effects on structures and energetics of guest molecules in zeolite structures [18-20].

We herein report the results of our theoretical study on interactions of nitrous oxide and methane with Fe-ZSM-5 using a DFT method with the aims of investigating the effects of the extended zeolitic framework on the structure and function of the Fe-ZSM-5 complex. This is the first case we know of where the explicit zeolite environment is included in calculations for this zeolite catalyst.

#### **METHODS**

Structures of cluster models were taken from the crystal structure of a ZSM-5 lattice with one aluminium atom substituted with a silicon atom at the T12 position and the negative charge of the cluster was balanced by either FeO or FeO<sub>2</sub> ion to form the active centre. In this study, the Fe-ZSM-5 structure was represented by a 5T quantum cluster (Fig. 1a, 1c) and a 46T ONIOM2 model [21,22] (Fig 1b, 1d). In the ONIOM2 model the 5T active centre is treated quantum chemically at the B3LYP/6-31G(d,p) level of theory, and the rest of the extended framework, up to 46T, is treated at the UFF.

All calculations have been performed by using the Gaussian98 code [23]. The basis set 6-31G(d,p) is utilized for the B3LYP calculations. During the structure optimization, only the portion of the active site region and the adsorbate are allowed to relax. In order to obtain more reliable interaction energies, the single-point energy calculations at the ONIOM2-46T(MP2/6-31G\*\*:UFF//B3LYP/6-31G\*\*:UFF) level were carried out.

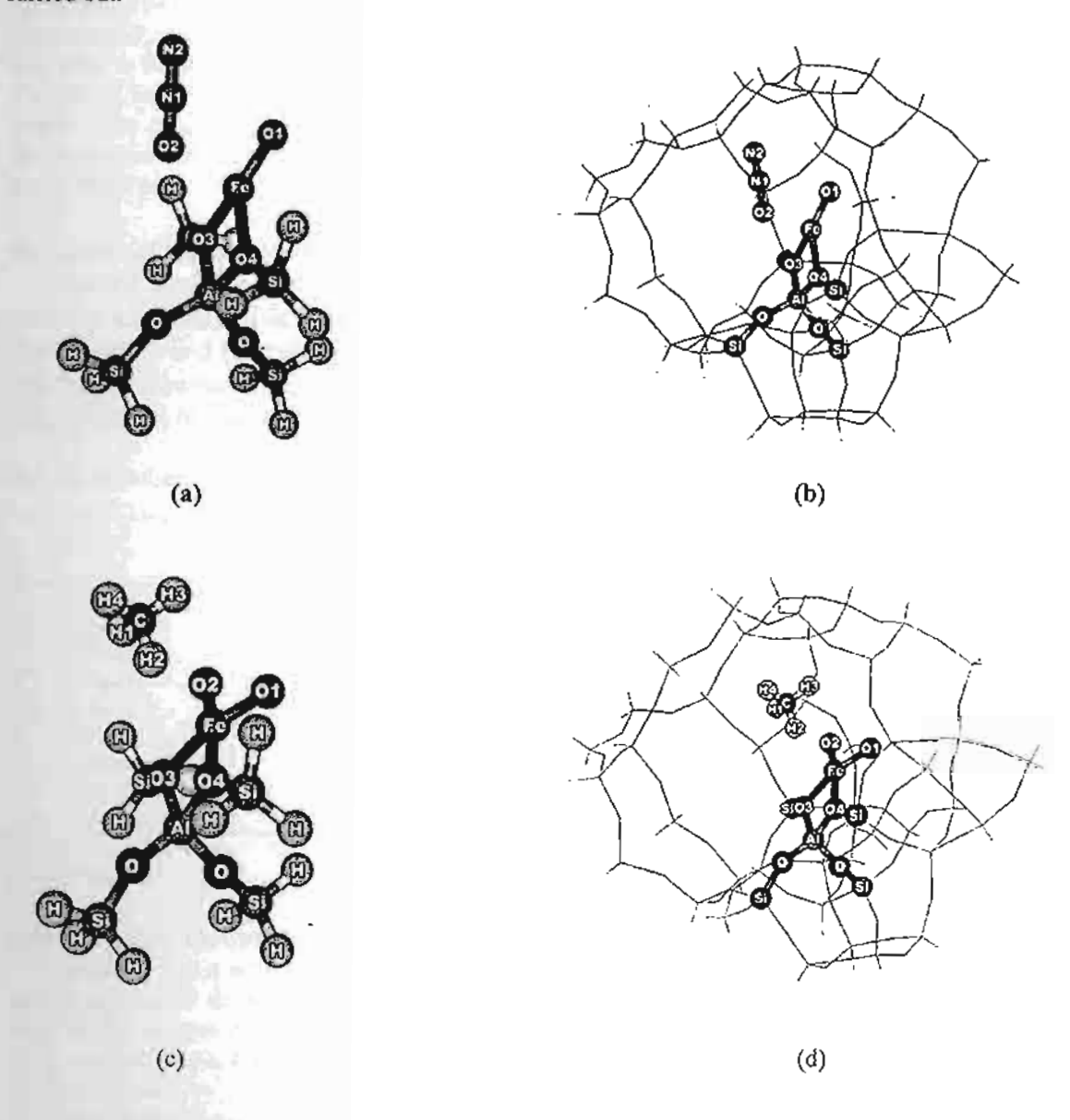


Figure 1 N<sub>2</sub>O/FeO-ZSM-5 and CH<sub>4</sub>/FeO<sub>2</sub>-ZSM-5 clusters, atoms belonging to the active region drawn as sphere, (a) 5T cluster of N<sub>2</sub>O/FeO-ZSM-5, (b) 46T ONIOM model of N<sub>2</sub>O/FeO-ZSM-5, (c) 5T cluster of CH<sub>4</sub>/FeO<sub>2</sub>-ZSM-5, (d) 46T ONIOM model of CH<sub>4</sub>/FeO<sub>2</sub>-ZSM-5.

#### RESULTS AND DISCUSSION

It has been found that with low iron content in Fe-ZSM-5, iron atoms are highly dispersed in the zeolite pores and present primarily in a form of isolated mononuclear iron oxide ion at the ion-exchange sites of the ZSM-5 [24]. Therefore, the α-site can be modeled as a divalent mononuclear Fe(II)O<sup>+</sup>/ZSM-5 and after N<sub>2</sub>O decomposition, the α-oxygen loaded active site can be modeled as Fe(III)O<sub>2</sub><sup>+</sup>/ZSM-5 [15]. In this work, two cluster sizes, 5T and 46T, were used to represent the Fe-ZSM-5 zeolite. In the 46T ONIOM2 model, the extended structure was included to cover the cavity at the intersection of the straight and zigzag channels where adsorbates are favorably adsorbed.

#### Structures of the α-site [Fe(II)O<sup>+</sup>/ZSM-5<sup>-</sup>]

At the active site, an iron ion (FeO<sup>+</sup>) is coordinated by the two bridging oxygen atoms in zeolite which act as Lewis bases via the formation of bidentate interactions (Fig 1a, 1b). These interactions are found to be approximately symmetric, with almost equal Fe-O2 and Fe-O3 bond lengths about 202 pm (Table 1). The iron atom is bound more tightly to its covalent oxygen ligand (O1) with a bond distance of about 164 pm. The Fe-O1 bond is aligned with the plane of the 10T windows of the zigzag pore channel. Increasing the cluster sizes causes the FeO+ to move farther from the zeolite framework and the distance Fe-A1 was increased from 281.3 pm to 287.1 pm and the Fe-O1 bond distance was also slightly increased from 163.9 pm to 164.4 pm.

#### Structures of the \alpha-oxygen loaded site [Fe(III)O2\*/ZSM-5]

Selected structure parameters of Fe(III)O<sub>2</sub><sup>+</sup>/ZSM-5<sup>-</sup> model and its adsorption complex with methane are tabulated in Table 2. In the  $\alpha$ -oxygen loaded active site, the bond distances between the iron atom and the two oxygen atoms are virtually the same (Fe-O1= 166.6 pm amd Fe-O2 = 166.7 pm). However, the  $\alpha$ -oxygen (O2) is pointed toward the free space in the intersection cavity and, therefore, it is more accessible by adsorbates (Fig 1c, 1d).

Table 1 Optimized geometries of isolated model and adsorption complex of nitrous oxide on FeO-ZSM-5 zeolite.

	ST(B3LYP/6-31G(d,p))	461(	B3LYP/6-31G(d,p):UFF	?)
	Isolated	Complex	Isolated	Complex
Fe-O1	165.1	166.4	164.9	166.2
Fe-O2	-	230.1	-	229.5
Fe-O3	202.7	203.4	202.7	203.9
Fe-O4	201.2	202.7	201.7	203.0
Fe-Al	282.5	282.8	283.1	283.3
Fe-N1	**	303.4	-	305.7
Fe-N2	-	394.8	-	398.8
N1-O2		120.6	-	121.0
N1-N2	-	112.9	-	112.5

 $N-O \text{ of } N_2O = 119.2 \text{ pm}$  $N-N \text{ of } N_2O = 113.4 \text{ pm}$ 

#### Adsorption of nitrous oxide on the a-site

It is known that a nitrous oxide molecule can be adsorbed on the FeO+ site via either the nitrogen-end or the oxygen-end of the molecule. In this study, we, however, only look at the case where adsorption takes place via the oxygen-end of the N<sub>2</sub>O molecule, since we are interested in studying interactions of N<sub>2</sub>O with the α-site (FeO<sup>+</sup>) that leads to the formation of the α-oxygen loaded site (FeO<sub>2</sub><sup>+</sup>). The N<sub>2</sub>O molecule adsorbs on the active site by having its oxygen atom pointing to the iron center and the nitrogen end pointing to the free space in the intersection cavity. In the 5T cluster calculation, the N-O bond distance is slightly increased from 119.2 to 120.6 pm while the N-N bond distance is contracted from 113.4 to 112.9 pm (see Table 1). Inclusion of the extended framework structure significantly enhances interactions between the adsorbed nitrous oxide and the active site. The adsorption energy is markedly increased from 41.2 kJ/mol to 57.3 kJ/mol, which is very close to an experimental estimate of 67 kJ/mol [21]. After correction with single point

energy calculations at the high level of theory and the high basis set, MP2/6-31G\*\*:UFF//B3LYP/6-31G\*\*:UFF, the adsorption energy is calculated to be 66.9 kJ/mol, which is apparently identical to the experimental estimate (see Table 3). The result indicates that the extended framework included by the UFF force field is sufficient to correct the absence of the framework effect in the DFT cluster calculation and, therefore, makes it possible to calculate accurate adsorption energy by using the ONIOM model.

Table 2 Optimized geometries of isolated model and adsorption complex of methane on FeO2-ZSM-5 zeolite.

	5T(B3LYP/6-31G(d,p))	46T(	B3LYP/6-31G(d,p):UFF	·)
	Isolated	Complex	Isolated	Complex
Fe-Ol	166.7	166.7	166.6	166.6
Fe-O2	166.6	166.6	166.5	166.5
Fe-O3	197.9	1 <b>9</b> 7.5	198.0	198.2
Fe-O4	197.5	198.7	197.8	199.1
O1-O2	228.1	227.4	228.2	227.0
Fe-Ai	281.5	277.4	279.8	278.7
Fe-C	-	343.7	-	342.6
Fe-H1	-	338.1	-	337.8
Fe-H2	-	282.1	-	281.1
Fe-H3	-	357.8	•	357.1
Fe-H4	-	444.1	-	443.7
O2-H1	-	295.3	-	294.8
O2-H2	-	328.1		327.7
O2-H3	-	331.8	_	331.2
O2-H4	-	444.0	-	443.6
C-H1	-	109.1	-	109.1
C-H2	-	109.5	-	109.7
C-H3	-	109.1	-	109.1
C-H4	-	109.2	-	109.2

C-H of CH<sub>4</sub> =109.2 pm

#### Adsorption of methane on the \alpha-oxygen loaded site

Methane adsorbs on the α-oxygen loaded site by having one hydrogen atom (H1) pointing toward the iron atom and another hydrogen atom (H2) pointing toward the α-oxygen atom (O2). In the 5T quantum cluster, the distance between Fe-H1 is evaluated to be 282.1 pm and that of O2-H1 is 295.3 pm. The weak interactions between the adsorbed methane and the active site do not significantly disturb the structure of the active site. On the other hand, the adsorbed methane molecule is partially activated by the adsorption as the C-H2 bond distance is slightly elongated from 109.2 to 109.5 pm. Including the extended framework increases interactions between adsorbed methane and the active center. The adsorption energy is increased from 15.5 kJ/mol to 27.2 kJ/mol and adsorbed methane is getting closer to the active iron site as reflected by decreasing in distance between Fe-C and Fe-H2 and O2-H1 (see Table 2) and also the increase of the C-H2 bond distance of the methane molecule from 109.5 to 109.7 pm. After correction with the single point energy calculations, the adsorption energy of methane on the active iron site in ZSM-5 is predicted to be -30.5 kJ/mol (see Table 3)

Table 3 The adsorption energies (kJ/mol) for the N2O/FeO-ZSM-5 and CH4/FeO-ZSM-5 systems

Method	Adsorption energies (kJ/mol)			
	N2O/FeO-ZSM-5	CH <sub>4</sub> /FeO-ZSM-5		
Full 5T(B3LYP/6-31G(d,p))	-41.2	-15.5		
ONIOM2-46T(B3LYP/6-31G(d,p): UFF)	-57.3	-27.2		
ONIOM2-46T(MP2/6-31G(d,p): UFF// B3LYP/6-31G(d,p): UFF)	-66.9	-30.5		
Experiment	-66.9			

#### CONCLUSIONS

The extended framework significantly enhances the adsorption energy of methane to the zeolites. With the ONIOM2(B3LYP/6-31G(d,p):UFF) scheme, the adsorption energy of N<sub>2</sub>O on Fe-ZSM-5 was accurately calculated to be -66.9 kJ/mol, the adsorption energy of -30.5 kJ/mol for the [CH<sub>4</sub>]/Fe-ZSM-5 complexes was predicted. From the structure and adsorption energy point of views, the B3LYP or MP2 combining with the UFF force fields method as a lower level is considered to be one of the best combinations for the ONIOM2 scheme. This efficient scheme provides a cost effective computational stategy for treating the effects of a large extended framework structure. The results obtained in the present study suggest that the ONIOM approach yields a more accurate and practical model in studying adsorption of hydrocarbons on zeolites and also in studying the mechanisms of oxidation of methane to methanol using N<sub>2</sub>O as oxidant. This challenging reaction is being actively pursued.

#### ACKNOWLEDGMENTS

This work was supported in part by grants from the Thailand Research Fund (TRF Senior Research Scholar to JL.) and the Kasetsart University Research and Development Institute (KURDI) as well as the Ministry of University Affairs under the Science and Technology Higher Education Development Project (MUA-ADB funds).

#### REFERENCES

- [1] Panov, G. I., Kharitonov, A. S., Sobolev, V. I., Appl. Catal. A, 98 (1993), 1-20.
- [2] Panov, G. I., Sobolev, V. I., Dubkov, K. A., Parmon, V. N., Ovanesyan, N. S., Shilov, A. E., Shteinman, A. A., React. Kinet. Catal. Lett., 61 (1997), 251-258.
- [3] Sobolev V. I., Panov G. I., Kharitonov A. S., Romannikov V. N., Volodin A. M., Ione K. G., J. Catal., 139 (1993), 435-443.
- [4] Perez-Ramirez, J., Kapteijn, F., Mul, G., Moulijn, J. A., Chem. Commun., (2001), 693-694.
- [5] El-Malki, E.-M., van Santen, R. A., Sachtler, W. M. H., J. Catal., 196 (2000), 212-223.
- [6] Chen, H.-Y., El-Malki, E.-M., Wang, X., van Santen, R. A., Sachtler, W. M. H., J. Mol. Catal. A, 162 (2000), 159-174.
- [7] Spoto, G., Zecchina, A., Berlier, G., Bordiga, S., Clerici, M. G., Basini, L., J. Mol. Catal. A, 158 (2000), 107-114.
- [8] Pannov, G. I., Sobolev, V. I., Kharitonov, A. S., J. Mol. Catal., 61 (1990), 85-97.
- [9] Zhidomirov, G. M., Yakovlev, A. L., Milov, M. A., Kachurovskaya, N. A., Yudanov, I. V., Catal. Today, 51 (1999), 397-410.
- [10] Dubkov, K. A., Ovanesyan, N. S., Shteinman, A. A., Starokon, E. V., Panov, G. I., J. Catal., 207 (2002), 341-352.
- [11] Panov, G. I., Sobolev, V. I., Dubkov, K. A., Parmon, V. N., Ovanesyan, N. S., Shilov, A. E., Shteinman, A. A., React. Kinet. Catal. Lett., 61 (1997), 251-258.
- [12] Marturano, P., Drozdova, L., Kogelbauer, A., and Prins, R., J. Catal. 192(2000), 236-247.
- [13] Berlier, G., Spoto, G., Bordiga, S., Ricchiardi, G., Fisicaro, P., Zecchina, A., Rossetti, I., Selli, E., Forni, L., Giamello, E., Lamberti, C., J. Catal., 208 (2002), 64-82.
- [14] Lobree, L.J., Hwang, I., Reimer, J.A. and Bell, A.T., J. Catal. 186(1999), 242-253.
- [15] Ryder, J. A., Chakraborty, A. K., Bell, A. T., J. Phys. Chem. B. 106(2002), 7059-7064.
- [16] Knops-Gerrits, P. P., Goddard, W. A., J. Mol. Catal. A, 166 (2001), 135-145.
- [17] Yoshizawa, K., Shiota, Y., Yumura, T. and Yamabe, T., J. Phys. Chem. B 104(2000), 734-740.
- [18] Pelmenschikov, A., Leszczynski, J., J. Phys. Chem. B, 103 (1999) 6886.
- [19] Raksakoon, C. and Limtrakul, J., J. Mol. Struct. (Theochem), 631 (2003), 147.
- [20] Kasuriya, S., Namuangruk, S., Treesukol, P., Tirtowidjojo, M. and Limtrakul, J., J. Catal., (2003), in press.
- [21] Basch, H., Musaev, D. G. and Morokuma, K., J. Phys. Chem. B 105(2001), 8452-8460.
- [22] Basch, H., Mogi, K., Musaev, D. G. and Morokuma, K., J. Am. Chem. Soc. 121(1999), 7249-7256.

[23] Frisch, M.J., Trucks, G.W., Schlegel, H.B., Scuseria, G.E., Robb, M.A., Cheeseman, J.R., Zakrzewski, V.G., Montgomery, J.A., Stratmann, Jr., R.E., Burant, J.C., Dapprich, S., Millam, J.M., Daniels, A.D., Kudin, K.N., Strain, M.C., Farkas, O., Tomasi, J., Barone, V., Cossi, M., Cammi, R., Mennucci, B. Pomelli, C., Adamo, C., Clifford, S., Ochterski, J., Petersson, G.A., Ayala, P.Y., Cui, Q., Morokuma, K., Salvador, P., Dannenberg, J.J., Malick, D.K., Rabuck, A.D., Raghavachari, K., Foresman, J.B., Cioslowski, J., Ortiz, J.V., Baboul, A.G., Stefanov, B.B., Liu, G., Liashenko, A., Piskorz, P., Komaromi, I., Gomperts, R., Martin, R.L., Fox, D.J., Keith, T., Al-Laham, M.A., Peng, C.Y., Nanayakkara, A., Challacombe, M., Gill, P.M.W., Johnson, B., Chen, W., Wong, M.W., Andres, J.L., Gonzalez, C., Head-Gordon, M., Replogle, E.S., Pople, J.A. Gaussian, Inc., Pittsburgh PA, 2001.

## ADSORPTION OF TOLUENE OVER FAUJASITE ZEOLITE INVESTIGATED BY THE COMBINED QUANTUM MECHANICS/MOLECULAR MECHANICS METHOD

Pinyo Wongthong, Chorchat Soonthornpalin, Piboon Pantu, and Jumras Limtrakul

Laboratory for Computational & Applied Chemistry, Chemistry Department, Kasetsart University, Bangkok 10900, THAILAND

#### **ABSTRACT**

The ONIOM (Our-own-N-layered Integrated molecular Orbital + molecular Mechanics) approach utilizing two-layer ONIOM2 schemes — ONIOM2(MP2/6-31G(d,p):HF/3-21G), ONIOM2(B3LYP/6-31G(d,p):HF/3-21G), ONIOM2(B3LYP/6-31G(d,p):UFF), and ONIOM2(HF/3-21G:UFF) — have been used to investigate adsorption properties of aromatics in faujasite zeolites (H-FAU). The active site has been modeled with realistic clusters sizes up to 84 tetrahedra. The predicted adsorption energy of H-FAU/toluene complexes for the ONIOM2(B3LYP/6-311++G(d,p):UFF) scheme is –81.34 kJ/mol, which is in line with the experimental values of –58.5 and –85.3 kJ/mol for H-FAU/benzene and H-FAU/ethylbenzene, respectively. Where the conventional 3T quantum cluster yields an underestimated value of –32.52 kJ/mol. This finding clearly demonstrates that acidity does not depend only on the Brønsted group center but also on the lattice framework surrounding the Brønsted site. The results obtained in this study suggest that the ONIOM2 approach yields a more accurate for studying the adsorption of aromatics on zeolites.

#### INTRODUCTION

Zeolites are widely used in petroleum and chemical industries as solid catalysts for a number of commercially important reactions due to their outstanding properties, i.e., Brønsted and Lewis acid sites, size-shape selectivity. Nowadays the many conventional acid-catalyzed processes have been progressively substituted with zeolite-based processes for the advantages of handling, safety, and environmental benign. Electrophilic aromatic substitution is one of the most industrially important processes that can be efficiently catalyzed by many zeolite catalysts, e.g., FAU, ZSM-5, beta [1]. For the alkylation of toluene with methanol catalyzed by zeolites, a variety of important petrochemical products can be obtained. The product selectivity is governed by many factors, such as the intrinsic reaction rate and steric constraint imposed by specific pore size and adsorption-desorption and diffusion of reactants and products. Therefore details of molecular interactions are needed to fully understand the reaction mechanism and product selectivity.

Since it is known that a significant fraction of energetics of aromatics in zeolites is derived from van der Waals interactions with the constricted zeolite pores, the effect of the extended zeolite framework is essential in accurately investigating interactions of aromatics in zeolites. Numerous theoretical models have been proposed to study the crystalline zeolite [2-3]. Nevertheless, zeolites that have a high impact in industrial processes usually possess hundreds of atoms per unit cell. This makes the use of sophisticated methods, such as periodic ab initio calculations, computationally too expensive and even impractical sometimes when very large zeolites are concerned. The recent development of hybrid methods, such as the embedded cluster or the combined quantum mechanics/molecular mechanics (QM/MM) methods, as well as the more general ONIOM (Our-own-N-layered Integrated molecular Orbital + molecular Mechanics) method has brought a larger system within reach of obtaining accurate results. Up to date, the ONIOM method is applied to the study of extended systems, for example, chemical reactions on surface [4-12], and in enzymes [13].

<sup>\*</sup> Corresponding author. Fax: 662-9428900 ext 324. E-mail addresses: fscijrl@ku.ac.th (J. Limtrakul)

In this report, we present the results of using the ONIOM model to represent the complicated structure of zeolites and to study the adsorption of benzene, and toluene, which is the first important step for a more comprehensive study of alkylation reaction. We are focusing on the systems of faujasite (H-FAU), which are of high importance in many industrial reactions. The faujasite's unit cell of 576 atoms limits the use of periodic calculation, thus we manage to use the ONIOM method to model the active site of H-FAU, the Brønsted acid site. The rational choice of the levels of calculations for the ONIOM scheme has been examined. The results are compared to experimental data to find efficient combinations to satisfactorily reproduce the adsorption energies of H-FAU zeolite. This should provide us with a better understanding of the role of H-FAU in the process of catalyzing reactions of aromatic hydrocarbons.

#### **METHOD**

Two different strategies have been employed to model the faujasite. First, the 3T cluster H<sub>2</sub>SiOAl(OH)<sub>2</sub>O(H)SiH<sub>3</sub> (see Figure 1a) which is considered as the smallest unit that is required to represent the active site of zeolite. The cluster models were obtained from the lattice structure of faujasite zeolite [14]. The effect from the framework structure of zeolite cannot be totally neglected if more accurate results are required. The more realistic cluster model created for this study is 84T (see Figure 1b) which includes two supercages that can act as a nanoscopic reaction vessel.

The accuracy of the QM/MM method, particularly the ONIOM method, depends significantly on the choice of the level of calculations for high- and low-level regions [15]. Using the B3LYP method for treating the quantum cluster, we varied the methods for the low-level region from the molecular mechanics force fields (UFF), semiempirical, over to the Hartree-Fock methods. Using the experimental observation as a benchmark, we found that the UFF method provides reasonable values corresponding to the experimental prediction [7-10]. This is due to the explicit consideration of van der Waals contribution, which is the dominant contribution in adsorption-desorption in zeolites [16-21]. Therefore, the UFF method is the practical choice for the low-level methodology when the high-level region is treated by the B3LYP/6-31G(d,p) method. All calculations have been performed by using the Gaussian98 code [22]. The basis set 6-31G(d,p) is utilized for the B3LYP calculations. During the structure optimization, only the active site region [=SiO(H)Al(O)<sub>2</sub>OSi=], and the adsorbate are allowed to relax. In order to obtain more reliable interaction energies, a single-point energy calculation at the ONIOM2(B3LYP/6-311++G(d,p)//B3LYP/6-31G(d,p):UFF) level of theory and basis sets superposition error (BSSE) corrections were also taken into account.

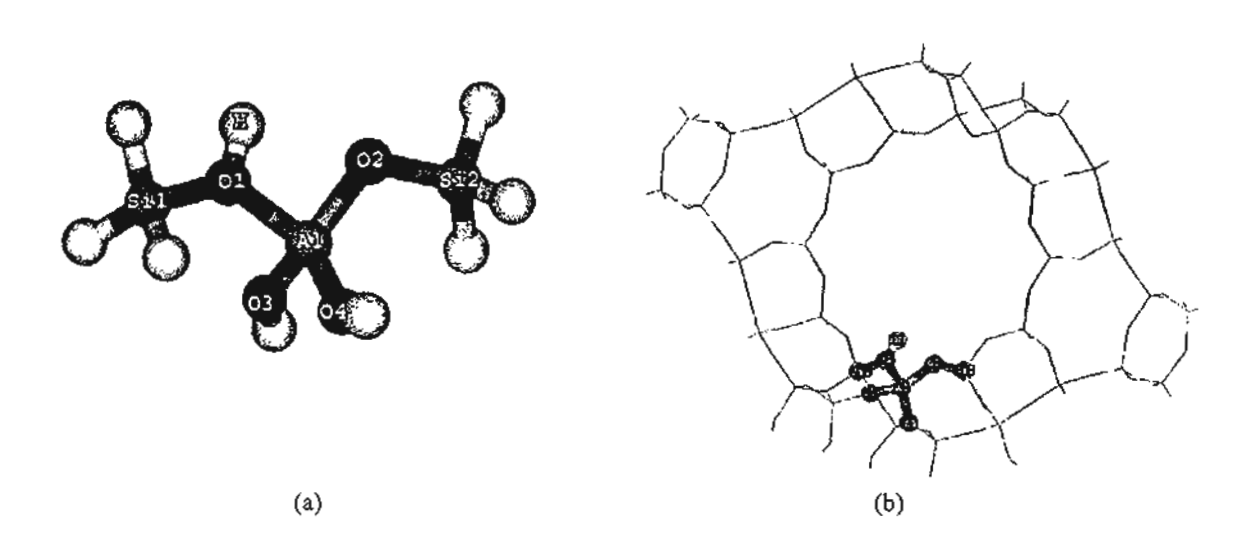


Figure 1: Presentation of cluster used to model the faujasite zeolite: (a) full 3T cluster model; (b) ONIOM2 model. The darker atoms in cluster 84T are treated at the higher level in the ONIOM2 approach.

#### RESULTS AND DISCUSSION

#### Structures of faujasite zeolite models

The faujasite zeolites were modeled by two different aluminosilicate clusters containing 3T and 84T tetrahedrally coordinated tetravalent atoms (see Figures 2-3). Table I lists some selected structural parameters derived at 3T quantum clusters and the ONIOM2 integrated schemes. By comparing the structure between the 3T quantum cluster and the 84T ONIOM2 models, it is seen that the cluster size environment has little effect on the structure of the active site. The extended framework slightly lengthens the O1-H bond distance (Brønsted acid site) from 96.7 pm in the 3T model to 96.8 pm in the 84T model. The bond distance between the aluminum and the proton nuclei in a Brønsted acid site, r(Al···H), of faujasite was computed to be 246.0 pm and 240.2 pm for the 3T cluster and 84T ONIOM2 models, respectively compared well with the experimental measurement value of 238.0 ± 4 pm reported in a literature [23]. Since the ONIOM2(B3LYP:UFF) method gives a good structural representation of the Brønsted acid site and the UFF force field is also a theoretically appropriate method for representing the effect of extended framework for this purpose (as discussed above) only the ONIOM models with the UFF force field will be discussed in detail hereafter.

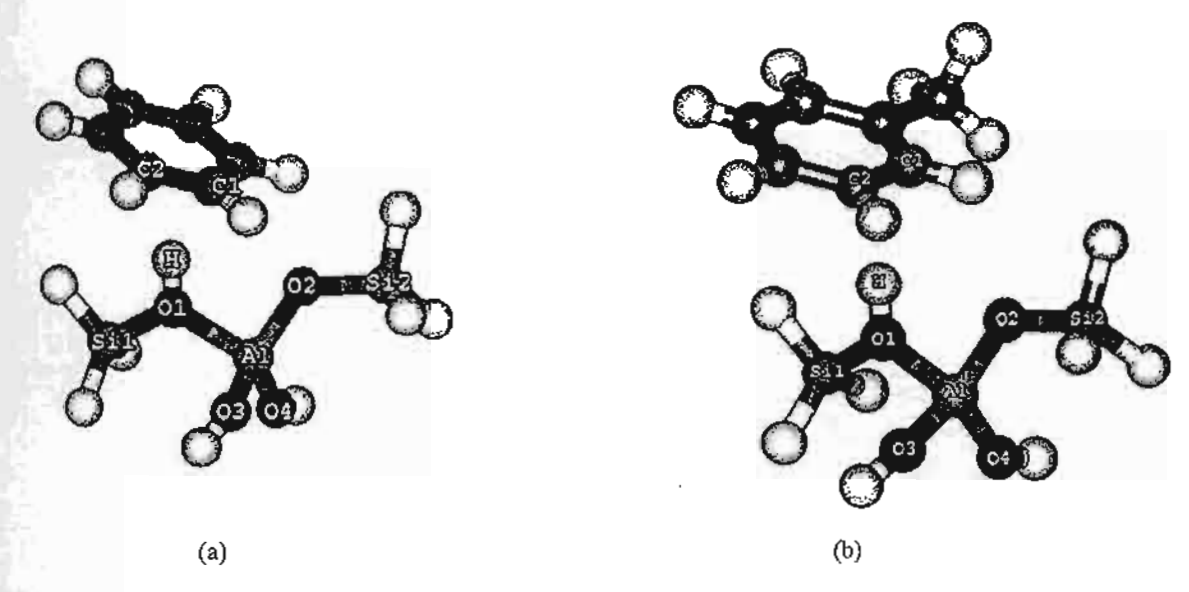


Figure 2: Presentation of models of faujasite and interacting with adsorbates: (a) full 3T cluster model interacting with benzene; (b) full 3T cluster model interacting with toluene.

Table 1: Structural parameters of faujasite obtained at full HF/3-21G, full B3LYP/6-31G(d,p) and various two-layer ONIOM2 schemes (bond distances in pm and bond angles in degrees).

Parameters	3T		84	τ
	Full HIF	Full B3LYP	HF:UFF	B3LYP:UFF
01-10	96.8	96.7	96.8	96.8
Al-OI	184.2	191.7	180.5	186.0
Si1-O1	171.9	170.9	169.4	168.6
Al-H	233.5	246.0	230.3	240.2
ZAI-OI-SiI	127.4	126.7	126.0	125 5

The HF is Hatree-Fock with 3-21G basis set.

The B3LYP is density functional theory with 6-31G(d,p) basis set.

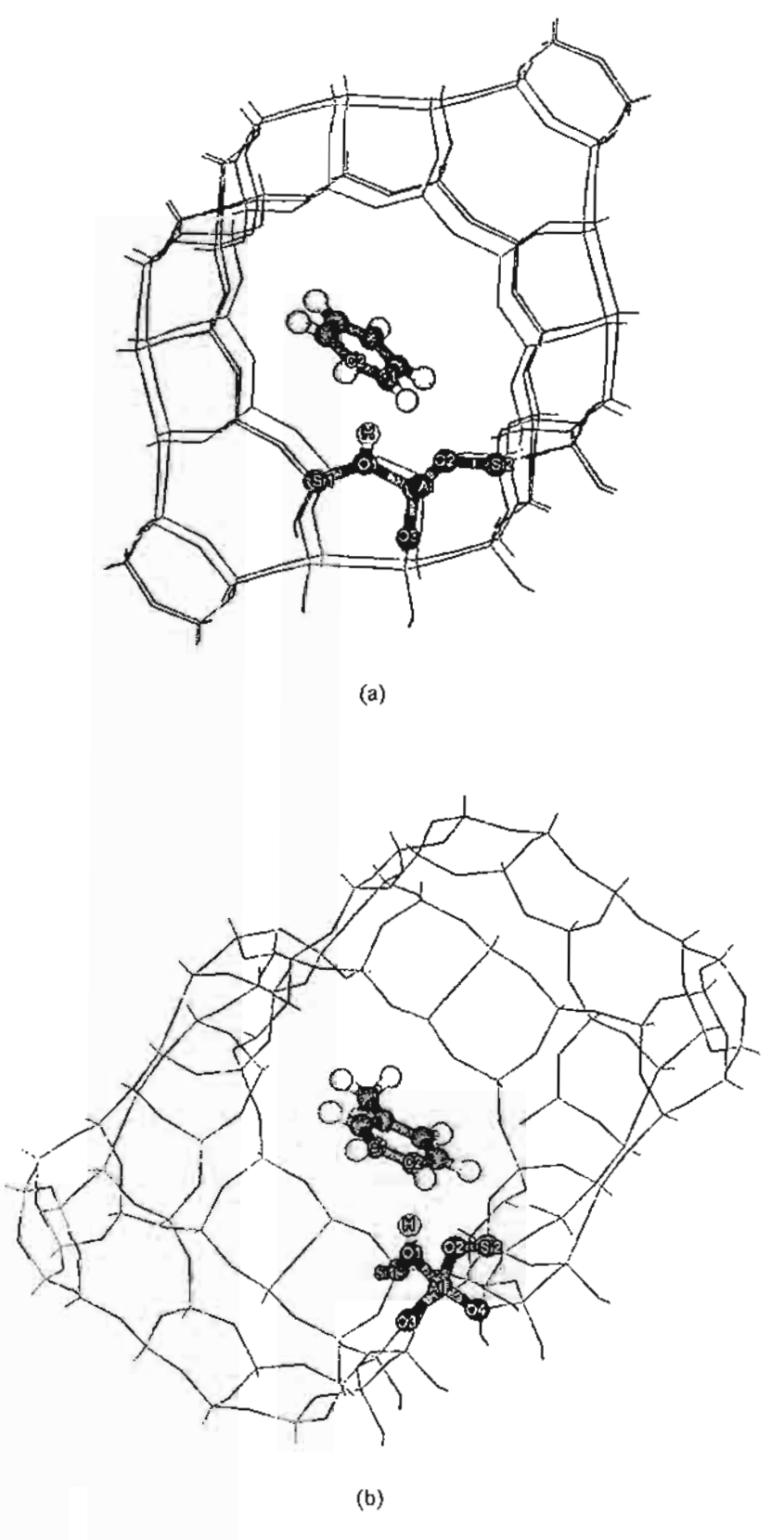


Figure 3: Presentation of models of faujasite and interacting with adsorbates: (a) ONIOM2 layer models of 84T cluster interacting with benzene; and (b) ONIOM2 layer models of 84T cluster interacting with toluene. Atoms belonging to the high-level regions are drawn as spheres.

#### Interactions of toluene with faujasite zeolites

Some structural parameters of the adsorption complexes calculated at finite clusters and at different ONIOM models (HF:UFF and B3LYP:UFF) are tabulated in Table 2. Table 2 presents the comparison between the 3T and 84T cluster models of the adsorption complexes indicating that adsorption does not significantly perturb structures of the adsorbed molecules or the zeolites due to the weak interactions between the hydrocarbons and the zeolite. Increasing of cluster size has only a small effect on the structure of the active site, but significantly affects the orientation of the adsorbed molecules. For the small cluster models, the adsorbed molecules are Pi-bonded to the active site with almost equal bond distances between the two double-bond carbons and the Brønsted proton. For the 84T cluster models, interactions with the extended framework cause the adsorbed molecules to move farther from the acid proton and lose the symmetrical bidentated structures.

Table 2: Structural parameters for adsorbate/zeolite cluster complexes, where adsorbates are benzene, and toluene.

Methods	Parameters		3T		84T		
		Benzene	Toluene	Benzene	Toluene		
HF	01-Н	97.5	97.6	97.3	97.2		
	Al-O1	182.9	182.8	179.4	197.4		
	Si1-O1	171.1	171.0	168.9	168.9		
	CI-H	220.8	218.3	222.5	226.0		
	C2-H	224.3	225.1	267.4	270.5		
	C=C	138.9	139.0	138.7	138.9		
	∠Al-O1-Si1	127.7	127.7	126.5	126.4		
B3LYP	OI-H	98.0	98.2	98.0	98.2		
	Al-O1	189.8	189.7	184.9	184.5		
	Si1-O1	171.0	170.1	168.4	167.9		
	C1-H	221.4	218.0	219.1	289.8		
	C2-H	224.1	224.8	259.4	211.6		
	C=C	140.1	140.0	140.1	140.0		
	∠Al-O1-Si1	126.5	126.5	124.9	125.1		

The zeolite clusters are 3T, 84T (bond distances in pm and bond angles in degrees). The B3LYP is density functional theory with 6-31G(d,p) basis set; HF is Hatree-Fock with 3-21G basis set.

The adsorption energies of benzene and ethylbenzene on H-Y zeolite were experimental measured to be -58.5 and -85.3 kJ/mol, respectively. Although the adsorption energy of toluene in faujasite zeolite is not available, it is expected to be between the values of the benzene and ethylbenzene adsorption. In the 3T cluster model, the DFT calculations predict the adsorption energies of benzene and toluene to be -31.21 and -32.52 kJ/mol, respectively which are considerably lower than the experimental measurements. Moreover, the small cluster calculations incorrectly predict comparable interaction energies of the zeolite with benzene and toluene molecules mistakenly indicating no shape selectivity between these two molecules. The erroneous results are due to the fact that the quantum cluster calculations omit the effect of the zeolite crystal structure.

In the more realistic 84T ONIOM2 model, the adsorption energies of benzene and toluene are calculated to be -71.69 and -88.66 kJ/mol, respectively. These interaction energies are somewhat overestimated as compared to the experimental results. After including the basis set correction by single point calculations at the higher basis set, 6-311++G(d,p), the corresponding interaction energies are computed to be of -63.41 and -81.34 kJ/mol. The BSSE corrections were also performed and gave similar results as the single point calculations at the high basis set (see Table 3).

It is noted that the choices of the methods using the high- and low-levels in the ONIOM scheme and also the sizes of the inner and outer regions are arbitrary. The size of the inner region employed in this study (3T cluster) is sufficient to represent the acid property of zeolites whilst small enough to guarantee that the van der Waals interactions between the hydrocarbon and the zeolite are well accounted for by the UFF force field, which is better than the DFT for this purpose [19-21]. From the structure and adsorption energy point of views, the B3LYP combining the UFF force fields method as a lower level is considered to be one of the best combinations for the ONIOM2 scheme. This efficient scheme provides a cost effective computational strategy for treating the effects of a large extended framework structure.

Table 3: Binding energy of benzene, and toluene on the Brønsted proton of faujasite zeolites (binding energy in kJ/mol)

Methods/Models	31	84T		
	Benzene	Toluene	Benzene	Toluene
HF/3-21G	-39.67	<del>-4</del> 1. <b>0</b> 7	-	-
B3LYP/6-31G(d,p)	-31.27	-32.52	•	-
HF/3-21G:UFF	-	-	-76.62	-91.96
B3LYP/6-31G(d,p):UFF	-	-	- 71.69	-88.66
B3LYP/6-31G(d,p):UFF+BSSE *	-	-	-67.51	-78.75
B3LYP/6-311++G(d,p):UFF <sup>6</sup>	•	-	-63.41	-81.34
$MP2/6-311++G(d,p):UFF^c$	-	-	-	-106.00
MP2/6-311++G(d,p):UFF+BSSE*	•	-	-	-89.54

Adsorption energies of benzene and ethylbenzene on H-FAU zeolites are experimentally observed to be -58.5 and -85.3 kJ/mol, respectively [24,25].

#### CONCLUSIONS

The extended framework significantly enhances the adsorption energy of toluene to the zeolites. With the ONIOM2(B3LYP/6-311++G(d,p):UFF) scheme, the adsorption energy of -81.34 kJ/mol for the H-FAU/toluene complexes was predicted. The results obtained in the present study suggest that the ONIOM approach yields a more accurate and practical model in studying adsorption of aromatics on zeolites.

#### ACKNOWLEDGMENTS.

This work was supported in part by grants from the Thailand Research Fund (TRF Senior Research Scholar to JL) and the Kasetsart University Research and Development Institute (KURDI) as well as the Ministry of University Affairs under the Science and Technology Higher Education Development Project (MUA-ADB funds). The support from the Dow Chemical Company (USA) is also acknowledged.

#### REFERENCES

- [1] Perego, C., Ingallina, P., Catal. Today, 73 (2002), 3-22.
- [2] Rozanska, X., Hutschka, F., van Santen, R.A., Saintigny, X., J. Catal., 202 (2001), 141-155.
- [3] Hutschka, F., van Santen, R.A., Rozanska, X., Hafner, J., J. Am. Soc., 123 (2001), 7655-7667.
- [4] Tang, H.R., Fan, K.N., Chem. Phys. Lett., 330 (2000), 509-514.
- [5] Roggero, I., Civalleri, B., Ugliengo, P., Chem. Phys. Lett., 341 (2001), 625-632.
- [6] Sillar, K., Burk, P., J. Mol. Struct. (Theochem.), 589 (2002), 281-290.
- [7] Raksakoon, C., Limtrakul, J., J. Mol. Struct. (Theochem), 631 (2003), 147-156.
- [8] Panjan, W., Limtrakul, J., J. Mol. Struct., 654 (2003), 35-45.
- [9] Kasuriya, S., Namuangruk, S., Treesukol, P., Tirtowidjojo, M., Limtrakul, J., J. Catal., 2003, in press.
- [10] Bobuatong, K., Limtrakul, J., Appl. Catal. A, 2003, in press.
- [11] Solans-Monfort, X., Bertran, J., Branchadell, V., Sodupe, M., J. Phys. Chem. B, 106 (2002), 10220-10266.

<sup>\*</sup> Basis set superposition error corrected.

b Indicates single-point energy with B3LYP/6-311++G(d,p)//B3LYP/6-31G(d,p)

<sup>&#</sup>x27;Indicates single-point energy with MP2/6-311++G(d,p)//B3LYP/6-31G(d,p)

- [12] Damin, A., Bonino, F., Ricchiardi, G., Bordiga, S., Zecchina, A., Lamberti, C., J. Phys. Chem. B, 106 (2002), 7524-7526.
- [13] Torrent, M., Vreven, T., Musaev, D.G., Morokuma, K., J. Am. Chem. Soc., 124 (2002), 192-193.
- [14] van Koningveld, H., van Bekkum, H., Jansen, J.C., Acta Crystallogr. B, 43 (1987), 127-132.
- [15] Dapprich, S., Komarmi, I., Byun, K.S., Morokuma, K., Frish, M.J., J. Mol. Struct. (Theochem), 461 (1999), 1-21.
- [16] Pelmenschikov, A., Leszczynski, J., J. Phys. Chem. B, 103 (1999), 6886-6890.
- [17] Wesolowski, T.A., Parisel, O., Ellinger, Y., Weber, J. J. Phys. Chem. A, 101 (1997), 7818-7825.
- [18] Derouane, E.G., Chang, C.D., Microporous Mesoporous. Mater., 425 (2000), 35-36.
- [19] Clark, L.A., Sierka, M., Sauer, J., J. Am. Chem. Soc., 125 (2003), 2136-2141.
- [20] Vos, A.M., Rozanska, X., Schoonheydt, R.A., van Santen, R.A., Hutschka, F., Hafner, J., J. Am. Chem. Soc., 123 (2001), 2799-2809.
- [21] Rozanska, X., van Santen, R.A., Hutschka, F., Hafner, J., J. Am. Chem. Soc., 123 (2001), 7655-7667.
- [22] Frisch, M.J., Trucks, G.W., Schlegel, H.B., Scuseria, G.E., Robb, M.A., Cheeseman, J.R., Zakrzewski, V.G., Montgomery, J.A., Stratmann, Jr. R.E., Burant, J.C., Dapprich, S., Millam, J.M., Daniels, A.D., Kudin, K.N., Strain, M.C., Farkas, O., Tomasi, J., Barone, V., Cossi, M., Cammi, R., Mennucci, B., Pomelli, C., Adamo, C., Clifford, S., Ochterski, J., Petersson, G.A., Ayala, P.Y., Cui, Q., Morokuma, K., Salvador, P., Dannenberg, J.J., Malick, D.K., Rabuck, A.D., Raghavachari, K., Foresman, J.B., Cioslowski, J., Ortiz, J.V., Baboul, A.G., Stefanov, B.B., Liu, G., Liashenko, A., Piskorz, P., Komaromi, I., Gomperts, R., Martin, R.L., Fox, D.J., Keith, T., Al-Laham, M.A., Peng, C.Y., Nanayakkara, A., Challacombe, M., Gill, P.M.W., Johnson, B., Chen, W., Wong, M.W., Andres, J.L., Gonzalez, C., Head-Gordon, M., Replogle, E.S., and Pople, J.A., Gaussian, Inc., Pittsburgh PA, 2001.
- [23] Frende, D., Klinowski, J., Hamdan, H., Chem. Phys. Lett., 149 (1988), 355-362.
- [24] O'Malley, P.J., Farnworth, K., J. Phys. Chem. B, 102 (1998), 4507-4515.
- [25] Dixit, L., Prasada Rao, T.S.R., J. Chem. Inf. Comput. Sci., 39 (1999), 218-223.

# A QUANTUM CHEMICAL STUDY OF THE INTERACTION OF CARBONYLS WITH H-ZSM-5 ZEOLITE

Bundet Boekfa, Jakkapan Sirijareansre, Piboon Pantu, and Jumras Limtrakul\*

Laboratory for Computational & Applied Chemistry, Chemistry Department, Kasetsart University, Bangkok 10900, THAILAND

#### **ABSTRACT**

The quantum cluster, ONIOM and embedded ONIOM models have been used to investigate adsorption properties of carbonyls in H-ZSM-5 zeolites. The active site has been modeled with realistic cluster sizes up to 46 tetrahedra. The predicted adsorption energies of ZSM-5/carbonyls complexes for the embedded ONIOM2(MP2/6-311G(d,p):UFF) scheme are -119.0 and -139.0 kJ/mol for acetaldehyde and acetone, respectively, the latter value compared well with the experimental estimated of 130 ± 4 kJ/mol, whereas the conventional quantum cluster yields an underestimate value of -68.2 kJ/mol. The results obtained in this study suggest that the new embedded ONIOM scheme provides a more accurate method of studying the interaction of carbonyls with zeolites.

#### INTRODUCTION

Aldol condensation of acetone and acetaldehyde is an important reaction in organic synthesis because it leads to C-C bond formation. This reaction can be catalyzed by acid and base catalysts such as NaOH, H<sub>2</sub>SO<sub>4</sub> etc. However, these corrosive catalysts cause a number of problems concerning handling, safety, corrosion, and waste disposal. Therefore, the conventional liquid-acid catalysts are progressively replaced by heterogeneous catalysts. Many types of catalysts have been used for this reaction such as various oxides [1-3] and various zeolites [4-14]. The zeolite catalysts also offer the advantage of high selectivity toward the desired product due to the shape selective properties of their microcrystalline pore structures. Several types of zeolites have been reported to have high activity for aldol condensation such as H-ZSM-5, HY, HX, etc. (refs) Numerous experiments have focused on investigating the interaction of acetaldehyde and acetone on H-ZSM5 zeolite by using different techniques such as NMR [15], FT-IR [16], <sup>13</sup>C-NMR [7-8, 14, 17-18], etc. From experimental data, it is indicated that the stoichiometric of adsorption of acetaldehyde and acetone on H-ZSM5 zeolite is 1:1 adsorption complex. The adsorption complex is in the form of a hydrogen-bonded complex which is the interaction between the carbonyl group and the Brønsted acid site of zeolite. Sepa et al. [17] found that the heat of adsorption energy of acetone on H-ZSM5 zeolite is 130 ± 4 kJ/mol.

There have been several theoretical studies on the adsorption of acetone in zeolite using quantum cluster calculations [16-17, 19]. These studies provided useful information on the mechanism and energetic properties of the reaction. However, none of these studies included the effects of the zeolite framework and, as a result, the predicted adsorption energies of acetone on H-ZSM-5 in a range of -55 to -64 kJ/mol were significantly lower than the experimental adsorption energy of acetone on the acidic H-ZSM-5 zeolite (-130 ± 4 kJ/mol). Such a large deviation indicates an important effect of the extended framework in stabilizing the adsorption complex. To accurately include the effects of the extended zeolite framework on the catalytic

\*Corresponding author, Fax: 662-9428900 ext 324. E-mail addresses: fscijrl@ku.ac.th (J. Limtrakul) properties, one can employ the periodic electronic structure methods such as the periodic density functional theory methodology. However, due to the large unit cells of typical zeolites, such calculations are often computationally unfeasible. The hybrid methods, such as the embedded cluster or combined quantum mechanics/molecular mechanics (QM/MM) methods, as well as the more general ONIOM (Our-own-N-layer Integrated molecular Orbital + molecular Mechanics) provide a cost effective computational strategy for including the effects of the zeolite framework [20-23].

In this study, the interactions between carbonyl compounds, acetaldehyde and acetone, with different models of H-ZSM5 have been studied with the aims of investigating; a) the effects of the zeolite framework on the interaction between carbonyl compounds with H-ZSM5 zeolite; b) efficient schemes of the ONIOM method. The models consist of an inner layer of active region, modeled by a small cluster using the density functional theory to account for interactions of the adsorbates with the acid site of zeolite, and a large outer layer of the zeolite framework, represented by a molecular mechanics force field, to account for the van der Waals interactions arising from confinement of the pore structure. Due to the large dipole moments of the adsorbates, the long-range electrostatic interactions are expected to contribute significantly to the adsorption process. Therefore, the electrostatic effect of the whole zeolite crystal lattice is additionally included using an electronic embedded method. This is the first time that the ONIOM method and long-range interacting method are being used in combination and, thus, we call it "embedded ONIOM."

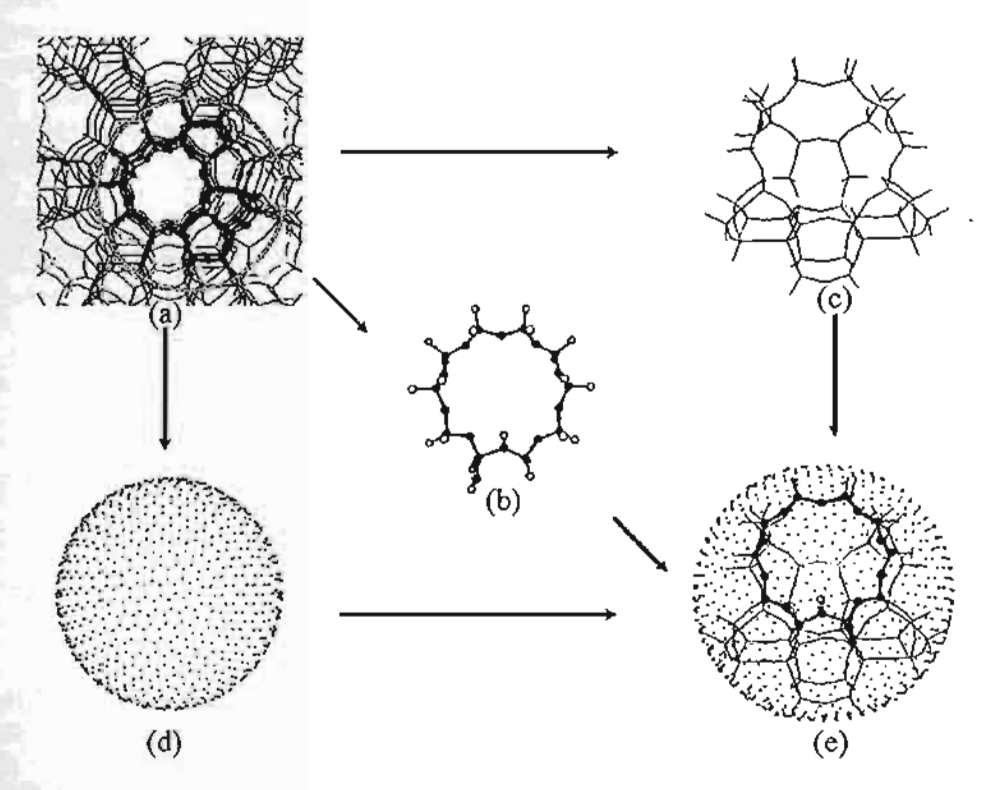


Figure 1: Schematic diagram of embedded ONIOM method: periodic structure of ZSM-5 framework (a) was subdivided into three parts: the innermost is the QM region (b); the next layer is UFF part (c) and the outermost is a set of point charges (d); complete model of embedded ONIOM (e).

#### **METHODS**

Three different models have been employed to model the H-ZSM5 zeolite and their complexes with the adsorbed carbonyl compounds. First, bare cluster models, 3T and 10T (Figures 2-3), were taken from the crystal structure of ZSM-5 lattice [24] to model the ZSM-5 system by using B3LYP/6-31G(d,p) level of theory for calculation. Second, a larger cluster of the 46T model were proposed for representing the system of H-ZSM5 treated by using the ONIOM (B3LYP/6-31G(d,p): UFF) approach. In the ONIOM2 (B3LYP/6-31G(d,p): UFF) scheme, the active Brønsted acid site of the zeolite is treated quantum chemically at the

B3LYP/6-31G(d,p) and MP2/6-311G(d,p) level of theory, and the other extended framework, up to 46T, is treated at the UFF.

In order to take into account the long-range interactions of the zeolite lattice beyond the 46T, the third model, called "embedded ONIOM2", calculations of the zeolite framework are developed. The embedded ONIOM2 models consist of three layers. The center layer is a ten-tetrahedral (10T) quantum chemical cluster. The next layer is the UFF force fields. The outermost layer of the model is a set of optimized point charges located to model the remaining Madelung potential from the extended zeolite crystal. Accuracy of the method for modeling the adsorption process has been compared to the experimental observation [17].

All calculations have been performed by using the Gaussian98 code [25]. The basis set 6-31G(d,p) is utilized for the B3LYP calculations. It is known that DFT does not account for the dispersion component of the interactions. Single point MP2/6-311G(d,p) calculations for the high-level active region were carried out at the B3LYP optimized geometries to improve the energetic information between benzene and the zeolite framework. During the structure optimization, only the active site region [=SiOHAI(O)<sub>2</sub>OSi=], and the adsorbate are allowed to relax.

#### RESULTS AND DISCUSSION

#### Comparisons of quantum cluster with ONIOM models

All cluster models of H-ZSM-5 of zeolite are illustrated in Figures 2-5 and their corresponding selected structure parameters are tabulated in Tables 1-2. Three different aluminosilicate clusters containing up to 46 tetrahedrally coordinated tetravalent atoms modeled the H-ZSM-5 zeolites. The more realistic 46T model covers the cavity at the intersection of the straight channel, and the zigzag channels, where the adsorbate is favorably adsorbed.

Table 1 Optimized geometries of the isolated model and adsorption complex of acetaldehyde on H-ZSM5 zeolite.
(Bond lengths are in pm and angles in degrees)

Parameters			N	(ethod		
	3T		<u> </u>	10T		6 T
	Isolated	Complex	Isolated	Complex	Isolated	Complex
Sil-Ol	169.3	168.0	167.3	165.7	165.8	164.1
OI-Al	186.5	183.4	184.1	180.8	185.5	180.8
Al-O2	169.6	170.6	168.1	168.9	166.9	167.5
O2-Si2	165.6	161.7	160.4	159.3	158.4	157.3
O1-H1	96.8	101.4	97.0	103.0	97.1	102.7
Al-H1	232.9	242.0	234.6	240.8	230.8	239.5
H1-O3	-	158.4	-	152.3	-	151.6
O3-C1	-	122.7	-	122.7	-	122.7
C1-H2	-	110.1	-	1 J 0.0	-	110.0
H2-O2	-	221.9	-	236.7	-	238.4
∠Si1-O1-AI	134.3	132.1	134.2	131.7	135.6	133.3
∠Al-O2-Si2	122.5	125.2	122.9	126.1	118.9	122.0
∠Al-O1-H1	106.2	113.2	109.2	113.3	105.2	112.3
∠O1-H1-O3	¥-	171.0	-	176.3		173.f

To assess the sensitivity of the active site structure with varying environments, we optimized the active site, [≡SiO(H)Al(O)₂OSi≡], for all the clusters, whilst the remaining atoms were kept fixed at the crystallographic positions. By comparing the structure between the full quantum cluster model of 3T and 10T models, it is seen that the cluster size environment has a little effect on the structure of the active site. The extended framework has the effect of lengthening the O1-H bond distance (Brønsted acid site) by 0.2 pm (full B3LYP). In the ONIOM2 schemes, specifically B3LYP/6-31(d,p):UFF, the O1-H bond distances are increased by 0.3 pm, thus enhancing the acidity of the Brønsted acid site. While the other bond distances of the active site region such as A1-O, Si-O (to O1 and O2) are affected by the increasing cluster size as shown in Tables 1-2.

#### The interactions of acetone and acetaldehyde with the H-ZSM5 zeolite

The structure of acetone and acetaldehyde adsorbed on different models of H-ZSM5 zeolite are shown in Figures 2a-4a. Acetaldehyde is adsorbed on the Brønsted acid site by forming a strong hydrogen bonding interaction between the carbonyl oxygen (O3), acidic proton (H1), and a weak hydrogen bonding interaction between the aldehyde hydrogen (H3) and the adjacent framework oxygen (O2) of the zeolite. Increasing the cluster sizes increases the interactions between the acetaldehyde and the zeolite as evidenced by the decrease of the H1-O3 bond distance from 158.4 to 152.3 and to 151.6 pm concurrently with the increase of the acidic O1-H1 bond distance from 96.8-97.1 pm for isolated acidic O1-H1 to 101.4, 103.0, and 102.7 pm as the cluster size is progressively increased. On the other hand, acetone is adsorbed by forming only one strong hydrogen bonding interaction between the carbonyl oxygen and the acidic proton. Increasing the cluster size has a more subtle effect on the adsorbed acetone.

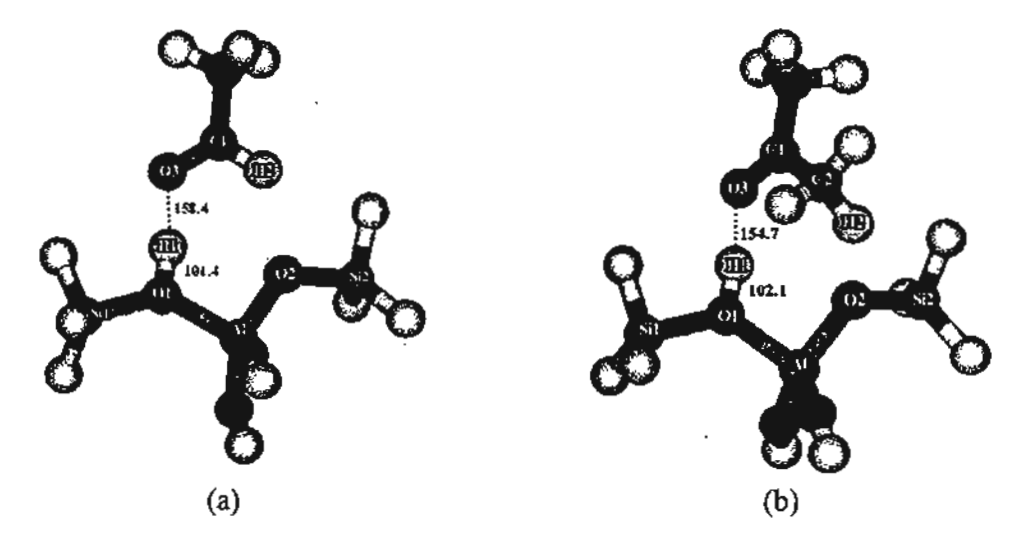


Figure 2: The interaction of carbonyls with the 3T bare cluster model of H-ZSM-5 zeolite: (a) acetaldehyde; (b) acetone.

Due to the increase in steric interactions between the methyl groups of the acetone and the zeolite framework as the cluster size increases, the adsorbed acetone is moved toward the intersection cavity, where it can be further stabilized. In all cases, the structure of the zeolite structure was not significantly changed by the adsorption of the adsorbates.

Table 2 Optimized geometries of the isolated model and their adsorption complexes of acetone on H-ZSM5 zeolite (Bond lengths are in pm and angles in degrees).

Parameters			M	ethod	11-1	
	3T			0T	10T / 46T	
	Isolated	Complex	Isolated	Complex	Isolated	Complex
Si1-O1	169.3	167.8	167.3	165.4	165.8	164.5
O1-Ai	186.5	183.3	184.1	180.3	185.5	180.9
A1-O2	169.6	170.4	168.1	168.4	166.9	166.9
O2-Si2	165.6	161.6	160.4	159.0	158.4	157.1
O1-H1	96.8	102.1	97.0	104.4	97.1	102.9
Al-H1	232.9	243.1	234.6	238.7	230.8	233.9
H1-O3	-	154.7	-	147.9		154.4
O3-C1	-	123.2	-	123.4	-	123.2
C1-C2	-	150.5	-	150.3	-	150.6
H2-O2	-	224.7	-	268.3	-	282.3
∠Si1-O1-Al	134.3	132.0	134.2	132.0	135.6	133.2
∠Al-O2-Si2	122.5	125.5	122.9	126.5	118.9	122.1
∠Al-O1-HI	106.2	113.8	109.2	111.2	105.2	107.8
∠01-H1-03	-	173.7	-	173.0	-	6.691

The adsorption energy is one of the most valuable data obtained from experimental observation which can be used to validate the theoretical data. The adsorption energies of acetone and acetaldehyde on H-ZSM-5 zeolite calculated from different models, as discussed above, and also those from the ONIOM models using the molecular mechanics force fields for the outer layer are documented in Table 3.

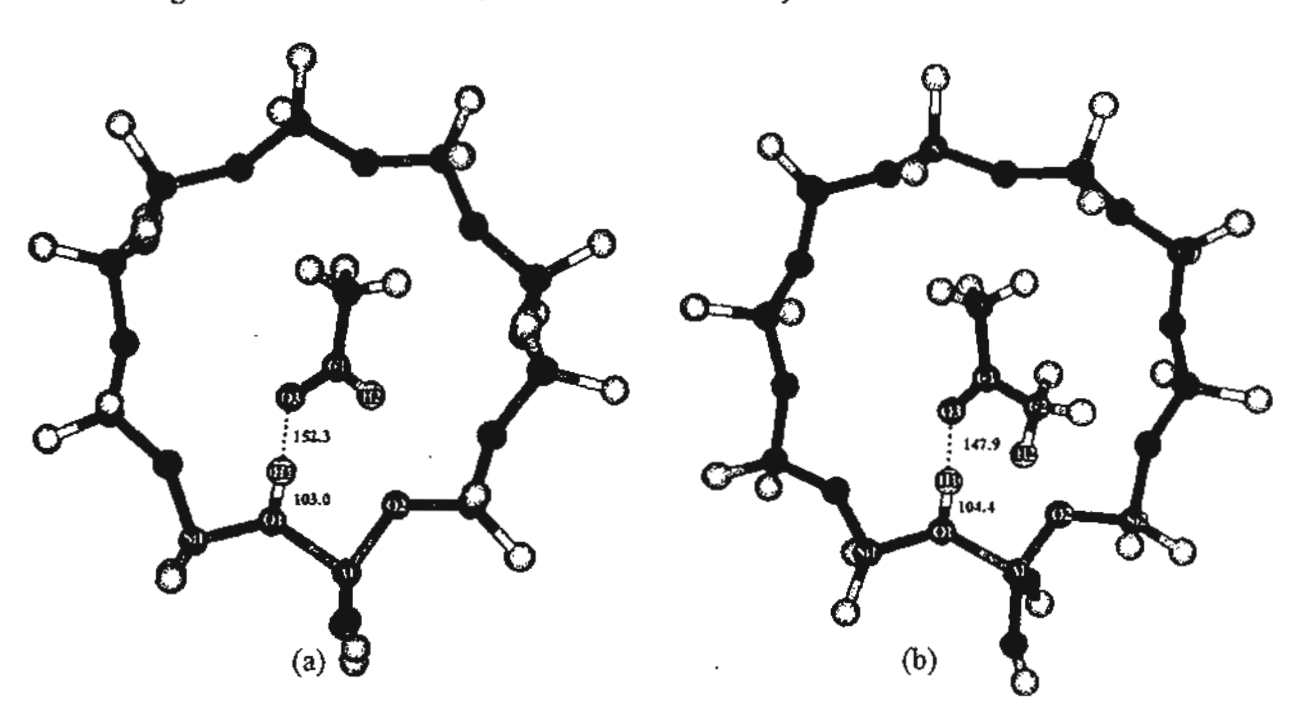


Figure 3: Presentation of carbonyl compounds interacted with the 10T bare cluster model of H-ZSM-5 zeolite: (a) acetaldehyde; (b) acetone.

Using the 3T cluster model, the DFT methods predict the adsorption energies of acetaldehyde and acetone to be -66.7 and -68.2 kJ/mol, respectively. These energy values are significantly lower than those of the experimental results. The adsorption energy of acetone on the acidic H-ZSM-5 zeolite was determined to be -130 kJ/mol [17]. Increasing the cluster size from 3T to 10T clusters, the calculated adsorption energies ( $\Delta E_{ads}$ ) of acetaldehyde and acetone interacted with zeolites is still well below the observation value, but somewhat differentiable (Table 3).

Table 3 Comparison of the adsorption energy,  $\Delta E_{ads}$  (in kJ/mol) along the adsorption of acetaldehyde and acetone on H-ZSM5 zeolite in different models and methods.

Methods/models	3T		10T		46T	
	Acetaldehyde	Acetone	Acetaldehyde	Acetone	Acetaldehyde	Acetone
B3LYP/6-31G(d,p)	-66.7	-68.2	-67.7	-71.1	-	-
B3LYP/6-31G(d,p):UFF	•	-	-	-	-83.0	-90.6
B3LYP/6-31G(d,p):UFF+charges1	-	•	-	-	-103.3 b	-125.6 <sup>b</sup>
MP2/6-311G(d,p):UFF+charges <sup>a</sup>	-	-	-	-	-119.0 <sup>ь</sup>	-139.0 <sup>b</sup>

Experimental adsorption energy of acetone on H-ZSM5 zeolite is 130 ± 4 kJ/mol from Ref. [17]

Increasing the cluster size from 10T up to the more realistic model, 46T, by enlarging the outer layer, the differences between each adsorption energy are pronounced. The adsorption energies of acetaldehyde and acetone calculated from the 46T cluster using ONIOM2 (B3LYP/6-31(d,p):UFF) are calculated to be -83.0

<sup>&</sup>lt;sup>a</sup>Set of point charges surrounding the 46T model

Indicates single-point energy at indicated level of theory on the optimized B3LYP/6-31G(d,p):UFF structure

and -90.6 kJ/mol, respectively. These interaction energies are still underestimated as compared to the experimental results.

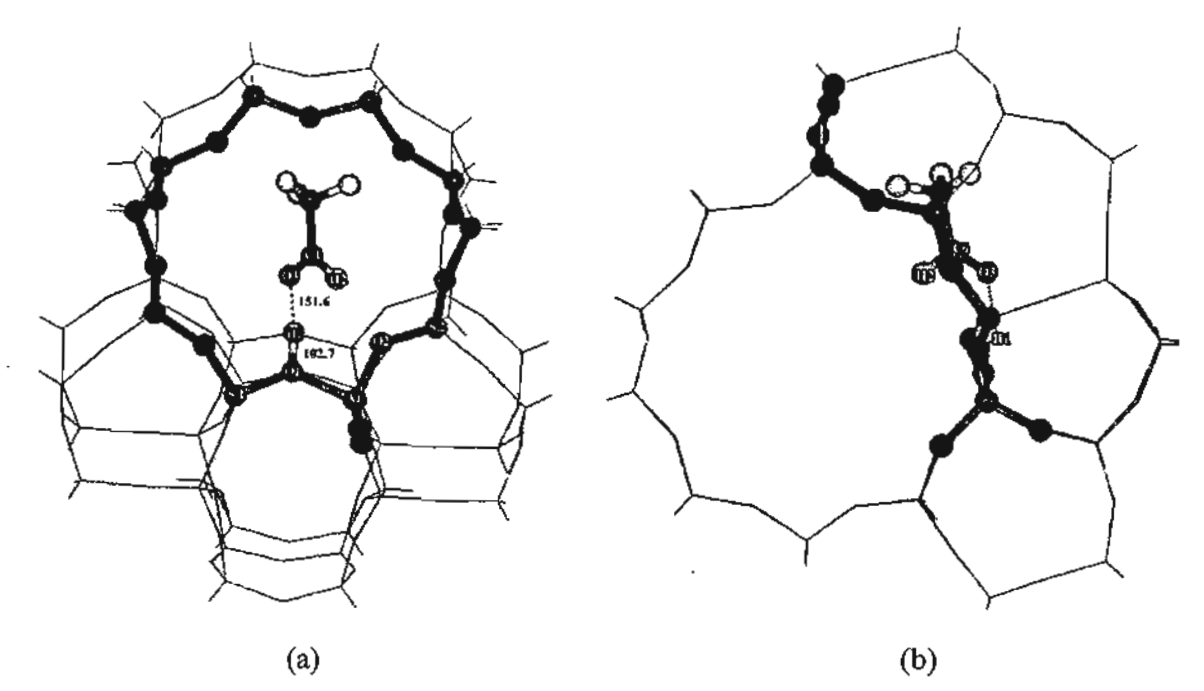


Figure 4: Presentation of acetaldehyde interacted with the 46T ONIOM model of H-ZSM-5 zeolite: viewed from the zigzag channel (a) and the straight channel (b).

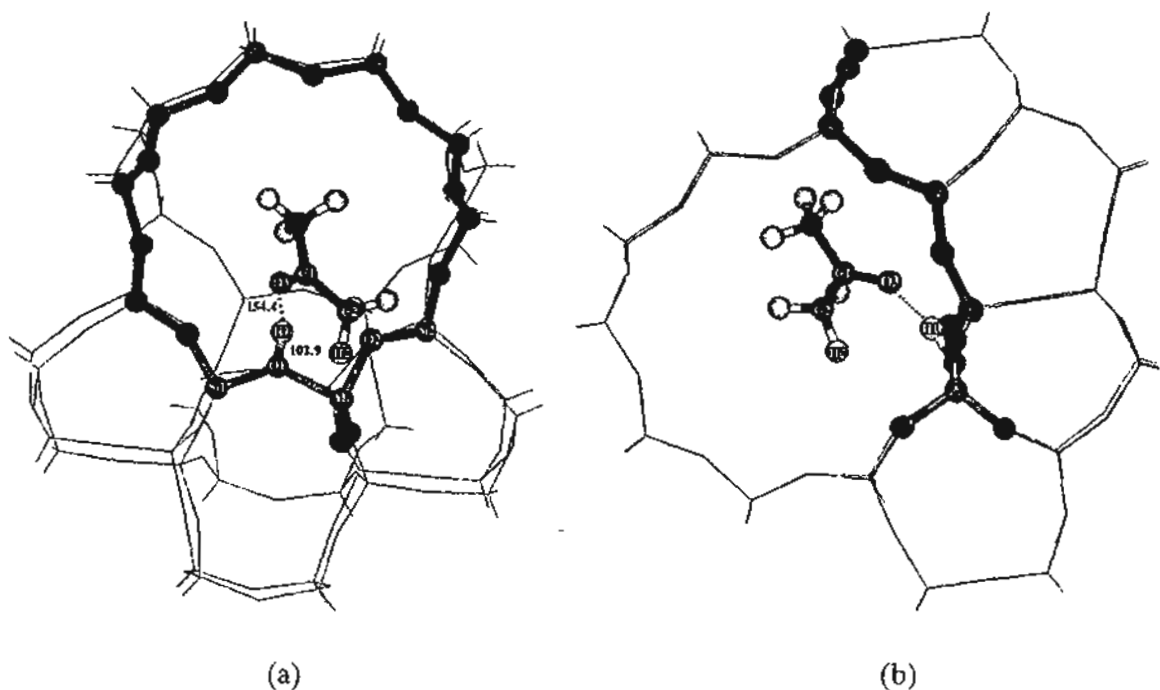


Figure 5: Presentation of acetone interaction with the 46T ONIOM model of H-ZSM-5 zeolite: viewed from the zigzag channel (a) and the straight channel (b).

It is known that DFT does not account for the dispersion component of the interactions. Single point MP2/6-311G(d,p) calculations for the high-level active region were carried out at the B3LYP optimized geometries to improve the energetic information between benzene and the zeolite framework. And in order

to take into account the long range interactions of the zeolite lattice beyond the 46T, the "embedded ONIOM2" calculations of the zeolite framework is employed. This yields the adsorption energies of -119.0 and -139.0 kJ/mol for acetaldehyde and acetone, respectively. Our predicted value for the latter system is in excellent agreement with the experimental estimate of  $-130 \pm 4$  kJ/mol obtained by Sepa et al.,[17], indicating that the MP2 combining the UFF force fields method as a lower level is considered to be one of the best combinations for the ONIOM2 scheme. This efficient scheme provides a cost effective computational strategy for treating the effects of a large extended framework structure.

#### CONCLUSIONS

The adsorption of acetaldehyde and acetone on H-ZSM5 zeolite has been investigated with three different cluster sizes and methods. The bare cluster models,3T and 10T, (B3LYP/6-31G(d,p) quantum cluster approach predicts to have the adsorption energies of -66.7 (3T) vs. -68.2 (10T) kJ/mol for acetaldehyde/H-ZSM5 and -68.2 (3T) vs. -71.1 (10T) kJ/mol for acetone/H-ZSM5. The effect of zeolite framework is modeled on the ONIOM2 and e-ONIOM method. We found that the extended framework significantly enhances their adsorption energy of adsorbate molecules to the zeolite. The most accurate model, embedded ONIOM predicts the adsorption energy to be -119.0 and -139.0 kJ/mol for acetaldehyde and acetone, respectively. The calculated adsorption of acetone/H-ZSM5 complex using the e-ONIOM approach is in good agreement with the experimental data. The results obtained in this study indicate that the embedded ONIOM approach yields a more accurate model for studying adsorption properties on periodic systems.

#### ACKNOWLEDGMENTS

This work was supported in part by grants from the Thailand Research Fund (TRF Senior Research Scholar to JL.) and the Kasetsart University Research and Development Institute (KURDI) as well as the Ministry of University Affairs under the Science and Technology Higher Education Development Project (MUA-ADB funds).

#### REFERENCES

- 1. Ai, M., Bull. Chem. Soc. Jpn., 64 (1991), 1342.
- 2. Malinowski, S., Jedrzejewska, H., Basniski, S. and Benebek, S., Chim. Ind. Genie Chim., 85 (1961), 885.
- 3. Malinowski, S., React. Kinet. Catal., 1 (1974), 73.
- 4. Durnitriu, E., Hulea, V., Bilba, N., Carge, G. and Azzouz, A., J. Mol. Catal., 79 (1993), 175.
- 5. Dumitriu, E., Bilba, N., Lupascu, M., Azzouz, A., Hulea, V., Carge, G. and Nibou, D., J. Catal., 174 (1994), 133.
- 6. Dumitriu, E., Azzouz, A., Hulea, V., Lutic, D. and Kessler, H., Micropor. Mater., 10 (1997), 12.
- 7. Biaglow, A. I., Sepa, J., Gorte, R. J. and White, D., J. Catal., 151 (1995), 373.
- 8. Xu, T., Munson, E. J. and Haw, J. F., J. Am. Chem. Soc., 116 (1994), 1962.
- Dumitriu, E., Hulea, V., Fechete, I., Auroux, A., Lacaze, J.-F. and Guimon, C., MICROPOR. MESOPOR. MAT., 43 (2001), 341.
- 10. Panov, A. G. and Fripiat, J. J., J. Catal., 178 (1998), 188.
- 11. Kubelkaova, L., Cejka, J. and Novakova, J., Zeolites, 11 (1991), 822.
- 12. Kubelkaova, L. and Novakova, J., Zeolites, 11 (1991), 48.
- 13. Bell, V. A. and Gold, H. S., J. Catal., 79 (1983), 286.
- 14. Biaglow, A. I., Gorte, R. J., Kokotailo, G. T. and White, D., J. Catal., 148 (1994), 779.
- 15. Bohlmann, W. and Michel, D., J. Catal., 202 (2001), 421.
- 16. Florian, J. and Kubelkava, L., J. Phys. Chem., 98 (1994), 8734.
- 17. Sepa, J., Lee, C., Gorte, R. J., White, D., Kassab, E., Evleth, E. M., Jessri, H. and Allavena, M., J. Phys. Chem., 100 (1996), 18515.
- Lee, S.-O., Kitchin, S. J., Harris, K. D. M., Sanker, G., Dugal, M. and Thomas, J. M., J. Phys. Chem. B, 106 (2002), 1322.
- 19. Kassab, E., Jessri, H., Allavena, M. and White, D., J. Phys. Chem. A, 103 (1999), 2766.

- 20. Bobuatong, K. and Limtrakul, J., Appl. Catal. A, (2003), in press.
- 21. Panjan, W. and Limtrakul, J., J. Mol. Struct., 654 (2003), 35.
- 22. Raksakoon, C. and Limtrakul, J., THEOCHEM, 631 (2003), 147.
- 23. Kasuriya, S., Namuangruk, S., Treesukol, P., Tirtowidjojo, M. and Limtrakul, J., J. Catal., (2003), in press.
- 24. Koningveld, H. v., Bekkum, H. v. and Jansen, J. C., Acta Crystallogr. B, 43 (1987), 127.
- Frisch, M. J., Trucks, G. W., Schlegel, H. B., Scuseria, G. E., Robb, M. A., Cheeseman, J. R., Zakrzewski, V. G., Montgomery, J. A., Stratmann, Jr. R. E., Burant, J. C., Dapprich, S., Millam, J. M., Daniels, A. D., Kudin, K. N., Strain, M. C., Farkas, O., Tomasi, J., Barone, V., Cossi, M., Cammi, R., Mennucci, B., Pomelli, C., Adamo, C., Clifford, S., Ochterski, J., Petersson, G. A., Ayala, P. Y., Cui, Q., Morokuma, K., Salvador, P., Dannenberg, J. J., Malick, D. K., Rabuck, A. D., Raghavachari, K., Foresman, J. B., Cioslowski, J., Ortiz, J. V., Baboul, A. G., Stefanov, B. B., Liu, G., Liashenko, A., Piskorz, P., Komaromi, I., Gomperts, R., Martin, R. L., Fox, D. J., Keith, T., Al-Laham, M. A., Peng, C. Y., Nanayakkara, A., Challacombe, M., Gill, P. M. W., Johnson, B., Chen, W., Wong, M. W., Andres, J. L., Gonzalez, C., Head-Gordon, M., Replogle, E. S., and Pople, J. A., Gaussian, Inc., Pittsburgh PA, 2001.

### ภาคผนวก ข.5

ผลงานในการประชุมนานาชาติ
"American Chemical Society National
Meeting ครั้งที่ 229"
จำนวน 12 เรื่อง

#### Adsorption of aromatics on nanoporous MCM-41

#### Bavornpon Jansang and Jumras Limtrakul\*

Laboratory for Computational & Applied Chemistry, Physical Chemistry Division, Department of Chemistry, Faculty of Science, Kasetsart University, Bangkok 10900, Thailand.

E-mail address: fscijrl@ku.ac.th (Limtrakul)

MCM-41 nanoporous materials have drawn tremendous interest from fields ranging from physics and chemistry to engineering, owing to their unique characteristics, i.e. shape- and size-selectivity. Here, the first of aromatic hydrocarbon adsorption inside in this nanonmaterials has been carried out and adsorption properties are compared to known behaviors in the MCM-41. The two-layer ONIOM (Our own N-layered Integrated molecular Orbital + molecular Mechanics) methods have been carried out on nanocluster models representing MCM-41 and their complex with benzene. When carefully calibrated, using the experimental observation as a benchmark, the ONIOM(B3LYP/6-311++G(d,p):UFF), in which a reaction site is treated at the B3LYP/6-311++G(d,p) level, and the rest using Universal Force Field (UFF) has been found to provide reliable information for evaluating the influence of the extended framework on the structure and energetic properties of the C6H6/MCM-41 nanosystem. The predicted interaction energy for this ONIOM scheme is -15.2 kcal/mol, which agrees well with the experimental result of -14.4 kcal/mol.

## Interaction of the different types of dienes with single wall carbon nanotube (SWNT) and $C_{60}$ : A QM/MM study

#### P. Khongpracha, C. Warakulwit, S. Bamrungsap, P. Luksirikul and J. Limtrakul\*

Laboratory for Computational & Applied Chemistry, Physical Chemistry Division, Department of Chemistry, Faculty of Science, Kasetsart University, Bangkok 10900, Thailand. E-mail address: fscijrl@ku.ac.th

The transition states and products of the Diels-Alder cycloadditions of the different types of dienes have been investigated within the framework of our-Own-N-layered-Integrated molecular Orbital and molecular Mechanic (ONIOM) approaches utilizing the two layered ONIOM scheme (B3LYP/6-31G\*:AM1). The structure and activity relationship for a series of different outer-ring dienes interacted with armchair (5,5) single wall carbon nanotubes (SWNT) were established. The reactivity of the Diels-Alder reaction has been related to the distance between the methylene carbons in the butadiene moiety (R<sub>1,4</sub>) of these outer-ring dienes. The reactivity is higher as the R<sub>1,4</sub> becomes shorter. Nevertheless, in the case of the most reactive diene considered in this study, 2,3-dimethylene-1,4-dioxane, the activation energy in SWNT reaction is still much higher than that of [60]fullerene. To enhance the capability of the Diels-Alder reaction of SWNT at the sidewall, the metal cation was introduced into the SWNTs. The decrease of activation energy of Diels-Alder is due mainly to the electron deficiency nature of the double bond of Na@SWNT and the stabilization of LUMO and HOMO orbitals.

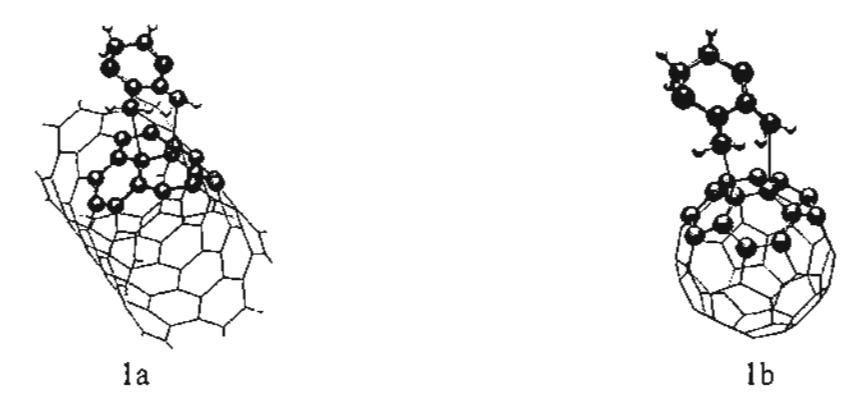
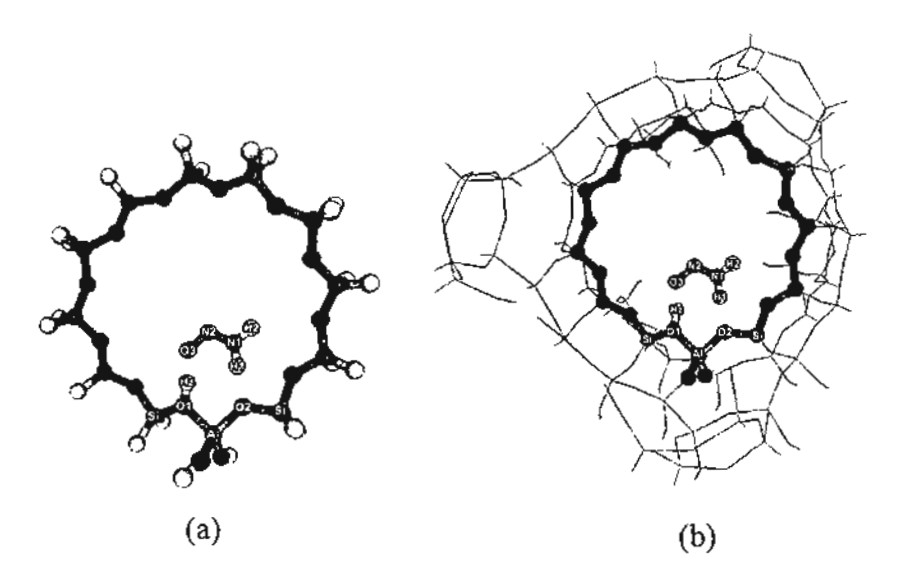


Fig. 1. The transition state structures of SWNT (1a) and C<sub>60</sub> (1b) with 2,3-dimethylene-1,4-dioxane.

## Model and ONIOM (QM/MM) studies of isomerization of nitrosamine over nanoporous catalysts

Chorchat Soonthornpalin and Jumras Limtrakul\*
Laboratory for Computational & Applied Chemistry, Physical Chemistry Division,
Kasetsart University, Bangkok 10900, Thailand;
e-mail address: fscijrl@ku.ac.th (J. Limtrakul)

To unravel isomerization and decomposition of nitrosamine over H-faujasite, the ab initio molecular orbital calculations (B3LYP/6-31G(d,p)) and the ONIOM2 method (B3LYP/6-31G(d,p):UFF) have been performed with three different cluster sizes, 3T, 12T and 84T. The reaction intermediates and reaction routes are defined. Nitrosamine can decompose via trans-diazene, cis-diazene, and cis-diazene-trans-H intermediates. These reaction intermediates are not stable and quickly decompose to N<sub>2</sub> and H<sub>2</sub>O. The zeolite framework stabilizes the intermediates via the formation of hydrogen bonds. These hydrogen bond interactions play an important role in the binding of intermediate species on the zeolite and the course of reaction. The interactions between the reaction intermediates and H-faujasite are relatively strong and evaluated to be 24.87, 23.49, 21.59, and 18.78 kcal/mol for the nitrosamine/H-FAU, trans-diazene/H-FAU, cis-diazene/H-FAU, and cis-diazene-trans-H/H-FAU complexes, respectively. The zeolite acid site facilitates the decomposition of nitrosamine via a series of proton transfer and isomerization reactions.



Presentation of NH<sub>2</sub>NO molecule interaction with the model of the faujasite zeolite clusters: (a) 3T cluster model; (a) 12T cluster model; and (b) ONIOM2 layer model of 84T cluster. The sphere atoms in cluster 84T are treated at the higher level in the ONIOM2 approach.

## Interaction of pyridine with nanoporous catalyst: An embedded ONIOM study

Jarun Lomratsiri<sup>1</sup>, Michael Probst<sup>2</sup>, Jumras Limtrakul<sup>1\*</sup>

<sup>1</sup>Laboratory for Computational & Applied Chemistry, Chemistry Department, Kasetsart University, Bangkok 10900, Thailand <sup>2</sup>Institut für Ionenphysik, Universität Innsbruck, Technikerstrasse 25, 6020 Innsbruck, Austria

#### **Abstract**

The adsorption properties of pyridine on H-ZSM-5 zeolites have been investigated by cluster calculations with the ONIOM and a new embedded ONIOM scheme. The active site has been modeled with realistic cluster sizes of up to 46 tetrahedra. Two different types of pyridine adsorption complexes on the zeolite models are found. If Zeolite is modeled by a small 3T quantum cluster, the adsorption energy of the hydrogen-bonded pyridine complex (Py---Hz), is found to be -18.5 kcal/mol. When a larger cluster or the ONIOM models are employed, the optimized geometries show the formation of pyrdinium cation [PyH<sup>+</sup>] bound as an ion-pair complex [PyH<sup>+</sup>][Z]. The calculated energy of formation for this ion-pair complex is -36.8 kcal/mol in the ONIOM (B3LYP/6-31G(d,p):UFF) model. Both values are considerably lower than the experimentally estimated heat of adsorption of pyridine in ZSM-5 zeolite of -47.6 kcal/mol. Inclusion of the electrostatic effects of the zeolite crystal lattice via the embedded ONIOM model increases the adsorption energy to -44.4 kcal/mol. Performing the quantum-chemical treatment at the MP2/6-31G(d,p) level instead of the B3LYP/6-31G(d,p) leads to a further small increase of the adsorption energy to -45.9 kcal/mol, suggesting that the new embedded ONIOM scheme provides an accurate method of studying the interaction of small organic molecules with zeolites.

The 1,3-dipolar cycloadditions of ozone on the cap of two series of [5,5] armchair and [9,0] zigzag single-walled carbon nanotubes capped with fullerene hemispheres

#### Montree Sawangphruk and Jumras Limtrakul

Laboratory for Computational & Applied Chemistry, Faculty of Science and Center of Nanotechnology, Kasetsart University, Bangkok 10900 Thailand

The 1,3-dipolar cycloadditions of ozone on the caps of [5,5] and [9,0] single-walled carbon nanotubes capped with fullerene hemispheres have been carried out with in the framework of ONIOM scheme (B3LYP/6-31G(d): AM1). Inclusion of the number of cyclic polyene chains have effects on the energetic and electronic properties of both the SWNT adducts and lead to conclusive findings in regard to the energies gab (HOMO-LUMO), reaction energies, and activation energies of the two series of finite length [5,5] armchair nanotube C60+10n (n=1-14) and the [9,0] zigzag nanotube C60+18n (n=1-8), both capped with fullerene hemisphere. The energies gap, reaction energies, and activation energies of the [5,5] SWNT adducts series are found to depend on the number of cyclic cis-polyene units lined up along the nanotube length while the [9,0] SWNT adducts series are predicted to be insensitive with the number of cyclic trans-polyene units. The ONIOM reaction energies of the series of [5,5] armchair SWNT adducts are oscillated within -46 to -49 kcal/mol, while the [9,0] zigzag SWNT adducts are about -48 kcal/mol, respectively. The predicted activation energies of the [5,5] SWNT adducts series are found to be oscillated between 1.5 to 3 kcal/mole, on the other hand, the corresponding values of the [9,0] zigzag SWNT adducts remains relatively unchanged at about 2 kcal/mol. Our results derived in this study suggest that the ONIOM2 scheme yields an accurate method for investigating the functionalized SWNT complexes and their applications in energy storage medium or various environmental issues.

ONIOM study of partial oxidation of methane to methanol on Co-ZSM-5 and Fe-ZSM-5 nanoporous catalysts

Nutcha Injan, Suwat Pabchanda, and Jumras Limtrakul\*

Laboratory for Computational and Applied Chemistry, Physical Chemistry Division,

Kasetsart University, Bangkok 10900, Thailand

\*Corresponding authors: fscijrl@ku.ac.th, (J. Limtrakul)

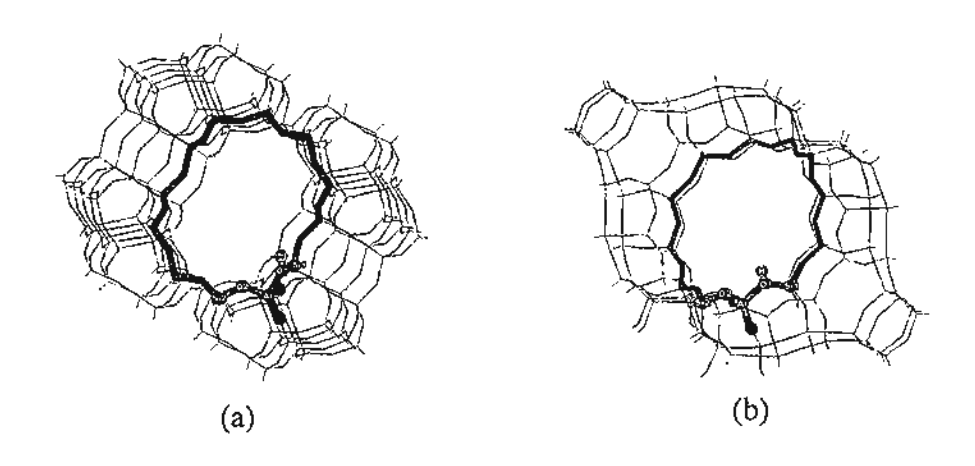
#### Abstract

Partial oxidation of methane to methanol on Fe-ZSM-5 and Co-ZSM-5 nanoporous catalysts has been investigated using the ONIOM (Our-own-N-layer Integrated molecular Orbital + molecular Mechanics) approach. A 46T cluster of ZSM-5 is modeled for the ONIOM2 (B3LYP/6-31G(d,p):UFF) method. Mononuclear [FeO2]+ and [CoO2]+ are modeled as the active sites located in the ion-exchanged site of Fe-ZSM-5 and Co-ZSM-5, respectively. When methane is adsorbed on the active site, the proton of CH4 is transferred to the active site yielding either methyl radical or methoxide intermediates, depending on the types of zeolite employed. Both intermediates can be derived via the Fe-ZSM-5 complex, while only the methoxide intermediates are obtained from the Co-complexes. The corresponding activation energies of both adducts are predicted to be 15.3 and 16.6 kcal/mol for the Fe-ZSM-5 and Co-ZSM-5, respectively. As for Fe-ZSm-5, the methyl radical reacts with the hydroxyl group of the active site, which generates a methanol product having the energy of methane formation of 11.1 kcal/mol, Alternatively, for both complexes, the strongly adsorbed methoxide species can be hydrolyzed to provide the methanol product. Our results derived in this study suggest that the reaction pathway of methane conversion occurred through the methoxide species for both type of catalysts.

#### Adsorption of light hydrocarbons on nanoporous mordenite and faujasite catalysts

Pinyo Wongthong and Jumras Limtrakul\*
Laboratory for Computational & Applied Chemistry, Physical Chemistry Division,
Kasetsart University, Bangkok 10900, Thailand;
E-mail address: fscijrl@ku.ac.th (J. Limtrakul)

The ONIOM (Our-own-N-layered Integrated molecular Orbital + molecular Mechanics) approach utilizing the three-layer ONIOM3(MP2/6-311++G(d,p):HF/6-31G(d):UFF) scheme has been used to investigate the adsorption properties of light hydrocarbons in two industrially important catalysts, such as mordenite (H-MOR) and faujasite (H-FAU). With the inclusion of the basis set superposition error (BSSE), the ONIOM3 adsorption energies are predicted to be -7.90, -9.68, -11.53, and -12.62 kcal/mol, respectively for H-MOR and -5.38, -8.73, -7.26, and -10.46 kcal/mol, respectively for H-FAU, which compare well with the experimental values of ethane, ethylene, and propane, which are -7.7, -9.7, and -10.7 kcal/mol, respectively for H-MOR and -5.7, -9.0, and -7.1 kcal/mol, respectively for H-FAU. The results derived in this study suggest that the ONIOM approach provides a more accurate method for investigating the adsorption of light hydrocarbons on these zeolites.



The ONIOM3 layer of 120T cluster models of H-MOR (a) and 84T cluster models of H-FAU (b). Atoms belonging to the 12T quantum cluster are drawn as bonds and sticks.

## Structural and electronic properties of the Rh/MgO(001) interface from periodic density functional calculations

Somkiat Nokbin<sup>1,2</sup>, Jumras Limtrakul<sup>2</sup> and Kersti Hermansson<sup>1,\*</sup>

<sup>1</sup>Materials Chemistry, The Ångström Laboratory, Box 538, SE-751 21 Uppsala, Sweden <sup>2</sup>Laboratory for Computational and Applied Chemistry, Department of Chemistry, Kasetsart University, Bangkok 10900, Thailand

Abstract: The Rh/MgO(001) system has been studied by means of periodic plane-wave density functional calculations using the VASP code and PAW potentials. Three surface coverages of Rh (1/8, 1/2 and 1 ML) were investigated at three different adsorption sites (on top of surface O, Mg and the hollow site). Three types of interaction energies have been calculated to help characterize the metal-oxide interaction: the energy of adsorption of Rh atoms ( $E_{ads}$ ), the energy of adhesion of a Rh overlayer ( $E_{adh}$ ) and the formation-of-the-Rh-layer energy. We find that Rh prefers to bind to the surface oxygen site. For 1 ML coverage, the metal-metal interactions within the Rh overlayer give the largest contribution to the stabilization of the Rh/MgO interface, while, naturally, the Rh-oxide interaction dominates at low coverage. The net result is that the adsorption energy (isolated MgO slab + isolated Rh atoms  $\rightarrow$  Rh/MgO interface) increases with increasing surface coverage. Moreover, electronic properties such as the density of states (DOS), electron density difference plot, spin density and the electron localization function (ELF) are presented to clarify the chemical bonding behavior of the Rh/MgO interface system.

Methodology: The Rh/MgO(001) system was investigated by means of periodic density functional theory (DFT) calculations using the Vienna Ab initio Simulations package, VASP, in which the electron density is expanded in a plane-wave basis set. The projector augmented-wave method (PAW) was used. In this study, both spin-polarized and non-spin-polarized calculations are reported to compare the effect of spin polarization on the Rh/MgO system. A cut-off energy of 500 eV was used in all cases. The electronic configurations of the atomic species employed in our calculations are Rh( $4p^6$ ,5 $s^1$ ,4 $d^8$ ), Mg( $2p^6$ ,3 $s^2$ ) and O( $2s^2$ ,2 $p^4$ ). The Brillouin zone integrations were performed using the Monkhorst-Pack (MP) algorithm with a Gaussian smearing factor with  $\sigma = 0.1$  eV and k-mesh points of 6x6x6 and 6x6x1 for the bulk and surface calculations, respectively.

A 2-dimensionally periodic slab model was mimicked using the 3-dimensionally periodic VASP code. A Rh layer was placed epitaxially on one side of the oxide slab and a vacuum-layer with a thickness of 15 Å was found to be sufficient for the surface calculations. Three different coverages (1/8, 1/2 and 1 ML) at three different sites (on top of O, Mg and the hollow) were explored. A 1x1 crystallographic supercell consisting of 8 layers of MgO(001) was selected as a model for the 1/2 and 1 ML coverages and for the lowest coverage (1/8 ML), a 2x2 supercell of 4 layers was used. The slab models were allowed to fully relax in all directions under the condition that the cubic unit cell was kept fixed at the optimized bulk lattice parameter of 4.25 Å (the experimental value is 4.21 Å).

<sup>\*</sup>E-mail address (corresponding author): kersti@mkem.uu.se

Results, Discussion and Conclusion: Our results show that Rh prefers to bind to the surface O atom site, which exhibits both a relatively large Rh-MgO interaction energy and a short Rh-surface distance. Also the hollow site is a rather attractive site for Rh, while adsorption on top of Mg is considerably less favourable. Our results for adsorption on the O sites are illustrated in Fig. 1. Our calculated adhesion energies over O are in good agreement with the scarce literature data existing. The adhesion energy [Rh layer + MgO slab  $\rightarrow$  Rh/MgO slab] is found to decrease with surface coverage and the adsorption energy [Rh(g) + MgO slab  $\rightarrow$  Rh/MgO slab] increases with coverage, thanks to the strong Rh-Rh interaction for large coverage. Rh adsorption at the O site introduces more electron density rearrangement in the oxide slab than adsorption at the Mg site.

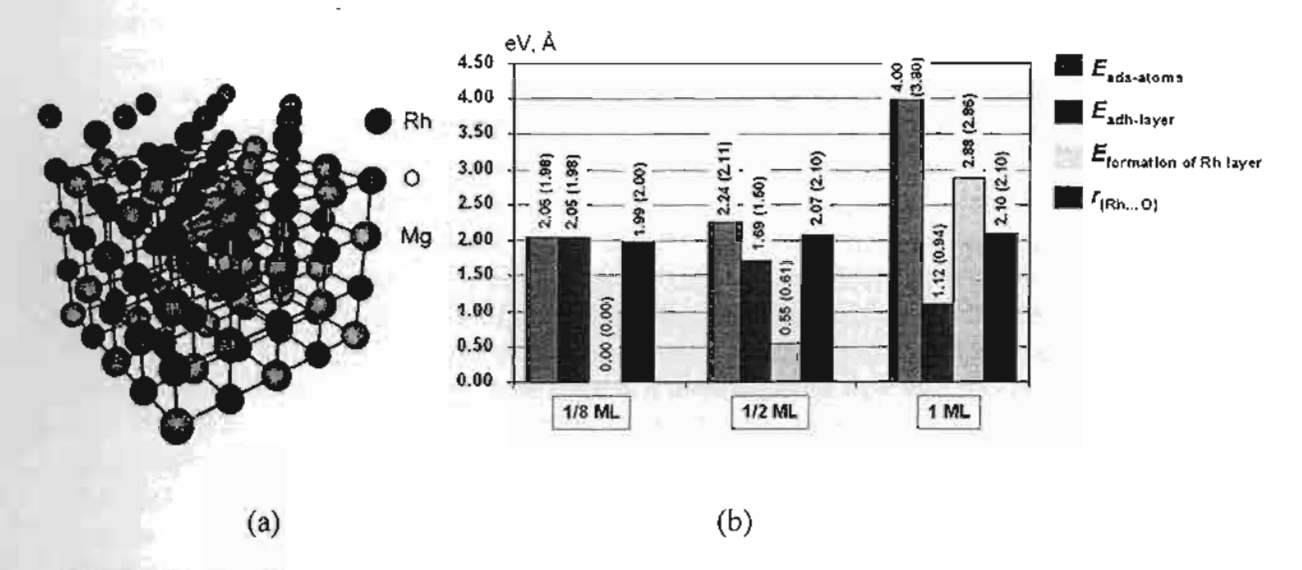


Figure 1. Rh/MgO(001) when Rh is placed on top of surface O: (a) 1 ML coverage of Rh above the surface oxygen, (b) the optimized Rh-O distance as well as the three different types of interaction energies for different Rh coverages at the O site. The energies are given per Rh atom.

Acknowledgements: Financial support from the Swedish Foundation for International Cooperation in Research and Higher Education (STINT) and the Swedish Research Council (VR) are gratefully acknowledged. S.N. wishes to thank the Thailand Research Fund (TRF) for a Royal Golden Jubilee Ph.D. fellowship. The authors also acknowledge the use of the Ngorongoro computer system at the Department of Information Technology, Uppsala University.

References: [1]. Nokbin, S., Limtrakul, J., Hermansson, K. Surf. Sci. 2004, in press.

[2]. Wu, R., Freeman, A. J. Phys. Rev. B 1995, 51, 5408.

[3]. Bogicevic, A., Jennison, D. R. Surf. Sci. 2002, 515, L481.

Keywords: Density functional calculations, VASP, MgO(001), Rhodium, adsorption, electron density, density of state, electron localization function.

## Computational study of carbonyl-ene reaction of encapsulated formaldehyde in Na-FAU zeolite

Winyoo Sangthong <jet\_world2003@hotmaif.com>,

The carbonyl-ene reaction between formaldehyde and propylene has been investigated theoretically. Three different models were employed to model the carbonyl-ene reaction system: (1) Na-exchanged faujasite zeolite system, (2) the naked Na(I) ion system and (3) the bare system. The reaction occurrs via a concerted mechanism which involves a proton transfer from propylene to formaldehyde and a carbon-carbon bond formation which occur simultaneously at one transition state. Carbonyl-ene reaction can proceed in Na-exchanged faujasite zeolite via concerted interactions in the coadsorbed complex of formaldehyde and propylene without any intermediate. The interaction between Na-exchanged faujasite zeolite and formaldehyde leads to a structure in which formaldehyde is stabilized in the zeolite framework. The energy barrier for this system is calculated to be 25.1 kcal/mol and the apparent activation energy is -3.2 kcal/mol. It is well established that carbonyl-ene reactions are catalyzed by Lewis acids. In order to gain some insight into the mechanism by which a Lewis acid can catalyze this reaction, we employed Na+ as a Lewis acid in order to compare these results (2) with the results from the Naexchanged zeolite system (1). The activation barrier in system (2) is 17.46 kcal/mol. due to the large electrostatic interaction between the naked Na ion and the complex. In the bare system (3) where no zeolite framework or electrostatic field from Na<sup>+</sup> are present, the structure of the transition state is a 6-membered ring and its energy barrier is 34.4 kcal/mol. The activation energy of the carbonyl-ene reaction of propylene with HCHO@Na-Faujasite (25.1 kcal/mol) lies between those of the bare model (34.4 kcal/mol) and the simple naked Na(I) model (17.5 kcal/mol). Theses results indicate that Na-exchanged faujasite can preserve formaldehyde in a monomeric form and can also act as a Lewis acid which can catalyze the carbonyl-ene reaction of formaldehyde with olefins without the presence of potentially harmful acidic chemicals.

ONIOM (QM/MM) study of hydrolysis reaction mechanism of methoxide species to methanol over Fe-ZSM-5 catalysts.

Suwat Pabchanda, Piboon Pantu, Jumras Limtrakul \*
Laboratory for Computational an Applied Chemistry, Physical Chemistry Division, Kasetsart University, Bangkok 10900, Thailand; e-mail address: fscijrl@ku.ac.th

The hydrolysis reaction mechanism of methoxide species to methanol over Fe-ZSM-5 catalysts has been investigated using the ONIOM (Our-own-N-layer Integrated molecular Orbital + molecular Mechanics) approach with a 46T cluster of Fe-ZSM-5 zeolite modeled by the ONIOM2(B3LYP/6-311+G(3df,2p):UFF) method. The activation energy for hydrolysis of methoxide species, Z[(HO)Fe(OCH<sub>3</sub>)] to form adsorbed methanol product, Z[Fe(OH)<sub>2</sub>(HOCH<sub>3</sub>)] is 13.7 kcal/mol. The Z[Fe(OH)<sub>2</sub>] then reacts with the excess water vapor to form the initial state of the active site Z[FeO]. The predicted activation energy for this process is 19.4 kcal/mol. These results are apparently identical to the experimental observation.

#### **Abstract Submitted to Program Officials**

Click to print this page now.

You have submitted the following abstract to 229th ACS National Meeting, San Diego, CA, March 13-17, 2005. Receipt of this notice does not guarantee that the submission was necessarily complete or correct; imply that any errors have been detected; or indicate that it has been accepted for presentation. Additional materials, such as a preprint, may be required by the division.

Influence of the framework and substituted group effects to the structures and energetic profiles of the vapor phase of the Beckmann rearrangement on nanoporous Faujasite zeolite

Jakkapan Sirijaraensre and Jumras Limtrakul, Department of Chemistry, Kasetsart University, Department of Chemistry, Faculty of Science, Kasetsart University, Phaholyothin Rd., Ladyao, Jatujak, Bangkok 10900, Thailand, Fax: 662-9428900 ext 324, jk\_om2002@yahoo.com, fscijrt@ku.ac.th

The reaction mechanism of the Beckmann rearrangement (BR) of four oximes, i.e. formaldehyde oxime, two stereoisomers (Z-, E- acetaldehyde oximes) and Propan-2-one oxime catalyzed by the H-Faujasite zeolite has been investigated by both the quantum cluster and embedded cluster approaches at the B3LYP level of theory using the 6-31G (d,p) basis set. Single point calculations were done at MP2/6-311G(d,p) to improve the energetic properties. By using the bare cluster model, the rate determining step of the whole reaction of these oxime molecules is the rearrangement step which has the energy barrier among 50-70 kcal/mol. Inclusion of zeolitic framework has effects on the adsorption properties of all complexes and lead to different reaction pathways than those obtained from the bare cluster model. The rate determining step of the reaction becomes the 1,2 H shift step for Z-acetaldehyde oxime (39.1 kcal/mol) and Propan-2-one oxime (31.2 kcal/mol), while, in the E-acetaldehyde oxime, the rate determining step is either the 1,2 H-shift (26.2 kcal/mol) or the rearrangement step (26.6 kcal/mol). Moreover, the embedded cluster model leads to differentiation of different types of zeolite, unlike the bare cluster model, which is not able to make this differentiation. From the above results, it is shown that the effect of the Madelung potential from the zeolite framework has an important effect on both the reaction mechanisms and the energetic profiles of the vapor phase of the Beckmann rearrangement on nanoporous faujasite zeolite.

#### 1. IF NECESSARY, CHANGE YOUR ABSTRACT BETWEEN NOW AND THE DEADLINE

- Point your browser to http://oasys.acs.org/acs/229nm/oasys.htm
- Log in using your special ID (842884) and password (931626).
- . Make all changes between now and the call for papers deadline date for this division.

#### 2. REMEMBER TO SUBMIT A PREPRINT or EXTENDED ABSTRACT, IF REQUIRED

If an extended abstract or a preprint manuscript is required for this program, submit it by clicking the appropriate link in the Abstract Control Panel to the left of these instructions. Your abstract will be rejected if an extended abstract or preprint is required by the division and you have not submitted it.

#### 3. REMEMBER TO REGISTER FOR THE MEETING

All presenters, including invited speakers, must register and are responsible for their meeting registration fees, unless otherwise notified in writing by a division officer. Advance <u>registration</u> will be available. Also use <u>this link</u> to look up housing information. See the <u>division home page</u> for a list of meetings and deadlines

#### 4. CHECK THE STATUS OF YOUR PAPER

You will be able to view your paper's acceptance status and its scheduled time after {{Program:ProgramEnd}}. Retrieve your paper using the instructions above for changing your abstract to view the status of your paper. Please do not contact ACS about whether your paper has been scheduled. Your session organizer or program chair can answer these questions.

Tell us what you think of online abstract submittal.

Tell us what you liked or what we need to improve and we'll work on new features for future meetings.

Back to ACS Meetings

Learn about how the abstract will appear in the printed abstract book.

#### **Abstract Submitted to Program Officials**

Click to print this page now.

You have submitted the following abstract to. Receipt of this notice does not guarantee that the submission was necessarily complete or correct; imply that any errors have been detected; or indicate that it has been accepted for presentation. Additional materials, such as a preprint, may be required by the division.

## Diffusion mechanism of p-xylene in nanoporous catalyst: A molecular dynamics simulation study

Tanin Nanok<sup>1</sup>, Philippe A. Bopp<sup>2</sup>, and **Jumras Limtrakul<sup>1</sup>**. (1) Department of Chemistry, Kasetsart University, Department of Chemistry, Faculty of Science, Kasetsart University, Phaholyothin Rd., Ladyao, Jatujak, Bangkok 10900, Thailand, Fax: 662-942-8900 ext 324, g4384022@ku.ac.th, fscijrl@ku.ac.th, (2) Laboratoire de Physico-Chimie Moléculaire, Université Bordeaux I

We report Molecular Dynamics computer simulations of the self-diffusion of p-xylene in silicalite, an aluminium-free MFI type zeolite, as a function of temperature and loading. Both the zeolite and the guest molecule are modeled as flexible entities. The calculated self-diffusion coefficients are of the order of  $10^{-7}$  to  $10^{-6}$  cm $^2$ /s, which are in the same order of magnitude as found by recent simulations. It is found that, at low loading and temperature, the diffusion is mainly controlled by the interaction between xylene and zeolitic wall. The mutual interaction becomes sufficiently important to affect the diffusion process when the loading is increased. The diffusion mechanism resembles the model process of jump diffusion. At the highest loading (4 molecules/unit cell), the microscopic picture of the diffusion mechanism provides the same conclusive finding of p-xylene adsorption in silicalite as reported by experimental studies.

#### 1. IF NECESSARY, CHANGE YOUR ABSTRACT BETWEEN NOW AND THE DEADLINE

- Point your browser to http://oasys.acs.org/acs//oasys.htm
- Log in using your special ID (850587) and password (654044).
- Make all changes between now and the call for papers deadline date for this division.

# 2. REMEMBER TO SUBMIT A PREPRINT or EXTENDED ABSTRACT, IF REQUIRED If an extended abstract or a preprint manuscript is required for this program, submit it by clicking the appropriate link in the Abstract Control Panel to the left of these instructions. Your abstract will be rejected if an extended abstract or preprint is required by the division and you have not submitted it.

#### 3. REMEMBER TO REGISTER FOR THE MEETING

All presenters, including invited speakers, must register and are responsible for their meeting registration fees, unless otherwise notified in writing by a division officer. Advance registration will be available. Also use this link to look up housing information. See the division home page for a list of meetings and deadlines

#### 4. CHECK THE STATUS OF YOUR PAPER

You will be able to view your paper's acceptance status and its scheduled time after

{{Program:ProgramEnd}}. Retrieve your paper using the instructions above for changing your abstract to view the status of your paper. Please do not contact ACS about whether your paper has been scheduled. Your session organizer or program chair can answer these questions.

Tell us what you think of online abstract submittal.

Tell us what you liked or what we need to improve and we'll work on new features for future meetings.

**Back to ACS Meetings** 

Learn about how the abstract will appear in the printed abstract book.



ภาคผนวก ค.

สรุปกิจกรรมอื่นๆ

### ภาคผนวก ค.1

## รายละเอียด "การประชุมเมธีวิจัยอาวุโส ครั้งที่ 1"



ที่ ทม 0406.03/ 0631

ภาควิชาเคมี คณะวิทยาศาสตร์ มหาวิทยาลัยเกษตรศาสตร์ เขตจตุจักร กรุงเทพฯ 10900

#### 4 พฤษภาคม 2547

เรื่อง ส่งรายงาน

เรียน ศ. ดร. วิชัย บุญแสง ผู้อำนวยการฝ่ายวิชาการ สกว.

**สิ่งที่ส่งมาด้วย** 1. โปรแกรมและบทคัดย่อของการสัมมานาวิชาการ 1 เล่ม

2. สำเนารายชื่อผู้เข้าร่วมสัมมนาวิชาการ 1 ชุด

3. สรุปค่าใช้จ่ายในการจัดสัมมนาวิชาการ 1 แผ่น

ตามที่ฝ่ายวิชาการสำนักงานกองทุนสนับสนุนการวิจัย (สกว.) ได้อนุมัติให้โครงการการศึกษา และการออกแบบสารประกอบที่มีโครงสร้างในระดับนาโนเมตร (เมธีวิจัยอาวุโส 2545) จัดสัมมนา วิชาการเรื่อง"การออกแบบโครงสร้างและกลไกการเกิดปฏิกิริยาของชีโอไลต์และสารประกอบที่มีโครง-สร้างในระดับนาโนเมตร" เมื่อวันที่ 11 พฤศจิกายน 2546 ณ โรงแรมรามา การ์เดน บัดนี้ การสัมมนา วิชาการครั้งนี้ได้สำเร็จลุล่วงไปแล้วด้วยดี กระผมในฐานะหัวหน้าโครงการฯ จึงขอสรุปผลการจัดสัมมนา วิชาการครั้งนี้มาให้ฝ่ายวิชาการได้ทราบ โดยมีผู้เข้าร่วมทั้งสิ้น 94 คน และมีค่าใช้จ่ายรวมทั้งสิ้น 42,896.25 บาท (สี่หมื่นสองพันแปดร้อยเก้าสิบหกบาทยี่สิบห้าสตางค์) ดังปรากฏในเอกสารที่แนบมา พร้อมกันนี้

จึงเรียนมาเพื่อโปรดพิจารณา

ขอแสดงความนับถือ

(รองศาสตราจารย์ คร. จำรัส ลิ้มตระกูล) หัวหน้าโครงการฯ

#### TRF Senior Research Scholar meeting on

### Molecular design, structures, adsorption, and reaction mechanism of catalysts and nanostructured materials systems

#### NOVEMBER 11, 2003 RAMA GARDEN HOTEL, BANGKOK

#### TECHNICAL PROGRAM

TUESESDAY MORNING Convention Center Room 001

Jumras Limtrakul, Presiding, Organizer

8:50 Introductory Remarks

9:00 A Technology-Oriented Application of Surface Simulations

**Michael Probst** 

Institute of Ion Physics, University of Innsbruck, Innsbruck

9:30 Fundamental Kinetic Modeling of Production Reactors

Max Tirtowidjojo

Dow Chemical Company, USA

#### Intermission

10:30 Reaction Mechanism of Selective Oxidation of Methane to Methanol on Fe-ZSM-5 Catalyst

Piboon Pantu, Suwat Pabchanda, and Jumras Limtrakul Laboratory of Computational and Applied Chemistry, Kasetsart University, Bangkok

11:00 Adsorption and Mechanisms of Zeolites: An Embedded Cluster Model

Jakkapan Sirijaraensre and Jumras Limtrakul

Laboratory of Computational and Applied Chemistry, Kasetsart University, Bangkok

11:30 Alkylation of Benzene with Ethylene Over Faujasite zeolite Investigated by the ONIOM Method

Supawadee Namuangruk and Jumras Limtrakul

Chemistry Department, Kasetsart University, Bangkok

#### Lunch

13:30 Industrial Applications of Computational Chemistry Rondan Nelson

Dow Chemical Company, USA

14:00 Magnetizabilities of Ring-Structured Molecules, [8]-Cyclacene, [8]-BN-Cyclacene and [8]-Collarene, and Their Effect on 3He Nuclear Shielding Tensor.

Yutthana Tantirungrotechai, Somsak Tonmunphean, Atchara Wijitkosoom, Narin Nuttavut and Jumras Limtrakul

Chemistry Department, Mahidol University

14:30 DFT Plane-Wave Calculations of the Rh/MgO(001) Interface Somkiat Nokbin, Kersti Hermansson, and Jumras Limtrakul Materials Chemistry, The Angström Laboratory, Uppsala University, Sweden

15:00 Structure and Reaction Mechanisms in Nanostructured Materials Systems: a New Embedded Study

Chardchalerm Raksakoon, and Jumras Limtrakul

Chemsitry Department, Kasetsart University, Bangkok

#### Intermission

- 15:30 Mathematical Models for TAP Experiments with Porous Catalyst: Theoretical Analysis Morudee Phongaksom, Nalinee Chaimongkol, Phungphai Phanawadee, and Jumras Limtrakul

  Chemical Engineering Dept, Kasetsart University
- 16:00 Production of Nanostructured Zeolite: a New Synthetic Approach
  Metta Charoenpanich, Rossana Thaneerat and
  Jumras Limtrakul
  Chemical Engineering Department, Kasetsart University, Bangkok
- 16:00 Conversion of Ethanol to Gasoline and Aromatics over- Metal-loading Zeolites Tawan Sooknoi, and Artit Ausavasukhi Chemistry Department, King Mongkut Institute of Technology, KMITL, Bangkok
- 17:00 A Unique Example of Hexa-coordinated Aqueous Zinc(II) Entrapped In Organically Hybrid Ionic Crystal
  Apinpus Rujiwatra, and Jumras Limtrakul
  Chemistry Department, Chiang-Mai University, Chiang-Mai

#### Registration Form

#### TRF Senior Research Scholar meeting

#### 11 November 2003

#### Rama Gardens Hotel, Bangkok

1.	Amornpattana	Wanida	
2.	Angkaew	Suppalak	Supply Angles
3.	Arayalert	Narongsak	Dow on
4.	Artrith	Nongnuch	Sor Obes
5.	Assawasuki	Artit	
6.	Assawasuki	Umaporn	Engove Juja.
7.	Ausavasukhi	Artit	Arhit Auscrealthi
8.	Amarin	Nat	Not Amon'n
9.	Aryuwat	Attawat	Atturit Aryunot
10.	Bamrungsap	Suwussa	grace 13 Bendador
11,	Baudin	Micael	Mar Mul
12.	Bobuatong	Karan	
13.	Boekfa	Bundet	Goorly half
14.	Boonsang	Vichai	Χ
15.	Boonsri	Pornthip	
16.	Bunsawansong	Pensri	from ds
17.	Chaimongkol	Nalinee	
18.	Chareonpanich	Metta	Mate Ing
19.	Chidthong	Rungtiwa	Ping thing
20.	Chuakheaw	Duangmanee	
21.	Chalermsuksri	Teerawat	Tecromont christoni

22.	Gotte	Anders	
23.	Hannongbua	Supa	Leyen
24.	Hermansson	Kersti	Kerel Remarks
25.	Herschend	Bjöm	200
26.	Hillier	lan H.	
27.	Hongkrengkai	Rattapon	
28.	Injan	Nutcha	nuth
29.	Jansang	Bavornporn	Elono Pulado
30.	Jaree	Attasak	Χ
31.	Jongkon	Nipa	म्ब
32.	Jiamesakul	Siriya	Siriya
33.	Karchanawanichakul	Pornsawan	אוקאות
34.	Kasuriya	Supawan	501751
35.	Kongkachuichay	Paisan	
36.	Limtrakul	Jumras	
37.	Lomratsiri	Jarun	
38.	Lorwongtragool	Panida	Panida
39.	Luksirikul	Patraporn	Potra pom
40.	Maitarad	Phompimon	
41.	Meeto	Wichanee	Will
42.	Mokmak	Wanwimon	x dest folor
43.	Mroz	Barbara	× hose follow
44.	Mungcharoen	Thumrongrat	
45.	Namuangruk	Supawadee	donos
46.	Na-Ranong	Duangkamol	who was
47.	Ngam-To	Teerapong	

Nokbin	Somkiat	Y Son kist Volclor n
Noppuang	Jutarat	Jota vat Roppions
Nunrium	Peerapol	
Nuttarut	Narin	
Pabchanda	Suwat	
Panjan	Wasinee	Hasinee Payjam.
Pannorad	Narong	~
Pantu	Piboon	ASI-W
Panyaburapa	Weerayuth	1. William
Phanawadee	Phungphai	P. Thana Le
Phongaksom	Monrudee	
Piam-aroon	Nipat	(L)
Poolmee	Potjaman	Patricus 2 1
Probst	Michael	Panida Prompinit
Prompinit	Panida	1 0
Raksakoon	Chadchalerm	handysneys
Roengsumran	Sophon	Some 1
Rondan	Nelson	Melson D. Korden
Rotpradit	Kanjana	Dow '
Rujiwatra	Ratana	
Rujiwatra	Apinpus	
Rungsirisakun	Ratana	som Johl Saa
Rungrotthear	Benjamas	<i>X</i>
Saenbandit	Kitipong	Sohn Sohn
Saetang	Darinee	2007 NEW 1
Sangma	Chak	gh /1/2 2_
	Noppuang Nunrium Nuttarut Pabchanda Panjan Pannorad Pantu Panyaburapa Phanawadee Phongaksom Piam-aroon Poolmee Probst Prompinit Raksakoon Roengsumran Rondan Rotpradit Rujiwatra Rujiwatra Rungsirisakun Rungrotthear Saenbandit Saetang	Noppuang Nunrium Peerapol Nuttarut Narin Pabchanda Suwat Panjan Wasinee Pannorad Narong Pantu Piboon Panyaburapa Weerayuth Phanawadee Piam-aroon Poolmee Prompinit Prompinit Panida Raksakoon Roengsumran Roengsumran Rujiwatra Rujiwatra Rungsirisakun Rungrotthear Raelana Rujiwatra Ratana Rungrotthear Raelana Rujiwatra Ratana Rungrotthear Raelana Rujiwatra Ratana

74.	Sangthong	Winyoo	shy z lon
<b>7</b> 5.	Sawangphruk	Montree	Olyd De
76.	Seehabua	Pirune	13.16
77.	Sirijaraensre	Jakkapan <	
78.	Siriwijitrakol	Kriangsak	Kriengsah
79.	Sooknoi	Tawan	-9
80.	Soontornpalin	Chorchat	CHORCHAT
81.	Srivub	Pensri	6g- 1 5 0/1 N
82.	Sudsakom	Kandis	Lendo Di
83.	Sunpetch	Boonruen	
84.	Surakarin	Thanyawit	2-/1
85.	Suramitr	Songwut	norgaly str.
86.	Suwannaran	Suratsawadee	Suratrawadee.
87.	Tantanak	Duangkamol	1 De m
88.	Tantirungrotechai	Yutthana	X grag
89.	Thachepan	Surachai	and me
90.	Thaneerat	Rossana	
91.	Thuensukon	Pracaya	Brachya.
92.	Tirtowidjojo	Max M./	x Marx Julianos 17
93.	Tonmunphean	Somsak	
94.	Treesuwan	Witcha	15 C-
95.	Vailikhit	Veeramol	<i>V P</i>
96.	Warakulwit	Chompunuch	Baggen
97.	Wasvanitsanong	Chatree	X wz
98.	Wijikosoom	Atchara	•••••
99.	Wongpaiboonwatana	Wayoon	May con

		,	
100.	Wongthong Piny	⁄о	pfy o.
101.	Wuttiham Book	nyawat	Boonymat
102.	weerayath Pany	aburapa	Phig
103.	Benjamas Rung	rotthera	Bey.
104.	Chimklub Passay	pan	Passapan
105.	Korpany Hanger; Han Kor	pong.	Kompany
106.	Sansawake Sut	ida	Sut-
107.	Aranyabandhu Sa	หา	<del>20</del> 2
108.	Nutthawat Chaithmaboo	m	
109.	Maneryong Versachai		Jr-
110.	Hanyotee Saifon		Sh
111.	Chatchawan Sookmon		
112.	Kiltchniga Prako	6	- Carl
113.	Koo-amormpattane Wan	ido	Maria.
114.	Monnot Chevakidak		tonnat
115.	Nalinec Chaimongkol		tralinee.
116.	HUNSALLORAPONS Chompanut		chompung
117.	Oorkhamand Bovornlag		last Dati
118.	Panikhakorn Jaiyong		Panithakorn Jalyong
119.	Pong patt Tongmite		long patt Tongmak
120.	0.11		Panida Surawatanawong
121.	Supachasee Roddacha	L	Suprachance Poddacha
122.	•		
123.			
124.			
125.			

RAMA GARDENS HOTEL, BANGKOK

#### A Technology-Oriented Application of Surface Simulations

#### **Michael Probst**

Institute of Ion Physics, University of Innsbruck, Technikerstraße 25, 6020 Innsbruck, Austria

(michael.probst@uibk.ac.at)

The author (normally not very much surface-oriented) is responsible for a small subtask of an international cooperation with the aim of constructing the prototype of a fusion reactor. The lecture consists of:

- A brief excursion into popular science
   (The background of the project and how it evolved)
- Which Materials?

(Why surface science plays a role in the project)

'Some people actually believe that simulations are useful ...'
 (What kinds of simulations are possible and, especially, which types of potentials are used <sup>II-iv</sup>:)

www.iter.org/

A. P. Sutton and J. Chen, Phil. Mag. Lett. 61, 139 (1990)

D. W. Brenner, Phys. Rev. B 42, 9458 (1990)

R. E. Cohen, M. J. Mehl and D. A. Papaconstantopoulos, Phys. Rev. B <u>50</u>, 14694 (1994)

RAMA GARDENS HOTEL, BANGKOK

#### Fundamental Kinetic Modelling of Production Reactors

#### Max M. Tirtowidjojo

Reaction Engineering, Engineering Science Lab., Core R&D, Dow Chemical Company, B-1226

(Freeport, TX77541, e-mail: maxt@dow.com)

Elementary reaction based kinetic models have been developed for gas-phase reaction system of interest to Dow. The fundamental kinetic model (FKM) considers greater than 50,000 reactions involving greater than 2000 species. The corresponding kinetic parameters and thermodynamic properties were determined using a combination of available data, empirical/semi-empirical methods (RRKM, group additivity, bond energy, transition states and others), and Ab Initio quantum mechanics calculations. Examples of successful application of FKM kinetic database to design and optimize production scale reactors will be discussed.

RAMA GARDENS HOTEL, BANGKOK

## Reaction Mechanism of Selective Oxidation of Methane to Methanol on Fe-ZSM-5 Catalyst

Piboon Pantu, Suwat Pabchanda, and Jumras Limtrakul

Laboratory for Computational and Applied Chemistry, Department of Chemistry, Faculty of Science, Kasetsart University, Bangkok 10900, Thailand

Selective oxidation of methane to methanol on Fe-ZSM-5 catalyst has been theoretically investigated using the ONIOM (Ourown-N-layer Integrated molecular Orbital + molecular Mechanics) approach with an 46T cluster of Fe-ZSM-5 zeolite modeled by the ONIOM2 (B3LYP/6-31G(d,p):UFF) method. The active iron center is modeled as an isolated iron site [FeO<sub>2</sub>]<sup>+</sup> at the ion exchange site of ZSM-5 zeolite. The geometric constraint of the zeolitic nanostructured pores plays a vital role in regulating the orientations of reactive species around the active iron center and significantly affects the energetic properties of the reactive species. In the ONIOM2 model, the adsorbed methane is activated by direct hydrogen abstraction leading to the methyl radical, which is greatly stabilized by the zeolite framework. The apparent activation energy is calculated to be 9.9 kcal/mol. The subsequent combination of the methyl radical with the hydroxyl group or oxide oxygen on the iron site is a rapid process and may proceed without energy barrier, as the transition state has not been identified. The resulting adsorbed methanol and methoxide species are strongly adsorbed on the iron site.

RAMA GARDENS HOTEL, BANGKOK

#### Adsorption and Mechanisms of Zeolites: An Embedded Cluster Model

#### Jakkapan Sirijaraensre and Jumras Limtrakul

Laboratory for Computational and Applied Chemistry, Department of Chemistry, Faculty of Science, Kasetsart University, Bangkok 10900. Thailand

The heterogeneous catalytic Beckmann rearrangement (BR) on ZSM-5 and FAU catalysts has been investigated by both the quantum cluster and embedded cluster approaches at the B3LYP level of theory using the 6-31G (d,p) basis set. On the FAU zeolite, the embedded cluster model suggests that the initial step of the Beckmann rearrangement is not the O-protonated oxime but the N-protonated oxime as same as obtained from investigated the BR on H-ZSM-5 zeolite. The energies barrier derived from the proton shuttle of the Nbound to the O-bound isomer are evaluated to be about 23.8 and 9.5 kcal/mol for the embedded cluster and quantum cluster approaches, respectively. The difference in the activation energy is due mainly to the effect of the Madelung potential from the zeolite framework. The overall activation energy, at the rearrangement step, is calculated to be about 58.1 and 60.0 kcal/mol for the embedded cluster and the quantum cluster approaches, respectively. While on the H-ZSM-5 zeolite, the activation energy of the rearrangement step is calculated to be 34.0 and 65.3 kcal/mol for the embedded cluster and the quantum cluster approaches, respectively. These calculated results suggest that the rate-determining step of the vapor phase of the Beckmann rearrangement on H-FAU is the rearrangement step. As compared the energetic profile with obtained from H-ZSM-5 zeolite, we found that the H-ZSM-5 zeolite is a better acid catalyst for the Beckmann rearrangement reaction of formaldehyde oxime than H-FAU zeolite.

RAMA GARDENS HOTEL, BANGKOK

#### Alkylation of Benzene with Ethylene over Faujasite Zeolite Investigated by the ONIOM Method

#### Supawadee Namuangruk, Piboon Pantu and Jumras Limtrakul

Laboratory for Computational and Applied Chemistry, Department of Chemistry, Faculty of Science, Kasetsart University, Bangkok 10900, Thailand

The alkylation of benzene with ethylene over faujasite zeolite has been investigated using an 84T cluster of faujasite zeolite serving as a nanometre-sized chemical reactor modeled by the ONIOM3 (MP2/6-311++G(d,p):HF/6-31G(d):UFF) method which gives accurate adsorption energies for the reactants and the product indicating the accuracy of the model in representing interactions between the adsorbates and the zeolite. The computed adsorption energies are -8.73, -13.91, and -20.11 kcal/mol which are compared well with experimentally reported values of -9.0, -14.0, and -20.4 kcal/mol for ethylene, benzene and ethylbenzene, respectively. The alkylation reaction starts with the protonation of the adsorbed ethylene by an acidic zeolite proton leading to the formation of the active ethoxide intermediate. Subsequently, the reaction proceeds via interactions between the surface ethoxide intermediate and a gaseous benzene molecule and this step is found to be the rate-determining step. The ONIOM3 model predicts the activation energy of 38.18 kcal/mol and the apparent activation energy of 27.67 kcal/mol.

RAMA GARDENS HOTEL, BANGKOK

#### Industrial Application of Computational Chemistry

#### **Nelson Rondan**

Computational Chemistry Group, Physical and Chemical Properties Division, Dow Chemical Company, B-1226

(Freeport, TX77541, e-mail: ngrondan@dow.com)

Molecular modeling or computational chemistry has played an important role in industry in shortening the time necessary to lunch new products in the marketplace. In the next century, modeling will even play a greater role in industrial research because in an ever increasingly competitive global market where the time required to deliver a product from laboratory to market is even shorter. Modeling will not only be used in the improvement of existing products and processes but most importantly, in the design of new materials and processes This talk will present some of the modeling tools and applications at the Dow Chemical Company with emphasis on epoxy polymerization.

RAMA GARDENS HOTEL, BANGKOK

Magnetizabilities of Ring-Structured Molecules, [8]-Cyclacene, [8]-BN-Cyclacene and [8]-Collarene, and Their Effect on 3He Nuclear Shielding Tensor

Yutthana Tantirungrotechai, Somsak Tonmunphean, Atchara Wijitkosoom, Narin Nuttavut, and Jumras Limtrakut

Department of Chemistry, Faculty of Science, Mahidol University, Rama 6 Road, Bangkok 10400, Thailand

The magnetizabilities of three ring-structured mols., [8]-cyclacene.

[8]-BN-cyclacene, and [8]-collarene, were subsequently calculated at the B3LYP/6-31G\* level with the CSGT gauge-origin treatment. The magnetizability of [8]-cyclacene shows a large diamagnetic nature in the direction parallel to the ring cylindrical axis, while the value of [8]-BN-cyclacene is nearly isotropic, and that of [8]-collarene is slightly more diamagnetic in the perpendicular direction than in the parallel direction. A large diamagnetic magnetizability in the parallel direction of [8]-cyclacene arises from the current flow around the ring circumference. The magnetic environment in the ring channel of these three molecules was investigated by calcg. the nuclear shielding tensor of the 3He atom when the atom moves through the ring channel. The GIAO nuclear shielding tensor changes significantly toward a prolate shape in [8]-cyclacene, but becomes a slightly oblate shape in [8]-BN-cyclacene and [8]-collarene. The changes correlate well with the magnetizabilities of the ring-structured mols.

RAMA GARDENS HOTEL, BANGKOK

## DFT Plane-Wave Calculations of the Rh/MgO(001) Interface

Somkiat Nokbin<sup>1,2</sup>, Kersti Hermansson<sup>1</sup>, and Jumras Limtrakul<sup>2</sup>

<sup>1</sup>Department of Materials Chemistry, The Ångström Laboratory, Box 538, SE-751 21 Uppsala, Sweden <sup>2</sup>Laboratory for Computational and Applied Chemistry, Department of Chemistry, Faculty of Science, Kasetsart University, Bangkok 10900, Thailand

(somkiat.nokbin@mkem.uu.se)

The interatomic interactions of the Rh/MgO(001) system have been studied by means of periodic plane-wave density functional calculations using the VASP code and the PAW method. Four starting adsorption sites and three different coverages were investigated.

Our results clearly demonstrate that Rh prefers to bind to the surface O atom rather than to the other sites; this is shown by the relatively large adsorption energy and the relatively short Rh-surface distance for this site. The adhesion energy for Rh on top of O, i.e. the interaction energy calculated with respect to a reference state consisting of the isolated metal and oxide slabs, is found to decrease as a function of coverage (from 1.8 to 1.1 eV as the coverage increases from 1/8 to 1 ML). The adsorption energy on the other hand, i.e. the interaction energy with respect to an oxide slab and a Rh(g) atom, is found to increase with surface coverage.

Electron difference density plots were calculated to display some of the electron rearrangement responsible for the Rh-oxide adhesion energy and the features of adsorption on the Mg and O sites were compared.

RAMA GARDENS HOTEL, BANGKOK

#### Structure and Reaction Mechanisms in Nanostructured Materials Systems: A New Embedded QM/UFF Study

#### Chadchalerm Raksakoon and Jumras Limtrakul

Laboratory for Computational and Applied Chemistry, Department of Chemistry, Faculty of Science, Kasetsart University, Bangkok 10900, Thailand

It is often necessary to calculate the electrostatic potential resulting from an infinite or extended array of charges in the interior of a region of interest. In case of a periodic potential this can, for example, be done by Ewald summation. An important alternative are those methods where arrays of auxiliary point charges are optimized with respect to charge and/or position in order to reproduce the original electrostatic potential. The optimized charges, determined by fitting, representation of electrostatic potential has been applied to study the structure and reaction mechanism in nanostructured zeolite catalysts. The periodic structure of nanostructured zeolite framework was subdivided into three parts: the innermost is QM region, the next layer is force field and the outermost is a set of point charges, determined by fitting, representation of electrostatic potential of the infinite lattice framework.

RAMA GARDENS HOTEL, BANGKOK

# Mathematical Models for TAP Experiments with Porous Catalyst: Theoretical Analysis

Monrudee Phongaksom<sup>1</sup>, **Phungphai Phanawadee**<sup>2</sup> Nalinee Chaimongkol<sup>2</sup>, and Jumras Limtrakul<sup>3</sup>

<sup>1</sup>Department of Industrial Chemistry, King Mongkut's Institute of Technology North Bangkok <sup>2</sup>Department of Chemical Engineering, Kasetsart University <sup>3</sup>Department of Chemistry, Kasetsart University

(fengphi@ku.ac.th)

TAP (Temporal Analysis of Products) Knudsen pulse response experiments (Gleaves, et al., 1997) have been used for heterogeneous catalytic reaction studies for non-porous and porous catalysts. Problems involving intraparticle and interparticle transport in porous catalytic systems have been studied using the TAP reactors (Huinink, 1995; Nijhuis et al., 1999; Keipert and Baerns, 1998; Schuurman et al., 1999). Analytical solutions for some domain of system parameters have been reported (Huinink, 1995; Huinink et al., 1996; Yablonsky, et al., 2001). In some articles, a macro-porous catalytic system was assumed a non-porous one (Schuurman and Gleaves, 1997; Dewaele and Froment, 1999).

In this paper, the mathematical model that describes the transport and kinetics for an irreversible reaction case in a TAP reactor packed with a porous catalyst sample is analyzed for one- and threezone reactors. The differential equations that describe the mass balances of the reactant in the interparticle and intraparticle void regions as well as the initial and boundary conditions are transformed into dimensionless form. Gas concentration profiles in the catalyst pore are calculated. It is found that a key parameter that governs the characteristics of the concentration profiles is the ratio of the interparticle characteristic time to the intraparticle characteristic time. When this ratio is sufficiently large, the gas concentration profile in the intraparticle void region at each time is similar to the corresponding profile in the steady state condition. A simplified TAP model can then be obtained by assuming a pseudo-steady state in the intraparticle void region. As a result, the set of mass balance equations is reduced to a single interparticle equation involving the effectiveness factor defined in typical steady state conditions. When the effectiveness factor is unity,

RAMA GARDENS HOTEL, BANGKOK

a uniform concentration distribution in the intraparticle void region is obtained.

This intraparticle pseudo-steady state model is also compared with the primary model by investigating the characteristics of the exit flow rate. Moment analysis of the exit flow rate for the diffusion-only case shows that the analytical expressions for the first moment from the two models are the same. The difference between the exit flow rates from the two models is then characterized by the second moment. For diffusion + irreversible reaction, the expressions for the zeroth moment from the two models are the same, and consequently the difference is characterized by using the first moment. The results show that the simplified model is valid in a wide domain of system parameters for both one- and three-zone reactors.

A special case in which the effectiveness factor is large enough to apply a uniform intraparticle concentration model is also analyzed in detail. The domain of system parameters in which the model can be applied is presented with corresponding errors of the determined rate constant. It is also shown that one can apply a non-porous assumption to a porous system when this model is valid. However, the rate constant determined from the experimental response needs to be multiplied by the ratio of the total (interparticle and intraparticle) void volume to the interparticle vold volume. Nevertheless, even if no correction is made to the rate constant, the determined activation energy from a series of responses at different temperatures needs no correction.

RAMA GARDENS HOTEL, BANGKOK

# Production of Nanostructured Zeolite: A New Synthetic Approach

# Metta Chareonpanich<sup>1</sup>, Rossana Thaneerat<sup>1</sup>, and Jumras Limtrakul<sup>2</sup>

<sup>1</sup>Department of Chemical Engineering, Kasetsart University, Bangkok 10900, Thailand <sup>2</sup>Department of Chemistry, Kasetsart University, Bangkok 10900, Thailand

Lignite fty ash and rice husk ash were used as raw materials for synthesis of ZSM-5 zeolite and zeolite Y. The effects of reaction temperature, mole ratio of silica to alumina, sodium hydroxide concentration, initial pressure and reaction time on yields of zeolite products are investigated. Maximum yields of ZSM-5 zeolite (59 wt.%) was obtained at SiO<sub>2</sub>/Al<sub>2</sub>O<sub>3</sub> mole ratio, 40; initial pressure, 4 atm; treatment temperature, 210°C and treatment period, 4 h. The maximum yield of zeolite Y of 37 wt.% was achieved at the following conditions: temperature, 90°C; SiO<sub>2</sub>/Al<sub>2</sub>O<sub>3</sub> ratio, 8; NaOH concentration, 5 M; synthesis period, 1 day; pressure, 1 bar.

RAMA GARDENS HOTEL, BANGKOK

# Conversion of Ethanol to Gasoline and Aromatics Over Metal-Loading Zeolites

#### Tawan Sooknoi<sup>1</sup> and Artit Ausavasukhi<sup>2</sup>

<sup>1</sup>Department of Chemistry, King Mongkut's Institute of Technology Ladkrabang, Chalongkrung Road, Ladkrabang, Bangkok 10520, Thailand

Conversion of Ethanol to Gasoline and Aromatics

<sup>2</sup>Program in Chemistry, Faculty of Science & Technology, Rajabbat
Institute Pelchburiwillayalongkom, Phabonyothin Road, Klong Luang
District Pathumthani, 13180 Thailand

The development of renewable sources of fuels and petrochemicals is special interest for agro-industrial countries. This study has been focussed on the conversation of ethanol to gasoline and aromatics using ZSM-5 zeolites incorporated with platinum, gallium, and silver. The experiments show that a higher contact time results in a higher selectivity for high molecular weight hydrocarbons. whereas at a lower contact time the gas products become predominant. At 350-375 °c, hydrocarbons can undergo oligomerization and isomerization to give high quality gasoline, while at a higher reaction temperature (400-450 °C), higher hydrocarbons shift toward the aromatic fraction. In the reaction using ethanol as feed, aromatic yields of 7.55, 9.83, and 6.59 %mol were obtained at 125 °C over HZSM-5, [Ag]HZSM-5, and [Ga]HZSMS, respectively. Addition of water as cofeeding in the reaction (95 wt% ethanol), decreases aromatic yields to 4.30 and 7.31 %mol over HZSM-5 and [Ag]HZSM5, respectively. However, the enhanced acitivity of [Ga]HZSM-55 can be obtained, yielding 8.16% mole of aromatic due to the additional acid sites which are readily produced by an interaction of gallium extra-framework with water. In the ethanol conversion, aromatic is namely produced by reforming of the oligomerized hydrocarbons. However, in the reaction using ethylene as feed, aromatic can be produced from small olefin aromatization over [Ga]HZSM-5. On the other hand, [Pt]HZSM-5 is found to inhibit the case of ethylene oligomerization, while silver impregnated ([Ag]HZSM-5) shows relatively low activity for the aromatic production.

RAMA GARDENS HOTEL, BANGKOK

# A Unique Example of Hexa-coordinated Aqueous Zinc(II) Entrapped In Organically Hybrid Ionic Crystal

#### Apinpus Rujiwatra<sup>1</sup> and Jumras Limtrakul<sup>2</sup>

<sup>1</sup>Department of Chemistry, Faculty of Science, Chiang Mai University, Chiang Mai, 50200 Thailand <sup>2</sup>Department of Chemistry, Faculty of Science, Kasetsart University, Bangkok, Thailand

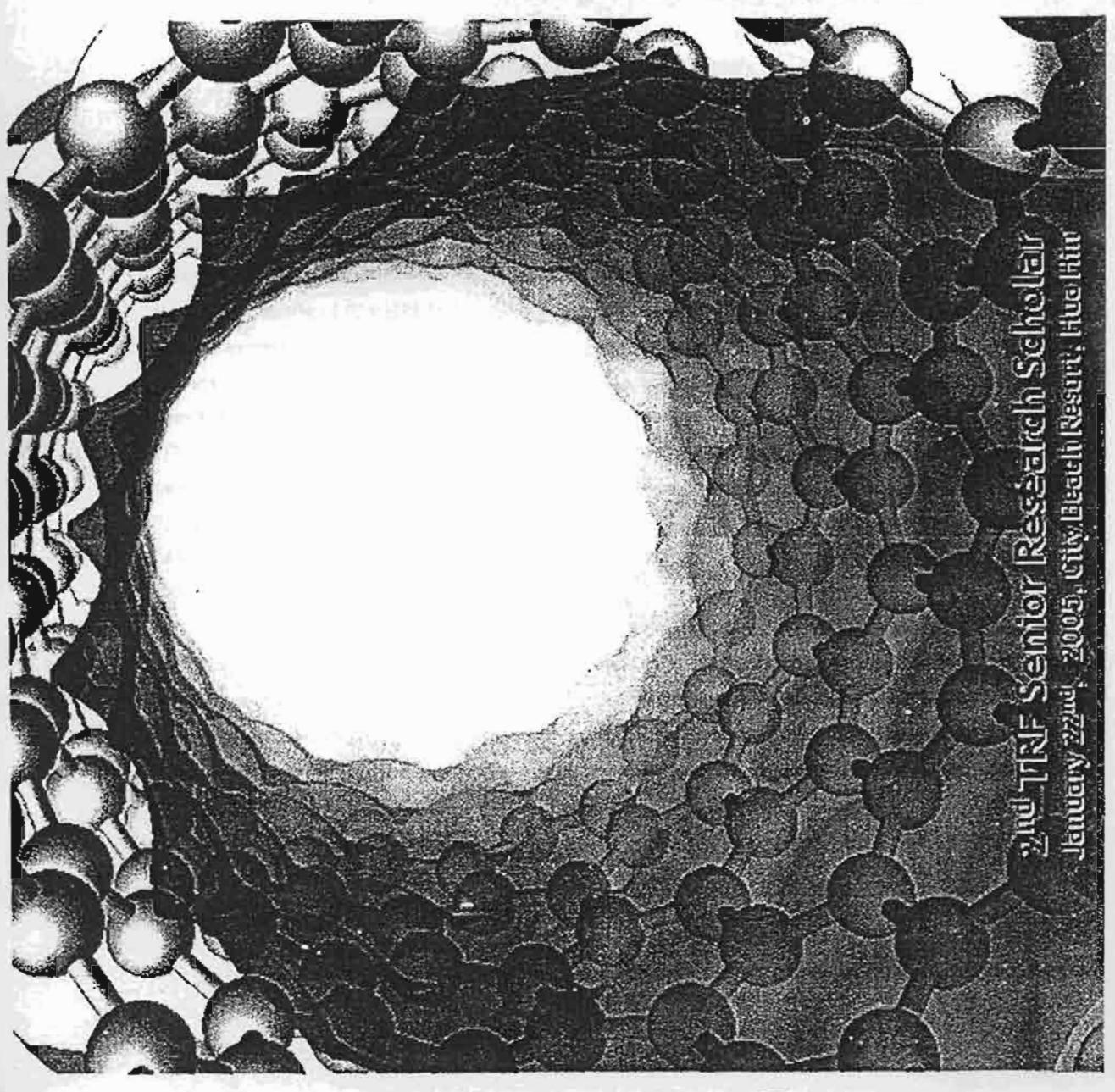
(apinpus@chiangmai.ac.th)

A unique example of an organically hybrid zinc sulfate ionic coordinated composed hexaaqua of n(H<sub>2</sub>O)<sub>6</sub>(SO<sub>4</sub>)<sub>2</sub>(C<sub>2</sub>N<sub>2</sub>H<sub>10</sub>), was prepared and structurally characterized by single crystal X-ray diffraction. The single crystals were observed after being crystallized for 24 hours in the filtrate, which was separated from the reaction between ZnSO<sub>4</sub>·7H<sub>2</sub>O, ethylenediamine (99%) and ethyl alcohol(95%) in the mole ratio of 1:0.1:100 refluxed over 6 hours at 80°C. Crystal Data for Zn(H<sub>2</sub>O)<sub>6</sub>(SO<sub>4</sub>)<sub>2</sub>(C<sub>2</sub>N<sub>2</sub>H<sub>10</sub>): monoclinic P21/c, a = 8.287(5) Å, b = 7.115(5) Å, c = 14.179(5) Å,  $\beta$  = 113.710(5)°, V = 765.5(8) Å<sup>3</sup>, Z = 2, d(calc) = 1.803 g cm<sup>-3</sup>; structure solution and refinement based on 1676 reflections with  $F_0 \ge 4\sigma(F_0)$  (Mo K $\alpha$ ,  $\lambda$  = 0.71073 Å) converged at R = 0.0864. The crystals are hygroscopic and readily dissolve in air. IR spectroscopy was used to confirm the presence of the organic cation and coordinated water.

### ภาคผนวก ค.2

# รายละเอียด "การประชุมเมชีวิจัยอาวุโส ครั้งที่ 2"

# Molecular Design, Structure and Reaction Mechanisms of Nanostructured Materials Systems















Molecular Design, Structure and Reaction Mechanisms of Nanostructured Materials Systems January 22<sup>rd</sup>, 2005, City Beach Resort, Hua Hin

05.30	Leave for Hua Hin, City Beach Resort	
09.00 - 09.15	Gathering of the participants & Registration	
09.15 09.45	Introduction Remarks by	
	Director, Academic Division, TRF (Prof. Dr. Vichai Boonsaeng)	
	Head, Chemistry Department, KU (Dr. Surapol Patharakom)	
	TRF Senior Research Scholar (Dr. Jumras Limtrakul)	
09.45 - 10.00	Intermission	
10.00 - 10.30	"Two-stage synthesis of pure ZSM-5 zeolite from lignite fly	1
	ash and rice husk ash"	
	N. Reanvattana, M. Chareonpanich and J. Limtrakul	
10.30 - 11.00	"Mild chemical approaches in the synthesis of new organically	2
	hybrid inorganic framework; growth and single crystal	
	structure of Zn(H <sub>2</sub> O) <sub>6</sub> ](SO <sub>4</sub> ) <sub>2</sub> (C <sub>2</sub> N <sub>2</sub> H <sub>10</sub> )"	
	A. Rujiwatra and J. Limtrakul	
11.00 - 11.30	"Validity of the Dirac delta function for describing the inlet	3
	flow in TAP pulse response models"	
	Y. Boonnumpha, P. Phanawadee, and J. Limtrakul	
11.30 - 12.00	"MAS NMR study of [Ga]HZSM-5 catalyst: Evidence for the	4
	change in catalytic behavior"	
	T. Sooknoi and A. Ausavasukhi	
12.00 - 13.00	Lunch and Check In	
13.00 - 13.30	"Theoretical investigation of selective oxidation of methane in	5
	nanostructured Fe-ZSM-5 catalyst using an ONIOM method"	
	P. Pantu, S. Pabchanda and J. Limtrakul	
13.30 ~ 14.00	"Ab Initio prediction of pK <sub>4</sub> and electronic spectra of dye	6
	indicators"	
	Y. Tantirungrotechai, S. Roddacha and J. Limtrakul	
14.00 ~ 14.30	"Probing the structural and electronic factors affecting the	7
	adsorption and reactivity of alkenes in acidic zeolites using	
	DFT calculations and multivariate statistical methods"	
	D. Tantanak, M. P. Gleeson and J. Limtrakul	

Molecular Design, Structure and Reaction Mechanisms of Nanostructured Materials Systems January 22<sup>M</sup>, 2005, City Beach Resort, Hua Hin

14.30 - 15.00	"Generating point charges that produce accurate electrostatic	8
	potential from the infinite crystal lattice for embedded cluster	
	approximations"	
	N. Pannorat and J. Limtrakul	
15.00 - 15.20	Intermission	
15.20 - 15.40	"The nucleoside bases attached on single wall carbon	9
	nanotube: an ONIOM investigation"	
	P. Khongpracha, W. Panchan and J. Limtrakul	
15.40 ~ 16.00	"Structural and electronic properties of the Rh/MgO(001)	10
	interface from periodic density functional calculations"	
	S. Nokbin, J. Limtrakul and K. Hermansson	
16.00 - 16.20	"Diffusion mechanism of p-xylene in nanoporous catalyst: A	11
	molecular dynamics simulation study"	
	T. Nanok, P. A. Bopp, and J. Limtrakul	
16.20 - 16.40	"Computational study of the carbonyl-ene reaction of	12
	encapsulated formaldehyde in Na-FAU zeolite"	
	W. Sangthong and J. Limtrakul	
16.40 - 17.00	"Interaction of Mordenite with aromatic hydrocarbon:	13
	A new embedded ONIOM study*	
	B. Jansang, T. Nanok and J. Limtrakul	
17.00 - 17.20	"Diels-Alder addition of single-wall carbon nanotubes and	14
	fullerenes with electron-rich dienes"	
	C. Warakulwit, S. Bamrungsap, P. Luksirikul, P. Khongpracha and	
	J. Limtrakul	
17.20 – 17.40	"Synthesis, characterization of the Fe-ZSM5/N2O complex"	15
	P. Prompinit, K. Sanbandit, P. Pantu, S. Vannarat and C. Sangma	
	Discussion Forums	
18.00 - 19.00	"The ethylene dimerization over Faujasite zeolite investigated	16
	by the ONIOM method"	
•	S Namuanguik P Pantu and I Limtrakul	

Molecular Design, Structure and Reaction Mechanisms of Nanostructured Materials Systems January 22<sup>nd</sup>, 2005, City Beach Resort, Hua Hin

19.00 - 21.00

Effects of substituted groups to the energetic profile of	17
Beckmann rearrangement of formaldehyde oxime on	
H-Faujasite zeolite"	
J. Sirijaraensre and J. Limtrakul	
"MAS NMR study of Ga-modified HZSM-5 catalyst: Evidence	18
for the additional of a new acid site"	
A. Ausawasuki and T. Sooknol	
"The production of gasoline and aromatics from ethanol over	19
AgHZSM5 catalysts"	
S. Suwannaran and T. Sooknoi	
"Active sites in the alkylation of methanoi with acetonitrile:	20
Study of basicity in alkali cation exchanged Faujasite zeolites"	
P. Tueonsukol and T. Sooknoi	
General Discussions	
Discussions concerning future collaborations	
Dinner	

Molecular Design, Structure and Reaction Mechanisms of Nanostructured Materials Systems January 22™, 2005, City Beach Resort, Hua Hin

Oral Presentation		
05.30	Leave for Hua Hin, City Beach Resort	
09.00 - 09.15	Gathering of the participants & Registration	
09.15-09.45	Introduction Remarks by	Prof. Dr. Vichai Boonsaeng Dr. Surapol Patharakorn Dr. Jumras Limtrakul
09.45 - 10.00	Intermission	
	Chairperson: Jumras Limtrakul and Chak Sangma	
10.00 - 10.30	Two-stage synthesis of pure ZSM-5 zeolite from lignite fly ash and rice husk ash	Metta Chareonpanich
10.30 - 11.00	Mild chemical approaches in the synthesis of new organically hybrid inorganic framework; growth and single crystal structure of $Zn(H_2O)_{\delta}](SO_4)_2(C_2N_2H_{10})$	Apinpus Rujiwatra
11.00 – 11.30	Validity of the Dirac delta function for describing the inlet flow in TAP pulse response models	Phungphai Phanawadee
11.30 – 12.00	MAS NMR study of [Ga]HZSM-5 catalyst: Evidence for the change in catalytic behavior	Tawan Sooknoi
12.00 – 13.00	Lunch and Check in	

Molecular Design, Structure and Reaction Mechanisms of Nanostructured Materials Systems January 22", 2005, City Beach Resort, Hus Hin

Chareonpanich
and Metta
Phanawadee
Phungphai
Chairperson:

Piboon Pantu	Yuthana Tantírungrotechai	Duangkamol Tantanak	Narong Pannorad			Pipat Kongpracha	Somkiat Nokbin	Tanin Nanok	Winyoo Sangthong
Theoretical investigation of selective oxidation of methane in nanostructured Fe-ZSM-5 catalyst using an ONIOM method	Ab initio prediction of pK, and electronic spectra of dye indicators	Probing the structural and electronic factors affecting the adsorption and reactivity of alkenes in acidic zeolites using DFT calculations and multivariate statistical methods	Generating point charges that produce accurate electrostatic potential from the infinite crystal lattice for embedded cluster approximations	Intermission	Chairperson: Supa Hannongbua and Tawan Sooknoi	The nucleoside bases attached on single wall carbon nanotube: an ONIOM investigation	Structural and electronic properties of the Rh/MgO(001) interface from periodic density functional calculations	Diffusion mechanism of p-xylene in nanoporous catalyst: A molecular dynamics simulation study	Computational study of the carbonyl-ene reaction of encapsulated formaldehyde in Na-FAU zeolite
13.00 13.30	13.30 – 14.00	14.00 – 14.30	14.30 – 15.00	15.00 – 15.20		15.20 – 15.40	15.40 – 16.00	16.00 – 16.20	16.20 – 16.40

Molecular Design, Structure and Reaction Mechanisma of Nanostructured Materials Systems January 22<sup>rd</sup>, 2005, City Beach Resort, Hua Hin

16.40 – 17.00 17.00 – 17.20	Interaction of Mordenite with aromatic hydrocarbon: A new embedded ONIOM study Diels-Alder addition of single-wall carbon nanotubes and fullerenes with electron-rich dienes	Bavornpon Jansang Chompunuch Warakulwit
17.20 - 17.40	Synthesis, characterization of the Fe-ZSM5/N <sub>2</sub> O complex	Panida Prompinit
	Discussion Forums	
18.00 - 19.00	The ethylene dimerization over Faujasite zeolite investigated by the ONIOM method	Supawadee Namuangruk
	Effects of substituted groups to the energetic profile of Beckmann rearrangement of formaldehyde oxime on H-Faujasite zeolite	Jakkapan Sirijaraensre
	MAS NMR study of Ga-modified HZSM-5 catalyst: Evidence for the additional of a new acid site	Artit Ausavasukhi
	The production of gasoline and aromatics from ethanol over AgHZSM5 catalysts	Suratsawadee Suwannaran
	Active sites in the alkylation of methanol with acetonitrile: Study of basicity in alkali cation exchanged Faujasite zeolites	Prachya Tueonsukol
19.00 – 21.00	General Discussions	

Discussions concerning future collaborations

Dinner

# บทคัดย่อของผลงานที่ได้แสดงในการ ประชุมเมธิวิจัยอาวุโส ครั้งที่ 2 จำนวน 20 เรื่อง

Molecular Design, Structure and Reaction Mechanisms of Nanostructured Materials Systems January 22<sup>rd</sup>, 2005, City Beach Resort, Hua Hin

## Two-stage synthesis of pure ZSM-5 zeolite from lignite fly ash and rice husk ash

N. Reanvattana<sup>1</sup>, M. Chareonpanich<sup>1</sup> and J. Limtrakul<sup>2</sup>

<sup>1</sup>Department of Chemical Engineering, Kasetsart University

<sup>2</sup>Laboratory for Computational and Applied Chemistry, Physical Chemistry Division, Kasetsart University

Many types of zeolites were possibly synthesized by conventional hydrothermal treatment of fly ash. However, the purity of zeolite products was low. In this research, pure ZSM-5 zeolite was synthesized from coal fly ash by two-stage synthesis process. In the first stage, in order to remove mineral contaminants, two methods including acid treatment and alkaline treatment were undertaken. With acid treatment, H2SO4 and HCl solutions were used to separate mineral matters, especially iron oxides from raw fly ash. In the case of alkaline treatment, NaOH solution was used to extract silica and alumina in raw fly ash to form a mixture of silicate and aluminate. The treated fly ash and silicate-aluminate mixture were consequently used for ZSM-5 zeolite synthesis in the second stage. It was found that 16.7 wt.% of Fe in fly ash can be reduced by the treatment with 3.5 M HCl for 60 min at 70°C and 15.9 wt.% of Fe can be reduced by the treatment with 2.5 M H<sub>2</sub>SO<sub>4</sub> for 50 min at the same temperature. The yield of ZSM-5 zeolite, approximately 15 wt.%, was obtained by the conventional one-stage synthesis. while those of 42 and 65 wt.% were obtained by treating the fly ash with HCl and H2SO4, respectively. In the case of fly ash treated with NaOH, the maximum yields of silicate and aluminate were obtained when fly ash was treated in autoclave at 80°C for 4 hrs. In this study, sodium silicate solution prepared from rice husk ash was used to adjust SiO<sub>2</sub>/Al<sub>2</sub>O<sub>3</sub> mole ratio. Zeolite formation was studied as a function of the SiO<sub>2</sub>/Al<sub>2</sub>O<sub>3</sub> mole ratios (5, 10, 20, 40, 80, 100 and 200) and pH of mixture (8 - 12). As the result, pure ZSM-5 zeolite was produced at SiO<sub>2</sub>/Al<sub>2</sub>O<sub>3</sub> mole ratio of 40 and pH of 12.

Molecular Design, Structure and Reaction Mechanisms of Nanostructured Materials Systems January 22<sup>nd</sup>, 2005, City Beach Resort, Hua Hin

Mild chemical approaches in the synthesis of new organically hybrid inorganic framework; growth and single crystal structure of [Zn(H<sub>2</sub>O)<sub>6</sub>](SO<sub>4</sub>)<sub>2</sub>(C<sub>2</sub>N<sub>2</sub>H<sub>10</sub>)

#### A. Rujiwatra<sup>1</sup> and J. Limtrakul<sup>2</sup>

<sup>1</sup>Department of Chemistry, Faculty of Science, Chlang Mai University

<sup>2</sup>Laboratory for Computational and Applied Chemistry, Physical Chemistry Division, Kasetsart University

Attempts to synthesizing and growing single crystals of new organically hybrid inorganic framework structures, especially those of the sulfate frameworks, were conducted employing mild chemical approaches e.g. reflux, precipitation and hydrothermal synthesis. The rare ethylenediammonium hybrid zinc sulfate ionic framework,  $[Zn(H_2O)_6](SO_4)_2(C_2N_2H_{10})$ , with zinc(ii) ion in hexa-aqua coordination environment was illustrated. The crystals of  $[Zn(H_2O)_6](SO_4)_2(C_2N_2H_{10})$  was prepared and structurally characterized by single crystal X-ray diffraction. The single crystals were observed after being crystallized for 24 hours in the filtrate, which was separated from the reaction between ZnSO<sub>4</sub>.7H<sub>2</sub>O, ethylenediamine and ethyl alcohol in the mole ratio of 1:0.1:100 refluxed over 6 hours at 80°C. Crystal Data for  $[Zn(H_2O)_6](SO_4)_2(C_2N_2H_{10})$ : monoclinic P21/c, a = 8.287(5) Å, b = 7.115(5) Å, c = 14.179(5) Å,  $\beta$  = 113.710(5)°, V = 765.5(8) ų, Z = 2, d(calc) = 1.803 g cm³; structure solution and refinement based on 1676 reflections with F0  $\geq$  4 $\sigma$ (F0) (Mo K $\alpha$ ,  $\lambda$  = 0.71073 Å) converged at R = 0.0864. The crystals are hygroscopic and readily dissolve in air. IR spectroscopy was used to confirm the presence of the organic cation and coordinated water.

Molecular Design, Structure and Reaction Mechanisms of Nanostructured Materials Systems

January 22<sup>nd</sup>, 2005, City Beach Resort, Hua Hin

## Validity of the Dirac delta function for describing the inlet flow in TAP pulse response models

#### Y. Boonnumpha<sup>1</sup>, P. Phanawadee<sup>1</sup>, and J. Limtrakul<sup>2</sup>

<sup>1</sup>Department of Chemical Engineering, Faculty of Engineering, Kasetsart University

<sup>2</sup>Laboratory for Computational and Applied Chemistry, Physical Chemistry Division, Kasetsart University

Temporal analysis of products or TAP has been recognized as an important transient experimental method for heterogeneous catalytic reaction studies. The experiment is performed by injecting a narrow gas pulse into an evacuated microreactor packed with catalyst pellets. The time-dependent exit flow rate of each gas is detected by a mass spectrometer. Interpretation of TAP response data including transport and kinetic parameter estimation requires mathematical models that describe the processes in the reactor. Parameter estimation can be accomplished by curve fitting between the experimental exit flow rate and the model exit flow rate calculated from an analytical solution or by a numerical method. Another alternative is the use of moment analysis of the exit flow rate.

TAP process modeling involves describing the gas inlet flow introduced by a pulse valve. The inlet flow is usually described by the Dirac delta function at the initial time. Many analytical solutions and moment expressions of the exit flow rate were determined for simple reactions using the Dirac delta function. However, many researchers used different mathematical descriptions of the inlet flow. In these cases, the solutions for the exit flow rate can be determined only by numerical methods.

In this paper, the validity of the Dirac delta function for TAP modeling is theoretically analyzed. For the diffusion-only case, the degree of validity is based on the difference in the diffusivities calculated from the exit flow rate using delta and non-delta functions. The dependence of the degree of validity of the delta function upon the system parameters, including the open duration time of the pulse valve, for the diffusion-only case is reported in a simple form. For typical TAP experimental domains, the delta function is shown to be valid. For the diffusion with irreversible reaction case, the conversion expression for the reactant gas is the same for all functions describing the inlet flow. The gas conversion expression for the delta function case can then be properly used for any non-delta function cases to determine the rate constant.

Molecular Design, Structure and Reaction Mechanisms of Nanostructured Materials Systems January 22<sup>nd</sup>, 2005, City Beach Resort, Hua Hin

MAS NMR study of [Ga]HZSM-5 catalyst: Evidence for the change in catalytic behavior

#### T. Sooknoi and A. Ausavasukhi

Department of Chemistry, Faculty of Science, King Mongkut's Institute of Technology

MAS NMR spectroscopy was employed to investigate Ga-modified HZSM-5 catalyst prepared by impregnation ([Ga]HZSM-5). It was found that the steam treatment of [Ga]HZSM5 results in a pronounced increase in the intensity of <sup>1</sup>H MAS NMR resonance of Brønsted acid sites in the catalyst, which is attributed to the interaction of gallium oxide with water. The additional of Brønsted acid sites that may be responsible for the change in the catalytic behavior of [Ga]HZSM-5 from ethylene aromatization to ethanol reforming activity for the production of aromatic.

Molecular Design, Structure and Reaction Mechanisms of Nanostructured Materials Systems January 22<sup>rd</sup>, 2005, City Beach Resort, Hua Hin

## Theoretical investigation of selective oxidation of methane in nanostructured Fe-ZSM-5 catalyst using an ONIOM method

#### P. Pantu, S. Pabchanda and J. Limtrakul

Laboratory for Computational and Applied Chemistry, Physical Chemistry Division, Kasetsart University

Selective oxidation of methane to methanol on Fe-ZSM-5 catalyst has been theoretically investigated using the ONIOM approach with a 46T cluster of Fe-ZSM-5 zeolite modeled by the ONIOM2 (B3LYP/6-311+G(3df,2p):UFF) method. The active iron center is modeled as a mononuclear iron species [FeO<sub>2</sub>]\* located at the ion exchange site of the ZSM-5 zeolite. The steric constraint of the zeolite nanostructured pores plays a vital role in regulating the orientation of reactive species around the active iron center and significantly affects the energetic of the reactive species. Methane is first weakly adsorbed on the active Iron site and then activated by direct hydrogen abstraction forming a methyl radical. The barrier energy for the hydrogen abstraction is calculated to be 15.3 kcal/mol. Subsequently, the methyl radical can rapidly recombine with the oxygen radical anion on the iron site resulting in a highly stable adsorbed methoxide product. The methyl radical can react with the hydroxyl group on the iron site with a small barrier energy of 11.1 kcal/mol producing strongly adsorbed methanol on the active iron site. However, direct desorption of the adsorbed methanol would require a high desorbing energy of 28.8 kcal/mol. On the other hand, the hydrolysis of methoxide can readily occur with an activation energy of 13.7 kcal/mol to produce a methanol molecule weakly adsorbed on the iron active site. The reaction is mildly exothermic by 5.2 kcal/mol. The adsorbed methanol can be desorbed requiring an energy of 13.2 kcal/mol.

Molecular Design, Structure and Reaction Mechanisms of Nanostructured Materials Systems January 22<sup>nd</sup>, 2005, City Beach Resort, Hua Hin

#### Ab initio prediction of pK, and electronic spectra of dye indicators

Y. Tantirungrotechai<sup>1</sup>, S. Roddacha<sup>1</sup> and J. Limtrakul<sup>2</sup>

<sup>1</sup>Department of Chemistry, Faculty of Science, Mahidol University

<sup>2</sup>Laboratory for Computational and Applied Chemistry, Physical Chemistry Division, Kasetsart University

We introduce in this work the combination of an extrapolated ONIOM(G2MS) method and a continuum solvation model as a practical choice for determining the  $\Delta G_{gas}$  and  $\Delta \Delta G_{sol}$  respectively as defined in thermodynamic cycle for the prediction of pK<sub>a</sub>. Our focus is on the determination of pK<sub>a</sub> values of dye indicators which have a large change in electronic structure upon the protonation process. The results indicate that our employed method can provide a reasonable estimation of pK<sub>a</sub> with the standard deviation of 0.94 among the molecules studied in a relatively short time. Additionally we investigated the change of electronic spectra, hence the colour, of the dye indicator upon the protonation process by using the ZINDO method. However this ZINDO can predict the colour change only qualitatively.

Molecular Design, Structure and Reaction Mechanisms of Nanostructured Materials Systems January 22<sup>nd</sup>, 2005, City Beach Resort, Hua Hin

Probing the structural and electronic factors affecting the adsorption and reactivity of alkenes in acidic zeolites using DFT calculations and multivariate statistical methods

#### D. Tantanak<sup>1</sup>, M. P. Gleeson<sup>2</sup> and J. Limtrakul<sup>2</sup>

<sup>1</sup>Chemistry Department, Faculty of Science, King Mongkut's Institute of Technology Ladkrabang <sup>2</sup>Laboratory for Computational and Applied Chemistry, Physical Chemistry Division, Kasetsart University

Quantum mechanical (QM) cluster calculations have been performed on a model of ZSM-5 at DFT and MP2 levels. We investigated how the adsorption energies and the energetics of alkoxide intermediate formation of six different alkene substrates; ethene, propene, 1-butene, cis/trans butene and isobutene vary in this zeolite model. Analysis of the DFT geometric, electronic and energetic parameters of the zeolite-substrate complexes, transition states and alkoxide intermediates is performed using principal components analysis (PCA) and partial least squares (PLS). These deliver an insight into the correlated changes that occur between molecular structure and energy along the reaction coordinate between the physisorped and chemisorbed species within the zeolite. To our knowledge this is the first occasion multivariate techniques such as PCA or PLS have been employed to profile the changes in electronics. distances and angles in QM calculations of catalytic systems such as zeolites. We find the calculated adsorption and the alkoxide intermediate energies correlate strongly with the absolute charge on the substrate and the length of the substrate double bond. The transition states energies are not affected by the zeolite framework as modeled which explains why they correlate strongly with the gas-phase substrate protonation energy. Our cluster results show that for ethene, propene, 1-butene and isobutene, the relative energetics associated with the formation of the alkoxide intermediate in ZSM-5 follow the same trends as calculations where the effects of the framework are included.

Molecular Design, Structure and Reaction Mechanisms of Nanostructured Materials Systems January 22<sup>nd</sup>, 2005, City Beach Resort, Hua Hin

Generating point charges that produce accurate electrostatic potential from the infinite crystal lattice for embedded cluster approximations

#### N. Pannorat and J. Limtrakul

Laboratory for Computational and Applied Chemistry, Physical Chemistry Division, Kasetsart University

The cluster approximation to calculate adsorption energies of molecule with zeolites requires less computational effort than the periodic approach but it neglects the effect of long range electrostatic interaction from infinite crystal lattice which plays a vital role along the adsorption process. We propose the simple but accurate method for including such effect into the calculation by generating a set of finite number of point charges placing upon the lattice sites. These point charges are to reproduce infinite electrostatic potential over the quantum cluster as the embedded ONIOM scheme. The method is applied to the adsorption of Pyridine on H-FAU zeolite giving adsorption energy well agree with its experimental result.

Molecular Design, Structure and Reaction Mechanisms of Nanostructured Materials Systems January 22<sup>nd</sup>, 2005, City Beach Resort, Hua Hin

# The nucleoside bases attached on single wall carbon nanotube: an ONIOM investigation

#### P. Khongpracha, W. Panchan and J. Limtrakul

Laboratory for Computational and Applied Chemistry, Physical Chemistry Division, Kasetsart University

The derivatives of nucleoside bases (Adenine and Guanine) attached on a (5,5) armchair single wall carbon nanotube (SWNT) have been theoretically examined by using our own N-layered integrated molecular orbital + molecular mechanics (ONIOM) techniques. The C<sub>130</sub>H<sub>20</sub> cluster has been used as a model of the SWNT and the B3LYP/6-31G(d):AM1 compound method has shown the advantages over the B3LYP/6-31G(d):UFF combination due to the more reliable binding energy outcomes. It has been found that purine bases bound with a single carbon atom and their double ring fused plane are arranged in the parallel direction along with the SWNT tube. In order to enhance the stability of covalently modified SWNT products, adjacent carbon atoms in the SWNT cluster have been replaced by boron (B) and nitrogen (N) atoms on behalf of the BN doped SWNT.

Molecular Design, Structure and Reaction Mechanisms of Nanostructured Materials Systems January 22<sup>nd</sup>, 2005, City Beach Resort, Hua Hin

# Structural and electronic properties of the Rh/MgO(001) interface from periodic density functional calculations

S. Nokbin<sup>1,2</sup>, J. Limtrakul<sup>2</sup> and K. Hermansson<sup>1</sup>

<sup>1</sup>Materials Chemistry, The Angström Laboratory, Box 538, SE-751 21 Uppsala, Sweden <sup>2</sup>Laboratory for Computational and Applied Chemistry, Physical Chemistry Division, Kasetsart University

The Rh/MgO(001) system has been studied by means of periodic plane-wave density functional calculations using the VASP code and PAW potentials. Three surface coverages of Rh (1/8, 1/2 and 1 ML) were investigated at three different adsorption sites (on top of surface O, Mg and the hollow site). Three types of interaction energies have been calculated to help characterize the metal-oxide interaction: the energy of adsorption of Rh atoms ( $E_{ads}$ ), the energy of adhesion of a Rh overlayer ( $E_{adh}$ ) and the formation-of-the-Rh-layer energy. We find that Rh prefers to bind to the surface oxygen site. For 1 ML coverage, the metal-metal interactions within the Rh overlayer give the largest contribution to the stabilization of the Rh/MgO interface, while, naturally, the Rh-oxide interaction dominates at low coverage. The net result is that the adsorption energy (isolated MgO slab + isolated Rh atoms  $\rightarrow$  Rh/MgO interface) increases with increasing surface coverage. Moreover, electronic properties such as the density of states (DOS), electron density difference plot, spin density and the electron localization function (ELF) are presented to clarify the chemical bonding behavior of the Rh/MgO interface system.

Molecular Design, Structure and Reaction Mechanisms of Nanostructured Materials Systems January 22<sup>™</sup>, 2005, City Beach Resort, Hua Hin

# Diffusion mechanism of p-xylene in nanoporous catalyst: A molecular dynamics simulation study

T. Nanok<sup>1</sup>, P. A. Bopp<sup>2</sup>, and J. Limtrakul<sup>1</sup>.

<sup>1</sup>Laboratory for Computational and Applied Chemistry, Physical Chemistry Division, Kasetsart University

<sup>2</sup>Laboratoire de Physico-Chimie Moléculaire, Université Bordeaux!

We report Molecular Dynamics computer simulations of the self-diffusion of p-xylene in silicalite, an aluminium-free MFI type zeolite, as a function of temperature and loading. Both the zeolite and the guest molecule are modeled as flexible entities. The calculated self-diffusion coefficients are of the order of  $10^{-7}$  to  $10^{-6}$  cm<sup>2</sup>/s, which are in the same order of magnitude as found by recent simulations. It is found that, at low loading and temperature, the diffusion is mainly controlled by the interaction between xylene and zeolitic wall. The mutual interaction becomes sufficiently important to affect the diffusion process when the loading is increased. The diffusion mechanism resembles the model process of jump diffusion. At the highest loading (4 molecules/unit cell), the microscopic picture of the diffusion mechanism provides the same conclusive finding of p-xylene adsorption in silicalite as reported by experimental studies.

Molecular Design, Structure and Reaction Mechanisms of Nanostructured Materials Systems January 22<sup>nd</sup>, 2005, City Beach Resort, Hua Hin

# Computational study of the carbonyl-ene reaction of encapsulated formaldehyde in Na-FAU zeolite

#### W. Sangthong and J. Limtrakul

Laboratory for Computational and Applied Chemistry, Physical Chemistry Division, Kasetsart University

The density functional theory (B3LYP/6-31G(d,p)) and the ONIOM (Our-own-N-layer Integrated molecular Orbital + molecular Mechanics) approach utilizing two-layer ONIOM schemes (B3LYP/6-31G(d,p):UFF) have been employed to investigate the structures of the Naexchanged zeolite-encapsulated formaldehyde (HCHO@Na-zeolite) and their interactions with propylene. Three model systems are considered for carbonyl-ene reactions of propylene and formaldehyde: 1) Na-exchanged zeolite model, HCHO@NaZeolite/CH<sub>3</sub>CH=CH<sub>2</sub>; 2) naked Na(I) model, Na(I)/HCHO/CH3CH=CH2; 3) bare model where the Na ion and zeolitic Faujasite framework are neglected, i.e., HCHO/CH<sub>3</sub>CH=CH<sub>2</sub>. Inclusion of the extended zeolite framework has an effect on the structure and energetic of the adsorption complexes and leads to a lower energy barrier of the reaction as compared to the bare model system. The simple, naked Na(I) interacted with the HCHO/CH<sub>3</sub>CH=CH<sub>2</sub> complex, obviously underestimated the energy barrier of the system as compared to the HCHO@Na-zeolite/CH<sub>3</sub>CH≈CH<sub>2</sub> due to the large electrostatic field generated by the naked Na(I) cation. The carbonyl-ene reaction of propylene using HCHO@Na-Faujasite takes place in a single reaction step. The concerted mechanism has an activation energy of 25.08 kcal/mol which lies between those of bare model (34.40 kcal/mol) and the simple, naked Na(I)/HCHO/CH3CH=CH2 (17.46 kcal/mol).

Molecular Design, Structure and Reaction Mechanisms of Nanostructured Materials Systems January 22<sup>nd</sup>, 2005, City Beach Resort, Hua Hin

Interaction of Mordenite with aromatic hydrocarbon: A new embedded ONIOM study

#### B. Jansang, T. Nanok and J. Limtrakul

Laboratory for Computational and Applied Chemistry, Physical Chemistry Division, Kasetsart University

The structure of mordenite (MOR) and its interaction with benzene has been investigated within the framework of Our-own-N-layered Integrated molecular Orbital + molecular Mechanics (ONIOM) approach utilizing the two-layer ONIOM scheme (B3LYP/6-31G(d,p):UFF). The effect of the long range interactions is also included via optimized point charges added on to the ONIOM2(B3LYP/6-31G(d,p):UFF), embedded ONIOM. Inclusion of the extended zeolitic framework covering the nanocavity has an effect on the adsorption properties. The adsorption energies estimated from 3T and 12T quantum clusters of -5.97 and -6.89 kcal/mol, respectively, are significantly lower than that obtained from the 120T ONIOM2 scheme of -16.55 kcal/mol. The completed adsorption model obtained at the embedded ONIOM2(MP2/6-31G(d,p):UFF) method predicts the adsorption energy of -23.41 kcal/mol, which is comparable to the estimated value of -21.53 kcal/mol.

Molecular Design, Structure and Reaction Mechanisms of Nanostructured Materials Systems January 22<sup>nd</sup>, 2005, City Beach Resort, Hua Hin

## Diels-Alder addition of single-wall carbon nanotubes and fullerenes with electron-rich dienes

C. Warakulwit, S. Bamrungsap, P. Luksirikul, P. Khongpracha and J. Limtrakul
Laboratory for Computational and Applied Chemistry, Physical Chemistry Division, Kasetsart University

The transition states and products of the Diels-Alder (DA) cycloaddition of different types of dienes have been investigated within the framework of Our own N-layered Integrated molecular Orbital and molecular Mechanics (ONIOM) approach utilizing the two layered ONIOM scheme (B3LYP/6-31G\*:AM1). The structure and activity relationship for a series of different types of dienes interacted with armchair (5,5) single wall carbon nanotube (SWNT) was established, i.e. the reactivity of the DA has been related to the distance between the methylene carbons in the butadiene moiety (R<sub>1,4</sub>). The reactivity becomes higher as the R<sub>1,4</sub> is shortened. Thus, the diene(2) (2,3-dimethylene-1,4-dioxane) with the shortest R<sub>1,4</sub> of 3.005 Å was found to be the most reactive one. Nevertheless, the activation energy in SWNTs reaction is still much higher than that of [60]fullerene complex, due to the increase of the curvature of dienophile. To enhance the reactivity of the DA reaction, the metal cation was introduced into the SWNTs. The decreasing of activation energy of the DA reaction seems to be due mainly to the electron deficiency nature of the double bond of Na@SWNT.

Molecular Design, Structure and Reaction Mechanisms of Nanostructured Materials Systems January 22<sup>rd</sup>, 2005, City Beach Resort, Hua Hin

#### Synthesis, characterization of the Fe-ZSM5/N2O complex

P. Prompinit, K. Sanbandit, P. Pantu, S. Vannarat and C. Sangma

Laboratory for Computational and Applied Chemistry, Physical Chemistry Division, Kasetsart University

A series of ZSM-5 samples containing Fe and AI in the framework positions with different molar ratios of Fe/AI was synthesized by hydrothermal method in 7 h. The XRD, FT-IR, SEM, N<sub>2</sub>-adsorption Isotherm and H<sub>2</sub>-TPR data show that the samples synthesized by this method have well crystallinity, high specific surface area and high dispersion of iron. The sample with Fe/AI ratio of 0.26 was activated by steam treatment with various water partial pressures at 650 °C to test as catalysts for N<sub>2</sub>O decomposition. We found that the sample pretreated with steam concentration of 300 mbar gives the best catalytic activity in N<sub>2</sub>O decomposition.

Molecular Design, Structure and Reaction Mechanisms of Nanostructured Materials Systems January 22<sup>nd</sup>, 2005, City Beach Resort, Hua Hin

### The ethylene dimerization over Faujasite zeolite investigated by the ONIOM method

#### S. Namuangruk, P. Pantu and J. Limtrakul

Laboratory for Computational and Applied Chemistry, Physical Chemistry Division, Kasetsart University

The ethylene dimerization has been investigated using an 84T cluster of faujasite zeolite modeled by the ONIOM3(MP2/6-311++G(d,p):HF/6-31G(d):UFF) method, which had been proved to be the accurate model for studying the reaction in zeolite. The concerted and stepwise mechanisms have been evaluated. For the stepwise mechanism, the reaction starts with the protonation of ethylene formed ethoxide intermediate followed by C-C bond formation between ethoxide and the second ethylene molecule leading to the butoxide product. The activation barrier of the first and the second step are almost equivalent and calculated to be 30.06 and 28.87 kcal/mol, respectively. The first step is the rate-determining step. For the concerted mechanism, there are no ethoxide intermediate occurring during the reaction (the protonation and C-C bond formation occur simultaneously at one transition state). The activation barrier of the concerted mechanism is evaluated to be 38.08 kcal/mol, which has an energy barrier higher than the stepwise mechanism. Therefore, the stepwise mechanism dominates overall the deactivation reaction.

The dominated mechanism of both benzene alkylation from previous study and the ethylene dimerization in this study are compared. The activation barrier of the concerted mechanism of benzene alkylation of 33.41 kcal/mol has an energy barrier higher than the stepwise mechanism of ethylene dimerization of 30.06 kcal/mol. Therefore, the ethylene dimerization occurs faster than the benzene alkylation.

Molecular Design, Structure and Reaction Mechanisms of Nanostructured Materials Systems

January 22<sup>rd</sup>, 2005, City Beach Resort, Hua Hin

# Effects of substituted groups to the energetic profile of Beckmann rearrangement of formaldehyde oxime on H-Faujasite zeolite

#### J. Sirijaraensre and J. Limtrakul

Laboratory for Computational and Applied Chemistry, Physical Chemistry Division, Kasetsart University

The heterogeneous catalytic Beckmann rearrangement (BR) on a FAU catalyst has been investigated by both the quantum cluster and embedded cluster approaches at the B3LYP level of theory using the 6-31G (d,p) basis set. Our calculation indicates that the rate determining step of reaction is the rearrangement step. Our finding found that the catalytic activity of zeolite depends on the suitable size of the adsorbate molecule with the pore size of the zeolite. Increasing the size of the oxime compound from formaldehyde oxime to Z- and E-methyl formaldehyde oxime, the activation energy, especially, in the rearrangement step is decreased from 58.0 to 27.1 and 31.1 kcal/mol for Z- and E- methyl formaldehyde oxime, respectively. This indicates that the shape-selectivity of zeolite plays an important role to the reaction as a catalyst.

Molecular Design, Structure and Reaction Mechanisms of Nanostructured Materials Systems January 22<sup>nd</sup>, 2005, City Beach Resort, Hua Hin

#### MAS NMR study of Ga-modified HZSM-5 catalyst: Evidence for the additional of a new acid site

#### A. Ausawasuki and T. Sooknoi

Department of Chemistry, Faculty of Science, King Mongkut's Institute of Technology

MAS NMR spectroscopy was employed to investigate Ga-modified HZSM-5 catalyst prepared by impregnation ([Ga]HZSM-5). It was found that the steam treatment of [Ga]HZSM-5 results in a pronounced increase in the intensity of 1H MAS NMR resonance of Brønsted acid sites in the catalyst, which is attributed to the interaction of gallium oxide with water. The additional of Brønsted acid sites that may be responsible for the change in the catalytic behavior of [Ga]HZSM-5 from small olefin aromatization to reforming activity for the production of aromatic. In the reaction using athylene as feed, aromatic can be produced from small olefin aromatization. However, in ethanol conversion, aromatic is mainly produced by reforming of the oligomerized hydrocarbons due to the additional acid sites.

Molecular Design, Structure and Reaction Mechanisms of Nanostructured Materials Systems January 22<sup>nd</sup>, 2005, City Beach Resort, Hua Hin

#### The production of gasoline and aromatics from ethanol over AgHZSM5 catalysts

#### S. Suwannaran and T. Sooknoi

Department of Chemistry, Faculty of Science, King Mongkut's Institute of Technology

The conversion of ethanol to hydrocarbons, over silver-modified HZSM5 catalyst (Si/Al=12), is described. Catalysts were prepared by an ion-exchange method using HZSM5 zeolite as the starting material. The study was carried out in a fixed bed reactor operating at atmospheric pressure over a temperature at 425 °C, W/F(0.2-0.39 h), Silver content in HZSM5 catalyst(1.76-7.68 wt%) and role of silver ions in HZSM5 were investigated. The reaction was tested and the products were analyzed by online to Gas Chromatography(GC).

The experiments show that higher contact time results in higher selectivity for high molecular weight hydrocarbon than lower contact time. The distribution of aromatics were 26.77, 32.71, 36.28 and 30.95 %mole over HZSM5, 1.76%AgHZSM5, 3.12%AgHZSM5 and 7.68%AgHZSM5, respectively. It is concluded that Ag<sup>+</sup> ions have a capacity of efficiently converting alkene intermediates into aromatic hydrocarbons.

Molecular Design, Structure and Reaction Mechanisms of Nanostructured Materials Systems January 22<sup>nd</sup>, 2005, City Beach Resort, Hua Hin

Active sites in the alkylation of methanol with acetonitrile: Study of basicity in alkali cation exchanged Faujasite zeolites

#### P. Tueonsukol and T. Sooknoi

Department of Chemistry, Faculty of Science, King Mongkut's Institute of Technology

The catalytic alkylation of methanol with acetonitrile in a fixed bed flow reactor was studied over basic zeolite catalysts. Solid base faujasite-type zeolites including NaX, KNaX, KX, and CsNaX were modified in order to increase their basicity. Samples prepared by ion exchange. Their physical and chemical characteristics were then determined by XRD, XRF, SEM, and Gas sorption analyzer. The effects on product selectivity, particularly the saturation/unsaturation ratio was found to depend on basicity of the zeolite framework. The saturation/unsaturation ratio was found to increase with increasing the catalyst basicity. Moreover, the excess cesium "clusters" present in the zeolite framework increases the hydrogenation activity of the catalyst. Further investigation on the hydrogenation activity of CsNaX shows that propionitrile and acetonitrile can be obtained from reaction of acrylonitrile and methanol or hydrogen, indicating that basic zeolite catalysts can be readily promoted hydrogenation and hydrogenolysis, respectively.

Molecular Design, Structure and Reaction Mechanisms of Nanostructured Materials Systems January 22<sup>rd</sup>, 2005, City Beach Resort, Hua Hin

#### List of Participants

1.	Apinpus	Rujiwatra	Chiang Mai University
2.	Artit	Ausavasukhi	King Mongkut's Institute of Technology
3.	Bavompon	Jansang	Kasetsart University
4.	Boonruen	Sunpetch	Kasetsart University
5.	Bundet	Boekfa	Kasetsart University
6.	Chadchalerm	Raksakoon	Kasetsart University
7.	Chak	Sangma	Kasetsart University
8.	Chatree	Vajwanitsanong	King Mongkut's Institute of Technology
9.	Chompunuch	Warakulwit	Kasetsart University
10.	Darinee	Saetang	Kasetsart University
<b>1</b> 1.	Duangkamol	Tantanak	King Mongkut's Institute of Technology
12.	Dumrongsak	Jasdapattarakul	King Mongkut's Institute of Technology
13.	Ekasith	Somsook	Mahidol University
14.	Jumras	Limtrakul	Kasetsart University
15.	Jakkapan	Sirijaraensre	Kasetsart University
16.	Jarun	Lomratsíri	Kasetsart University
17.	Kanjana	Rotprodit	Kasetsart University
18.	Karan	Bobuatong	Kasetsart University
19.	Kraiwan	Panya-inn	Mahidol University
20.	Kronvika	Tangpong	Kasetsart University
21.	Maneepom	Saiduang	Kasetsart University
22,	Metta	Chareonpanich	Kasetsart University
23.	Montree	Sawangphruk	Kasetsart University
24.	Narong	Pannorad	Kasetsart University
25.	Nongnuch	Artrith	Kasetsart University
26.	Norawit	Grainara	Kasetsart University
27.	Nutcha	Injan	Kasetsart University
28.	Panida	Prompinit	Kasetsart University
29.	Panida	Lorwongtragool	Kasetsart University
30.	Panvika	Pannopard	Kasetsart University
31.	Patchreenart	Saparpakom	Kasetsart University
32.	Patraporn	Luksirikul	Kasetsart University

### Molecular Design, Structure and Reaction Mechanisms of Nanostructured Materials Systems January 22<sup>nd</sup>, 2005, City Beach Resort, Hua Hin

33.	Pensri	Srivub	Kasetsart University
34.	Phompimon	Maitarad	Kasetsart University
35.	Phungphai	Phanawadee	Kasetsart University
36.	Piboon	Pantu	Kasetsart University
37.	Ріпуо	Wongthong	Kasetsart University
38.	Pinsuda	Viravathana	Kasetsart University
39.	Pipat	Kongpracha	Kasetsart University
40.	Pomthip	Boonsri	Kasetsart University
41.	Potjaman	Poolmee	Kasetsart University
42.	Prachya	Tueonsukol	King Mongkut's Institute of Technology
43.	Prapasiri	Pongprayoon	Kasetsart University
44.	Ratana	Rungsirisakun	Kasetsart University
45.	Rattinan <sup></sup>	Meemavit	Kasetsart University
<b>4</b> 6.	Rungtiwa	Chidthong	Kasetsart University
47.	Sani	Arannabandhu	Kasetsart University
48.	Sirirat	Jitkamka '	Chulalongkorn University
49.	Somsak	Tonmunphean	Chulalongkorn University
50.	Somkiat	Nokbin	Kasetsart University
51.	Sukhontip	Thaomola	Kasetsart University
52.	Supa	Hannongbua	Kasetsart University
<b>5</b> 3.	Supawadee	Namuangruk	Kasetsart University
54.	Suphacharee	Roddecha	Mahidol University
55.	Suratsawadee	Suwannaran	King Mongkut's Institute of Technology
56.	Suwat	Pabchanda	Kasetsart University
57.	Suwussa	Bamrungsap	Kasetsart University
58.	Tanin	Nanok	Kasetsart University
59.	Tawan	Sooknoi	King Mongkut's Institute of Technology
60.	Thanyada	Rungrotmongkol	Kasetsart University
61.	Thapanic	Gongprom	Kasetsart University
62.	Veeramol	Vailikhit	Kasetsart University
63.	Vichai	Boonsaeng	The Thailand Research Fund
64.	Wanwimon	Mokmak	Kaselsart University

Molecular Design, Structure and Reaction Mechanisms of Nanostructured Materials Systems January 22<sup>rd</sup>, 2005, City Beach Resort, Hua Hin

65. Wayoon	Wongpaiboonwatana	Kasetsart University
66. Wasinee	Panjan	Kasetsart University
67. Weerayuth	Рапуавигара	Kasetsart University
68. Wichanee	Meeto	Kasetsart University
69. Winyoo	Sangthong	Kasetsart University
70. Witcha	Treesuwan	Kasetsart University
71. Yuthana	Tantirungrotechai	Mahidol University

Molecular Design, Structure and Reaction Mechanisms of Nanostructured Materials Systems January 22<sup>nd</sup>, 2005, City Beach Resort, Hua Hin

#### TRF senior research scholar's output (2003-2004)

- Pantu, P., Pabchanda, S., and Limtrakul, J. (2004) "Theoretical Investigation of Selective Oxidation of Methane to methanol on Nanostructured Fe-ZSM-5 by ONIOM method", ChemPhysChem, 5, 1901-1906.
- Namuangruk, S., Pantu, P., Limtrakul, J. (2004) "Alkylation of benzene with ethylene over faujasite zeolite investigated by the ONIOM method", *Journal of Catalysis*, 2004, 225(2), 523-530.
- Limtrakul, J., Inntam, C., Truong, T.N. (2004) "Density functional theory study of the ethylene epoxidation over Ti-substituted silicalite (TS-1)", Journal of Molecular Catalysis A: Chemical, 207(2), 139-148.
- Nokbin, S., Limtrakul, J., Hermansson, K. (2004) \*DFT plane-wave calculations of the Rh/MgO(001) interface\*, Surface Science, 566-568, 977-982.
- Rungsirisakun, R., Jansang, B., Pantu, P. and Limtrakul, J. (2004) "The adsorption of Benzene on industrially important nanostructured catalysts (H-BEA, H-ZSM-5, and H-FAU): confinement effects", J. Mol. Struct., 733, 239-246.
- Sirijaraensre, J., Limtrakul, J. (2004) "The influence of the framework to structures and energetic profiles of the vapor phase of the Beckmann rearrangement on different types of zeolite", Petroleum Chemistry, Preprints, 49(2), 222-226.
- Chareonpanich, M., Namto, T., Kongkachuichay, P., Limtrakul, J. (2004) "Synthesis of ZSM-5 zeolite from lignite fly ash and rice husk ash", Fuel Processing Technology, 85(15), 1623-1634.
- Feil, S., Gluch, K., Matt-Leubner, S., Scheier, P., Limtrakul, J., Probst, M., Deutsch, H., Becker, K., Stamatovic, A., Märk, T.D. (2004) "Partial cross sections for positive and negative ion formation following electron impact on uracil", *Journal of Physics B*, 37, 3013-3020.
- Ketrat, S., Limtrakul, J. (2003) "Theoretical study of the ethylene on alkali-exchanged zeolites", International Journal of Quantum Chemistry, 94(6), 333-340.
- Kasuriya, S., Namuangruk,S., Treesukol, P.,Tirtowidjojo, M., Limtrakul, J., (2003)
   "Adsorption of ethylene, benzene and ethylbenzene over faujasit zeolite investigated by the ONIOM method", *Journal of Catalysis*, 219, 320-328.
- Bobuatong, K., Limtrakul, J. (2003) "Effects of the zeolite framework on the adsorption of ethylene and benzene on alkali-exchanged zeolite: an ONIOM study", *Applied Catalysis A: General*, 253, 49-64.

Molecular Design, Structure and Reaction Mechanisms of Nanostructured Materials Systems January 22<sup>nd</sup>, 2005, City Beach Resort, Hua Hin

- 12. Sailer, W., Pelc, A., Probst, M., Limtrakul, J., (2003) \*Dissociative electron attachment to acetic acid (CH₃COOH)\*, Chemical Physics Letters, 378 (3-4), 250-256.
- Tonmunphean, S., Wijitkosoom, A., Tantirungrotechai, Y., Nuttavut, N., Limtrakul, J. (2003) "Magnetizabilities of Ring-structured Molecules, [8]-cyclacene, [8]-BN-cyclacene and [8]-Collarene, and their Effect on <sup>3</sup>He Nuclear Shielding Tensor", Bulletin of the Chemical Society of Japan, 76, 1537-1541.
- Dungsrikaew, V., Limtrakul, J., et. al. (2003) "Comparison of methods for point charge representation of electrostatic fields", *International Journal of Quantum Chemistry*, 96, 17-22.
- Sailer, W., Pelc, A., Limao-Vieira, P., Mason, N.J., Limtrakul, J, and Probst, M., (2003) "Low energy electron attachment to CH<sub>3</sub>CN", Chemical Physics Letters, 381(1,2), 216-222.
- Panjan, W., Limtrakul, J. (2003) "The influence of the framework on adsorption properties of ethylene/H-ZSM-5 system: an ONIOM study", *Journal of Molecular Structure*, 654(1-3), 35-45.
- Raksakoon, C., Limtrakul, J. (2003) "Adsorption of aromatic hydrocarbon onto H-ZSM-5 zeolite investigated by ONIOM study" THEOCHEM 631, 147-156.
- Boekfa, B., Sirijareansre, J., Pantu, P. and Limtrakul, J., (2004) "A quantum chemical study of the interaction of carbonyls with H-ZSM-5 zeolite", Stud Surf Sci Catal. 154, 1582-1588.
- Wongthong, P., Soonthompalin, C., Pantu, P. and Limtrakul, J., (2004) "Adsorption of Toluene over Faujasite zeolite investigated by the combined quantum mechanics/molecular mechanics method", Stud Surf Sci Catal., 154, 1817-1822.
- Pabchanda, S., Pantu, P., Tantanak, D. and Limtrakul, J., (2004) "Structure and energetics
  of nitrous oxide and methane adsorption on the Fe-ZSM-5 zeolite: ONIOM and density
  functional studies". Stud Surf Sci Catal., 154, 1844-1848.
- Warakulwit, C., Bamrungsap, S., Luksirikul, P., Khongpracha, P. and Limtrakul, J., (2005)
   "Diels-Alder cycloadditions of single-wall carbon nanotubes and with electron-rich dienes", Surface Science, in press.
- Jansang, B., Limtrakul, J., (2005) "Adsorption of Benzene on MCM-41-type Material: A QM/MM Study", Surface Science, in press.

Molecular Design, Structure and Reaction Mechanisms of Nanostructured Materials Systems January 22<sup>nd</sup>, 2005, City Beach Resort, Rua Hin

#### Submitted

- 23. Lomratsiri, J., Probst, J., Limtrakul, J., "Structure and adsorption of a basic probe molecule on H-ZSM-5 zeolite: An embedded ONIOM study", *Chemical Physics Letters*, submitted.
- Sinjaraensre, J., Limtrakul, J., "Density functional study of mechanism of the Beckmann rearrangement catalyzed by H-ZSM-5: A cluster and embedded cluster study", *Journal of Physical Chemistry B*, submitted.
- Jungsuttiwong, S., Limtrakul, J., Truong, T. N., "Theoretical Study of Modes of Adsorption of Water Dimer on H-ZSM-5 and H-Faujasite Zeolites", Journal of Physical Chemistry B, submitted
- Treesukol, P., Srisuk, K., Limtrakul, J., "Understanding Metal-Support Interaction in Bifunctional Catalytic Pt/H-ZSM-5 Zeolite", Journal of Physical Chemistry B, submitted.
- 27. Namuangruk, S., Pantu, P., Limtrakul, J., "The ethylene dimerization over faujasite zeolite investigated by the ONIOM method", *ChemPhysChem.*, submitted.
- Pabchanda, S., Pantu, P., Tantanak, D. and Limtrakui, J., "Hydrolysis of methoxide species and regeneration of active site in Fe-ZSM-5 catalyst by the ONIOM method", J Mol Catal A: General, submitted.
- Sangthong, W., Probst, M., Limtrakul, J., "Computational study of the carbonyl-ene reaction of encapsulated formaldehyde in Na-FAU zeolite", J Chem Phys., submitted.

#### In Preparation

- Nokbin, S., Limtrakul, J., Hermansson, K., "Structural and Electronic peoperties of Rh/MgO(001): A periodic density functional study", in preparation.
- Khongpracha, P., Panjan W and Limtrakul, J., "Covalent Attachment of DNA on Single-Walled Carbon Nanotubes", in preparation.
- 32. Phanawadee, P., Phongaksom, M., Chaimonkol, N., Jaree, A., Limtrakul, J., "Interpretation of TAP pulse responses from a porous catalytic system: Theoretical analysis"; *Chemical Engineering Science, In preparation.*
- Tantanak, D., Gleeson, M. P., Limtrakul, J., "Probing the structural and electronic spectra affecting the adsorption and reactivity of alkenes in acidic zeolites using DFT calculations and Multivariate statistical methods", In preparation.
- 34. Nanok, T., Bopp, P.A., Limtrakul, J., "Molecular Dynamics Simulation Studies of Adsorption and Diffusion of p-Xylene in Si-MCM-41", *In preparation*.